Table of Contents

List of Tables

List of Figures

2.5 GEOLOGY, SEISMOLOGY, AND GEOTECHNICAL ENGINEERING

This section presents information on the geological, seismological, and geotechnical engineering properties of the {Nine Mile Point 3 Nuclear Power Plant (NMP3NPP)} site. Section 2.5.1 describes basic geological and seismologic data, {focusing on those data developed since the publication of the Final Safety Analysis Report (FSAR) for licensing Nine Mile Point (NMP) Unit 1 and Unit 2.} Section 2.5.2 describes the vibratory ground motion at the site, including an updated seismicity catalog, description of seismic sources, and development of the Safe Shutdown Earthquake and Operating Basis Earthquake ground motions. Section 2.5.3 describes the potential for surface faulting in the site area, and Section 2.5.4 and Section 2.5.5 describe the stability of surface materials at the site.

Appendix D of Regulatory Guide 1.165, "Geological, Seismological and Geophysical Investigations to Characterize Seismic Sources," (NRC, 1997) provides guidance for the recommended level of investigation at different distances from a proposed site for a nuclear facility.

- The site region is that area within 200 mi (322 km) of the site location
- The site vicinity is that area within 25 mi (40 km) of the site location
- The site area is that area within 5 mi (8 km) of the site location
- The site is that area within 0.6 mi (1 km) of the site location

These terms, site region, site vicinity, site area, and site, are used in Section 2.5.1 through Section 2.5.3 to describe these specific areas of investigation. These terms are not applicable to other sections of the FSAR.

The geological and seismological information presented in this section was developed from a review of previous reports prepared for the existing units, published geologic literature, interpretation of aerial photography, and a subsurface investigation and field and aerial reconnaissance conducted for preparation of this application. {Previous site-specific reports reviewed include the NMP Unit 2 Updated Final Safety Analysis Report (CEG, 1998) and Dames & Moore geologic reports for NMP Unit 2 (Niagara Mohawk, 1978a; Niagara Mohawk 1978b; Niagara Mohawk, 1978c and Niagara Mohawk, 1980).} A review of published geologic literature was used to supplement and update the existing geological and seismological information. In addition, relevant unpublished geologic literature, studies, and projects were identified by contacting the U.S. Geological Survey (USGS), State geological surveys and universities. The list of references used to compile the geological and seismological information is presented in the applicable section.

{Extensive geologic and related explorations were conducted, and can be categorized as: 1) general exploration; 2) bedrock investigation and mapping; 3) supplementary geologic exploration; and 4) rock mechanics investigation. Extensive geophysical surveys were performed, including seismic refraction profiling. Field reconnaissance of the site and within a 25 mi (40 km) radius of the site was conducted by geologists.

The investigations of regional and site physiographic provinces and geomorphic processes, geologic history, stratigraphy, tectonics and structural geology and geotechnical engineering were conducted by GEI Consultants, Inc. and AREVA NP. Risk Engineering Inc. conducted probabilistic seismic hazard analyses and Weston Geophysical Engineers conducted geophysical surveys and seismicity catalog updates.

The results of the investigations indicate that the site is relatively tectonically stable and the site area and region are generally free of major active tectonic structures. There are no known capable faults within the site vicinity, and there is no potential for surface faulting within the site area. The subsurface materials at the NMP3NPP site are not adversely affected by collapse, subsidence, or uplift and present no adverse foundation conditions for site structures. The ground motion level for the SSE was calculated using conservative correlations sufficiently representative of seismic wave transmission characteristics of the site.}

This section is intended to demonstrate compliance with the requirements of paragraph c of 10 CFR 100.23, "Geologic and Seismic Siting Criteria" (CFR, 2007).

2.5.1 BASIC GEOLOGIC AND SEISMIC INFORMATION

The U.S. EPR FSAR includes the following COL Item in Section 2.5.1:

> A COL applicant that references the U.S. EPR design certification will use site-specific information to investigate and provide data concerning geological, seismic, geophysical, and geotechnical information.

The COL Item is addressed as follows:

This section presents information on the geological and seismological characteristics of the site region (200 mi (322 km) radius), site vicinity (25 mi (40 km) radius), site area (5 mi (8 km) radius) and site (0.6 mi (1 km) radius). Section 2.5.1.1 describes the geologic and tectonic characteristics of the site region. Section 2.5.1.2 describes the geologic and tectonic characteristics of the site vicinity and location. The geological and seismological information was developed in accordance with the following NRC guidance documents:

- Regulatory Guide 1.70, Section 2.5.1, "Basic Geologic and Seismic Information," (NRC, 1978)
- Regulatory Guide 1.206, "Combined License Applications for Nuclear Power Plants (LWR Edition)," (NRC, 2007a) and
- Regulatory Guide 1.165, "Identification and Characterization of Seismic Sources and Determination of Safe Shutdown Earthquake Ground Motion," (NRC, 1997).

2.5.1.1 Regional Geology (200 mi (322 km) radius)

The U.S. EPR FSAR includes the following COL Item in Section 2.5.1.1:

> Regional geology is site specific and will be addressed by the COL applicant.

This COL Item is addressed as follows:

This section discusses the physiography, geologic history, stratigraphy, and tectonic setting within a 200 mi (322 km) radius of the site (Figure 2.5-1). The regional geologic map as shown in Figure 2.5-2 contains information on the geology, stratigraphy, and tectonic setting of the region surrounding the {NMP3NPP site (Schruben, 1994).} Summaries of these aspects of regional geology are presented to provide the framework for evaluation of the geologic and seismologic hazards presented in the succeeding sections.

{Section 2.5.1.1.1 through Section 2.5.1.1.4 are added as a supplement to the U.S. EPR FSAR.

2.5.1.1.1 Regional Physiography and Geomorphology

The NMP3NPP site lies within the Physiographic Provinces shown in Figure 2.5-3 (Fenneman, 1946; GSC, 1975). The area within a 200 mile (322 km) radius of the NMP3NPP site encompasses parts of five other physiographic provinces in the United States and three other physiographic provinces in Canada. In the United States these provinces are: The Central Lowland; the Adirondack Massif, the Appalachian - Allegheny Plateau, the Valley and Ridge (including the Great Valley), and the Northern Appalachians - New England Province (Fenneman, 1946; NYSM, 1990). In Canada the provinces within the 200-mile (322 km) radius of the NMP3NPP site are: The West St. Lawrence Lowland, The Central St. Lawrence Lowland and The Laurentian Highlands (GSC, 1975).

Each of these physiographic provinces is briefly described in the following sections. The physiographic provinces in the site region are shown on Figure 2.5-3 and Figure 2.5-4 (Fenneman, 1946; GSC, 1975).

2.5.1.1.1.1 Central Lowland Physiographic Province - Central St. Lawrence Lowland

The Central Lowland Physiographic Province includes large portions of the U.S. Mid-west, including the area around the Great Lakes. The NMP3NPP site is located on a northeast extension of the U.S. Central Lowland Physiographic Province, which extends to the north of Lake Ontario, into Canada, where it is known as the West St. Lawrence Lowland. The Central Lowland is bounded by Appalachian Plateau to the south. To the east, the Central Lowland is bounded by the Tug Hill Plateau (a small portion of the Appalachian Plateau), and by the Adirondack Mountains. To the northeast the Central Lowland is bounded by the Frontenac Arch of the Grenville Province, beyond which is located the Central St. Lawrence Lowland in Canada (Figure 2.5-3 and Figure 2.5-4). To the north, the Central Lowland is bounded by the Laurentian Highlands of the Canadian Shield in Ontario and Quebec in Canada. To the south the Central Lowland is bounded by the main potion of the Appalachian Plateau.

The portion of the Central Lowland in New York is also known as the Erie-Ontario Plain (USGS, 1982a), the Erie - Ontario Lowlands (Isachsen, 2000) and the Lake Ontario Plain (USGS, 2002a). These refer to a smaller area of the Central Lowland in New York. The most common term in New York geologic literature is the Erie-Ontario Lowland.

The Erie-Ontario Lowlands extend southward from the site about 35 miles (56 km) to the Portage Escarpment which forms the boundary between the lowlands and the Allegheny Escarpment portion of the Appalachian-Allegheny Plateau Province, and westward into Canada near Niagara Falls. Differential erosion of southerly dipping, relatively more resistant carbonate rock of the Lockport and Onondaga Formations has resulted in east-west trending cuestas within the lowlands (CEG, 1998).

The generally flat to gently undulating topography of the Central Lowland is superimposed upon erosional bedrock surface of irregular, low relief. The land surface rises gradually to the south and southeast from an elevation of 246 feet (75 m) above msl at the southern shore of Lake Ontario to an elevation of approximately 500 feet (152 m) above msl at the base of the Allegheny Escarpment.

Four main periods of continental glaciation occurred in the site region during the Pleistocene. Glaciers advanced as far south as northeastern Pennsylvania and central New Jersey. Thus the topography is dominated by glacial landforms (Isachsen, 2000).

A veneer of glacial deposits such as tills, glaciofluvial deposits, and proglacial lake sediments covers most of the area. The deposits occur as drumlin fields and recessional moraines. Postglacial weathering and stream erosion have modified the terrain only slightly.

2.5.1.1.1.2 Laurentian Highlands Province

The Laurentian Highlands are bordered to the southwest by the West St. Lawrence Lowland and to the southeast by the Central St. Lawrence Lowland. The Laurentian Highlands of Canada include the Grenville Province and extend to the east along the Frontenac Arch to connect with the Adirondack Mountains. The Grenville Province is underlain by highly deformed Precambian metamorphic bedrock (Davidson, 1998).

2.5.1.1.1.3 West St. Lawrence Lowland Province

The West St. Lawrence Lowland of Canada is the northwestern extension of the Central Lowland - Central St. Lawrence Lowland. The West St. Lawrence Lowland is that part of the St. Lawrence drainage basin underlain by gently dipping Paleozoic bedrock (Karrow, 1989). The West St. Lawrence Lowland includes land on both sides of the St. Lawrence River and trends parallel to the St. Lawrence River (Figure 2.5-3). The region is long and narrow and trending southwest-northeast, with its central area characterized by generally low relief and extensive glacial drift cover which is commonly 98 feet (30 m) to 197 feet (60 m) thick.

2.5.1.1.1.4 Northern Appalachians - New England

The Northern-Appalachians-New England Province includes the Taconic Mountains located along the New York, Connecticut, Massachusetts and Vermont borders which are within a 200 mile (322 km) radius of the NMP3NPP site. The Northern Appalachians are bordered to the west by the Great Valley of the Valley and Ridge Province and by the Atlantic Ocean to the east (Figure 2.5-4). The Northern Appalachian Province includes folded and faulted Paleozoic sedimentary rocks (Karrow, 1989; Williams, 1995; Hibbard, 2007), metamorphic rocks and igneous rocks. The New England Province includes: the White Mountain section of residual mountains in New Hampshire and Maine, The Green Mountain section which is a linear north-south uplift which extends from Canada, through Vermont to northern Massachusetts and the Taconic section of New York, Massachusetts and Vermont which includes mountains and limestone valleys (Fenneman, 1938).

2.5.1.1.1.5 Adirondack Mountains

The Adirondack Mountains are the eastern extension of the Grenville Province of the Laurentian Highlands. The two provinces are connected by the Frontenac Arch and Adirondack Lowlands and are underlain by high grade Precambrian metamorphic bedrock (Tollo, 2004). The Adirondack Province covers approximately 10,000 square miles. The Great Valley of the Valley and Ridge Province borders the Adirondacks to the east, while the Central Lowland Province of the St. Lawrence Valley borders the Adirondacks to the west. To the north (Figure 2.5-3) the Adirondacks are bordered by the Central St. Lawrence Lowland of Canada and the Adirondacks are bordered to the south by the Appalachian Plateau (Fenneman, 1938).

2.5.1.1.1.6 Valley and Ridge Physiographic Province

The Valley and Ridge Physiographic Province forms the 900 mile (1,500 km) long, central portion of the Appalachian Mountains. It lies south and east of the Appalachian Plateau Province as shown in Figure 2.5-3 and Figure 2.5-4. Valleys and ridges are aligned in a northeast-southwest direction in this province, which is between 25 and 50 miles (40 and 80 km) wide. The sedimentary rocks underlying the Valley and Ridge Province are tightly folded and, in some locations, faulted (Milici, 1988). Sandstone units that are more resistant to

weathering are the ridge formers, while less resistant shales and limestones underlie most of the valleys (Faill, 1997a; Faill 1997b). The Great Valley Section of the province as shown in Figure 2.5-3. The Valley and Ridge Province is divided into many distinct lowlands by ridges or knobs, the largest lowland being the Shenandoah Valley in Virginia. This broad valley is underlain by shales and by limestones in the southern portion that are prone to dissolution, resulting in the formation of sinkholes and caves (NYSM, 2004). Elevations within the Shenandoah Valley typically range between 500 and 1,200 feet (152 and 366 m) msl. The northern extension of The Great Valley is known as the Hudson - Mohawk Lowlands in New York and the Champlain Lowlands in Vermont (Isachsen, 2000). The western portion of the Valley and Ridge Province is characterized by a series of roughly parallel ridges and valleys, some of which are long and narrow. Elevations within the ridges and valleys range from about 1,000 to 4,500 feet (305 to 1,372 m) msl.

2.5.1.1.1.7 Appalachian - Allegheny Plateau Physiographic

Located north and west of the Valley and Ridge Province, the Appalachian Plateau Physiographic Province includes the western part of the Appalachian Mountains, stretching from New York to Alabama as shown in Figure 2.5-3. The Allegheny Front is the topographic and structural boundary between the Appalachian Plateau and the Valley and Ridge Province. It is a bold, high escarpment, underlain primarily by clastic sedimentary rocks capped by sandstone and conglomerates. In eastern West Virginia, elevations along this escarpment reach 4,790 feet (1,460 m) (Hack, 1989). West of the Allegheny Front, the Appalachian Plateau's topographic surface slopes gently to the northwest and merges imperceptibly into the Interior Low Plateaus. The Tug Hill Plateau, northeast of the NMP3NPP site, is the northern most extension of the Allegheny Plateau. The Catskill Mountains represent the northeastern extent of the Allegheny Plateau.

The Appalachian Plateau Physiographic Province is underlain by sedimentary rocks such as sandstone, shale, and coal of Cambrian to Permian age (Milici, 1988). These strata are generally subhorizontal to gently folded into broad synclines and anticlines and exhibit relatively little deformation (Faill, 1998). These sedimentary rocks differ significantly from each other with respect to resistance to weathering. Sandstone units tend to be more resistant to weathering and form topographic ridges. The relatively less resistant shales and siltstones weather preferentially and underlie most valleys. The Appalachian Plateau is deeply dissected by streams into a maze of deep, narrow valleys and high narrow ridges. Limestone dissolution and sinkholes occur in the southern portion where limestone units with high karst susceptibility occur at or near the ground surface.

2.5.1.1.2 Regional Geologic History

The geologic history of the NMP3NPP site region, located within the northern Appalachian Basin, began circa (ca.) 1.3 Ga (billion years ago) in the late Precambrian (Isachsen, 2000; NYSM, 1990). Through the Paleozoic, compressional events (orogenies) and rifting were the predominant tectonic forces occurring to the east. Deformation and rifting is clearly visible in the rock record of the northern and eastern part of the site region. These orogenic and rifting events to the east drove the relatively slower nonorogenic vertical crustal movements at the NMP3NPP site and the record of deposition and erosion within the northern Appalachian Basin reflects the vertical movements of the region (CEG, 1998).

The following paragraphs outline the major regional geologic events. Regional tectonics are discussed in more detail in more detail in Section 2.5.1.1.4 and discussion of the resulting stratigraphic sequences of the region can be found in Section 2.5.1.1.3. The Geologic Time Scale, which lists the major periods in geologic time, is presented in Figure 2.5-5.

A series of figures illustrating the geologic evolution of the Eastern Margin of North America is presented in Figure 2.5-6 through Figure 2.5-16. These figures, beginning in the mid-Proterozic and continuing through to the present, illustrate the major tectonic events which provided the growth of the eastern North American continent.

2.5.1.1.2.1 Grenville Orogeny

The Grenville Orogeny refers to the period ca. 1.3-1.0 Ga when multiple collision events occurred along the southeastern margin of Laurentia. At this time, Laurentia, or proto-North America, was covered in shallow seas where sand, mud, and lime-rich sediments accumulated (Isachsen, 2000). Prior to the Grenville Orogeny, oceanic crust to the east of Laurentia began subducting beneath it, which led to the formation of a magmatic arc (Isachsen, 2000). Eventually the oceanic crust completely subducted and the ocean basin closed leading to a continent-continent collision, marking the onset of the Grenville Orogeny. Figure 2.5-17 is a crustal-scale cross-section of the Grenville Orogeny in Southern Ontario.

The complex series of events, termed the Grenville orogenic cycle, can be further broken down into the Elzevirian Orogeny, anorthosite-mangerite-charnockite-granite (AMCG) magmatism, and the Ottawan Orogeny, three regional pulses of activity analogous to the Appalachian orogenic cycle (Tollo, 2000). The Elzevirian and Ottawan orogenies brought about crustal uplift and compressional deformation while the AMCG magmatism led to contact metamorphism from the heat of the intrusive body (Hughes, 1991; Hughes, 1992). The Grenville Orogeny led to the formation of a Himalayan-size mountain range at the margin of the continent-content collision with an uplifted plateau to the west, similar to the modern Tibetan Plateau, which may have extended as far as Texas and Mexico (Isachsen, 2000).

The protolith of the metamorphosed Grenville basement in a portion of the Central Metasedimentary Belt (CMB) has a formation age of ca. 2.7 Ga which is equivalent to the ages of rock in the Canadian Superior Province (Isachsen, 2000). The Grenville basement rocks, now exposed to the north and east of the NMP3NPP site in the Adirondack Lowlands and Highlands are, therefore, a southern extension of the CMB (Rankin, 1993; Carr, 2000). Thus the effects of the Grenville Orogeny are visible only in bedrock outcrops in the northern portion of the NMP3NPP 200 mi (322 km) site radius. Grenville basement rocks are also exposed to the south in the northern Blue Ridge Province and episodes of metamorphism and deformation in these rocks have been correlated to those further north (Tollo, 2004).

2.5.1.1.2.2 Late Precambrian Subsidence and Rifting

The Grenville Orogen subsided ca. 1.0 Ga and erosion and spreading became the predominant tectonic forces due to the absence of crustal thickening and compression (Reed, 1993). Erosion removed approximately 16 miles (25 km) of Grenville basement crust during the late Proterozoic prior to rifting along the Grenville suture zone approximately 660 Ma (million years ago) (Isachsen 2000). The rifting left the east coast of the proto-North American continent as a passive margin with a vast basin extending eastward (Figure 2.5-6, Figure 2.5-7, Figure 2.5-8 and Figure 2.5-9). At the basin extended, a divergent margin formed which produced basalt and formed new oceanic crust. The oceanic crust continued to build and the Iapetus Ocean was formed with a central divergent margin (Isachsen, 2000) (Figure 2.5-10). Sedimentation in the Iapetus Ocean along the margin of North America was derived from beach sands and the marine life along the coast. During Late Cambrian time, as the now tectonically stable continental margin continued to subside, micro-continents and volcanic arcs, characteristic of an intra-oceanic island-arc terrane, began to develop in the proto-Atlantic Ocean as a result of east-directed oceanic subduction and initial closing of the proto-Atlantic. The Penobscot Orogeny (documented in the Maritime Provinces of Canada) is thought to have been caused by crustal convergence and accretion of these volcanic arcs thrust over micro-continents along

the North American plate margin (Williams, 1995). This orogeny is considered to represent the beginning of the convergent phase in the closing of the proto-Atlantic Ocean. Subsequent convergent phases in the closing of the proto-Atlantic include the Taconic and Acadian orogenies and the Allegheny orogeny that finally closed the proto-Atlantic in the Permian (Reed, 1993).

2.5.1.1.2.3 Taconic Orogeny

The Taconic Orogeny occurred during Middle to Late Ordovician time and was caused by continued collision of micro-continents and volcanic arcs with eastern North America along an eastward dipping subduction zone during progressive closure of the proto-Atlantic Ocean (Figure 2.5-11 and Figure 2.5-12). The Iapetus Ocean began to close ca. 550 Ma as the tectonic forces reversed. Reversal of the divergent margin in the central Iapetus Ocean led to subduction of the western portion of the ocean (the proto-North American Plate) below the eastern portion (Isachsen, 2000). The subducting plate formed the Taconic island arc. The Iapetus Ocean basin separated the proto-North American continent from the Taconic arc (Figure 2.5-12). Once the Iapetus Ocean basin had fully subducted, the Taconic Orogeny began to build the Taconic Mountains during an island arc collision.

During and after the Taconic Orogeny, the Taconic Mountains eroded rapidly. The mountains provided the material that filled Appalachian Basin and the shallow inland sea covering central North American, including western New York. The resulting sedimentary sequence records a transgressive marine environment extending from the Cambrian to the Middle Ordovician followed by a regressive marine environment during the Middle and Late Ordovician (Isachsen, 2000; Sloss, 1988).

The marine transgressive sequence is represented by relatively shallow water Cambrian sandstone units followed by deeper water Ordovician carbonate units while the marine regressive sequence is represented by deep water siltstone and shale followed by relatively shallow water sandstone units (Millici, 1988). Deposition continued in the eastern part of the Appalachian basin into Early Devonian time (Faill, 1997b). The deposition of these units is also discussed in Section 2.5.1.2.

The present-day Taconic Mountains are a portion of the New England physiographic province and are considered part of the Appalachian Mountains, trending northeast-southwest along the eastern border of New York/Western border of New England.

2.5.1.1.2.4 Acadian Orogeny

The Acadian Orogeny occurred ca. 410 Ma as the micro-continent Avalon collided with eastern North America (Figure 2.5-12). At its peak, the orogeny produced a continuous chain of mountains along the east coast of North America and brought with it associated volcanism and metamorphism. The Acadian orogeny ended the largely quiescent environment that dominated the Appalachian Basin during the Silurian, as vast amounts of terrigenous sediment from the Acadian Mountains were introduced into the basin and formed the Catskill clastic wedge in New York and Pennsylvania as shown (Isachsen, 2000). Thick accumulations of clastic sediments belonging to the Catskill Formation are spread throughout the Valley and Ridge Province (Faill, 1997b). During the Mississippian Period, the Acadian Mountains were completely eroded, and the basement rocks of the Avalon terrane were exposed.

Although much of the adjacent New England Province contains bedrock highly affected by the Acadian Orogeny, bedrock in New York state was unaffected by the tectonic event and evidence of the Acadian Orogeny is not observed at the NMP3NPP site.

2.5.1.1.2.5 Allegheny Orogeny

The Allegheny Orogeny (also historically referred to as the Appalachian Orogeny) occurred ca. 330 Ma and represents the final convergent phase in the closing of the proto-Atlantic Ocean in the Paleozoic Era (Isachsen, 2000). Metamorphism and magmatism were significant events during the early part of the Allegheny Orogeny. The Allegheny orogeny was caused by the collision of the North American and African plates, and it produced the Allegheny Mountains (Figure 2.5-13). As the African continent was thrust westward over North America, the Taconic and Acadian terranes became detached and also were thrust westward over Grenville basement rocks. The northwest movement of the displaced rock mass above the thrust was progressively converted into the deformation of the rock mass, primarily in the form of thrust faults and fold-and-thrust structures, as seen in the Blue Ridge and Piedmont Plateau Provinces (Faill, 1997b). The youngest manifestation of the Allegheny orogeny was northeast-trending strike-slip faults and shear zones in the Piedmont Province. The extensive, thick, and undeformed Appalachian Basin and its underlying sequence of carbonate sediments were deformed and a fold-and-thrust array of structures, long considered the classic Appalachian structure, was impressed upon the basin (Figure 2.5-13). The tectonism produced the Allegheny Mountains and a vast alluvial plain to the northwest (Faill, 1998). The Allegheny Front along the eastern margin of the Appalachian Plateau Province is thought to represent the western most extent of the Allegheny orogeny (Hatcher, 1987). Rocks throughout the Valley and Ridge Province are thrust faulted and folded up to this front, whereupon they become relatively flat and only slightly folded west of the Allegheny Front (Faill, 1998).

2.5.1.1.2.6 Early Mesozoic Extensional Episode (Triassic Rifting)

2.5.1.1.2.6.1 Opening of the Atlantic Ocean

The Allegheny Orogeny marked the last collision event in proto-North America. The result of which, along with other orogenies around the world, was the supercontinent, Pangaea (Figure 2.5-13 and Figure 2.5-14). Pangaea began to break up ca. 220 Ma during a worldwide rifting event, which rapidly separated the modern continents. One of these divergent margins occurred along eastern North America as Africa rifted away creating a basin and range topography similar to that of the western United States (Isachsen, 2000). As the divergent margin progressed, the widening gap between North America and Africa gave rise to the Atlantic Ocean, similar to the formation of the Iapetus Ocean (Figure 2.5-13).

Crustal extension during Early Mesozoic time (Late Triassic and Early Jurassic) marked the opening of the Atlantic Ocean. This extensional episode produced numerous local, closed basins ("Triassic basins") along eastern North America (Faill, 1998). The elongate basins generally trend northeast, parallel to the pre-existing Paleozoic structures. The basins range in length from less than 20 miles (32 km) to over 100 miles (161 km) and in width from less than 5 miles (8 km) to over 50 miles (80 km). Mesozoic basins closest to the NMP3NPP site include the Newark Basin in New Jersey and New York and the Connecticut River basin of Connecticut and Massachusetts. The New York Basin contains sedimentary rocks of the Newark Group and the igneous rock of the Palisades Sill (Isachsen, 2000). Valleys in these Mesozoic basins are developed on sandstone and shale units and trend northeast-southwest, parallel to the strike of the bedrock. Generally, the basins are asymmetric half-grabens with principal faults located along the western margin of the basins. Triassic and Jurassic rocks that fill the basins primarily consist of conglomerates, sandstones, and shales interbedded with basaltic lava flows. At several locations, these rocks are cross-cut by basaltic dikes. The basaltic rocks are generally more resistant to erosion and form local topographically higher landforms (Isachsen, 2000).

2.5.1.1.2.6.2 Cenozoic History

The Early Mesozoic extensional episode gave rise to the Cenozoic Mid-Atlantic spreading center. The Atlantic seaboard presently represents the trailing passive margin related to the spreading at the Mid-Atlantic ridge (Figure 2.5-15 and Figure 2.5-16). Ridge push forces resulting from the Mid-Atlantic spreading center are believed to be responsible for the northeast-southwest directed horizontal compressive stress presently observed in the northeastern U.S.; however, these stresses do not appear to be responsible for joint systems observed in the region, as discussed in Section 2.5.1.1.4.4.2)

During Cenozoic time, as the Atlantic Ocean opened, the newly formed continental margin cooled and subsided, leading to the present day passive trailing divergent continental margin. As the continental margin developed, continued erosion of the Appalachian Mountains produced extensive sedimentation within the Coastal Plain, slightly beyond the 200 mile (322 km) radius of the NMP3NPP site.

During the Quaternary Period, much of the northern United States and Canada experienced multiple glaciations interspersed with warm interglacial episodes (Karrow, 1989). The last (Wisconsinan) Laurentide ice sheet advanced over much of North America during the Pleistocene. The southern limit of glaciation extended into parts of northern Pennsylvania and New Jersey and covered the NMP3NPP site vicinity. Present-day Holocene landscapes, therefore, are partially the result of glacial geologic processes responding to isostatic uplift.

Figure 2.5-18 is a tectonic map of New York and the surrounding area. This figure illustrates the current physical extent of each of the geologic episodes discussed above and summarizes the dominant rock types in each domain. The glacial till and other glacial deposits in the NMP3NPP site region are due to the Laurentide glacial advance or retreat. The basins of the Great Lakes themselves were scoured out by Laurentide ice sheets or possibly earlier glacial advances.

2.5.1.1.3 Regional Stratigraphy

This section contains information on the regional stratigraphy within each of the physiographic provinces. The regional geology and generalized stratigraphy within a 200 mile (322 km) radius of the NMP3NPP site is shown on Figure 2.5-2.

The NMP3NPP site is located on Paleozoic sedimentary rocks ranging in age from Middle Ordovician to Late Ordovician, which, in turn, were deposited unconformably on the Precambrian basement rock. The Paleozoic section shown on the site stratigraphic column in Section 2.5.1.2 (Figure 2.5-57) is projected to the site from proximal deep borings which intersect the Precambrian basement.

Paleozoic sedimentary rocks were deposited in the Appalachian Basin extending from New York to Alabama (Milici, 1988; Swezey, 2002). The sedimentary rocks at NMP3NPP were deposited during a period of marine regression and exhibit lateral and vertical variation in both lithology and texture.

The closest deep boring which extends through the Paleozoic sedimentary sequence and advances to Precambrian gneissic basement is approximately 7 miles (11 km) southwest of the NMP3NPP site in Oswego County (Flagler, 1966; Kreidler, 1972). This boring penetrated the Trenton Group and Black River Group and the underlying Precambrian crystalline gneissic basement. The Cambrian Theresa dolomite/sandstone/orthoquartzite and Potsdam orthoquartzite/sandstone were not present at this location.

Additional deep borings are located between approximately 12 and 42 miles (19 and 68 km) from the NMP3NPP site. These additional deep borings close to NMP3NPP indicate that the Cambrian Potsdam Sandstone and Theresa Formation are not present at these locations.

Section 2.5.1.2.3 presents an area-specific stratigraphic column (Figure 2.5-57) based on correlations by Flagler (Flagler, 1966), Fischer (Fischer, 1978), Fisher (Fisher, 1977), and Rickard (Rickard, 1973).

Near surface bedrock in the region consists of nearly flat-lying Paleozoic sedimentary rock with horizontal homogeneity. The sedimentary rock formations dip regionally to the south-southwest with a gradient of approximately 50 ft/mi (9 m/km) (roughly 1 foot per hundred feet)).

The bedrock formations at the NMP3NPP site are, in order of increasing depth:

- Oswego Sandstone (sandstone, Late Ordovician)
- Pulaski Formation (interbedded dark gray siltstone, gray sandstone, and dark gray argillaceous sandstone, Late Ordovician)
- Whetstone Gulf Formation (alternating dark gray siltstone, gray sandstone, and dark gray argillaceous sandstone, Late Ordovician)
- Trenton and Black River Groups (carbonate sequence, limestone with minor shale, Ordovician)
- Grenville Province (crystalline gneissic rock, Precambrian)

The estimated elevation of the top of the Trenton Group at the site is 800 feet (213 m) below mean sea level, plus or minus 200 feet (61 m). The estimated elevation of the top of the Precambrian crystalline rock is 1,500 feet (457 m) below mean sea level, plus or minus 200 feet (61 m).

All of these Ordovician formations consist primarily of gently dipping sandstone, siltstone, and shale. The boundary between units is often gradational, and the units are lithologically similar.

2.5.1.1.3.1 Central Lowland - St. Lawrence Lowland Physiographic Province

There are two distinct divisions of the bedrock of the Central Lowland -St. Lawrence Lowland Physiographic Province of the U.S. and Canada. These are a set of predominantly Precambrian crystalline basement rocks and Paleozoic age sedimentary rocks.

2.5.1.1.3.1.1 Crystalline Rocks (Precambrian)

Crystalline rocks of the Central Lowland - St. Lawrence Lowland Physiographic Province primarily occur beneath the cover of overlying Paleozoic sedimentary rocks. The crystalline rocks consist of deformed and metamorphosed meta-sedimentary, meta igneous, and meta-volcanic rocks intruded by mafic dikes and granitic plutons. Proterozoic Grenville rocks in the U.S. have been summarized by Reed (Reed, 1993), Rankin (Rankin, 1993) and Tollo (Tollo, 2004). An overview of the Grenville Province Precambrian rocks of the Canada has been described by Davidson (Davidson, 1998).

2.5.1.1.3.1.2 Sedimentary Rocks (Paleozoic)

Sedimentary rocks of the Central Lowland-St. Lawrence Lowland Physiographic Province primarily form the bedrock of the province. The sedimentary rocks consist of relatively undeformed, flat lying sandstone, limestone and shale. Salt deposits are also present in New York State. Sedimentary rocks in the Appalachian Basin, including the Central Lowland Physiographic Province have been summarized by Milici (Milici, 1988) and Sloss (Sloss, 1988). Sedimentary rocks of the St. Lawrence Lowland Physiographic Province in Canada have been described by Atken (Atken, 1993), Stott (Stott, 1993) and Sanford (Sanford, 1993a; Sanford, 1993b).

2.5.1.1.3.1.3 Precambrian Basement Rock

Precambrian Basement

Crystalline basement rocks of Precambrian age are exposed north and northeast of the NMP3NPP site in three areas:

1. The Adirondack Massif 50 miles (80 km) northeast.

2. The Frontenac Arch of the Thousand Islands region 75 miles (121 km) north.

3. The Canadian Shield of Ontario and Quebec Provinces, Canada 90 miles (145 km) north.

In general, the Precambrian basement rocks of these three areas are divided into two broad geologic provinces and several subprovinces and belts (Carr, 2000) which are illustrated on the regional geologic map (Figure 2.5-2). In western Ontario, the Superior subprovince of the Canadian Shield is separated from the neighboring Grenville subprovince of central and eastern Ontario and Quebec by the Grenville Front (Davidson, 1998). The crystalline rocks of the Superior subprovince (metamorphosed igneous and sedimentary rock) are of Archean age, that is, more than approximately 2.5 Ga. Southeast of the Grenville Front, the Grenville subprovince consists of largely high-grade metamorphic rocks, whose ages range from Archean in the northwest to Early and Medial Proterozoic (2.5 to 1.1 Ga) near the St. Lawrence valley. The Grenville subprovince consists of both orthogneiss (metamorphosed igneous rock) and paragneiss (metamorphosed sedimentary rock) surrounding a central belt of paragneiss. This belt is termed the Central Metasedimentary Belt (Hughes, 1992). The terrain of mixed gneisses of Canada and the Adirondacks is understood to represent the pre-Grenville Precambrian "basement" shallow platform upon which the protolithic sediments and volcanics were deposited in Proterozoic time (1.1 to 1.4 Ga) (Sanford, 1993b). These particular paragneisses are termed the Grenville Series or the Grenville Supergroup (Williams, 1995). The Late Precambrian sediments underwent progressive, high-grade metamorphism culminating approximately 1.1 Ga, during an event known as the Grenville Orogeny. The sediments were altered to marble, quartzite, quartzofeldspathic gneiss, granulite, leucogranitic gneiss, and amphibolite. The gneisses bordering the Central Metasedimentary Belt in western Ontario consist largely of quartzofeldspathic paragneisses, whereas those in the Adirondack Massif consist of intermediate igneous rocks with granitic rocks and marbles. Local igneous intrusives ranging from felsic to mafic occur throughout the Grenville subprovince (Rankin, 1993).

The erosional surface developed on the Precambrian rocks of the Canadian Shield slopes gradually southward, beneath the Paleozoic cover rocks of the Appalachian Basin at a gradient of 45 to 50 ft/mi (8.5 to 9.5 m/km). This slope gradually steepens to 90 to 100 ft/mi (17 to 19 m/km) in south central New York. As the erosional surface dips southward, the Paleozoic cover becomes thicker in the Appalachian Basin (Swezey, 2002)

Direct knowledge of the composition of the Precambrian basement beneath the cover rocks is very limited, consisting of core samples from widely-spaced boreholes that penetrated the basement complex. The long geological history of the rock, which includes intensive metamorphism, makes interpretation of the distribution and structure of the covered basement rocks very difficult. More information is gained from studies of regional Bouguer gravity and aeromagnetic anomalies (Figure 2.5-19, Figure 2.5-20, and Figure 2.5-30).

Deep well data from central New York State (Flagler, 1966; Kreidler, 1972) indicate that the basement rocks are typically of gneissic composition (biotite-quartz-feldspar gneiss). Marble, amphibolite, and quartz-feldspar granulite have also been reported. Granite was reported from a well near Oswego. A geothermal test well drilled in Spring 1982 penetrated the basement near Auburn, New York. Core retrieved from the Auburn Geothermal Test well at 1560-m depth consisted of a coarse-grained, light gray massively-bedded dolomite marble with occasional trace amounts of pyrite, chalcopyrite with bornite and chalcocyte. This basement rock type is consistent with rock types previously extracted from deep wells in southern Ontario and Central and Western New York State.

Deep well data from western New York State (Flagler, 1966; Kreidler, 1972) indicate extensive areas of granite and marble. Locally, gabbroic intrusives surrounded by areas of metavolcanics are known.

The Central Metasedimentary Belt of the Canadian Shield in Ontario consists of rock types similar to those extracted from deep wells in central and western New York State. In the belt, local mafic intrusives and extensive felsic intrusive bodies are surrounded by highly-deformed gneisses, marbles, and schists. This information suggests that prominent local density and magnetic contrasts may exist in the basement rocks. Moreover, the pattern of regional Bouguer gravity anomalies (Figure 2.5-20) and regional aeromagnetic anomalies (Figure 2.5-19) confirms such contrasts. From these observations, it appears reasonable to suggest that the Central Metasedimentary Belt extends southward from the Canadian Shield into central and western New York. It is uncertain, however, how far south this belt continues.

The Precambrian basement rocks of the Grenville Province are located approximately 1,770 feet (540 m) deep at the NMP3NPP site. A contour map of the top of the Precambrian basement rock is presented in Figure 2.5-21. It is likely that the Precambrian rock underlying the NMP3NPP site is similar to Precambrian rock noted from deep wells located in Oswego County. Precambrian basement rocks have been described from wells located approximately 7 miles (11 km) (Beckwith well), 17 miles (27 km) (Fee #1 well), 28 miles (45 km) (Slayton 2 well) and 42 miles (68 km) (Ainsworth well) from the NMP3NPP site. The Precambrian metamorphic rocks from the Beckwith well have been described as pink quartz-feldspar gneiss, sparsely biotitic and chloritic (Flagler, 1966). The Precambrian metamorphic rocks from the Fee #1 well have been described as white calc-silicate rocks (Flagler, 1966). The Precambrian metamorphic rocks from the Slayton 2 well have been described as pink quartz-feldspar granulite, sparsely magnetitic, pyroxenic, chloritic (Flagler, 1966). The Precambrian metamorphic rocks from the Ainsworth well have been described as white quartz-feldspar gneisses, sparsely biotitic, muscovitic, hornblendic (Flagler, 1966).

2.5.1.1.3.1.4 Paleozoic Sedimentary Rocks

The Paleozoic formations in northern central New York State form a wedge that thickens to the south, away from the Canadian Shield. The strata are relatively flat-lying but have been rotated slightly, exhibiting a gentle, regional gradient to the south (approximately 50 ft/mi, 9.5 m/km). In the vicinity of the Nine Mile Point Nuclear Station (NMPNS) site, Late Ordovician formations have been exposed by erosion that removed younger units (Figure 2.5-12). Farther south,

younger Silurian, Devonian, and Carboniferous formations are still preserved in the central part of the Appalachian Basin.

The basal units of this sedimentary wedge consist of an Early Cambrian clastic sequence (the Potsdam Sandstone) and an Ordovician carbonate sequence (the Beekmantown, Black River, and Trenton Groups), both of which were deposited in a relatively stable shelf environment . These strata are overlain by a Late Ordovician-Early Silurian clastic sequence, which constitutes the Utica Shale and the Lorraine Group (Whetstone Gulf and Pulaski Formations), the Oswego Sandstone, the Queenston Formation, and the Grimsby Formation. This sedimentary sequence represents a transition from a shelf to a terrestrial environment of deposition, reflecting a westward regression of the Ordovician sea, which was synchronous with development of the Taconic highlands from the time of development of the Middle Ordovician unconformity (on the top of the Beekmantown Group).

Following the deposition of the Late Ordovician-Early Silurian clastic sequence, a marine transgression occurred and produced a second carbonate sequence. This Silurian-Devonian sequence includes the Clinton, Lockport, Salina, and Helderberg Groups, which are presently exposed in central New York (Figure 2.5-18 and Figure 2.5-22). Above the Helderberg Group, a sequence of clastic deposits was deposited unconformably above the Onondaga Group (carbonates), namely the Hamilton through Conewango sequence. These are syn-orogenic deposits related to the Acadian Orogeny and formation of the Catskill delta.

Farther south a clastic sequence of younger Paleozoic formations (Mississippian-Pennsylvanian) is exposed (Swezey, 2002). These formations are also syn-orogenic sedimentary rocks, deposited synchronously with the Alleghanian deformation.

The youngest rocks of the Appalachian Basin are of Early Permian age and are exposed in southwestern Pennsylvania and West Virginia.

2.5.1.1.3.2 Ordovician Stratigraphic Units

2.5.1.1.3.2.1 Late Ordovician Oswego Sandstone

The Oswego Sandstone at the NMP3NPP site ranged in thickness from 29 to 79 feet (8.8 to 24 m) with typical thicknesses of about 45 to 60 feet (13.7 to 18 m). The Oswego Sandstone consisted of hard, fresh to slightly weathered, unfossiliferous, greenish-gray, fine to medium grained, massive to distinctly bedded or cross-bedded sandstone. Thin dark gray siltstone and shale beds were minor and siltstone clasts were common. The sandstone was typically composed of subangular to subrounded quartz grains, sometimes with well-rounded lithic fragments, feldspar crystals, and a clay matrix (CEG, 1998). The depositional environments of the Oswego Sandstone in Oswego County have been previously presented by Patchen (Patchen, 1978).

At the NMP3NPP site, the lower portion of the Oswego Sandstone has been informally designated as the Oswego Transition Zone (CEG, 1998). At NMP3NPP this sub-unit was found to range from 9 to 60 feet (2.7 to 18 m) thick in the borings with typical thicknesses of 15 to 30 feet (4.6 to 9 m) The Oswego Transition Zone consists of medium hard to hard, slightly weathered to fresh, alternating, laminated to thickly bedded, fine to medium-grained sandstone, argillaceous sandstone, and siltstone. Trace fossils are present. At the the NMP3NPP site, there is a general trend toward bed thinning and increasing clay content, downward through the sub-unit. A 3 to 12-inch (7.6 to 30.5 cm) thick shale bed was often noted near the base of the Oswego Transition Zone.

The Oswego Transition Zone at NMP Unit 2 is very similar and consists of alternating, laminated to thickly bedded, fine to medium grained sandstone, argillaceous sandstone and siltstone. Trace fossils are present. There is a general trend toward bed thickening and decreasing clay content, upward through the unit. (CEG, 1998).

2.5.1.1.3.2.2 Late Ordovician Pulaski Formation

The Pulaski Formation was approximately 100 feet (30.48 m) thick at the NMP3NPP site.

The Pulaski Formation was informally subdivided into Units A, B, and C during the investigation for NMP Unit 2 (CEG, 1998) and similar divisions were made for the NMP3NPP studies. Each unit was typically in the range of 20 to 35 feet (6.1 to 10.7 m) thick at the NMP3NPP site. All three units consisted of interbedded sandstone, siltstone, and shale. The relative amount of siltstone and shale increased in the lower portions of the Pulaski Formation. All three units contained marine fossil shell debris.

Unit A is the uppermost unit and consisted of slightly weathered, medium hard, dark gray argillaceous sandstone interbedded with light gray sandstone and a few beds of dark gray shale and siltstone. Unit A had abundant marine fossil debris and disturbed bedding layers indicating soft sediment deformation. A distinctive 1/2-inch to 2-inch (.3 to 5.1 cm) thick green layer of smectite and chlorite was noted near the base of Unit A or near the top of Unit B in many of the borings.

Unit B consisted of slightly weathered, medium hard, interbedded light gray sandstone, dark gray siltstone, and shale. Unit B had relatively more sandstone than Unit A and relatively less fossil debris than Unit A.

Unit C consisted of slightly weathered, medium hard dark gray siltstone and shale, interbedded with light gray sandstone. Unit C was darker and had more siltstone and shale than Units A and B.

2.5.1.1.3.2.3 Late Ordovician Whetstone Gulf Formation

The Whetstone Gulf Formation is estimated to be approximately 770 feet (235 m) thick at the NMP3NPP site. The top of the Whetstone Gulf Formation is lithologically very similar to the Pulaski Formation Unit C. The Whetstone Gulf Formation contains marine fossil shell debris. The differentiation among the formations is made in the literature based on the types of fossils in the rock (Bretsky, 1970). The Whetstone Gulf Formation was informally subdivided into Units A and B during the investigation for NMP Unit 2 (CEG, 1998). The upper unit (Unit A) consisted of dark gray siltstone and shale with occasional light gray sandstone beds and was observed to be 60 feet (18 m) thick. The lower unit (Unit B) consisted of siltstone and shale interbedded with sandstone. Sandstone interbeds became more common in Unit B.

2.5.1.1.3.2.4 Middle Ordovician Groups

The combined Trenton Group and Black River Group carbonates are approximately 800 feet (244 m) thick at the NMP3NPP site based on scattered deep wells within Oswego County. The outcrop localities of the Trenton and Black River Groups in New York have been recently described (Cornell et. al., 2005).

The Trenton Group carbonate unit includes multiple formations across New York (Fisher, 1977 and Flagler, 1966). Contour maps of the top of the Trenton Group are presented in Figure 2.5-22 and Figure 2.5-23. An isopach map depicting the thickness of the Trenton Group is presented in Figure 2.5-24. The formations comprising the Trenton Group include the Utica shale, the Canajoharie calcareous shale, the Dolgeville calcareous shale and limestone and the Trenton

limestone and Chaumont unit. The Utica Shale, Canajoharie calcareous shale and Dolgeville calcareous shale are thicker to the east of the and may not be present in the site area, leaving the Trenton Limestone and Chaumont unit as those portions of the Trenton Group present at the NMP3NPP site.

The Utica Shale consists of a sequence of dark gray to black non-calcareous silty shales. The Utica shale becomes slightly calcareous downward and grades into the underlying calcareous Canajoharie shale. The Canajoharie calcareous shale consists of dark gray to black calcareous to highly calcareous shale. The carbonate content increases with depth and the shale becomes highly calcareous directly above the Dolgeville limestone. The Dolgeville calcareous shale and limestone consists of black calcareous to highly calcareous shale, interbedded with dark gray to dark brown or black, finely crystalline non-fossiliferous argillaceous limestone. Shale predominates in the upper portion of the formation, while limestone is predominant in the lower portion of the formation. The Trenton limestone consists of gray or brown aphanitic to finely crystalline fossiliferous limestone with black argillaceous limestone, black aphanitic limestone, dark brown aphanitic limestone, brown mottled limestone and gray finely crystalline limestone. The Chaumont unit is a very dark gray to black limestone at the base of the Trenton Group.

The Black River Group carbonate unit includes multiple formations across New York (Fisher, 1977; Flagler, 1966). An isopach map depicting the thickness of the Black River Group is presented in Figure 2.5-25. The formations comprising the Black River Group include the Lowville lithographic limestone and the Pamelia limestone. The Lowville consists of light tan colored lithographic limestone with minor light brown to brown aphanitic non-fossiliferous limestone and light tan to light gray finely crystalline dolomite. The Pamelia unit consists of dark gray to black oolitic limestone, varicolored arenaceous carbonates, dolomitic to calcareous sandstones, variegated shales and dark argillites. The carbonates of the Black River Group underlie the carbonates of the Trenton Group at the NMP3NPP site.

2.5.1.1.3.2.5 Mesozoic Sedimentary Rocks and Intrusive Igneous Rocks

There is no record of Mesozoic (Triassic and Jurassic) sedimentation preserved within 200 miles (320 km) of the NMPNS site. A regional, erosional unconformity occurs in New York State that was developed on the Paleozoic sedimentary strata. Mesozoic sediment and basic igneous intrusive and extrusive rocks are known to occur, however, in narrow, extensive fault-bounded basins in southeastern Pennsylvania, New Jersey, and New York, and in the Connecticut River Valley of New England. Moreover, Cretaceous marine strata are exposed in the Atlantic Coastal Plain of New Jersey.

Igneous rocks are rare in the Western Appalachian Mountains. In New York State, small kimberlite-alnoite dikes occur near Ithaca, striking roughly north-south. These dikes yielded radiometric ages of 136 to 145 million years (CEG, 1998). Lamprophyre dikes are reported along the borders of the Adirondack Massif that are generally oriented east-west and have yielded isotopic ages of 118 to 150 million years (CEG, 1998). Larger alkaline intrusions of the Monteregian Hills of Canada occur in an east-west trending belt east of Montreal. These intrusions yielded isotopic ages of 90 to 150 million years (CEG, 1998). Alkalic intrusive bodies have been classically interpreted as characteristic of the rift tectonic environment. Their parent magmas are believed to have been generated from very deep levels in the crust or from within the upper mantle.

2.5.1.1.3.2.6 Cenozoic Sedimentary Rocks

Tertiary Deposits

There are no Tertiary strata known within 320 kilometers (200 mi) of the NMP3NPP site because the region was uplifted and undergoing widespread erosion during that time. However, Tertiary strata do comprise the major portion of the Atlantic Coastal Plain formations exposed in New Jersey and Delaware. Early Tertiary igneous activity occurred in Virginia and West Virginia. This is the youngest igneous event in the eastern United States.

2.5.1.1.3.2.7 Plio-Pleistocene and Quaternary Deposits

Quaternary Deposits

It is generally believed that there were several advances of continental ice sheets in New York State during the Pleistocene Epoch. The ice advances were separated by warm interglacial stages.

Glacial scour and periglacial slope processes were such that virtually all New York State's unlithified sediments are of late Wisconsinan (the latest glacial advance) or more recent derivation. Only in narrow transverse valleys cut deeply enough to escape intense glacial scour might preglacial paleosol be preserved. In southwestern New York State a reentrant in the Wisconsinan terminal moraine near Salamanca may contain materials related to pre-Wisconsinan glaciation, perhaps Illinoian (CEG, 1998). These materials include glacial drift, possible end moraine deposits, plus outwash, kame terrace, and deltaic deposits. However, these deposits may also be earliest Wisconsinan.

During the advance and retreat of the Wisconsinan ice sheet, the bedrock surface was scoured and till was deposited unconformably on the older Paleozoic strata of New York State. Minor readvances resulted in additional till being laid down, in some areas, covering glaciofluvial or glaciolacustrine deposits above the lowermost till. During stages of retreat of the Wisconsinan ice sheet, glaciolacustrine sediment from proglacial lakes such as Lake Iroquois, together with glaciofluvial sediment, were also deposited.

Soil at the NMP3NPP site consists primarily of glacial till or weathered soil derived from the till.

The Quaternary geology of the St. Lawrence Lowlands in Canada has been summarized by Karrow (Karrow, 1989).

Unlithified Soils

Unlithified soils have been identified at NMP Unit 2 and their approximate ages determined on the basis of stratigraphic position, sediment type, pollen stratigraphy, C-14 dating, grain size distribution, and mineralogical analyses. The soils in order of decreasing age are: till, Lake Iroquois clay and silt, Sandy Creek time-equivalent sands, and marls, silts, and peat (CEG, 1998). With the exception of the till, these soils were not identified during the site characterization studies of the NMP3NPP site.

Pleistocene Surficial Deposits

At NMP3NPP, surficial deposits were encountered at the ground surface and ranged in thickness from 0.5 to 10.6 feet (0.15 to 3.2 m). Surficial deposits can be subdivided into two categories based on engineering properties. The two categories are topsoil and fine-grained soil near wetland areas. The topsoil typically consisted of silty sand to sandy silt with varying amounts of organics and gravel. The topsoil was encountered throughout the site and typically ranged from 0.5 to about 2 feet (0.15 to about 0.6 m) thick.

Fine grained soils were encountered to depths of up to 10.6 feet (3.2 m) in areas near wetlands to the north of the proposed reactor complex. The fine grained soils generally consisted of low plasticity silts and clays with varying amounts of sand and gravel. Occasional layers or pockets of organic materials were observed in these fine grained soils to depths of up to 10 feet (3.0 m).

2.5.1.1.3.2.8 Sandy Creek Equivalent Sand

Shallow water deposits overlie Lake Iroquois sediments, till, or bedrock. The shallow water sediments consist of up to 3 feet (0.9 m) of thin bedded silt, fine to medium sand, and clay, and do not occur above el 270 feet (82 m). The bedding varies from planar to wavy rippled and cross-laminated ripple drift (CEG, 1998).

The Sandy Creek shoreline was formed during the lowering of lake level in the Ontario Basin to the Admiralty stage. Terraces between el 270 and 290 feet (82 and 88 m) along streams in the site area and near Mexico Bay were identified from air photos, topographic maps, and field reconnaissance and are inferred to be equivalent to Sutton's shoreline identification further north. Just west of Demster Beach a distinct break in slope and change in air photo tone occurs at el 270 feet (82 m). The slope gradient above 270 feet (82 m) is steeper than the slope gradient below this elevation. This break in slope as well as the terraces suggests a possible relation to the Sandy Creek stillstand, therefore placing the shoreline at approximately el 270 feet (82 m) in the Mexico Bay area (CEG, 1998).

The relative ages inferred for samples of the shallow water sediments and the aforementioned pollen stratigraphy indicate that they are representative of the middle to upper A pollen zone. This, in conjunction with the observation that these sediments have not been identified above el 270 feet (82 m) at the site, suggests that the shallow water sediments were deposited during or just prior to the Sandy Creek lake level stillstand (CEG, 1998).

Marl

The shallow water deposits locally grade into a marl unit up to 2 feet (0.6 m) thick. The light tan marl consists of silt to fine sand-size calcite fragments, clay, and abundant freshwater fossil fragments. The macrofossil content increases upward culminating in a highly fossiliferous zone in the upper 3 inches (7.6 cm). The pollen assemblage within the marl is similar to that of the shallow water deposits, suggesting that it also falls in the A zone. A C-14 date of 12,545 + 330 radiocarbon yr B.P. was obtained from pelecypod and gastropod shells in the top 2 inches (5.1 cm) of the marl. C-13 analysis suggests that the fossils may have been naturally contaminated by older carbon. Thus, the C-14 age probably is older than the true age of the marl; however, the error of the date would probably be less than about 2,000 years. This suggests the marl is time-equivalent with the lower part of the peat (CEG, 1998).

No soils of this type were encountered during the site characterization studies of the NMP3NPP site.

Silt

Outside the area of marl deposition, the shallow water deposits grade into nonorganic massive to medium bedded silts and silty fine sands which in turn grade into organic silts. This sequence represents a transition from a high energy environment of the Sandy Creek time-equivalent sands to marshy areas above lake level. In part, these may be aeolian silts and fine sands and are probably time equivalent with the marl (CEG, 1998).

Peat

Peat was observed in thicknesses up to 3 feet (0.9 m). However, the peat was restricted to a depression where it overlies, and is in gradational contact with, the shallow water deposits identified as Sandy Creek time-equivalent sands.

C-14 dates obtained using samples from this peat provide minimum absolute ages of the shallow water deposits. One reliable date of 11,260 + 190 radiocarbon yr B.P. was obtained using samples from the basal woody peat. The basal woody peat is overlain by approximately 8 inches (20 cm) of peat composed almost entirely of sphagnum moss. Samples of this mass yielded ages of 10,400 + 255 and 10,060 + 125 radiocarbon yr B.P., which are consistent with the age of the underlying wood, and the pollen assemblage, which suggests the base of the peat is in the A pollen zone. The decrease in spruce pollen and the increase in hemlock and hardwood suggests that the top of the peat falls close to the B-C pollen zone boundary or about 8,500 years B.P. Therefore, deposition of the peat began before 11,260 + 190 radiocarbon yr B.P., continued at least through 10,400 + 255 years B.P. and possibly through 8,500 years B.P. Thus, a minimum absolute age can be inferred for the underlying shallow water sediments (Sandy Creek sands) as 11,260 + 190 radiocarbon years B.P. Because the peat is overlain by artificial fill, no minimum age of peat deposition could be obtained (CEG, 1998).

No soils of this type were encountered during the site characterization studies of the NMP3NPP site.

Lake Iroquois Deposits

The deposits of proglacial Lake Iroquois are deep water sediments up to 4 feet (1.2-m) thick which directly overlie gray till, bedrock, or ice marginal lake till. These sediments consist of laminated to massive, reddish brown or gray clayey silt or silty fine sand with lenses and laminations of fine to medium sand and a little gravel (CEG, 1998).

The age of Lake Iroquois is bracketed by C-14 dates from various locations along the shoreline. At Lewiston, NY, wood from a spit was dated at 12,600 + 400 radiocarbon years B.P. This date represents a maximum age for the initiation of Lake Iroquois. Karrow et al date a post-Iroquois lake level stand, 12 meters (40 ft.) below the crest of the Iroquois beach in the Hamilton area, at 11,570 + 260 radiocarbon years B.P. This date gives a minimum age for the extinction of the Iroquois high stand. If the deep water sediments on-site are Lake Iroquois sediments, they probably were deposited between 12,600 + 400 and 11,570 + 260 radiocarbon years B.P. However, no organic material was found within the Iroquois sediments that was suitable for C-14 dating. Hence, the minimum age of these sediments is inferred as pre-Sandy Creek shallow water deposits (CEG, 1998).

The pollen stratigraphy of the deep-water lacustrine sediments has been correlated with C-14 dates, and it also suggests that the deep water sediments were deposited approximately 12,000 years B.P. These Iroquois sediments are generally low in total pollen content; however, the pollen that does exist is dominantly spruce and pine. Data from samples illustrate a decrease in the percent of spruce pollen found in the shallow water deposits (Sandy Creek) when compared to the underlying deep water Iroquois sediments. The relative percentages of spruce pollen suggest that the shallow water sediments (Sandy Creek) are similar in age to the upper spruce pollen zone (Zone A4, about 10,000 years B.P.), and that the Iroquois sediments are similar in age to the lower spruce pollen zones (Zones A1 and A2, about 12,000 years B.P.) (CEG, 1998).

Pleistocene Glacial Till

Where encountered, glacial till extended down to the top of bedrock. The glacial till ranged in thickness from 2.1 to 21.3 feet (0.6 to 6.5 m) thick, but was typically between 5 and 15 feet (1.5 and 4.6 m) thick. The glacial till typically consisted of silty or clayey sand with gravel, with occasional cobbles and boulders. The results of grain size tests performed on glacial till samples indicated a widely graded soil with between 20 and 60 percent fines (passing the # 200 sieve). Atterberg limits tests performed on glacial till samples indicated the plasticity ranged from non-plastic to low plasticity. Four tests on glacial till samples indicated a specific gravity of 2.74 to 2.75, and one test indicated a specific gravity of 2.68. SPTs performed in the borings typically indicated a medium dense to very dense soil. Many of the SPTs encountered refusal on cobbles and boulders.

The upper portion of the glacial till layer was typically a light brown to tan color and the lower portion was light to dark gray. The grain size test results and the field classifications indicate that the gradations of the two different colored till soils are similar. The color difference appears to be related to site groundwater levels and the long-term degree of saturation of the soils.

Four geological varieties of till are present on the NMP Unit 2 site. Two types of gray till, a brown till, and a proglacial lake till are distinguishable on the basis of color, texture, and composition. Field relationships and mineralogic analyses indicate that till from only the Late Wisconsinan glacial stage is present at the site. These tills were most likely deposited immediately prior to and during the existence of Lake Iroquois, and are probably equivalent in age to tills deposited during the Port Huron glacial advance (12,900 to 12,000 years B.P.) (CEG, 1998).

Generally, gray till up to 6 feet (1.8-m) thick has been deposited across the NMP Unit 2 site and directly overlies either bedrock or, in places, a 1-inch (2.5 cm) layer of gray sand. Two units of gray till are distinguished primarily by the size, angularity, and composition of the rock clasts. Notably, one unit contains exotic clasts (CEG, 1998).

A distinctive brown till as much as 10 feet (3-m) thick overlies the gray till and bedrock in the southeastern portion of the NMP Unit 2 site. Locally, the brown till also interfingers with, and is in vertical contact with, the gray till. The brown till consists of rounded to subrounded exotic rock fragments in a fine-grained silty sand matrix. It is distinguished from the gray till on the basis of color, inclusions of stratified drift, larger percentages of well-rounded foreign clasts, and a coarser texture, and may, in part, represent an ablation till (CEG, 1998).

Locally, up to 2 feet (0.6 m) of till that was deposited in an ice marginal lake overlies both the gray till and the bedrock. This till consists of a dark gray silty sand with subrounded rock fragments of mostly gray sandstone and minor percent black limestone. It interfingers with and is overlain by as much as 1 foot (0.3 m) of light gray stratified silt and sand with some subrounded to rounded gravel and light gray silt clasts. This till is poorly stratified and grades upward into the laminated clayey silts of Lake Iroquois. It was deposited as the ice margin receded northward and sediment from the receding ice was reworked and redeposited in the Lake Iroquois basin (CEG, 1998).

2.5.1.1.3.3 Appalachian Plateau Physiographic Province

The Appalachian Plateau Province is underlain by rocks that are continuous with those of the Central Lowland and the Valley and Ridge Provinces. But in the Appalachian Plateau, the layered rocks are nearly flat-lying or gently tilted and warped, rather than being intensely folded and faulted as in the Valley and Ridge Province. Rocks of the Allegheny Front along the eastern margin of the province consist of thick sequences of sandstone and conglomerate, interbedded with shale, ranging in age from Devonian to Pennsylvanian. Rocks of the

Appalachian Plateau west of the Allegheny Front are less resistant and consist of Permian age sandstone, shale and coal (Hack, 1989). Sedimentary rocks in the Appalachian Basin, including the Appalachian Plateau Province have been summarized by Milici, 1988 and Sloss, 1988.

2.5.1.1.3.4 Valley and Ridge Physiographic Province

The Valley and Ridge Physiographic Province is underlain primarily by layered sedimentary rock that has been intensely folded and locally thrust faulted. The sedimentary rocks are similar to those of the Appalachian Plateau Physiographic Province and range in age from Cambrian to Pennsylvanian. The valley areas within the Great Valley are underlain predominantly by thick sequences of limestone, dolomite and shale. The upland areas of the Valley and Ridge Province (Appalachian Mountains) to the west of the Great Valley are underlain predominantly by resistant sandstones and conglomerates, while the lowland areas are underlain predominantly by less resistant shale, siltstone, sandstone and limestone (Colton, 1970). Sedimentary rocks in the Appalachian Basin, including the Valley and Ridge Physiographic Province have been summarized by Milici, 1988 and Sloss, 1988.

2.5.1.1.3.5 Laurentian Highlands Physiographic Province

The Laurentian Highlands Physiographic Province is characterized by the Precambrian metamorphic rocks of the Grenville Orogen. Proterozoic Grenville rocks in the Grenville Province of Canada, including the Laurentian Highlands Physiographic Province, have been summarized by Davidson (Davidson, 1998) and Tollo (Tollo, 2004). Refer to Section 2.5.1.1.3.1 (Central Lowland - St. Lawrence Lowlands) for a discussion of Precambrian Grenville Age rocks.

2.5.1.1.3.6 Adirondack Mountains Physiographic Province

The Adirondack Mountains Physiographic Province is characterized by the Precambrian metamorphic rocks of the Grenville Orogen. Proterozoic Grenville rocks in the U.S., including the Adirondack Mountains Physiographic Province, have been summarized by Reed (Reed, 1993), Rankin (Rankin, 1993) and Tollo (Tollo, 2004). Refer to Section 2.5.1.1.3.1 (Central Lowland - St. Lawrence Lowlands) for a discussion of Precambrian Grenville Age rocks.

2.5.1.1.4 Regional Tectonic Setting

In 1986, the Electric Power Research Institute (EPRI) developed a seismic source model for the Central and Eastern United States (CEUS), which included the NMP3NPP site region (EPRI, 1986). The CEUS is a stable continental region (SCR) characterized by low rates of crustal deformation and no active plate boundary conditions. The EPRI source model included the independent interpretations of six Earth Science Teams and reflected the general state of knowledge of the geoscience community as of 1986. The seismic source models developed by each of the six teams were based on the tectonic setting and the occurrence, rates, and distribution of historical seismicity. The original seismic sources identified by EPRI are thoroughly described in the EPRI study reports (EPRI, 1986) and are summarized in Section 2.5.2.2.

Since 1986, additional geological, seismological, and geophysical studies have been completed in the CEUS and in the NMP3NPP site region. The purpose of this section is to summarize the current state of knowledge on the tectonic setting and tectonic structures in the site region and to highlight new information acquired since 1986 that is relevant to the assessment of seismic sources.

A global review of earthquakes in SCRs shows that areas of Mesozoic and Cenozoic extended crust are positively correlated with large SCR earthquakes. Nearly 70 percent of SCR earthquakes with M 6 occurred in areas of Mesozoic and Cenozoic extended crust (Johnston,

1994). Additional evidence shows an association between Late Proterozoic rifts and modern seismicity in eastern North America (Johnston, 1994) (Wheeler, 1995) (Ebel, 2002).

Paleozoic and Mesozoic extended crust underlies only a small portion of the 200 miles (322 km) NMP3NPP site region (Figure 2.5-1). As discussed in this section, there is no evidence for late Cenozoic seismogenic activity of any tectonic feature or structure in the site region (Crone, 2000) (Wheeler, 2005). No new structures or features have been identified in the site region since 1986 that show clear evidence of seismogenic potential greater than what was recognized and incorporated in the EPRI study (EPRI, 1986) seismic source model.

The following sections describe the tectonic setting of the site region by discussing the: (1) plate tectonic evolution of eastern North America at the latitude of the site, (2) origin and orientation of tectonic stress, (3) gravity and magnetic data and anomalies, (4) principal tectonic features, and (5) seismic sources defined by regional seismicity. Historical seismicity occurring in the site region is described in Section 2.5.2.1. The geologic history of the site region was discussed in Section 2.5.2.1.1.

The NMP3NPP site is in a region characterized by rocks at the surface which, although very old, have not been subjected to large-scale orogenic processes. In consequence, few major structural features are known within 200 miles (322 km) of the NMP3NPP site.

Low-level seismicity is known to occur throughout the northeastern region of the United States, but the distribution of historic and instrumentally detected events appears in most instances to be unrelated to movement on either specific or known geological structures. The site region exhibits very low seismicity. The lack of a well-defined relationship between seismicity and geologic structure leads to a conservative assessment of the design values for vibratory ground motion at the site based upon the delineation of tectonic provinces as required by Appendix A to 10 CFR 100.

2.5.1.1.4.1 Plate Tectonic Evolution of the Appalachian Basin

The Late Precambrian to Recent plate tectonic evolution of the site region is summarized in Section 2.5.1.1.2. Most of the present-day understanding of the plate tectonic evolution comes from research performed prior to the 1986 EPRI report (EPRI, 1986). Fundamental understanding about the timing and architecture of major orogenic events was clear by the early 1980s, after a decade or more of widespread application of plate tectonic theory to the evolution of the Appalachian orogenic belt (e.g., Rodgers, 1970). Major advances in understanding of the plate tectonic history of the Northern Appalachian Basin since the EPRI study report (EPRI, 1986) include the imaging of deep crustal structure in the United States (e.g. Brown, 1983; Braile, 1989; Fakundiny, 2002b; Forsyth, 1994a; Forsyth, 1994b; Herman, 1992; Hughes, 1991; Hughes, 1992; Levin, 1995; Musacchio, 1997; Ouassaa, 2002; Spencer, 1987; Hibbard, 2007) and in Canada (Carr, 2000; Eaton, 2006; Perry, 2002; White, 1994; White 2000; Zelt, 1994a; Zelt, 1994b). Figures including cross sections of deep crustal structure are presented in Figure 2.5-26, Figure 2.5-27 and Figure 2.5-28.

The following subsections divide the regional plate tectonic history into: (1) Late Proterozoic and Paleozoic tectonics and assembly of North American continental crust, (2) Mesozoic rifting and passive margin formation, and (3) Cenozoic vertical tectonics associated with exhumation, deposition, and flexure.

2.5.1.1.4.1.1 Late Proterozoic and Paleozoic Plate Tectonic History

The NMP3NPP site is situated within the Eastern Stable Platform sub-province of the Central Stable Region. The Central Stable Region tectonic province is a vast area represented by the

interior portion of the North American craton. The cratonic part of the continent was affected by only convergent, diastrophic processes. The central eastern portion of the craton is represented both by exposed and buried continental crust ranging in age from 1,000 to 1,450 Ma. The exposed basement rocks occur as part of the Grenville Geologic Province of the Canadian Shield and the Adirondack Massif. The buried Grenvillian rocks in this tectonic province are covered by Paleozoic sedimentary rock (Cambrian to Permian) deposited in a downwarped basin. This basin is bounded on the west by a broad structural rise, the Findlay Arch. The strata of this basin extend eastward, beyond the Eastern Stable Platform Sub-Province, until they meet the Hudson Highlands anticlinoria, which separate non- or slightly metamorphosed basinal facies from the more intensely altered ones. These strata form a sedimentary wedge, thickening to the southeast, reflecting the asymmetry of the basin floor. The eastern boundary of this sub-province marks the transition to the region of thin-skinned folding and thrust faulting of the Fold Belt.

West of the Findlay Arch-Algonquin Axis (outside of the Eastern Stable Platform Sub-Province) lie the Michigan and Illinois Basins, contemporaries of the Appalachian Basin. The Anna, OH, area lies at the confluence of three reentrant zones of these contemporary basins: 1) the boundary of the Kankakee and Findlay Arches with the Michigan Basin, 2) the boundary of the Kankakee Arch and Indiana-Ohio Platform (northern portion of the Cincinnati Arch) with the Illinois Basin, and 3) the boundary of the Findlay Arch and the Indiana-Ohio Platform with the Appalachian Basin. Studies by Dames & Moore (CEG, 1998) indicate that, just as in the vicinity of Attica, NY, along the Clarendon-Linden Fault, the basement rocks in the Anna area reflect a strong north-south magnetic anomaly, coincident with the Bowling Green Fault. Likewise, a focal mechanism solution for the March 8, 1937, MMI VII-VIII shock at Anna has a nodal plane (north-south orientation) that is in agreement with postulated basement faulting. On the basis of regional geophysical studies and the results described above, the Anna seismogenic zone was defined as lying between 84° and 84°30' longitude, north of the northwesterly-trending Champaign Fault and south of the northern limit of a band of acidic igneous intrusive rocks which contrast strongly with other basement rocks in the region.

The deformational history of the basement rocks is long and complex involving both ductile and brittle episodes; nevertheless, the overlying Paleozoic sedimentary rocks of the Appalachian Basin within the site province reflect a long history of very minor deformation. Broad upwarps like the Findlay Arch-Algonquin Axis are bordered by moderately deep depositional basins containing Paleozoic strata. These upwarps and complementary basins developed gradually throughout Paleozoic time under stress conditions that reflect vertical tectonic movement of the crust. Local stress concentrations developed and resulted in high-angle faulting and mild folding. In this subprovince, the Clarendon-Linden Fault (Section 2.5.1.1.3) and the Bowling Green and Champaign Faults in the Anna, Ohio, area are examples of the effect of these conditions in Paleozoic time.

2.5.1.1.4.1.2 Ottawa Basin Sub-Province

The Ottawa River Basin is characterized by a west-northwest striking zone of faults called the Ottawa-Bonnechere Graben. The character of this feature is unlike the other portions of the Central Stable Region tectonic province lying east of the Findlay Arch-Algonquin Axis. Consequently, one can subdivide this portion of the Central Stable Region with another subprovince, namely the Ottawa Basin Sub-Province, which is distinct from the site subprovince.

The Ottawa Basin Sub-Province lies immediately to the north of the site tectonic province. The boundary between them marks the position of the extension of the New England Salient into the Eastern Stable Platform. The Ottawa Basin is characterized by the development of a deep, Cambro-Ordovician structural basin along an older zone of crustal weakness. This basin was

subsequently deformed by a branching system of normal faults: one west-northwesterly branch formed the Ottawa-Bonnechere Graben, and the other the St. Lawrence Rift Valley with northeasterly trending normal faults. The eastern border of the Ottawa Basin corresponds to Logan's Line.

2.5.1.1.4.1.3 Northern Appalachian Fold Belt

The Northern Appalachian Fold Belt tectonic province adjoins the site province on the south and east. The province consists of strongly folded Paleozoic sedimentary strata 1.9 to 6.2 miles (3 to 10 km) thick, broken by low-angle thrust faults (decollement structures) that are largely confined to the sedimentary strata and rarely involve the Precambrian basement rocks. The fold belt changes considerably in width along its length from the southern Appalachians to New England. It is nearly 118 miles (190 km) wide in Pennsylvania and only about 19 miles (30 km) wide in eastern New York State. The tectonic assembly of the central Appalachians occurred during the late Paleozoic (Valentino, 1994). The western boundary of the province delineates the point where orogenic folding of the Paleozoic sedimentary strata of the basin dies out. The eastern tectonic province boundary is marked by the abrupt change to basement rocks in the cores of the Hudson Highlands anticlinoria and highly altered metasediments that characterize the eugeosynclinal deposits of the Appalachian Geosyncline.

This tectonic province has been subdivided into two parts: the faulted and nonfaulted fold belts. Moreover, the tectonic style of deformation in the northern portion of this province differs notably from the southern portion. This change of tectonic style is related to the geological evolution of the province, and is manifested by the dominance of folding in the north as compared to overthrust faulting in the south.

The northeast structural trends of the Appalachian Fold Belt are transected by an east-northeast trending belt in southern Pennsylvania known as the Central Appalachian Salient.

This salient was likely developed during late Precambrian time in association with rifting and the concomitant development of the proto-Atlantic Ocean. Whether this feature is related to an aulocogen or to transcurrent or transform faulting is uncertain. However, it seems to be a fundamental crustal feature with no evidence of post-Cretaceous deformation.

The compressional forces that led to the development of folds and thrust faults in this tectonic province were generated during the continental convergence represented by the Taconian, Acadian, and Alleghanian orogenies during the Paleozoic Era. During the late stages of the Alleghanian event, the effects of compressional forces were more pronounced in the southern Appalachians (south of the Central Appalachian Salient) than they were in the northern Appalachians.

2.5.1.1.4.1.4 Appalachian Mobile Belt

The Blue Ridge, Piedmont, and Green Mountain Belt may be considered to be part of a single, unnamed tectonic province. The rocks of this province were affected in the geologic past by initial divergent and convergent diastrophic processes in Precambrian and Paleozoic time, as well as the final divergent diastrophism in the Mesozoic Era. For this reason, it is termed the Appalachian Mobile Belt. The province corresponds to the eugeosynclinal belt and includes the ancient continental margins. The western edge is parallel to and lies west of the eastern edge of the North American continent of Cambro-Ordovician time as defined by Rodgers (Rodgers, 1970).

The Appalachian Mobile Belt is underlain by both sialic crust of Grenvillian age and by thick, dense, and presumably mafic crust. Additionally, metasedimentary and metavolcanic rocks of

Avalonian age (approximately 600 Ma) occur in this province in eastern New England. In the southern and western portions of the Mobile Belt, the Avalonian rocks, with mafic intrusives, unconformably overlie Grenvillian basement as an eastward-thickening sequence. The origin of the Avalonian rocks is believed related to the rifting that led to the opening of the proto-Atlantic Ocean.

Unconformably above these two sequences of basement rocks are various metamorphosed early- and late-Paleozoic marine sedimentary rocks (mio- and eugeosynclinal) which were deformed during both the Medial Ordovician Taconic Orogeny (450 million years ago) and the Devonian Acadian Orogeny (300 million years ago).

Continental clastic and volcanic rocks of late-Paleozoic Age (late-Carboniferous to Permian) were deposited in southern and central-eastern New England within rift basins along the ancient western margin of the Avalon Platform during the translational stage of Paleozoic continental convergence.

Although details about the kinematics, provenance, and histories of lithostratigraphic units within the Appalachian orogenic belt continue to be debated and reclassified (e.g., Hatcher, 1989; Hibbard, 2006; Hibbard, 2007), it is well accepted that plate boundary deformation has occurred repeatedly in the site region since late Precambrian time. Suturing events that mark the welding of continents to form supercontinents and rifting events that mark the breakup of supercontinents to form ocean basins have each occurred twice during this interval. Foreland strata, deformation structures, and metamorphism associated with the Grenville (Middle Proterozoic) and Allegheny (Late Paleozoic) orogenies record the closing of ocean basins and welding of continents to form the supercontinents Rodinia and Pangaea, respectively. Synrift basins, normal faults, and postrift strata associated with the opening of the Iapetus (Late Proterozoic to Early Cambrian) and Atlantic (Early Mesozoic) Ocean basins record the break-up of the supercontinents. The principal structures that formed during the major events are salient to the current seismic hazards in that: (1) they penetrate the seismogenic crust, (2) they subdivide different crustal elements that may have contrasting seismogenic potential, and (3) their associated lithostratigraphic units make up the North American continental crust that underlies most of the site region. Many of the principal structures are inherited faults that have been reactivated repeatedly through time. Some are spatially associated with current zones of concentrated seismic activity and historical large earthquakes. For example, the 1811-1812 New Madrid earthquake sequence ruptured a failed Late Proterozoic rift that also may have been active in the Mesozoic.

During the interval between opening of the Iapetus Ocean and opening of the Atlantic Ocean, the eastern margin of the ancestral North America continent was alternately (1) an active rift margin accommodating lithospheric extension with crustal rift basins and synrift strata and volcanism; (2) a passive continental margin accumulating terrestrial and shallow marine facies strata; and (3) an active collisional margin with accretion of microcontinents, island arcs, and eventually the African continent. Major Paleozoic mountain building episodes associated with the collision and accretion events included the Taconic, Acadian, and Allegheny Orogenies. More localized collisional events in the site region include the Avalon, Virgilina and Potomac (Penobscot) orogenies (Hatcher, 1987) (Hatcher, 1989). The geologic histories of these orogenies are described in Section 2.5.1.1.2.

Tectonic structures developed during the interval between the Late Proterozoic and Triassic Periods are variable in sense of slip and geometry. Late Proterozoic and early Cambrian rifting associated with the breakup of Rodinia and development of the Iapetus Ocean formed east-dipping normal faults through Laurentian (proto-North American) crust. Late Proterozoic extended crust of the margin probably underlies the Appalachian fold belt southeastward to

beneath much of the Piedmont Province (Wheeler, 1996). Paleozoic compressional events associated with the Taconic, Acadian, and Allegheny orogenies formed predominantly west-vergent structures that include (1) Valley and Ridge Province shallow folding and thrusting within predominantly passive margin strata, (2) Blue Ridge Province nappes of Laurentian crust overlain by lapetan continental margin deposits, (3) Piedmont Province thrust-bounded exotic and suspect terranes including island arc and accretionary complexes interpreted to originate in the lapetus Ocean, and (4) Piedmont Province and sub-Coastal Plain Province east-dipping thrust, oblique, and reverse fault zones that collectively are interpreted to penetrate much of the crust and represent major sutures that juxtapose crustal elements (Hatcher, 1987) (Hibbard, 2006). Many investigators recognize significant transpressional components to major faults bounding lithostratigraphic units (Hatcher, 1987) (Hibbard, 2006).

2.5.1.1.4.1.5 Mesozoic and Cenozoic Plate Tectonic Evolution

Brittle faulting occurred in this subprovince during Mesozoic time also; the association of normal faults, alkaline igneous activity, and the formation of domes indicates that the crust was subjected to extensional strain to great depth.

2.5.1.1.4.1.6 Northern Appalachian Fold Belt

During the divergent rifting of the continent (opening of the Atlantic Ocean) in the Mesozoic Era, rocks of the Northern Appalachian Fold Belt tectonic province were subjected to extensional strains that were most pronounced along its eastern boundary and manifest in the development of the Triassic-Jurassic basins of Maryland, Pennsylvania, and New Jersey. Minor igneous activity associated with rifting also affected the province, as scattered diabase dikes of Triassic and Jurassic Age, plus kimberlite and peridotite dikes of late-Jurassic Age that were intruded into upper levels of the crust. Mild folding recognized along the western border of this province may have occurred in late-Jurassic time. During this era, the orientation of stresses of the northern Appalachians differed significantly from that of the southern Appalachians, as evidenced by the regional change in strikes of Mesozoic diabase dikes.

2.5.1.1.4.1.7 Appalachian Mobile Belt

Lastly, the Mobile Belt contains continental clastic, volcanic, and intrusive mafic rocks in rift basins formed in Triassic to Jurassic time and associated with opening of the Atlantic Ocean. Concomitant with the formation of these basins in southern New England, New York, New Jersey, Pennsylvania, and Maryland, alkaline intrusive rocks invaded the crust in northern New England and Quebec Province, Canada, known as the White Mountain and Monteregian Hills intrusive complexes.

2.5.1.1.4.1.8 Cenozoic Plate Tectonic Evolution

Since Mesozoic time, the Eastern Stable Platform (and adjoining tectonic provinces) has undergone extensive epeirogenic uplift and concomitant erosion. These processes have resulted in tilting of the basin floor and sedimentary strata southward with a gentle dip of 1/2 to 1 deg (Figure 2.5-22). This structural feature is known in the site region as the Lake Ontario Homocline.

The contemporary stress conditions in the site tectonic subprovince (Eastern Stable Platform) are characterized by high (subhorizontal compressive) stress near the upper free surface of the crust. The NMP3NPP site occurs within the Mid-Continent stress province, which is characterized by east-northeast trending, maximum compressive stress, essentially parallel to the absolute motion of the North American Plate.

2.5.1.1.4.1.9 Northern Appalachian Fold Belt

From Cretaceous time to the present, the province has been subjected to epeirogenic uplift and erosion. The majority of this province occurs within the Central Lowland Canadian Shield stress province of Zoback (Zoback, 1992), which they believe is characterized by high subhorizontal, compressive stress, with the maximum stress oriented east-northeast.

Appalachian Mobile Belt

The Cretaceous and Cenozoic clastic wedge of the Atlantic Coastal Plain covers a major portion of this province south of New York City. The majority of these sediments were deposited as a result of episodes of epeirogenic uplift and erosion of the eastern craton and subsidence with deposition as its margin.

Central Stable Region Eastern Stable Platform Eastern Stable Platform Sub-Province

In 1929, a MMI VII earthquake occurred near Attica, New York, approximately 90 miles (145 km) west of the site. This shock and an accompanying concentration of lesser events has been attributed to movement along the Clarendon-Linden Fault (Ebel, 2002).

A shock of MMI VI in 1853 near Lowville, New York, about 50 miles (80 km) northeast of the site, may be related to faulting expressed in the Paleozoic strata at the western edge of the Adirondack Massif. The faults are oriented northeast-southwest, downthrown an unknown amount to the southeast.

MMI VII-VIII shocks in the area of Anna, OH, should not be assumed to occur at the site because they have been attributed to movement along known basement faults in the Anna region (CEG, 1998). Furthermore, this active zone lies west of the boundary (Findlay Arch-Algonquin Axis) of the site subprovince.

2.5.1.1.4.1.10 Ottawa Basin Sub-Province

The early record indicates that events of MMI IX and X occurred in the 1600s and 1700s in the St. Lawrence River Region, and a MMI IX event occurred in 1925 near LaMalbaie, Quebec. In 1944, a maximum MMI VIII shock occurred between Massena, NY, and Cornwall, Ontario, a distance of 110 miles (177 km) from the site. These events, if migrated to the boundary of the Ottawa Basin Sub-Province with the site tectonic subprovince (109 mi, 175 km from the site), would subject the site to about MMI VI using attenuation relationships.

Northern Appalachian Fold Belt

The Northern Appalachian Fold Belt tectonic province, as is true for the Central Stable Region, exhibits both a relatively aseismic area (the nonfaulted fold belt) and a moderately seismic area (the faulted fold belt). The faulted fold belt has been described in detail (USNRC, 1980). Based upon the Southern Appalachian Seismic Zone, they further recognize that the southern portion of the faulted fold belt is more seismic than its northern counterpart. Hence, it seems reasonable that the Central Appalachian Salient divides the Fold Belt province with respect to the distribution of seismic events. The largest event known in the Southern Fold Belt tectonic province was the 1897 Giles County, Virginia, earthquake (MMI VIII). To the north of the salient, no events greater than MMI VI have been recorded within the Northern Appalachian Fold Belt tectonic province. (The February 1954 localized shock near Wilkes Barre, Pennsylvania, (MMI VII) has been attributed to mine collapse).

Appalachian Mobile Belt

The foregoing summary indicates that this tectonic province has undergone major changes in regional stress conditions since late-Precambrian time. The changes have been cyclic, ranging from episodes of crustal extension to major compression. Since the Cretaceous Period, strain

developed in the crust has been attributed to motion related to lateral spreading from the Mid-Atlantic Ridge and to vertical crustal uplift and subsidence. Zoback and Zoback (Zoback, 1989) have interpreted that the Atlantic Coast region, Coastal Plain, and Piedmont represent a contemporary stress province in which the maximum horizontal stress and least horizontal stress are perpendicular and parallel to the coastline, respectively. The western boundary of this stress province is approximately coincident with the peak of the steep Appalachian gravity gradient which separates the highly metamorphosed, plutonized, and upthrust rocks of the core of the orogen on the east (Mobile Belt) from the miogeosynclinal rocks to the west (Fold Belt).

The largest earthquake recorded in the Appalachian Mobile Belt was the 1886 MMIX event near Charleston, South Carolina. This event is not considered relevant to the NMP3NPP site, because the earthquake is considered to be associated with structure in the Charleston, South Carolina area. The MMI VIII Boston-Cape Ann event of 1755 occurred nearer to the site. This event appears to be restricted to the northwestern boundary of the Avalon Platform near Boston. This event may be associated with the Boston-Ottawa seismic trend which includes the Ottawa-Bonnechere Graben area. Delineation of the Ottawa Basin subprovince of the Central Stable Region is consistent with this seismic trend. The closest approach of the boundary of the Appalachian Mobile Belt Province is 162 miles (260 km) from the site.

Additionally, a number of MMI VII events have occurred in historic and recent time in the Mobile Belt. Some have occurred within the Connecticut Basin, some within the central Piedmont, and some along the Fall Line boundary of the Piedmont and the Atlantic Coastal Plain. These events would approach no closer than 162 miles (260 km) to the site.

2.5.1.1.4.2 Tectonic Stress in the Mid-Continent Region

Expert teams that participated in the 1986 EPRI evaluation of intra-plate stress generally concluded that tectonic stress in the CEUS region is characterized by northeast-southwest directed horizontal compression. In general, the expert teams concluded that the most likely source of tectonic stress in the northeast region was ridge-push force associated with the Mid-Atlantic ridge, transmitted to the interior of the North American plate by the elastic strength of the lithosphere. Other potential forces acting on the North American plate were judged to be less significant in contributing to the magnitude and orientation of the maximum compressive principal stress. Some of the expert teams noted that deviations from the regional northeast-southwest trend of principal stress may be present along the east coast of North America and in the New Madrid region. They assessed the quality of stress indicator data and discussed various hypotheses to account for what were interpreted as variations in the regional stress trajectories.

Since 1986, an international effort to collate and evaluate stress indicator data has resulted in publication of a new world stress map (Zoback, 1989). Data for this map are ranked in terms of quality, and plate-scale trends in the orientations of principal stresses are assessed qualitatively based on analysis of high-quality data (Zoback, 1992). Subsequent statistical analyses of stress indicators confirmed that the trajectory of the maximum compressive principal stress is uniform across broad continental regions at a high level of statistical confidence. In particular, the northeast-southwest orientation of principal stress in the CEUS inferred by the EPRI experts is statistically robust, and is consistent with the theoretical trend of compressive forces acting on the North American plate from the mid-Atlantic ridge (Coblentz 1995).

More recent assessments of lithospheric stress do not support inferences by some EPRI expert teams that the orientation of the principal stress may be locally perturbed in the New England area, along the east coast of the United States, or in the New Madrid region. A variety of data

was summarized (Zoback, 1989), including well-bore breakouts (Zoback, 1985), results of hydraulic fracturing studies, and newly calculated focal mechanisms, which indicate that the New England and eastern seaboard regions of the U.S. are characterized by horizontal northeast-southwest to east-west compression. Similar trends are present in the expanded set of stress indicators for the New Madrid region. Zoback and Zoback (Zoback, 1989) grouped all of these regions, along with a large area of eastern Canada, with the CEUS in an expanded "Mid-Plate" stress province characterized by northeast-southwest directed horizontal compression.

In addition to better documenting the orientation of stress, research conducted since 1986 has addressed quantitatively the relative contributions of various forces that may be acting on the North American plate to the total stress within the plate. Richardson and Reding (Richardson, 1991) performed numerical modeling of stress in the continental U.S. interior, and considered the contribution to total tectonic stress to be from three classes of forces:

1. Horizontal stresses that arise from gravitational body forces acting on lateral variations in lithospheric density. These forces commonly are called buoyancy forces. Richardson and Reding (Richardson, 1991) emphasize that what is commonly called ridge-push force is an example of this class of force. Rather than a line-force that acts outwardly from the axis of a spreading ridge, ridge-push arises from the pressure exerted by positively buoyant, young oceanic lithosphere near the ridge against older, cooler, denser, less buoyant lithosphere in the deeper ocean basins (Turcotte, 2002). The force is an integrated effect over oceanic lithosphere ranging in age from about 0 to 100 million years (Dahlen, 1981). The ridge-push force is transmitted as stress to the interior of continents by the elastic strength of the lithosphere.

2. Shear and compressive stresses transmitted across major plate boundaries (strike-slip faults and subduction zones).

3. Shear tractions acting on the base of the lithosphere from relative flow of the underlying asthenospheric mantle.

Richardson and Reding (Richardson, 1991) concluded that the observed northeast-southwest trend of principal stress in the CEUS dominantly reflects ridge-push body forces. They estimated the magnitude of these forces to be about 2 to 3 x 10^{12} Newton-meters (N/m) (i.e., the total vertically integrated force acting on a column of lithosphere 1 m wide), which corresponds to average equivalent stresses of about 40 to 60 MPa (373 to 559 tsf) distributed across a 30 miles (50 km) thick elastic plate. The fit of the model stress trajectories to data was improved by the addition of compressive stress (about 5 to 10 MPa) acting on the San Andreas Fault and Caribbean plate boundary structures. The fit of the modeled stresses to the data further suggested that shear stresses acting on these plate boundary structures is in the range of 5 to 10 MPa (47 to 93 tsf).

Richardson and Reding (Richardson, 1991) noted that the general northeast-southwest orientation of principal stress in the CEUS also could be reproduced in numerical models that assume a shear stress, or traction, acting on the base of the North American plate. Richardson and Reding (Richardson, 1991) and Zoback (Zoback, 1989) do not favor this as a significant contributor to total stress in the mid-continent region. A basal traction predicts or requires that the horizontal compressive stress in the lithosphere increases by an order of magnitude moving east to west, from the eastern seaboard to the Great Plains. Zoback and Zoback (Zoback, 1989) noted that the state of stress in the southern Great Plains is characterized by north-northeast to south-southwest extension, which is contrary to this prediction. They further observed that the level of background seismic activity is generally higher in the eastern

United States than in the Great Plains, which is not consistent with the prediction of the basal traction model that compressive stresses (and presumably rates of seismic activity) should be higher in the middle parts of the continent than along the eastern margin.

Site specific studies in-situ studies were conducted during geologic investigation for NMP Unit 2 (Niagara Mohawk, 1978c).

The stress field determined from overcoring measurements in a block of limited volume at the NMP Unit 2 site (CEG, 1998) clearly demonstrates this complexity. Nevertheless, some useful general characteristics of the regional stress field are noted.

The entire region surrounding Lake Ontario is characterized by a stress field that is considerably different than that to be expected solely due to present gravitational loading. The state of stress is manifested by the development of postglacial deformational structures (popup structures), and by the occurrence of shallow seismic events of low magnitude (Section 2.5.2). The presence of high horizontal stress is confirmed by the in situ measurements made at many locations (Karrow, 2002).

The regional stress field appears to be spatially continuous and homogeneous in its character from one locality to the other. The most consistent observation regarding this field is that the greatest and intermediate principal stresses are generally horizontal or subhorizontal. The least principal stress tends to be nearly vertical. The trend of the greatest principal stress, as indicated by focal mechanism solutions, hydrofracture testing, and the average orientation of postglacial folds, is consistently northeast to east-northeast. However, for many possible reasons, overcore measurements made at shallow depths reveal a widespread variation of the orientation of the maximum horizontal stress, making it difficult to identify a representative trend (CEG, 1998). This characterization is in general accordance with the definition of the Central Lowland/Canadian Shield stress province.

Focal mechanism solutions of earthquakes that occurred in the region indicate that the greatest principal stress may be inclined at a shallow angle with respect to the horizontal plane. A southward plunge of this stress is suggested for the area north of the NMPNS site (CEG, 1998). The slip planes associated with shallow seismic events generally strike northwest or north-northeast, and dip steeply in most instances. Slip has been either reverse, strike-slip, or a combination thereof. Two focal mechanism solutions with oblique-normal slip have been recorded in central New York (CEG, 1998). Section 2.5.2 presents a discussion of the distribution of regional seismicity and the correlations of certain seismic events with known geological structures.

The magnitude of the maximum horizontal normal stress in the region is high in the depth interval from the surface to about 518 meters (1,700 ft) (CEG, 1998). Refer to Section 2.5.4. for additional discussion. Magnitudes range from several hundred to several thousand psi. Averaging the data gives a magnitude of this stress in excess of 98 kg/sq cm (1,400 psi), which is a fair indication of the order of stress to be expected in the Lake Ontario region. The average stress difference in the horizontal plane is also high, and is approximately equal to 70 kg/sq cm (1,000 psi).

It is not possible to assess the relative stability of geological structures on the basis of this limited knowledge of the regional stress field. One would not expect reverse-slip on high-angle faults (such as the Clarendon-Linden fault) with the maximum principal stress being horizontal to subhorizontal However, the focal solutions by Hermann (CEG, 1998) for two Attica events indicate that the intermediate principal stress is sharply inclined with respect to the earth's surface. From this analysis, one must infer that a component of strain in a vertical plane is

related to this shear displacement on the fault. For this reason, it is important to consider the distribution of contemporary vertical crustal movements in the region of the NMP3NPP site, and the possible influence of these movements on the tectonic features in the region.

To summarize, analyses of regional tectonic stress in the CEUS since EPRI (1986) have not significantly altered the characterization of the northeast-southwest orientation of the maximum compressive principal stress. The orientation of a planar tectonic structure relative to the principal stress direction determines the magnitude of shear stress resolved onto the structure. Given that the current interpretation of the orientation of principal stress is similar to that adopted in EPRI (1986), a new evaluation of the seismic potential of tectonic features based on a favorable or unfavorable orientation to the stress field would yield similar results. Thus, there is no significant change in the understanding of the static stress in the CEUS since the publication of the EPRI source models in 1986, and there are no significant implications for existing characterizations of potential activity of tectonic structures.

2.5.1.1.4.3 Gravity and Magnetic Data and Features of the Site Region and Site Vicinity

Gravity and magnetic anomaly datasets of the site region have been published following the 1986 EPRI study. A magnetic anomaly map of North America was published in 2002 that featured improved reprocessing of existing data and compilation of a new and more complete database (Bankey, 2002) (Figure 2.5-19)

These maps present the potential field data at 1:5,000,000-scale, and thus are useful for identifying and assessing gravity and magnetic anomalies with wavelengths on the order of tens of kilometers or greater (USGS, 2002c). Regional gravity anomaly maps are based on Bouguer gravity anomalies onshore and free-air gravity anomalies offshore. The primary sources of magnetic data reviewed for this NMP3NPP study are from aeromagnetic surveys onshore and offshore (Bankey, 2002).

Most of the contributed gravity and magnetic data that went into the regional compilations were collected prior to the 1986 EPRI study; thus, most of the basic data were available for interpretation at local and regional scales. Large-scale compilations (1:2,500,000-scale) of the free-air anomalies offshore and Bouguer anomalies onshore were published in 1982 by the Society of Exploration Geophysicists (Lyons, 1982). The DNAG magnetic anomaly maps were based on a prior analog map of magnetic anomalies of the U.S. published in the early 1980s (Zietz, 1982).

Recent magnetic maps of Canada and North America have been published by the Geological Survey of Canada. A 1:5,000,000-scale Magnetic Anomaly Map of Canada was published by the Geological Survey of Canada (GSC, 1987). A 1:2,000,000 -scale Residual Total Field Magnetic Map of the Superior and Grenville Provinces was published by the Geological Survey of Canada (GSC, 1998). A 1:3,000,000-scale map of Magnetic Anomalies and Major Structural Features of Southeastern Canada and the Atlantic Continental Margin was also published by the Geological Survey of Canada (Shih, 1993). A 1:7,500,000-scale Magnetic Anomaly Map for Canada was published by the Geological Survey of Canada (Miles, 2000) and a 1:10,000,000-scale Magnetic Field Intensity Map of North America was published by the Geological Survey of Canada (Pilkington, 1992a).

Recent gravity maps of Canada and North America have been published by the Geological Survey of Canada. A 1:10,000,000-scale Vertical Gradient of the Bouguer Anomaly Map of North America was published by the Geological Survey of Canada (Pilkington, 1992b). A 1:3,000,000-scale Gravity Anomalies and Major Structural Features of Southeastern Canada and

The Atlantic Continental Margin map was published by the Geological Survey of Canada (Shih, 1993). A 1:10,000,000-scale Gravity Anomaly Map with Shaded Relief of Gradient of North America (Pilkington, 1992a) was published by the Geological Survey of Canada. A 1:7,500,000-scale Gravity Anomaly Map for Canada was published by the Geological Survey of Canada (Miles, 2006).

In summary, the gravity and magnetic data published since 1986 do not reveal any new anomalies related to geologic structures that were not identified prior to the 1986 EPRI study. Post-EPRI publications have only refined the characteristics and tectonic interpretation of the anomalies. Discussion of the gravity and magnetic anomalies is presented in the following sections.

2.5.1.1.4.3.1 Gravity Data and Features

The pattern of regional Bouguer gravity anomalies and regional aeromagnetic anomalies confirms local density contrasts and magnetic contrasts in the Precambrian Central Metasedimentary Belt (CMB) of the Canadian Grenville Province (CEG, 1998). Rocks in the CMB consist of local mafic intrusive, extensive felsic intrusives, highly deformed gneisses, marbles and schists. The patterns of gravitational and magnetic anomalies extends into central and western New York suggesting that the Grenville CMB extends beneath the NMP3NPP site.

The extent of major Paleozoic shortening is to some degree evident from regional gravity studies. Figure 2.5-20 shows the configuration of Bouguer gravity anomalies of New York State and adjacent Canada. At the east edge of this map, a pronounced and steep gravity gradient separates the broad area of negative gravity anomalies to the west from higher magnitude anomalies to the east. This gradient represents a fundamental change from the sedimentary rock of the basin to the highly-metamorphosed, plutonized, and faulted rocks of the core of the crystalline Appalachians. Because of the thrusting of large rock masses to the west of this gradient during orogenesis, the resultant increased loading depressed the light crust into the asthenosphere, perhaps accounting for the negative gravity anomalies in the Appalachian Basin region.

In Pennsylvania, the southeast boundary of the Greene-Potter zone nearly coincides with the major aeromagnetic lineament of King and Zietz (CEG, 1998), the New York-Alabama lineament, which seems to indicate a profound crustal break.

Gravity and magnetic investigations of the Clarendon-Linden fault zone suggest that some control of the Paleozoic structure by the Precambrian basement is evidenced by the location of the structure on the western flank of a series of gravity and magnetic highs (Figure 2.5-19 and Figure 2.5-20) that are probably caused by mafic intrusives in the basement. The distribution of these geophysical anomalies suggests that the fault may indeed extend to Pennsylvania. This possibility is further strengthened by some Devonian depositional patterns in Pennsylvania.

The Ottawa-Bonnechere graben (Figure 2.5-31) is largely confined to the Ontario and Quebec Provinces of Canada, and consists of major west-northwest and east-northeast-striking faults, with as much as 457 meters (1,500 ft) of vertical displacement. This fault system is aligned with a series of Mesozoic, alkalic, intrusive rocks which compose the Monteregian Hills. The isotopic ages yielded by these rocks range between 90 and 150 million years before present (B.P.) (CEG, 1998). Two faults of this system, the Gloucester and the Winchester Springs, have been extended into northern New York on the basis of geophysical investigations. The Gloucester fault (Figure 2.5-31 is a member of the Ottawa-Bonnechere fault system. It trends west-northwest. The northeast side is downthrown about 1,800 feet (549 m). In Canada, the fault cuts through early Paleozoic sedimentary rocks and is believed to be a member of a zone of extension that had been active repeatedly long ago in the geological past. Radiometric dates

of igneous rocks occurring within the Ottawa-Bonnechere indicate activity from Late Precambrian to Middle Ordovician and, again, in Mesozoic time (CEG, 1998).

Four prominent cross-strike features are postulated in Pennsylvania, New York, and southern Ontario based principally on the regional configuration of simple Bouguer gravity anomalies and the regional aeromagnetic signature (Figure 2.5-32). There is little compelling geologic evidence to support the speculation that these lineaments are direct manifestations of fundamental discontinuities emanating from the Precambrian basement. However, what evidence there is may be significant. The possible relationship of the New York-Pennsylvania lineaments to historic seismicity is speculative. The regions of intense seismic activity may coincide with one or more of these lineaments, implying that the crust is segmented by both northwest and northeast discontinuities, and that the interior portions of these blocks are relatively aseismic. These blocks are approximately 90 miles (145 km) square. Moreover, Fakundiny (CEG, 1998) recognizes possibly less distinct east-west discontinuities extending across central New York through the Finger Lakes. It is noteworthy that the NMP3NPP site is situated within the interior of one of these crustal blocks. The geologic evidence of the nature of the New York-Pennsylvania lineaments is briefly reviewed here.

Lineament G (Figure 2.5-32) is one of several lineaments in this area of Pennsylvania. Mapping along the lineament has revealed:

- Localized structural disturbance in the form of complex thrust and tear fault combinations.
- A down-faulted structural block in the Paleozoic strata, the Tipton Zone, bounded by northwest strike-slip faults.
- Localized zones of high fracture density.
- Water and wind gaps in topographic ridges.
- Pb-Zn and Cu mineralization of fractures and fault.
- Localized, abrupt termination of small-scale folds and fault.

Studies in the vicinity of Lineament X (Figure 2.5-32) have detected possible north-northwest-trending horsts and grabens, generally below the Salina salt, but also above it. High magnetic contrasts across the edge of a block bounded by the lineament are also present. In addition, a small fault along the west edge of Lake Cayuga, New York, appears to exhibit a change in movement sense from pre- to post-Ordovician time. These three lines of evidence suggest basement structural control along the lineament. Podwysocki and others report evidence for a different, namely thrust-faulting, origin of this block. This consists of: 1) seismic well log and mine data that show thrust faults originating in the salt, 2) deformed fossils along the block's margins, and 3) change of fold axis attitude near the margins of the block.

There is little corroborative evidence of northwest structure along Lineament F (Figure 2.5-32). A system of Hadrynian diabase dikes near the Frontenac Axis (Figure 2.5-32) outlines a transverse fracture pattern with deep crustal connections extant in early Paleozoic time. However, no major northwest discontinuities are known in the area along Lineament F. Focal mechanism solutions from the southwestern Adirondacks indicate northwest-striking nodal planes (Section 2.5.2).

Lineament E (Figure 2.5-32) coincides approximately with the region of the Ottawa River Valley wherein the Ottawa-Bonnechere System occurs. Major displacements, emanating from the basement, and deep-seated intrusives of Cretaceous age along strike of the fault zone, all suggest that this lineament is a fundamental structural discontinuity in Canada. Evidence is less compelling in New York State, except for the Gloucester and Winchester Springs faults (mentioned above), which appear to terminate in the central highlands of the Adirondack Massif.

Bouguer gravity values increase eastward from about -80 milligals (mgal) in the Valley and Ridge Province of western Virginia to about +10 mgal in the Coastal Plain Province, corresponding to an approximately 90 mgal regional anomaly across the Appalachian Orogen (Figure 2.5-33. This regional gradient is called the "Piedmont gravity gradient", and is interpreted to reflect the eastward thinning of the North American continental crust and the associated positive relief on the Moho discontinuity with proximity to the Atlantic margin.

In summary, gravity data published since the mid-1980s confirm and provide additional documentation of previous observations of a gradual "piedmont gravity gradient" across the Blue Ridge and Piedmont Provinces of Virginia and a prominent gravity anomaly at the seaward margin of the continental shelf. Shorter-wavelength anomalies such as the SGA also are recognized in the data. All anomalies were known at the time of the 1986 EPRI study. The "piedmont gravity gradient" is interpreted to reflect eastward thinning of the North American crust and lithosphere. The free-air anomaly at the outer shelf edge is interpreted as reflecting the transition between continental and oceanic crust. Second-order features in the regional field, such as the Salisbury geophysical anomaly and the short discontinuous northeast-trending anomaly east of the site, primarily reflect density variations in the upper crust associated with the boundaries and geometries of Appalachian thrust sheets and accreted terranes.

2.5.1.1.4.3.2 Magnetic Data and Features

Magnetic data compiled for the 2002 Magnetic Anomaly Map of North America reveal numerous northeast-southwest-trending magnetic anomalies, generally parallel to the structural features of the Appalachian orogenic belt (Bankey, 2002) (Figure 2.5-19). Unlike the gravity field, the magnetic field is not characterized by a regional, long-wavelength gradient that spans the east-west extent of the site region.

Prominent north- to northeast-trending magnetic anomalies in the NMP3NPP site region include the interior New York-Alabama lineaments (King, 1978) (Bankey, 2002).

King and Zietz (King 1978) identified a 1,000 mile (1,600 km) long lineament in aeromagnetic maps of the eastern U.S. that they referred to as the "New York-Alabama lineament" (NYAL) (Figure 2.5-19). The NYAL primarily is defined by a series of northeast-southwest-trending linear magnetic anomalies in the Valley and Ridge province of the Appalachian fold belt that systematically intersect and truncate other magnetic anomalies. The NYAL is located southeast of the NMP3NPP site.

King and Zietz (King, 1978) interpreted the NYAL to be a major strike-slip fault in the Precambrian basement beneath the thin-skinned fold-and-thrust structures of the Valley and Ridge province, and suggested that it may separate rocks on the northwest that acted as a mechanical buttress from the intensely deformed Appalachian fold belt to the southeast. Shumaker (Shumaker, 2000) interpreted the NYAL to be a right-lateral strike-slip fault that formed during an initial phase of Late Proterozoic continental rifting that eventually led to the opening of the Iapetus Ocean.

The East Coast magnetic anomaly (ECMA) is a prominent, linear, segmented magnetic high that extends the length of the Atlantic continental margin from the Carolinas to New England (Figure 2.5-19). The anomaly is about 65 miles (105 km) wide and has an amplitude of about 500 nT. This anomaly approximately coincides with the seaward edge of the continental shelf, and has been considered to mark the transition from continental to oceanic crust. Klitgord et al. (Klitgord, 1995) note that the anomaly is situated above the seaward edge of the thick Jurassic volcanic wedge and lower crustal zone of magmatic under plating along the boundary between rift-stage and marginal oceanic crust. The ECMA is not directly associated with a fault or tectonic feature, and thus is not a potential seismic source.

In summary, magnetic data published since the mid-1980s confirm and provide additional documentation of previous observations (i.e., pre-EPRI) across this region of eastern North America, and do not reveal any new anomalies related to geologic structures previously unknown to EPRI (EPRI, 1986).

2.5.1.1.4.4 Principal Tectonic Structures

Research since the EPRI study (EPRI, 1986) has advanced the understanding of the character and timing of the crustal architecture and tectonic history of the eastern United States and Canada. The research has clarified the timing and kinematics of tectonic processes from the Late Precambrian through the Cenozoic. Since the EPRI study (EPRI, 1986) was completed, new Cenozoic tectonic features have not been proposed in the site region. Based on the absence of published literature documenting Quaternary tectonic deformation and spatially associated with seismicity, we conclude that these features are not a capable tectonic source.

In the sections below, specific tectonic features and their evidence for activity published since the EPRI (1986) study are discussed. We find that no new information has been published since 1986 on any tectonic feature within the NMP3NPP site region that would cause a significant change in the EPRI seismic source model.

We divide principal tectonic structures within the 200 mile (322 km) NMP3NPP site region into five categories based on their age of formation or most recent reactivation. These categories include Late Proterozoic, Paleozoic, Mesozoic, Tertiary, and Quaternary. Late Proterozoic, Paleozoic, and Mesozoic structures are related to major plate tectonic events and generally are mapped regionally on the basis of geological and/or geophysical data. Late Proterozoic structures include normal faults active during post-Grenville orogeny rifting and formation of the lapetan passive margin. Paleozoic structures include thrust and reverse faults active during Taconic, Acadian, Alleghenian, and other contractional orogenic events. Mesozoic structures include normal faults active during break-up of Pangaea.

Tertiary and Quaternary structures within the NMP3NPP site region are related to the glaciation of the site region. This stable province is characterized by northeast-southwest oriented, horizontal principal compressive stress, and vertical crustal motions. The vertical crustal motions are associated with glacial isostatic rebound and erosion. Commonly, these structures are localized. Zones of seismicity not clearly associated with a tectonic feature are discussed separately in Section 2.5.1.1.4.5.

2.5.1.1.4.4.1 Late Proterozoic Tectonic Structures

Extensional structures related to Late Proterozoic-Early Cambrian rifting of the former supercontinent Rodinia and formation of the lapetus Ocean basin are located along a northeast-trending belt between Alabama and Labrador, Canada, and along east-west-trending branches cratonward (Wheeler, 1995). Major structures along this northeast-trending belt include the Reelfoot rift, the causative tectonic feature of the

1811-1812 New Madrid earthquake sequence. Within the 200-mile (322 km) site region, a discrete Late Proterozoic feature includes the New York-Alabama lineament (King, 1978) (Shumaker, 2000). The Rome Trough is located beyond the 200-mile (322 km) site region.

Extended crust of the lapetan passive margin extends eastward beneath the Appalachian thrust front approximately to the eastern edge of Mesozoic extended crust within the eastern Piedmont physiographic province (Wheeler, 1995). This marks the western boundary of major Paleozoic sutures that juxtapose Laurentian crust against exotic crust amalgamated during the Paleozoic orogenies (Wheeler, 1995).

The earthquake potential of lapetan normal faults was recognized by the EPRI team members due to the association between the Reelfoot rift and the 1811 to 1812 New Madrid earthquake sequence (EPRI, 1986). Seismic zones in eastern North America spatially associated with lapetan normal faults include the Giles County seismic zone of western Virginia, and the Charlevoix, Quebec seismic zone. The Giles County seismic zone is located outside the NMP3NPP site region (Wheeler, 1995). Because the lapetan structures are buried beneath Paleozoic thrust sheets and/or strata, their dimensions are poorly known except in isolated, well studied cases.

Although published literature since the EPRI study (EPRI, 1986) has made major advances in showing the association between local seismic sources and Late Proterozoic structures (Wheeler, 1995) and has highlighted the extent of extended lapetan passive margin crust (Wheeler, 1995), no new information has been published since 1986 on any Late Proterozoic feature within the NMP3NPP site region that would cause a significant change in the EPRI study (EPRI, 1986) seismic source model.

The Carthage-Colton mylonite zone (Figure 2.5-21) separates the Adirondack Highlands from the Adirondack Lowlands of the Frontenac Terrane and is characterized by grain-size reduction accompanied by a strong northwest-dipping foliation (Baird, 2004). The zone varies from 10 feet to 3 miles (3 m to 5 km) wide and is approximately 68 miles (110 km) long. The Adirondacks Lowlands deformation includes folding events associated with the Ottawan Orogen (1090 - 1030 Ma) compression within the Grenville Province, but the kinematics and style of deformation are cryptic and cannot conclusively be connected to metamorphic fabrics (Baird, 2004). Early formed shear zones recorded predominantly right lateral oblique-to-strike slip motion while later events recorded oblique-to-dip slip motions prior to 1020 Ma (Johnson, 2004; Streepey, 2004).

2.5.1.1.4.4.2 Paleozoic Tectonic Structures

The southern and eastern portions of the NMP3NPP site region encompass portions of the Valley and Ridge and Appalachian Plateau physiographic provinces (Figure 2.5-3). Structures within these provinces are associated with thrust sheets, shear zones, and sutures that formed during convergent and transpressional Appalachian orogenic events of the Paleozoic Era. Paleozoic structures include: 1) sutures juxtaposing allochthonous (tectonically transported) rocks against proto-North American crust, 2) regionally extensive Appalachian thrust faults and oblique-slip shear zones, and 3) a multitude of smaller structures that accommodated Paleozoic deformation within individual blocks or terranes (Figure 2.5-2). The majority of these structures dip eastward and sole into one or more levels of low angle, basal Appalachian decollement. Below the decollement are rocks that form the North American Grenville basement complex.

Researchers have observed that much of the sparse seismicity in eastern North America occurs within the North American basement below the basal decollement. Therefore, seismicity within the Appalachians may be unrelated to the abundant, shallow thrust sheets mapped at the surface (Wheeler, 1995). For example, seismicity in the Giles County seismic zone, located in the

Valley and Ridge Province, is occurring at depths ranging from 3 to 16 miles (5 to 25 km) which is generally below the Appalachian thrust sheets and basal decollement.

The Clarendon-Linden fault system located in western New York, is one of a few fault systems in the northeastern United States that has been recognized as a probable earthquake source. The fault system extends from the Lake Ontario shoreline south to Allegany County, New York and from the Lake Ontario shoreline north beneath Lake Ontario to Prince Edward County, Ontario Canada. It has been proposed that Clarendon-Linden fault system is a reactivated basement structure formed as an Iapetan normal fault (Tuttle, 2002). The Clarendon-Linden fault system may define a fundamental boundary between seismically active continental margin and the less active craton (Wheeler, 1995). Interpretation of seismic reflection data suggests that the fault system is a broad zone of small faults with small displacements in the lower Paleozoic bedrock and that the zone is at least 48 miles (77 km) long and 4 to 10 miles (7 to 17 km) wide (Fakundiny, 2002). Near Attica, New York, the relative offset across the faults of the system is more than 298 feet (91 m). The fault system is the expression of tectonic crustal adjustments within the Paleozoic rock above the boundary between the Rochester basement megablock and the Niagara basement megablock.

The locations of brittle bedrock structures within the site radius of 25 miles (40 km) are presented in Figure 2.5-36 and Figure 2.5-37 (Isachsen, 1977a, b, c, d, e, f, g).

In general, the two dominant orientations of brittle structures trend east-northeast and northwest (Figure 2.5-38). These dominant joint orientations in New York have been documented extensively (Parker, 1942; Parker, 1969; Engelder, 1979; Engelder, 1980; Engelder, 1982a, b); Engelder, 1985; Engelder, 1993; Engelder, 2001; Engelder, 2006; Engelder, 2007; Gross, 1991; Hancock, 1989; Lash, 2007; Scheidegger, 1991; Younes, 1999; Zhao, 1997). The northwest striking joints have been associated with the Paleozoic Alleghenian Orogeny. The east-northeast striking joints are parallel to the maximum horizontal stress orientation of the contemporary stress field (Evans, 1989a; Evans, 1989b; Hickman, 1985; Plumb, 1985; Plumb, 1991; Whitaker, 2005; Zoback, 1985; Zoback, 1989). A discussion of joint orientations is presented in Section 2.5.1 and Section 2.5.3.

2.5.1.1.4.4.3 Appalachian Structures

Paleozoic faults in the Appalachians are for the most part beyond 200 miles (322 km) from the NMP3NPP site (see Section 2.5.2 for a complete discussion of seismicity). Faults have been mapped within the Appalachian provinces (Valley and Ridge), but no new information has been published since 1986 on any Paleozoic fault in the site region that would cause a significant change in the EPRI study (EPRI, 1986) seismic source model.

2.5.1.1.4.4.4 Mesozoic Tectonic Structures

Mesozoic basins have long been considered potential sources for earthquakes along the eastern seaboard and were considered by most of the EPRI teams in their definition of seismic sources (EPRI, 1986). A series of elongate rift basins of early Mesozoic age are exposed in a belt extending from Nova Scotia to South Carolina and define the area of extended Mesozoic crust. These Mesozoic rift basins, also commonly referred to as Triassic basins, exhibit a high degree of parallelism with the surrounding structural grain of the Appalachian orogenic belt. The parallelism generally reflects reactivation of pre-existing Paleozoic structures. The rift basins formed during extension and thinning of the crust as Africa and North America rifted apart to form the modern Atlantic Ocean.

Generally, the rift basins are asymmetric half-grabens with the primary rift-bounding faults on the western margin of the basin (Withjack, 1998). Rift basins with rift-bounding faults on the western margin (e.g. Newark Basin, Connecticut Basin) are located beyond the 200 mile (322

km) NMP3NPP site region. The rift-bounding normal faults are interpreted by some authors to be listric at depth and merge into Paleozoic low angle basal decollement (Manspeizer, 1989). Other authors interpret rift-bounding faults to penetrate deep into the crust following deep crustal fault zones.

Aside from the global finding of Johnston et al. (1994) that areas of Mesozoic extended crust are correlated with large magnitude earthquakes within stable continental regions (e.g.., New Madrid seismic zone), there are no specific Mesozoic basin-bounding faults that have demonstrable associated seismic activity or evidence for recent fault activity. Seismicity potentially associated with reactivation of faults bordering or beneath the Mesozoic basins is captured in the existing EPRI seismic source model. No new data have been developed to demonstrate that any of the Mesozoic basins are currently active, and Crone and Wheeler (Crone, 2000), Wheeler (Wheeler, 2005) and Wheeler (Wheeler, 2006) do not recognize any basin-margin faults that have been reactivated during the Quaternary in the site region. No Mesozoic basin in the site region is associated with a known capable tectonic source, and no new information has been developed since 1986 that would require a significant revision to the EPRI seismic source model.

2.5.1.1.4.4.5 Tertiary Tectonic Structures

Capable faults are not known to have been active during the Tertiary Period within the 200 mile (322 km) NMP3NPP site region. There is no new capable fault information that would require a significant revision to the EPRI (1986) seismic source model.

2.5.1.1.4.4.6 Quaternary Tectonic Features

In an effort to provide a comprehensive database of Quaternary tectonic features, Crone and Wheeler (Crone, 2000), Wheeler (Wheeler, 2005), and Wheeler (Wheeler, 2006) compiled geological information on Quaternary faults, liquefaction features, and possible tectonic features in the CEUS. Crone (Crone, 2000) and Wheeler (Wheeler, 2005) evaluated and classified based on strength of evidence for Quaternary activity.

Category	Description
Class A	Geologic evidence demonstrates the existence of a Quaternary fault of tectonic origin, whether the fault is exposed for mapping or inferred from liquefaction to other deformational features.
Class B	Geologic evidence demonstrates the existence of a fault or suggests Quaternary deformation, but either (1) the fault might not extend deeply enough to be a potential source of significant earthquakes, or (2) the currently available geologic evidence is too strong to confidently assign the feature to Class C but not strong enough to assign it to Class A.
Class C	Geologic evidence is insufficient to demonstrate (1) the existence of tectonic fault, or (2) Quaternary slip or deformation associated with the feature.
Class D	Geologic evidence demonstrates that the feature is not a tectonic fault or feature; this category includes features such as demonstrated joints or joint zones, landslides, erosional or fluvial scarps, or landforms resembling fault scarps, but of demonstrable non-tectonic origin.

~~Within a 200 mile (322 km) radius of the NMP3NPP site, Crone and Wheeler (Crone, 2000), Wheeler (Wheeler, 2005) and Wheeler (Wheeler, 2006) identified 6 potential Quaternary features. An additional 6 potential Quaternary features were identified just beyond the 200 mile (322 km) radius. Work performed as part of the NMP3NPP investigation, including literature review, interviews with experts, and geologic reconnaissance, did not identify any additional potential Quaternary tectonic features within the NMP3NPP site region. Within approximately 200 miles (322 km) of the site, Crone and Wheeler (Crone, 2000) found no features described in the literature that exhibited potential evidence for Quaternary activity.~~

~~The following sections provide descriptions of the 12 potential Quaternary features identified by Crone and Wheeler (Crone, 2000), Wheeler (Wheeler, 2005) (Wheeler, 2006). Out of the 12 features evaluated for this NMP3NPP study, all are classified as Class C or D features.~~

Within a 200 mile (322 km) radius of the NMP3NPP site, Crone and Wheeler (Crone, 2000), Wheeler (Wheeler, 2005), and Wheeler (Wheeler, 2006) identified four potential Quaternary features. All of these features are at a distance of well over 100 miles (161 km) from the NMP3NPP site. An additional eight potential Quaternary features were identified just beyond the 200 mile (322 km) radius. Work performed as part of the NMP3NPP site investigation, including literature review, personal communication with experts, and geologic reconnaissance, did not identify any additional potential Quaternary tectonic features within the NMP3NPP site region. Review of literature concentrated on those publications issued after the original 1978 publication of the NMP Unit 2 USAR (CEG, 1998). Personal communication with experts included meeting with Dr. David Valentino of SUNY Oswego to discuss New York geology and e-mail correspondence with Dr. Martitia Tuttle to obtain paleoliquefaction studies in the CEUS. Within approximately 200 miles (322 km) of the site, Crone and Wheeler (Crone, 2000) found no features described in the literature that exhibited potential evidence for Quaternary activity.

The following sections provide descriptions of the twelve potential Quaternary features identified by Crone and Wheeler (Crone, 2000), and Wheeler (Wheeler, 2005) (Wheeler, 2006). Out of the twelve features evaluated for this NMP3NPP study, all are classified as Class C features. Class C features are characterized by insufficient geologic evidence to demonstrate the existence of a tectonic fault or insufficient geologic evidence to demonstrate Quaternary slip or deformation associated with the feature.

The features are labeled with the reference numbers utilized in Figure 2.5-39:

- Clarendon-Linden fault zone (Class C)
- Cornwall-Massena earthquake liquefaction features (Class C)
- Catlin Lake-Goodnow Pond Lineament (Class C)
- Champlain lowlands normal faults (Class C)
- Offset glacial surfaces (Class C)
- Ramapo fault system (Class C)
- Kingston fault (Class C)
- Dobbs Ferry fault zone (Class C)
- Mosholu fault (Class C)
- New York Bight fault (offshore) (Class C)
- Cacoosing Valley earthquake (Class C)
- Lancaster seismic zone (Class C)

Clarendon-Linden Fault Zone

~~The north-striking Clarendon-Linden fault zone extends at least 56-62 miles (90-100 km) across western New York State. Damaging earthquakes of M 4.9 in 1929, M 4.2 in 1966, and M 4.1 in 1967 occurred in the vicinity of the fault zone. Damage consisted of minor damage to fragile structures. Focal mechanisms of the 1966 and 1967 earthquakes have nodal planes parallel to adjacent strands of the fault zone and epicenters of other small earthquakes cluster between and near the strands of the fault zone. Field evidence of Quaternary faulting has not been found (Tuttle, 2002), although a readily detectable surface rupture is unlikely in the humid, highly vegetated area (Wheeler, 2001). Wheeler, 2001, concluded that it is unclear whether earthquakes larger than any historical shocks can occur in the Clarendon-Linden fault zone.~~

The north-striking Clarendon-Linden fault zone extends at least 56-62 miles (90-100 km) across western New York State (Jacobi, 1993) and has been interpreted as extending north beneath Lake Ontario to southern Canada (McFall, 1993) (Mohajer, 1993). The Clarendon-Linden fault zone has been identified as the northwestern limit of Iapetan normal faults associated with Late Proterozoic to Cambrian rifting (Wheeler, 1995). Earthquakes in the Clarendon-Linden fault zone may represent compressional reactivation of Iapetan faults (Wheeler, 1995).

Apparent deformation of sediments has been observed in the bottom sediments of western and southeastern Lake Ontario (Thomas, 1993) (Hutchinson, 1993). However, none of the features appear to be spatially correlative with the diffuse seismicity that characterizes the lake area or with deeper structures such as Paleozoic bedrock faults or crustal-penetrating faults in the Precambrian basement (Hutchinson, 1993).

Damaging earthquakes of M 4.9 in 1929, M 4.2 in 1966, and M 4.1 in 1967 occurred in the vicinity of the fault zone (Herrmann, 1978). Damage consisted of minor damage to fragile structures. Focal mechanisms of the 1966 and 1967 earthquakes have nodal planes parallel to adjacent strands of the fault zone and epicenters of other small earthquakes cluster between and near the strands of the fault zone. Earthquakes associated with hydraulic mining and fluid injection have also been recorded associated with this feature (Fletcher, 1977) (Seeber, 1993).

Field evidence of Quaternary faulting has not been found (Tuttle, 2002), although a readily detectable surface rupture is unlikely in the humid, highly vegetated area (Wheeler, 2001). Tuttle concluded that the lack of earthquake induced liquefaction features in sand and gravel pits and along river cutbanks demonstrates that the Clarendon-Linden fault zone probably did not generate large events during the Late Wisconsin and Holocene (Tuttle, 2002). Wheeler (Wheeler, 2001) concluded that it is unclear whether earthquakes larger than any historical shocks can occur in the Clarendon-Linden fault zone.

Cornwall-Massena Earthquake

~~In 1944, a damaging M 5.8 earthquake occurred in the Cornwall, Ontario - Massena, New York area. Paleoseimological studies in the epicentral area failed to find clear evidence for or against historic or prehistoric liquefaction and the locations of reported sand venting liquefaction could not be confirmed (Wallach, 2002; Wheeler, 2001). Wheeler, 2001, concluded that the result, occurrence, magnitude, and timing of possible prehistoric earthquakes in the area remain uncharacterized.~~

In 1944, a damaging M 5.8 earthquake occurred in the Cornwall, Ontario – Massena, New York area (Bent, 1996). Paleoseimological studies in the epicentral area failed to find clear evidence for or against historic or prehistoric liquefaction and the locations of reported sand venting liquefaction could not be confirmed with surface observation, ground-penetrating radar and trenching (Tuttle, 1996) (Wallach, 2002) (Wheeler, 2001). Wheeler (Wheeler, 2001) concluded

that the result, occurrence, magnitude, and timing of possible prehistoric earthquakes in the area remain uncharacterized.

Catlin Lake-Goodnow Pond Lineament

The Catlin Lake-Goodnow Pond lineament has been mapped as a lineament from topographic maps and imagery in the Adirondack Mountains of northern New York State. In 1983, an earthquake of moment magnitude M 4.9 occurred 7.5 km beneath the lineament (Nabelek, 1989) (Dawers, 1991)(Wheeler, 2001). The lineament has not been studied for paleoseimological evidence of Quaternary tectonic faulting. Wheeler, 2001, concluded that no reported results demonstrate either the occurrence of prehistoric earthquakes significantly larger than the 1983 earthquake or the presence of a continuous fault zone beneath the lineament that would accommodate rupture zones.

Champlain Lowlands Normal Faults

The Champlain lowlands normal faults in eastern New York State and western Vermont comprise a system of east-facing, normal faults (Oliver, 1970). The faults cut~~t~~ flat-lying, Cambrian and Ordovician, sedimentary rocks that step down to the east, between Proterozoic metamorphic rocks in the Adirondack Mountains to the west and west-verging, early Paleozoic rocks and thrust sheets in the Green and Taconic Mountains to the east (Isachsen, 1977a) (Isachsen, 1977b) (Isachsen, 1977c) (Isachsen, 1977d) (Isachsen, 1977e) (Isachsen, 1977f) (Isachsen, 1977g) (Wheeler, 2001). Marine seismic reflection profiles in Lake George and Lake Champlain found no clear evidence of Quaternary faulting in glacial and post-glacial deposits and Wheeler (Wheeler, 2001) concluded that the normal faults have not been investigated paleoseismologically for evidence of Quaternary faulting.

Offset Glacial Surfaces

Offset glacial surfaces have been documented in the Albany-Schenectady-Troy New York and Glens Falls New York areas (Oliver, 1970). Small, steeply dipping faults offset the smoothed, striated, or polished surfaces of many glaciated outcrops in the Northeast (Wheeler, 2006). The formation of the faults has been attributed to nontectonic processes such as frost-wedging. Crone and Wheeler (Crone, 2000) demonstrated that the reported sizes of the faults would present negligible seismic hazard, even if the faults are of tectonic origin.

Ramapo Fault System

The Ramapo fault system is located in northern New Jersey and southern New York State, approximately 200 miles (322 km) south-southeast of the NMP3NPP site. This fault system consists of northeast-striking, southeast-dipping, normal faults that bound the northwest side of the Mesozoic Newark basin that to the northeast become a single 40 mile (64 km) long northeast-striking fault (Ratcliffe, 1971) (Schlische, 1992) (Drake, 1996). Bedrock mapping shows primarily northwest-dipping Lower Jurassic and Upper Triassic Newark Supergroup rocks in the hanging wall and tightly folded and faulted Paleozoic basement rocks in the footwall of the fault. The Ramapo fault splays into several fault strands southwest of Bernardsville and merges with the Flemington Fault zone. This fault zone also splays into several northeast- to east-trending faults in Rockland and Westchester Counties, New York.

The Ramapo fault system has been considered a potentially active tectonic feature because the fault: (1) exhibits repeated reactivation during the Paleozoic, (2) bounds the Mesozoic Newark basin (i.e. the region is composed of extended crust), and (3) aligns with earthquake epicenters (Wheeler, 2006) (Aggarwal, 1978) (Sykes, 2008). In cross section and map view, the seismicity data and focal mechanisms illustrate a 60° to 65° southeast-dipping fault zone that projects upward to the mapped trace of the Ramapo fault. In addition, 14 focal mechanism solutions have orientations that are consistent with the present-day stress field and suggest reverse

reactivation of the Ramapo fault. Collectively, these data led Aggarwal, 1978 to conclude that the Ramapo fault is likely active.

Many of the assumptions and conclusions made by Aggarwal, 1978, were later reevaluated with alternative interpretations suggesting the fault probably has not been active during the Quaternary. Subsequent fault activity studies included several types of geophysical and geologic techniques. First, a modified velocity model and a carefully re-evaluated earthquake catalog refined the location of the earthquakes previously inferred as aligned with the Ramapo fault, and demonstrated that approximately half of the reported earthquakes occur near the margins of the Newark Basin, far from the Ramapo fault, but still within the Ramapo fault system proper (Kafka, 1985) (Thurber, 1985) (Wheeler, 2006). In addition, a reassessment of the eastern U.S. stress field demonstrated that the present-day stress field is oriented east-southeast (Zoback, 1989), which would be inconsistent with the previously inferred reverse reactivation of the fault. Kinematic analysis of fault zone samples collected from deep exploratory boreholes provides evidence that the latest style of deformation probably included extensional faulting during the Mesozoic (Ratcliffe, 1982) (Ratcliffe, 1990). The borehole data also confirm that the dip of the Ramapo fault is 10° to 15° shallower than inferred by Aggarwal, 1978.

In summary, several papers infer that evidence for Quaternary deformation exists near the Ramapo fault zone, however, Crone and Wheeler (Crone, 2000) and Wheeler (Wheeler, 2006) argue convincingly that none of the data used to infer seismic slip can be used to differentiate seismic from aseismic slip.

Additionally, trenches excavated across the up-dip projection of the fault zone revealed no evidence for Quaternary faulting (Stone, 1984) (Ratcliffe; 1990). Besides the presence of microseismicity within the vicinity of the Ramapo fault zone, there is no clear evidence of Quaternary tectonic faulting (Crone, 2000) (Wheeler, 2006), thus the Ramapo fault system is assigned a Class C designation by Crone and Wheeler (Crone, 2000). The Ramapo fault zone was a known structure for the EPRI study (EPRI, 1986). Based on the review of post-EPRI literature and seismicity, there is no new information developed since 1986 that would require a significant change to the EPRI seismic source model.

Kingston Fault

The Kingston fault is located in central New Jersey, approximately 200 miles (322 km) southeast of the NMP3NPP site. The Kingston fault is a 7 mile (11 km) long north to northeast-striking fault that offsets Mesozoic basement and is overlain by Coastal Plain sediments. Borehole and geophysical data have been used to interpret a thickening of as much as 80 feet (24 m) of Pliocene Pennauken Formation across the surface projection of the Kingston fault. The thickening of the Pennauken Formation gravel may be a result of faulting rather than fluvial processes. Geologic cross sections do not show that the bedrock-Pennauken contact is vertically offset across the Kingston fault. Therefore, it seems reasonable to conclude that faulting of the Pennauken Formation is not required and that apparent thickening of the Pliocene gravels may represent a channel-fill from an ancient pre-Pliocene channel. Furthermore, Pleistocene glaciofluvial gravels that overlie the fault trace are not offset, thus indicating the fault is not a capable tectonic source. Wheeler, 2006, reports that the available geologic evidence does not exclusively support a fault versus a fluvial origin for the apparent thickening of the Pennauken Formation. Wheeler, 2005, assigns the Kingston fault as a Class C feature based on a lack of evidence for Quaternary deformation. Given the absence of evidence for Quaternary faulting and the presence of undeformed Pleistocene glaciofluvial gravels overlying the fault trace, we conclude that the fault is not a capable tectonic feature.

Dobbs Ferry fault zone

The Dobbs Ferry fault zone is a northwest striking zone located near Westchester County, New York approximately 200 miles (322 km) southeast of the NMP3NPP site. The northwest trending, steeply dipping, zone is 5-6 miles (8-10 km) long and approximately 1,300 feet (400 m) wide. In 1985, the Ardsley earthquake M 4.1) occurred in the Westchester County. The fault zone is a member of a family of faults that also includes the Mosholu fault. Wheeler (Wheeler, 2006) concludes that there is no reported evidence of ground cracking or liquefaction during the Ardsley earthquake or from larger prehistoric earthquakes.

Mosholu Fault

The Mosholu Fault is located near New York City, approximately 200 miles (322 km) southeast of the NMP3NPP site. The 5.6-mile (9 km) long fault strikes northwest, is steeply dipping and is a member of a family of faults that also includes the Dobbs Ferry fault zone. It has been reactivated at various times with diverse slip directions in the New York City area (Wheeler, 2006). Wheeler, 2006 concluded that it cannot be proved that post-glacial uplift of the northeast side occurred by seismic slip instead of aseismic creep.

New York Bight Fault

On the basis of seismic surveys, the New York Bight fault is characterized as an approximately 31 mile (50 km) long, north-northeast-striking fault, located offshore of Long Island, New York (Schwab, 1997). The fault is located about 200 miles (322 km) southeast of the NMP3NPP site. Seismic reflection profiles indicate that the fault originated during the Cretaceous and continued intermittently with activity until at least the Eocene. The sense of displacement is northwest-side down and displaces bedrock as much as 280 feet (85 m), and Upper Cretaceous deposits about 150 feet (46 m). High-resolution seismic reflection profiles that intersect the surface projection of the fault indicate that middle and late Quaternary sediments are undeformed within a resolution of 3 feet (1 m) (Schwab, 1997). Only a few, poorly located earthquakes are spatially associated within the vicinity of the New York Bight fault (Wheeler, 2006). Wheeler, 2006, defines the fault as a feature having insufficient evidence to demonstrate that faulting is Quaternary and assigns the New York Bight fault as a Class C feature. Based on the seismic reflection surveys of Schwab, 1997 and the absence of Quaternary deformation, we conclude that the New York Bight fault is not a capable tectonic source.

Cacoosing Valley Earthquake Sequence

The 1993 to 1997 Cacoosing Valley earthquake sequence occurred along the eastern margin of the Lancaster seismic zone with the main shock occurring on January 16, 1994, near Reading, Pennsylvania, about 200 miles (322 km) southeast of the NMP3NPP site (Seeber, 1998). This earthquake sequence also is discussed as part of the Lancaster seismic zone discussion. The maximum magnitude earthquake associated with this sequence is an event of m_{bLg} 4.6 (Seeber, 1998). Focal mechanisms associated with the main shock and aftershocks define a shallow subsurface rupture plane confined to the upper 1.5 miles (2.4 km) of the crust. It appears that the earthquakes occurred on a pre-existing structure striking N 45° W in contrast to the typical north-trending alignment of microseismicity that delineates the Lancaster seismic zone. Seeber (Seeber, 1998) use the seismicity data, as well as the shallow depth of focal mechanisms, to demonstrate that the Cacoosing Valley earthquakes likely were caused by anthropogenic changes to a large rock quarry. Based on the findings of Seeber, 1998, we interpret this earthquake sequence to be unrelated to a capable tectonic source.

Lancaster Seismic zone

Wheeler (Wheeler, 2006), defines the fault of the Lancaster Seismic zone as a feature having insufficient evidence to demonstrate that faulting is Quaternary and assigns the Cacoosing Valley earthquake sequence as a Class C feature. Seismicity associated with the Lancaster

Seismic zone is presented in Armbruster (Armbruster, 1987). Additional discussion of the Lancaster Seismic zone is presented in Section 2.5.1.1.4.5 .

2.5.1.1.4.5 Seismic Sources Defined by Regional Seismicity

Within 200 miles (322 km) of the NMP3NPP site, 3 potential seismic sources are defined by a concentration of small to moderate earthquakes. These seismic sources include Eastern Canada (Charlevoix Zone and Western Quebec Zone), the Adirondack Massif of New York, and the Lancaster seismic zone in southeast Pennsylvania. The seismic zones are discussed below and in Section 2.5.2. The NMP3NPP site is located within the Eastern Great Lakes Basin. The occurrence rate of earthquakes in the Eastern Great Lakes Basin is lower than that of the surrounding regions (Ebel, 2002).

2.5.1.1.4.5.1 Eastern Canada - Quebec seismicity

The St. Lawrence Valley is frequently affected by earthquakes of low, medium, or, rarely, high magnitude. These shocks are concentrated in the area of the Charlevoix Astrobleme, in the area of Montreal, and in the Gatineau Valley. It has been suggested that the Charlevoix activity may be related to residual stress release associated with a Devonian impact feature. In addition recent vertical crustal movements have been proposed for the southern Laurentians and there is other evidence of neotectonic, possibly residual glacial isostatic uplift in the area. Postglacial faulting has been reported in southern Quebec (Karrow, 1989).

Earthquakes are frequent in eastern Canada. Major ones were noted as early as 1534-1535 and tremors of greater than magnitude 7 have occurred periodically during the last 300 years. Five earthquakes in the Charlevoix Seismic Zone of magnitude 6 or larger include the events of 1663 (M 7), 1791 (M 6), 1860 (M 6), 1870 (M 6.5), and 1925 (Ms 6.2). These earthquakes are expressions of tectonic activity believed to be partly related to plate tectonic movements and possible also to vertical uplift resulting from the stress relief caused by the melting of the last ice sheet. Strain energy appears to be dissipating in zones of crustal weakness. For example, the Charlevoix area of Quebec was the locus of a meteorite impact 350 Ma ago. The strain energy imparted by this impact is coupled with the regional tectonic stress to induce in situ principal stress ratios greater than 1 in many areas. These deviatoric stresses can exceed the shear strength of the rock, resulting in popouts (Jackson, 1989).

The Charlevoix Seismic Zone is the most seismically active region of eastern Canada. Most earthquakes occur under the St. Lawrence River, between Charlevoix County on the north shore and Kamoursaka County on the south shore and the zone is also referred to as the Charlevoix-Kamouraska Seismic Zone. The seismicity of the Charlevoix Seismic Zone has been summarized in a three-dimensional P wave velocity model (Vlahovic, 2003).

The Western Quebec Zone constitutes a large territory that encompasses the Ottawa Valley from Montreal to Temiscaming, as well as the Laurentian mountains and eastern Ontario. The approximately 160-km (99-mi) wide band of intraplate seismicity extends approximately 500 km (311-mi) from the Adirondack Highlands of New York to the Laurentian Uplands of Canada (Ma, 2007). Historical seismicity in the Western Quebec Seismic Zone includes events in 1732 (M 5.8), 1935 (M 6.2), 1944 (M 5.6), 1990 (M 5), 1996 (M 4.4) and 1997 (M 4.3). The occurrence of seismicity in the Western Quebec Seismic Zone has been recently summarized as occurring along a Mesozoic hot spot track (Ma, 2007)

2.5.1.1.4.5.2 Lancaster Seismic Zone

The Lancaster seismic zone, as defined by Armbruster, 1987, of southeast Pennsylvania has been a persistent source of seismicity for at least two centuries. The seismic zone is about 80 miles (129 km) long and 80 miles (129 km) wide and spans a belt of allochthonous Appalachian

crystalline rocks between the Great Valley and Martic Line about 200 miles (322 km) southeast of the NMP3NPP site. The Lancaster seismic zone crosses exposed Piedmont rocks that include thrust faults and folds associated with Paleozoic collisional orogenies. It also crosses the Newark-Gettysburg Triassic rift basin which consists of extensional faults associated with Mesozoic rifting. Most well-located epicenters in the Lancaster seismic zone lie directly outside the Gettysburg-Newark basin. The epicenters of 11 events with magnitudes 3.04 to 4.61 rmb from 1889 to 1994 from the western part of Lancaster seismic zone define a north-south trend that intersects the juncture between the Gettysburg and Newark sub-basins. This juncture is a hinge around which the two sub-basins subsided, resulting in east-west oriented tensile stress. Numerous north-south trending fractures and diabase dikes are consistent with this hypothesis. It is likely that seismicity in at least the western part of the Lancaster seismic zone is due to present-day northeast-southwest compressional stress which is activating the Mesozoic fractures, with dikes perhaps serving as stress concentrators (Armbruster, 1987).

It also is probable that some recent earthquakes in the Lancaster seismic zone have been triggered by surface mining. For instance, the 16 January 1994 Cacoosing earthquake (m_b 4.6) is the largest instrumented earthquake occurring in the Lancaster seismic zone. This event was part of a shallow (depths generally less than 1.5 miles (2.4 km)) earthquake sequence linked to quarry activity (Seeber, 1998). The earthquake sequence that culminated in the January 16 event initiated after a quarry was shut down and the quarry began to fill with water. Seeber, 1998, interprets the reverse-left lateral oblique earthquake sequence to be due to a decrease in normal stress caused by quarrying followed by an increase in pore fluid pressure (and decrease in effective normal stress) when the pumps were turned off and the water level increased.

Prior to the Cacoosing earthquake sequence, the 23 April 1984 Martic earthquake (m_b 4.1) was the largest instrumented earthquake in the seismic zone and resembles pre-instrumental historical events dating back to the middle 18th century. The 1984 earthquake sequence appears centered at about 2.8 miles (4.5 km) in depth and may have ruptured a steeply east-dipping, north-to northeast-striking fault aligned subparallel to Jurassic dikes with a reverse-right lateral oblique movement, consistent with east-northeast horizontal maximum compression. These dikes are associated with many brittle faults and large planes of weakness suggesting that they too have an effect on the amount of seismicity in the Lancaster seismic zone. Most of the seismicity in the Lancaster seismic zone is occurring on secondary faults at high angles to the main structures of the Appalachians. The EPRI study (EPRI, 1986) source models do not identify the Lancaster seismic zone as a separate seismic source. However, the 5.3 to 7.2 M_b maximum magnitude distributions of EPRI source zones are significantly greater than any reported earthquake in this Lancaster seismic zone. Thus, the EPRI study (EPRI, 1986) models adequately characterized this region and no significant update is required.

2.5.1.1.4.5.3 Pymatuning Earthquake

Since 1986, the largest and closest earthquake to the NMP3NPP site is the Pymatuning Pennsylvania event located approximately 230 miles (370 km) southwest of the NMP3NPP site. This 1998 m_{bLg} 5.2 event occurred near Jamestown, PA. Intensity VII minor damage was observed near the epicenter and hydrologic changes have been documented (Fleeger, 1999). The earthquake was a northeast-southwest directed thrust along a northwest striking fault. The epicentral area is thought to be at the edge of a Paleozoic rift system that extends along the St. Lawrence River and may extend into Ohio. Section 2.5.2 presents a more detailed discussion of seismicity related to the NMP3NPP site.}

2.5.1.1.4.5.4 Recent Northeastern U.S. Seismicity Research

Results of recent deterministic seismicity research for the northeastern U. S. and adjacent Canada, postulating increased magnitudes for historic events and large magnitudes for hypothesized pre-historic events were evaluated (Ebel, 1996)(Ebel, 2000)(Ebel, 2006). These

references focus on the following areas: Charlevoix-La Malbaie Zone, central and northern NH, and western Maine and coastal Massachusetts. All of these areas are outside the 200-mile radius surrounding NMP3NPP. Sensitivity analyses performed in the PSHA for NMP3NPP demonstrate that Charlevoix has a small contribution to seismic hazard at NMP3NPP site, especially at lower ground motion frequencies. The Charlevoix Zone was then used in the PSHA for calculations of uniform hazard response spectra. Sensitivity analyses performed in 1986 show that EPRI seismic zones in eastern New England do not contribute significantly (< 1%) to seismic hazard at NMP3NPP.

One finding from the research is relocation of a 1638 earthquake from the Charlevoix Zone to an uncertain location in central New Hampshire or western Maine (Ebel, 1996). This relocation of an historical earthquake does not impact any seismic zone that contributes significantly (>1%) to seismic hazard at NMP3NPP. In a separate paper on "paleoseismicity" (Ebel, 2000) a hypothesis is offered that all observed present-day small magnitude earthquakes are aftershocks of very large (M 6.5 or greater) earthquakes that occurred at some unknown time before the historical period (pre-1600 for the northeast). It is further stated in this paper that historically observed (since 1600) moderate earthquakes of about M = 5 to 6 could also be aftershocks of much larger earthquakes that occurred perhaps thousands of years ago. It is then concluded that the presented paleoseismicity model is a new way to view some of the seismicity of an intraplate region, while at the same time looking for clues of past seismic activity;however, the identification of which clusters of earthquake activity may indeed be aftershocks and of how large the past earthquakes were is speculative at best without independent confirming evidence.

The magnitude of the Cape Ann (Massachusetts coastline) 1755 earthquake is re-evaluated based on apparent paleoliquefaction features and other data, postulating a somewhat higher magnitude for that event (Ebel, 2006). No impact on seismic risk for the NMP3NPP site is interpreted from this premise due to the large distance of about 300 miles (482 km) from the NMP3NPP site to the location. In summary, the historical seismicity re-evaluations and hypotheses offered in the evaluated research papers (Ebel 1996) (Ebel, 2000) (Ebel, 2006) do not affect the performance and results of the PSHA performed for the NMP3NPP mainly because impacts, if any, are to zones located considerably beyond the 200 mile (320 km) site radius.

A new deterministic study (Sykes, 2008) provides updating of historic and instrumental seismicity information for an area around New York City and Philadelphia at a distance from the NMP3NPP site of about 190 to 250 miles (306 to 402 km) from the NMP3NPP site. The area covers in southeastern New York, southwestern Connecticut, northern New Jersey, and eastern Pennsylvania. The events considered include three large earthquakes (greater than a magnitude 5), all documented historic events which would have been considered for the EPRI-SOG seismic model. The reference also updates the apparent relationship of the Ramapo Fault with instrumentally detected seismicity. Results of this study are not determined to affect the PSHA for the NMP3NPP site due to the distance from the site and the magnitudes and distribution of the events involved. Other recent seismicity research for the St. Lawrence seismic zone is presented by Wallach (Wallach, 2002), and discussed in Section 2.5.2.2.2.1. Sensitivity analyses performed in 1986 show that EPRI seismic zones encompassing the St. Lawrence and Ramapo areas do not contribute significantly (< 1%) to seismic hazard at NMP3NPP. }

2.5.1.2 Site Geology

The U.S. EPR FSAR includes the following COL Item in Section 2.5.1.2:

Site-specific geology information will be addressed by the COL applicant.

This COL Item is addressed as follows:

{Section 2.5.1.2.1 through Section 2.5.1.2.6 are added as a supplement to the U.S. EPR FSAR.

2.5.1.2.1 Site Area Physiography and Geomorphology

The NMP3NPP site area is defined as the area within a 5 mile (8 km) radius of the NMP3NPP site. The NMP3NPP site area is located within the Eastern Lake Section of the Central Lowland and the Mohawk Section of the Appalachian Plateau Physiographic Province (Fenneman, 1946). The physiographic province in which the NMP3NPP site is located is referred to as (variously): the Ontario Lowlands (NYGS, 2000), the Interior Lowlands (NYSM, 1990) and the Central Lowlands (Fenneman, 1946) (Figure 2.5-3 and Figure 2.5-4).

The NMP3NPP site vicinity is defined as the region within a 25 mile (40 km) radius of the NMP3NPP site. The NMP3NPP site vicinity topography is presented in Figure 2.5-40. The NMP3NPP site area topography is presented in Figure 2.5-41. The NMP3NPP site is defined as a 0.6 mile (1 km) radius surrounding the location of NMP3NPP. The NMP3NPP site topography is presented in Figure 2.5-42.

The site vicinity bedrock geologic map (Figure 2.5-46, Figure 2.5-47, Figure 2.5-48), from the Geologic Map of New York Adirondack Sheet (NYSM, 1970a) and Finger Lakes Sheet (NYSM, 1970b), indicates that the NMP3NPP site is underlain by the Ordovician age Oswego Sandstone. The site vicinity to the north and east is underlain by the Ordovician age Pulaski Formation of the Lorraine Group, the Ordovician age Whetstone Gulf Formation of the Lorraine Group, the Ordovician age Utica Shale, the Ordovician age Trenton Group and the Ordovician age Black River Group.

To the south and west, the site vicinity is underlain by the Late Ordovician to Early Silurian age Queenston Formation-Medina Group, the Silurian age Clinton Group, the Silurian age Lockport Group and the Silurian age Vernon Formation. The bedrock geology is shown in greater detail on the scale of the site area (8 km (5 mi)) geologic map (Figure 2.5-46, Figure 2.5-47, Figure 2.5-48).

Geologic cross sections presented in Section 2.5.1.1 indicate that the Paleozoic age sedimentary rocks in the site vicinity dip gently to the southwest as described Section 2.5.1.2.2.

The site vicinity surficial geologic map (Figure 2.5-49, Figure 2.5-50, Figure 2.5-51), from the Surficial Geologic Map of New York Adirondack Sheet (NYSM, 1991) and the Finger Lakes Sheet (NYSM, 1986) indicates that the NMP3NPP site is underlain by Pleistocene age glacial till. The site vicinity to the north and east is predominantly underlain by Pleistocene age till, Pleistocene age lacustrine silt and clay, Pleistocene age lacustrine sand, Pleistocene age outwash sand and gravel, Pleistocene age kame deposits and Pleistocene age till moraine.

To the south and west, the site vicinity is underlain predominantly by Pleistocene age till, Pleistocene age lacustrine silt and clay and Pleistocene age lacustrine sand. The surficial geology is shown in greater detail on the scale of the site area (5 mile (8 km)) surficial geologic map (Figure 2.5-52, Figure 2.5-53, Figure 2.5-54).

The surficial geology is also depicted on a site area geologic map compiled from U.S.G.S. surficial geology of Texas, West of Texas, Mexico, Oswego West, Oswego East, and New Haven, Oswego County, New York, quadrangles (U.S.G.S., 1980) (Figure 2.5-55). The NMP3NPP site is

underlain by lodgement till. The immediately adjacent NMP Unit 1 and Unit 2 sites to the east are underlain by artificial fill and the immediately adjacent Ontario Bible Camp to the west of the site is underlain by lacustrine silt and fine sand. In the site area, to the east, south and west, ablation till and lodgement till are predominant with smaller areas of lacustrine silt and fine sand, peat, marl, muck and clay. The surficial geology is shown in greater detail on the scale of the site in the site geologic map (Figure 2.5-56).

Elevations in Oswego County range from approximately 250 feet (76 m) above msl at Lake Ontario to greater than 1,700 feet (518 m) msl on the Tug Hill Plateau (USGS, 1985a; USGS, 1985b; USGS, 1985c; USGS, 1985d). As shown on the site area and site topographic and geologic maps, the local site topography is fairly flat, ranging from approximately El. 280 feet (85 m) msl (on the south) to El. 260 feet (79 m) msl (on the north) (USGS, 1982). At the lake shore there is a small bluff that drops from the site to lake level of approximately El. 245 feet (75 m). During the investigation, the lake level ranged from approximately El. 243 to 247 feet (74 to 75 m) (as measured by NOAA Station ID 9052030 in Oswego, NY, which is approximately 8 miles (13 km) west of the NMP3NPP site (NOAA, 2008).

Oswego County lies in the Erie-Ontario Plain and the Tug Hill Plateau portion of the Appalachian Plateau (NYSM, 2000). The Erie-Ontario Plain is a relatively low and flat area that borders Lake Erie and Lake Ontario on the south and extends up to the Tug Hill Plateau. The topography within 5 miles (8 km) of the site rises eastward and southward from Lake Ontario to about 1,000 to 1,500 feet (305 to 457 m) msl along the Allegheny Plateau, which forms the boundary with the Appalachian Uplands to the south (NYSM, 1990). The Tug Hill Plateau is an isolated upland located on the eastern part of the Erie-Ontario Lowlands (NYSM, 2000). Elevations range from approximately 1,800 to 2,000 feet (549 to 610 m) msl and the topographic relief is very low (USGS, 1985a; USGS, 1985b; USGS, 1985c; USGS, 1985d). The Tug Hill Aquifer is an approximately north-south trending ridge of glacial drift materials at the base of the western edge of the plateau (NYSM, 2000).

The significant surface water body at the NMPNS site is Lake Ontario. Surface water and groundwater flow regionally towards the lake, with some minor seasonal drainage across the northern part of the site from northeast to southwest. During wet seasons, surface water and groundwater flow across the site and during dry seasons water collects in pools, which make up the wetlands. Water in the wetland pools appears to be perched at an elevation close to the local groundwater table in the soil and Oswego Sandstone.

The Lake Ontario shoreline forms the northern boundary of the NMP3NPP site and generally consists of low steep bluffs with narrow beaches at their base. The narrow beaches consist of cobbles and bedrock outcrops on promontories and glacio-lacustrine sediments in embayments.

Field observations indicate that these steep slopes fail along steep irregular surfaces. The slope failure appears to be caused by shoreline erosion along the base of the cliffs. Shoreline processes and slope failure along Lake Ontario are discussed in Section 2.4.9.

Much of the shoreline along the existing NMP Unit 1 and Unit 2 and James A. Fitzpatrick Nuclear Power Plant intake structures eastward to the existing barge slip is stabilized against shoreline erosion (See Section 2.4). NMP3NPP will be constructed at a final grade elevation of approximately 270 feet (82 m) msl and will be set back approximately 1,300 feet (396 m) from the Lake Ontario shoreline.

As described in Section 2.5.1.1, Lake Ontario was formed toward the end of the Wisconsinan glacial stage, which marked the end of the Pleistocene epoch. As the glaciers retreated, the

huge volumes of melting ice fed the large ancestral Glacial Lake Iroquois. The lake level of Glacial Lake Iroquois was significantly above the current level of Lake Ontario. Following glacial retreat, isostatic rebound of the Earth's crust led to a lowering of the lake level, significantly below the current lake level, to approximately elevation -50 feet (-15 m) msl during the Admiralty Stage. The Lake Ontario level then rose to its current elevation of approximately 245 feet (75 m) msl. Refer to Section 2.4 for additional discussion.

2.5.1.2.2 Site Area Geologic History

The site area geologic history prior to the Late Ordovician is inferred from limited but deep petroleum exploration borehole data, geophysical surveys and a synthesis of published information. Geophysical data and borehole data indicate that the basement rock beneath the site consists of crystalline gneissic Precambrian rock of the Grenville Province (Tollo et al, 2004; Ouassaa, 2002; Carr, 2000; White et al, 2000; Musacchio, 1997; Forsyth, 1994; Zelt, 1994; Rankin, 1993; Reed, 1993; Hughes and Luetgert, 1992;; Brown, 1983; Kreidler, 1972; Flagler, 1966). The most recent detailed site area (5 mi (8 km) radius) geologic history is presented in the NMP Unit 2 USAR and is summarized here (CEG, 1998).

The NMP Unit 2 detailed geologic history was made possible through detailed geologic study of rock excavations and cleared bedrock surfaces during initial construction of NMP Unit 2. Cleared bedrock surfaces and excavations for NMP3NPP will also be mapped during initial construction and the site area geologic history will be refined for the NMP3NPP site.

The NMP3NPP site is located within a region that has been subjected to nonorogenic tectonic deformation, due to formation of the Atlantic Ocean, and glacioisostatic adjustments, both of which are characterized by vertical crustal movements. These broad-scale movements precipitated a geologically simple, yet mechanically complex, sequence of events at the NMP Unit 2 site (CEG, 1998).

Although the Precambrian basement has not been penetrated directly beneath the NMP3NPP site with drill holes, regional geologic cross sections developed from geophysical, gravity and aeromagnetic, as well as limited deep borehole stratigraphic data near the site area, suggest Precambrian rocks are most likely present at a depth of about 1,770 feet (539 m) beneath the site (Section 2.5.1.2.3 and Section 2.5.1.2.4).

Tectonic models discussed in Section 2.5.1.2.4 hypothesize that the Grenville Province crystalline basement was formed by convergent tectonics along the southeastern margin of Laurentia during multiple episodes of orogenesis within the Grenville Orogen circa 1.3-1.0 billion years ago (Ga). The protoliths of the metamorphosed crystalline Grenville basement rocks have formation ages of circa 2.7 Ga (Isachsen, 2000). This age of protolith formation is equivalent to the ages of rocks of the Superior Province of the Canadian Shield.

Therefore, the crystalline basement beneath the Paleozoic sedimentary rocks in the site area consists of the southern extension of the Central Metasedimentary Belt (CMB) of the Precambrian Grenville Province. The CMB is composed of the Frontenac Terrane and the New York Adirondack Lowlands. Grenville CMB rocks are exposed approximately 62 miles (100 km) to the north of the site area in Canada and in the Adirondack Lowlands and Adirondack Highlands of New York (Rankin et al, 1993).

Following uplift of the Grenville Plateau, erosion removed approximately 16 miles (25 km) of Grenville basement crust in the Late Proterozoic prior to rifting of the Grenville suture zone outboard of New York State approximately 660 million years ago (Ma) (Isachsen, 2000). The rifting of the Grenville province led to the formation of the Iapetus Ocean.

During early Paleozoic time the previous trend toward uplift was reversed and subsidence began. This downwarping of the crust signaled the initial development of the Appalachian Orogen and the closing of the Iapetus Ocean. Throughout most of early to middle Paleozoic time, the site was situated in the midst of a vast subsiding sedimentary basin. Within the basin a westward thickening wedge of predominantly clastic lithologies was being deposited as a result of the intense orogenesis occurring to the east. Approximately 1,700 feet (518 m) of this sedimentary sequence accumulated prior to the deposition of the site strata. These strata, which are currently exposed at the site, represent a shallow water phase of deposition in the basin history coincident with the culmination of the Late Ordovician Taconic Orogeny in the Valley and Ridge Appalachians Province. Subsidence and deposition continued, and it is estimated that 8,000 to 10,000 feet (2,440 to 3,050 m) (Section 2.5.1.1) of younger sedimentary rocks buried the site strata before deposition within the basin ceased. This maximum depth of burial at NMP Unit 2 is interpreted on the basis of regional relationships (Section 2.5.1.1) and the homogenization temperatures (349 °F to 297 °F, 176 °C to 147 °C) of fluid inclusions within grains of the host rock and secondary fracture-filling minerals (CEG, 1998).

Paleozoic sedimentary rocks were deposited in the northern part of the Appalachian Basin unconformably on the Precambrian erosional surface. Sediments were shed from the Taconic Mountains located in eastern New York State. The Taconic Mountains were formed during an Island Arc collision during the Taconic Orogeny.

The sediments from the western slopes of the Taconic Mountains were deposited in the relatively shallow sea that covered western New York State. The Paleozoic sedimentary sequence at the site records a marine transgression extending from the Cambrian to the Middle Ordovician followed by marine regression during the Middle Ordovician through the Late Ordovician. The marine transgressive sequence is represented by relatively shallow water Cambrian sandstone units (e.g. Potsdam Sandstone and Theresa Formation) followed by deeper water Ordovician carbonate units (e.g. Black River Group and Trenton Group). The marine regressive sequence is represented by deep water siltstone and shale units (e.g. Utica Shale and Whetstone Gulf and Pulaski Formations of the Lorraine Group) followed by relatively shallow water sandstone units (e.g. Oswego Sandstone and Queenston Formation). The deposition of these units is also discussed in Section 2.5.1.1.2 and Section 2.5.1.2.4. The Potsdam Sandstone and Theresa Formation are not present at the NMP3NPP site.

In the site area it is estimated that approximately 8,000 to 10,000 feet (2438 to 3048 m) of Paleozoic sedimentary rock were conformably deposited on top of the currently exposed Late Ordovician Oswego Sandstone bedrock during the Paleozoic (CEG, 1998), prior to erosion of those formations. There is no record of Mesozoic sedimentary rocks preserved within 200 miles (320 km) of the NMPNS site. The Paleozoic rocks were uplifted and eroded during the Mesozoic and Cenozoic Eras. Differential uplift resulted in a southward regional tilt of 50 ft/mi (9.5 m/km) (0.5 deg). The eroded sediments were likely deposited in the Triassic Basins and the Coastal Plain to the southeast. Pleistocene glacial till and lacustrine sediments were deposited unconformably upon this erosional surface. Quaternary geologic history is discussed in Section 2.5.1.2.1.

Subsidence and deposition ended during middle- to late-Paleozoic time and reflect the cessation of the regional orogenesis. The first deformation (D1-D2) of the NMP Unit 2 site rocks is interpreted to have occurred in late-Paleozoic time. The conjugate fractures and strike-slip faults (Section 2.5.1.2.3) within relatively brittle lithologic layers developed at this time. The homogenization temperatures of mineralization associated with these deformations range from 320 °F to 248 °F (160 °C to 120 °C) (CEG, 1998). Mineralization within the Demster Structural Zone displayed similar temperatures; hence it is interpreted that this structure was also active at the time (Section 2.5.1.2.4).

A second phase of deformation (D3-D4) affected the NMP Unit 2 site vicinity probably during early- to late-Mesozoic time. This episode of deformation resulted in normal faulting along the strike-slip faults (Section 2.5.1.2.3), extending them into previously unaffected strata. Structural relationships described in Section 2.5.1.2.3, as well as mineralization associated with normal faulting with homogenization temperatures of 241 °F to 163 °F (116 °C to 73 °C), confirm that this deformation postdated the strike-slip faulting (CEG, 1998).

At NMP Unit 2 there is a definite relationship between the structural fabric associated with the normal faults, and evidence of a major geochemical change during crystallization of the calcite minerals on the faults. This relationship is exhibited by the transformation from sulfide minerals to goethite at decreasing temperatures which represents a change from reducing conditions to oxidizing conditions caused by the influx of convective, air-saturated ground waters. It is believed that the change, more importantly than the distribution of homogenization temperatures, must be regarded as a time-line of regional extent because it is also recorded in the mineral data from the New Haven, New York site (Section 2.5.1.2.4) (CEG, 1998).

Apparently, the regional environmental change to oxidizing conditions corresponds to the cessation of the tendency for the northern Appalachian Basin to subside. The history of sedimentation ceased in conjunction with the late stages of mountain building processes in the Appalachian geosyncline in the site area during late-Paleozoic time. The literature documents that the region around the site was subjected to extension in Mesozoic time as evidenced by the occurrence of ultramafic dikes that intruded the crust in the area of the Finger Lakes and Syracuse (Section 2.5.1.1.2). Hence, deformational events D3 and D4, representing normal faulting at NMP Unit 2, are interpreted to be of late-Paleozoic to Mesozoic age. Furthermore, the data from both the structural fabric and mineralization studies from the Demster Structural Zone (Section 2.5.1.2.4) are in accordance with those from NMP Unit 2, and imply a similar age for the normal faulting at the New Haven site (CEG, 1998).

Uplift and erosion of the NMP3NPP site vicinity continued through the Tertiary and Quaternary Periods. During the Pleistocene Epoch the site underwent repeated glaciations. The crustal depression and rebound associated with each glaciation were superimposed on the continuous tectonic uplift. Glacioisostatic movements and accompanying environmental effects played an important role in the buckling along the preexisting north-dipping, high-angle faults at NMP Unit 2 and in the development of the low-angle thrust structures (Section 2.5.1.2.3). The development of these structures appears to be interrelated. It is certain that both developed at relatively shallow levels in the crust because of the character of deformation. In particular, the study of the Radwaste and Intake Shaft faults has shown that calcite minerals are present along shear planes and on some open vertical fractures within the zone of deformation. These minerals are deformed (D5-D6). Studies of this mineralization indicate that all of the calcite occurring on the low-angle structures is younger than the latest stage of epigenetic (high-temperature) calcite reported from the NMP Unit 2 site (CEG, 1998).

Initial buckling on the high-angle faults had occurred prior to the Wisconsinan glaciation (Section 2.5.1.2.3). This initial buckling, together with the erosion of the Wisconsinan or older bedrock valley, has been interpreted to be necessary for the development of the thrust structures (Section 2.5.1.2.3). The NMP Unit 2 USAR (CEG, 1998) has concluded that:

1. The structure was initially developed in pre-Holocene time and in the Illinoian time interval between 500,000 and 140,000 yr B.P. with glacial erosion of rock and consequent reduction of vertical confining pressure. That at least most of its movement occurred in pre-Holocene time is indicated by the partial filling of structurally-formed openings by silts that are about 11,000 yr old.

2. Initial formation of the structure probably was abrupt, with displacements at a given place relatively large at first and attenuating with time.

3. Movements along the structure probably occurred during Pleistocene time, as prompted by episodes of glacial loading and unloading. Fluid pressure changes accompanying the draining of Late-Wisconsinan proglacial Lake Iroquois augmented the second stage of buckling on the high-angle faults. This stage postdates lacustrine sediment, dated to be 12,200 to 10,400 yr old.

The Holocene history of the site is predominated by crustal uplift principally related to glacial rebound. Holocene movements have been small, if they have occurred at all.

2.5.1.2.3 Site Area Stratigraphy

The NMP3NPP site is located on Paleozoic sedimentary rocks ranging in age from Middle Ordovician to Late Ordovician, which, in turn, were deposited unconformably on the Precambrian basement rock. The Paleozoic section shown on the site stratigraphic column is projected to the site from proximal deep borings which intersect the Precambrian basement (Figure 2.5-57). Engineering geology conducted by Dames & Moore at the NMPNS site has previously been presented by Fisher and Laird (Fischer, 1978).

Paleozoic sedimentary rocks were deposited in the Appalachian Basin extending from New York to Virginia (Figure 2.5-4) (Milici, 1988). The sedimentary rocks at NMP3NPP were deposited during a period of marine regression and exhibit lateral and vertical variation in both lithology and texture on a regional scale.

Site specific information on the stratigraphy underlying the NMP3NPP site is limited by the total depths of the various borings advanced by site investigators over the years. Geotechnical borings have not extended beneath the Whetstone Gulf Formation of the Lorraine Group.

The deepest boring known to have been advanced at the NMPNS site was drilled to a total depth of approximately 400 feet (122 m) during investigation for NMP Unit 2 (CEG, 1998). This boring penetrates the Whetstone Gulf Formation Unit A and terminates in the upper portion of the Whetstone Gulf Formation Unit B.

The closest boring which extends through the Paleozoic sedimentary sequence and advances to Precambrian gneissic basement is approximately 7 miles (11 km) southwest of the NMP3NPP site in Oswego County (Flagler, 1966; Kreidler, 1972). This boring penetrated the Trenton Group and Black River Group and the underlying Precambrian crystalline gneissic basement. The Cambrian Theresa dolomite/sandstone/orthoquartzite and Potsdam orthoquartzite/sandstone were not present at this location.

Additional deep borings are located between approximately 12 and 42 miles (19 and 68 km) from the NMP3NPP site. These additional deep borings close to NMP3NPP indicate that the Cambrian Potsdam Sandstone and Theresa Formation are not present at these locations.

Figure 2.5-58 is a site specific stratigraphic column compiled from the NMP3NPP boring log information. Figure 2.5-57 is an area-specific stratigraphic column based on correlations by Flagler (Flagler, 1966), Fischer (Fischer, 1978), Fisher (Fisher, 1977), and Rickard (Rickard, 1973).

Figure 2.5-59 shows the Site Plan. Figure 2.5-60, Figure 2.5-61 and Figure 2.5-62 show the locations of the various borings at the site and identify those completed as observation wells.

Many of these borings were drilled to 150 feet (46 m) in total depth; 18 were advanced to a total depth of greater than 200 feet (61 m). Boring logs are provided in Part 11E.

Near surface bedrock in the region consists of nearly flat-lying Paleozoic sedimentary rock with horizontal homogeneity. The sedimentary rock formations dip regionally to the south-southwest with a gradient of approximately 50 ft/mi (9 m/km) (roughly 1 foot per hundred feet)).

Locally at the NMP3NPP site, the bedrock erosional surface slopes to the northwest toward Lake Ontario.

The bedrock formations at the site are, in order of increasing depth:

- Oswego Sandstone (sandstone, Late Ordovician)
- Pulaski Formation (interbedded dark gray siltstone, gray sandstone, and dark gray argillaceous sandstone, Late Ordovician)
- Whetstone Gulf Formation (alternating dark gray siltstone, gray sandstone, and dark gray argillaceous sandstone, Late Ordovician)
- Trenton and Black River Groups (carbonate sequence, limestone with minor shale, Ordovician)
- Grenville Province (crystalline gneissic rock, Precambrian)

The top elevations of the Oswego Sandstone, Pulaski Formation, and Whetstone Gulf Formation, as encountered in the borings, are presented in Figure 2.5-41.

The estimated elevation of the top of the Trenton Group at the site is 700 feet (213 m) below mean sea level, plus or minus 200 feet (61 m). The estimated elevation of the top of the Precambrian crystalline rock is 1,500 feet (457 m) below mean sea level, plus or minus 200 feet (61 m).

The various layers of fill, natural soils, and bedrock encountered in the borings are described in the following paragraphs in order of increasing depth. The elevations of the top of the soil and bedrock layers encountered in the borings at the site are presented in Figure 2.5-41. Subsurface profiles at the locations of structures and along the alignment of the cooling water intake pipeline are presented in Figure 2.5-63 through Figure 2.5-67. Elevation contours of the top of the Oswego Sandstone (top of bedrock) and the top of the Pulaski Formation are presented in Figure 2.5-68 and Figure 2.5-69.

The top of the bedrock encountered in the borings varied between El. 283.2 to 238.4 feet (86.3 and 72.7 m). The top of bedrock is highest in the southern portion of the site near the Strike Road and drops to the north-northwest towards Lake Ontario. Contours of the top of the Oswego Sandstone (top of bedrock) are presented in Figure 2.5-68.

Bedrock was cored with NQ wireline coring equipment. Rock recoveries in the core runs were almost always greater than 90%, and often were 100%. Instances of low recoveries (less than 90%) were rare and may have been due to coring techniques that had not been adjusted to changes in rock quality or to rock core jamming in the core barrel.

Rock quality designation (RQD) for the rock cores were measured in accordance with GEI Procedures. The RQD values are reported on the boring logs. In general, RQD values of the bedrock cored for this project were above 80%, indicating high quality rock.

The bedrock formations encountered in the borings were:

- Oswego Sandstone (including Oswego Transition Zone)
- Pulaski Formation (subdivided into Units A, B, and C)
- Whetstone Gulf Formation

All of these formations consist primarily of gently dipping sandstone, siltstone, and shale. The boundary between units is often gradational, and the units are lithologically similar.

These uniform, nearly flat-lying, Paleozoic strata can be traced continuously for a significant distance horizontally from the James A. Fitzpatrick Nuclear Power Plant site beneath NMP Unit 2 to NMP Unit 1 where prior nuclear plant site investigations have provided great detail (CEG, 1998). At the NMP3NPP site, continuous geologic units can be traced from the southeastern most portion of the site to the shore of Lake Ontario. The strata can also be traced continuously from the shore of Lake Ontario offshore along the length of the proposed cooling water tunnels. Geologic cross sections (Figure 2.5-63 through Figure 2.5-67) demonstrate the lack of significant vertical offset, an indication of possible faulting, and the lateral and vertical uniformity of the bedrock units at the NMP3NPP site.

A total of fourteen samples from five boreholes were analyzed by petrographic microscopy. At least one sample was analyzed from each geological unit encountered during drilling. More than one sample was analyzed from the Oswego Formation because most safety-related structures will involve excavation into the Oswego Formation. Petrographically analyzed samples were chosen to coincide with samples analyzed for geotechnical parameters. The descriptions from the field boring logs differ slightly from the thin section descriptions because the field boring logs represent the entire core sample, while the petrographic descriptions represent a small sub-sample.

Of the five boreholes chosen for petrographic analysis; four samples were chosen from the 200-series reactor complex borings (B201 (MW), B207, B224, and B238 (MW)), and one sample was chosen from the 300-series pipeline borings (B301). Two samples were selected for petrographic analysis from each of the five boreholes except B207 and B224. B207 only had one sample selected for analysis, while B224, the center of the reactor, had seven samples selected (at least one from each geological unit). The samples selected generally provided a representative horizontal and vertical distribution of site borings and geological units encountered while drilling. Specific geological units were targeted in the samples from B207, B238 (MW) and B301. Samples from B207 and B238 (MW) targeted the green marker bed seen in several borings, and only shallow samples were selected from B301, a boring along the cooling water pipeline.

2.5.1.2.3.1 Late Ordovician Units

2.5.1.2.3.1.1 Late Ordovician Oswego Sandstone

The Oswego Sandstone at NMP3NPP ranged in thickness from 29 to 79 feet (8.8 to 24 m) with typical thicknesses of about 45 to 60 feet (13.7 to 18 m). The Oswego Sandstone consisted of hard, fresh to slightly weathered, unfossiliferous, greenish-gray, fine to medium grained, massive to distinctly bedded or cross-bedded sandstone. Thin dark gray siltstone and shale

beds were minor and siltstone clasts were common. The sandstone was typically composed of subangular to subrounded quartz grains, sometimes with well-rounded lithic fragments, feldspar crystals, and a clay matrix. The depositional environments of the Oswego Sandstone in Oswego County have been previously presented by Patchen (Patchen, 1978).

The Oswego Sandstone at NMP Unit 2 is very similar and consists of unfossiliferous, greenish-gray, fine to medium grained, massive to cross-bedded sandstone. Thin dark gray siltstone and shale beds are minor and siltstone clasts are common. The sandstone is characteristically composed of subangular to subrounded quartz grains, sometimes with well rounded lithic fragments, feldspar and a clay matrix (CEG, 1998).

The lower portion of the Oswego Sandstone has been informally designated as the Oswego Transition Zone (CEG, 1998). At NMP3NPP this sub-unit was found to range from 9 to 60 feet (2.7 to 18 m) thick in the borings with typical thicknesses of 15 to 30 feet (4.6 to 9 m) The Oswego Transition Zone consists of medium hard to hard, slightly weathered to fresh, alternating, laminated to thickly bedded, fine to medium-grained sandstone, argillaceous sandstone, and siltstone. Trace fossils are present. There is a general trend toward bed thinning and increasing clay content, downward through the sub-unit. A 3 to 12-inch (7.6 to 30.5 cm) thick shale bed was often noted near the base of the Oswego Transition Zone.

The Oswego Transition Zone at NMP Unit 2 is very similar and consists of alternating, laminated to thickly bedded, fine to medium grained sandstone, argillaceous sandstone and siltstone. Trace fossils are present. There is a general trend toward bed thickening and decreasing clay content, upward through the unit (CEG, 1998).

A total of five samples from the Oswego Sandstone were analyzed by petrographic microscopy (B224 (26.0 to 26.08 ft (7.92 to 7.95 m)), (60.61 to 60.90 ft (18.47 to 18.56 m)), and B301 (23.15 to 23.70 ft) (7.06 to 7.22 m)) and from the Oswego Transition Zone (B224 (84.6 to 84.8 ft) (25.79 to 25.85 m)) and B301 (65.95 to 66.40 feet (20.10 to 20.24 m)). All five of the samples were classified as "altered sandstone" by petrographic analysis. The boring log descriptions for these samples varied from "sandstone" to "sandstone with interbedded siltstone and shale." The texture of the samples showed no alteration and none to a weakly directed fabric, and typically quartz, potassium feldspar and plagioclase grains in a clay matrix held together by dolomite/ferroan dolomite cement. The mineral content consisted of quartz (31% to 62%), dolomite (up to 42%) clay (5% to 25%), potassium feldspar (12% to 15%), and minor amounts (<10%) of plagioclase, ferroan dolomite, opaques and zircon.

2.5.1.2.3.1.2 Late Ordovician Pulaski Formation

The Pulaski Formation was approximately 100 feet (30.48 m) thick at the NMP3NPP site. Elevation contours of the top of the Pulaski Formation are presented in Figure 2.5-69.

The Pulaski Formation was informally subdivided into Units A, B, and C during the investigation for NMP Unit 2 (CEG, 1998). Each unit was typically in the range of 20 to 35 feet (6.1 to 10.7 m) thick at the NMP3NPP site. All three units consisted of interbedded sandstone, siltstone, and shale. The relative amount of siltstone and shale increased in the lower portions of the Pulaski Formation. All three units contained marine fossil shell debris.

Unit A is the uppermost unit and consisted of slightly weathered, medium hard, dark gray argillaceous sandstone interbedded with light gray sandstone and a few beds of dark gray shale and siltstone. Unit A had abundant marine fossil debris and disturbed bedding layers indicating soft sediment deformation. A distinctive 1/2-inch to 2-inch (1.3 to 5.1 cm) thick green layer of smectite and chlorite was noted near the base of Unit A or near the top of Unit B in many of the borings.

Two samples from the Pulaski Formation Unit A were analyzed by petrographic microscopy: B201 (MW) (97.08 to 97.45 feet) (29.59 to 29.70 m), and B224 (115.60 to 115.99 feet) (35.23 to 35.35 m). The sample collected from B201 (MW) was described on the field boring log as 'argillaceous sandstone interbedded with siltstone and sandstone.' The rock sample was identified, using petrographic analysis, as 'altered siltstone and sandstone.' The texture was considered to be a finely bedded sedimentary rock with quartz, potassium feldspar and plagioclase grains held together in a clay matrix by ferroan dolomite cement. The sample was found to have the following mineral composition: quartz (42%), clay (illite) (20%), potassium feldspar (15%), ferroan dolomite (15%), and 5% or less (each) of plagioclase, unidentifiable opaques, and zircon.

The second sample analyzed from the Pulaski Formation Unit A was from B224 (115.60 to 115.99 ft) (35.23 to 35.35 m). This sample was described on the field boring log as "argillaceous sandstone with mottling" and was given the more specific name of "altered mudstone" based on detailed petrographic analysis. The texture of the sedimentary rock sample was a weakly directed fabric with no alteration features, and consisted of an equal amount of quartz/potassium feldspar/plagioclase grains and clay matrix, with a very minor amount of ferroan dolomite cement. The mineral content was clay (50%), quartz (27%), potassium feldspar (18%), and 5% or less of (each) plagioclase, ferroan dolomite and opaques.

Samples B207 (110.9 to 110.95 feet) (33.80 to 33.82 m) and B238 (MW) (132.15 to 132.18 feet (40.28 to 40.29 m) were selected for petrographic analysis to identify the green marker bed seen in several rock core samples during drilling. Both samples were identified as altered claystone by petrographic analysis. The boring log description for B207 at this depth was "sandstone with layers of siltstone and shale", while the boring log description for B238 (MW) at this depth was "argillaceous sandstone and siltstone". The texture of the samples was defined as altered sedimentary rock with moderately directed fabric, and mostly clay matrix/cement with grains of various forms of potassium feldspar and quartz. The mineral content of the samples was 83% to 89% clay (smectite) with less than 10% of some or all of the following minerals: potassium feldspar, quartz, biotite, chlorite, rutile, zircon and unidentifiable opaques.

Unit B consists of slightly weathered, medium hard, interbedded light gray sandstone, dark gray siltstone, and shale. Unit B had relatively more sandstone than Unit A and relatively less fossil debris than Unit A.

One sample from the Pulaski Formation Unit B was analyzed by petrographic microscopy, B224 (138.54 to 138.75 ft) (42.23 to 42.29 m). On the field boring log, the sample was described as "siltstone interbedded with sandstone and argillaceous sandstone." The petrographic sample was given the more specific name of "altered mudstone" based on detailed petrographic analysis. The texture of the sample was altered (deformed) and weakly directed with equal amounts of quartz/potassium feldspar/plagioclase grains and clay matrix, with a very minor amount of ferroan dolomite cement. The mineral content consisted of: clay (50%), quartz (35%), potassium feldspar (12%), and 3% or less of (each) plagioclase, ferroan dolomite and opaques.

Unit C consists of slightly weathered, medium hard dark gray siltstone and shale, interbedded with light gray sandstone. Unit C is darker and has more siltstone and shale than Units A and B.

Two samples from the Pulaski Formation Unit C were analyzed by petrographic microscopy: B224 (167.14 to 167.35 feet (50.94 to 51.0 m)) and B238 (MW) (173.95 to 174.1 ft) (53.02 to 53.06 m)). The sample from B224 was described on the field boring log as "siltstone interbedded with sandstone and argillaceous sandstone", and by petrographic analysis as "altered clayey sandstone." The texture of the sample is altered (deformed) with a weakly directed fabric and quartz, potassium feldspar and plagioclase grains in a clay matrix held together by ferroan

dolomite cement. The mineral content consists of: clay (45%), quartz (35%), potassium feldspar (13%), and <10% of ferroan dolomite, plagioclase, zircon and unidentifiable opaques.

The sample from B238 (MW) (173.95 to 174.1 ft) (53.02 to 53.06 m) is classified as "siltstone with interbedded sandstone" on the field boring log and as "claystone" by petrographic analysis. The texture of the sample is unaltered but had a moderately directed fabric and is almost all clay matrix/cement with a minor amount of quartz and potassium feldspar grains. The mineral content consists of: clay (smectite) (93%), and 3% or less of unidentifiable opaques, quartz, and potassium feldspar.

2.5.1.2.3.1.3 Late Ordovician Whetstone Gulf Formation

The Whetstone Gulf Formation is estimated to be approximately 770 feet (235 m) thick at the NMP3NPP site. Seventeen of the borings extend into the Whetstone Gulf Formation. The deepest boring (B101) extended to a depth of 255 feet (78 m), which penetrated 73 feet (22 m) into the Whetstone Gulf Formation.

The top of the Whetstone Gulf Formation is lithologically very similar to the Pulaski Formation Unit C. The Whetstone Gulf Formation contains marine fossil shell debris. The differentiation among the formations is made in the literature based on the types of fossils in the rock (Bretsky, 1970). The Whetstone Gulf Formation was informally subdivided into Units A and B during the investigation for NMP Unit 2 (CEG, 1998). The upper unit (Unit A) consists of dark gray siltstone and shale with occasional light gray sandstone beds. The lower unit (Unit B) consists of siltstone and shale interbedded with sandstone. Sandstone interbeds became more common in Unit B. One boring for NMP3NPP (B102) penetrated through Unit A into the top of Unit B. In B102, Unit A was observed to be 60 feet (18 m) thick.

Two samples from the Whetstone Gulf Formation Unit A were analyzed by petrographic microscopy; B201 (MW) (188.2 to 188.75 feet (57.36 to 57.53 m) and B224 (200.79 to 200.90 feet (61.20 to 61.23 m). The petrographic description of B201 (MW) was "altered siltstone" and the boring log description was "alternating sandstone and siltstone". The texture of the sample is slightly altered and deformed with weakly directed clay minerals with quartz, potassium feldspar and plagioclase grains held together in a clay matrix by ferroan dolomite cement. The mineral content of the sample consists of: clay (illite) (40%), quartz (30%), potassium feldspar (15%), and 10% or less of ferroan dolomite, plagioclase, and unidentifiable opaques.

The second sample from the Whetstone Gulf Formation Unit A, B224 (200.79 to 200.90 feet (61.20 to 61.23 m)) is described as "siltstone with occasional layers of argillaceous sandstone" on the field boring log and as "silty claystone" by petrographic analysis. The texture of the sedimentary rock is an unaltered but moderately directed fabric with mostly a clay matrix/cement and minor amounts of quartz and potassium feldspar. The mineral content consists of: clay (85%), and less than 10% each of quartz, potassium feldspar, unidentifiable opaques, and carbonaceous matter.

2.5.1.2.3.2 Middle Ordovician Groups

The combined Trenton Group and Black River Group carbonates are approximately 800 feet (244 m) thick at the NMP3NPP site based on scattered deep wells within Oswego County. The outcrop localities of the Trenton and Black River Groups in New York have been recently described by Cornell et al (Cornell, 2005).

The Trenton Group carbonate unit includes multiple formations across New York (Fisher, 1977 and Flagler, 1966). An isopach map depicting the thickness of the Trenton Group in New York is presented in Figure 2.5-70. The formations comprising the Trenton Group include the Utica

shale, the Canajoharie calcareous shale, the Dolgeville calcareous shale and limestone and the Trenton limestone and Chaumont unit. The Utica Shale, Canajoharie calcareous shale and Dolgeville calcareous shale are thicker to the east of the site area and may not be present in the site area.

The Utica Shale consists of a sequence of dark gray to black non-calcareous silty shales. The Utica shale becomes slightly calcareous downward and grades into the underlying calcareous Canajoharie shale. The Canajoharie calcareous shale consists of dark gray to black calcareous to highly calcareous shale. The carbonate content increases with depth and the shale becomes highly calcareous directly above the Dolgeville limestone. The Dolgeville calcareous shale and limestone consists of black calcareous to highly calcareous shale, interbedded with dark gray to dark brown or black, finely crystalline non-fossiliferous argillaceous limestone. Shale predominates in the upper portion of the formation, while limestone is predominant in the lower portion of the formation. The Trenton limestone consists of gray or brown aphanitic to finely crystalline fossiliferous limestone with black argillaceous limestone, black aphanitic limestone, dark brown aphanitic limestone, brown mottled limestone and gray finely crystalline limestone. The Chaumont unit is a very dark gray to black limestone at the base of the Trenton Group.

The Black River Group carbonate unit includes multiple formations across New York (Fisher, 1977 and Flagler, 1966). An isopach map depicting the thickness of the Black River Group is presented in Figure 2.5-71. The formations comprising the Black River Group include the Lowville lithographic limestone and the Pamelia limestone. The Lowville consists of light tan colored lithographic limestone with minor light brown to brown aphanitic non-fossiliferous limestone and light tan to light gray finely crystalline dolomite. The Pamelia unit consists of dark gray to black oolitic limestone, varicolored arenaceous carbonates, dolomitic to calcareous sandstones, variegated shales and dark argillites.

The Cambrian Potsdam Sandstone and Theresa Formation are not present at the NMP3NPP site.

2.5.1.2.3.3 Precambrian Geology

The Precambrian basement rocks of the Grenville Province are located approximately 1,770 feet (540 m) deep at the NMP3NPP site. A contour map of the top of the Precambrian basement rock is presented in Figure 2.5-72 (Flagler, 1966). It is likely that the Precambrian rock underlying the NMP3NPP site is similar to Precambrian rock noted from deep wells located in Oswego County. Precambrian basement rocks have been described from wells (Flagler, 1966) located approximately 7 miles (11 km) (Beckwith well), 17 miles (27 km) (Fee #1 well), 28 miles (45 km) (Slayton 2 well) and 42 miles (68 km) (Ainsworth well) from the NMP3NPP site. The Precambrian metamorphic rocks from the Beckwith well have been described as pink quartz-feldspar gneiss, sparsely biotitic and chloritic (Flagler, 1966). The Precambrian metamorphic rocks from the Fee #1 well have been described as white calc-silicate rocks (Flagler, 1966). The Precambrian metamorphic rocks from the Slayton 2 well have been described as pink quartz-feldspar granulite, sparsely magnetitic, pyroxenic, chloritic (Flagler, 1966). The Precambrian metamorphic rocks from the Ainsworth well have been described as white quartz-feldspar gneisses, sparsely biotitic, muscovitic, hornblendic (Flagler, 1966).

2.5.1.2.3.4 Quaternary Units

Soil at the NMP3NPP site is less than 25 feet (7.6 m) thick, and the surficial deposits consist primarily of glacial till.

2.5.1.2.3.4.1 Unlithified Sediments

Unlithified sediments have been identified at NMP Unit 2 and their approximate ages determined on the basis of stratigraphic position, sediment type, pollen stratigraphy, C-14 dating, grain size distribution, and mineralogical analyses. The sediments in order of decreasing age are: till, Lake Iroquois clay and silt, Sandy Creek time-equivalent sands, and marls, silts, and peat (CEG, 1998).

The surficial sediments in the NMP Unit 2 site area were examined and mapped in the Cooling Tower Excavation, Pit 1, and Trenches 3, 4, and 5. Descriptions of the units composing the stratigraphic sequence of unlithified sediments are presented below.

2.5.1.2.3.4.2 Artificial Fill

At NMP3NPP, fill was encountered at the ground surface in 11 of the 59 sampled borings and ranged in thickness from 4 to 13.5 feet (1.2 to 4.1 m). Fill was generally encountered in the borings located on and around the southern ball field (the area on the south side of the proposed reactor building) and in one boring advanced near the firing range (B116). Fill generally consisted of varying amount of silts, sands, and gravels with cobbles and boulders. Typically, the upper 6 to 12 inches (15 to 30 cm) of the fill layer was finer grained and had some organic material. Construction debris was not noted in the soil borings.

Soils were characterized as fill based on a higher quantity of cobbles and boulders, variability of SPT (Standard Penetration Test) blow counts, and the general surficial topography around the boring location. NMPNS site personnel indicated that rock fill from the construction of NMP Unit 2 might have been used to fill the area of the southern ball field. The NMPNS site is also known to have been filled during the late 1930s or early 1940s when the area was known as Camp Oswego and was used for military training. Foreign matter or construction debris was not observed in the soils characterized as fill.

2.5.1.2.3.4.3 Pleistocene Surficial Deposits

At NMP3NPP surficial deposits were encountered in 38 of the 59 sampled borings at the ground surface and ranged in thickness from 0.5 to 10.6 feet (0.15 to 3.2 m). Surficial deposits can be broken down into two categories: topsoil and fine-grained soil near wetland areas. The topsoil typically consisted of silty sand to sandy silt with varying amounts of organics and gravel. The topsoil was encountered throughout the site and typically ranged from 0.5 to about 2 feet (0.15 to about 0.6 m) thick. Approximately 70 percent of the site is covered with a thin layer of topsoil.

Fine grained soils were encountered to depths of up to 10.6 feet (3.2 m) in areas near wetlands to the north of the proposed reactor complex. These soils were typically observed in the 300-series borings that were performed along the proposed water intake alignment. The fine grained soils generally consisted of low plasticity silts and clays with varying amounts of sand and gravel. Occasional thin layers or pockets of organic materials were observed in these fine grained soils to depths of up to 10 feet (3.0 m).

2.5.1.2.3.4.4 Sandy Creek Equivalent Sand at NMP Unit 2

In the southern portion of the NMP Unit 2 site, shallow water deposits overlie Lake Iroquois sediments, till, or bedrock. The shallow water sediments consist of up to 3 feet (0.9 m) of thin bedded silt, fine to medium sand, and clay, and do not occur above el 270 feet (82 m). The bedding varies from planar to wavy rippled and cross-laminated ripple drift (CEG, 1998).

The Sandy Creek shoreline was formed during the lowering of lake level in the Ontario Basin to the Admiralty stage. Terraces between el 270 and 290 feet (82 and 88 m) along streams in the

site area and near Mexico Bay were identified from air photos, topographic maps, and field reconnaissance and are inferred to be equivalent to Sutton's shoreline identification further north. Just west of Demster Beach a distinct break in slope and change in air photo tone occurs at el 270 feet (82 m). The slope gradient above 270 feet (82 m) is steeper than the slope gradient below this elevation. This break in slope as well as the terraces suggests a possible relation to the Sandy Creek stillstand, therefore placing the shoreline at approximately el 270 feet (82 m) in the Mexico Bay area (CEG, 1998).

The relative ages inferred for samples of the shallow water sediments and the aforementioned pollen stratigraphy indicate that they are representative of the middle to upper A pollen zone. This, in conjunction with the observation that these sediments have not been identified above el 270 feet (82 m) at the site, suggests that the shallow water sediments were deposited during or just prior to the Sandy Creek lake level stillstand (CEG, 1998). At NMP3NPP sand was categorized as fine-grained soil surficial deposit.

2.5.1.2.3.4.5 Marl at NMP Unit 2

At NMP Unit 2, the shallow water deposits locally grade into a marl unit up to 2 feet (0.6 m) thick. The light tan marl consists of silt to fine sand-size calcite fragments, clay, and abundant freshwater fossil fragments. The macrofossil content increases upward culminating in a highly fossiliferous zone in the upper 3 inches (7.6 cm). The pollen assemblage within the marl is similar to that of the shallow water deposits, suggesting that it also falls in the A zone. A C-14 date of 12,545 + 330 radiocarbon yr B.P. was obtained from pelecypod and gastropod shells in the top 2 inches (5 cm) of the marl. C-13 analysis suggests that the fossils may have been naturally contaminated by older carbon. Thus, the C-14 age probably is older than the true age of the marl; however, the error of the date would probably be less than about 2,000 yr. This suggests the marl is time-equivalent with the lower part of the peat in Trench 4 (CEG, 1998). Marl was not noted in the borings at NMP3NPP.

2.5.1.2.3.4.6 Silt at NMP Unit 2

Outside the area of marl deposition at NMP Unit 2, the shallow water deposits grade into nonorganic massive to medium bedded silts and silty fine sands which in turn grade into organic silts. This sequence represents a transition from a high energy environment of the Sandy Creek time-equivalent sands to marshy areas above lake level. In part, these may be aeolian silts and fine sands and are probably time equivalent with the marl (CEG, 1998). At NMP3NPP silt was categorized as fine-grained soil surficial deposits.

2.5.1.2.3.4.7 Peat at NMP Unit 2

In the Cooling Tower Piping Trench at NMP Unit 2 and in Trench 4, peat was exposed in thicknesses up to 3 feet (0.9 m). However, in Trench 4, the peat was restricted to a depression on the west wall where it overlies, and is in gradational contact with, the shallow water deposits identified as Sandy Creek time-equivalent sands. Peat was not noted in the borings at NMP3NPP.

C-14 dates obtained using samples from this peat provide minimum absolute ages of the shallow water deposits. One reliable date of 11,260 + 190 radiocarbon yr B.P. was obtained using samples from the basal woody peat. The basal woody peat is overlain by approximately 8 inches (20 cm) of peat composed almost entirely of sphagnum moss. Samples of this mass yielded ages of 10,400 + 255 and 10,060 + 125 radiocarbon yr B.P., which are consistent with the age of the underlying wood, and the pollen assemblage, which suggests the base of the peat is in the A pollen zone. The decrease in spruce pollen and the increase in hemlock and hardwood suggests that the top of the peat falls close to the B-C pollen zone boundary or about 8,500 yr B.P. Therefore, deposition of the peat began before 11,260 + 190 radiocarbon yr B.P., continued

at least through 10,400 + 255 yr B.P. and possibly through 8,500 yr B.P. Thus, a minimum absolute age can be inferred for the underlying shallow water sediments (Sandy Creek sands) as 11,260 + 190 radiocarbon yr B.P. Because the peat is overlain by artificial fill, no minimum age of peat deposition could be obtained (CEG, 1998).

2.5.1.2.3.4.8 Lake Iroquois Deposits at NMP Unit 2

The deposits of proglacial Lake Iroquois are deep water sediments up to 4-feet (1.2-m) thick which directly overlie gray till, bedrock, or ice marginal lake till where they occur in the NMP Unit 2 site area. These sediments consist of laminated to massive, reddish brown or gray clayey silt or silty fine sand with lenses and laminations of fine to medium sand and a little gravel (CEG, 1998). At NMP3NPP silt and sand were categorized as fine-grained soil surficial deposits.

The age of Lake Iroquois is bracketed by C-14 dates from various locations along the shoreline. At Lewiston, NY, wood from a spit was dated at 12,600 + 400 radiocarbon yr B.P. This date represents a maximum age for the initiation of Lake Iroquois. Karrow et al date a post-Iroquois lake level stand, 40 feet (12 m) below the crest of the Iroquois beach in the Hamilton area, at 11,570 + 260 radiocarbon yr B.P. This date gives a minimum age for the extinction of the Iroquois high stand. If the deep water sediments on-site are Lake Iroquois sediments, they probably were deposited between 12,600 + 400 and 11,570 + 260 radiocarbon yr B.P. However, no organic material was found within the Iroquois sediments that was suitable for C-14 dating. Hence, the minimum age of these sediments is inferred as pre-Sandy Creek shallow water deposits (CEG, 1998).

The pollen stratigraphy of the deep-water lacustrine sediments at NMP Unit 2 has been correlated with C-14 dates, and it also suggests that the deep water sediments were deposited approximately 12,000 yr B.P. These Iroquois sediments are generally low in total pollen content; however, the pollen that does exist is dominantly spruce and pine. Data from samples illustrate a decrease in the percent of spruce pollen found in the shallow water deposits (Sandy Creek) when compared to the underlying deep water Iroquois sediments. The relative percentages of spruce pollen suggest that the shallow water sediments (Sandy Creek) are similar in age to the upper spruce pollen zone (Zone A4, about 10,000 yr B.P.), and that the Iroquois sediments are similar in age to the lower spruce pollen zones (Zones A1 and A2, about 12,000 yr B.P.) (CEG, 1998).

2.5.1.2.3.4.9 Pleistocene Glacial Till

Glacial till at the NMP3NPP site is present at the ground surface in 10 of the 59 sampled borings, and occurs below fill or surficial deposits in 45 of the 59 sampled borings. Where encountered, glacial till extends down to the top of bedrock. (Glacial till was not encountered in four borings. In those four borings, the fill or surficial deposits extended to bedrock.) The glacial till ranges in thickness from 2.1 to 21.3 feet (0.6 to 6.5 m) thick, but is typically between 5 and 15 feet (1.5 and 4.6 m) thick. The glacial till typically consists of silty or clayey sand with gravel, with occasional cobbles and boulders. The results of grain size tests performed on glacial till samples indicates a widely graded soil with between 20 and 60% fines (passing the # 200 sieve). Atterberg limits tests performed on glacial till samples indicate a plasticity range from non-plastic to low plasticity. Four tests on glacial till samples indicate a specific gravity of 2.74 to 2.75, and one test indicated a specific gravity of 2.68. SPTs performed in the borings typically indicated a medium dense to very dense soil. Many of the SPTs encountered refusal on cobbles and boulders.

The upper portion of the glacial till layer is typically a light brown to tan color and the lower portion was light to dark gray. The grain size test results and the field classifications indicate that the gradations of the two different colored till soils are similar. The color difference appears to be related to site groundwater levels and the long-term degree of saturation of the soils. At

NMP3NPP glacial till is considered to be one unit based on similar and consistent geotechnical engineering properties in the upper and lower portions.

Four varieties of till are present on the NMP Unit 2 site. Two types of gray till, a brown till, and a proglacial lake till are distinguishable on the basis of color, texture, and composition. Field relationships and mineralogic analyses indicate that till from only the Late Wisconsinan glacial stage is present at the site. These tills were most likely deposited immediately prior to and during the existence of Lake Iroquois, and are probably equivalent in age to tills deposited during the Port Huron glacial advance (12,900 to 12,000 yr B.P.) (CEG, 1998).

Generally, gray till up to 6-feet (1.8-m) thick has been deposited across the NMP Unit 2 site and directly overlies either bedrock or, in places, a 1-inch (2.5 cm) layer of gray sand. Two units of gray till are distinguished primarily by the size, angularity, and composition of the rock clasts. Notably, one unit contains exotic clasts (CEG, 1998).

A distinctive brown till as much as 10 feet (3-m) thick overlies the gray till and bedrock in the southeastern portion of the NMP Unit 2 site. Locally, the brown till also interfingers with, and is in vertical contact with, the gray till. The brown till consists of rounded to subrounded exotic rock fragments in a fine-grained silty sand matrix. It is distinguished from the gray till on the basis of color, inclusions of stratified drift, larger percentages of well-rounded foreign clasts, and a coarser texture, and may, in part, represent an ablation till (CEG, 1998).

Locally, up to 2 feet (0.6 m) of till that was deposited in an ice marginal lake overlies both the gray till and the bedrock. This till consists of a dark gray silty sand with subrounded rock fragments of mostly gray sandstone and minor percent black limestone. It interfingers with and is overlain by as much as 1 foot (0.3 m) of light gray stratified silt and sand with some subrounded to rounded gravel and light gray silt clasts. This till is poorly stratified and grades upward into the laminated clayey silts of Lake Iroquois. It was deposited as the ice margin receded northward and sediment from the receding ice was reworked and redeposited in the Lake Iroquois basin (CEG, 1998).

2.5.1.2.4 Site Area Structural Geology

The NMP3NPP site is situated within the Eastern Stable Platform Tectonic Province (Sections 2.5.1.1 and 2.5.2.2). The site area is considered relatively tectonically stable and is free of major tectonic structures. The relatively undeformed nature of the rocks at the site reflects this stability. Since the beginning of Paleozoic time, about 542 million yr ago, the site has been subjected to little more than epeirogenic crustal movements. The broad-scale effects of these movements have resulted in the accumulation of a thick sequence of sedimentary rocks at the site and the subsequent rotation of these strata to the south with an average gradient of 50 ft/mi (9.5 m/km) (0.5 deg). During the Cenozoic Era, the site bedrock was also affected by broad crustal warping induced by isostatic loading as a result of continental glaciation.

The foregoing geologic processes have produced a number of relatively small structures observed at the NMP Unit 2 site. The NMP Unit 2 geologic structures are depicted on Figure 2.5-73. These structures consist of systematic fracture sets, moderately to steeply dipping faults, and shallowly dipping faults with associated low amplitude folds. Investigations of the age, origin, extent, and significance of these geologic structures were conducted at the NMP Unit 2 site. None of the faults was determined to be a capable fault (CEG, 1998).

While faults were not encountered during the drilling program for NMP3NPP, it is anticipated that some fault structures or deformed zones may be encountered in foundation excavations for the plant. Based on the prevalence of non-capable faults in excavations at NMP Unit 2 and

the similar lithology and structure at NMP3NPP. The faults documented at NMP Unit 2 do not appear to extend to the NMP3NPP site (CEG, 1998), but if faults are encountered at NMP3NPP they are likely to be structures similar in character to those well documented at NMP Unit 2. The investigation of the structures at NMP Unit 2 is described in detail in Section 2.5.1.2 and summarized in section 2.5.3.

The NMP Unit 2 detailed structural geology was made possible through detailed geologic study of rock excavations and cleared bedrock surfaces during initial construction of NMP Unit 2 (Niagara Mohawk, 1978a; Niagara Mohawk, 1980). Cleared bedrock surfaces and excavations for NMP3NPP will also be mapped during initial construction and the site area structural geology will be refined for the NMP3NPP site.

2.5.1.2.4.1 Nine Mile Point Unit 2 Structural Geology

2.5.1.2.4.1.1 Fractures at NMP Unit 2 and NMP3NPP

The attitudes of 282 fractures were measured at NMP Unit 2 to detect site-wide fracture trends. Poles to these fractures were plotted and contoured on lower hemisphere equal area projections. In the northern part of the NMP Unit 2 site two predominant vertical fracture sets are present and are oriented N 42 W and N 72 E. In the southern part of the NMP Unit 2 site (cooling tower piping trench) similar fracture trends are present. There, the greatest number of fractures strike about N 50 W, effectively the same northwest trending set as in the northern part of the site. Smaller concentrations of data points define sets with average strikes ranging between N 68 E and N 24 E, which are all considered the equivalent of the east-northeast oriented set in the northern part of the site (CEG, 1998). Because of their predominance across the entire site, the northwest and east-northeast trending vertical fractures will be the focus of the remainder of this discussion.

Similar northwest and east-northeast striking fracture orientations were observed in bedrock outcrops at the NMP3NPP site. These two dominant fracture patterns have also been measured throughout the site area in Oswego County (Stilwell et al, 2005) and were documented during geological reconnaissance conducted by GEI (refer to Section 2.5.3).

Members of both fractures sets are very similar in character. They are generally nearly planar and developed approximately normal to bedding. Fractures of each set on-site commonly contain calcite and sulfide mineralization. They are best developed within the sandstone members of the stratigraphic section. At boundaries with more argillaceous strata, the fracture attitudes either change or they terminate. Very few members of these two fracture sets extended continuously through significant thicknesses of strata. However, their occurrence was noted throughout the stratigraphic section (CEG, 1998).

The acute angle between nearly vertical fracture sets at NMP Unit 2 is about 58 to 70 degrees. This suggests that the fractures formed, at least locally, as conjugate fractures with the greatest and least principal compressive stresses oriented west to west-northwest and north to north-northeast, respectively (CEG, 1998).

No data are available from the site that would permit a direct determination of the age(s) of the major fracture sets. However, studies in the literature provide the basis for interpreting the site fractures as being related to late Paleozoic Alleghanian tectonics (Section 2.5.1.1.3)

Parker (1942; 1969) concluded that the three regional fracture sets (I, II, III) are all older than the time of emplacement of numerous periodotite and kimberlite dikes in the early and medial Paleozoic rocks in central New York. One such dike, at Portland Point, NY, near Ithaca, yielded a

potassium-argon (K/Ar) mineral age on phlogopite of 155 + 4 million yr. Zartman has obtained similar dates with the rubidium-strontium (R/SR) technique (Section 2.5.1.1.2) (CEG, 1998).

Investigations by Engelder and Geiser (Engelder, 1980), Engelder (1982a), Engelder (1985), Hancock (1989) Scheidegger (1991), Hancock (1991), Gross (1991), Engelder (1993), and Zhao (1997), are in accordance with the observed direction of joint sets, however, Fracture Set III is interpreted to postdate Alleghanian tectonics, forming, instead, in response to the contemporary stress field.

Fracture Set III strikes east-northeast nearly ubiquitously. Nevertheless, the fractures on-site at NMP Unit 2 are equivalent in their time of origin to the older fractures of Sets I and II of Parker (1942, 1969) and Ia, Ib, and II of Engelder (1980) (CEG, 1998).

Mineralization of the fractures at NMP Unit 2 provides further information regarding the age of the fractures, which is consistent with the foregoing conclusion (Section 2.5.1.2.6). A study of the fluid inclusion temperatures from the calcite on fracture surfaces indicates that these minerals were deposited by fluids with a temperature range of approximately 320 °F to 212 °F (160 °C to 100 °C). Based on these temperatures, it may be inferred that these minerals were formed at burial depth of 1.2 to 1.8 miles (2 to 3 km). It may also be inferred that such great burial depth is more consistent with the pre-Jurassic age suggested by Parker than the time of development of the contemporary stress field as inferred by Engelder (CEG, 1998).

The most recent studies (Engelder, 2001; Whitaker, 2005; Engelder, 2006; Lash, 2007) have reinterpreted these joint set orientations. These works have concluded that the ENE striking joints are actually pre-Alleghanian joints formed during an Appalachian-wide stress field prior to the Alleghanian Orogeny. The joints were then rotated during the Alleghanian Orogeny to be coincident with the orientation of the contemporary stress field. The coincident directions led to the erroneous interpretation during the 1980s and 1990s that the ENE striking joints were produced by the contemporary stress field.

2.5.1.2.4.1.2 High-Angle Faults at NMP Unit 2

~~Three high-angle faults striking west-northwest, namely, the Barge Slip fault, the Drainage Ditch fault, and the Cooling Tower fault, occur at or adjoining the NMP Unit 2 site. The Barge Slip fault dips 60 to 65 degrees southward; the other two faults dip 55 to 70 degrees to the north. All three faults have similar structural characteristics. Most of the information concerning these faults was gained from a detailed investigation of the Cooling Tower fault. However, all available surficial exposures of the Barge Slip and Drainage Ditch faults were examined, together with reports of previous investigations of these structures (CEG, 1998).~~

Three high-angle faults striking west-northwest, namely, the Barge Slip fault - Normal Fault, the Drainage Ditch fault, and the Cooling Tower fault, occur at or adjoining the NMP Unit 2 site. The Barge Slip fault – Normal Fault dips 60 to 65 degrees southward; the other two faults dip 55 to 70 degrees to the north. All three faults have similar structural characteristics. Most of the information concerning these faults was gained from a detailed investigation of the Cooling Tower fault. However, all available surficial exposures of the Barge Slip – Normal Fault and Drainage Ditch faults were examined, together with reports of previous investigations of these structures (CEG, 1998; Stone and Webster, 1978).

The high-angle faults display several common characteristics. All three appear to be subvertical strike-slip faults in surficial exposures within the Oswego Sandstone. However, they display the geometry and displacement of a normal fault within the Lorraine Group. They each contain occurrences of calcite and sulfide mineralization associated with the strike-slip and normal slip deformational fabrics. Furthermore, the homogenization temperatures and paragenesis of the

mineralization associated with the different episodes of deformation are similar for each fault (CEG, 1998).

Some aspects of the geometry and deformation along the Drainage Ditch and Cooling Tower faults (the two north-dipping faults) differ from those of the Barge Slip fault - Normal fault. Each of these faults is coincident with the axial plane of an asymmetric chevron fold or monocline. They exhibit reverse slip, stratigraphic displacements in addition to the aforementioned deformation. Also, in surficial exposures of each of the north dipping structures, the plane of the fault was displaced by translation of the adjacent strata along bedding planes (bedding plane slip). The Drainage Ditch and Cooling Tower faults were not determined to be capable faults (CEG, 1998).

Of the three high-angle faults at the NMP Unit 2 site, only the Cooling Tower fault had clearly deformed the overlying Pleistocene sediments. The effects and mechanism of this deformation are presented under the heading Reverse-Slip Displacements. The Cooling Tower fault was not determined to be a capable fault (CEG, 1998).

The total inferred lateral extent of the high-angle faults is represented by the fault traces shown on Figure 2.5-73. The fault traces are assumed to be relatively linear. This assumption proved to be valid by direct observations elsewhere, especially along the Cooling Tower fault. Few data are available regarding the southeast extent of the Barge Slip fault - Normal fault. To the northwest, the Barge Slip fault was named the Normal Fault when encountered during construction of the intake and discharge tunnels at the James A. Fitzpatrick plant. The minimum lateral extent of this feature is about 2,200 feet (670 m) (Figure 2.5-73). The west-northwest extent of the Barge Slip fault can only be inferred to be located west of its intersection with the excavation for the lake water tunnels of the James A. Fitzpatrick Nuclear Power Plant. The fault was mapped in the James A. Fitzpatrick Nuclear Power Plant intake and discharge tunnels ~~(CEG, 1998).~~ as the Normal Fault (CEG, 1998; Stone and Webster, 1978). An extension of the Barge Slip - Normal Fault was not encountered in borings done for the intake and discharge tunnels at NMP3NPP.

The inferred western extent of the Drainage Ditch fault is located as shown on Figure 2.5-73 because the lake water tunnels for the NMP Unit 2 site did not encounter the fault. The east-southeastern extent of the Drainage Ditch fault was determined when the extension of the compression buckle or tepee fold at the James A. Fitzpatrick Nuclear Power Plant site was investigated by examination of aerial photographs, seismic refraction surveys, and test excavations. These studies led to the conclusion that, east of the James A. Fitzpatrick Nuclear Power Plant, the buckling (of the bedrock layers) dies out and the fracture resolves into a local system of close jointing (CEG, 1998).

Seven trenches and pits were dug to investigate the lateral extent of the Cooling Tower fault (CEG, 1998). The western extent of the fault is inferred, as shown, because Trenches 1 and 2 revealed no evidence of faulting (Figure 2.5-73 in Section 2.5.1.2).

Two trenches at NMP Unit 2, located along the western projection of the Cooling Tower fault, showed no evidence of the fault as part of the investigation at that plant, indicating it was unlikely to extend into the NMP3NPP site. Investigations for the offshore tunnels for the NMP3NPP included off shore boring locations along the strike direction of the cooling tower fault. No evidence of the fault (e.g. significant sub vertical fracturing, fault gouge, slickensides or weathering) was noted. Additionally, land-based and marine seismic refraction studies showed no anomalies that could be interpreted as faults or significant discontinuities. Therefore, it the extension of the NMP Unit 2 Cooling Tower fault beyond the excavation mapping in Trench 1 and Trench 2 at NMP Unit 2 (CEG, 1998) seems unlikely.

The Cooling Tower and Drainage Ditch faults were investigated by performing proton precession magnetometer surveys across the established traces of both faults. The surveys found no magnetic gradients that could be interpreted to represent faults across the traces of the structures or at a hypothetical projection to the basement (CEG, 1998).

The depths of the high-angle faults at NMP Unit 2 are inferred on the basis of information gathered from the subsurface investigation of the Cooling Tower fault. This fault was investigated by drilling two rows of closely spaced vertical boreholes perpendicular to the strike of the fault. Detailed stratigraphic and structural logs were prepared from the cores extracted from the boreholes. From these logs, detailed correlation charts were prepared and these charts were used to prepare geologic cross sections. The principal structural element in the subsurface is a 60- to 65-degree northward dipping discontinuity. The structure extends from the top of the bedrock down to the explored depth of 270 feet (82 m). Below a depth of 200 feet (60 m), the sense of fault displacement is normal and the magnitude of offset is about 1 foot (0.3 m). Because of the similar structural character of the high-angle faults, it is inferred that they all extend to a depth similar to that attained by the Cooling Tower fault. Based on the small magnitude of the observed displacement and the relatively short length of this structure, it seems inappropriate to infer that this fault extends much deeper than 270 feet (82 m). Therefore, it is believed that the high-angle faults only extend to depths of several hundred feet and that they do not extend to the basement. The results of the magnetometer survey discussed above support this inference because magnetic anomalies represent magnetic contrasts in the basement rock, and there are no magnetic anomalies to provide evidence of any offset (CEG, 1998).

The investigations of the three high-angle faults (i.e. Barge Slip fault - Normal fault, Cooling Tower Fault and Drainage Ditch fault) at and adjoining the NMP Unit 2 site revealed evidence of a history of multiple displacements with different senses of movement along the faults. It was found that the three faults had moved simultaneously. They initially experienced strike-slip movement followed by normal slip movement. In addition, the two northward-dipping faults (Cooling Tower and Drainage Ditch faults) have been affected by buckling of the bedrock along the fault planes both laterally and with depth. The buckling mechanism resulted in the development of reverse-slip displacements along the fault planes, but restricted to the upper 200 feet (60 m) of the bedrock mass (CEG, 1998).

2.5.1.2.4.1.3 NMP Unit 2 Strike-Slip Deformation

The three high-angle faults commonly display characteristics indicative of strike-slip deformation. The amount of lateral displacement is known only for the Cooling Tower fault. In one exposure a sedimentary channel crest (an interfluve ridge) within the Oswego Sandstone was displaced 3 feet (0.9 m) in a left-lateral sense across this fault. Indirect evidence of strike-slip faulting, such as the character of the shear and fracture fabric in proximity to the faults, as well as the occurrence of both horizontal slickensides and slickensides with gentle rakes on fracture surfaces, are also present (CEG, 1998).

In surface exposures, the high-angle faults are vertical, or nearly so. However, subsurface investigation with vertical borings demonstrated the presence of a fault dipping approximately 60 degrees. Two inclined borings were drilled to investigate whether a vertical strike-slip fault, independent of the moderately dipping fault, also existed at depth. The angle borings demonstrated that a vertical fault does not exist below a depth of 90 feet (27 m). Apparently, the vertical, strike-slip portion of the fault exists only in the massive strata of the Oswego Sandstone (CEG, 1998).

Strike-slip displacements predate other deformations that occurred on the high-angle faults. This interpretation is supported by both mineralogical and structural relationships. The

strike-slip faults probably formed at the same time as the systematic fracture sets at the site. Both the fracture sets and the strike-slip faults contain vein mineralization with homogenization temperatures (320 °F to 248 °F, 160 °C to 120 °C) similar to those determined for quartz grain clasts in the host rock (349 °F to 297 °F, 176 °C to 147 °C). This indicates that this deformation occurred after diagenesis and represents the onset of brittle bedrock deformation (CEG, 1998).

2.5.1.2.4.1.4 NMP Unit 2 Normal-Slip Deformation

Each of the high-angle faults also exhibits some characteristics of normal-slip deformation. Normal-slip stratigraphic displacements on the Barge Slip - Normal fault and Cooling Tower faults are 16 inches (40 cm) and 6 to 12 inches (15 to 30 cm), respectively. No normal-slip displacement was detected along the Drainage Ditch fault. However, several indirect indicators of normal-slip were observed along these faults. Shear fracture geometry consistent with normal faulting was observed in a number of exposures. Moreover, slickensides with steep rakes are present on some of these surfaces as well as on the main shear surfaces of the brecciated zones. Drag folds with normal shear sense were detected during both the surface and subsurface investigations of the Cooling Tower fault. Many fractures associated with normal-slip deformation contain calcite and sulfide mineralization (CEG, 1998).

The results of field studies indicate that normal-slip deformation postdates strike-slip faulting but predates other deformations that affected the high-angle faults. Structural relationships such as the overprinting of slickensides with steep rakes on slickensides with gentle rakes, and the truncation of strike-slip fracture sets by shear zones with a normal-slip fabric, suggest that normal-slip followed the strike-slip deformation. Mineralization studies at the site confirm this relationship. Homogenization temperatures of calcite mineralization associated with normal fault deformation fabric (249 °F to 163 °F, 116 °C to 73 °C) were typically lower than those associated with diagenesis and strike-slip faulting (349 °F to 248 °F, 176 °C to 120 °C). Based on the paragenetic sequence developed for the site (Section 2.5.1.2.6), mineralization of the lower temperature range was emplaced later than diagenesis and strike-slip faulting (CEG, 1998).

2.5.1.2.4.1.5 NMP Unit 2 Bedding-Plane-Slip Displacement

The effects of displacements resulting from bedrock translation along bedding planes has been noticed at numerous locations at the site. Bedding-plane-slip accompanied reverse-slip displacements on the high-angle faults as well as the development of the low-angle thrust structures. The age and relationship of bedding-plane-slip to these deformations is included in the discussions specifically addressing these topics (CEG, 1998).

Excluding the thrust structures, the most prominent examples of bedding-plane-slip displacement were observed in the surficial exposures of the high-angle faults. These displacements distorted the original configuration of the faults, resulting in considerable variation in the thickness and attitudes of the breccia zones of these originally steeply dipping faults (CEG, 1998).

2.5.1.2.4.1.6 NMP Unit 2 Reverse-Slip Displacements

The Drainage Ditch and Cooling Tower faults are both coincident with the axial plane of an asymmetric chevron-like fold or monocline. These folds resulted from a third episode of deformation occurring along the north-dipping high-angle faults. It was characterized by reverse-slip displacements accompanied by bedding plane slip and dilation of the bedrock within 200 feet (60 m) of the surface. Field evidence clearly indicates that this deformational episode consisted of two phases: 1) preglacial buckling along high-angle faults, and 2) postglacial buckling on the fault (CEG, 1998).

The total reverse separations across the Drainage Ditch and Cooling Tower faults are 1.5 feet (0.46 m) and 5 to 6 feet (1.5 to 1.8 m), respectively. However, the reverse stratigraphic separations along the shear zones in surficial exposures vary from zero to 3 feet (0.9 m). These displacements are less than the total separation because they do not include all the reverse separation resulting from monoclinal rotation. The shear sense indicated by drag folds, within the breccia zones and in the adjacent bedrock, is consistent with this reverse displacement sense (CEG, 1998).

At five exposures along the Cooling Tower fault, the layered sequence of glaciolacustrine sediments was deformed. The deformation occurs generally within a 20-feet (6-m) wide zone straddling the bedrock fault. The numerous small-scale deformational features in the sediments consist of fluidized flow and sediment flow structures, as well as small faults. The most prominent of these faults exhibits maximum displacements of several inches. Structural analysis indicates that the deformation was accomplished by relative vertical movements consisting of broad arching and monoclinal flexuring of the sediments resulting from reverse-slip displacements on the bedrock fault. In Pit 1, the Cooling Tower Trench, Trench 4, and Trench 5, the vertical separation, caused by arching and generally accompanied by compensatory normal faults in the sediments, is estimated to range from 0.5 to 1 foot (0.15 to 0.30 m). In Trench 3 the separation that resulted from monoclinal flexuring is 2.70 to 3.25 feet (0.82 to 0.99 m). As a result of the flexuring at this location, many small-scale normal, thrust, and high-angle reverse faults developed in the sediments, especially in the area of the short limb of the monocline (CEG, 1998).

The subsurface character of displacements on the Cooling Tower fault was also the subject of a detailed investigation (CEG, 1998).

In the upper part of the section, the structure resembles a kink band or monocline, consistent with the surficial exposures. The reverse stratigraphic separation of about 5.5 feet (1.7 m) is accomplished mainly by southward rotation of bedding by up to 50 deg within a bedrock sliver bounded by two shear planes. Deeper in the section the separation has resulted from shear directly on the bounding planes, as well as rotation of the bedrock sliver. The bounding planes of the sliver merge at a depth of approximately 140 feet (43 m). Below this depth, the reverse stratigraphic separation results from direct shear displacement along a single shear plane. The magnitude of reverse displacement decreases progressively from the surface to nearly zero at a depth of approximately 200 feet (60 m) . Below this depth, a normal displacement of 0.5 to 1 foot (0.15 to 0.30 m) occurs (CEG, 1998).

As noted previously, the displacement adjacent to the fault (0 to 3 ft, 0 to 0.9 m,) is less than the displacement measured away from the structure (5 to 6 ft, 1.5 to 1.8 m) near the bedrock surface. In contrast, at the base of the Oswego Sandstone and below, the measured amount of displacement is significantly less away from the structure than it is adjacent to the fault. On opposite sides of the structure it is always possible to find two points on the same stratigraphic horizon that do not appear to be displaced. The horizontal distance between two such points becomes progressively smaller with depth. Hence, the reverse dislocation of strata occurred only within a narrow zone contained almost entirely in the hanging wall block. In cross section, this zone has roughly the shape of a right triangle with the Cooling Tower fault forming the hypotenuse. The vertical leg of the triangle is approximately 200 feet (60 m) long; the horizontal leg is at least 60 feet (18 m) long (CEG, 1998).

Prior to the development of the structure, the stratigraphic thickness must have been equal on each side. However, the present stratigraphic thickness of the section between Markers 1 and 3 on the hanging wall is about 6 feet (1.8 m) greater than on the footwall. Notably, the magnitude of this difference in thickness (dilation) is nearly equal to the overall reverse stratigraphic

displacement. The amounts of both the displacement and the dilation decrease progressively downward and do not appear to be present below a depth of approximately 200 feet (60 m). Hence, the reverse displacement at any point along the structure is approximately equal to the amount of dilation of the section on the hanging wall. It should be noted that this is true not only for the zone of flexural shear displacement but also for the direct shear displacement observed below this zone (CEG, 1998).

Analysis of the information from the investigation of the Drainage Ditch and Cooling Tower faults provides the basis for understanding the relative age of the reverse and bedding-plane-slip displacements. It must be noted that the principal mechanism for the deformation was buckling. The dilation of the bedrock and slip of the strata toward the crest of the buckle resulted in the observed reverse displacements (CEG, 1998).

Buckling along the north dipping high-angle faults postdated the strike-slip and normal fault deformations, as indicated by several structural relationships. Structural fabrics resulting from both strike-slip and normal fault episodes were deformed by bedding-plane-slip related to the buckling. Conjugate strike-slip and normal fracture sets have been rotated in conjunction with the limbs of the buckle. The buckling deformation and absence of associated mineralization indicates the deformation occurred near the surface, whereas the homogenization temperatures of mineralization associated with the episodes of strike-slip and normal faulting indicate that deformation occurred at considerable depths of burial (CEG, 1998).

The reverse-slip deformation occurred during more than one phase of movement. Field data from precise surveys show that some of the bedrock deformation occurred prior to deposition of the Late Wisconsinan and Holocene sediments above the Cooling Tower fault. Specifically, it has been demonstrated that in the Cooling Tower Piping Trench and Pit 1 exposures, bedding on the south side of the fault dips 7 to 9 deg southward marking the tilted limb of a monocline. Varved lacustrine sediments spanning this limb were not structurally affected by this rotation. However, there is obvious evidence of deformation of the sediment as described above. Hence, a second phase of deformation must have occurred later than that of the monocline development, and later than 12,000 yr B.P., the approximate age of the layered sediment (CEG, 1998).

It is uncertain how many deformational events affected the overburden sediments. The effects of arching and monoclinal flexuring, with associated small-scale reverse and normal faults, all may be the result of one deformation. The elements of deformation are emphasized by local well-defined shear planes where the sediments have been faulted because of arching or flexuring. However, there are present in several exposures a number of diapiric structures caused by fluidization. In Pit 1 and Trench 3, these features are clearly deformed by the small faults formed during arching of the sediments. Thus, they predate the formation of small-scale normal faults. It has been observed that, although some diapiric structures do occur in sediments away from the fault, they are mostly concentrated in the area of the fault zone. It is possible that the formation of these structures was related to fluid pressure changes as a result of water level fluctuations in the Ontario Basin (CEG, 1998).

2.5.1.2.4.2 NMP Unit 2 Mechanism of Reverse-Slip Deformation (Pre-Wisconsinan)

The expansion of the stratigraphic section on the north limb of the structure is an important aspect of the deformation that was detected in the subsurface. The cross-sectional area affected can be approximated as a right triangle equal to at least 6,000 square feet (557 sq m). Unidirectional dilation resulted in an increase of area in this zone that is equal to a minimum of 165 square feet (15 sq m). The amount of expansion on the hanging wall then is approximately 2 to 3 percent. It is also likely that expansion affects the strata of the footwall or south limb,

particularly for the strata above the apex of the two shear planes within the zone of flexural shear displacement. However, uncertainties in the amount of stratigraphic separation due to the direct shear displacement and in the geometric arrangement of strata on the south limb do not permit an estimate of the amount of expansion that might exist there (CEG, 1998).

Dilation of the bedrock is associated with the presence of voids or partings along bedding planes, as corroborated by observations in both the surface and subsurface investigations. These have been observed in the excavated bedrock slots. Similarly dilated strata have also been noticed in the subsurface. They commonly occur as voids into which the drilling rods suddenly dropped and water circulation was lost. The presence of these voids was further substantiated by a downhole impression packer survey (CEG, 1998).

Although the cumulative effect of the bedding plane separations appears to account for most of the expansion of 5 or 6 feet (1.5 or 1.8 m), it is believed that time-dependent deformation of the rock also contributed to the total displacement. Disharmonic, concentric drag folds that occur outside the bedrock sliver and adjacent to the shear fractures bounding the sliver attest to this. Structural shortening of these folds is approximately 20 to 30 percent, based on that observed in Trench 3 (CEG, 1998).

As discussed in Section 2.5.4, a rock specimen can undergo an increase in its original dimensions during and after removal from the in situ stress field. This increase is elastic or instantaneous as well as time dependent. It has been shown by unconfined swelling tests that the rock specimen expands when removed from the bedrock and placed in an environment of constant temperature and high humidity. The rate of this expansion varies with the lithology of the specimen and is greatest in the direction perpendicular to bedding. The swelling process is caused by the development of very high negative pore pressures in response to the elastic strain relief. This results in the flow of water to the available dilated pore species of the rock. The swelling, and concomitant flow of water, can be time dependent as a function of gradual changes in permeability of the rock mass related to time-dependent change in the stored strain energy. Considering these results, it appears reasonable to assume that the perturbation of the stress field at the Cooling Tower fault did cause swelling in the bedrock. Therefore, the total expansion very likely may be the combined result of both factors: the separation along bedding planes and the internal volumetric changes. This internal dilation is relatively small or nonexistent on the footwall (excluding the rotated sliver), but may be considerable on the hanging wall. Hence, these postulated volumetric changes may be differential and could have enhanced and prolonged the deformation process by providing an additional source of incremental, distortional, strain energy (CEG, 1998).

Considering the observations and relationships provided above, buckling is the mechanism of reverse-slip deformation on the Cooling Tower fault. Buckling is also related to the bedding-plane-slip distortion of the normal fault observed in the excavations. It is important to note, therefore, that the direct shear displacement is only a secondary effect of the buckling instability (CEG, 1998).

The entire structure can actually be accurately described as a sequence of full-wave length (l) buckles in the upper part and a sequence of half-wave length (l/2) buckles in the lower part. These buckles are superimposed upon a preexisting normal fault that dips 60 deg northward. The amplitudes and wavelengths of each type of buckle diminish progressively with depth. Concomitantly, 1) the reverse-slip displacements decrease to zero with depth, 2) the displacement decreases to zero in a lateral direction away from the structure, and 3) the zone of dilation on the hanging wall narrows with depth (CEG, 1998).

2.5.1.2.4.3 NMP Unit 2 Mechanical Theory (Stages of Development)

To evaluate the possibility of reactivation, the mechanics of buckling along the Cooling Tower fault have been treated by applying the theory of folding of stratified viscoelastic media, as developed by Biot (CEG, 1998); by reconstructing the buckling process across the fracture plane.

The geologic data indicate that the pre-Wisconsinan buckling proceeded through four states: the deflection, amplification, rotation, and stabilization stages. During the initial stage, a deflection of small amplitude occurred in one or a sequence of layers on the hanging wall of the north-dipping fault. The geometry of this feature indicates that the initial deflection did not occur at the bedrock surface, but instead at the base of the massive sandstone or else within the thinner beds of the Transition Zone. The initial wavelength was approximately 60 feet (18 m) (CEG, 1998).

During the second (amplification) stage of buckling, the amplitude of the initial deflection increased as a function of time and the acting compressive stress. The result of this stage was the formation of a monocline in the massive sandstone, such as that seen in the initial Cooling Tower Trench exposure of the fault. Consequently, the more thinly bedded strata beneath the sandstone began to deflect upward along the discontinuity because of the reduced vertical load. This process (development of 2 buckles) affected successively deeper strata, thereby propagating the buckling instability downward (CEG, 1998).

The third (rotation) stage was characterized by the development of a second (lower) shear plane across the strata. This second shear occurred when progressive buckling, accompanied with reverse-slip along the preexisting discontinuity, induced an incremental bending moment caused by the shear force acting in the plane of the fault. However, the second shear plane formed only below the depth of the initial deflection, and converged with the old, normal fault plane (at a depth of 140 feet, 43 m) where buckle amplification was insufficient in magnitude to generate a critical bending moment. Despite a certain geometric similarity, it should be noted that the Cooling Tower and Drainage Ditch faults are not kink structures (CEG, 1998).

The stabilization stage is characterized by minor deformation that followed the rotation of the bedrock sliver of the footwall. Evidence from the subsurface indicates that the rotation of the bedrock sliver on the footwall did not terminate the development of the structure. Further strain is indicated by the formation of concentric drag folds in the strata adjacent to the lower and upper shear planes based on interpretation of bedding dip versus depth in boreholes drilled through the fault. It is possible that the rotation of the southern limb occurred prior to the attainment of the final depth by the buckling process. The evident continuation of the development of the structure may reflect the deformation that was extending the buckling instability to that depth. This was accompanied with further amplification of the individual l/2 deflections below the zone of rotation. As the south limb had become locked after it was rotated to the critical angle with the shear plane, the strain resulting from the continuation of buckling had to be accommodated by a mechanism of deformation other than rotation, such as the bedrock swelling associated with the perturbations of the stress field in proximity to the fault zone. Consequently, the bedrock continued to experience differential (different magnitudes in different parts of the rock mass) and time-dependent internal expansion. This process introduced additional incremental quantities of distortional strain energy into the buckling system. This thereby increased the time required for its stabilization by partly compensating for energy loss due to the rotation of the bedrock sliver between the shear planes (CEG, 1998).

2.5.1.2.4.4 NMP Unit 2 Mechanical Analysis

The analysis was performed to determine whether or not: 1) the buckling can propagate to greater depth, and 2) the feature is seismogenic (CEG, 1998).

Buckling in the site area was noted to occur on only two of the three high-angle faults. These two faults dip northward (Cooling Tower and Drainage Ditch faults), whereas the third fault dips southward (Barge Slip fault - Normal fault). Ironically, however, the south-dipping fault could be inferred to have the greatest potential for developing this type of deformation, assuming that the stresses on-site prior to buckling were horizontal and uniform (CEG, 1998).

A possible explanation for the absence of reverse-slip deformation and associated buckling on the Barge Slip fault - Normal fault is likely related to the direction of its dip. However, for this factor to be significant, the trajectory of the greatest principal stress must be inclined with respect to the earth's surface. The occurrence of the l/2 sequence of buckles on the hanging wall of the northward dipping faults and the sense of bedding-plane-slip indicate that if the stress trajectory were inclined during development of these buckles, it would have to be inclined toward the south. In this situation neither the hanging wall nor the footwall of the Barge Slip fault - Normal fault was susceptible to the reverse-slip deformation because the sense of shear stress acting in a plane parallel to the fault was incompatible with the sense of shear stress in a plane parallel to bedding (CEG, 1998).

Thus, the southward inclination of the stress trajectory is a factor that controlled the selective development of the deformation. Changes of this inclination also probably influenced the stability of the northward dipping faults. Such changes have been shown to be related to glacially-induced downwarping associated with the growth of the continental ice sheet known to have affected the site area (Section 2.5.1.1). Hence, the tendency of the plunge of the s1 trajectory to increase southward ceased a few thousand years ago (CEG, 1998).

During glacially-induced crustal downwarping, as the plunge of the s1 trajectory increased progressively southward, changes in the magnitudes of the stresses occurred and affected the stability of the bedrock. These changes are related to the boundary conditions of the bedrock on-site. The site strata crop out to the north on the floor of Lake Ontario or on its north shore. This boundary appears to be a free (or deformable) boundary. By contrast, the southern boundary is assumed to be a non-deformable boundary because the average structural gradient of 50 ft/mi (9.5 m/km) to the south provides a confined boundary condition (CEG, 1998).

Furthermore, the ability of bedding to accommodate shear stress without developing shear failure increases with depth. Therefore, the amount of shear stress on bedding is too small to cause instability. The difference between the layer-parallel shear stress and the strength of a bedding plane decreases southward as the layer attains a greater depth. Thus, the excess shear stress developing in the shallower part of the layer is not being relieved by bedding-plane-slip. This results in additional shortening of the layer above the point for which the difference between the shear stress and shear strength is equal to zero. In this situation the normal stress parallel to layering attains progressively greater values in time. When this stress reaches a certain critical value, it will facilitate stress relief by a mechanism other than bedding-plane-slip, such as buckling (CEG, 1998).

From the foregoing discussion, it is evident that slip of a given layer southward toward the fault relative to another layer beneath it is required to accomplish the buckling along the discontinuity. The question of the stresses necessary to initiate buckling has been considered utilizing a simple model. In general, it may be shown that the layer-parallel normal stress must

be large enough to overcome the frictional resistance to sliding of a layer along the inclined fault, the body weight of the layer, and the critical buckling stress of the layer. Moreover, layer-parallel shear stress must exceed the bedding plane shear strength to initiate frictional sliding between layers (CEG, 1998).

The buckle amplitudes and wavelengths decrease progressively to a depth of 200 feet (60 m) where they die out. For the stress levels extant prior to glaciation, as inferred from stress measurements at the Unit 2 site (Section 2.5.4) which are believed to be less than 3,000 psi (210 kg/sq cm), the analysis indicates that, at the site, typical strata with an average thickness of 1 foot (0.3 m) would buckle with length-to-thickness ratios (L/t) less than 200:1. At the level where the smallest L/t occurs, the magnitude of the layer-parallel normal stress must have been much greater than 3,000 psi (210 kg/sq cm) at the time of buckling (CEG, 1998).

The foregoing information is relevant to the assessment of the possibility that the amplification process may propagate to a greater depth than where presently detected (200 ft, 60 m). This depends upon the magnitudes of two controlling factors referred to as the potential depth of amplification (Da), and the potential depth of reverse-slip deflection (Dr). The relationships between the subhorizontal compressive stress, the layer-parallel shear stress, and the slenderness ratio (L/t) can be used to evaluate the present Dr for the Cooling Tower fault, a quantity is necessary for one to determine if the structure is capable of propagating to greater depth. The characteristic relationship displayed by the wavelength of individual buckles to the depth of their occurrence is an important factor in this determination (CEG, 1998).

The buckle wavelengths progressively diminish with depth, and this corresponds to a similar decrease in the slenderness ratio because the thicknesses of the strata are relatively constant throughout the section in which the structure is developed. The layer-parallel stress required to initiate a deflection is least if the body weight of only a single stratum is considered, ignoring that of the overlying strata. However, this is true only if a layer beneath the given stratum is deflected with a smaller wavelength (slenderness ratio) than that of the overlying stratum. Thus, it follows that Dr is governed by the wavelength of the uppermost deflections, and is directly dependent upon the magnitude of the layer-parallel stress (CEG, 1998).

Considering this relationship, it can be shown that, for the Cooling Tower fault, Dr today is smaller than the depth to which the structure developed in the past (CEG, 1998).

Prior to the glacial advance, the s1 trajectory had probably been parallel to bedding. Hence, the layer-parallel shear stress was zero. Under these conditions, as soon as downwarping of the land surface was initiated, the layer-parallel shear stress attained a value greater than zero. Consequently, the strata of the Transition Zone were susceptible to folding. As the downwarping continued, the layer-parallel shear stress increased progressively so that deflections could form at a greater depth. Therefore, the maximum potential depth of development of the reverse-slip deflections occurs when the amount of distortional strain energy in the bedrock is greatest, which occurs concomitantly at the time of maximum crustal downwarping. During glacioisostatic rebound, the amount of distortional strain energy gradually diminishes and Dr, therefore, decays with time accordingly. Hence, it can be justifiably concluded that Dr is presently much smaller than it was during the development of the structure at the time of crustal downwarping (CEG, 1998).

Biot (CEG, 1998) has shown that the amplification of folding in layered, viscoelastic media will be restricted to a finite depth termed herein the potential depth of amplification (Da). Da is dependent upon the lateral compressive stress.

The in situ stress may exceed 2,000 psi (140 kg/sq cm) at the Unit 2 site (Section 2.5.4.). Hence, Da may presently exceed 200 feet (60 m), and amplification can theoretically occur below this depth. However, Da actually depends on the magnitude of Dr. If Dr is less than Da, the Da is effectively equal to Dr, which is currently less than 200 feet (60 m) (CEG, 1998).

The considerations of the rates of deformation, and resultant accumulation of distortional strain energy, which are believed to have been extant during the progressive development of the Cooling Tower fault, suggest that the folding process may be seismogenic only during the rotation stage which is a stage of unstable growth (formation of the rotated bedrock sliver). Hence, the present ability of the structure to generate vibratory ground motion of noticeable intensity appears to be dependent upon whether or not the structure can reenter the rotation stage. This renewed folding cannot be accommodated on those parts of the fault that have already experienced this phase, because the structure has become locked and the rotation is completed. Thus, the folding would have to occur in the area where only the l/2 stack of buckles is developed, that is, below a depth of 140 feet (43 m) (CEG, 1998).

To generate a seismic shock, the renewed folding would require a volume of rock mass sufficient to create another rotated limb or bedrock sliver in this zone. This would require that the depth at which the original amplification was terminated be extended downward to a minimum depth of 280 feet (85 m), or approximately twice the thickness of the stratigraphic section involved in the original folding during unstable growth. However, an amplification depth of 280 feet (85 m) would be realized only if both Da and Dr equal or exceed 280 feet (85 m), which is not the case. Hence, the recurrence of unstable growth folding on the Cooling Tower and Drainage Ditch faults with a concomitant seismic event is a very unlikely possibility, and there is no rational basis to consider the structure to be a fault presently capable of generating vibratory ground motion (CEG, 1998).

2.5.1.2.4.5 NMP Unit 2 Mechanism of Postglacial Deformation

In light of the foregoing discussion, it is very possible that the disturbance of the overburden sediments reflects movements along the fault caused by changes of fluid pressure in the bedrock. These changes may have been caused by the fluctuation of the water level in the Ontario Basin following glacial retreat. It seems very unlikely that the deformation of the overburden sediments indicates that the Cooling Tower fault buckles were propagating downward within the past 10,000 yr. The reasons for this are twofold. First, the postglacial movements occurred when the differential crustal downwarping was reduced due to glacioisostatic uplifeetor rebound. Hence, the amount of distortional strain energy stored in the bedrock was reduced from its former value. Consequently, the potential depth of development of the structure at this time was smaller than that to which the structure had already developed. Second, the dilated openings in the bedrock would prevent propagation of any movement to the surface from a depth of more than 140 feet (43 m). Hence, even if these movements had occurred at depth, one would not expect to find them expressed at the surface (CEG, 1998).

The maximum Lake Iroquois water level was approximately 300 feet (91 m) above the land surface at the NMPNS site. As the ice sheet receded to the north and opened the lowest lake outlet in the Thousand Islands region, Lake Iroquois was drained through the St. Lawrence Valley. The water level subsequently assumed a low stand commonly referred to as the Admiralty Stage. The water level of Lake Iroquois dropped approximately 450 feet (137 m) to reach this latter stage. The bedrock in the site area is covered by a thin, but relatively impervious veneer of unconsolidated sediments which would prevent a rapid flow of fluids to the surface or into the lake from the bedrock. Hence, it may be inferred that, at a time after deposition of the deformed lacustrine sediments, the fluid pressure in the bedrock could be

much greater than the water pressure exerted by the lake. It may be further inferred that after the deposition of the unlithified sediments (including the upper sequence of Sandy Creek), this excess fluid pressure, DP, underwent incremental changes. Consequently, the effective stress normal to bedding (s3-P) was modified accordingly (CEG, 1998).

Such changes in the effective normal stress influenced the stability of the Cooling Tower feature by temporarily reducing the effective shear strength of bedding. The problem has been analyzed using a model showing a bedrock stratum with thickness (h) that is situated above a shear zone and that can move along this zone as a solid block. With the assumption that there was no change of in situ stress during the time between the completion of the preglacial movements on the Cooling Tower fault and the high stand of Lake Iroquois, the model presents the equilibrium conditions for sliding on bedding planes in the vicinity of the fault prior to the buildup of fluid pressure. The stratum modeled corresponds to a layer or sequence of layers forming one of the two limbs of the buckle feature. When the buckle feature was formed, stress-drop normal to the fault occurred. The modeled layer attained equilibrium for a particular value of the effective stress normal to bedding, and a point near the axial plane region of the fold was thereby displaced toward the region of greatest stress relief. If there was no change in DP until the end of the high stand of Lake Iroquois, then the equilibrium would endure until that time, and the displacement would remain constant. At the end of the high stand of Lake Iroquois, DP was progressively increasing, thereby causing an incremental reduction of the effective normal stress. This, in turn, caused an incremental reduction of the effective shear strength of bedding. Consequently, the equilibrium of the limb could not be maintained and additional incremental translations must have occurred toward the region of low stress, that is, toward the axial plane. The translation was greatest near the axial plane, and gradually decreased away from it (CEG, 1998).

One notable exception to this occurred in Trench 3 exposure where the north limb is unopposed by the south limb which was removed by glacial erosion. The north limb migrated southward, displacing the older fault plane about 4 feet (1.2 m) leading to the folding of the unlithified sediments with ancillary faults. Conversely, if the margin of one limb was equally opposed by another, the lateral translations of this limb would be restricted, and most effectively so, if the axial plane (fault plane) separating the limbs were vertical. This situation existed during deformation of the overburden sediments at the Cooling Tower Piping Trench and Pit 1 (and other locations along the trace of the fault). Thus, at these locations, the lateral displacements at the margins of each limb could not be freely accomplished, and thereby resulted in an incremental buildup of layer-parallel normal stress in the strata contiguous with the fault. When this stress attained a certain value in conjunction with the high buildup of fluid pressure, both limbs of the structure buckled further, and formed a gentle arch with the fault along the crest (CEG, 1998).

Arching and compensatory normal faults developed in the overlying sediments in response to arching of the bedrock. The disturbance of the unlithified sediments very likely occurred as the result of a buildup of fluid pressure in the bedrock which equaled or exceeded the pressure due to the body weight of the rocks. The deformation does not, therefore, indicate that the Cooling Tower buckle was propagating downward during recent glacioisostatic uplift. The present maximum possible value of the fluid pressure in the bedrock is equal to approximately 40 percent of the pressure due to the body weight of the rock. Hence, it can be concluded that movements with a similar origin to those which caused the postglacial deformation are not likely to occur at the present time (CEG, 1998).

2.5.1.2.4.6 Conclusions

On the basis of the analysis of the deformation process and its origin, the following principal conclusions are drawn with respect to the Cooling Tower fault:

1. The development of the pre-Wisconsinan, reverse-slip deformation is attributed to the combined effects of three factors:

   a. In situ bedrock stress field.

   b. Changes in the stress field induced by the crustal downwarping caused by glacial loading.

   c. Pronounced anisotropy of the bedrock at the site.

2. In the present tectonic environment of the site area, it is not possible for the structure to propagate downward below its original depth of development. On this basis, the structure is considered to be presently incapable of generating vibratory ground motion (CEG, 1998).

3. The disturbance of the glaciolacustrine sediments (Lake Iroquois and Sandy Creek Stage of Lake Iroquois) is attributed to the excessive buildup of fluid pressure in the bedrock caused by postglacial fluctuations of the water level in the Ontario Basin. The present value of the fluid pressure has no significant influence on the stability of bedding adjoining the Cooling Tower fault. Hence, movements of similar origin are unlikely.

4. Based on the present understanding of the site conditions and the mechanism of deformation, it cannot be ruled out that minor, subsurface adjustments may occur within the zone of buckling along the Cooling Tower fault. If these minor adjustments occur, they will involve a relatively low strain rate and only limited volumes of the rock mass, and thus should be considered to be inconsequential in terms of vibratory ground motion. These adjustments are expected to be restricted to the rock mass within the depth interval defined by the location of the Transition Zone (depth of approximately 50 ft, 15 m) and a depth of 200 feet (60 m). Furthermore, it is believed that the adjustments will not be expressed at the bedrock surface because of the presence of voids between layers that first must be closed (CEG, 1998).

2.5.1.2.4.7 NMP Unit 2 Thrust Faults

A series of shallowly dipping faults, referred to as thrust structures, are exposed in the bedrock excavations at the NMP Unit 2 site. They appear to be interrelated because of striking similarities in structural style, mechanism of deformation, and relative age. A series of detailed structural, mineralogic, isotopic, and palynologic studies were conducted to investigate the nature of these thrust structures (CEG, 1998).

The faults are predominantly developed in the area of the erosional valley in the bedrock surface. All field evidence suggests that they are confined between the Cooling Tower fault and the Drainage Ditch fault. The Radwaste fault was traced to the east with borings. The results indicate that the thrust structure extends in its dip direction a minimum distance of 100 feet (30 m) to the east of its exposure in the North Radwaste Trench. The position of the thrust structures appears related to the presence of three prominent lithologic interfaces within the stratigraphic section penetrated by the site excavations. The Radwaste thrust structure was exposed in several shallow excavations at the site from the North Radwaste Trench to the

Circulating Water Piping Trench. This structure is situated between the lower Oswego Sandstone and the upper portion of Unit A of the Pulaski Formation. The Unit B slip zone was exposed in the walls of the reactor containment excavation, and in rock cores from borings drilled in the vicinity of the reactor complex. It is located near the interface between Units B and C of the Pulaski Formation. The thrust faults in the tunnels are exposed at the base of the intake shaft and in both lake water tunnels. Stratigraphically, these structures are located within the upper portion of Unit C of the Pulaski Formation (CEG, 1998).

The thrust faults are all similar in overall appearance and display common structural characteristics. The structures consist of small zones of brecciation and folding that are at most several feet wide. The dips of these zones range from nearly horizontal to approximately 30 deg. The configuration of the thrust structures resembles a stack of tabular bedrock elements displaced to the west along bedding planes. These structures appear to be confined to specific stratigraphic units. They generally occur as planes of slip, parallel to bedding, with short intervals where the discontinuity transects the layering at a low angle and then merges with bedding at a higher stratigraphic level. The most intense deformation occurs along the inclined portions of the discontinuities. Locally, there may be no shear dislocation of the beds along the fault (CEG, 1998). The mode of displacement typically consists of:

1. Discontinuous shear dislocation of individual beds or groups of beds.

2. Rigid body rotation of beds to form small folds.

3. Broad arching of the hanging wall strata.

4. Dilation of the bedrock along bedding planes and variously oriented fractures.

Numerous indicators of dilation within the bedrock mass, such as voids, open fractures of various attitudes, and zones of loose bedrock rubble, were encountered during the investigation of the thrust structures. This is possibly the most important characteristic of the structures and is significant because it clearly indicates that an environment of low confining pressure was necessary for their development (CEG, 1998).

The sense of dislocation on these structures is generally similar to the upper strata typically displaced to the west. Locally, slip down the dip has been noted for some of the ancillary shears in lake water tunnel no. 1. Curiously, reverse-slip was observed on different parts of the same ancillary shear with normal slip in some places. The principal stratigraphic dislocation in the tunnels, however, is reverse-slip toward the west. The slip direction of all the thrust structures appears to vary from west-southwest to west-northwest progressively from the cooling tower area to the tunnel exposure. This variation apparently depends either on the location of a particular exposure and/or depth of development, that is, upon the stratigraphic position of the faults. The variation of slip direction attests to the heterogeneous nature of the strain along these structures. It is possible that this has resulted from a progressive change in the stress trajectories either laterally or with depth (CEG, 1998).

The magnitude of displacement also varies along both the strike and dip of the Radwaste fault. For example, 5 to 7 feet (1.5 to 2.1 m) of displacement is present near the upper limit of the ramp of the structure in the North Radwaste Trench; however, in the deepest part of the excavation, an apparent dip separation of 4.5 feet (1.4 m) was noted. The faults in the lake water tunnels exhibit small displacements typically less than several inches. The magnitude of displacement along the Unit B slip zone has not been established. However, one may infer that the displacement is at least equivalent to that of the tunnel faults because it occurs at a higher level in the stratigraphic section (CEG, 1998).

Secondary materials commonly occur within the thrust structures. These materials consist of several types of calcite mineralization and glaciolacustrine sediment. The calcite occurs along dilated bedding planes and fractures, as well as along shear surfaces. On shear planes, the calcite commonly cements breccia fragments and displays dip-slip slickensides. Calcite within dilated fractures occurs as concretionary nodules or patches of euhedral, drusy crystals. In one case, laminated clays deposited within a dilated bedding plane are cemented by the calcite (CEG, 1998).

Two types of unlithified sediment fill openings in the bedrock near the thrust structures: a gray to tan laminated silty clay, and a gray massive plastic clay. The latter type was most commonly present in zones of intensely shattered bedrock along the ramp portions of the faults. The laminated clay typically fills dilated bedding planes. Similar occurrences were noted to depths as great as 270 feet (82 m) in rock cores recovered from borings. Within the North Radwaste Trench, laminated clay was found mixed with the breccia along bedding planes where it appeared to be contorted. Another example of deformation of the laminated clays within the Radwaste fault occurs in the exposure of a small monocline in the North Radwaste Trench. At this location, clay layers 0.25 to 1 inch (0.6 to 2.5 cm) thick dip from 20 to 70 deg, parallel to the steep limb of the monocline (CEG, 1998).

The age of development of the Radwaste fault (and other thrusts) was evaluated by considering the age and origin of the secondary filling materials. Specimens of calcite minerals were analyzed using geothermometry, isotope ratio analysis, and radiometric dating. These results were compared with similar data obtained from analyses of mineralization occurring in proximity to the high-angle faults. The paragenetic study of the calcite found in association with the thrust structures strongly suggests that the four principal varieties identified may be different facies of the same depositional stage. Fluid inclusion analysis of this calcite indicated that it crystallized very near the ground surface at temperatures only slightly greater than present ambient temperatures, that is, 50 °F to 86 °F (10 °C to 30 °C). This calcite contrasts with the epigenetic calcite along the high-angle faults whose formation temperatures ranged from 158 °F to 320 °F (70 °C to 160 °C), indicating an origin at greater depth, and thus geologically older. Isotopic analysis confirmed the fresh water origin of the low temperature calcite and revealed that some of it (the calcitic breccias) probably formed below the groundwater table, whereas some (the travertine) apparently formed in the vadose zone. Radiometric dating of the former, using the Thorium-230/Uranium-234 technique, indicated only that the material is younger than 300,000 yr old. However, radiocarbon dating of the travertine yielded a C-14 age of 14,180 ±550 radiocarbon yr B.P. These radiometric dates confirm the interpretation that the low-temperature calcite is younger than the high-temperature calcite and is likely Quaternary in age (CEG, 1998).

The interstitial sediment within openings in the bedrock is similar in appearance to surficial glaciolacustrine sediments of Pleistocene age (Section 2.5.1.2.). Therefore, it was suspected to be of similar origin. Specimens of the interstitial sediment were collected for grain size analysis, compositional and heavy mineral analysis, and pollen analysis. These results were compared with similar analyses of specimens from the surficial sediments. The conclusion of principal importance is that the tan, laminated sediment is derived from material of glaciolacustrine origin. This material contained pollen and spores similar to those found in portions of the Late-Pleistocene age surficial sediments. A Late-Pleistocene age of the interstitial sediment was confirmed by a C-14 date of 11,060 ±360 radiocarbon yr B.P. for organic material in the sediment collected from within the Radwaste fault. The age of similar laminated clay encountered at a depth of 250 feet (76 m) in the borings is uncertain. However, palynologic analysis of this material also suggests a late-Quaternary age (CEG, 1998).

A minimum age of approximately 11,000 yr B.P. can be interpreted for the development of the Radwaste fault on the basis of the radiocarbon date of laminated clays encountered within the zone of deformation. Dilation of the bedrock associated with development of the structure clearly had to have occurred prior to emplacement of the clays. Nevertheless, the exact age of latest deformation is uncertain because the time of deformation of the laminated clay is unclear. Based on his observations in the North Radwaste Trench, Dr. L. Sirkin concluded that the lacustrine sediments were deposited in the bedrock openings and were subsequently deformed. In contrast, the prevailing opinion is that of Drs. T. L. Pewe, R. H. Jahns, and S. S. Philbrick, namely that the deformation in the bedrock had occurred prior to the deposition of the clays on the basis of observations of the clay overlying the hinge of a fold (CEG, 1998).

2.5.1.2.4.8 Mechanics of Thrust Structure Development

Many factors indicate that the thrust structures developed near the ground surface under similar conditions extant at the time of development of buckling along the north-dipping faults. Also, the thrust structures are only recognized within the bedrock block bounded by the high-angle faults. The possible age and spatial relationships between these two groups of structures must be inferred because the absolute age of formation of the thrusts is not known, and there are no data which allow an interpretation of their relative ages. Analysis of the possible relationships between these deformations led to the inference of a mechanism of development for the thrust structures (CEG, 1998).

The thrust structures appear to have resulted from the relief of stored strain energy which is assumed to be remnant gravitational and/or tectonic in origin. Development of the structures was triggered by an environmental change that reduced the ability of the bedrock block to retain the stored strain energy. This ability is controlled by the resistances to shearing along the boundaries and the lateral restraining forces. Hence, reduction of the restraints precipitated release of stored strain energy resulting in the development of the thrust structures (CEG, 1998).

Two factors, consisting of lateral restraining force and shear resistance along the block boundaries, controlled the initial strain energy stored in the bedrock. The lateral restraining force was provided by the bedrock which has since been removed during formation of the erosional valley. The shear resistance along the block boundaries consisted of shear resistance along the Drainage Ditch fault (Boundary 1), shear resistance along the Cooling Tower fault (Boundary 2), and shear resistance along the base of the block (Boundary 3). In the instance of Boundary 3, the shear resistance is the sum of the integrated shear strength on the boundary and the shear stress acting along bedding planes (CEG, 1998).

Significant changes in the values of normal stress (sn1 and sn2) and shear stress parallel to bedding must have occurred in response to gravitational loading of the lithosphere by glaciation(s) and other related phenomena. Changes in the value of shear stress parallel to bedding resulted from shear straining of the lithosphere caused by glacially-induced differential vertical movements. Reduction in the value of normal stress perpendicular to bedding may have accompanied changes in the water level of ice-marginal lakes (CEG, 1998).

Considering the foregoing, the following three-part scenario for development of the Radwaste fault is inferred. Initially, downwarping of the crust in relation to glacial advance created conditions favorable for buckling of the hanging wall blocks of northward dipping high-angle faults (as discussed previously). This reduced normal stresses acting across the high-angle faults. Hence, the shear resistances along the Drainage Ditch and Cooling Tower faults were reduced. Next, formation of the erosional valley reduced the lateral restraining force. Finally, removal of the load imposed by the continental ice sheet reduced normal stress perpendicular

to bedding, and thus reduced shear resistance along the base of the block (Boundary 3). Further reduction of these restraints may have occurred during the drainage of Lake Iroquois as a result of the development of high fluid pressure in the bedrock (CEG, 1998).

The mechanics of deformation of the thrust structures in the intake shaft and lake water tunnels are inferred to be similar to the Radwaste fault. Studies have suggested that these structures consist of a principal fault with numerous nearby ancillary splays or subparallel shears. The attitude, curviplanar nature, and lateral extent of all the shears are similar. Slickensides indicate instances of oblique slip. All exhibit some occurrences of calcite mineralization of a type shown to have precipitated from groundwater at ambient surface temperature (CEG, 1998).

As noted above, some instances of slip down the dip occur on these shears. Most of these occur structurally beneath the principal thrust fault exposed in the shaft. They can be generically explained in either of two ways:

1. They could be developed as the result of, and in proximity to, a differential, vertical displacement, for example, low-angle "normal" faults that are formed in response to development of a high-angle reverse fault.

2. It is also possible that they represent a secondary response to bedding-slip thrusting deformation. The slip down the dip of low-angle faults in the westernmost tunnel can best be explained by the latter possibility because: 1) the strain along the thrust faults is heterogeneous, this manner of strain supports the possibility of rotational slip on the thrusts where reverse-slip at one location is accompanied by normal-slip at another location, and 3) the spatial relation of shears with normal-slip below the main structure and reverse-slip above it. Furthermore, no differential vertical displacement, as in the explanation 1 above, is present.

In summary, detailed studies of the site conditions strongly suggest that the thrust faults do not cut the Cooling Tower and Drainage Ditch faults. It appears that the thrust faults together with the high-angle faults form an integrated, but sequential, system of bedrock deformation (CEG, 1998).

The postulated equilibrium conditions of the thrust structures imply that the development of buckling (the pre-Wisconsinan phase of the reverse-slip deformation) along the Cooling Tower and Drainage Ditch faults contributed to the instability of the intervening bedrock block. Hence, it can also be inferred that the development of the thrust faults postdates the first phase of reverse-slip movement along the Cooling Tower fault (CEG, 1998).

2.5.1.2.4.9 Conclusions

The results of detailed geologic investigation of the Radwaste fault resulted in the following conclusions regarding the nature and origin of the thrust structures. The following conclusions and results are supported by a panel of consultants (CEG, 1998).

1. Movements along the Radwaste fault (and similar thrust faults) have been recurrent.

2. The initial development of the structure is believed to be associated with crustal loading and unloading during episodes of glaciation. This suggests that the thrust was initiated sometime between 12,000 and 2,000,000 yr ago. Based on experience with similar structures, Drs. Jahns and Philbrick believe that the age of initial formation can be narrowed to between 150,000 and 400,000 yr B.P. (CEG, 1998).

3. The minimum age of development of the Radwaste fault is approximately 11,000 yr B.P. However, the exact age of the latest deformation is uncertain because the relationship of the lacustrine clays to the bedrock deformation does not provide certain resolution of the age of latest deformation (CEG, 1998).

4. The thrust faulting results from the release of stored strain energy caused by the reduction in vertical confining pressure by erosion. The faulting occurs on the flanks of the small bedrock valley. It is postulated that formation of the valley disturbed equilibrium conditions and removed the lateral restraint that had prevented the expansion of the strata on either side of the valley. Furthermore, the development of the thrust faults was facilitated by buckling across the lateral boundaries of the thrust sheet (i.e., Cooling Tower and Drainage Ditch faults). The buckling resulted in a significant reduction of the normal stress acting perpendicular to these boundaries, thus lowering the resistance to frictional sliding of the thrust sheet relative to the surrounding bedrock (CEG, 1998).

5. As stated in the consultant report, "the faulting is not related to current tectonic processes that could introduce additional amounts of strain energy." In addition, it is stated that "it can be concluded that no increase in the amount of stored strain energy will occur during the coming centuries" (CEG, 1998).

6. Based on observations of analogous geologic structures, Drs. Philbrick and Jahns conclude that because of the inability of the structure to build up significant amounts of strain energy, the Radwaste structure is so nearly dead at present levels of exposure that its participation in such future movements would amount to no more than a small fraction of an inch (CEG, 1998).

Drs. Jahns and Philbrick also conclude that any future movements should not exceed 0.25 in (0.64 cm), based on their experience. Based on studies including mathematical modeling, it has been concluded that 1 in (2.54 cm) is a conservative allowance for future maximum credible movement. Thus, an allowance of 1 in is used for design purposes (CEG, 1998). The maximum allowable total settlement of 3 inches and differential settlement of 1.5 inches for EPR design purposes for NMP3NPP are presented in Section 2.5.4.

2.5.1.2.5 Broad Low-Amplitude Folds and Associated Normal Faults

Demster Structural Zone - New Haven, New York)

2.5.1.2.5.1 Introduction

The Demster Structural Zone trends northeast. Associated with this zone of locally intense fracturing and faulting is a sequence of gently southwest-plunging, broad, asymmetric anticlines and synclines. The locations of the Demster Structural Zone features are depicted on Figure 2.5-55. This zone of complex deformation is in the Late Ordovician Oswego Sandstone, the youngest site area rock unit in outcrop and subcrop. Post-Ordovician deformation was identified during subregional and site subsurface mapping investigations at the New York State Electric & Gas Corporation (NYSEG) proposed New Haven nuclear site approximately 8 km (5 mi) southeast of NMP (NYSEG, PSAR, 1978).

Subsurface mapping defined and delimited the major bedrock structures within an 5-miles (8 km) radius of the New Haven site. Deep well data for the region east of the New Haven site substantiate subsurface interpretations reported in the 1979 investigations.

Field investigations, data synthesis, and conclusions of the New Haven site study are reported in the NYSE&G PSAR (NTSE&G, 1978). This section is a summary and concentrates primarily on the structural characteristics of the Demster Structural Zone.

Studies associated with the exploration of the Demster Structural Zone included 29 diamond drill core borings; site area geologic mapping at a scale of 1:24,000 with supplemental reconnaissance mapping in and adjacent to the Adirondack Mountains; geologic mapping of a 240 feet (73 m) long trench excavated across the Demster Zone; geophysical surveys including natural gamma logging of boreholes, offshore seismic refraction and reflection surveys, land refraction surveys and land magnetic surveys; review and update of regional gravity and aeromagnetic data; mineralogical, petrographic, isotope, and radiometric age analyses of representative samples obtained from the Demster fault zone; and analysis interpretation of available subsurface data in central and northern New York (CEG, 1998).

In summary, the interpretation and evaluation of the combined geologic and geophysical data support the following conclusions:

1. The Demster Structural Zone is not capable.

2. Broad folding, reverse faulting, and normal faulting associated with the Demster Zone developed sequentially through a series of three events or phases that occurred in Middle to Late Paleozoic and, possibly, Mesozoic time.

3. Ordovician strata in the site area are folded into a series of essentially parallel, southwestward-plunging anticlines and synclines. The Demster Beach Anticline is intensely deformed and faulted within part of the eastern oversteepened limb designated the Demster Structural Zone. Stratigraphic offset is due primarily to folding, but steeply northwest-dipping small faults and fold axial fractures account for the intense brittle deformation.

4. Assuming ambient depositional conditions, fluid inclusion data are indicative of calcite mineralization emplaced at temperatures greater than 212 °F (100 °C). Paragenetic and structural element correlation demonstrate the deposition of calcite after bacteriological reduction of sulfides, in part contemporaneous with and soon after the deformation.

Early calcite mineralization indicates deposition prior to completion of structural development and late calcite is undeformed.

2.5.1.2.5.2 Geologic Setting of the Demster Zone

2.5.1.2.5.2.1 Demster Zone Stratigraphic Setting

The area adjacent to and including the Demster Zone is underlain at a relatively shallow depth by Grenville crystalline rocks of the Precambrian basement. The basement complex is apparently similar to lithologically and genetically equivalent strata cropping out in the Grenville Province of Canada and the Adirondack Mountains of New York (Section 2.5.1.1).

The Precambrian basement is overlain by approximately 1,500 to 1,800 feet (457 to 549 m) of Cambrian-Ordovician strata which, in the site area, from oldest to youngest, are the Theresa Sandstone, Black River Group, Trenton Group, Utica Shale, Whetstone Gulf Formation, Pulaski Formation, and the Oswego Sandstone (Section 2.5.1.1). The Late Ordovician Queenston Formation, a sequence of red beds overlying the Oswego Sandstone to the south of the site area, completes the progradational character of this sedimentary succession from limestone to

shale to sandstone. This sedimentary sequence rests unconformably on a Precambrian crystalline basement surface that slopes southward at 50 ft/mi (9.5 m/km) and results in a south-dipping homoclinal sequence of Paleozoic strata that thicken to the south and southwest. The site area, except for infrequent exposures, is overlain by several types of glacial deposits that include till, undifferentiated ice-contact stratified drift, glaciolacustrine, and peat deposits (CEG, 1998).

Subdivision of the near surface stratigraphic succession at both the NMPNS and New Haven sites is nearly identical, although the nomenclature differs. The New Haven site nomenclature includes five zones within the Oswego Sandstone (sensu lato). Zone 5 correlates with the NMP Oswego Sandstone and Oswego Transition Zone. Zone 2 correlates with the NMP Pulaski Formation Unit A, Zone 3 correlates with the Pulaski Formation Unit B, Zone 2 correlates with the Pulaski Formation Unit C and Zone 1 correlates with the Whetstone Gulf Formation Unit A. At the New Haven site the Whetstone Gulf Formation Unit B of NMP is known at Pulaski Shale (CEG, 1998).

2.5.1.2.5.2.2 Demster Zone Subsurface Structure

Subsurface stratigraphic investigations in the New Haven site area were carried out in order to divide the section into mappable units to define the subsurface structure. The section represents a continuum of marine deposition in which unit boundaries are assumed to have been essentially horizontal as deposited, except on a very local scale, and therefore are considered reliable horizons. Structure contour maps of the unit boundaries, or key horizons, were constructed and examined for evidence of structural trends. The Pulaski Formation-Oswego Sandstone boundary was selected as the primary horizon because of its mappability resulting from lithologic differences between the Oswego Sandstone and Pulaski Formation. The boundaries of five mappable subzones within the Oswego Sandstone (sensu lato) were also utilized in the structural analysis. Structurally, the top of the Pulaski Formation is a gently sloping surface consistent with the marine conditions of its deposition, as modified by subsequent regional tilting. Within the areal limits of stratigraphic control the Pulaski Formation appears to strike west-northwest and dips to the south-southwest approximately 60 ft/mi (11 m/km). Both the New Haven and the NMPNS sites overlie a gently sloping, mildly downwarped rock sequence whose south-southwest dip reflects the regional homoclinal structure (CEG, 1998).

Based on closely spaced Pulaski Formation control points, the contour patterns southeast of the NMPNS are indicative of abrupt changes in the strike and dip of the Pulaski Formation - Oswego Sandstone boundary. These changes, together with the pronounced linearity and the steep contour gradient, are suggestive of faulting. Inclined boreholes in the zone of suspected faulting traversed a crushed zone several tens of feet wide, including intervals of gouge and breccia, confirming the occurrence of a fault zone. Deep exploration data east of the New Haven site confirm the Mexico Anticline and suggest associated deformation on the eastern limb of this fold (CEG, 1998).

The contour pattern of the formation boundary and boring data define the position and orientation of a northeast-trending fault zone and associated folding. Figure 2.5-50, Figure 2.5-51, and Figure 2.5-52 indicates the effects of tectonism on the Pulaski Formation-Oswego Sandstone boundary on the eastern limb of the Demster Beach Anticline, herein designated the Demster Structural Zone. Spacing and alignment of the contour pattern are indicative of folding, rather than faulting, as the dominant process in the formation of the Demster Structural Zone. The fold is markedly asymmetrical with little net displacement on the fault. Southward deflections of the contour pattern occur west-northwest and east-southeast of the New Haven site. To reestablish the regional strike and correlate with stratigraphic control at the NMPNS site, the structural contours must return to a northerly trend. Stratigraphic

control west of the New Haven site indicates a repeated pattern. The contour pattern is undulatory along regional strike. To the west of the NMPNS site, the continuity of the pattern is uncertain (CEG, 1998).

Examination of the individual structure contour maps indicates clearly the marked compression and linearity of contours for all mapped horizons in the vicinity of the Demster Zone. This anomalous contour pattern as well as the site area pattern indicate that the Upper Ordovician age strata are folded into a series of broad, low amplitude, southwest-plunging folds designated the Demster Beach Anticline and Mexico Anticline and an unnamed inferred syncline at the NMPNS site and the New Haven Syncline (CEG, 1998).

Structural contours of all horizons examined indicated that a linear zone of deformation separates the Demster Anticline from the New Haven Syncline. This was shown to be a relatively narrow zone of flexure characterized by considerable stratigraphic displacement, brittle deformation, and calcite mineralization (CEG, 1998).

The configuration, location, trend, and extent of the three folds named above are shown on Figure 2.5-50, Figure 2.5-51, and Figure 2.5-52; they trend N 45 E, plunge southwest, and extend a minimum of several miles. Dip angle and direction of the fault zone were defined through analysis of sedimentary and tectonic structures in core. Excavation of a 240-feet (73-m) long trench exposed the bedrock across the most intensely deformed zone. Detailed studies were made of the type of deformation, the amount of stratigraphic displacement due to faulting, the relationship between faulting and broad folding, and the nature and condition of surficial units overlying the bedrock faults (CEG, 1998).

2.5.1.2.5.3 Demster Zone Detailed Geologic Studies, Trench II and Vicinity

2.5.1.2.5.3.1 Demster Zone Surface Geology

Excavations, detailed geophysical investigations, and drilling enabled an evaluation of mechanism, cause, style, extent, and apparent age of deformation. Bedrock exposure and overlying surficial deposits were mapped in detail. Trench II was the second bedrock trench excavated during the New Haven site studies (CEG, 1998).

The bedrock/till interface at faults mapped on the trench floor was closely examined for evidence of displacement. The till fabric was random and the bedrock surface smooth over mapped faults. A distinct pair of silt laminae occur continuously near the base of the lake sediments over the fault between along the northeast trench wall. The laminae are undisturbed and follow the topography of the lower till upon which they were deposited. These laminae were most likely laid down in proglacial Lake Iroquois, 12,500 to 10,000 yr B.P. (CEG, 1998).

The silt laminae are locally contorted and warped where draped over cobbles or boulders or where rafted material has settled. Faulting and folding associated with the development of the Demster Structural Zone have not disturbed the overlying Pleistocene deposits exposed in Trench II (CEG, 1998).

2.5.1.2.5.3.2 Demster Zone Subsurface Structure

Stratigraphic and structural interpretation of data from borings, combined with trench excavations, indicate that major stratigraphic offset in the section explored is caused by the development of the Demster Beach Anticline and not by faulting. As the structure contours indicate, the Oswego Sandstone and Pulaski Formation folding is not a single fold but a series of folds. Drilling, stratigraphic interpretation, and seismic studies surrounding the Demster

Zone demonstrate an apparent dying out of faulting to the northeast and southwest along the Demster Zone. Only one boring to the west of the zone intersected minor faults (CEG, 1998).

Subsurface data show two styles and phases of deformation, large-scale reverse-slip and small-scale normal-slip. Fracturing, calcite mineralization, and faulting decrease away from the fault zone. Offsets diminish away from the fault zone, as well as to the southwest along the zone. Principal reverse stratigraphic offsets across the zone vary from 130 to 160 feet (40 to 49 m). Within the zone of intense deformation 10 to 15 feet (3 to 4.6 m) of normal displacement was found (CEG, 1998).

At the fault zone proper, the exact amount of offset is uncertain due to complex folding, fracturing, and the necessary extrapolation of data. The vertical component of normal faulting is suspected to be no more than approximately 10 feet (3 m). This 10 feet (3 m) normal throw is in agreement with boring alignment data (CEG, 1998).

2.5.1.2.5.3.3 Demster Zone Structure Trench II

Bedrock along the entire 240 feet (73 m) exposure of bedrock in the trench is affected by the two phases of deformation mentioned above. Resultant bedrock deformation, in and adjacent to this exposed zone, is principally due to areal folding, not faulting (CEG, 1998).

The observed gentle bedding dips (2 to 10 deg southeast) reflect the fold structural dip and not the regional homoclinal dip. Dips in the trench areas average 2 to 10 deg southeast and represent the southeast limb of a southwest-plunging asymmetric anticline (CEG, 1998)..

Faulting exposed in the trench is not a single structural break, but a zone of variable deformation approximately 70 feet (21 m) wide. Detailed mapping indicates the bedrock structures exposed in Trench II can be subdivided into three small-scale structural domains for description and analysis. These domains are delineated on the basis of deformation style and structural elements. The continuity of these domains along the entire length of the fault is uncertain. However, similar domains are inferred for the boring alignment. The southeast domain is characterized by relatively steep southeast-dipping strata (locally up to 50 deg). No faults or folds are observed in the southeast domain. Joints and minor bedding plane shears are the only structural elements recognized (CEG, 1998).

The central domain rocks, bounded by faults with normal movement, are intensely fractured, faulted, and folded. This domain contains the greatest amount of deformation exposed in the trench and characteristically exhibits bedding plane gouge, flexural slip folding, and high-angle faulting (CEG, 1998).

The northwest domain consists of gentle, southeast-dipping, Zone 1 strata. Small-scale reverse faults and joints are the predominant structural elements. Shallow bedding dips recorded in this structural domain reflect the limb of the Demster Beach Anticline; this dip appears in core boring data northwestward (CEG, 1998).

2.5.1.2.5.3.4 Demster Zone Rock Pit I

Rock Pit I, excavated 20 feet (6.1 m) to the south of the Trench II centerline, provided a three-dimensional evaluation of the fold/fault deformation and allowed sampling of geological materials for age analysis and observation of any crosscutting mineralization. The excavated limits of Rock Pit I are primarily the central structural domain with limited vertical exposures of the other two structural domains in Trench II. The strata exposed in Rock Pit I are essentially upper Zone I with minor amounts of Zone 2 strata (CEG, 1998).

The principal brittle structural features exposed in Rock Pit I are faults, folds, and fractures.

2.5.1.2.5.3.5 Demster Zone Rock Pit II

Rock Pit II was excavated along the toe of the northeast trench wall to aid in evaluation of three-dimensional aspects of the deformation and to explore for crosscutting mineralization. This rock pit is in the central structural domain of Trench II and primarily exposes flexural slip folds and normal faults. Drag of beds associated with the normal faulting is prominent on both walls. The dragged Zone 2 strata show minor small-scale thrusts with flexural and bedding slip (CEG, 1998).

2.5.1.2.5.3.6 Demster Zone Joints

Six joint sets were identified in the vicinity of the Demster Structural Zone with orientations as follows, in order of abundance:

	Strike	Dip
Set I	N7 4E	High-angle
Set II	N44E	High-angle
Set III	N44W	High-angle
Set IV	N13E	High-angle
Set V	N38E	Low-angle
Set VI	N6 9W	High-angle

Fractures in the immediate vicinity of the Demster Structural Zone exhibit pervasive calcite and minor sulfide mineralization. Calcite mineralized joints decrease in abundance away from the Demster Structural Zone.

Analysis of the joint trends suggests a relationship between folding, faulting, and jointing of the Demster area. Folds identified from analysis of borehole data trend approximately N 45 E. Joint Sets II and III are essentially parallel and perpendicular, respectively, to the fold axis and are apparently tensional in origin. Joint Sets I and IV occur at approximately 30-deg angles to the N 45 E fold trend and apparently originated due to shear (CEG, 1998).

Set V is mainly confined to the Demster Structural Zone and appears to be associated with flexuring and bedding-plane-slip. These joints are probably contemporaneous with reverse faulting. Joint Set VI may be related to the folding (CEG, 1998).

Reverse fault movement appears to accentuate the dip of Set II in the upturned beds of the southeast domain. Also, faults coinciding with the trend of Set I reflect the reverse displacement observed throughout the northwest section of Trench II. Thus it appears that Joint Sets I and II developed prior to reverse faulting and are related to folding. Joint Sets I and II also served as planes of weakness during the normal phase of deformation. Within Trench II, these trends coincide with those of faulting (CEG, 1998).

Based on structural evidence from areas investigated, Joint Sets I, II, III, and IV appear to be contemporaneous with the regional northeast folding. These four sets were further accentuated during the subsequent reverse faulting phase, and Set V, localized joints, may have developed at this time. Within the central structural domain, a readjustment of Joint Sets I and II occurred at the time of normal faulting, the second phase of deformation (CEG, 1998).

2.5.1.2.5.3.7 Demster Zone Mineralization

Epigenetic mineralization in the trench proper and adjacent borings is primarily calcite with varying amounts of sulfides. Epigenetic calcite and sulfide assemblages are well developed in breccia zones, joints, and faults. This mineral assemblage is predominantly associated with

sandstones and, to a lesser extent, siltstones. Gouge and shales are barren of visible calcite veins but are, themselves, calcareous (CEG, 1998).

Sulfide assemblages are essentially undeformed and generally predate calcite. Recognized sulfides are pyrite, marcasite, sphalerite, and chalcopyrite. Sulfur isotope analysis indicates that these sulfides were derived primarily by bacteriological reduction of sulfate in the sedimentary environment. Thus, isotope data preclude a hydrothermal source for these sulfides (CEG, 1998).

Fluid inclusion studies on vein calcite indicate a range of temperatures from 167 °F to 356 °F (75 °C to 180 °C). Diagenetic temperatures of the Oswego Sandstone range from 345 °F to 349 °F (174 °C to 176 °C) based on the studies of the NMP Unit 2 site (Section 2.5.1.2.6). Fluid inclusion data indicate that the vein calcite was deposited at temperatures similar to those during diagenesis.

Petrologic studies indicate a definite paragenetic sequence for the calcite mineralization. Field data concerning fractures and breccias and the paragenetic sequence indicate that deformation occurred after sediment lithification and prior to last stage of calcite mineralization. The paragenesis of the vein calcite demonstrates two minor deformation events, but the last stage of calcite mineralization is postdeformation. Further evidence for this is recorded in Rock Pit I where a small vein of calcite intrudes the main gouge zone and is not offset. Petrologic and fluid inclusion data indicate that the postlithification deformation and mineralization have not been disturbed since the formation of late-stage calcite (CEG, 1998).

2.5.1.2.5.3.8 Demster Zone Mineralogical Studies

Mineralogical studies were undertaken to determine the type, origin, and possible age(s) of minerals associated with folding and faulting in the Demster Structural Zone. Several techniques and investigations were used to identify the mineral assemblages and distinct mineralogical episodes and to determine the possible age(s) of faulting.

The studies consisted of two separate approaches: one examined the formation and nature of the vein minerals, and the other examined the gouge minerals for suitable material to be dated by the K-Ar method. Investigation of the vein minerals included: microscopic examination in transmitted and reflected light; inspection of the cathodoluminescence of the calcites; study of the fluid inclusions in the calcites; and an analysis of the sulfur isotope ratios from the sulfides. Investigation of the gouge minerals included X-ray diffraction and radiometric age determination by the K-Ar method.

An exact age of faulting and last movement cannot be assigned based on the mineralogical studies; yet, the cumulative evidence does demonstrate reasonable consistency. Fluid inclusion studies indicate that the calcite formed at depth, with an overlying rock column of approximately 1.2 miles (2 km) or more. Sulfur isotope data indicate very high d34S values, and most of the sulfide was produced by bacterial reduction of limited sulfate. Sulfur isotope data eliminate the possibility of an igneous mass as the source of the mineralizing fluid for the sulfides and calcite. Explanation of the fluid inclusion temperatures involving unknown magmatic activity must be precluded, because only nonmagnetic sulfides are present in the veins. Detailed petrographic studies of the vein minerals agree with this hypothesis (CEG, 1998).

All deformational features in the calcite are minor. Deformation occurs in the middle of the mineral sequence. Furthermore, deformation apparently was not sufficiently pervasive to open new fractures in the preexisting mineralized areas. The last stages of the mineral sequence are not deformed. Detritus deposited during this sequence may be related to the stress relaxation interval of the structures (CEG, 1998).

Potassium-Argon (K-Ar) age determinations yield an age of approximately 400 million yr for samples of clays. However, the similarities of the clay mineralogy of the gouge samples to control samples, and the probability of partial resetting of argon in the analyzed clays, prevent a conclusive quantitative determination of the age of minerals and time of last movement of the Demster Structural Zone (CEG, 1998).

2.5.1.2.5.3.9 Structural Synthesis of Demster Zone

Structural data substantiated by the stratigraphic sequence in the trench vicinity indicate two phases of folding and faulting for the Demster Structural Zone. These multiple deformation events have produced three separate, small-scale deformation zones. Each deformation zone in part exhibits the effects of the overall fold/fault deformation and no movement has been identified since late calcite mineralization (CEG, 1998).

Sequentially, the structural deformation appears to be of two stages or phases. The first stage of apparent compression resulted in a series of broad, low-amplitude, eastward-verging, southwest-plunging folds (Demster Beach and Mexico Anticlines and New Haven Syncline) which account for the main stratigraphic offset. This stage is manifested by a gentle southeast dip at the extremities of Trench II. With continuing compression, the steep limb of the Demster Beach Anticline was faulted in a reverse sense rather than in a left-lateral strike-slip sense. Associated with the reverse faulting are small-scale, eastward-verging, northeast-plunging folds. This folding style is recognized only in the intensely deformed strata of the central structural domain of Trench II and may not have developed along the entire length of the Demster Structural Zone. The exact stratigraphic displacement due to reverse faulting could not be ascertained at the trench exposure because the second-stage structural deformation, normal faulting, modified the offset due to reverse faulting (CEG, 1998).

Normal faulting resulting from apparent extension, the final deformational event, truncated the limbs of the small-scale folds and displaced the main reverse fault at Trench II. This relaxation of the compressional forces resulted in outliers of Zone 2 strata in the central structural domain (CEG, 1998).

Based on petrologic evidence and bedrock mapping of the structural features, the last stage of epigenetic calcite mineralization was emplaced after the normal fault movement. However, the earliest phases of mineralization may have occurred prior to the end of the deformation, as shown by the twinning, crushing, and detritus events identified in the paragenetic sequence. Fracturing associated with the folding and faulting provided channelways for the calcite mineralization (CEG, 1998).

Subsurface data reveal the same structural style as that exposed in Trench II, and stratigraphic offset due to faulting is also apparently similar. Normal faulting appears to die out several thousand feet to the southwest, and the main stratigraphic offset there is caused by folding. Geophysical studies along the projected deformation trace indicate a lack of continuity of fracturing (CEG, 1998).

2.5.1.2.5.4 Demster Zone Structural Contour Anomalies and Geophysical Correlations

2.5.1.2.5.4.1 Demster Zone Structure Contours

Stratigraphic and sedimentological studies infer an early-Paleozoic northeast-trending subsurface structure. Rickard, using selected deep well data, studied the subsurface stratigraphy and structure of the Cambrian and Ordovician carbonates of New York (Rickard 1977). Structure contours were drawn on the tops of the Precambrian basement, the Knox unconformity, and the Trenton Group. As pointed out by Rickard, subsurface data in many areas are sparse; however, his structure contour maps demonstrate apparent north-trending

subsurface faulting and folding and may show only a small portion of those structures actually present.

To confirm these structure contour anomalies and to contour horizons higher than the Trenton top and possibly relate these anomalies to the Demster Zone, deep exploration borehole data from Kreidler et al (1972) were contoured (CEG, 1998).

Subsurface data demonstrate three salient results: 1) Ordovician through Devonian strata are deformed by folding with or without faulting; however, the true style and nature of these structure contour flexures are indeterminate, 2) the apparent north-trending anomalies of Rickard are more north-northeast to northeast in orientation, and 3) the Clarendon-Linden structure, although not included on these maps, is expressed in all horizons up to Mid-Devonian where the structure apparently becomes a monoclinal element (CEG, 1998).

Interpretation of the subsurface data not only verified Rickard's Trenton anomalies but extended the contours higher into the stratigraphic section. The northeasterly trend is coincident with regional geophysical and basement anomalies. Whether structure contour anomalies are due to faulting or folding or both is uncertain. Many could be interpreted as faults, and indeed drilling data, supported by geophysical data, infer basement involvement. Basement deformation is inferred particularly where retrogressive metamorphism of amphibolite grade Grenville basement is coincident with both structure contour and gravity anomalies. The deformation style of this apparent basement involvement on the overlying Paleozoics is uncertain and may include compaction structures, growth faulting, folding, and faulting (CEG, 1998).

2.5.1.2.5.4.2 Demster Zone and Nine Mile Point Geophysical Correlations

The gravity and aeromagnetic data covering the region surrounding the NMPNS site are mutually consistent in defining a northeast-trending structural fabric in the crystalline basement. Previously, Rickard (1973) had identified essentially north-south basement trends based on limited boring data. The northeast trend is similar to the structural fabric of the Central Metasedimentary Belt (CMB) of the Grenville Province located north of the site and in the region west of the site (CEG, 1998).

The geophysical data consist of gravity and aeromagnetics. The gravity data are responsive to density changes, whereas magnetic data are responsive to susceptibility changes in the basement rock. Although it is an oversimplification, the gravity anomalies in this area can be attributed, at least in part, to basement rock topography whereas aeromagnetic data are more related to basement lithologies. In some instances, gravity highs are coincident with magnetic lows, whereas in other locales gravity lows are located in the same area as magnetic highs. However, this apparent inconsistency is resolved with borehole data and regional geologic information. Several of the broad and "simple" gravity anomalies are characterized by a complex series of magnetic anomalies. The geophysical data indicate that the crystalline basement in this portion of New York State is composed of a complex assemblage of rock types within a dominantly northeast-trending structural fabric (CEG, 1998).

The gravity and magnetic data for central New York provide confirmation of inferred structures and indicate a northeast fabric for the region. The geophysical data support the interpretation that the probable faulting in the Cross Lake area is related to basement uplift and probable alteration of the basement rocks along a northeast trend. The structural high inferred in the Camden area is supported by a gravity high at the same locality. The Demster Zone proper does not have a distinctive geophysical signature. This would suggest either limited or no direct basement control; however, it could have resulted as an indirect consequence of basement deformation (CEG, 1998).

2.5.1.2.5.4.3 Demster Zone Summary

Structural and stratigraphic relationships in the Demster Structural Zone show that the New Haven area has been deformed by two sequences of paleotectonic activity: initial broad folding culminating in reverse faulting and later normal faulting. No other tectonic activity is documented at the Demster Structural Zone. Calcite paragenesis indicates no deformation subsequent to the youngest sequence of minerals, and Pleistocene surficial sediments overlying the fault zone are not deformed (CEG, 1998).

The K-Ar data may suggest a Middle-Paleozoic (Silurian) time of deformation for the Demster Structural Zone. The reconstructed geologic column, associated geologic history, and other interpretations of data suggest a Middle- to Late-Paleozoic age. A younger Late-Jurassic age cannot be ruled out, although the sulfur isotope data do not strongly support this age. The uncertainty of the timing of alkaline emplacement based on the geochemical data, plus lack of documented high-angle Late-Mesozoic faulting, place constraints on this time interval. Consequently, a Middle- to Late-Paleozoic age is inferred for the final development of the Demster Structural Zone (CEG, 1998).

The deformation style, the northeast trend of the structural elements, regional stratigraphy, and analytical data are in agreement that the Ordovician strata in northern Oswego County, and conceivably the underlying Cambrian and Ordovician strata in central New York, have undergone broad areal folding with variable reverse and normal faulting. Combined geologic and geophysical data indicate that the Demster Structure is not capable (CEG, 1998).

2.5.1.2.6 Relationship of NMP Unit 2 Site Structures to Near-Site Structures

The Demster Structural Zone of folding and faulting trends northeastward. Its surface trace is approximately 2.8 miles (4.6 km) southeast of the NMPNS site. This zone is characterized by tight to broad, eastward-verging, asymmetric, locally-overturned folds; flexural slip; reverse faulting; normal faulting; and associated drag folding. The deformation resulted from at least two phases of essentially contemporaneous movement: an initial stage of folding and reverse faulting followed by a stage of relaxation and normal faulting (CEG, 1998).

The Demster faults, both normal and reverse, strike northeasterly and dip steeply to the northwest; maximum throws are no more than a few feet. They occur in an elongate domain of closely jointed and highly broken rock that is transected by several zones of breccia-free gouge with trends both parallel and normal to the strike of bedding and the strike of the faults. In this ground there is no evidence of dilation such as that observed at NMP Unit 2, where the gouge and breccia are packed tightly along the nearly vertical faults. None of the faults offset the surface of bedrock or cut the overlying Quaternary glacial and lacustrine sediments. These faults are probably Paleozoic (possibly Alleghanian) in age, and certainly are no younger than Mesozoic in age. They are not capable faults (CEG, 1998).

The geologic structure at the NMP Unit 2 site (Section 2.5.1.2.3) is expressed by two steeply dipping, northwesterly striking normal faults that bound a block of gently dipping sedimentary rocks that are cut at shallow depths by a series of subparallel thrust faults grossly concordant with the host-rock bedding. The uppermost thrust fault dips southeastward at low angles across the bedrock strata where it is exposed in the excavation for the NMP Unit 2 Radwaste building. There the leading portion of the faulted rock is crumpled and dilated in very close similarity to the valley-bottom faults of the Upper Ohio River valley that were produced as a result of erosion of the bedrock in the river valley and the consequent reduction of the least principal stress in the bedrock (s3). The relationships observed along the thrust zone also are similar to those associated with shallow-seated breaks noted in many New England granite

quarries, where small thrust movements and numerous expressions of dilatancy also represent geologically young stress relief related to the ground surface (CEG, 1998).

The openwork along the NMP Unit 2 Radwaste fault contains in-fillings of lacustrine sediments containing pollen, which indicates a late-Wisconsinan age (10,000 to 13,500 yr B.P.) for those sediments. The faulting appears to have been geologically young, with movements that probably occurred during Pleistocene time in response to episodes of glacial loading and unloading. Holocene (post-Pleistocene) movements have been small if they have occurred at all. It cannot be demonstrated that no Holocene movements have occurred, as no dated in-filling sediments or other reference features extend entirely across the zones of disturbance (CEG, 1998).

Displacement of late-Pleistocene lake sediments has occurred along the southerly bounding fault, the NMP Unit 2 Cooling Tower fault. Both of the normal faults are marked by thin zones of gouge, and both have displacements of a few feet or less (CEG, 1998).

The strata at the NMP Unit 2 site are essentially undisturbed except right at the faults, in contrast to the broken and highly disturbed strata in the Demster Zone. The faulting in the Demster Zone may well have been of direct tectonic origin, whereas the much younger faulting at the NMP Unit 2 site, and especially that along the NMP Unit 2 Radwaste thrust, is readily explainable as a result of local stress relief unrelated to major or contemporary tectonic activity. Such relief, as widely expressed in this and other regions, derives through failure, within a highly anisotropic stress field, of rocks containing a combination of residual strain energy and strain energy inherited from earlier tectonic activity (CEG, 1998).

As discussed in Section 2.5.1.2.3, reduction of the vertical load (s3) as a result of Pleistocene glacial erosion facilitated westward slip of the NMP Unit 2 Radwaste structure's hanging wall block by reducing the shear resistance of the block to stresses acting subhorizontally (s1). This is similar to the mechanics of formation of the valley-bottom faults in the Upper Ohio River basin and of sheet structure and associated exfoliation phenomena in more massive rocks of the northeastern United States (CEG, 1998).

Formation of the bounding normal faults at NMP Unit 2 probably resulted from adjustments during late stages of the Appalachian Basin as the bottom ceased to subside and oxidizing processes began. Minor Quaternary movements could be expected in the form of much younger readjustments associated with erosional unloading of the bedrock section (CEG, 1998).

The Demster folds and faults and the NMP Unit 2 Radwaste thrust faulting are quite different geologic structures in terms of respective sizes, extents, attitudes, degrees of brecciation, origins, and ages. The Demster Zone is tectonic in origin, whereas the NMP Unit 2 Radwaste structure is a result of much younger unloading by accelerated erosion. In both occurrences the causative processes are no longer active, and the faults are not capable (CEG, 1998).

The steeply dipping normal faults, striking northeasterly at New Haven and northwesterly at NMP Unit 2 , are related in origin to late-stage processes in the evolution of the Appalachian Basin, and perhaps to the extensional forces that opened near-vertical channels for emplacement of ultrabasic dikes in the adjacent Finger Lakes and Syracuse region during Mesozoic time. Deformation of the Quaternary lake sediments along the Cooling Tower fault at NMP Unit 2 evidently resulted from localized buckling related to removal of the ice load following recession of the Wisconsinan ice sheet. These normal faults are not tectonically capable (Section 2.5.1.2.3) (CEG, 1998).

The most detailed subsurface exploration of the site was performed by Dames & Moore as part of the original FSAR (Niagara Mohawk, 1978a; Niagara Mohawk, 1980) for the existing NMP Unit 2 foundation and supporting structures (CEG, 1998).

2.5.1.2.7 Site Area Geologic Hazard Evaluation

No geologic hazards have been identified within the NMP3NPP site area. No geologic units at the site are subject to dissolution. Localized deformation zones, associated with minor faults, were encountered in the excavations for NMP Unit 2 (CEG, 1998). Deformation zones have not been encountered in the site investigation for NMP3NPP. Because the NMP3NPP plant site is located at an elevation of approximately 270 feet (83 m) msl and approximately 1,300 feet (396 m) from the Lake Ontario shoreline, it is unlikely that shoreline erosion or flooding will impact the NMP3NPP site. Geological hazards within the site region are described in Section 2.5.1.1. The hazards discussed are not considered to have an adverse impact on the site. However, several phenomena are considered to be potentially capable of resulting in small movements within the site bedrock. The potential impact of these phenomena has been considered in the design of the site foundations.

2.5.1.2.8 Site Engineering Geology Evaluation

2.5.1.2.8.1 Engineering Soil and Rock Properties and Behavior of Foundation Materials

Engineering soil and rock properties, including index properties, static and dynamic strength, and compressibility are discussed in Section 2.5.4. Variability and distribution of properties for the foundation bearing rock and soils will be evaluated and mapped as the excavation is completed. Settlement monitoring will be based on analyses performed for the final design.

All safety-related engineering structures at the NMP3NPP site are founded on bedrock. Detailed evaluations of the engineering geology aspects of the geologic features at the NMP Unit 2 site indicate that conditions of in situ stress, bedrock lithology, rock mass anisotropy, and groundwater fluctuations are important elements that had to be considered in the design. In addition to the above, the dynamic behavior of the site during earthquakes is discussed in Section 2.5.2.5 and Section 2.5.4.2.2. Specific discussion of the subsurface materials is provided in Section 2.5.4.

In situ stresses in the bedrock, ranging from low-magnitude tensile stresses to compressive stresses of more than 2,000 psi (141 kg/sq cm), were measured at the NMP Unit 2 site. The NMP Unit 2 reports detailed interpretations of the wide range of stresses with respect to the geologic structures at the site (CEG, 1998). Section 2.5.4.1.4 discusses these results with regard to the engineering geology of the site.

The anisotropic character of the bedrock is related to the variation of physical properties of the rock resulting from compositional variations. Static properties have been determined and are presented in Section 2.5.4.2. Dynamic properties were determined from geophysical surveys, and the results are contained in Section 2.5.4.4.

The design criteria developed in consideration of various aspects of the site engineering geology are discussed in Section 2.5.4.

2.5.1.2.8.2 Zones of Alteration, Weathering, and Structural Weakness

No unusual weathering profiles have been encountered during the site investigation. Rock obtained from borings was generally fresh and unweathered. No dissolution is expected to

affect foundations. Any noted desiccation, weathering zones, joints or fractures will be mapped during excavation and evaluated.

2.5.1.2.8.3 Deformational Zones

Localized deformation zones, associated with minor faults, were encountered in the excavations for NMP Unit 2. There are several zones of bedrock deformation that intersect the NMP Unit 2 site excavations. The cooling tower at NMP Unit 2 (Figure 2.5-72) was relocated to avoid being founded above a fault along which Quaternary buckling had occurred (Section 2.5.1.2.3). Several Quaternary, low-angle thrust faults intersect the main site excavations (Figure 2.5-72) and are described in Section 2.5.1.2.3. These faults were judged by a panel of experts to have a negligible impact on the site engineering structures (CEG, 1998). Surface faulting is discussed in Section 2.5.3.

Deformation zones have not been encountered in the site investigation for NMP3NPP. Excavation mapping is required during construction and any noted deformational zones will be evaluated. No capable tectonic sources as defined by Regulatory Guide 1.165 (NRC, 1997) and Regulatory Guide 1.208 (NRC, 2007b) exist in the NMP3NPP site region.

2.5.1.2.8.4 Prior Earthquake Effects

Studies of the NMP Unit 1 and Unit 2 excavations, available outcrops, and exposures along the shore of Lake Ontario have not indicated any evidence for earthquake activity that affected the unconsolidated deposits. There is no evidence of earthquake-induced liquefaction in the State of New York (Crone, 2000; Wheeler, 2005).

2.5.1.2.8.5 Effects of Human Activities

No mining operations, excessive extraction or injection of groundwater or impoundment of water has occurred within the site area that can affect geologic conditions. Hazards related to man's activities within the site region are a described in Section 2.5.1.1. The hazards discussed are not considered to have an adverse impact on the site. However, several phenomena (e.g. rock squeeze) are considered to have the potential to create small movements within the site bedrock. The potential impact of these phenomena has been considered in the design of the site foundations in Section 2.5.4 and in Section 2.5.5.

2.5.1.2.8.6 Site Groundwater Conditions

A detailed discussion of groundwater conditions is provided in Section 2.5.4.12. Potential large-scale prehistoric fluctuation of the groundwater table is a factor which, because of the stress conditions at the site, could influence the stability of planes of structural weakness in the bedrock mass. This aspect is discussed with respect to historical geology of the site in Section 2.5.1.1. Further information on groundwater conditions is presented in Section 2.5.4.}

2.5.1.3 References

{This section is added as a supplement to the U.S. EPR FSAR.

Aggarwal, 1978. Earthquakes, Faults, and Nuclear Power Plants in Southern New York and Northern New Jersey, Science, Volume 200, April 28, 1978, Pages 425-429, Y.P. Aggarwal and L.R. Sykes.

Atken, 1993. Chapter 13: Evolutionary Models and Tectonic Comparisons, In: Sedimentary Cover of the Craton in Canada, D.F. Stott and J.D. Aitken (ed), Geological Survey of Canada, Geology of Canada, No 5, 1993, Pages 799-808, J.D. Aitken.

Alter, 1985. In Situ Velocity Estimates for Shallow Crystalline Rocks in the Adirondack Mountains, New York and the Laramie Range, Wyoming, Bulletin of the Seismological Society of America, Volume 75, No. 5, 1985, Pages 1363-1369, B. Alter.

Anderson, 1978. Punctuated Aggradational Cycles (PACS) in Middle Ordovician and Lower Devonian Sequences, New York State Geological Association Guidebook 50th Annual Meeting, Syracuse New York, 1978, Pages 204-224, E.J. Anderson and P.W. Goodwin.

Andrews, 1993. Chapter 8: Quaternary Geodynamics in Canada, In: Quaternary Geology of Canada and Greenland, R.J. Fulton (ed), Geological Survey of Canada, Geology of Canada, No 1, 1989, Pages 543-572, J.T. Andrews and W.R. Peltier.

Armbruster, 1987. The 23 April 1984 Martic Earthquake and the Lancaster Seismic Zone in Eastern Pennsylvania, Bulletin of the Seismological Society of America, Volume 77, No. 3, June 1987, Pages 877-890. J.G. Armbruster and L. Seeber.

Baird, 2004. Deformation of the Diana Syenite and Carthage-Colton Mylonite Zone: Implications For Timing of Adirondack Lowlands Deformation. In: Tollo R.P., Corriveau, L., McLelland, J. and Bartholomew, M.J. (eds), Proteozoic Tectonic Evolution of the Grenville Orogen in North America, Geological Society of America Memoir 197, 2004, pp. 285-297. G.B. Baird and W.D. MacDonald.

Bankey, 2002. Magnetic Anomaly Map of North America, U.S. Geological Survey, 1 sheet, scale 1:10,000,000, V. Bankey, A. Cuevas, D. Daniels, C. Finn, I. Hernandez, P. Hill, R. Kucks, W. Miles, M. Pilkington, C. Roberts, W. Roest, V. Rystrom, S. Shearer, S. Snyder, R. Sweeney, and J. Velez, 2002.

Barber, 1978. Deformation Structures in Lower Paleozoic Rocks, Northwestern New York, New York State Geological Association Guidebook 50th Annual Meeting, Syracuse New York, 1978, Pages 48-57, B.G. Barber and J.T. Bursnall.

Bent, 1996. Source Parameters of the Damaging Cornwall-Massena Earthquake of 1944 from Regional Waveforms, Bulletin of the Seismological Society of America, Volume 86, No. 2, Pages 489-497, A.L. Bent, 1996.

Boyce, 2002. Basement-controlled Faulting of Paleozoic Strata in Southern Ontario, Canada: New Evidence from Geophysical Lineament Mapping, Tectonophysics, Volume 353, 2002, Pages 151-171, J.I. Boyce and W.A. Morris.

Braile, 1989. Chapter 28: Seismic Properties of the Crust and the Uppermost Mantle of the Conterminous United States and Adjacent Canada, In: Pakiser, L.C.; Mooney, W.D., Geophysical Framework of the Continental United States, Geological Society of America, Memoir 172, 1989, L.W. Braile, W.J. Hinze, R.R.B. von Frese and G.R. Keller.

Bretsky, 1970. Late Ordovician Benthic Marine Communities in North-Central New York, Bulletin 414, New York State Museum and Science Service, 34 pp, P. Bretsky, 1970.

Bretsky, 1978. Benthic Marine Communities in the Upper Ordovician Clastics of the Tug Hill Region, New York, New York State Geological Association Guidebook 50th Annual Meeting, Syracuse New York, 1978, Pages 189-2003, P. Bretsky and D. Thomas.

Brown, 1983. Adirondack-Appalachian Crustal Structure: The COCORP Northeast Traverse, Geological Society of America Bulletin, Volume 94, No. 10, 1983, Pages 1173-1184, L. Brown, C. Ando, S. Klemperer, J. Oliver, S. Kaufman, B. Czuchra, T. Walsh and Y.W. Isachsen.

Carr, 2000. Geologic Transect Across the Grenville Orogen of Ontario and New York, Canadian Journal of Earth Sciences, Volume 37, 2000, Pages 193-216, S.D. Carr, R.M. Easton, R.A. Jamieson and N.G. Culshaw, .

CEG, 1998. Nine Mile Point Unit 2 USAR, 1998, Docket No. 50-410, Constellation Energy Group

CFR, 2007. Geologic and Seismic Siting Criteria, Title 10, Code of Federal Regulations, Part 100.23.

Coblentz, 1995. Statistical Trends in the Intraplate Stress Field, Journal of Geophysical Research, Volume 100, No B10, October 10, 1995, Pages 20,245-20,255, D.D. Coblentz and R.M. Richardson.

Cornell, 2005. Classic Localities of the Black River and Trenton Groups (Upper Ordovician) in the Black River Valley: Revisited Through Traditional and Sequence Stratigraphy, New York State Geological Association Guidebook 77th Annual Meeting, Oswego New York, 2005, Pages 45-74, S. Cornell, Andrews, J., Agle, P., and D. Thomas.

Crone, 2000. Data for Quaternary faults, liquefaction features, and possible tectonic features in the Central and Eastern United States, east of the Rocky Mountain front, Open File Report 00-260, U.S.G.S., 2000. A. J. Crone and R. L. Wheeler.

Dahlen, 1981. Isostacy and the ambient state of stress in the oceanic lithosphere, Dahlen, F. A., Jour Geophys Res. V 86 No. B9, Pages 7801-7807.

Daneshfar, 2002. Spatial Relationships between Natural Seismicity and Faults, Southeastern Ontario and North-Central New York State, Tectonophysics, Volume 353, 2002, Pages 31-44, B. Daneshfar and K Benn.

Davidson, 1998. Chapter 3: An Overview of Grenville Province Geology, Canadian Shield, In: Geology of the Precambrian Superior and Grenville Provinces and Precambrian Fossils in North America, S.B. Lucas and M.R. St-Onge, Geological Survey of Canada, Geology of Canada, No 7, 1998, Pages 205-270, A. Davidson.

Dawers, 1991. Intraplate Faults Revealed in Crystalline Bedrock in the 1983 Goodnow and 1985 Ardsley Epicentral Areas, New York, Tectonophysics, Volume 186, Pages 115-131, N.H. Dawers and L. Seeber, 1991.

Dewey, 1989. Chapter 25: Earthquakes, Faults, and the Seismo Tectonic Framework of the Contiguous United States, In: Pakiser, L.C.; Mooney, W.D., Geophysical Framework of the Continental United States, Geological Society of America, Memoir 172, 1989, J.W. Dewey, D.P. Hill, W.L. Ellsworth and E.R. Engdahl.

Dineva, 2004. Seismicity of the Southern Great Lakes: Revised Earthquake Hypocenters and Possible Tectonic Controls, Bulletin of the Seismological Society of America, Volume 94, No. 5, 2004, Pages 1902-1918, S. Dineva, D. Eaton and R. Mereu.

Drake, 1989. The Taconic Orogen, in Hatcher, R.D., William T., and Viele, G.W. eds., The Appalachian-Ouachita Orogen in the United States, DNAG, Volume F-2, Pages 101-177, A. Drake Jr., A. Sinha, J. Laird, and R. Guy, 1989.

Eaton, 2006. Crustal Thickness and V_P/V_S Variations in the Grenville Orogen (Ontario, Canada) from Analysis of Teleseismic Receiver Functions, Tectonophysics, Volume 420, 2006, Pages 223-238, D.W. Eaton, S. Dineva and R. Mereu.

Ebel, 1996. The Seventeenth Century Seismicity of Northeastern North America, Seismological Research Letters, Volume 67, No 3, May/June, 1996, Pages 51-68, J.E. Ebel.

Ebel, 2000. Paleoseismicity: Seismicity Evidence for Past Large Earthquakes, Seismological Research Letters, Volume 71, No 2, March/April 2000, Pages 283-294, J.E. Ebel, K. Bonjer, M. Oncescu.

Ebel, 2002. Earthquakes in the Eastern Great lakes Basin from a Regional Perspective, Tectonophysics, Volume 353, 2002, Pages 17-30, J.E. Ebel and M. Tuttle.

Ebel, 2006. The Cape Ann, Massachusetts Earthquake of 1755: A 250th Anniversary Perspective, Seismological Research Letters, Volume 77, No 1, Jan/Feb 2000, Pages 74-86, J.E. Ebel.

Engelder, 1979. The Nature and Deformation Within the Outer Limits of the Central Appalachian Foreland Fold and Thrust Belt in New York State, Tectonophysics, Volume 55, June, 1979, Pages, 289-310, T. Engelder.

Engelder, 1980. On the Use of Regional Joint Sets as Trajectories of Paleostress Fields During the Development of the Appalachian Plateau, New York, Journal of Geophysical Research, Volume 85, No B11, November, 1980, Pages 6319-6341, T. Engelder and P. Geiser.

Engelder, 1982a. Is There a Genetic Relationship Between Selected Regional Joints and Contemporary Stress Within the Lithosphere of North America?, Tectonics, Volume1, No 2, April, 1982, Pages 161-177, T. Engelder.

Engelder, 1982b. Reply, Tectonics, Volume 1, No 5, October, 1982, Pages 465-470, T. Engelder.

Engelder, 1985. Loading Paths to Joint Propagation During a Tectonic Cycle: an Example From the Appalachian Plateau, U.S.A., Journal of Structural Geology, Volume 7, Nos. 3 / 4, 1985, Pages 459-476, T. Engelder

Engelder, 1993. Curving Cross joints and the Lithospheric Stress Field in Eastern North America, Geology, Volume 21, September, 1993, Pages 817-820, T. Engelder and M.R. Gross.

Engelder, 2001. Horizontal Slip Along Alleghanian Joints of the Appalachian Plateau: Evidence Showing That Mild Penetrative Strain Does Little to Change the Pristine Appearance of Early Joints, Tectonophysics, Volume 336, July, 2001, Pages 31-41, T. Engelder, B.F. Haith and A. Yo

Engelder, 2006. Early Jointing in Coal and Black Shale: Evidence for an Appalachian-Wide Stress Field as a Prelude to the Alleghanian Orogeny, Geology, Volume 34, No 7, July, 2006, Pages 581-584, T. Engelder and A. Whitaker

Engelder, 2007. Propagation Velocity of Joints: A Debate Over Stable vs. Unstable Growth of Cracks in the Earth, in: Quinn, G.D.; Varner, J.R.; Wightman, M., eds., Fractography of Glasses and Ceramics V, American Ceramic Society, Westerville, OH, 2007, Pages 500- 525, T. Engelder.

EPRI, 1986. Seismic Hazard Methodology for the Central and Eastern United States, EPRI Report NP-4726, Electric Power Research Institute, July 1986.

Evans, 1989a. Appalachian Stress Study 1, A Detailed Description of In Situ Stress Variations in Devonian Shales of the Appalachian Plateau, Journal of Geophysical Research, Volume 94, No B6, June 10, 1989, Pages 7129-7154, K.F. Evans, T. Engelder and R.A. Plumb.

Evans, 1989b. Appalachian Stress Study 2, Analysis of Devonian Shale Core: Some Implications for the Nature of Contemporary Stress Variations and Alleghanian Deformation in Devonian Rocks, Journal of Geophysical Research, Volume 94, No B6, June 10, 1989, Pages 7155-7170, K.F. Evans, G. Oertel and T. Engelder.

Faill, 1997a. A Geologic History of the North-Central Appalachians. Part 1: Orogenesis from the Mesoproterozoic through the Taconic Orogeny, American Journal of Science, Volume 297, June, 1997, Pages 551-619, R.T. Faill.

Faill, 1997b. A Geological History of the North-Central Appalachians, Part 2: The Appalachian Basin from the Silurian through the Carboniferous, American Journal of Science, Volume 297, Summer, 1997, Pages 729-761, R.D. Faill.

Faill, 1998. A Geologic History of the North-Central Appalachians, Part 3: The Alleghany Orogeny, American Journal of Science, Volume 298, February, 1998, Pages 131-179, R.T. Faill.

Fakundiny, 2002a. Editorial, Neotectonics and Seismicity in the Eastern Great Lakes Basin: Introduction, Tectonophysics, Volume 353, 2002, Pages 1-2, R.H. Fakundiny, C.F. M. Lewis and R.D. Jacobi

Fakundiny, 2002b. Seismic-reflection Profiles of the Central Part of the Clarendon-Linden Fault System of Western New York in Relation to Regional Seismicity, Tectonophysics, Volume 353, 2002, Pages 173-213, R.H. Fakundiny and P.W. Pomeroy.

Fenneman, 1938. Physiography of the Eastern United States, McGraw Hill, 714 pp., N.M. Fenneman.

Fenneman, 1946. Physical Divisions of the United States, U.S. Geological Survey, 1:7,000,000-scale map, N. Fenneman and D. Johnson, 1946.

Fischer, 1978. Engineering Geology at Nine Mile Point, New York, New York State Geological Association Guidebook 50th Annual Meeting, Syracuse New York, 1978, Pages 257-272, J.A. Fisher and H.S. Laird.

Fisher, 1977. Correlation of the Hadrynian, Cambrian and Ordovician Rocks in New York State, New York State Museum, Map and Chart Series No. 25, D.W. Fisher, 1977.

Flagler, 1966. Subsurface Cambrian and Ordovician Stratigraphy of the Trenton Group - Precambrian Interval in New York State, New York State Museum and Science Service, Map and Chart Series No. 8, C.W. Flagler, 1966.

Fleeger, 1999. Hydrologic Effects of the Pymatuning Earthquake of September 25, 1998, in Northwestern Pennsylvania, USGS, WRIR 99-4170, G.M. Fleeger and D.J. Goode, August 1999.

Fletcher, 1977. Earthquakes Related to Hydraulic Mining and Natural Seismic Activity in Western New York State, Journal of Geophysical Research, Volume 82, No. 26, Pages 3767-3780, J.B. Fletcher and L.R. Sykes, 1977.

Forsyth, 1994a. Deep Structure Beneath Lake Ontario: Crustal-scale Grenville Subdivisions, Canadian Journal of Earth Sciences, Volume 31, 1994, Pages 225-270, D.A. Forsyth, B. Milkereit, C.A. Zelt, D.J. White, R.M. Easton and D.R. Hutchinson.

Forsyth, 1994b. Seismic Images of a Tectonic Subdivision of the Grenville Orogen Beneath Lakes Ontario and Erie, Canadian Journal of Earth Sciences, Volume 31,1994, Pages 229-242, D.A. Forsyth, B. Milkereirt, A. Davidson, S. Hanmer, D. R. Hutchinson, W.J. Hinze and R.F. Mereu.

Gross, 1991. A Case for Neotectonic Joints Along the Niagara Escarpment, Tectonics, Volume 10, No 3, June, 1991, Pages 631-641, M.R. Gross and T. Engelder.

GSA, 1999. 1999 Geologic Time Scale, Geological Society of America, Compiled by A.R. Palmer and J. Geissman.

GSC, 1975. Physiographic Map of Eastern Canada and Adjacent Areas, Geological Survey of Canada, Map 1399A, 1:2,000,000-scale map, 1975.

GSC, 1987. 1:5,000,000-scale Magnetic Anomaly Map of Canada, Geological Survey of Canada.

GSC, 1998. 1:2,000,000-scale Residual Total Field Magnetic Map of the Superior and Grenville Provinces, Geological Survey of Canada.

Hack, 1989. Geomorphology of the Appalachian Highlands, R. Hatcher Jr., W. Thomas, and G. Viele, eds., The Geology of North America, Volume F-2, The Appalachian-Ouachita Orogen in the United States, Geological Society of America, J. Hack, 1989.

Hancock, 1989. Neotectonic Joints, Geological Society of America Bulletin, Volume 101, October, 1989, Pages 1197-1208, P.L Hancock and T. Engelder.

Hancock and Engelder, 1991. Meglis, I.L., Engelder, T., and Graham, E.K., 1991, The effect of stress-relief on ambient microcrack porosity in core samples from the Kent Cliffs (New York) and Moodus (Connecticut) scientific research boreholes, Tectonophyiscs, v. 186, p. 163-173.<http //www.geosc.psu.edu/~engelder/references/link089.pdf>

Harris, 1979. Sequential Development of the Appalachian Orogen Above a master Decollement - A Hypothesis, Geology, Volume 7, December, 1979, Pages 568-572, L.D. Harris and K.C. Bayer.

Hatcher, 1987. Tectonics of the Southern and Central Appalachian Internides, Annual Reviews Earth Planet Science, Volume 15, 1987, Pages 337-362, R. D. Hatcher Jr.

Hatcher, 1989. Alleghenian Orogen, in Hatcher, R.D., William, A., Viele, G., eds., The Appalachian-Ouachita Orogen in the United States, Geological Society of America DNAG, Volume F-2, p.233-318, R. Hatcher, W. Thomas, P. Geiser, A. Snoke, S. Mosher, and D. Wiltschko, 1989.

Hemant, 2007. Magnetic Anomaly Map of the World: Merging Satellite, Airborne, Marine and Ground-based Magnetic Data Sets, Earth and Planetary Science Letters, Volume 260, 2007, Pages 56-71, K Hemant, E. Thebault, M. Mandea, D. Ravat and S Maus.

Herrman, 1978. A Seismological Study of Two Attica, New York Earthquakes, Bulletin of the Seismological Society of America, Volume 68, No. 3, Pages 641-651, R.B. Herrman, 1978.

Herman, 1992. Deep Crustal Structure and Seismic Expression of the Central Appalachian Orogenic Belt, Geology, Volume 20, March 1992, Pages 275-278, G.C. Herman.

Hibbard, 2006. Hibbard, J. P., van Staal, C.R. Rankin, D.W., and Williams, H. Lithotectonic map of the Appalachian Orogenm Canada-United States of America; Geological Survey of Canada, Map 2096A, scale 1:1,500,000

Hibbard, 2007. A. Comparative Analysis of Pre-Silurian Crustal Building Blocks of the Northern and Southern Appalachian Orogen, American Journal of Science, Volume 307, p. 23, J. Hibbard, C. van Staal, and D. Rankin, 2007.

Hickman, 1985. In Situ Stress, Natural Fracture Distribution, and Borehole Elongation in the Auburn Geothermal Well, Auburn, New York, Journal of Geophysical Research, Volume 90, No B7, June 10, 1985, Pages 5497-5512, S.H. Hickman, J.H. Healy and M.D. Zoback.

Hughes, 1991. Crustal Structure of the Western New England Appalachians and the Adirondack Mountains, Journal of Geophysical Research, Volume 96, No B10, 1991, Pages 16,471-16,494, S. Hughes and J.H. Luetgert.

Hughes, 1992. Crustal Structure of the Southeastern Grenville Province, Northern New York State and Eastern Ontario, Journal of Geophysical Research, Volume 97, No B12, 1992, Pages 17,455-17,479, S. Hughes and J.H. Luetgert.

Hutchinson, 1993. Regional Stratigraphic Framework of Surficial Sediments and Bedrock Beneath Lake Ontario, Geographie Physique et Quaternaire, Volume 47, No. 3, Pages 337-352, D.R. Hutchinson, D.F.M. Lewis and G.E. Hund, 1993.

Isachsen, 1977a. Preliminary Brittle Structures Map of New York - Adirondack Sheet, New York State Museum Map and Chart Series Number 31A, 1977. Y.W. Isachsen, and W.G. McKendree.

Isachsen, 1977b. Preliminary Brittle Structures Map of New York - Hudson-Mohawk Sheet, New York State Museum Map and Chart Series Number 31B, 1977. Y.W. Isachsen and W.G. McKendree.

Isachsen, 1977c. Preliminary Brittle Structures Map of New York - Lower Hudson Sheet, New York State Museum Map and Chart Series Number 31C, 1977. Y.W. Isachsen and W.G. McKendree.

Isachsen, 1977d. Preliminary Brittle Structures Map of New York - Niagara-Finger Lakes Sheet, New York State Museum Map and Chart Series Number 31D, 1977. Y.W. Isachsen and W.G. McKendree.

Isachsen, 1977e. Preliminary Brittle Structures Map of New York, New York State Museum Map and Chart Series Number 31E, 1977. Y.W. Isachsen and W.G. McKendree.

Isachsen, 1977f. Generalized Map of Recorded Joint Systems in New York, New York State Museum Map and Chart Series Number 31F, 1977. Y.W. Isachsen and W.G. McKendree.

Isachsen, 1977g. Sources of Information for Preliminary Brittle Structures Map of New York and Generalized Map of Recorded Joint Systems in New York, New York State Museum Map and Chart Series Number 31G, 1977. Y.W. Isachsen and W.G. McKendree.

Isachsen, 2000. Geology of New York, A Simplified Account, Second Edition, New York State Museum Educational Leaflet 28, 294 pp, Y.W. Isachsen, E. Landing, J.M. Lauber, L.V. Rckard, and W.B. Rogers, 2000.

Jachens, 1989. Chapter 19: Isostatic Residual Gravity and Crustal Geology of the United States, In: Pakiser, L.C.; Mooney, W.D., Geophysical Framework of the Continental United States, Geological Society of America, Memoir 172, 1989, R.C. Jachens, R.W. Simpson, R.J. Blakely and R.W Saltus.

Jackson, 1989. Chapter 12: The Influence of The Quaternary Geology of Canada On Man's Environment, In: Quaternary Geology of Canada and Greenland, R.J. Fulton (ed), Geological Survey of Canada, Geology of Canada No. 1, Pages 701 - 738. L.E. Jackson, Jr.

Jacobi, 1993. The Southern Extension and Reactivations of the Clarendon-Linden Fault System, Geographie Physique et Quaternaire, Volume 47, No. 3, Pages 285-302, R. Jacobi and J. Fountain, 1993.

Jacobi, 2002a. Basement Faults and Seismicity in the Appalachian Basin of New York State, Tectonophysics, Volume 353, 2002, Pages 75-113, R.D. Jacobi.

Jacobi, 2002b. The Character and Reactivation History of the Southern Extension of the Seismically Active Clarendon=Linden Fault System, Western New York State, Tectonophysics, Volume 353, 2002, pages 215-262, R.D. Jacobi and J. Fountain.

Johnson, 2004. Right Lateral Oblique Slip Movements Followed by Post-Ottawan (1050-1020 Ma) Orogenic Collapse Along the Carthage-Colton Shear Zone: Data From the Dana Hill Metagabbro Body, Adirondack Mountains, New York, In: Tollo R.P., Corriveau, L., McLelland, J. and Bartholomew, M.J. (eds), Proteozoic Tectonic Evolution of the Grenville Orogen in North America, Geological Society of America Memoir 197, 2004, Pages 357-378, E.L. Johnson, E.T. Goergen, B.L. Fruchey.

Johnston, 1994. The Earthquakes of Stable Continental Regions: Volume 1 - Assessment of Large Earthquake Potential, EPRI, TR-102261-V1, A. Johnston, K. Coppersmith, L. Kanter, and C. Cornell.

Kafka, 1985. Earthquake Activity in the Greater New York City Area: Magnitudes, Seismicity, and Geologic Structures, Bulletin of the Seismological Society of America, Volume 75, No 7, October 1985, pages 1285-1300, A.L. Kafka, E.A. Schlesinger-Miller and N.L. Bartstow.

Kane, 1989. Chapter 18: A Crust/Mantle Structural Framework of the Conterminous United States Based on Gravity and Magnetic Trends, In: Pakiser, L.C.; Mooney, W.D., Geophysical Framework of the Continental United States, Geological Society of America, Memoir 172, 1989, M.F. Kane and R.H. Godson.

Karrow, 1989. Chapter 4: Quaternary Geology of the St Lawrence Lowlands, In: Quaternary Geology of Canada and Greenland, R.J. Fulton (ed), Geological Survey of Canada, Geology of Canada, No 1, 1989, P.F. Karrow and S. Occhietti.

Karrow, 2002. A History of Neotectonic Studies in Ontario, Tectonophysics, v. 353, pp. 3-15, P.F. Karrow and O.L White.

King, 1978. The New York - Alabama Lineament: Geophysical Evidence for a Major Crustal Break in the Basement Beneath the Appalachian Basin, Geology, Volume 6, May 1978, Pages 31-318, E.R. King and I. Zietz.

Klemperer, 1985. Some Results of COCORP Seismic Reflection Profiling in the Grenville-age Adirondack Mountains, New York State, Canadian Journal of Earth Sciences, Volume 22, No. 2, 1985, Pages 141-153, S.L. Klemperer, L.D. Brown, J.E. Oliver, C.J. Ando, B.L. Czuchra and S. Kaufman.

Klitgord, 1995. Mid-Atlantic Continental Margin: the Mesozoic-Cenozoic Ocean Boundary in L. Glover and K Klitgord, chief compilers, E-3 southwest PA to Baltimore Canyon Trough, GSA Continental/Ocean Transect No. 19.

Kreidler, 1972. Deep Wells in New York State, New York State Museum and Science Service, Bulletin Number 418A, 335 pp, W.L. Kreidler, A.M. Van Tyne and K.M. Jorgensen, 1972.

Lash, 2007. Jointing within the Outer Arc of a Forebulge at the Onset of the Alleghanian Orogeny, Journal of Structural Geology, Volume 29, May, 2007, pages 774-786, G.G Lash and T. Engelder.

Levin, 1995. Seismic Velocities in the Shallow Crust of Western New England and Northern New York, Bulletin of the Seismological Society of America, Volume 85, No. 1, 1995, Pages 207-219, V. Levin, W.Y. Kim and W. Menke.

Levin, 2000a. No Regional Anisotropic Domains in the Northeastern U.S. Appalachians, Journal of Geophysical Research, Volume 105, No B8, 2000, Pages 19,029-19,042, V. Levin, W. Menke and J. Park.

Levin, 2000b. Thinning of the Upper Mantle During Late Paleozoic Appalachian Orogenesis, Geology, Volume 28, No. 3, 2000, Pages 239-242, V. Levin, J. Park, M.T. Brandon and W. Menke.

Lyons, 1982. Gravity Anomaly Map of the United States, Society of Exploration Geophysicists, Scale 1:2,500,000, P. Lyons and N. O'Hara, 1982.

Ma, 2007. Western Quebec Seismic Zone (Canada): Clustered, Midcrustal Seismicity Along a Mesozoic Hot Spot Track, Journal of Geophysical Research, Volume 112, B06305, S. Ma and D.W. Eaton, 2007.

Manspeizer, 1989. Post-Paleozoic Activity, Geology of North America, Volume F-2, The Appalachian-Ouachita Orogen in the United States, Geological Society of America, W. Manspeizer, J. DeBoer, J. Costain, A. Froelich, C. Coruh, P. Olsen, G. McHone, J. Puffer, and D. Prowell, 1989.

McFall, 1993. Structural Elements and Neotectonics of Prince Edward County, Southern Ontario, Geographie Physique et Quaternaire, Volume 47, No. 3, Pages 303-312, G.H. McFall, 1993.

Miles, 2000a. Magnetic Anomaly Map, Canada, Geological Survey of Canada, Open File 3829a, 1:7,500,000-scale map, 2000, W.F. Miles, W.R. Roest and M.P. Vo.

Miles, 2000b. Gravity Anomaly Map, Canada, Geological Survey of Canada, Open File 3830a, 1:7,500,000-scale map, 2000, W.F. Miles, W.R. Roest and M.P. Vo.

Milici, 1988. Chapter 15: The Appalachian Basin, In: The Geology of North America, Volume D-2, Sedimentary Cover-North American Craton: U.S., The Geological Society of America, 1988, R.C. Milici and W. de Witt Jr.

Mohajer, 1993. Seismicity and Seismotectonics of the Western Lake Ontario Region, Geographie Physique et Quaternaire, Volume 47, No. 3, Pages 353-362, A.A. Mohajer, 1993.

Musacchio, 1997. Composition of the Crust in the Grenville and Appalachian Provinces of North America inferred from V_P/V_S Ratios, Journal of Geophysical Research, Volume 102, No B7, 1997, Pages 15,225-15,242, G. Musacchio, W.D. Mooney, J.H. Luetgert and N.I. Christensen.

Nabelek, 1989. The 1983 Goodnow Earthquake in the Central Adirondacks, New York: Rupture of a Simple, Circular Crack, Bulletin of the Seismological Society of America, Volume 79, No B6, Pages 1762-1777, J. Nabelek and G. Suarez, 1989.

New York State Electric and Gas, 1978. NYSE&G 1 and 2, Preliminary Safety Analysis Report, New Haven Site, Oswego County, New York, November 1978.

Niagara Mohawk, 1978a. Nine Mile Point Nuclear Station Unit 2, Geologic Investigation, Volume I, Geology, Syracuse, New York.

Niagara Mohawk, 1978b. Nine Mile Point Nuclear Station Unit 2, Geologic Investigation, Volume II, Geomorphology, Vertical Crustal Movement, Seismicity, Syracuse, New York.

Niagara Mohawk, 1978c. Nine Mile Point Nuclear Station Unit 2, Geologic Investigation, Volume III, Stresses, Syracuse, New York.

Niagara Mohawk, 1980. Nine Mile Point Nuclear Station Unit 2, Geologic Investigation, Radwaste Thrust Structure, Syracuse, New York.

NOAA, 2008. Great Lakes Water Level Data, Website: http://tidesandcurrents.noaa.gov, Date accessed: April 22, 2008.

NRC, 1978. Standard Format and Content of Safety Analysis Reports for Nuclear Power Plants (LWR Edition), U. S. Nuclear Regulatory Commission, Regulatory Guide 1.70, Section 2.5.1, November 1978.

NRC, 1997. Identification and Characterization of Seismic Sources and Determination of Safe Shutdown Earthquake Ground Motion, U. S. Nuclear Regulatory Commission, Regulatory Guide 1.165, March 1997.

NRC, 2007a. Combined License Applications for Nuclear Power Plants, U. S. Nuclear Regulatory Commission, Regulatory Guide 1.206, Section 2.5.1, June 2007.

NRC, 2007b. A Performance-Based Approach to Define the Site-Specific Earthquake Ground Motion, U. S. Nuclear Regulatory Commission, Regulatory Guide 1.208, March 2007.

NYSDEC, 2007. New York State Department of Environmental Conservation - Oil & Gas Database, Website: http://www.dec.ny.gov/cfmx/extapps/GasOil, Date accessed: December, 2007.

NYSM, 1970a. Reprinted 1995, Geologic Map of New York - Adirondack Sheet, New York State Museum and Science Service, Map and Chart Series No. 15, Y.W. Isachsen and D.W. Fisher, 1970

NYSM, 1970b. Geologic Map of New York - Finger Lakes Sheet, New York State Museum and Science Service, Map and Chart Series No. 15, Rickard, L.V. and D.W. Fisher, 1970.

NYSM, 1971. Simple Bouguer Gravity Anomaly Map of Western New York. New York State Museum and Science Service, Geological Survey Map and Chart Series No. 17. F. Revetta and W.H. Diment, 1971.

NYSM, 1973a. Simple Bouguer Gravity Anomaly Map of Northern New York, New York State Museum and Science Service Geological Survey Map and Chart Series No. 17A, G. Simmons and W.H. Diment, 1973.

NYSM, 1986. Surficial Geologic Map of New York - Finger Lakes Sheet, New York State Museum - Geological Survey, Map and Chart Series No. 40, E. H. Muller and D.H. Cadwell, 1986.

NYSM, 1990. New York State Geological Highway Map, The University of the State of New York, The State Education Department, New York State Geological Survey, New York State Museum, Cultural Education Center, Albany, NY 12230, 1990.

NYSM, 1991. Surficial Geologic Map of New York - Adirondack Sheet, New York State Museum - Geological Survey, Map and Chart Series No. 40, D.H. Cadwell and D.L. Pair, 1991.

NYSM, 2000. Geology of New York, A Simplified Account, Second Edition, New York State Museum Educational Leaflet 28, 294 pp, Y.W. Isachsen, E. Landing, J.M. Lauber, L.V. Rckard, and W.B. Rogers, 2000.

Obermeier, 1996. Use of Liquefaction-Induced Features for Paleozeismic Analysis - An Overview of How Seismic Liquefaction Features Can Be Distinguished From Other Features And How Their Regional Distribution And Properties of Source Sediment Can Be Used To Infer The Location And Strength of Holocen Paleo-Earthquakes, Enginering Geology, v. 44, pp. 1-76, S.F. Obermeier.

Oliver, 1970. Postglacial Faulting and Seismicity in New York and Quebec, Canadian Journal of Earth Sciences, Volume 7, Pages 579-590, J. Oliver, T. Johnson and J. Dorman, 1970.

Ouassaa, 2002. Interpretation of Seismic and Potential Field Data From Western New York State and Lake Ontario, Tectonophysics, Volume 353, 2002, Pages 1115-149, K. Ouassaa and D.S. Forsyth.

Parker, 1942. Regional Systematic Jointing in Slightly Deformed Sedimentary Rocks, Geological Society of America Bulletin, v. 53, p. 381-408.

Parker, 1969. Jointing in South-Central New York: Discussion, Geological Society of America Bulletin, Volume 80, May, 1969, Pages 919-922, J.M. Parker III.

Patchen, 1978. Depositional Environments of the Oswego Sandstone (Upper Ordovician), Oswego County, New York, New York State Geological Association Guidebook 50th Annual Meeting, Syracuse New York, 1978, Pages 368-386, D.G. Patchen.

Perry, 2002. LITH5.0: A Revised Crustal Model for Canada Based on Lithoprobe Results, Geophysical Journal International, Volume 150, Issue 1, 2002, Pages 285-294, H.K.C. Perry, D.W.S. Eaton and A.M. Forte.

Pilkington, 1992a. 1:10,000,000-scale Magnetic Field Intensity Map of North America, Geological Survey of Canada.

Pilkington, 1992b. 1:10,000,000-scale Vertical Gradient of the Bouguer Anomaly Map of North America, Geological Survey of Canada.

Pilkington, 1992c. 1:10,000,000-scale Gravity Anomaly Map with Shaded Relief of Gradient of North America, Geological Survey of Canada.

Plumb, 1985. Stress-Induced Borehole Elongation: A Comparison Between the Four-Arm Dipmeter and the Borehole Televiewer in the Auburn Geothermal Well, Journal of Geophysical Research, June, 1985, Pages 5514-5221 R.A. Plumb and S.H. Hickman.

Plumb, 1991. Geophysical Log Responses and Their Correlation With Bed-to-Bed Stress Contrasts in Paleozoic Rocks, Appalachian Plateau, New York, Journal of Geophysical Research, Volume 96, No B9, August 10, 1991, Pages 14,509-14,528, R.A. Plumb, K.F. Evans and T. Engelder.

Prowell, 1983. Index of Faults of Cretaceous and Cenozoic Age in the Eastern United States, USGS Map MF-1269, 1983. D.C. Prowell.

Rankin, 1993. Chapter 5: Proterzoic Rocks East and Southeast of the Grenville Front, In: the Geology of North America, Volume C-2, Precambrian: Conterminous U.S., the Geological Society of America, 1993, D.W. Rankin, J.R. Chiarenzelli, A.A. Drake, R. Goldsmith, L. M. Hall, Y.W. Isachsen, E.G. Lidiak, J. McLelland, S. Mosher, N.M. Ratcliffe, .J. Secpor Jr. and P.R. Whitney.

Ratcliffe, 1971. The Ramapo Fault System in New York and Adjacent Northern New Jersey: A Case of Tectonic Heredity, Geological Society of America Bulletin, v. 82, p.125-142, January, 1971. N.M. Ratcliffe.

Ratcliffe, 1982. Results of Core Drilling of the Ramapo Fault at Sky Meadow Road, Rockland County, New York, and Assessment of Evidence For Reactivation to Produce Current Seismicity, U.S.G.S. Miscellaneous Investigations, Map 1-1401, 1 Sheet, N. Ratcliffe.

Ratcliffe, 1990. Orientation, Movement History, And Cataclastic Rocks of Ramapo Fault Based On Core Drilling And Trenching Along The Western Margin of The Newark Basin Near Bernadsville, New Jersey, U.S.G.S. Miscellaneous Investigations, Map I-1982, 1 Sheet, N. Ratcliffe, W. Burton, and M. Pavich.

Reed, 1993. Chapter 1: Introduction, In: the Geology of North America, Volume C-2, Precambrian: Conterminous U.S., the Geological Society of America, 1993, J.C. Reed Jr. and J.E. Harrison.

Richardson, 1991. North American Plate Dynamics, Journal of Geophysical Research, Volume 96, No B7, July 10, 1991, Pages 12,201-12,223, R.M. Richardson and L.M. Reding.

Rickard, 1973. Stratigraphy and Structure of the Subsurface Cambrian and Ordovician Carbonates of New York, New York State Museum and Science Service, Map and Chart Series Number 18, L.V. Rickard, 1973.

Rodgers, 1970. The Tectonics of the Appalachians, Wiley-Intersciens: New York, NY, p. 271, J. Rodgers, 1970.

Sanford, 1993a. Chapter 10: St. Lawrence Platform - Introduction, In: Sedimentary Cover of the Craton in Canada, D.F. Stott and J.D. Aitken (ed), Geological Survey of Canada, Geology of Canada, No 5, 1993, Pages 709-722, B.V. Sanford.

Sanford, 1993b. Chapter 11: St. Lawrence Platform - Geology, In: Sedimentary Cover of the Craton in Canada, D.F. Stott and J.D. Aitken (ed), Geological Survey of Canada, Geology of Canada, No 5, 1993, Pages 723-786, B.V. Sanford, W.R. Cowan and K.L. Currie.

Scheidegger, 1991. Neotectonic Joints: Discussion and Reply, Geological Society of America Bulletin, Volume 103, March, 1991, Pages 432-433, A.E. Scheidegger.

Schlische, 1992. Structural and Stratigraphic Development of the Newark Extensional Basin, Eastern North America: Evidence for the Growth of the Basin and its Bounding Structures, Geological Society of America Bulletin, v. 104, Pages 1246-1263, October 1992. R. W. Schlische.

Schwab, 1997. Mapping The Sea Floor Offshore of The New York-New Jersey Metropolitan Area Using Sidescan Sonar - Preliminary Report, USGS Open File Report, OFR-97-61, Plate 003, W. Schwab, W. Corso, M. Allison, B. Butman, J. Denny, L. Lotto, W. Danforth, D. Foster, T. O'Brien,

Scruben, 1994. Scruben, Paul G.; Arndt, Raymond E.; and Bawiec, Walter J. 1994. Geology of the conterminous United States at 1:2,500,000 scale - a digital representation of the 1974 P.B. King and H.M. Beikman map. Reston VA : U.S. Geological Survey. (U.S. Geological Survey digital data series DDS-11).

Seeber, 1993. Natural and Induced Seismicity in the Lake Erie-Lake Ontario Region: Reactivition of Ancient Faults with Little Neotectonic Displacement, Geographie Physique et Quaternaire, Volume 47, No. 3, Pages 363-378, L. Seeber and J.G. Armbruster, 1993.

Seeber, 1998. The 1994 Cacoosing Valley Earthquakes Near Reading, Pennsylvania: A Shallow Rupture Triggered by Quarry Unloading, Journal of Geophysical Research, v. 103, No. B10, pp. 24,505-24,421, October 10, 1998, L. Seeber, J.G. Armbruster, W.Y. Kim, N. Barstow, and C. Scharnberger.

Shih, 1993. 1:3,000,000-scale map of Magnetic Anomalies and Major Structural Features of Southeastern Canada and the Atlantic Continental Margin, Geological Survey of Canada.

Shih, 1993. 1:3,000,000-scale map of Gravity Anomalies and Major Structural Features of Southeastern Canada and the Atlantic Continental Margin, Geological Survey of Canada.

Shumaker, 2000. The New York-Alabama Lineament; An Early Iapetian Wrench Fault, American Association of Petroleum Geolgoists Bulletin, Volume 84, Number 9, AAPG v. 84 No. 9 p. 1393

Sloss, 1988. Chapter 1: Introduction, In: The Geology of North America, Volume D-2, Sedimentary Cover - North American Craton: U.S., The Geological Society of America, 1988, L.L. Sloss.

Spencer, 1987. More Seismic Evidence on the Location of Grenville Basement Beneath the Appalachians of Quebec-Maine, Geophysical Journal International, Volume 89, Issue 1, 1987, Pages 177-182, C. Spencer, A. Green and J. Luetgert.

Stillwell, 2005. Fractures and Faults in the Eastern Lake Ontario Basin, Oswego County, New York, New York State Geological Association Guidebook 77th Annual Meeting, Oswego New York, 2005, Pages 29-44, S.M. Stillwell, Valentino, J.D., J.M. Gawron and D.W. Valentino

Stone, 1984. Faults in Pleistocene Sediments at Trace of Ramapo Fault in Geological Survey Research, Fiscal Year 1981, U.S.G.S. Professional Paper 1375, p. 49, B. Stone and N. Ratcliffe, 1984.

Stone and Webster, 1978. Stone and Webster Engineering Corporation, 1978. Report of Fault Investigation at Fitzpatrick Nuclear Power Plant, Scriba, New York, Power Authority of the State of New York, February, 1978.

Stott, 1993. Chapter 1: Introduction, In: Sedimentary Cover of the Craton in Canada, D.F. Stott and J.D. Aitken (ed), Geological Survey of Canada, Geology of Canada, No 5, 1993, Pages 1-7, D.F. Stott and J.D. Aitken.

Stover, 1987. Seismicity Map of the State of New York, USGS Map MF-1282, 1987. C.W. Stover, B.G. Reagor, L.M. Highland, and S.T. Algermissen.

Streepy, 2004. Exhumation of a Collisional Orogen: A Perspective From The North American Grenville Province, , In: Tollo R.P., Corriveau, L., McLelland, J. and Bartholomew, M.J. (eds), Proteozoic Tectonic Evolution of the Grenville Orogen in North America, Geological Society of America Memoir 197, 2004, pp. 391-410. M.M. Streepy, C. Lithgow-Bertelloni, B.A. van der Pluijm, E.J. Essene and J.f. Magloughlin.

Swezey, 2002. Regional Stratigraphy and Petroleum Systems of the Appalachian Basin, North America. U.S.G.S Geologic Investigations Series Map I-2768. C.S. Swezey.

Sykes, 2008. Observations and Tectonic Setting of Historic and Instrumentally Located Earthquakes in the Greater New York City - Philadelphia Area, Bulletin of the Seismological Society of America, Volume 98, No 4, August 2008, Pages 1696-1719, L.R. Sykes, J.G. Armbruster, W-Y Kim, and L. Seeber.

Taylor, 1989. Chapter 16: Geophysical Framework of the Appalachians and Adjacent Grenville Province, In: Pakiser, L.C.; Mooney, W.D., Geophysical Framework of the Continental United States, Geological Society of America, Memoir 172, 1989, S.R. Taylor.

Thomas, 1993. Recent Deformation in the Bottom Sediments of Western and Southeastern Lake Ontario and its Association with Major Structures and Seismicity, Geographie Physique et Quaternaire, Volume 47, No. 3, Pages 325-335, R.L. Thomas, J.L. Wallach, R.K. McMillan, J.R. Bowlby, S. Frape, D. Keyes and A.A. Mohajer, 1993.

Thomas, 2006. Tectonic Inheritance at a Continental Margin, GSA Today, Volume 16, No 2, February 2006, Pages 4-11, W.A. Thomas.

Thurber, 1985. Crustal Structure Along the Ramapo Fault Zone, New York State, Earthquake Notes, Volume 56, Pages 145-152, C. Thurber and T. Caruso, 1985.

Tollo, 2004. Proterozoic Tectonic Evolution of the Grenville Orogen in North America: An Introduction, In: Tollo, R.P., Corriveau, L. , McLelland, J. and Bartholomew, M.J., eds, Proterozoic Tectonic Evolution of the Grenville Orogen in North America: Boulder, Colorado, Geological Society of America, Memoir 197, 2004, R.P. Tollo, L. Corriveau, J. McLelland and M.J. Bartholomew.

Turcotte, 2002. Geodynamics, Cambridge University Press, p. 456, D. Turcotte and G. Schubert, 2002.

Tuttle, 1996. Case Study of Liquefaction Induced by the 1944 Massena, New York – Cornwall, Ontario Earthquake, Lamont – Doherty Earth Observatory of Columbia University, NUREG/CR-6495, M.P. Tuttle, 1996.

Tuttle, 2002. Paleoliquifaction Study of the Clarendon-Linden Fault, Western New York State, Tectonophysics, Volume 353, 2002, Pages 263-286, M.P. Tuttle, K. Dyer-Williams and N.L. Barstow.

USGS, 1978. Oswego East, NY, Topographic 7.5 Minute Series, 1:24,000-scale map, 1978, USGS.

USGS, 1980. Surficial Geology of New Haven Quadrangle, Oswego County, New York, Water-Resources Investigations Open-File Report 80-1208, 1:24,000-scale map, 1979, E.H. Muller and T. S. Miller.

USGS, 1980. Surficial Geology of Oswego East Quadrangle, Oswego County, New York, Water-Resources Investigations Open-File Report 80-1209, 1:24,000-scale map, 1980, E.H. Muller and T.S. Miller.

USGS, 1980. Surficial Geology of Oswego West Quadrangle, Oswego County. New York, Water-Resources Investigations Open-File Report 80-968, 1:24,000-scale map, 1980, T.S. Miller.

USGS, 1980. Surficial Geology of Texas Quadrangle, Oswego County, New York, Water-Resources Investigations Open-File Report 80-760, 1:24,000-scale map, 1980, E.H. Muller and T.S. Miller.

USGS, 1980. Surficial Geology of Mexico Quadrangle, Oswego County, New York, Water-Resources Investigations Open-File Report 80-2040, 1:24,000-scale map, 1980, E.H. Muller, D. Andrews and T.S. Miller.

USGS, 1980. Surficial Geology of West of Texas Quadrangle, Oswego County, New York, Water-Resources Investigations Open-File Report 80-1113, 1:24,000-scale map, 1974, E.H. Muller.

USGS, 1982. West of Texas, NY, Topographic 7.5 Minute Series, 1:24,000-scale map, 1982, USGS.

USGS, 1985a. Pulaski, NY, Metric Topographic Series, 1:100,000-scale map, 1985.

USGS, 1985b. Syracuse, NY, Metric Topographic Series, 1:100,000-scale map, 1985.

USGS, 1985c. Utica, NY, Metric Topographic Series, 1:100,000-scale map, 1985.

USGS, 1985d. Watertown, NY, Metric Topographic Series, 1:100,000-scale map, 1985.

USGS, 2002a. Documentation for the 2002 Updated of the National Seismic Hazard Maps, Open File Report 02-420, U.S. Geological Survey, A.D. Frankel, M.D. Petersen, C.S. Mueller, K.M. Haller, R.L. Wheeler, E.V. Leyendecker, R.L. Wesson, S.C. Harmsen, C.H. Cramer, D.M. Perkins and K.S. Rukstales, 2002

USGS, 2002b. Examples of the Utility of Magnetic Anomaly Data for Geologic Mapping, USGS Open-File Report 02-400, U.S. Geological Survey, C. Finn, M. Pilkington, R. Blakely, S. Johnson, W. Cannon, M. Gettings and W. Roest, 2002.

USGS, 2002c. Magnetic Anomaly Map of North America: Booklet to Accompany Map, U.S. Geological Survey, North American Magnetic Anomaly Group (NAMAG), 2002.

USGS, 2007a. Landsat Thematic Mapper, Landsat 5, Landsat Scene Identifier: LT50160302007214EDC00, Date Acquired: 8/2/2007, USGS.

USGS, 2007b. Landsat Thematic Mapper, Landsat 5, Landsat Scene Identifier: LT50150302007223EDC00, Date Acquired: 8/11/2007, USGS

USNRC, 1980. A Characterization of Faults in the Appalachian Foldbelt, Division of Siting, Health, and Safeguards Standards, U.S. Nuclear Regulatory Commission, A.L. Odom and R.D. Hatcher, Jr., September, 1980

Valentino, 1994. Late Paleozoic Transcurrent Tectonic Assembly of the Central Appalachian Piedmont, Tectonics, Volume 13, No 1, February, 1994, Pages 110-126, D.W. Valentino, A.E. Gates and L. Glover III.

Vlahovic, 2003. A Three-Dimensional P Wave Velocity Model for the Charlevoix Seismic Zone, Quebec, Canada, Journal of Geophysical Research, Volume 108, No. B9, 2439, G. Vlahovic, C. Powell and M. Lamontagne, 2003.

Wallach, 2002. The Presence, Characteristics and Earthquake Implications of the St Lawrence Fault Zone within and Near lake Ontario (Canada - U.S.), Tectonophysics, Volume 353, 2002, pages 45-74, J.L. Wallach.

Wheeler, 1995. Earthquakes and the Cratonward Limit of Iapetan Faulting in Eastern North America, Geology, Volume 23, No 2, February 1995, Pages 105-108, R.L. Wheeler.

Wheeler, 1996. Geological Map of Canada, Geological Survey of Canada, Map 1860A, Scale 1:5,000,000, J.O. Wheeler, P.F. Hoffman, K.D. Card, A. Davidson, B.V. Sanford, A.V. Okulitch and W.R. Roest.

Wheeler, 2001. Known and Suggested Quaternary Faulting in the Midcontinent United States, Engineering Geology, Volume 62, October, 2001, Pages 51-78, R.L. Wheeler and A.J. Crone.

Wheeler, 2005. Known or Suggested Quaternary Tectonic Faulting, Central and Eastern United States - New and Updated Assessments for 2005, Open File Report 2005-1336, U.S.G.S., 2005. R.L. Wheeler.

Wheeler, 2006. Quaternary Tectonic Faulting in the Eastern United States, Engineering Geology, Volume 82, January, 2006, Pages 165-186, R.L. Wheeler.

Whitaker, 2005. Characterizing Stress Fields in the Upper Crust Using Joint Orientation Distributions, Journal of Structural Geology, Volume 27, October, 2005, Pages 1778-1787, A.E. Whitaker and T. Engelder.

White, 1994. Seismic Images of the Grenville Orogen in Ontario, Canadian Journal of Earth Sciences, Volume 31, 1994, Pages 293-307, D.J. White, R.M. Easton, N.G. Culshaw, B. Milkereit, D.A. Forsyth, S. Carr, A.G. Green and A. Davidson.

White, 2000. A Seismic-based Cross-section of the Grenville Orogen in Southern Ontario and Western Quebec, Canadian Journal of Earth Sciences, Volume 37, No. 2-3, 2000, Pages 183-192. D.J. White, D.A. Forsyth, I. Asudeh, S.D. Carr, H. Wu, R.M. Easton and R.F. Mereu.

Williams, 1995. Chapter 1: Introduction, In: Geology of the Appalachian-Caledonian Orogen in Canada and Greenland, H. Williams (ed.), Geological Survey of Canada, Geology of Canada, No 6, 1995, Pages 1-19, H. Williams.

Withjack, 1998. Diachronous Rifting, Drifting, and Inversion on the Passive Margin of Central Eastern North America: An Analog for Other Passive Margins, AAPG Bulletin, Volume 82, No 5A, May 1998, Pages 817-835, M.O. Withjack, R.W. Schlische and P.E. Olsen.

Younes, 1999. Fringe Cracks: Key Structures for the Interpretation of the Progressive Alleghanian Deformation of the Appalachian Plateau, Geological Society of America Bulletin, Volume 111, No 2, February, 1999, Pages 219-239, A.I. Younes and T. Engelder.

Zelt, 1994a. Seismic Structure of the Central Metasedimentary Belt, Southern Grenville Province, Canadian Journal of Earth Sciences, Volume 31, 1994, Pages 243-254, C.A. Zelt, D.A. Forsyth, B. Milkereit, D.J. White, I. Asudeh and R.M. Easton.

Zelt, 1994b. Modeling Wide-angle Seismic Data for Crustal Structure: Southeastern Grenville Province, Journal of Geophysical Research, Volume 99, 1994, Pages 11,687-11,704, C.A. Zelt and D.A. Forsyth

Zhao, 1997. Formation of Regional Cross-Fold Joints in the Northern Appalachian Plateau, Journal of Structural Geology, Volume 19, No 6, June, 1997, Pages 817-834, M. Zhao and R. Jacobi.

Zhu, 1994. Tomographic Inversion for the Seismic Velocity Structure Beneath Northern New England Using Seismic Refraction Data, Journal of Geophysical Research, Volume 99, No B8, 1994, Pages 15,331-15,358, H. Zhu and J.E. Ebel.

Zietz, 1982. Composite Magnetic Anomaly Map of the United States, 1:2,500,000 - scale map, U.S.G.S. Map GP-954A, I. Zietz, J.D. Corbett, G.P. Eaton, M.D. Fuller, R.H.Godson, W.F. Hanna, J.R. Heirtzler, W.J. Hinze and J.A. Schwartz.

Zoback, 1985. Well Bore Breakouts and In Situ Stress, Journal of Geophysical Research, Volume 90, No B7, June 10, 1985, Pages 5523-5530, M.D. Zoback, D. Moos and L. Mastin.

Zoback, 1989. Chapter 24: Tectonic Stress Field of the Continental United States, In: Pakiser, L.C.; Mooney, W.D., Geophysical Framework of the Continental United States, Geological Society of America, Memoir 172, 1989 M.L. Zoback and M.D. Zoback.

Zoback, 1992. Stress Field Constraints on Intraplate Seismicity in Eastern North America, Journal of Geophysical Research, Volume 97, No B8, July 30, 1992, Pages 11,761-11,782, M.L. Zoback. }

2.5.2 VIBRATORY GROUND MOTION

The U.S. EPR FSAR includes the following COL Items for Section 2.5.2:

A COL applicant that references the U.S. EPR design certification will review and investigate site-specific details of the seismic, geophysical, geological, and geotechnical information to determine the safe shutdown earthquake (SSE) ground motion for the site and compare site-specific ground motion to the Certified Seismic Design Response Spectra (CSDRS) for the U.S. EPR.

This COL Item is addressed as follows:

This section provides a detailed description of the vibratory ground motion assessment that was carried out for the {NMP3NPP} site, resulting in the development of the {NMP3NPP} site Safe Shutdown Earthquake (SSE) ground motion response spectra. {This section provides a detailed description of the vibratory ground motion assessment that was carried out for the NMP3NPP site, resulting in the development of the NMP3NPP site Safe Shutdown Earthquake (SSE) ground motion response spectra. The starting point for this site assessment is the EPRI-SOG probabilistic seismic hazard analysis (PSHA) methodology outlined in EPRI NP-4726-A 1988 (EPRI, 1988) and tectonic interpretations in EPRI NP-4726 1986 (EPRI, 1986).

Nuclear Regulatory Commission (NRC) Regulatory Guide 1.165, "Identification and Characterization of Seismic Sources and Determination of Safe Shutdown Earthquake Ground Motion," March, 1997, (NRC, 1997) states in Section B, Discussion:

> *"The CEUS is considered to be that part of the United States east of the Rocky Mountain front or east of Longitude 105 West (Refs. 4 and 5). To determine the SSE in the CEUS, an accepted PSHA methodology with a range of credible alternative input interpretations should be used. For sites in the CEUS, the seismic hazard methods, the data developed, and seismic sources identified by Lawrence Livermore National Laboratory (LLNL) (Refs. 4-6) and the Electric Power Research Institute (EPRI) (Ref. 7) have been reviewed and accepted by the staff."*

Reference 7 is Electric Power Research Institute, "Probabilistic Seismic Hazard Evaluations at Nuclear Power Plant Sites in the Central and Eastern United States," NP-4726, All Volumes, 1989-1991. The title and number of the referenced document are not in agreement. The title of EPRI-4726 is "Seismic Hazard Methodology for the Central and Eastern United States." No document could be found that had the title provided by the NRC.

In lieu of the reference 7, i.e., EPRI document, NP-4726, All Volumes, 1989-1991, Section 2.5.2 will implement EPRI NP-4726, "Seismic Hazard Methodology for the Central and Eastern United States," 1986 and EPRI-4726-A, "Seismic Hazard Methodology for the Central and Eastern United States," 1988. EPRI NP-4726-1986 and EPRI-4726-A, 1988 have been determined to be acceptable as described below.

Additionally, the PSHA methodology used for the NMP3NPP site is described in EPRI NP-6395-D-1989 (EPRI, 1989a). EPRI NP-6395-D has been determined to be an acceptable PSHA methodology by the NRC is also described below.

The NRC has accepted the use of the following, which were included in the North Anna Early Site Permit Application by Dominion Nuclear North Anna, LLC, which was approved in NUREG-1835, Safety Evaluation Report for an Early Site Permit (ESP) at the North Anna Site, 2005 (NRC, 2005).

- EPRI 4726, 1986, "Seismic Hazard Methodology for the Central and Easter United States" was included in the Early Site Permit Application as reference 120. It is also specifically included as a reference in Section C of NUREG-1835.

- EPRI-NP-6395-D, 1989, "Probabilistic Seismic Hazard Evaluation At Nuclear Plant Sites In The Central And Eastern United States, Resolution Of The Charleston Earthquake Issue."

    a. Early Site Permit Application as reference 115.

b. Generic Letter 88-20, "Individual Plant Examinations of External Events (IPEEE) for Severe Accident Vulnerabilities" (NRC, 1991)

The NRC has accepted the use of the EPRI NP-4726-A, 1988 in the letter dated October 31, 2005, T. Mundy, Exelon to NRC, Subject: Response Supplemental Draft Safety Evaluation Report (DSER) Item, page 16 of 112 and page 54 of 112, (Adams Accession No. ML053120131) (Exelon, 2005).

The EPRI-SOG tectonic interpretations in EPRI NP-4726 1986 (EPRI, 1986) were updated with more recent geological, seismological, and geophysical data under the guidance of NRC Regulatory Guide 1.165, (NRC, 1997). Section 2.5.2.1 through Section 2.5.2.3 document this review and update, as needed, of the EPRI-SOG seismicity, seismic source, and ground motion models.

Section 2.5.2.4 develops PSHA parameters at the site assuming the very hard rock foundation conditions implied by currently accepted ground motion attenuation models.

Section 2.5.2.5 summarizes information about the seismic wave transmission characteristics of the NMP3NPP site with reference to more detailed discussion of all engineering aspects of the subsurface in Section 2.5.4.

Section 2.5.2.6 describes the development of the horizontal SSE ground motion for the NMP3NPP site. The selected SSE ground motion is based on the risk-consistent/ performance-based approach of Regulatory Guide 1.208, A Performance-Based Approach to Define the Site-Specific Earthquake Ground Motion (NRC, 2007), with reference to NUREG/CR-6728 (NRC, 2001), NUREG/CR-6769 (NRC, 2002), and ASCE/SEI 43-05 (ASCE, 2005). Horizontal ground motion amplification factors are developed using site-specific data and estimates of near-surface soil and rock properties. These amplification factors are then used to scale the hard rock spectra to develop Uniform Hazard Spectra accounting for site-specific conditions using Approach 2A of NUREG/CR-6728 (NRC, 2001) and NUREG/CR-6769 (NRC, 2002). Horizontal SSE spectra are developed from these soil Uniform Hazard Spectra using the performance-based approach of ASCE/SEI 43-05 (ASCE, 2005), as implemented in Regulatory Guide 1.208 (NRC, 2007). The SSE motion is defined at the free ground surface of a hypothetical outcrop at the base of the nuclear island foundation. See Section 2.5.4 and Section 2.5.2.5 for further discussion of the subsurface conditions.

Section 2.5.2.6 also describes vertical SSE spectra, which are developed by scaling the horizontal SSE by a frequency-dependent vertical-to-horizontal (V:H) factor.

The SSE spectra that are described in this section are considered performance goal-based (risk-informed) site specific safe shutdown earthquake response spectra. The SSE spectra, and its specific location at a free ground surface, reflect the seismic hazard in terms of a PSHA and geologic characteristics of the site and represent the site-specific ground motion response spectrum (GMRS) of Regulatory Guide 1.208 (NRC, 2007). These spectra are expected to be modified as appropriate to develop ground motion for design considerations.

The SSE developed in this section meets the requirements of paragraph (d) of 10 CFR 100.23 (CFR, 2007).}

2.5.2.1 Seismicity

The U.S. EPR FSAR includes the following COL Item in Section 2.5.2.1:

Seismicity is site specific and will be addressed by the COL applicant.

This COL Item is addressed as follows:

{The seismic hazard analysis conducted by EPRI as delineated in NP-6395-D 1989 (EPRI, 1989a) relied, in part, on an analysis of historical seismicity in the central and eastern United States (CEUS) to estimate seismicity parameters (rates of activity and Richter b-values) for individual seismic sources. The historical earthquake catalog used in the EPRI analysis was complete through 1984. The earthquake data for the site region that has occurred since 1984 was reviewed and used to update the EPRI catalog (EPRI, 1988).

Geologic evidence for prehistoric seismicity in the site region is discussed in Section 2.5.2.2.1.7.

The EPRI seismic hazard analysis (EPRI, 1989a) forms the starting point for the current probabilistic seismic hazard analysis (PSHA)., ~~and t~~The EPRI study developed and relied upon a historical earthquake catalog for the ~~central and eastern United States (~~CEUS~~)~~. This catalog of earthquakes is complete through 1984 and includes regions of southern Canada bordering the CEUS. One task of the current study was to update this earthquake catalog through current times, as a database to determine if rates of earthquake occurrence have changed in the intervening 23+ years.

At the longitude of the NMPNS site, the EPRI catalog extends north into Canada to latitude 49° (and farther north for some longitudes) as shown in Figure 2.5-74. This means that historical earthquakes within 310 miles (500 km) of the NMPNS site (latitude 43.52°N) are included in the EPRI catalog.

To extend the EPRI earthquake catalog to current times, the following earthquake catalogs were examined:

Advanced National Seismic System (ANSS)

The ANSS composite catalog is an earthquake catalog that is created by merging the master earthquake catalogs from contributing ANSS institutions and removing duplicate solutions for the same event. The ANSS earthquake catalog grew out of the efforts of the Council of the National Seismic System.

National Earthquake Database (NEDB)

The NEDB comprises a number of separate databases that together act as the Canadian national repository for all raw seismograph data, measurements, and derived parameters that are derived from the Canadian National Seismograph Network (CNSN), the Yellowknife Seismological Array (YKA), previous regional telemetered networks in eastern and western Canada (ECTN and WCTN), local telemetered networks (CLTN and SLTN), the Regional Analogue Network, and the former Standard Seismograph Network (CSN). This database supports the monitoring and verification of the Comprehensive Nuclear Test Ban Treaty as well as international data exchange. This database also supports the Nuclear Explosion Monitoring project.

National Earthquake Information Center (USGS/NEIC)

The NEIC produces the monthly listing Preliminary Determination of Epicenters (PDE), which is the most compete computation of hypocenters and magnitudes published by the USGS/NEIC. This is normally produced a few months after the events occur. The publication is called "Preliminary" because the "final" computation of hypocenters for the world is considered to be the Bulletin of the International Seismological Centre (ISC), which is produced about two years

after the earthquakes occur. The NEIC PDE program contributes about one-third of all data used by the ISC.

Lamont-Doherty Cooperative Seismographic Network (LCSN)

The LCSN monitors earthquakes occurring in the eastern United States, centered around New York and Pennsylvania, with several sub-networks operating in the region and reporting local earthquakes.

New England Seismic Network (NESN)

The NESN is operated by the Weston Observatory of Boston College. The mission of the NESN is to operate and maintain a regional seismic network with digital recording of seismic ground motions in and adjacent to New England, in order to record earthquakes in that region and conduct research on earthquakes, crustal properties, and seismic hazard.

Ohio Seismic Network (OhioSeis)

The OhioSeis catalog lists all know earthquakes that were felt or had instrumental magnitudes greater than 2.0 and that occurred within Ohio's borders, including the area beneath Lake Erie.

The original EPRI catalog lists earthquakes in terms of body-wave magnitude m_b, which is equivalent to Lg magnitude (m_{bLg}) and to body-wave magnitude (m_N). For consistency, m_b was taken as the preferred magnitude measure for extending the EPRI catalog. For the NMPNS site region, all six catalogs were filtered to keep only earthquakes with m_b>3.0 within latitudes 40°-47° N and longitudes 71°-81° W. This captured all recorded earthquakes within approximately 230 miles (370 km) of the site. In addition, the Charlevoix seismic zone lies some 435 miles (700 km) to the northeast of the NMPNS site, and this zone is recognized as a potential contributor to seismic hazard at the site. Therefore the first five catalogs above were also searched for earthquakes with m_b>3.0 within latitudes 46°-49° N and longitudes 68°-72.5° W (The last catalog, documenting Ohio earthquakes, did not include any events in the Charlevoix seismic zone). The catalogs available from NESN extend through 2005, so the combined catalog was limited to the period 1985-2005.

To obtain a catalog of independent earthquakes in the site region (latitudes 40°-47° N and longitudes 71°-81° W), the catalogs were processed as follows. The catalogs were combined in sequence, flagging potential duplicates and dependent events (foreshocks and aftershocks), and removing duplicates and dependent events by inspection. The ANSS and NEDB catalogs both listed earthquakes by Nuttli magnitude m_N, and these magnitude values were used. The OhioSeis catalog also listed m_N, but all of these earthquakes were duplicates of events from the ANSS and NEDB catalogs. The catalogs from Weston Observatory extend from 1985 through 2005 and list events by m_N. Earthquakes from the PDE catalog were largely duplicative of events in other catalogs. Ultimately only four independent PDE earthquakes were identified, and of these, three had m_{bLg} or m_b assigned, and the remaining earthquake had a duration magnitude assigned. The LCSN earthquakes were largely duplicative of events in other catalogs, and these events had m_N, m_C, m_{bLg}, and m_b assigned. Ultimately only two independent earthquakes were identified from the LCSN catalog, and these were assigned the largest magnitude value among the scales listed.

The combined catalog yielded 233 earthquakes with m_b>3.0 within latitudes 40°-47°N and longitudes 71°-81° W. Of these, 231 earthquakes had m_b (or an equivalent value) assigned, and for these events, the standard deviation measure SMB was taken to be zero (per EPRI 1989). The remaining two earthquakes had a duration magnitude assigned, and these were converted to an equivalent m_b value using the conversion relationships of EPRI (1989a). For these events, SMB was taken to be 0.3 (per EPRI 1989a). Finally, an RMB estimate was calculated (m_b* in the

terminology of EPRI, 1989a) as RMB = EMB + 0.5 ln(10) b SMB2, where a generic b-value of 1.0 was assumed. Thus RMB differs from EMB for only two earthquakes, those for which EMB was estimated from duration magnitude. For the remaining 231 earthquakes, the RMB estimate is equivalent to the EMB estimate.

For the Charlevoix area, a similar procedure was followed to obtain a combined catalog of events. The ANSS and NEDB catalogs were the primary source of information for this area, yielding 86 earthquakes with m_b>3.0. The NESN catalogs added one independent earthquake, and the PDE and LCSN events were all duplicates of these 87 earthquakes. For the 1988 Saguenay earthquake, a moment magnitude M=5.9 was listed in the NEDB catalog, and this was converted to m_b=6.2 which is consistent with the magnitude conversions (m_b to M) used in ground motion estimates for hazard calculations. All estimates of SMB for these 87 earthquakes were taken to be zero, because m_b was listed or because (in the case of the Saguenay earthquake) the m_b value was chosen to be consistent with how ground motions are calculated. Thus the RMB estimate is equivalent to the EMB estimate for these 87 earthquakes.

Table 2.5-1 lists earthquakes in the final composite catalog within 200 miles (320 km) of the NMPNS site, for m_b>3.0. Table 2.5-2 lists earthquakes in the composite catalog for the Charlevoix region (latitudes 46°-49° N and longitudes 68°-72.5° W) for m_b>3.0. Depth information is not available from the EPRI catalog (events up to 1984), and all EPRI magnitudes are listed as m_b. Figure 2.5-74 and Figure 2.5-75 show epicenters within the site region (230 miles (~370 km)) and closer (50 miles (~80 km)), and Figure 2.5-76 shows epicenters in the Charlevoix seismic zone.}

2.5.2.2 Correlation of Earthquake Activity with Seismic Sources

The U.S. EPR FSAR includes the following COL Item in Section 2.5.2.2:

> Geologic and tectonic characteristics of site and region are site specific and will be addressed by the COL applicant.

This COL Item is addressed as follows:

{As described in Section 2.5.1, a comprehensive review of available geological, seismological, and geophysical data has been performed for the NMP3NPP site region and adjoining areas. As discussed in Section 2.5.1.2.6, excavation mapping is required during construction and any noted deformational zones will be evaluated and NRC notified when excavations are open for inspection. The following sections summarize the seismic source interpretations (EPRI, 1986) from the 1989 EPRI PSHA study (EPRI, 1989a), relevant post-EPRI seismic source characterization studies, and updated interpretations of new and existing sources provided by the more recent data. Based on evaluation of this information, no new information was found that would suggest potentially significant modifications to the EPRI seismic source model (EPRI, 1989a).

The seismic sources used for modeling are those that lie within the 200-mile radius of the NMP3NPP site. Although the La Malbaie/Charlevoix source lies outside the site region (200-mi radius), a sensitivity analysis performed for the NMP3NPP site shows that this source contributes a small fraction of the hazard for ground motions, and thus the La Malbaie/Charlevoix source has been included in the PSHA study for the site. The following sections present a summary of the EPRI NP-4726 (EPRI, 1986) seismic sources (Section 2.5.2.2.1) and post-EPRI seismic source characterization studies (Section 2.5.2.2.2).

2.5.2.2.1 Summary of EPRI Seismic Sources

Summarized in this section are the seismic sources and parameters used in the 1989 EPRI project EPRI NP-6452-D (EPRI, 1989b). The following description of seismic sources is limited to those sources within 200 mi (320 km) of the NMP3NPP site (the "site region") followed by the one significant source at distance greater than 200 mi (320 km) (i.e., La Malbaie/Charlevoix) (Section 2.5.2.2.2) that appear to impact the hazard at the NMP3NPP site. In the 1986 EPRI project (EPRI, 1986), six independent Earth Science Teams (ESTs) evaluated geological, geophysical, and seismological data to develop seismic sources in the CEUS. These sources were used to model the occurrence of future earthquakes and evaluate earthquake hazards at nuclear power plant sites across the CEUS. The six ESTs involved in the EPRI project were Bechtel Group, Dames & Moore, Law Engineering, Rondout Associates, Weston Geophysical Corporation, and Woodward-Clyde Consultants. Each team produced a report which was included in EPRI NP-4726, 1986 (EPRI, 1986) that provides detailed descriptions of how they identified and defined seismic sources. The results were implemented into a probabilistic seismic hazard analysis (PSHA) reported in EPRI NP-6395-D (EPRI, 1989a). EPRI NP-6452-D (EPRI, 1989b) summarized the parameters used in the final PSHA calculations and this reference is the primary source for the seismicity parameters used in this current NMP3NPP COL application. For the computation of hazard in the 1989 study (EPRI, 1989a) a few of the seismic source parameters were modified or simplified from the original parameters determined by the six ESTs as discussed in EPRI NP-6452-D (EPRI, 1989b).

The seismic source models developed for each of the six EST teams are shown on Figure 2.5-77 through Figure 2.5-88. These twelve figures illustrate the EST's seismic source zones compared to the EPRI-SOG seismicity catalog for the time period pre-1985, and to the updated seismicity catalog for the time period from 1985 to 2007. For example, Figure 2.5-77 illustrates the Bechtel team seismic sources overlaid on the pre-1985 EPRI-SOG seismicity map; Figure 2.5-78 shows the Bechtel team source zones and recent seismicity since 1985. Seismic source zones and seismicity maps for pre-1985 and post-1985 time periods are shown for each of the six ESTs. The sources that contributed 99 percent of the NMP3NPP site hazard are identified in the discussions in this Section. For the 1989 EPRI seismic hazard calculations, a screening criterion was implemented to identify those sources whose combined hazard exceeded 99 percent of the total hazard from all sources for two ground motions measurements (EPRI, 1989a). These sources are identified in the descriptions below as "primary" seismic sources. Other sources, which together contributed less than one percent of the total hazard from all sources for the two ground motion measures, are identified in the descriptions below as "additional" seismic sources. Earthquakes with m_b (body-wave magnitude: see below for discussion of this concept) > 3.0 are also shown in Figure 2.5-75 through Figure 2.5-88 to show the spatial relationships between seismicity and seismic sources. Earthquake epicenters include events from both the EPRI earthquake catalog (EPRI, 1988) and for the period between 1985 and 2007, as described in Section 2.5.2.1.2.

Earthquake epicenters from the EPRI earthquake catalog include events from the period between 1663 and 1984, updated with seismicity in the CEUS from the period between 1985 and 2006, as described in Section 2.5.2.1 and provided in Table 2.5-1 and Table 2.5-2. The maximum magnitude, the closest distance to the NMP3NPP site, and the probability of activity of each EST's seismic sources is summarized in Table 2.5-3. This table presents the parameters assigned to each source and specifies whether or not the source contributed to 99 percent of the site hazard in the original EPRI seismic hazard analyses. The tables also indicate that no new information has been identified that would lead to a significant revision of the source's geometry, maximum earthquake magnitude, or recurrence parameters. The seismicity recurrence parameters (a- and b-values) used in the EPRI seismic hazard study were computed for each one-degree latitude and longitude cell that intersects any portion of a seismic source.

The validity of the EPRI-SOG seismic source zone information with respect to seismicity that has occurred since that work was completed in 1984 is further discussed in Section 2.5.2.3.

Each EST used separate nomenclature to describe the seismic sources in the CEUS and the NMP3NPP site region. A number of different names may have been used by the EPRI teams to describe the same or similar tectonic features or sources, or one team may describe seismic sources that another team does not. Each team's source names, data, and rationale are included in their team-specific documentation (EPRI, 1986). Brief descriptions of the seismic sources that contribute 99 percent of the site seismic hazard are described in the following sections.

As indicated in this section, the EPRI PSHA study (EPRI, 1989a) expressed maximum magnitude (M_{max}) values in terms of body-wave magnitude (m_b), whereas most modern seismic hazard analyses describe M_{max} in terms of moment magnitude (M). To provide a consistent comparison between magnitude scales, this study relates body-wave magnitude to moment magnitude using the arithmetic average of three equations, or their inversions, presented by Atkinson (Atkinson, 1995) and by Frankel (USGS, 1996) and in EPRI TR-102293 (EPRI, 1993).

The conversion relations are very consistent for magnitudes 4.5 and greater and begin to show divergence at lower magnitudes. Throughout this section, the largest assigned values of M_{max} distributions assigned by the ESTs to seismic sources are presented for both magnitude scales (m_b and M) to give perspective on the maximum earthquakes that were considered possible in each seismic source. For example, EPRI m_b values of M_{max} are followed by the equivalent M value.

The most significant EPRI sources for each of the six ESTs, with respect to the NMP3NPP site, are described below. For each team, the listed sources contributed to 99 percent of the total seismic hazard for that team at the NMP3NPP site. The assessment of these and other EPRI sources within the site region has found that the EPRI source parameters (maximum magnitude, geometry, recurrence rate) are sufficient to capture the current understanding of the seismic hazard in the site region.

No new seismological, geological, or geophysical information in the literature published since the 1986 EPRI source model (EPRI, 1986) suggests that these sources should be modified for the NMP3NPP site.

The most significant sources, deemed to be those that contribute 10% or more to hazard are as follows:

Bechtel:	BEC-07, BEC-C, BEC-BZ7, BEC-03
Dames & Moore:	DAM-03, DAM-38, DAM-C09, DAM-C10, DAM-59
Law:	LAW-11, LAW-17, LAW-111, LAW-12
Rondout:	RND-33, RND-35, RND-47, RND-37
Woodward-Clyde:	WCC-19, WCC-33, WCC-34, WCC-B14, WCC-12
Weston Geophysical:	WGC-05, WGC-C13, WGC-01

2.5.2.2.1.1 Sources Used for EPRI PSHA – Bechtel Group

Bechtel Group identified and characterized four discrete seismic sources and three background zones that contribute to 99 percent of the hazard at the NMP3NPP site. All of these sources are within the site region and include the zones listed below that are 99% contributors to site hazard at 0.394 in/s (0.394 in/s (1 cm/s). The Bechtel seismic source zones from pre-1985 and 1985-2007 are shown in Figure 2.5-77 and Figure 2.5-78, respectively. Seismic sources identified by the Bechtel Group team within the site region are listed in Table 2.5-3 along with properties for each source.

The heading for each source zone includes the percentage source contribution for each team's zones. A brief discussion of each of the seismic sources that contribute to 99 percent of the site hazard is provided below.

BEC-03

The Charlevoix-La Malbaie source zone is highly localized but active seismic zone about 100 by 150 miles (161-241 km) in area along the course of the St. Lawrence River in southern Quebec, Canada. Its historic large events have magnitudes estimated at 7. There is a good correlation between locations for most of the seismic events and faults striking parallel to the river. The seismic activity may be related to the impact of a large meteorite in the Devonian or Ordovician which weakened the crust at this location. The source zone's geologic expression is defined by a crater structure and associated faulting, St. Lawrence paleo-rift faults, and its position at the contact between the margin of the ancient Grenville cratonic rocks and rocks representing the Appalachians along the paleo-rift.

BEC-07 - Bonnechere Graben

The Ottawa- Bonnechere Graben runs from the Ottawa–Montreal area on the east to near Sudbury and Lake Nipissing on the west. On the east, it joins the St. Lawrence rift system, a half-graben which extends more than 1,000 km along the St. Lawrence River valley and links the Ottawa and Saguenay Grabens.

The Ottawa-Bonnechere Graben a branch of the Timiskaming Graben, is an ancient rift valley in the Canadian Shield of Northeastern Ontario and Quebec, Canada. This rift valley is bounded the Mattawa and Petawawa faults. The graben appears to be the source of occasional release stress in the form of earthquakes, such as the 1935 Timiskaming earthquake. The length of the graben is about 700 km (435 mi).

BEC-11 - Clarendon-Linden Fault

The Clarendon-Linden fault system is a major series of fault lines in western New York. It extends through Orleans, Genesee, Wyoming, and into Allegany counties. The Clarendon-Linden fault is located on the western flank of gravity and magnetic anomalies that traverse western New York.

While the seismicity in this zone is largely confined to the area near Attica and Dale, New York the entire Clarendon/Linden-Scotch Bonnet-Rise is considered to act as a single zone. The zone is one of distributed movement along several major north-south trending high angle faults.

BEC-C - Western Quebec Seismic Zone

The Western Quebec Seismic Zone which extends from northern New York into western Quebec is a large and homogeneous seismotectonic region, although geologically complex. This source zone is based essentially on the observed concentration of seismicity. It is approximately rectangular in shape with a length of about 400 km and a width of about 200 km. The seismic potential of this zone is assigned at 15%.

Source zone C is presented as an alternative to source zones 07, 10, and 12 with which it shares the same area.

BEC-D - Niagara area/peninsular

Also termed the western Lake Ontario-Niagara-Attica and the Niagara-Pickering Zone, this is a discreet narrow area of geophysical features that crosses Lake Ontario with a north-south trend in western New York.

Sources of earthquakes for this zone may be limited to the intersections of small faults with either the gravity or magnetic lineaments located here. With most of the faulting shallow, large earthquakes are not expected, with moderate earthquakes only occasional events. The zone has experienced sporadic seismicity during its history; a few small earthquakes may occur over several months and then years go by before occurrence of another temporal cluster.

BEC-BZ5 - Southern Appalachians Region

This large background zone is source-independent. Seismic sources within this background zone are 13, 15, 16, 17, 19, 23, 24, 25, E, F, and G.

BEC-BZ6 - Southern Eastern Craton Region

This large background zone is source-independent. Seismic sources within this background zone are 11, 27, 45, D, and N1.

BEC-BZ7 - Northern Eastern Craton Region

This large background zone is source-independent. This zone is made up of two principal groups of sources: (1) The St. Lawrence rift/La Malbaie group and (2) The western Quebec group. Source zones 02, 03, 07, 10, 12, and C are located within this background zone.

The following is a Bechtel source zone that is a less than 1% contributor at 0.394 in/s (1 cm/s).

BEC-C05 - Combination Zone 5

This zone consists of a combination of zones D and 11.

2.5.2.2.1.2 Sources Used for EPRI PHSA – Dames & Moore

Dames & Moore identified and characterized three seismic sources and four combination zones that contribute to 99 percent of the hazard at the NMP3NPP site. The Dames and Moore seismic source zones from pre-1985 and 1985-2007 are shown in Figure 2.5-79 and Figure 2.5-80, respectively. Seismic sources identified by the Dames & Moore team within the site region are listed in Table 2.5-3 along with properties for each source. The following are Dames and Moore source zones that are 99% contributors at 0.394 in/s (1 cm/s).

DAM-01 (through C09, 10 and 11) - Western Quebec Seismic Zone

See BEC-C

DAM-03 - Adirondacks Zone

This large dome exposure of Precambrian basement, lacks evidence of a group of structures responsible for its seismic activity. Seismicity is concentrated in the northeastern two-thirds of feature; the southwestern third of the dome is relatively quiet for both large and small events. The Adirondack zone generates moderate sized earthquakes. Seismicity appears to be associated with border of dome structure at depth as opposed to dome interior.

DAM-09 - Clarendon-Linden Zone

See BEC 11.

DAM-38 - Gloucester Fault

The Gloucester fault is part of the Ottawa-Bonnechere fault system.

DAM-39B - Gloucester and Winchester Springs Faults

Zone 39B encompasses zones 38 and 39 (The Gloucester Fault and the Winchester Springs Fault. The Gloucester and Winchester Springs Faults Seismic Zone is drawn primarily on the basis of the zone of seismicity trending west-north-westerly from northern New York State through the Timiskaming region in eastern Ontario. The western Quebec seismic zone also encompasses portions of the failed rift area of the St. Lawrence Rift as well as the Ottawa Bonnechere Graben.

DAM-59

See BEC-03.

DAM-C09 - Combination Zone 09

This zone consists of a combination of Zones 01 and 38.

DAM-C10 - Combination Zone 10

This zone consists of a combination of Zones 01 and 39.

DAM-C11 - Combination Zone 11

This zone consists of a combination of Zones 01 and 39B.

The following is a Dames and Moore source zone that is a less than 1% contributor at 0.394 in/s (1 cm/s).

DAM-C02 - Combination Zone 02

This zone consists of a combination of Zones 08 and 09.

2.5.2.2.1.3 Sources Used for EPRI PSHA – Law Engineering

Law Engineering identified and characterized three seismic sources that contribute to 99 percent of the hazard at the NMP3NPP site. The Law Engineering seismic source zones from pre-1985 and 1985-2007 are shown in Figure 2.5-81 and Figure 2.5-82, respectively. Seismic sources identified by the Law team within the site region are listed in Table 2.5-3 along with properties for each source.

The following are source zones that are 99% contributors at 0.394 in/s (1 cm/s).

LAW-11 - Ottawa-Bonnechere Graben

See the Bechtel B-07 source description.

LAW-12

See BEC-03.

LAW-17 - Eastern Basement including Giles County – Eastern Tennessee Seismic Zone

This zone contains a large number of tectonic features however; the pattern of seismicity allows consideration as a single background source.

LAW-111 - Laurentian

This background zone has a western boundary at the Grenville front as interpreted from magnetic and gravity data. The southern edge is a belt of abundant high frequency magnetic anomalies in New York and the eastern boundary is along the St. Lawrence Lowlands.

2.5.2.2.1.4 Sources Used for EPRI PSHA – Rondout Associates

Rondout identified and characterized five seismic sources that contribute to 99 percent of the hazard at the NMP3NPP site. The Rondout seismic source zones from pre-1985 and 1985-2007 are shown in Figure 2.5-83 and Figure 2.5-84, respectively. Seismic sources identified by the Rondout team within the site region are listed in Table 2.5-3 along with properties for each source.

The following are Rondout source zones that are 99% contributors at 0.394 in/s (1 cm/s).

RND-33 - Niagara-by-the-Lake

This rectangular zone extends beyond the west end of Lake Ontario into central New York State. Sources of earthquakes may be limited to the intersections of small faults with either the gravity or magnetic lineaments mapped here. See BEC-D.

RND-34 - Nessmuk

See DAM-03. The Adirondack Mountains, this large exposure of Precambrian basement, lacks evidence of a group of structures responsible for its seismic activity.

RND-35 - Tramblant

See BEC-07

Rondout-37

See BEC-03.

RND-47 - Cornwall/Massena/Montreal

It is at a triple junction with the Ottawa-Bonnechere Graben intersecting the St. Lawrence Rift and the Champlain graben bridging far northern New York into Canada. This is a zone of moderate seismicity.

RND-C02 - Combination Zone 2

This zone consists of background zone 50 with zones 12 and 33 excluded.

2.5.2.2.1.5 Sources Used for EPRI PSHA – Weston Geophysical

Weston Geophysical identified and characterized 6 seismic sources that contributed to 99 percent of the hazard at the NMP3NPP site. The Weston Geophysical seismic source zones from pre-1985 and 1985-2007 are shown in Figure 2.5-85 and Figure 2.5-86, respectively. Seismic sources identified by the Weston team within the site region are listed in Table 2.5-3 along with properties for each source.

WGC-01

See BEC-03.

WGC-05 - The Western Quebec Zone

See BEC-C.

WGC-07 - Niagara Peninsula

This source zone is located between Lakes Erie and Ontario. Magnetic anomalies coincide with aeromagnetic lineaments to define it. See BEC-D.

WGC-08 - Clarendon-Linden Structure

See BEC 11.

WGC-C12 - Combination Zone 12

This zone consists of a combination of zones 101 and 7.

WGC-C13 - Combination Zone 13

This zone consists of a combination of zones 101 and 8.

WGC-C14 - Combination Zone 14

This zone consists of a combination of zones 101 and 29.

WGC-C16 - Combination Zone 16

This zone consists of a combination of zones 101, 7.

The following is a Weston Geophysical source zone that is a less than 1% contributor at 0.394 in/s (1 cm/s).

WGC-04 - The St. Lawrence Rift

A narrow zone along the St. Lawrence River in Canada, this source zone is restricted to the portion of the rift located between the La Malbaie source and Western Quebec sources, both of which have distinctively higher seismicity. The observed seismicity in this zone is very low and almost indistinguishable from that of the background and the western New England Foldbelt.

WGC-29 (through C14) Anna Ohio

A historically continuous but isolated source of seismic activity in western Ohio unrelated to any obvious tectonic features.

WGC-101 (through C12, 13 and 14) S. Ontario, Ohio, Indiana

This large background zone is source-independent. Seismic sources within this background zone are

2.5.2.2.1.6 Sources Used for EPRI PSHA – Woodward-Clyde Consultants

Woodward-Clyde Consultants identified and characterized seven seismic sources that contributed to 99 percent of the hazard at the NMP3NPP site. The Woodward-Clyde seismic source zones from pre-1985 and 1985-2007 are shown in Figure 2.5-87 and Figure 2.5-88, respectively. Seismic sources identified by the Woodward-Clyde team within the site region are listed in Table 2.5-3 along with properties for each source. The following are Woodward-Clyde source zones that are 99% contributors at 0.394 in/s (1 cm/s).

WCC-1 - Greater Western Quebec

This source zone, which extends from northern New York into western Quebec, is based on the observed concentration of seismicity. The seismic potential of this zone is assigned at 15%.

WCC-12

See BEC-03.

WCC-18 - Adirondack Dome/Uplift

See DAM-03.

WCC-19 - Western Quebec Crustal Block

Western Quebec Seismic Zone is largely confined to this block. SW trend of activity extends beyond block boundaries; other scattered activity also outside of block (may be result of location uncertainties, especially for older events). Seismicity more concentrated within southeastern half of block, and along the northeast edge of block. Activity includes moderate-to-large and small magnitude earthquakes.

WCC-33 - Western New York – Southern Ontario Trend

A WNW trending zone of seismicity, extending from western New York into southern Ontario south of Toronto, this zone may be confined to a crustal block or broad zone along a crustal block boundary.

WCC-34 – Attica, NY Intersection

This source zone is defined as a region in which a number of features intersect. Its plan view is roughly circular and has a 75 km diameter. Seismic potential along the portion of the Clarendon-Linden fault system included within this source zone may be elevated, while along the rest of the system it may be low.

WCC-B14 – Background source for NMPNS site

This zone was constituted around the NMPNS site itself by the WCC team. This approach was a standard element of this teams approach to seismic zonation.

WCC-C10 - Combination Zone 10

This zone consists of a combination of zones 32 and 34.

2.5.2.2.2 Recent Neotectonic Studies

Recent studies address the existence of regional faulting or seismicity not previously studied. These are outlined below.

2.5.2.2.2.1 St. Lawrence Rift Faulting

Wallach (Wallach, 2002) discusses the inferred existence of paleotectonic faults beneath Lake Ontario and their potential for continuity with the St. Lawrence Rift faulting. These features, found in one lake-bottom location, range from meters to tens of kilometers in length. Wallach suggests that these features may represent a continuation of the St. Lawrence Rift Zone into the Lake Ontario basin, a topographically deep and parallel physiographic structure. The patterns of historic seismicity as shown in Figure 2.5-74, Figure 2.5-75, and Figure 2.5-76, show historic epicenters for events within the site region that have a magnitude of 3.0 or greater. The presence of historic seismic events is very low in the area of that study, suggesting the features identified are not historically related to seismicity.

Wallach~~, 2002~~ suggests consideration for regional occurrence of earthquakes up to magnitude 7 based on conjecture that these identified faults are directly related to the St. Lawrence Rift fault zone. Wallach states that seismic activity would be most likely at the intersection of the postulated extension of the St. Lawrence Fault Zone with other major faults. Known or suspected seismically active features that intersect the postulated extension of St. Lawrence Fault Zone are located in far western Lake Ontario (Wallach, 1998). The intersecting features are, from east to west, the Clarendon-Linden fault, the Wilson – Port Hope magnetic lineament, the Niagara-Pickering and Georgian Bay linear zones and the Hamilton-Lake Erie lineament. These

intersections are all located significantly west (by more than 50 miles) of the NMP3NPP site. In the absence of any historic seismicity, large earthquakes have been considered by the EPRI (EPRI, 1986) teams with an appropriate low probability as shown in Table 2.5-3. However, the uneven distribution of historic seismicity, as shown on Figure 2.5-77 through 88, is not consistent with Wallach's extrapolation of the St. Lawrence seismic zone to the area of Lake Ontario or its designation as a single, coherent zone.

2.5.2.2.2.2 Appalachian Basin of New York State

Jacobi (Jacobi, 2002), using lineament and related outcrop studies, argues for the presence of more faults and more active faults in the Appalachian Basin of New York State than are currently accounted for by prior studies. Jacobi also provides a comprehensive compendium of faults and related structures for New York State, noting the correspondingly located seismic events. The events cited are generally those with magnitudes less than 2 or 3. Jacobi's speculation that many of these faults are "active" is based on regional rather than local study and for many locations, geographic correlation with low level seismicity which may be a consequence of background level events. This study also assumes an inherent genetic link between surface faulting and seismicity, a concept that has not found general support in CEUS fault studies. The USGS on-line database of Quaternary faults (USGS, 2006) contains no known Quaternary faults (younger than 1.6 million years) in the site's region at the earth's surface. Refer to Section ~~2.5.1.1~~ 2.5.3.1 for a discussion of paleoliquefaction studies in New York State.

2.5.2.2.2.3 Lancaster Seismic Zone

The Lancaster Seismic Zone (LSZ) of southeastern Pennsylvania, discussed in Section 2.5.1.1, is identified as a post-EPRI seismic zone located about 200 mi (322 km) south of the NMP3NPP site. This region of seismicity is in the Appalachian mountains of Pennsylvania and includes roughly two centuries of seismicity. Despite its moderate rate of activity, the largest known earthquake was magnitude m_{bLg} 4.1 (SSA, 1987). One larger event has been attributed to anthropogenic causes (i.e. Cacoosing Valley Earthquake m_{bLg} 4.6; (Seeber, 1998). No evidence of larger prehistoric earthquakes, such as paleoliquefaction features, has been discovered (Wheeler, 2006). While the lack of large earthquakes in the relatively short historical record cannot preclude the future occurrence of large events, there is a much higher degree of uncertainty associated with the assignment of M_{max} for the LSZ than other CEUS seismic source zones, such as New Madrid and Charleston, where large historical earthquakes are known to have occurred.

Although the Lancaster seismic zone is not explicitly included in the original EPRI source model (EPRI, 1986), various EPRI source geometries and parameters provide conservative M_{max} distributions for the LSZ. A wide range of M_{max} values and associated probabilities were assigned to these EPRI sources to reflect the uncertainty of multiple experts from each EST. The body-wave magnitude (m_b) M_{max} values assigned by the ESTs for source geometries that envelop the LSZ range from m_b 5.3 to 7.2 (M 4.88 to 7.5). The Dames & Moore sources that envelop the LSZ include an upper-bound M_{max} value of m_b 7.2 (M 7.5). Sources from the Woodward-Clyde and Rondout teams that envelop the LSZ were also assigned large upper-bound M_{max} values of m_b 6.8 to 7.1 (M 6.8 to 7.33). Thus, the maximum magnitude distributions of EPRI source zones are significantly greater than the largest reported earthquake in the LSZ.

Despite the identification of the LSZ by Armbruster and Seeber (SSA, 1987), subsequent post-EPRI seismic source characterizations studies (Chapman, 1994) (USGS, 1992) (USGS, 2002) do not identify the zone as a seismic source zone. The M_{max} distribution assigned to the seismic source zones that cover, but do not define, the LSZ are m_b 7.2 (M 7.5) (Chapman, 1994), m_b 5.78 (M 5.4) (Bollinger, 1992), and m_b 7.2 (M 7.5) (USGS, 1996) (USGS, 2002). Like the EPRI models,

these magnitude distributions are larger than any instrumented or pre-instrumental historical events dating back to the 18th century (SSA, 1987). However, all of the post-EPRI (EPRI, 1986) background sources zones that encompass the LSZ effectively capture the EPRI background zones for the LSZ. Based on the available seismological and geologic evidence and available published literature for the LSZ, the existing EPRI seismic source model does not require a significant change. Therefore, it is concluded that no new information has been developed since 1986 that would require a significant revision to the EPRI seismic source model.

2.5.2.2.2.4 United States Geological Survey (USGS) Model

In 2002, the USGS produced updated seismic hazard maps for the conterminous United States based on new seismological, geophysical, and geological information (USGS, 2002). The 2002 maps reflect changes to the source model used to construct the previous version of the national seismic hazard maps (USGS, 1996). The most significant modifications to the CEUS portion of the source model include changes in the recurrence, M_{max}, and geometry of the Charleston and New Madrid sources. Further changes were adopted in USGS, 2008.

Unlike the EPRI models that incorporates many local sources, the USGS source model in the NMP3NPP site region (200 mi (320 km) radius) includes only two background sources that are important to the site hazard: the Eastern Extended Margin background and the Stable Craton. The former zone contains the Charlevoix subzone which was considered for the NMP3NPP site using the EPRI model, although outside of the site's 200-mile radius and subzones for the Eastern Tennessee, Charleston SC and New Madrid zones. For the latter subzones the earthquake recurrence is modeled using paleoliquefaction data so that the hazard for the large background or "maximum magnitude" zones is largely based on historical seismicity and the variation of that seismicity. This characteristic of the model is termed Smoothed Gridded Seismicity and it serves to generate results exclusively on the basis of historic seismicity.

The USGS model is intended for use building codes for ordinary building and construction and target probability levels range from .0021/year (475 y event) to .0004/year (2,500 year event), referred to as the maximum considered event (MCE) for ordinary buildings. The nuclear power industry targets more remote probabilities (.0001 to .00001 /yr) for seismic design specifications; thus the EPRI model developed for determining ground motions at very low probabilities of exceedance continues to be the most suitable probabilistic model for the NMP3NPP project and is used for many other new nuclear plant sites. This choice is also due to its highly detailed technique and its broader approach, using integrated opinions from six separate teams of geologic, seismologic and tectonic experts, weighted to obtain a most objective integration of facts and opinion. Further evidence for the quality and accuracy of the EPRI model is confirmed by the NMP3NPP project's investigation of recent seismicity, 1985-2007. Recent events in the site region consistently occur spatially in the EPRI zones and they are also consistent with magnitudes predicted for the model.}

2.5.2.3 CORRELATION OF EARTHQUAKE ACTIVITY WITH SEISMIC SOURCES

The U.S. EPR FSAR includes the following COL Item in Section 2.5.2.3:

> Correlation of earthquake activity with seismic sources is site specific and will be addressed by the COL applicant, consistent with the guidance of RG 1.208 and RG 1.165, as appropriate.

This COL Item is addressed as follows:

{The updated EPRI seismicity catalog was reviewed in order to evaluate the spatial pattern of seismicity relative to the EPRI seismic source model (EPRI, 1986) and potential correlation of

seismicity to possible geologic or tectonic structures. The EPRI seismicity catalog covers earthquakes in the CEUS for the time period from 1627 to 1984, as described in Section 2.5.2.1. This catalog has been updated for this NMP3NPP site investigation for the time period from 1985 to 2007, as described in Section 2.5.2.1. Figure 2.5-74 through Figure 2.5-88 show the distribution of earthquake epicenters from both the EPRI (pre-1985) and updated (post-1984) earthquake catalogs in comparison to the seismic sources identified by each of the EPRI ESTs.

Figure 2.5-188 illustrates a spatial interpretation of density pattern of seismicity determined for the EPRI-SOG catalog for the time period from 1627 through 1984. The map was prepared with no lower magnitude threshold of earthquake size; thus it includes earthquakes in the magnitude range of approximately 2 to 7 m_b. This was the earthquake history known to the 6 ESTs, and which was applied in combination with geologic and tectonic data to define their regional seismic source zones. Regions of enhanced seismic activity within 200 miles of NMP3NPP include the Adirondack Highlands and Western Quebec Zone to the east and north, the Niagara Peninsula and western Lake Ontario to the west, and the area of northern New Jersey and adjacent NY State, inclusive of the Ramapo Fault Zone, to the south. Additional regions of enhanced seismic activity beyond 200 miles (320 km) from the NMP3NPP site include the Northern Appalachians that extend through central and eastern New England into New Brunswick Province Canada. The most seismically active region on Figure 2.5-188 is the Charlevoix Zone located 435 miles (700 km) northeast of the NMP3NPP site along the St Lawrence River in Quebec Province Canada.

Comparison of ESTs seismic source zones (Figure 2.5-77 through Figure 2.5-88) with the patterns of enhanced seismic activity illustrated on Figure 2.5-188 demonstrate that each EST introduced seismic sources and various alternative sources to account for the known pattern of seismic activity. Differences in source zone boundaries among the ESTs arise from uncertain or poorly defined correlations of earthquake activity to local geologic and tectonic features to explain the observed patterns of seismic activity.

Seismic sources defined by the ESTs are compared to recent seismic activity from 1985 to 2007 on the even-numbered figures from Figure 2.5-78 to Figure 2.5-88. Also, Figure 2.5-189 illustrates a spatial interpretation of earthquake epicenter densities for the recent quarter century time period since completion of the EPRI-SOG seismic hazard study. This recent time period can be characterized as being completely 'instrumental' in that earthquake location and magnitude parameters are entirely determined using data from regional and national seismographic networks. The EPRI-SOG pre-1985 catalog has a significant 'historical' component for which earthquake location and size parameters are determined based on ground motion effects on people and infrastructure as evaluated on the Modified Mercalli Intensity Scale. Zones of enhanced seismic activity using more accurate seismicity data shown on Figure 2.5-189 repeats the seismicity pattern on Figure 2.5-188 determined from the 'historical' and partly instrumental EPRI-SOG catalog. Seismic source zones identified by the ESTs in 1986 within 200 miles of the NMP3NPP site (e.g. Adirondacks, Western Quebec, Niagara Peninsula, northern New Jersey and southeast New York) represent predictions of locations of future seismic events. It is concluded based on comparisons of Figure 2.5-188 and Figure 2.5-189 that the EPRI-SOG source zones have been reliable predictors of the most recent 25 years of seismic activity. No modifications of the ESTs seismic source boundaries were made for performance of the NMP3NPP PSHA.

One deviation from the historical seismicity pattern occurred beyond the 200-mile (320-km) radius of the NMP3NPP site. The 5.9 M Saguenay earthquake in 1988, located more than 450 miles (724 km) northeast of NMP3NPP, occurred west of the Charlevoix Zone in a region that exhibited background seismicity levels based on the EPRI-SOG pre-1985 catalog. Due to the distance from the NMP3NPP site no zone modifications were made to EST source zones to

include a zone for the Saguenay earthquake. The more seismically active Charlevoix Zone located closer to NMP3NPP was included in the NMP3NPP PSHA.

Figure 2.5-190 illustrates the current seismicity pattern using the combined EPRI-SOG pre-1985 catalog and the catalog update for the time period from 1985 to 2007. Also shown on the figure are locations of earthquakes with magnitude 5 m_b or greater. Recent earthquakes within 200 miles of the site of magnitude 5 and larger are located within the Adirondack Highlands and Western Quebec Zone.

Seismic activity rates for the 200-mile (320 km) radius region surrounding the NMP3NPP site are compared for the EPRI-SOG pre-1985 catalog and for the catalog updated through 2007. Using events listed in Table 2.5-1, the rate of earthquakes in the magnitude range of 4.0 to 4.99 for the EPRI-SOG catalog is 18 events since 1917, or 0.269 per year (e.g 18 in 67 years). Earlier time periods in the EPRI-SOG catalog are likely incompletely reported for magnitude 4 earthquakes; thus the activity rate was determined for the period since 1917. Eleven additional events in this magnitude range occurred since 1985. The activity rate through 2007 is 0.320 (e.g. 29 in 91 years). These annual activity rates represent a small variation in mean return period of magnitude 4 m_b earthquakes of 3.7 years (EPRI-SOG) to 3.1 years (through 2007).

Activity rates for magnitude 5 m_b earthquakes were determined for the time period since 1732. Resulting mean return periods for 5 m_b also show small variation for the region with 200 miles (320 km) of the NMP3NPP site. The return period for the pre-1985 catalog is 50 years compared to 46 years determined for the updated catalog spanning 1732 through 2007. The recent seismic activity since 1985 repeats the spatial pattern as well as earthquake activity rates determined from the EPRI-SOG pre-1985 catalog. These facts support a conclusion to use the EST seismic source zone and seismicity parameters intact for performance of the NMP3NPP PSHA. Following is a summary of conclusions related to usage of the EPRI-SOG models.

~~Comparison of the updated earthquake catalog to the EPRI earthquake catalog (EPRI, 1988) yields the following conclusions:~~

- The updated catalog does not show any earthquakes within the site region that can be associated with a known geologic or capable tectonic structure. Low-level seismicity is known to occur throughout the northeastern region of the United States, but the distribution of historic and instrumentally detected events appears in most instances to be unrelated to movement on either specific or known geological structures. The site region (to a 50 mile (80 km) radius) exhibits very low Seismicity.

- The updated catalog does not show a unique cluster of seismicity that would suggest a new seismic source outside of the EPRI seismic source model (EPRI, 1986), except for the Saguenay earthquake, which is located more than 450 miles (724 km) from the NMP3NPP site.

- The updated catalog does not show a pattern of seismicity that would require significant revision to the EPRI seismic source geometry.

- The updated catalog does not show or suggest any increase in M_{max} for any of the EPRI seismic sources (EPRI, 1986).

- The updated catalog does not show any increase in seismicity parameters (rate of activity, b value) for any of the EPRI seismic sources (see Section 2.5.2.6.5) (EPRI, 1986).}

2.5.2.4 Probabilistic Seismic Hazard Analysis and Controlling Earthquake

The U.S. EPR FSAR includes the following COL Item in Section 2.5.2.4:

> The probabilistic seismic hazard analysis is site specific and will be addressed by the COL applicant, consistent with the guidance of NUREG/CR-6372, RG 1.165 and RG 1.208, as appropriate.

This COL Item is addressed as follows:

{Sections 2.5.2.4.1 through 2.5.2.4.6 are added as a supplement to the U.S. EPR FSAR.

2.5.2.4.1 1989 EPRI Probabilistic Seismic Hazard Analysis

Following the recommendation of Regulator Guide 1.165 (NRC, 1997)), the 1989 EPRI study, EPRI NP-6395-D (EPRI, 1989a) forms a basis with which to start seismic hazard calculations. The first step was to replicate the results published from the 1989 EPRI study (EPRI, 1989a), to verify that seismic sources were modeled correctly and that the current seismic hazard software could accurately reproduce the 1989 results. The PSHA software used determines the annual frequency of exceedance as a function of minimum ground motion in an integration of hazard contribution of seismic sources - characterized by various parameters, including spatial extent and location, magnitude frequency recurrence, and tectonic environment - propagating the ground motion from the sources to the site through an appropriate attenuation relation. This software and the manner in which it is used allows for the incorporation of numerous elements of modeling and parametric variability, including alternative models and parametric distributions, as well as consideration of statistical uncertainties. This replication was made using the ground motion equations from the 1989 EPRI study, and it was made for rock hazard conditions in order to remove any effect that soil amplification might have on the comparison.

PSHA results were published in the 1989 EPRI study for the NMPNS site, and the first task was to replicate those PSHA results using the same assumptions on seismic sources and ground motion equations, to ensure that seismic sources were modeled correctly and that the software being used (Risk Engineering, Inc.'s FRISK88 software) could accurately reproduce the 1989 study results. Table 2.5-4 compares the total mean annual frequencies of exceedence calculated for the NMPNS site to published annual frequencies of exceedence from the 1989 EPRI site for this site, for peak ground acceleration (PGA) amplitudes of 100, 250, and 500 cm/s^2. All results are for hard rock conditions. The "% diff" column shows the percent difference of hazard calculated for current calculations at the NMPNS site compared to the 1989 results. Comparisons are shown for mean PGA hazard and for the 15th fractile, median, and 85th fractile hazard curves. For the mean hazard curves, the current calculation indicates the same or slightly higher hazard, with up to 4% difference at 0.5g (where the annual mean hazard is less than 10^{-6}. This implies that the difference in mean ground motion for a fixed annual frequency of exceedence will be even smaller, about 1% or less. This is excellent agreement. Differences in hazard are also very small for the median and 85th fractile hazard, being (in absolute value) 7% or less. For the 15th fractile hazard, differences are higher, with the current results indicating up to 56% less hazard than the 1989 EPRI results. The largest differences (more than 10% in absolute value) occur when the 15th fractile annual hazard is less than 10^{-6} and probably relate to unstated conservative assumptions in the 1989 EPRI results that are important only at these very low annual frequencies.

The comparisons shown in Table 2.5-4 are considered excellent agreement, given that independent software is being used, that the difference in mean hazard is slightly positive, and that final recommendations for seismic spectra are made using the mean hazard. Differences in

seismic hazard for the 15th fractile, median, and 85th fractile are also small, except for the 15th fractile at annual frequencies less than 10^{-6}, which is of less concern.

Updates to some of the inputs to PSHA might lead to changes in the level of seismic hazard at the NMPNS site compared to what would be calculated based on the EPRI (1989) evaluation. Seismic source characterization data and ground motion assumptions that could affect the calculated level of seismic hazard include:

- Updates in the characterization of the rate of earthquake occurrence as a function of magnitude for one or more seismic sources.
- Updates in the characterization of the maximum magnitude for seismic sources.
- Identification of a possible new seismic source in the site vicinity.
- Updates to models used for estimating strong ground shaking and its variability in the central and eastern US.

Possible changes to seismic hazard caused by changes in these areas are addressed in the following sections.

2.5.2.4.2 Effects of New Regional Earthquake Catalog

One of the important sensitivity studies examined the effect of earthquakes that have occurred since the 1989 EPRI study (EPRI, 1989a) was performed in order to determine if activity rates have changed. Seismicity rates in the EPRI study were based on an earthquake catalog that extended through 1984. This sensitivity study examined additional earthquakes that occurred during the period of 1985 to 2005 and calculated rates of activity in regions surrounding the NMP3NPP site.

The effect of the updated earthquake catalog on earthquake occurrence rates was assessed by computing earthquake recurrence parameters for three test areas shown in Figure 2.5-89 and Figure 2.5-90. These consisted of a rectangular area (Region 1) encompassing seismicity in the vicinity of the site and Lake Ontario, a polygon (Region 2) encompassing seismicity in northeastern New York, Ontario, and Quebec, to the north and east of the site, and sources used by the EPRI teams to represent seismicity in the Charlevoix seismic zone. The truncated exponential recurrence model was fit to the seismicity data using the EPRI EQPARAM program, which uses the maximum likelihood technique. Earthquake recurrence parameters were computed first using the original EPRI catalog and periods of completeness, and then using the updated catalog and extending the periods of completeness to 2007, assuming that the probability of detection for all magnitudes is unity for the time period 1985 to 2005. The resulting earthquake recurrence rates for Regions 1 and 2 are compared in Figure 2.5-91 and Figure 2.5-92. The comparison for Region 1 shows that the extended earthquake catalog results in lower estimated earthquake reoccurrence rates. For Region 2, the calculated recurrence rate is about the same using the updated catalog as it is for the original 1989 EPRI catalog.

Table 2.5-5 compares the seismicity rates for m_b>6.8, 7.0, and 7.2 for the six EPRI teams. Each of the six teams used a different geometry for the Charlevoix seismic zone, as shown in Figure 2.5-90, and each of these geometries included a different set of earthquakes. One of the teams (Weston Geophysical Corporation) used two sources to represent Charlevoix seismicity. Table 2.5-5 compares seismicity rates for m_b values of 6.8 to 7.2 because this zone is some 700 km from the NMPNS site, so only the largest earthquakes will affect the site. Individual team estimates of maximum magnitude in the Charlevoix seismic zone ranged from 6.4 to 7.5.

Table 2.5-5 shows that, for three of the EPRI teams, the updated catalog indicates that the mean rate of occurrence of large earthquakes decreased, and for three EPRI teams the rate of occurrence increased. On average over all teams, the updated rates of occurrence of large earthquakes increased by 1.2% or less. This will not have a significant effect on seismic hazard at the NMPNS site, in part because the Charlevoix seismic zone contributes only a fraction of the total hazard.

On the basis of the comparisons shown in Figure 2.5-91 and Figure 2.5-92 and in Table 2.5-5, it is concluded that the earthquake occurrence rate parameters developed in the EPRI (1989) evaluation adequately represent seismicity rates for regions that will contribute to seismic hazard at the NMPNS site.

2.5.2.4.3 New Maximum Magnitude Information

As discussed in Section 2.5.2.3, no new scientific information has been published that would lead to a change in the EPRI seismic source characterization or parameters, including the assessment of maximum magnitude. As a result, the maximum magnitude distributions assigned to the 1989 EPRI sources have not been modified for the calculation of seismic hazard.

2.5.2.4.4 New Seismic Source Characterizations

Section 2.5.2.2 reviews new geological, geophysical, and seismological information related to seismic source characterization models developed for post-EPRI seismic hazard analyses. Section 2.5.2.3 describes the updated earthquake catalog that was developed to augment the EPRI (1989) earthquake catalog. Based on these evaluations, no additional specific seismic sources have been identified.

The Nine Mile Point seismic hazard analysis is based on the hazard calculation documented in the 1989 EPRI-SOG report (EPRI, 1989). The electronic files used for the Nine Mile Point site from the 1989 study were used as the starting point for the hazard calculations reported in the COL application.

In the EPRI-SOG study, all of the EPRI teams derived a source representing the St. Lawrence rift, as follows:

Bechtel source BEC-02

Dames & Moore source DAM-58

Law Engineering source LAW-9

Rondout source RND-39

Weston source WGC-04

Woodward-Clyde source WCC-14

None of these sources was included in the 1989 EPRI-SOG hazard calculation for Nine Mile Point. Because they were not considered to be significant contributors to the seismic hazard at the Nine Mile Point site.

Only four of the six EPRI teams derived a source representing earthquakes restricted to the southern New York area that might be representative of the Ramapo fault, as follows:

Dames & Moore source DAM-43

Rondout source RND-31

Weston source WGC-21

Woodward-Clyde source WCC-24

The EPRI-SOG methodology considered all sources within 200 km of each site, and considered the New Madrid, Charleston, and La Malbaie sources if they were within 500 km of the site (EPRI, 1989a). All sources were included in the analysis so that the combined hazard from all excluded sources was less than 1% of the total hazard. For this purpose, the hazard ("annual frequency of exceedence") at one PGA acceleration ("annual frequency of exeedance") and at one 1 Hz spectral velocity were considered. The St. Lawrence and Ramapo fault sources listed above lie outside the 200 km limit and were not included in the original EPRI-SOG analysis, and thus were not included in the hazard analysis for the COL application for Nine Mile Point.

To evaluate the potential contribution of these sources, several hazard sensitivity calculations were made that calculated seismic hazard from the Ramapo fault sources and from the St. Lawrence sources listed above. These sensitivity hazard calculations were made for 1 Hz and 10 Hz spectral accelerations, using the ground motion equations documented in the COL application and using the non-CAV rock hazard analysis. These are the assumption used to determine rock input motions for the site amplification study.

Figure 2.5-195 shows the mean 1 Hz seismic hazard calculated for the COL application (labeled "Total mean") along wth several curves representing the Ramapo fault. The mean annual frequency of exceedance from the four sources listed above are shown (each team source is weighted by the factor 1/6), and the total Ramapo annual frequency of exceedance curve (labeled "Ramapo") is shown as a dashed line. At the spectral acceleration corresponding to the 1E-4 annual frequency of exceedance for the "Total mean" curve, the Ramapo curve indicates an annual frequency of exceedance that is about a factor of 0.005 of the total annual frequency of exceedance. At higher spectral accelaerations, the relative annual frequency of exceedance of the Ramapo curve to the total annual frequency of exceedance is even lower. This means that the potential contribution of Ramapo annual frequency of exceedance to the total 1 Hz annual frequency of exceedance at Nine Mile Point is about 0.5% or less. Figure 2.5-196 shows a similar plot for 10 Hz spectral accelration, where the contribution from the Ramapo fault sources is even lower than for 1 Hz. The conclusion is that the Ramapo fault, as modeled by the EPRI teams, is not a significant contributor to annual frequency of exceedance at the Nine Mile Point site.

For the St. Lawrence sources, Figure 2.5-197 shows the mean annual frequency of exceedance curve for 1 Hz spectral acceleration calculated for the COL application (labeled "Total mean") along with several curves representing the St. Lawrence source. The mean annual frequency of exceedance from the six St. Lawrence sources listed above are shown (each team source is weighted by the factor 1/6), and the total St. Lawrence annual frequency of exceedance is shown as a dashed line. At the spectral acceleration corresponding to 1E-4 "annual frequency of exceedance" for the "Total mean" curve, the total St. Lawrence curve indicates an annual frequency of exceedance that is about a factor of 0.04 times the total annual frequency of exceedance. At higher spectral accelerations there is also a relative factor of about 0.04. This means that the potential contribution of the St. Lawrence faults of about 0.04. This means that the potential contribution of the St. Lawrence faults to the total 1 Hz annual frequency of exceedance at Nine Mile Point would be about 4%. Figure 2.5-198 shows a similar plot for 10 Hz spectral acceleration, where the contribution from the St. Lawrence fault sources is lower than

for 1 Hz (for 10 Hz it is less than 2% at the spectral acceleration corresponding to the 1E-4 "annual frequency of exceedance," and less than 1% at the spectral acceleration corresponding to 1E-5 "annual frequency of exceedance").

The log-log slope of the 1 Hz total mean hazard curve between 1E-4 and 1E-5 is about -2.5, meaning that if the seismic hazard curve is increased by a factor of 1.04 on the vertical (annual frequency of exceedance) axis (call this increase ΔH), the corresponding increase on the spectral acceleration (horizontal) axis can be calculated by the following relation:

$$\Delta A = \Delta H^{1/2.5}$$

where ΔA is the factor increase in spectral acceleration for a fixed annual frequency of exceedance. This means that an increase of 4% in the hazard curve would result in an increase in amplitudes corresponding to the 1E-4 and 1E-5 annual frequencies of exceedance of about $1.04^{0.4} = 1.016$, or about a 1.6% increase in UHRS amplitudes.

For the Nine Mile Point site, this increase caused by including the seismic hazard contribution from the St. Lawrence seismic sources would result in a very small increase in the ground motion response spectrum (GMRS) for the site. The GMRS would increase about 1.6%, which is very small compared to the exceedence of the EUR CSDRS over the GMRS (see FSAR Figure 3.7-1), which is approximately 500% at 1 Hz. Thus, the inclusion of St. Lawrence sources will have a negligible impact on the safety of the seismic design.

2.5.2.4.5 New Ground Motion Models

Ground motion models for the central and eastern US (CEUS) have been evolved since the EPRI (1989) study. An EPRI project was conducted to summarize knowledge about CEUS ground motions, and results were published in EPRI (EPRI, 2004). These updated equations estimate median spectral acceleration and its uncertainty as a function of earthquake magnitude and distance. Epistemic uncertainty is modeled using multiple ground motion equations with weights, and multiple estimates of aleatory uncertainty, also with weights. Different sets of sources are recommended for seismic sources that represent rifted versus (vs.) non-rifted regions of the earth's crust. Equations are available for hard rock site conditions at spectral frequencies of 100 hertz (Hz) (which is equivalent to peak ground acceleration, PGA), 25 Hz, 10 Hz, 5 Hz, 2.5 Hz, 1 Hz, and 0.5 Hz. All ground motion estimates are for spectral response with 5% of critical damping.

Aleatory uncertainties published in the EPRI (2004) model were re-examined by Abrahamson and Bommer (Abrahamson and Bommer, 2006), because it was thought that the EPRI (2004) aleatory uncertainties were probably too large, resulting in over-estimates of seismic hazard. The Abrahamson and Bommer (2006) study recommends a revised set of aleatory uncertainties and weights that can be used to replace the original EPRI (2004) estimates of aleatory uncertainty.

To correctly model the damageability of small magnitude earthquakes to engineered facilities, the Cumulative Absolute Velocity (CAV) model of Hardy et al. (Hardy, 2005) was used. The CAV model in effect filters out the fraction of small magnitude earthquakes that will not cause damage, and includes in the hazard calculations only those ground motions with CAV values greater than 0.15 g-sec. The filter that is used is based on empirical ground motion records and depends on ground motion amplitude, duration of motion (which depends on earthquake magnitude), and shear-wave velocity in the top 100 ft (30 m) at the site. The ground motions for frequencies other than 100 Hz are assumed to be correlated with the ground motions at 100 Hz, so that the filtering is consistent from frequency to frequency.

In summary, the ground motion model used in the seismic hazard calculations consisted of the median equations from EPRI (2004) combined with the updated aleatory uncertainties of the Abrahamson and Bommer (2006) study. The CAV filter was applied to account for the damageability of small magnitude earthquake ground motions.

2.5.2.4.6 Updated Probabilistic Seismic Hazard Analysis and Deaggregation for Rock

A PSHA for the NMPNS site was conducted using the six EPRI team's seismic source zone models with the updated ground motion model for the CEUS. The first calculation was made for hard rock conditions, which is consistent with the EPRI (2004) ground motion model, and was made without applying the CAV filter.

A PSHA consists of calculating annual frequencies of exceeding various ground motion amplitudes for all possible earthquakes that are hypothesized in a region. The seismic sources specify the rates of occurrence of earthquakes as a function of magnitude and location, and the ground motion model estimates the distribution of ground motions at the site for each event. Multiple weighted hypotheses on seismic source zone characteristics, including rates of occurrence and magnitude distribution, and ground motions (characterized by the median ground motion amplitude and its uncertainty) result in multiple weighted seismic hazard curves. From this family of weighted curves, the mean and fractile seismic hazard can be determined. The calculation is made separately for each of the six EPRI teams, and the seismic hazard distribution for the teams is combined, weighting each team equally. This combination gives the overall mean and distribution of seismic hazard at the site.

Figure 2.5-93 through Figure 2.5-99 show mean and fractile (5th, 16th, median, 84th, and 95th) seismic hazard curves for hard rock from this calculation for the spectral frequencies of 100, 25, 10, 5, 2.5, 1, and 0.5 Hz, respectively. Table 2.5-6 through Table 2.5-12 documents the digital fractile and mean seismic hazard curves for the seven spectral frequencies. Table 2.5-13 documents the UHRS values for this calculation. The calculation of rock hazard without CAV was used to deaggregate hazard and identify the magnitudes and distances appropriate to represent rock spectral shapes for site response calculations. The reason the non-CAV calculations were used for this purpose is that the CAV filter depends at each frequency on surface amplitude (among other parameters), and site amplification affects the surface amplitude. Thus, the appropriate time to apply the CAV filter is when performing hazard calculations that include site amplification, as described below.

The rock seismic hazard without CAV was deaggregated following the guidelines of Regulatory Guide 1.208 (NRC, 2007). Specifically, the mean contributions to seismic hazard for 1 Hz and 2.5 Hz were deaggregated by magnitude and distance for the mean 10^{-4} ground motion amplitude at 1 Hz and at 2.5 Hz, and these deaggregations were combined (contributions for each magnitude and distance bin were averaged). Figure 2.5-100 shows this combined deaggregation. Similar deaggregations of the mean hazard were performed for 5 and 10 Hz spectral accelerations (Figure 2.5-101). Deaggregations of the mean hazard for 10^{-5} and 10^{-6} ground motions are shown in Figure 2.5-102 through Figure 2.5-105. Table 2.5-14 through Table 2.5-19 show the percent contributions for various magnitude and distance bins for the six deaggregations, and Table 2.5-20 summarizes the mean magnitude and distance resulting from these deaggregations, for all contributions to hazard and for contributions with distances exceeding 62 miles (100 km). (Note that Table 2.5-20 gives mean distances computed using linear distance, not the exponent of mean logarithmic distance. The effect on the rock spectra described below is insignificant; differences in interpolated amplitudes using the two measures of mean distance are <0.5%.) For Figure 2.5-100 through Figure 2.5-105 and Table 2.5-14 through Table 2.5-19 and Table 2.5-20, deaggregation is given in terms of moment magnitude.

The deaggregation plots in Figure 2.5-100 through Figure 2.5-105 indicate that local earthquakes are the major contributor to seismic hazard at the NMPNS site for high frequencies (5 and 10 Hz). Seismicity to the north and east of the site (see Figure 2.5-89), at about 93-125 miles (150-200 km) distance, also contributes to high-frequency hazard. At low frequencies (1 and 2.5 Hz), these sources also dominate the hazard, but the Charlevoix seismic zone also has an important contribution for the 10^{-4} deaggregation (see Figure 2.5-96). This source lies about 435 miles (700 km) from the site (see Figure 2.5-91) but contributions are plotted in the last distance bin in Figure 2.5-100 through Figure 2.5-105.

Table 2.5-20 indicates mean magnitudes and distances calculated from the deaggregations, both for all distances and for R>100 km (62 miles). For the 1 and 2.5 Hz results, contributions from events with R>100 km (62 miles) exceed 5% of the total hazard. As a result, following the guidance of RG 1.208, the controlling earthquake for low-frequency (LF) ground motions was selected from the R>100 km (62 miles) calculation, and the controlling earthquake for high-frequency (HF) ground motions was selected from the overall calculation. The values of M and R selected in this way are shown in shaded cells in Table 2.5-20.

Smooth UHRS were developed from the UHRS amplitudes in Table 2.5-13, using controlling earthquake M and R values shown in Table 2.5-20 and using the hard rock spectral shapes for CEUS earthquake ground motions recommended in NUREG/CR-6728 (NUREG/CR-6728, 2001). Separate spectral shapes were developed for high frequencies (HF) and low frequencies (LF). In order to reflect accurately the UHRS values calculated by the PSHA as shown in Table 2.5-13, the HF spectral shape was anchored to the UHRS values from Table 2.5-13 at 100 Hz, 25 Hz, 10 Hz, and 5 Hz. In between these frequencies, the spectrum was interpolated using shapes anchored to the next higher and lower frequency and using weights on the two shapes equal to the inverse logarithmic difference between the intermediate frequency and the next higher or lower frequency. Below 5 Hz, the HF shape was extrapolated from 5 Hz. For the LF spectral shape a similar procedure was used except that the LF spectral shape was anchored to the UHRS values at 2.5 Hz, 1 Hz, and 0.5 Hz. Below 0.5 Hz and above 2.5 Hz, the LF shape was extrapolated from those frequencies. To create these spectral shapes, the single-corner and double-corner models recommended in NUREG/CR-6728 were weighted equally. For frequencies below 0.5 Hz, the spectral shape was extrapolated from the value at 0.5 Hz assuming a constant spectral velocity (i.e. spectral accelerations were assumed to scale linearly with frequency) down to 0.125 Hz (8 sec). From 0.125 Hz to 0.1 Hz, spectral accelerations were assumed to scale as $(\text{frequency})^2$. This follows the recommendation of FEMA 450 (FEMA 450, 2003) for long periods.

An evaluation of the deaggregation results prepared for the NMP3NPP site to those presented in Table 3.9 of NUREG/CR-6606 (NRC, 1998) for Nine Mile Point was performed. In general, the magnitude of the controlling earthquake at the 1E-4 and 1E-5 event probability is seen to be similar, with the NMP3NPP "controlling" earthquake magnitudes being only slightly higher than those presented in NUREG/CR-6606. However, the distance to the "controlling" earthquake was noticeably higher for the NMP3NPP deaggregation, as shown below.

Table 3.9 of NUREG/CR-6606 reports the following "controlling" magnitudes and distances for Nine Mile Point:

LLNL results: Magnitude of Controlling Earthquake = 5.5

Distance of Controlling Earthquake = 19 km

EPRI results: Magnitude of Controlling Earthquake = 5.3

Distance of Controlling Earthquake = 15 km

The NMP3NPP analysis resulted in the following high-frequency (5-10 Hz) deaggregation magnitudes and distances (Table 2.5-20):

1E-4 deaggregation:Magnitude of Controlling Earthquake = 5.7
Distance of Controlling Earthquake = 150 km.
1E-5 deaggregation:Magnitude of Controlling Earthquake = 5.4
Distance of Controlling Earthquake = 62 km

There are several reasons for the difference between the NMP3NPP deaggregation results and those presented in NUREG/CR-6606.

1. Mean vs. median. The NUREG/CR-6606 deaggregations are based on deaggregating the median hazard (example: Section 2.3.2 of NUREG/CR-6606), whereas the NMP3NPP site deaggregations are based on the mean hazard (per Appendix D of Regulatory Guide 1.208 (NRC, 2007)). This difference in deaggregation will cause a difference in the calculated magnitude and distance.

2. Deaggregation reference probability. NUREG/CR-6606 deaggregates at a reference annual probability of 1E-5 (see Step 2 in Section 2.3.2 of NUREG/CR-6606). NMP3NPP deaggregates are provided at both the 1E-4 and 1E-5 event probability. The 1E-4 deaggregation distance will be farther than the 1E-5 deaggregation distance.

3. Distant sources. The NMP3NPP deaggregation includes the effect of distant seismic sources, such as the Charlevoix source at about 700 km (see Figure 2.5-101). The 1989 EPRI-SOG calculations did not include these distant sources. The inclusion of distant sources will increase the deaggregation distance.

4. Effect of logarithmic distance. The NMP3NPP deaggregations represent mean distance, whereas the NUREG/CR-6606 deaggregations represent the antilogarithm of mean logarithmic distance (see equations in Section 2.3.1 of NUREG/CR-6606). Using the logarithmic distance method for the seismic sources in the NMP3NPP deaggregation, the deaggregations would be

   E-4 deaggregation:Magnitude of Controlling Earthquake = 5.7
   Distance of Controlling Earthquake = 73 km
   1E-5 deaggregation:Magnitude of Controlling Earthquake = 5.4,
   Distance of Controlling Earthquake = 23 km

5. The difference in interpolated rock spectra between using these logarithmic distances vs. the original mean distances ranges from +0.2% to -0.5%, for the 1E-4, 1E-5, and 1E-6 spectra. Thus there is not a significant difference in spectral shape between the two distance measures.

The NUREG/CR-6606 deaggregations are based on ground motion equations developed in the 1980's. The NMP3NPP deaggregations are based on EPRI ground motion equations from 2004-2006. Differences in magnitude scaling and consideration of Moho bounce effects will cause differences in deaggregation results.

Figure 2.5-106 through Figure 2.5-108 show the horizontal HF and LF spectra calculated in this way for 10^{-4}, 10^{-5}, and 10^{-6} annual frequencies of exceedence, respectively. As mentioned

previously, these spectra accurately reflect the rock UHRS amplitudes in Table 2.5-13 that were calculated for the seven spectral frequencies at which PSHA calculations were done.}

2.5.2.5 Seismic Wave Transmission Characteristics of the Site

The U.S. EPR FSAR includes the following COL Item in Section 2.5.2.5.

> Seismic wave transmission characteristics are site specific and will be addressed by the COL applicant.

This COL Item is addressed as follows:

{The NMPNS site is underlain by rock with shear-wave velocities (V_S) less than 9,200 feet per second (fps), so the potential amplification of these rock units had to be determined, taking into account the low- and high-strain dynamic characteristics of the underlying rock, and the associated uncertainties. This characterization was performed by means of the following 4 steps: (1) Develop a base-case geologic column, in which mean low-strain shear wave velocities, material damping ratios, and strain-dependent properties are estimated for relevant layers from hard rock to the top of sandstone, using information from Section 2.5.4. At the NMPNS site, hard rock (V_S=9,200 fps) is at a depth of approximately 1,800 ft (550 m). (2) Develop a probabilistic model that describes the uncertainties in the above properties, locations of layer boundaries, and correlation between the velocities in adjacent layers, using information from Section 2.5.4, supplemented with generic model parameters when necessary. This model was used to generate a set of 60 artificial profiles. (3) Use an equivalent-linear site-response formulation together with Random Vibration Theory (RVT) to calculate the dynamic response of the site for each of the 60 artificial profiles, using as input rock motions the rock spectra described in the previous section. This model calculates the mean and standard deviation of site response for each of the six input motions (10^{-4}, 10^{-5}, and 10^{-6} annual frequencies, HF and LF smooth spectra). These steps are described in the following sections.

Section 2.5.2.5.1 is added as a supplement to the U.S. EPR FSAR.

2.5.2.5.1 Base-Case Rock Column

The development of a base case rock column is described here. This includes summaries of the low strain shear wave velocity, material damping, and strain-dependency properties of the base case materials, as these parameters are used in the site response analyses.

Two separate columns are created. The column to be used for the calculation of the Ground Motion Response Spectrum (GMRS) extends from bedrock to elevation 228.67 ft (70 m) (or 41.33 ft (16 m) below site grade). This is the elevation of the bottom of the Nuclear Island common basemat). The column to be used for the calculation of the Foundation Input Response Spectrum (FIRS) extends from bedrock to elevation 254 ft (or 16 ft below site grade). This is the elevation of the top of the Oswego sandstone and will be taken as representative of structures founded on rock with foundation elevations above that of the GMRS.

The subsurface materials at the NMP3NPP site are described in detail in Section 2.5.4. The material characterization is summarized in the following groups:

- Till (not considered in these calculations)
- Oswego Sandstone
- Pulaski Formation

- Whetstone Gulf Formation
- Trenton Group / Black River Group
- Precambrian Grenville crystalline basement rock (V_S> 9200 fps, treated as bedrock)

The depths associated with the transitions between the Whetstone and Trenton formations and between the Trenton and Grenville are uncertain. This uncertainty is incorporated by means of step-wise transitions in the base-case V_S profile. The depths and V_S values at these transitions are constructed so that they represent discrete approximations to uniform probability distributions Miller and Rice (Miller and Rice, 1983). The thicknesses, low-strain V_S, and unit weights are given in Table 2.5-21 and Table 2.5-22

All rock formations are given the same base-case degradation curves for shear modulus and damping. These curves were developed on the basis of generic curves for rock and on test data for tuffs with similar V_S, as documented in Section 2.5.4.

2.5.2.5.2 Characterization of Uncertainty in Site Properties.

To account for variations in shear-wave velocity and other dynamic properties across the site, two sets of 60 artificial profiles were generated using the stochastic model developed by Toro (Toro, 1996), with some modifications to account for the conditions at the NMPNS site. These artificial profiles represent the site column from the top of bedrock (with a shear-wave velocity of 9,200 fps) to the elevations where the GMRS and FIRS are defined. This model uses as inputs the following quantities: (1) the median shear-wave velocity profile, which is equal to the base-case rock profiles described above; (2) the standard deviation of $\ln(V_S)$ (the natural logarithm of the shear-wave velocity) as a function of depth, which is given a value of 0.10 (this value corresponds to the 10% standard deviation provided in Section 2.5.4 on the basis of available site and regional data); (3) the correlation coefficient between $\ln(V_S)$ in adjacent layers, which is taken from generic results for rock and firm soil in Toro (1996); (4) the probabilistic characterization of layer thickness as a function of depth, which is also taken from generic results in Toro (1996), and then modified to allow for sharp changes in the base-case velocity profile; and (5) the depth to bedrock, which is randomized to account for epistemic uncertainty in the depth of the transition between the Trenton and Grenville formations.

The correlation coefficient between $\ln(V_S)$ in adjacent layers is estimated using the inter-layer correlation model from Toro (1996) for category USGS A+B (this category was selected on the basis of V_S30; category A was not selected because it contains too few data).

In the V_S randomization scheme employed, it is possible for the calculated artificial V_S in the Trenton or other formations to be greater than 9,200 fps. When this happens for a certain artificial profile, the randomization scheme sets that V_S to 9,200 fps and defines the corresponding depth to be the depth to bedrock.

The probabilistic characterization of layer thickness consists of a function that describes the rate of layer boundaries as a function of depth. This study utilized a generic form of this function, taken from Toro (1996), and then modified to allow for sharp changes in the adopted base-case velocity profile. The interplay between the layer thickness randomization and the step-wise transitions described earlier between the Whetstone and Trenton and between the Trenton and Grenville provides a representation of the uncertainty in the depths of the corresponding transitions, as defined in Section 2.5.4.

Figure 2.5-109 illustrates the V_S values for artificial profiles 1 through 10 for the GMRS, using the median, logarithmic standard deviation, correlation model, and layer-thickness model described above. These profiles include uncertainty in depth to bedrock. In total, 60 artificial profiles were generated for the GMRS calculations and 60 for the FIRS calculations. Figure 2.5-110 compares the median of these 60 V_S profiles to the median V_S profile described in the previous section, indicating excellent agreement. This figure also shows the +1 σ values of the 60 profiles, reflecting the standard deviations and comparing them to the 10% standard deviation specified in Section 2.5.4.

Median values of shear modulus degradation (G/G_{MAX}) and damping for each geologic unit are described in the previous section. The uncertainty in damping is specified as 25% in Section 2.5.4. The uncertainty in modulus reduction is specified as 10%, which is typical of the values obtained by Costantino (Costantino, 1996). The artificial damping curves are capped at 1% damping, as specified in Section 2.5.4. The correlation coefficient between $\ln(G/G_{MAX})$ and ln(damping) is specified as -0.75, so that curves with higher than average G/G_{MAX} tend to have lower than average damping. The degradation and damping properties are treated as fully correlated among layers in the same geological unit, but independent between different units. Figure 2.5-111 and Figure 2.5-112 illustrate the 60 artificial shear stiffness and damping curves generated for the Oswego Sandstone (soil Unit 1) for the GMRS profiles.

Each set of 60 artificial profiles, consisting of V_S and unit weight vs. depth, depth to bedrock, stiffness, and damping curves, is used to calculate and quantify site response and its uncertainty, as described in the following sections.

2.5.2.5.3 Site Response Calculations

Site response calculations were performed for each of the 60 artificial GMRS profiles and for the 60 artificial FIRS profiles. These results were then used to calculate the logarithmic mean and standard deviation of the amplification factor for each structural frequency. These calculations were performed for six separate sets of bedrock motions, corresponding to the 10^{-4}, 10^{-5}, and 10^{-6} high-frequency (HF) and low-frequency (LF) rock spectra determined in Section 2.5.2.4.6.

The site response calculations were performed using the Random Vibration Theory (RVT) approach. In many respects, the inputs and assumptions are the same for an RVT analysis and for a time-history based analysis (e.g. an analysis with the program SHAKE). Both the RVT and time-history (SHAKE) procedures use a horizontally-layered half-space representation of the site and use an equivalent-linear representation of dynamic response to vertically propagating shear waves. Starting from the same inputs (in the form of response spectra), both procedures will lead to similar estimates of site response (see, for example, Rathje and Ozbey, (1996). The main advantage of the RVT approach is that it avoids the process of spectral matching of multiple time histories to a given rock response spectrum. Instead, the approach uses a probabilistic representation of the ensemble of all input motions corresponding to that given response spectrum and then calculates the response spectrum of the ensemble of dynamic responses.

In addition to the artificial profiles, their corresponding degradation curves, and the rock response spectra, the RVT site-response calculations require the following inputs: (1) the strong-motion duration associated with the rock spectrum; and (2) the equivalent-strain ratio to use in the equivalent-linear calculations (this input is required for both the time-history and RVT approaches) and depends on magnitude. The duration is calculated from the de-aggregation results in Section 2.5.2.4.6, using standard seismological relations between magnitude, seismic moment, magnitude, corner frequency, and duration (see, for example, Rathje and Ozbey, (2006), and using stress-drop and crustal V_S values typical of the eastern

United States. The effective strain ratio is calculated using the expression (M-1)/10 (Idriss, 1992). Values smaller than 0.5 or greater than 0.65 were brought into the 0.5-0.65 range, which is the range recommended by Kramer (Kramer, 1996). The calculation of duration and effective strain ratio are documented in Table 2.5-23.

Figure 2.5-112 through Figure 2.5-136 plot the results of the site-response calculations at the GMRS elevation for the various rock input motion. The following results are shown for each input motion: response spectrum obtained with each profile (with logarithmic sigma), Spectral acceleration (Sa) amplification factor obtained with each profile (with logarithmic sigma), maximum strain versus depth, and damping ratio versus depth. Figure 2.5-113 through Figure 2.5-136 present plots for the following input motions:

Figure 2.5-113 through Figure 2.5-116:	1E-4 HF input motion
Figure 2.5-117 through Figure 2.5-120:	1E-4 LF input motion
Figure 2.5-121 through Figure 2.5-124:	1E-5 HF input motion
Figure 2.5-125 through Figure 2.5-128:	1E-5 LF input motion
Figure 2.5-129 through Figure 2.5-132:	1E-6 HF input motion
Figure 2.5-133 through Figure 2.5-136:	1E-6 LF input motion

The calculated responses at the FIRS elevation to the six input motions were very similar to those plotted in Figure 2.5-113 through Figure 2.5-136 for the GMRS elevation. This similarity is shown in Figure 2.5-137 through Figure 2.5-140, which summarizes the calculated medians (calculated as the logarithmic means) and standard deviations of amplification factors for the GMRS and FIRS elevations. Figure 2.5-141 shows the ratio of the FIRS/GMRS Sa amplification factors for the 1E-4 input motions. The differences between these ratios are less than 2% for frequencies below 20 Hz, and they are less than 5% at higher frequencies except for a few high frequencies where they vary up to +8%. The amplification factors and standard deviations in Figure 2.5-137 through Figure 2.5-140 are used in the calculation of site-specific hazard at the GMRS and FIRS locations, as documented below in Section 2.5.2.6.}

2.5.2.6 Ground Motion Response Spectra

The U.S. EPR FSAR includes the following COL Item in Section 2.5.2.6:

> A COL applicant that references the U.S. EPR design certification will verify that the site-specific seismic parameters are enveloped by the CSDRS (anchored at 0.3 g PGA) and the 10 generic soil profiles discussed in Section 2.5.2 and Section 3.7.1 and summarized in Table 3.7.1-6.

This COL Item is addressed as follows:

{With the site-specific amplification described in the previous section, the seismic hazard model described in Section 2.5.2.4.6 was re-run incorporating the site amplifications into the hazard calculations. For ground motions below the 10^{-4} amplitudes shown in Table 2.5-13, site amplification was assumed to be the same as for the 10^{-4} amplitudes. For ground motions greater than the 10^{-6} amplitudes, site amplification was assumed to be the same as for the 10^{-6} amplitudes. The logarithmic standard deviations described in the previous section were used to represent uncertainties in site response. The CAV filter was applied to these calculations, using V_S30 for surface conditions and using amplitudes at the surface after site effects have been taken into account.

The amplification factors for the HF input spectra were used for hazard calculations at 5, 10, 25 and 100 Hz (PGA), and the amplification factors for the LF input spectra were used for hazard calculation at 0.5, 1, and 2.5 Hz. The reason is that the HF rock spectra dominate the high frequencies and the LF rock spectra dominate the low frequencies.

Figure 2.5-142 through Figure 2.5-148 show seismic hazard curves for the 7 spectral frequencies at which ground motion equations are available, for the GMRS elevation. The mean hazard curves roll over to an annual frequency of exceedence that is less than 10^{-4}, because the CAV calculation indicates that many small-magnitude earthquakes will not be damaging. Seismic hazard curves for the GMRS elevation are documented in Table 2.5-24 through Table 2.5-30. Table 2.5-31 shows mean amplitudes for annual frequencies of 10^{-5} and 10^{-6}.

A similar seismic hazard calculation was conducted for the FIRS elevation, using the amplification factors appropriate for the FIRS elevation, as described in the previous section. Because the amplification factors are similar, the calculated UHRS amplitudes at the FIRS elevation are very close to those calculated at the GMRS elevation. This is apparent in Table 2.5-31, which shows both sets of UHRS amplitudes. The hazard curves for the FIRS elevation are similar to those shown in Figure 2.5-142 through Figure 2.5-148 and are not shown separately. However, the digital hazard curves for the FIRS elevation are documented in Table 2.5-32 through Table 2.5-38.

To calculate the GMRS spectrum, the envelope spectrum of the HF and LF amplification calculations was used as a spectral shape, defined at 335 frequencies at which amplification calculations were done. This spectral shape was scaled to the UHRS values at the seven spectral frequencies at which hazard calculations were done. Because the 10^{-4} mean amplitudes were undefined for the GMRS elevation (see Figure 2.5-142 through Figure 2.5-148), this scaling was done for the 10^{-5} amplitudes only. At intermediate frequencies, the 10^{-5} spectrum was calculated by weighting the scaled shapes from the next higher and lower frequency, using a weighting that was inversely proportional to the logarithmic difference between frequencies. This defined a 10^{-5} UHRS spectrum for the GMRS elevation. An initial GMRS spectrum was calculated as 0.45 times the 10^{-5} UHRS spectrum, which is appropriate when the 10^{-4} spectrum is not defined. The initial GMRS spectrum was smoothed using a frequency window that was approximately +10% in frequency, to eliminate peaks and valleys that were thought to be a result only of the numerical calculations. The 335 frequencies were reduced to 38 frequencies for reporting purposes. An identical process was followed using the spectral shape and UHRS amplitudes calculated for the FIRS elevation.

Figure 2.5-149 shows the horizontal 10^{-5} UHRS and GMRS (for the GMRS elevation), and Figure 2.5-150 shows the horizontal 10^{-5} UHRS and FIRS (for the FIRS elevation).

Vertical spectra were scaled from the horizontal spectra using scaling factors for hard rock published in NUREG/CR-6728 (NUREG/CR-6728, 2001). These scaling factors (V/H ratios) depend on the PGA of the horizontal motion, and the scaling factors for PGA < 0.2g apply (see Figure 2.5-149 and Figure 2.5-150). These V/H ratios were developed for hard rock conditions and are considered applicable to the GMRS and FIRS elevations because shear wave velocities at those elevations are reasonable high (please refer to the discussion in Section 2.5.2.4.6). Figure 2.5-151 shows the V/H ratios from NUREG/CR-6728 as a function of structural frequency that apply to the three ranges of PGA values defined in that reference.

The vertical GMRS and FIRS were calculated by multiplying the horizontal GMRS and FIRS by the V/H ratio shown in Figure 2.5-151 for PGA<0.2g. Figure 2.5-152 shows the horizontal GMRS and the vertical GMRS calculated this way, and Figure 2.5-153 shows a similar plot for the FIRS. Because the 10^{-5} UHRS at both elevations is less than 0.2g, this calculation is numerically

equivalent to scaling the 10^{-5} horizontal UHRS to a 10^{-5} vertical UHRS, and then calculating the vertical GMRS as 0.45 times the 10^{-5} vertical UHRS.

Table 2.5-39 documents the horizontal 10^{-5} UHRS at the GMRS elevation, the calculated horizontal GMRS, and the vertical GMRS. Table 2.5-40 documents similar spectra for the FIRS elevation.}

2.5.2.7 Conclusions

{This section is added as a supplement to the U.S. EPR FSAR.

Nine Mile Point 3 Nuclear Project, LLC and UniStar Nuclear Energy used the seismic source and ground motion models published by the Electric Power Research Institute (EPRI) for the central and eastern United States (CEUS), Seismic Hazard Methodology for the Central and Eastern United States, (EPRI, 1986). As such, FSAR Section 2.5.2 focuses on those data developed since publication of this 1986 EPRI report. Regulatory Guide 1.165, Identification and Characterization of Seismic Sources and Determination of Safe Shutdown Earthquake Ground Motion, (NRC, 1997), indicates that applicants may use the seismic source interpretations developed by Lawrence Livermore National Laboratory (LLNL) in the "Eastern Seismic Hazard Characterization Update," published in 1993, or the EPRI document as inputs for a site-specific analysis.

Nine Mile Point 3 Nuclear Project, LLC and UniStar Nuclear Energy also used the guidance of Regulatory Guide 1.208, A Performance–Based Approach to Define the Site-Specific Earthquake Ground Motion, (NRC, 2007) to develop the Ground Motion Response Spectrum (GMRS) used for the development of the Safe Shutdown Earthquake (SSE).

Nine Mile Point 3 Nuclear Project, LLC and UniStar Nuclear Energy has provided a characterization of the seismic sources surrounding the site, as required by 10 CFR 100.23. Nine Mile Point 3 Nuclear Project, LLC and UniStar Nuclear Energy has adequately addressed the uncertainties inherent in the characterization of these seismic sources through a PSHA, and that this PSHA followed the guidance provided in Regulatory Guide 1.208 (NRC, 2007).

The GMRS developed by UniStar Nuclear Energy uses the performance-based approach described in Regulatory Guide 1.208 (NRC, 2007), adequately representing the regional and local seismic hazards and accurately includes the effects of the local NMP3NPPsubsurface properties.

The performance-based approach outlined in Regulatory Guide 1.208 (NRC, 2007) is an advancement over the solely hazard-based reference probability approach recommended in Regulatory Guide 1.165 (NRC, 1997) and it was used where appropriate in the determination of the GMRS. The performance-based approach uses not only the seismic hazard characterization of the site from the PSHA but also basic seismic fragility SSC modeling in order to obtain an SSE that directly targets a structural performance frequency value. Nine Mile Point 3 Nuclear Project, LLC and UniStar Nuclear Energy conclude that the application for the NMP3NPP site is acceptable from a geologic and seismologic standpoint and meets the requirements of 10 CFR 100.23(d) (CFR, 2007).}

2.5.2.8 References

{This section is added as a supplement to the U.S. EPR FSAR.

Abrahamson and Bommer, 2006. "Why do modern Probabilistic Seismic-Hazard Analyses often lead to increased hazard Estimates?" Bull. Seismol. Soc Am. 96, 1976 -1977.

ASCE, 2005. American Society of Civil Engineers, "Seismic Design Criteria for Structures, Systems, and Components in Nuclear Facilities," American Society for Civil Engineers/Structural Engineering Institute, Report ASCE/SEI 43-05, 2005.

Atkinson, 1995. Ground-Motion Relations for Eastern North America, G. M. Atkinson and D. M. Boore, Seismological Society of America, Bulletin, Volume 85, Number 1, pp 17-30, 1995.

CEG, 1998. "Nine Mile Point Unit 2 USAR", 1998, Docket No. 50-410, Constellation Energy Group.

CFR, 2007. "Geologic and Seismic Siting Criteria" Title 10, Code of Federal Regulations, Part 100.23

Chapman, 1994. Seismic Hazard Assessment for Virginia, M. C. Chapman and F. Krimgold, Virginia Tech Seismological Observatory, Department of Geological Sciences, February 1994.

Costantino, 1996. "Recommendations for Uncertainty Estimates in Shear Modulus Reduction and Hysteretic Damping Relationships", C. J. Costantino, (1996). Published as an appendix in "Description and validation of the stochastic ground motion model, "W. J. Silva, N. Abrahamson, G. Toro and C. Costantino. (1997). Report Submitted to Brookhaven National Laboratory, Associated Universities, Inc. Upton, New York 11973, Contract No. 770573.

Dames & Moore, 1976a. "Before the ASLAB on Behalf of Consolidated Edison Company of New York, Seismic "Show Cause" Hearings on Issue 1, Indian Point Station, Units 1, 2, and 3; Docket n 50-3, 50-247, and 50-286". Filed March 19, 1976.

Dames & Moore, 1976b. "Potential Relationship of the White Mountains to Tectonic Provinces and Earthquake Occurrence in the Northeastern United States". Report to Boston Edison Co., 1976.

EPRI, 1986. "Seismic Hazard Methodology for the Central and Eastern United States, Tectonic Interpretations, Electric Power Research Institute, Report NP-4726, Volumes 5-10, July 1986".

EPRI, 1988. "Seismic Hazard Methodology for the Central and Eastern United States, Electric Power Research Institute, Report NP-4726-A, Revision 1, Volume 1, Part 2, 1988".

EPRI, 1989a. "Probabilistic Seismic Hazard Evaluations at Nuclear Plant Sites in the Central and Eastern United Sites: Resolution of the Charleston Earthquake Issue," Elec. Power Res. Inst. Rept. NP-6395-D, Palo Alto, CA, April 1989.

EPRI 1989b. "EQHAZARD Primer, Elec. Power Res. Inst. Rept. NP-6452-D, Palo Alto, CA, June 1989.

EPRI, 1993. Guidelines for Determining Design Basis Ground Motions, Volume 5: Quantification of Seismic Source Effects, Electric Power Research Institute, Report TR-102293, November 1993.

EPRI, 2004. CEUS Ground Motion Project Final Report, Elec. Power Res. Inst., Palo Alto, Ca, Rpt. 1009684, December 2004.

Exelon, 2005. "Letter dated October 31, 2005, T. Mundy, Exelon to NRC, Subject: Response Supplemental Draft Safety Evaluation Report (DSER) Item, page 16 of 112 and page 54 of 112, (Adams Accession Number ML053120131)", 2005.

FEMA 450, 2004. "NEHRP Recommended Provisions for Seismic Regulations for New Buildings and Other Structures 2003 Edition" Building Seismic Safety Council, Wash, DC

Hadley, 1974. "Seismotectonic Map of the Eastern United States, U.S. Geologic Survey". Hadley, J. B. and Devine, J. F., Map MF-620, Washington, DC, 1974.

Hardy, 2005. "Program on Technology Innovation: Use of Cumulative Absolute Velocity (CAV) in Determining Effects of Small Magnitude Earthquakes on Seismic Hazard Analyses," Hardy, G., K. Merz, N. Abrahamson, and J. Watson-Lamprey, 2006. Elec. Power Res. Inst., Palo Alto, Rept. 1014099. US Nuc. Reg. Comm. document accession no. ML062350456, June 30, 2006.

Hatcher, 1987. "Tectonics of the Southern and Central Appalachian Internides, Annual Reviews Earth Planet Science", Volume 15, 1987, Pages 337-362, R. D. Hatcher Jr.

Hatcher, 1989. Alleghenian Orogen, in Hatcher, R.D., William, A., Viele, G., eds., "The Appalachian-Ouachita Orogen in the United States", Geological Society of America DNAG, Volume F-2, p.233-318, R. Hatcher, W. Thomas, P. Geiser, A. Snoke, S. Mosher, and D. Wiltschko, 1989.

Hibbard, 2006. "A Comparative Analysis of Pre-Silurian Crustal Building Blocks of the Northern and Southern Appalachian Orogen", American Journal of Science, Volume 307, p. 23, J. Hibbard, C. van Staal, and D. Rankin, 2007.

Hibbard, 2007. "A Comparative Analysis of Pre-Silurian Crustal Building Blocks of the Northern and Southern Appalachian Orogen", American Journal of Science, Volume 307, p. 23, J. Hibbard, C. van Staal, and D. Rankin, 2007.

Idriss, 1992. SHAKE91: "A computer program for conducting equivalent linear seismic response analyses of horizontally layered soil deposits", I. M. Idriss, and J. I Sun, Department of Civil and Environmental Engineering, Center for Geotechnical Modeling, University of California, Davis, Calif., 1992

Jacobi, 2002a. Basement Faults and Seismicity in the Appalachian Basin of New York State, Tectonophysics, Volume 353, 2002, Pages 75-113, R.D. Jacobi.

Kramer, 1996. Geotechnical Earthquake Engineering, Prentice Hall, Inc., Upper Saddle River, New Jersey, 653 pp.

Miller and Rice, 1983. "Discrete Approximations of Probability Distributions", Management Science, 29, 3, 352-362, March 1983.

New York State Electric and Gas Corporation, 1979. "Geologic Investigation, Demster Structural Zone; Appendix 2.5A, of Preliminary Safety Analysis Report, New Haven Units 1 and 2, Docket Nos. STN50-596 and STN50-597", 1979.

NRC, 1991. "Generic Letter 88-20, Individual Plant Examinations of External Events (IPEEE) for Severe Accident Vulnerabilities", U. S. Nuclear Regulatory Commission, 1991.

NRC, 1997. "Identification and Characterization of Seismic Sources and Determination of Safe Shutdown Earthquake Ground Motion, U. S. Nuclear Regulatory Commission, Regulatory Guide 1.165", March 1997.

NRC, 2001. NUREG/CR-6728, 2001. "Technical Basis for Revision of Regulatory Guidance on Design Ground Motions: Hazard- and Risk-consistent Ground Motion Spectra Guidelines," U.S. Nuclear Regulatory Commission, by Risk Engineering, Inc., October 2001.

NRC, 2002. "Technical Basis for Revision of Regulatory Guidance on Design Ground Motions: Development of Hazard- & Risk-Consistent Seismic Spectra for Two Sites", U. S. Nuclear Regulatory Commission, NUREG/CR-6769, 2002.

NRC, 2005. "Safety Evaluation Report for an Early Site Permit (ESP) at the North Anna ESP Site, U. S. Nuclear Regulatory Commission, NUREG-1835", September 2005.

NRC, 2007. "A Performance-Based Approach to Define the Site-Specific Earthquake Ground Motion", U. S. Nuclear Regulatory Commission, Regulatory Guide 1.208, March 2007.

NRC, 2007. Regulatory Guide 1.208, 2007. A performance Based Approach to Define the Site-Specific Earthquake Ground Motion, U.S. Nuclear Regulatory Commission, March 2007.

NUREG/CR-6728, 2001 "Technical Basis for Revision of Regulatory Guidance on Design Ground Motions: Hazards- and Risk-consistent Ground Motion Spectra Guidelines," U.S. Nuclear Regulatory Commission, by Risk Engineering, Inc. October 2001.

Rathje, 2006. "Site Specific Validation of Random Vibration Theory-Based Site Response Analysis," Rathje, E.M., and Ozbey, M.C., Journal of Geotechnical and Geoenvironmental Engineering, ASCE, 132(7), pp. 911-922.

Rodgers, 1970. "The Tectonics of the Appalachians", Wiley-Intersciens: New York, NY, p. 271, J. Rodgers, 1970.

SSA, 1987. The 23 April 1984 Martic Earthquake and The Lancaster Seismic Zone In Eastern Pennsylvania, Bulletin of the Seismological Society of America, Vol. 77, No. 2, Pages 877-890, J. Armbruster and L. Seeber, 1987.

Seeber, 1998. The 1994 Cacoosing Valley earthquakes near Reading, Pennsylvania: A shallow rupture triggered by quarry unloading, L. Seeber, J. G. Armbruster, W. Y. Kim, N. Barstow, C. Scharnberger, Journal of Geophysical Research, Volume 103, Number B10, Pages 24,505-24,521, 1998.

Toro, 1996. "Probabilistic Models of Site Velocity Profiles for Generic and Site-Specific Ground Motion Amplification Studies", G. R. Toro, Published as an appendix in W. J. Silva, N. Abrahamson, G. Toro and C. Costantino, (1997), Description and validation of the stochastic ground motion model, Report Submitted to Brookhaven National Laboratory, Associated Universities, Inc. Upton, New York 11973, Contract No. 770573, 1996.

USGS, 1992. Specification of Source Zones, Recurrence Rates, Focal Depths, and Maximum Magnitudes for Earthquakes Affecting the Savannah River Site in South Carolina, U.S. Geological Survey, Bulletin 2017, G. A. Bollinger, 1992.

USGS, 1996. National seismic-hazard maps: documentation, U. S Geological Survey, Open-File Report 96-532, A. Frankel, T. Barnhard, D. Perkins, E. V. Leyendecker, N. Dickman, S. Hanson, and M. Hopper, 1996.

USGS, 2002. Documentation for the 2002 Update of the National Seismic Hazard Maps, U.S. Geological Survey Open-File Report 02-420, A. D. Frankel, M. D. Petersen, C. S. Mueller, K. M Haller, R. L. Wheeler, E. V. Leyendecker, R. L. Wesson, S. C. Harmsen, C. H. Cramer, D. M. Perkins, and K. S. Rukstales, 2002.

USGS, 2006. U.S. Geological Survey, 2006, Quaternary fault and fold database for the United States, accessed DATE, from USGS web site: http//earthquakes.usgs.gov/regional/qfaults/.

USGS, 2008. Documentation for the 2008 Update of the National Seismic Hazard Maps, U.S. Geological Survey Open-File Report 00-1128, M. D. Petersen, A. D. Frankel, , S. C. Harmsen , C. S. Mueller, K. M. Haller, R. L. Wheeler, R. L. Wesson, Y. Zeng, O. S. Boyd, , D. M. Perkins, N. Luco, E. Fields, C. Wills and K. S. Rukstales, 2008.

Valentino, 1994. "Late Paleozoic Transcurrent Tectonic Assembly of the Central Appalachian Piedmont, Tectonics," Volume 13, No 1, February, 1994, Pages 110- 126, D.W. Valentino, A.E. Gates and L. Glover III.

Wallach, 1998. Wallach, J. L., A. A. Mohajer, and R. L Thomas (1998). Linear zones, seismicity and the possibility of a major earthquake in the intraplate western Lake Ontario area of eastern North America. Can. J. Earth Sci. 35, 762-786.

Wallach, 2002. Wallach, J. L. <http://europa.sim.ucm.es/compludoc/AA?a=Wallach%2c+J+L&donde=otras&zfr= 0> , 2002, The presence, characteristics and earthquake implications of the St. Lawrence fault zone within and near Lake Ontario (Canada-USA) , Tectonophysics, 2002; 353 (1) <http://europa.sim.ucm.es/compludoc/GetSumario?r=/W/10209/00401951_1.htm &zfr=0> , p. 45-74

Wheeler, 1996. "Geological Map of Canada, Geological Survey of Canada", Map 1860A, Scale 1:5,000,000, J.O. Wheeler, P.F. Hoffman, K.D. Card, A. Davidson, B.V. Sanford, A.V. Okulitch and W.R. Roest.}

2.5.3 SURFACE FAULTING

The U.S. EPR FSAR includes the following COL Item in Section 2.5.3:

> A COL applicant that references the U.S. EPR design certification will investigate site-specific surface and subsurface geologic, seismic, geophysical, and geotechnical aspects within 25 miles around the site and evaluate any impact to the design. The COL applicant will demonstrate that no capable faults exist at the site in accordance with the requirements of 10 CFR 100.23 and 10 CFR 50, Appendix S. If non-capable surface faulting is present under foundations for safety-related structures, the COL applicant will demonstrate that the faults have no significant impact on the structural integrity of safety-related structures, systems or components.

This COL Item is addressed as follows:

{There is no potential for tectonic fault rupture and there are no capable tectonic sources within a 25 mi (40 km) radius of the NMP3NPP site.} A capable tectonic source is a tectonic structure that can generate both vibratory ground motion and tectonic surface deformation, such as faulting or folding at or near the earth's surface in the present seismotectonic regime (NRC, 1997). The following sections provide the data, observations, and references to support this conclusion. Information contained in these sections was developed in accordance with RG 1.208 (NRC, 1997), and is intended to satisfy 10 CFR 100.23, "Geologic and Seismic Siting

Criteria" (CFR, 2007a) and 10 CFR 50, Appendix S, "Earthquake Engineering Criteria for Nuclear Power Plants" (CFR 2007b).

{The NMP3NPP site vicinity is shown in Figure 2.5-40. Faults of small displacement are present on the nearby NMP Unit 2 site, and a structural zone, known as the Demster Structural Zone, occurs about 4 miles (6.4 km) of the NMP3NPP site (Figure 2.5-55). The detailed results of the investigations of the Cooling Tower fault and Radwaste thrust fault at the NMP Unit 2 site were presented in the NMP Unit 2 USAR (CEG, 1998) (Niagara Mohawk, 1978a) (Niagara Mohawk, 1978b) (Niagara Mohawk, 1978c) (Niagara Mohawk, 1980). A summary is presented in Section 2.5.1.2. Figure 2.5-73 presents the locations of these faults with small displacement located at NMP Unit 2. In the NMP Unit 2. In the NMP Unit 2 USAR (CEG, 1998) these faults are shown to be non-capable due to the ages of the faults. It was concluded in each case that the potential for surface faulting at the site proper is negligible (Section 2.5.1.2.3). Investigations for a proposed nuclear power plant site at New Haven, NY, located about 7 mi (11 km) east of the NMP3NPP site, disclosed the existence of broad, low-amplitude folds and associated faults also shown to be non-capable (Section 2.5.1.2.4) (NYSE&G, 1978). Further detailed investigation of the Demster Structural Zone has led to the conclusion that the faults within the zone are not capable, and that no potential for surface faulting is associated with these structures (CEG, 1998).}

Sections 2.5.3.1 through 2.5.3.9 are added as a supplement to the U.S. EPR FSAR.

2.5.3.1 Geological, Seismological, and Geophysical Investigations

{The following investigations have been performed to assess the potential for surface fault rupture at and within a 25 mi (40 km) radius of the NMP3NPP site:

- Compile and review existing geologic and seismologic data
- Interpret aerial photography (New York State GIS Clearing House, 2008)
- Interpret satellite imagery (EarthSat, 1997) (USGS, 2007)
- Field reconnaissance
- Review of pre-EPRI and post-EPRI (EPRI, 1986) seismicity (i.e., earthquake catalog used in EPRI (EPRI, 1986) ended in 1983. Pre-EPRI catalog is 1500's through 1983; post-EPRI catalog is 1983 through 2006)
- Discuss site area geology with researchers at the New York Geological Survey and academic institutions.

The geologic and geotechnical information available for the existing NMP Unit 1 and Unit 2 sites, as well as the proposed NMP3NPP site, is contained in three principal sources:

1. Work performed for the existing NMP Unit 1 and Unit 2 and complementary structures (CEG, 1998).
2. Published geologic mapping performed primarily by the USGS and New York Geological Survey (USGS, 1980a) (USGS, 1980b) (USGS, 1980c) (USGS, 1980d) (USGS, 1980e) (USGS, 1980f) (NYSM, 1970a) (NYSM, 1970b).

3. Seismicity data compiled and analyzed in published journal articles and, more recently, as part of Section 2.5.2.

Existing information was supplemented by field reconnaissance within a 25 mile (40 km) radius of the site, and interpretation of aerial photography within a 25 mile (40 km) radius of the site.

Satellite raster imagery (Landsat 5 Thematic Mapper) (USGS, 2007a; USGS, 2007b) of the NMP3NPP site vicinity also was acquired for review and interpretation. These field and office-based studies were performed to verify, where possible, the existence of mapped bedrock faults in the NMP3NPP site area and to assess the presence or absence of geomorphic features suggestive of potential Quaternary fault activity or previously undetected faults. Features reviewed during the field reconnaissance and office-based analysis of aerial photography and satellite imagery were based on existing regional geologic information, as well as discussions with experts at the State University of New York in Oswego and at the New York Geological Survey who have worked in the vicinity of the NMP3NPP site.

Field reconnaissance of the site and within a 25 mile (40 km) radius of the site was conducted by project geologists. Reconnaissance visits in fall 2007 and spring 2008 focused on exposed portions of bedrock at Nine Mile Point, exposures along Lake Ontario, exposures along the Salmon River, and exposures along the Little Sandy River near Lorraine Gulf. Localities within the 25 mile (40 km) site vicinity were selected based on papers, including New York State Geological Association Guidebooks from 1978 and 2005, and suggestions from Dr. David Valentino at SUNY Oswego. Localities within the 5 mile (8 km) site area were selected based on the NMP Unit 2 USAR (CEG, 1998), Dames & Moore geologic reports (Niagara Mohawk, 1978a)(Niagara Mohawk, 1978b)(Niagara Mohawk, 1978c), and the New Haven PSAR (NYSE&G, 1978). Figure 2.5-191 shows the geographic extent of geologic reconnaissance studies done as part of site investigation for the NMP3NPP site.

These investigations included regional and site physiography and geomorphic process, geologic history, and stratigraphy as well as investigations of regional and site tectonics and structural geology.

The exposures of bedrock at Nine Mile Point have been previously described by Fisher (Fisher, 1978) and Patchen (Patchen, 1978). Exposures of bedrock at NMP3NPP including Oswego Sandstone along the shore of Lake Ontario, isolated small outcrops of Oswego Sandstone at the NMP3NPP site, and Oswego Sandstone along the Drainage Ditch Structure at NMP Unit 2 were examined and photographed. The Oswego Sandstone is heavily fractured in a limited section of the Drainage Ditch exposure. Oswego Sandstone exposed in the Drainage Ditch to the north and south is relatively unfractured. The fracturing represents the Drainage Ditch Structure which is an extension of the Tepee Fold located at the adjacent Fitzpatrick Plant (CEG, 1998). The observed lithology and structure agrees with that previously published (Fisher, 1978)(Patchen, 1978)(Niagara Mohawk, 1978a)(Niagara Mohawk, 1978b)(Niagara Mohawk, 1978c)(CEG, 1998). The projection of the Drainage Ditch Feature is located north of NMP Unit 2 and does not intersect the NMP3NPP site. No evidence of surface expression of the Cooling Tower Fault was observed at NMP Unit 2 . The lack of surficial expression of the Cooling Tower Fault was previously reported in the NMP Unit 2 USAR (CEG, 1998) and by Dames & Moore (Niagara Mohawk, 1978a)(Niagara Mohawk, 1978b)(Niagara Mohawk, 1978c).

The exposures of bedrock along Lake Ontario to the west and east of NMP3NPP have been previously described by Patchen (1978) and Stillwell (2005). Exposures of the Oswego Sandstone along Lake Ontario at the SUNY Oswego campus were examined with Dr. David Valentino of SUNY Oswego. Exposures of Oswego Sandstone along Lake Ontario at Fort Ontario in Oswego, NY and along Lake Ontario at Noyes Sanctuary at Nine Mile Point in Lycoming, NY

were also examined and photographed. The observed sandstone lithology and structure agrees with that previously published by Patchen (Patchen, 1978). Measurements were taken of the near vertical east-northeast striking joints and northwest striking joints which agree with measurements previously published by Stillwell (Stillwell, 2005). At Fort Ontario the dominant joint orientation is easterly and the secondary joint orientation is northwesterly. In the thick bedded Oswego Sandstone, joint spacing is on the order of 5 feet, while joint length is on the order of 50 feet. At Noyes Sanctuary, joints in the sandstone and siltstone of Oswego Transition Zone are near vertical.

The exposures of bedrock along the Salmon River have been previously described by Bretsky (Bretsky, 1978), Patchen (Patchen, 1978) and Stillwell (Stillwell, 2005). Exposures of the Pulaski Formation along the Salmon River at Pulaski, NY were examined and photographed. Exposures of the Oswego Transition Zone and Pulaski Formation at Salmon River Falls in Altmar, NY were also examined and photographed. Along the Salmon River, and at Salmon River Falls, the dominant joint orientation is easterly and the secondary joint orientation is northwesterly. The observed interbedded sandstone, argillaceous sandstone, siltstone, and shale lithology and structure agrees with that previously published by Bretsky (Bretsky, 1978) and Patchen (Patchen, 1978). Measurements were taken of the near vertical east-northeast striking joints and northwest striking joints which agree with those previously published by Stillwell (Stillwell, 2005). Joint spacing is on the order of five to ten feet and joint length is on the order of tens of feet.

The exposures of bedrock along the Little Sandy River near Lorraine Gulf about 30 miles north of the NMP3NPP site, have been previously described by Bretsky (Bretsky, 1978). Exposures of the Lorraine Group, including the Pulaski Formation and Whetstone Gulf Formation, along the Little Sandy River were examined and photographed. The observed siltstone, shale and sandstone lithology and structure agrees with that previously published by Bretsky (Bretsky, 1978) and the near vertical east-northeast striking joints and northwest striking joints are consistent with the regional joint pattern. In the Lorraine Group, joint spacing is on the order of a few feet and joint length is on the order of tens of feet.

Reconnaissance was also conducted along roads traversing the site and along roads to the southwest, south and southeast in the area of the Demster Structural Zone located about 4 miles (6.4 km) southeast of the NMP3NPP site. No evidence of surficial expression of the Demster Structural Zone was observed. The lack of surficial expression of the Demster Structural Zone was previously reported in the New Haven PSAR (NYSE&G, 1978) and NMP Unit 2 USAR (CEG, 1998).

Field reconnaissance studies did not identify the presence of any paleoliquefaction features in the NMP3NPP site area. The absence of these features in the site area is expected for a number of reasons:

1. A lack of occurrence sufficient size historic earthquakes in the NMP3NPP site area. The development of paleoliquefaction features requires a minimum earthquake magnitude of 5.5 to 6. Additionally, paleoliquefaction features will only occur at a maximum distance of 20 km from the epicenter of an event (Obermeier, 1996). Table 2.5-1 is a listing of the seismic events that have occurred within approximately a 300-mile (483 km) radius of the NMP3NPP site. This includes only two earthquakes with magnitudes estimates over 5.5; both of which are magnitude 5.7, and they occurred at distances of about 200 and 300 miles distant from the NMP3NPP site. Thus the required level of seismic activity for development of paleoliquefaction is essentially absent from the region.

2. Absence of abundant liquefiable soils from the site area. The predominant soil types in the NMP3NPP site vicinity include glacial till with some lacustrine silts and clays and glacial outwash. The occurrence of sediments that might provide a suitable host for paleoliquefaction features is thus limited (NYSM, 1986). Exposures of suitable materials are thus commensurately restricted in availability.

Geologic reconnaissance for the NMP3NPP site characterization studies focused on examination of low laying areas to look for stream cuts, bank cuts on the side of the glacial hills, and low relief glacial features that would be more likely to offer exposures of finer sediments such as sand and silt that might sustain liquefaction features if the appropriate seismic event had occurred. These geologic reconnaissance locations are shown on Figure 2.5-191. No good exposures of finer sediments were found other than the limited stream deposits, and these did not identify the presence of any paleoliquefaction features.}

~~Field reconnaissance of the site and within a 25 mile (40 km) radius of the site was conducted by project geologists. Reconnaissance visits in fall 2007 and spring 2008 focused on exposed portions of bedrock at Nine Mile Point, exposures along Lake Ontario, exposures along the Salmon River, and exposures along the Little Sandy River near Lorraine Gulf.~~

~~The exposures of bedrock at Nine Mile Point have been previously described by Fisher (1978) and Patchen (1978). The exposures of bedrock along Lake Ontario have been previously described by Patchen (1978) and Stillwell (2005). The exposures of bedrock along the Salmon River have been previously described by Bretsky (1978), Patchen (1978) and Stillwell (2005). The exposures of bedrock along the Little Sandy River near Lorraine Gulf about 30 miles north of the NMP3NPP site, have been previously described by Bretsky (1978).~~

~~Reconnaissance was also conducted along roads traversing the site and in the area of the Demster Structural Zone about 4 miles (6.4 km) southeast within a 25 mile (40 km) radius of the NMP3NPP site. Key observations and discussion items were documented in field notebooks and photographs. Field locations were logged by hand on topographic base maps and with a hand-held Global Positioning System (GPS) receiver.~~

~~The investigations of regional and site physiographic provinces and geomorphic process, geologic history, and stratigraphy were conducted by AREVA, NP and GEI Consultants, Inc. The investigations of regional and site tectonics and structural geology were also conducted by AREVA, NP and GEI Consultants, Inc.~~

2.5.3.1.1 Previous Site Investigations

{Localized deformation zones, associated with minor faults, were encountered in the excavations for NMP Unit 2. There are several zones of bedrock deformation that intersect the NMP Unit 2 site excavations. The cooling tower at NMP Unit 2 (Figure 2.5-73) was relocated to avoid being founded above a fault along which Quaternary buckling had occurred (Section 2.5.1.2.3). Several Quaternary, low-angle thrust faults intersect the main site excavations (Figure 2.5-73) and are described in Section 2.5.1.2.3. These faults were judged by a panel of experts to have a negligible impact on the site engineering structures (CEG, 1998).

Deformation zones have not been encountered in the site investigation for NMP3NPP. Excavation mapping is required during plant construction and any encountered faults or deformed zones will be mapped in detail and evaluated. No capable tectonic sources as defined by Regulatory Guide 1.165 (NRC, 1997) and Regulatory Guide 1.208 (NRC 2007) are known to exist in the NMP3NPP site vicinity.

While faults were not encountered during the drilling program for NMP3NPP, it is anticipated that some fault structures or deformed zones may be encountered in foundation excavations for the NMP3NPP plant, based on the prevalence of non-capable faults in excavations at NMP Unit 2 and the similar lithology and structure at NMP3NPP. The faults documented at NMP Unit 2 do not appear to extend to the NMP3NPP site (CEG, 1998), but if faults are encountered at NMP3NPP they are likely to be structures similar in character to those well documented at NMP Unit 2. The investigation of the structures at NMP Unit 2 is described in detail in Section 2.5.1.2 and summarized later in this section (2.5.3).

Previous site investigations performed for the existing units are summarized in the NMP Unit 2 Updated Safety Analysis Report (USAR) (CEG, 1998). As described in the NMP Unit 2 USAR, these previous investigations provide the following results documenting the absence of capable Quaternary faults at and within the area of the NMP3NPP site:

- Interpretation of air photos and topographic maps. This interpretation revealed no evidence of surface rupture, surface warping, or offset of geomorphic features that would be indicative of active faulting.

- Interviews with personnel from government agencies and private organizations. These interviews concluded that no known faults are present beneath the NMP3NPP site.

- Seismicity Analysis -This analysis showed that: no significant historic seismic activity has occurred in the site area; the site is located in a region that has experienced only infrequent minor historic earthquake activity; the closest epicentral location is greater than 25 mi (40 km) away. No earthquake within 25 mi (40 km) of the NMP3NPP site has been large enough to cause significant damage since the region has been populated. Section 2.5.2 provides a full discussion on the seismicity analysis for the NMP3NPP site.

- Exploratory boreholes were drilled at the NMP Unit 1 and Unit 2 and James A. Fitzpatrick Nuclear Power Plant site areas. Borehole data have provided evidence for the large scale lateral continuity of strata across the existing NMP Unit 1 and Unit 2 site areas and the inspection of soil and rock samples has revealed no adverse effects indicative of geologically recent or active faulting.

At the time of the original studies for the NMP Unit 2 USAR (CEG, 1998), there were no published maps showing bedrock faults within a 5 mile (8 km) radius of the NMP3NPP site. The Geologic Map of New York (NYSM, 1970a; NYSM, 1970b) does not show faults within a 25 mile (40 km) radius of the NMP3NPP site. The USGS's Quaternary Fault and Fold Database of the United States (USGS 2006) lists no capable faults in the state of New York. The NMP Unit 2 USAR (CEG, 1998) and the New Haven New York PSAR (NYSE&G, 1978) document minor non-capable faults that do not appear on previously published geologic maps. Jacobi (Jacobi, 2002a) presents recently identified lineaments (EarthSat, 1997) associated with fracture intensification domains and faults in New York. These lineaments associated with fracture intensification domains and faults are located beyond the 25 mile (40 km) radius and have not been shown to be capable faults.}

2.5.3.1.2 Regional and Local Geological Studies

{Extensive mapping of the NMP3NPP site region by Dames & Moore (NMPC, 1978a; NMPC, 1978b; NMPC, 1978c, NMPC, 1980) has improved the industry's knowledge of the Central Lowlands and geologic structure within the site's region.

In the immediate site area, geologic cross sections across the NMP Unit 2 site were based on excavation mapping and borehole data. This compilation of previous mapping and exploration studies, coupled with site-specific reconnaissance for NMP3NPP, provides the principal basis for the few minor off-set bedrock faults recognized within the site area.

In addition, the USGS recently completed a compilation of all Quaternary faults, liquefaction features, and possible tectonic features in the eastern U.S. (Crone, 2000) (Wheeler, 2005) (Wheeler, 2006). These compilations do not show any Quaternary faults or related features within a 25 mi (40 km) radius of the site as shown in Figure 2.5-39.

The nearest potential Quaternary faulting features located within a 200 mi (322 km) radius of NMP3NPP are: the Clarendon–Linden fault zone; the Cornwall–Massena earthquake surface features, the Catlin Lake–Goodnow Pond Lineament, the Champlain lowlands normal faults and Offset glacial surfaces near Albany, Schenectady and Troy, New York. (Crone, 2000; Wheeler, 2001; Wheeler, 2005; Wheeler, 2006). These features are discussed in detail in Section 2.5.1.1 and are shown in Figure 2.5-73.

No documented paleoliquefaction sites (Wheeler, 2001; Tuttle, 2002), are located within a 200 mi (322 km) radius from the NMP3NPP site as reflected in Figure 2.5-73. Paleoliquefaction features and studies are discussed in Section 2.5.3.1.

A review of a PSAR for a proposed nuclear power plant located east of the NMP3NPP site near the shore of Lake Ontario in New Haven, New York, reported faults and folds within a 5 mi (8 km) radius of the NMP3NPP site (NYSE&G, 1978). These structures are shown in Figure 2.5-55 and include the Demster Structural Zone, the New Haven Syncline and the Demster Beach Anticline. However, no surface faulting was noted during field reconnaissance and none of those recognized faults was judged to be a capable fault based on the age of faulting (CEG, 1998).

The most detailed subsurface exploration of the NMP3NPP site area was performed by Dames and Moore for the NMP Unit 2 foundation and supporting structures (NMPC, 1978a; NMPC, 1978b; NMPC, 1978c; NMPC, 1980; CEG, 1998). This study included drilling geotechnical and exploratory geological boreholes to characterize faults at depth, collecting down-hole geophysical data, and acquiring seismic refraction data across the site. As summarized in the NMP Unit 2 USAR (CEG, 1998), geologic cross sections were developed extending from New Haven, New York to Lake Ontario. The geologic cross section presented in Figure 2.5-154 incorporates the structures observed near New Haven New York and at NMP Unit 2. The cross section summarizes the subsurface structure across the site area radius of 5 mi (8 km).

Geologic cross-sections developed from geotechnical data collected from boreholes as part of the NMP3NPP study also provide additional detailed information for the upper approximately 250 ft (76 m) of strata on the presence or absence of structures directly beneath the footprint of the site. These cross-sections are presented and discussed in Section 2.5.1.2. Similar to the previous cross sections prepared for the site vicinity, the new geologic borehole data from NMP3NPP support an interpretation of gently-dipping to flat-lying Paleozoic sedimentary rock.

These uniform nearly flat-lying Paleozoic strata can be traced continuously for a significant distance horizontally from the James A. Fitzpatrick Nuclear Power Plant site beneath NMP Unit 2 to NMP Unit 1 where prior nuclear plant site investigations have provided great detail (CEG, 1998). At the NMP3NPP site, continuous geologic units can be traced from the southeastern most portion of the site to the shore of Lake Ontario . The strata can also be traced continuously from the shore of Lake Ontario offshore along the length of the proposed cooling water tunnels. Geologic cross sections (Figure 2.5-63 through Figure 2.5-67 and Figure 2.5-154)

demonstrate the lack of significant vertical offset, an indication of possible faulting and the lateral and vertical uniformity of the bedrock units at the NMP3NPP site.

The locations of brittle bedrock structures are presented as dashed lines in Figure 2.5-36 (Isachsen, 1977a; Isachsen, 1977b; Isachsen, 1977c; Isachsen, 1977d; Isachsen, 1977e; Isachsen, 1977f; Isachsen, 1977g). A Circle showing the 25 mi (40 km) radius around the site is also shown on the figure. The legend for Figure 2.5-36 is provided in Figure 2.5-37.

In general, the two dominant orientations of brittle structures trend east-northeast and northwest. These dominant joint orientations in New York have been documented extensively (Parker, 1942; Parker, 1969; Engelder, 1979; Engelder, 1980; Engelder, 1982a; Engelder, 1982b; Engelder, 1985; Engelder, 1993; Engelder, 2001; Engelder, 2006; Engelder, 2007; Gross, 1991; Hancock, 1989; Lash, 2007; Scheidegger, 1991; Younes, 1999; Zhao, 1997). The northwest striking joints have been associated with the Paleozoic Alleghenian Orogeny. The east-northeast striking joints are parallel to the maximum horizontal stress orientation of the contemporary stress field (Evans, 1989a; Evans, 1988b; Hickman, 1985; Plumb, 1985; Plumb, 1991; Whitaker, 2005; Zoback, 1985; Zoback, 1989). A discussion of joint orientations is presented in Section 2.5.1. Brittle structures within the site area radius of 5 mi (8 km) are shown to be the structures documented at NMP Unit 2 and discussed below. }

2.5.3.2 Geological Evidence, or Absence of Evidence, for Surface Deformation

{In addition to the small faults at NMP Unit 2, several other structures have been proposed within the 5 mile (8 km) radius of the site and are shown on Figure 2.5-55 (CEG, 1998; NYSE&G, 1978). None of these features are considered capable tectonic sources (CEG, 1998; NYSE&G, 1978), as defined in Appendix A of Regulatory Guide 1.165 (NRC, 1997) and Regulatory Guide 1.208.

No deformation or geomorphic evidence indicative of potential Quaternary activity has been reported in the literature for the Demster Structural Zone (NYSE&G, 1978). No evidence of Quaternary deformation along these inferred structures was identified during field reconnaissance or during air photo and satellite imagery review undertaken for the NMP3NPP study.

- Field reconnaissance of limited surface outcrops at the site and along the shore of Lake Ontario, coupled with geophysical surveys, provided no evidence of faulting at the NMP3NPP site.

2.5.3.2.1 Demster Structural Zone

The following presents a summary of the structures documented in the area of New Haven, New York based on studies conducted for a proposed plant at that location. Refer to Section 2.5.1.2 for detailed discussion of structural geology within a 5 mi (8 km) radius of the NMP3NPP site.

The Demster Structural Zone is located east of the NMP3NPP site and trends northeast. Associated with this zone of locally intense fracturing and faulting is a sequence of gently southwest-plunging, broad, asymmetric anticlines and synclines on the order of a few miles in length. The locations of the Demster Structural Zone features are depicted on Figure 2.5-55. This zone of complex deformation is located in the Late Ordovician Oswego Sandstone, the youngest site area rock unit in outcrop and subcrop. Post-Ordovician deformation was identified during subregional and site subsurface mapping investigations at the New York State Electric & Gas Corporation (NYSE&G) proposed New Haven nuclear site approximately 5 mi (8 km) southeast of the NMPNS site (NYSE&G, 1978).

Structural and stratigraphic relationships in the Demster Structural Zone show that the New Haven area has been deformed by two sequences of tectonic activity: initial post-Ordovician Paleozoic broad folding culminating in reverse faulting and later possibly Mesozoic normal faulting. No other tectonic activity is documented at the Demster Structural Zone. Calcite paragenesis indicates no deformation subsequent to the youngest sequence of minerals, and Pleistocene surficial sediments overlying the fault zone are not deformed (CEG, 1998).

K-Ar dating suggests a Middle-Paleozoic (Silurian) time of deformation for the Demster Structural Zone. The reconstructed geologic column, associated geologic history, and other interpretations of data suggest a Middle- to Late-Paleozoic age. A younger Late-Jurassic age cannot be ruled out, although sulfur isotope data do not strongly support this age. The uncertainty of the timing of alkaline emplacement based on the geochemical data, plus lack of documented high-angle Late-Mesozoic faulting, place constraints on this time interval. Consequently, a Middle- to Late-Paleozoic age is inferred for the final development of the Demster Structural Zone (CEG, 1998).

The deformation style, the northeast trend of the structural elements, regional stratigraphy, and analytical data are in agreement that the Ordovician strata in northern Oswego County, and conceivably the underlying Cambrian and Ordovician strata in central New York, have undergone broad areal folding with variable reverse and normal faulting. Combined geologic and geophysical data indicate that the Demster Structure is not capable and seismic activity has not been associated with the Demster Structure (CEG, 1998).

Demster Zone Subsurface Structure

Stratigraphic and structural interpretation of data from borings, combined with trench excavations, indicate that major stratigraphic offset in the section explored is caused by the development of the Demster Beach Anticline and not by faulting. As structure contours indicate, the Oswego Sandstone and Pulaski Formation folding is not a single fold but a series of folds. Drilling, stratigraphic interpretation, and seismic studies surrounding the Demster Zone demonstrate an apparent dying out of faulting to the northeast and southwest along the Demster Zone. Only one of several borings to the west of the zone intersected minor faults (CEG, 1998).

Subsurface data show two styles and phases of deformation, large-scale reverse-slip and small-scale normal-slip. Fracturing, calcite mineralization, and faulting decrease away from the fault zone. Offsets diminish away from the fault zone, as well as to the southwest along the zone. Principal reverse stratigraphic offsets across the zone vary from 130 to 160 ft (40 to 49 m). Within the zone of intense deformation 10 to 15 ft (3 to 4.6 m) of normal displacement was found (CEG, 1998).

At the fault zone proper, the exact amount of offset is uncertain due to complex folding, fracturing, and the necessary extrapolation of data. The vertical component of normal faulting is interpreted to be small, at no more than approximately 10 ft (3 m). This 10 ft (3 m) normal throw is in agreement with boring alignment data (CEG, 1998).

Structural Synthesis of Demster Zone

Structural data substantiated by the stratigraphic sequence in the trench vicinity indicate two phases of folding and faulting for the Demster Structural Zone. These multiple deformation events have produced three separate, small-scale deformation zones. Each deformation zone in part exhibits the effects of the overall fold/fault deformation and no movement has been identified since late calcite mineralization (CEG, 1998).

Sequentially, the structural deformation appears to be of two stages or phases. The first stage of apparent compression resulted in a series of broad, low-amplitude, eastward-verging, southwest-plunging folds (Demster Beach and Mexico Anticlines and New Haven Syncline) which account for the main stratigraphic offset. This stage is manifested by a gentle southeast dip. With continuing compression, the steep limb of the Demster Beach Anticline was faulted in a reverse sense rather than in a left-lateral strike-slip sense. Associated with the reverse faulting are small-scale, eastward-verging, northeast-plunging folds. This folding style is recognized only in the intensely deformed strata of the central structural domain and may not have developed along the entire length of the Demster Structural Zone. The exact stratigraphic displacement due to reverse faulting could not be ascertained at the trench exposure because the second-stage structural deformation, normal faulting, modified the offset due to reverse faulting (CEG, 1998).

Normal faulting resulting from apparent extension, the final deformational event, truncated the limbs of the small-scale folds and displaced the main reverse fault (CEG, 1998).

The bedrock/till interface at faults was closely examined for evidence of displacement. The till fabric was random and the bedrock surface smooth over mapped faults. A distinct pair of silt laminae occurs continuously near the base of the lake sediments over the fault between along the northeast trench wall. The laminae are undisturbed and follow the topography of the lower till upon which they were deposited. These laminae were most likely laid down in proglacial Lake Iroquois, 12,500 to 10,000 years Before Present (B.P.) (CEG, 1998).

The silt laminae are locally contorted and warped where draped over cobbles or boulders or where rafted material has settled. Faulting and folding associated with the development of the Demster Structural Zone have not disturbed the overlying Pleistocene deposits (CEG, 1998). Therefore, the most recent faulting and folding within the Demster Structural Zone occurred prior to the Pleistocene.

In summary, the interpretation and evaluation of the combined geologic and geophysical data support the following conclusions:

1. The Demster Structural Zone is not capable.

2. Broad folding, reverse faulting, and normal faulting associated with the Demster Zone developed sequentially through a series of three events or phases that occurred in Middle to Late Paleozoic and, possibly, Mesozoic time.

3. Ordovician strata in the site area are folded into a series of essentially parallel, southwestward-plunging anticlines and synclines. The Demster Beach Anticline is intensely deformed and faulted within part of the eastern oversteepened limb designated the Demster Structural Zone. Stratigraphic offset is due primarily to folding, but steeply northwest-dipping small faults and fold axial fractures account for the intense brittle deformation.

4. Fluid inclusion data are indicative of calcite mineralization emplaced at high temperatures greater than 212 °F (100 °C) which demonstrates a significant depth of burial. Paragenetic and structural element correlation demonstrates the deposition of calcite after bacteriological reduction of sulfides, in part contemporaneous with and soon after the deformation in the Middle to Late Paleozoic, and, possibly, Mesozoic.

5. Early calcite mineralization indicates deposition prior to completion of structural development and late calcite is undeformed, thus constraining the age of deformation as Mesozoic or older.

Field reconnaissance, coupled with interpretation of aerial photography (review and inspection of features preserved in aerial photos) shows that there are no geomorphic features indicative of Quaternary activity along the surface-projection of the Demster Structural Zone.

There is no pre-EPRI or post-EPRI (EPRI, 1986) study of seismicity spatially associated with this feature, or any geomorphic evidence of Quaternary deformation as shown in Figure 2.5-39. Thus, based on the absence of geomorphic expression, absence of seismicity, and lack of offset of Quaternary surficial deposits, it is concluded that the Demster Fault Zone is not a surface-fault rupture or deformation hazard for the NMP3NPP site.

2.5.3.2.2 NMP Unit 2 Cooling Tower, Barge Slip - Normal, and Drainage Ditch Faults

The following presents a summary of the three steeply dipping structures documented in the area of NMP Unit 2. Refer to Section 2.5.1.2 for detailed discussion of structural geology within a 5 mi (8 km) radius of the NMP3NPP site.

Three, approximately parallel, high-angle faults striking west-northwest, namely, the Barge Slip - Normal fault, the Drainage Ditch fault, and the Cooling Tower fault, occur at or adjoining the NMP Unit 2 site . The Barge Slip - Normal fault dips 60 to 65 deg southward; the other two faults dip 55 to 70 deg to the north. All three faults have similar structural characteristics. Most of the information concerning these faults was gained from a detailed investigation of the Cooling Tower fault. However, all available surficial exposures of the Barge Slip - Normal and Drainage Ditch faults were examined, together with reports of previous investigations of these structures (CEG, 1998).

Buckling in the site area was noted to have occurred on only two of the three high-angle faults. These two faults dip northward (Cooling Tower and Drainage Ditch faults), whereas the third fault dips southward (Barge Slip - Normal fault). However, the south-dipping fault could be inferred to have the greatest potential for developing this type of deformation, assuming that the stresses on-site prior to buckling were horizontal and uniform (CEG, 1998).

The high-angle faults display several common characteristics. All three appear to be subvertical strike-slip faults in surface and excavation exposures within the Oswego Sandstone. However, they display the geometry and displacement of a normal fault within the Lorraine Group. They each contain occurrences of calcite and sulfide mineralization associated with the strike-slip and normal slip deformational fabrics. Furthermore, the homogenization temperatures and paragenesis of the mineralization associated with the different episodes of deformation are similar for each fault (CEG, 1998).

Some aspects of the geometry and deformation along the Drainage Ditch and Cooling Tower faults (the two north-dipping faults) differ from those of the Barge Slip - Normal fault. Each of these two faults is coincident with the axial plane of an asymmetric chevron fold or monocline. The Drainage Ditch feature is coincident with the Teepee Fold noted at the James A. Fitzpatrick Nuclear Power Plant site. The faults exhibit reverse slip, stratigraphic displacements in addition to the aforementioned deformation. Also, in surficial exposures of each of the north dipping structures, the plane of the fault was displaced by translation of the adjacent strata along bedding planes (bedding plane slip). The Drainage Ditch and Cooling Tower faults were not determined to be capable faults based on their age (NMPC, 1978a; NMPC, 1978b; NMPC, 1978c,

NMPC, 1980; CEG, 1998). The Barge Slip - Normal fault was also determined to be a non-capable fault based on its age (NMPC, 1978a; NMPC, 1978b; NMPC, 1978c; NMPC, 1980; CEG, 1998).

Of the three high-angle faults at the NMP Unit 2 site, only the Cooling Tower fault had clearly deformed the overlying Pleistocene sediments. The effects and mechanism of this deformation are presented under the heading Reverse-Slip Displacements. The total inferred lateral extent of the high-angle faults is represented by the fault traces shown on Figure 2.5-73. The fault traces are assumed to be relatively linear. This assumption proved to be valid by direct observations elsewhere, especially along the Cooling Tower fault. Few data are available regarding the southeast extent of the Barge Slip - Normal fault. The minimum lateral extent of this feature is about 2,200 ft (670 m) (Figure 2.5-73). The west-northwest extent of the Barge Slip - Normal fault can only be inferred to be located west of its intersection with the excavation for the lake water tunnels of the James A. Fitzpatrick Nuclear Power Plant. The fault was mapped in the James A. Fitzpatrick Nuclear Power Plant intake and discharge tunnels (CEG, 1998).

The inferred western extent of the Drainage Ditch fault is located as shown on Figure 2.5-73 because the lake water tunnels for the NMP Unit 2 site did not encounter the fault. The east-southeastern extent of the Drainage Ditch fault was determined when the extension of the compression buckle or Tepee Fold at the James A. Fitzpatrick Nuclear Power Plant site was investigated by examination of aerial photographs, seismic refraction surveys, and test excavations. These studies led to the conclusion that, east of the James A. Fitzpatrick Nuclear Power Plant, the buckling (of the bedrock layers) dies out and the fracture resolves into a local system of close jointing (CEG, 1998).

Seven trenches and pits were dug to investigate the lateral extent of the Cooling Tower fault as part of studies for NMP Unit 2. The western extent of the fault is inferred, as shown, because Trenches 1 and 2 revealed no evidence of faulting.

Two trenches at NMP Unit 2 located along the western projection of the Cooling Tower fault showed no evidence of the fault as part of the investigation at that plant, indicating it ~~was~~is unlikely to extend into the NMP3NPP site. Investigations for the offshore tunnels for the NMP3NPP included boring locations along the strike direction of the Cooling Tower fault. These borings included two angle borings which were lay~~er~~ed out perpendicular to the strike direction of the fault. No evidence of the fault (e.g. significant sub vertical fracturing, fault gouge, slickensides or weathering) was noted. Additionally, land-based and marine seismic refraction studies showed no anomalies that could be interpreted as faults or significant discontinuities. ~~Therefore, it the~~Thus, an extension of the NMP Unit 2 Cooling Tower fault beyond the excavation mapping in Trench 1 and Trench 2 at NMP Unit 2 (CEG, 1998) ~~seems It is difficult to precisely locate the east-southeastern extent of the Cooling Tower fault because the deformation becomes diffuse~~has not been found. ~~However~~Because, most of the characteristics of this fault, including magnitude of displacement and degree of cataclasis, appear to be similar to those of the Drainage Ditch fault. Hence, it ~~may be~~is logical to assume that the length of the Cooling Tower fault may be similar to that of the Drainage Ditch Fault. This reasoning suggests that the surface extent of the Cooling Tower fault is essentially limited to the northeast to southwest trace as shown on Figure 2.5-73 (CEG, 1998).

The Cooling Tower and Drainage Ditch faults were also investigated by performing proton precession magnetometer surveys across the established traces of both faults. The surveys found no magnetic gradients that could be interpreted to represent faults across the traces of the structures or at a hypothetical projection to the basement (CEG, 1998).

The depths of the high-angle faults at NMP Unit 2 are inferred on the basis of information gathered from the subsurface investigation of the Cooling Tower fault. This fault was investigated by drilling two rows of closely spaced vertical boreholes perpendicular to the strike of the fault. Detailed stratigraphic and structural logs were prepared from the cores extracted from the boreholes. From these logs, detailed correlation charts were prepared and these charts were used to prepare geologic cross sections. The principal structural element in the subsurface is a 60- to 65-degrees northward dipping discontinuity. The structure extends from the top of the bedrock down to the explored depth of 270 ft (82 m). Below a depth of 200 ft (60 m), the sense of fault displacement is normal and the magnitude of offset is about 1 ft (0.3 m). Because of the similar structural character of the high-angle faults, it is inferred that they all extend to a depth similar to that attained by the Cooling Tower fault. Based on the small magnitude of the observed displacement of (~~(~~1 ft (0.3 m~~)~~) and the relatively short length of this structure's surface trace, it seems appropriate to infer that this fault extends more than 270 feet (82 m) deep. Based on the Cooling Tower fault study, it is believed that the high-angle faults only extend to depths of several hundred feet and that they do not extend to the basement. The results of the magnetometer survey discussed above support this inference because magnetic anomalies represent magnetic contrasts in the basement rock, and there are no magnetic anomalies to provide evidence of any offset (CEG, 1998).

The investigations of the three high-angle faults (i.e., Barge Slip - Normal fault, Cooling Tower Fault and Drainage Ditch fault) at and adjoining the NMP Unit 2 site revealed evidence of a history of multiple displacements with different senses of movement along the faults. It was found that the three faults had moved simultaneously. They initially experienced strike-slip movement followed by normal slip movement. In addition, the two northward-dipping faults (Cooling Tower and Drainage Ditch faults) have been affected by buckling of the bedrock along the fault planes both laterally and with depth. The buckling mechanism resulted in the development of reverse-slip displacements along the fault planes, but restricted to the upper 200 ft (60 m) of the bedrock mass (CEG, 1998). Buckling may be associated the contemporary stress field which has a maximum horizontal compressive stress oriented northeast – southwest. Refer to Section 2.5.1.1 for a more detailed discussion of the contemporary stress field and to Section 2.5.4 for the magnitude of in-situ stresses measured at NMP Unit 2.

NMP Unit 2 Strike-Slip Motion

The three high-angle faults commonly display characteristics indicative of strike-slip deformation. The amount of lateral displacement is known only for the Cooling Tower fault. In one exposure a sedimentary channel crest (an interfluve ridge) within the Oswego Sandstone was displaced 3 ft (0.9 m) in a left-lateral sense across this fault. Indirect evidence of strikeslip faulting, such as the character of the shear and fracture fabric in proximity to the faults, as well as the occurrence of both horizontal slickensides and slickensides with gentle rakes on fracture surfaces, are also present (CEG, 1998).

In surface exposures, the high-angle faults are vertical, or nearly so. However, subsurface investigation with vertical borings demonstrated the presence of the Cooling Tower fault dipping approximately 60 degrees. Two inclined borings were drilled to investigate whether a vertical strike-slip fault, independent of the moderately dipping fault, also existed at depth. The angle borings demonstrated that a vertical fault does not exist below a depth of 90 ft (27 m). Apparently, the vertical, strike-slip portion of the Cooling Tower fault exists only in the massive strata of the Oswego Sandstone (CEG, 1998).

Strike-slip displacements predate other deformations that occurred on the high-angle faults. This interpretation is supported by both mineralogical and structural relationships. The strikeslip faults probably formed at the same time as the systematic fracture sets at the site (Stillwell, 2005; Engelder, 2006). Both the fracture sets and the strike-slip faults contain vein

mineralization with homogenization temperatures (320 °F to 248 °F (160 °C to 120 °C)) similar to those determined for quartz grain clasts in the host rock (349 °F to 297 °F (176 °C to 147 °C)). This indicates that this deformation occurred after diagenesis and represents the onset of brittle bedrock deformation (CEG, 1998). Strike-slip deformation is most likely associated with the Late Paleozoic Alleghenian Orogeny.

NMP Unit 2 Normal-Slip Motion

Each of the high-angle faults also exhibits some characteristics of normal-slip deformation. Normal-slip stratigraphic displacements on the Barge Slip - Normal and Cooling Tower faults are 16 in (40 cm) and 6 to 12 in (15 to 30 cm), respectively. No normal-slip displacement was detected along the Drainage Ditch fault. However, several indirect indicators of normal-slip were observed along these high-angle faults. Shear fracture geometry consistent with normal faulting was observed in a number of exposures. Moreover, slickensides with steep rakes are present on some of these surfaces as well as on the main shear surfaces of the brecciated zones. Drag folds with normal shear sense were detected during both the surface and subsurface investigations of the Cooling Tower fault. Many fractures associated with normalslip deformation contain calcite and sulfide mineralization (CEG, 1998).

The results of field studies indicate that normal-slip deformation postdates strike-slip faulting but predates other deformations that affected the high-angle faults. Structural relationships such as the overprinting of slickensides with steep rakes on slickensides with shallow rakes, and the truncation of strike-slip fracture sets by shear zones with a normal-slip fabric, suggest that normal-slip followed the strike-slip deformation. Mineralization studies at the site confirm this relationship. Homogenization temperatures of calcite mineralization associated with normal fault deformation fabric (249 °F to 163 °F (116 °C to 73 °C)) were typically lower than those associated with diagenesis and strike-slip faulting (349 °F to 248 °F (176 °C to 120 °C)). Based on the paragenetic sequence developed for the site (Section 2.5.1.2.6), mineralization of the lower temperature range was emplaced later than diagenesis and strike-slip faulting (CEG, 1998). Normal-slip deformation may be associated with a Mesozoic extensional environmental.

NMP Unit 2 Bedding-Plane-Slip Motion

The effects of displacements resulting from bedrock translation along bedding planes have been noticed at numerous locations at the site. Bedding-plane-slip accompanied reverse-slip displacements on the high-angle faults as well as the development of the low-angle thrust structures. The age and relationship of bedding-plane-slip to these deformations is included in the discussions specifically addressing these topics (CEG, 1998).

Excluding the thrust structures, the most prominent examples of bedding-plane-slip displacement were observed in the surficial exposures of the high-angle faults. These displacements distorted the original configuration of the faults, resulting in considerable variation in the thickness and attitudes of the breccia zones of these originally steeply dipping faults (CEG, 1998).

NMP Unit 2 Reverse-Slip Motion

The Drainage Ditch and Cooling Tower faults are both coincident with the axial plane of an asymmetric chevron-like fold or monocline. These folds resulted from a third episode of deformation occurring along the north-dipping high-angle faults. It was characterized by reverse-slip displacements accompanied by bedding plane slip and dilation of the bedrock within 200 ft (60 m) of the surface around the fault. Field evidence clearly indicates that this deformational episode consisted of two phases: 1) preglacial buckling along high-angle faults, and 2) postglacial buckling on the fault (CEG, 1998).

The total reverse-motion separations across the Drainage Ditch and Cooling Tower faults are 1.5 ft (0.46 m) and 5 to 6 ft (1.5 to 1.8 m), respectively. However, the reverse stratigraphic separations along the shear zones in surficial exposures vary from 0 to 3 ft (0 to 0.9 m). These displacements are less than the total separation because they do not include all the reverse separation resulting from monoclinal rotation. The shear sense indicated by drag folds, within the breccia zones and in the adjacent bedrock, is consistent with this reverse displacement sense (CEG, 1998).

At five exposures along the Cooling Tower fault, the layered sequence of glaciolacustrine sediments was deformed. The deformation occurs generally within a 20-ft (6-m) wide zone straddling the bedrock fault. The numerous small-scale deformational features in the sediments consist of fluidized flow and sediment flow structures, as well as small faults. The most prominent of these faults exhibits maximum displacements of several inches. Structural analysis indicates that the deformation was accomplished by relative vertical movements consisting of broad arching and monoclinal flexuring of the sediments resulting from reverseslip displacements on the bedrock fault. In Pit 1, the Cooling Tower Trench, Trench 4, and Trench 5, the vertical separation, caused by arching and generally accompanied by compensatory normal faults in the sediments, is estimated to range from 0.5 to 1 ft (0.15 to 0.30 m). In Trench 3 the separation that resulted from monoclinal flexuring is 2.70 to 3.25 ft (0.82 to 0.99 m). As a result of the flexuring at this location, many small-scale normal, thrust, and high-angle reverse faults developed in the sediments, especially in the area of the short limb of the monocline (CEG, 1998).

The subsurface character of displacements on the Cooling Tower fault was also the subject of a detailed investigation (CEG, 1998).

In the upper part of the section, the structure resembles a kink band or monocline, consistent with the surficial exposures. The reverse stratigraphic separation of about 5.5 ft (1.7 m) is accomplished mainly by southward rotation of bedding by up to 50 degrees within a bedrock sliver bounded by two shear planes. Deeper in the section the separation has resulted from shear directly on the bounding planes, as well as rotation of the bedrock sliver. The bounding planes of the bedrock sliver merge at a depth of approximately 140 ft (43 m). Below this depth, the reverse stratigraphic separation results from direct shear displacement along a single shear plane. The magnitude of reverse displacement decreases progressively from the surface to nearly zero at a depth of approximately 200 ft (60 m). Below this depth, a normal displacement of 0.5 to 1 ft (0.15 to 0.30 m) occurs (CEG, 1998).

As noted previously, the displacement adjacent to the fault (0 to 3 ft (0 to 0.9 m)) is less than the displacement measured away from the structure (5 to 6 ft (1.5 to 1.8 m)) near the bedrock surface. In contrast, at the base of the Oswego Sandstone and below, the measured amount of displacement is significantly less away from the structure than it is adjacent to the fault. On opposite sides of the structure it is always possible to find two points on the same stratigraphic horizon that do not appear to be displaced. The horizontal distance between two such points becomes progressively smaller with depth. Hence, the reverse dislocation of strata occurred only within a narrow zone contained almost entirely in the hanging wall block. In cross section, this zone has roughly the shape of a right triangle with the Cooling Tower fault forming the hypotenuse. The vertical leg of the triangle is approximately 200 ft (60 m) long; the horizontal leg is at least 60 ft (18 m) long (CEG, 1998).

Prior to the development of the structure, the stratigraphic thickness must have been equal on each side. However, the present stratigraphic thickness of the hanging wall is now about 6 ft (1.8 m) greater than on the footwall. Notably, the magnitude of this difference in thickness (dilation) is nearly equal to the overall reverse stratigraphic displacement. The amounts of both

the displacement and the dilation decrease progressively downward and do not appear to be present below a depth of approximately 200 feet (60 m). Hence, the reverse displacement at any point along the structure is approximately equal to the amount of dilation of the section on the hanging wall. It should be noted that this is true not only for the zone of flexural shear displacement but also for the direct shear displacement observed below this zone (CEG, 1998).

Analysis of the information from the investigation of the Drainage Ditch and Cooling Tower faults provides the basis for understanding the relative age of the reverse and bedding-planeslip displacements. It must be noted that the principal mechanism for the deformation was buckling. The dilation of the bedrock and slip of the strata toward the crest of the buckle resulted in the observed reverse displacements (CEG, 1998).

Buckling along the north dipping high-angle faults postdated the strike-slip and normal fault deformations, as indicated by several structural relationships. Structural fabrics resulting from both strike-slip and normal fault episodes were deformed by bedding-plane-slip related to the buckling. Conjugate strike-slip and normal fracture sets have been rotated in conjunction with the limbs of the buckle. The buckling deformation and absence of associated mineralization indicates the deformation occurred near the surface, whereas the homogenization temperatures of mineralization associated with the episodes of strike-slip and normal faulting indicate that deformation occurred at considerable depths of burial (CEG, 1998).

The reverse-slip deformation occurred during more than one phase of movement. Field data from precise surveys show that some of the bedrock deformation occurred prior to deposition of the Late Wisconsinan and Holocene sediments above the Cooling Tower fault. Specifically, it has been demonstrated that in the Cooling Tower Piping Trench and Pit 1 exposures, bedding on the south side of the fault dips 7 to 9 degrees southward marking the tilted limb of a monocline. Varved lacustrine sediments spanning this limb were not structurally affected by this rotation. However, there is obvious evidence of deformation of the sediment as described above. Hence, a second phase of deformation must have occurred later than that of the monocline development, and later than 12,000 yr B.P., the approximate age of the layered sediment (CEG, 1998).

It is uncertain how many deformational events affected the overburden sediments. The effects of arching and monoclinal flexuring, with associated small-scale reverse and normal faults, all may be the result of one deformation. The elements of deformation are emphasized by local well-defined shear planes where the sediments have been faulted because of arching or flexuring. However, there are present in several exposures a number of diapiric structures caused by fluidization. In Pit 1 and Trench 3, these features are clearly deformed by the small faults formed during arching of the sediments. Thus, they predate the formation of small-scale normal faults in the sediment. It has been observed that, although some diapiric structures do occur in sediments away from the fault, they are mostly concentrated in the area of the fault zone. It is possible that the formation of these structures was related to fluid pressure changes as a result of water level fluctuations in the (Lake) Ontario Basin (CEG, 1998).

NMP Unit 2 Mechanism of Reverse-Slip Deformation (Pre-Wisconsinan)

The expansion of the stratigraphic section on the north limb of the structure is an important aspect of the deformation that was detected in the subsurface. Expansion of the stratigraphic section on the north limb would have resulted in reverse-slip motion along the pre-existing Cooling Tower fault. The cross-sectional area affected can be approximated as a right triangle equal to at least 6,000 ft^2 (557 m^2). Unidirectional dilation resulted in an increase of area in this zone that is equal to a minimum of 165 ft^2 (15 m^2). The amount of expansion on the hanging wall then is approximately 2 to 3 percent. It is also likely that expansion affects the strata of the footwall or south limb, particularly for the strata above the apex of the two shear planes within

the zone of flexural shear displacement. However, uncertainties in the amount of stratigraphic separation due to the direct shear displacement and in the geometric arrangement of strata on the south limb do not permit an estimate of the amount of expansion that might exist there (CEG, 1998).

Dilation of the bedrock close to the fault is associated with the presence of voids or partings along bedding planes, as corroborated by observations in both the surface and subsurface investigations. These have been observed in the excavated bedrock slots. Similarly dilated strata have also been noticed in the subsurface. They commonly occur as voids into which the drilling rods suddenly dropped and water circulation was lost. The presence of these voids was further substantiated by a downhole impression packer survey (CEG, 1998).

Although the cumulative effect of the bedding plane separations appears to account for most of the expansion of 5 or 6 ft (1.5 or 1.8 m), it is believed that time-dependent deformation of the rock also contributed to the total displacement. Disharmonic, concentric drag folds that occur outside the bedrock sliver and adjacent to the two shear fractures bounding the bedrock sliver attest to this. Structural shortening of these folds is approximately 20 to 30 percent, based on that observed in Trench 3 (CEG, 1998).

As discussed in Section 2.5.4, a rock specimen can undergo an increase in its original dimensions during and after removal from the in situ stress field. This increase is elastic or instantaneous as well as time dependent. It has been shown by unconfined swelling tests that the rock specimen expands when removed from the bedrock and placed in an environment of constant temperature and high humidity. The rate of this expansion varies with the lithology of the specimen and is greatest in the direction perpendicular to bedding. The swelling process is caused by the development of very high negative pore pressures in response to the elastic strain relief. This results in the flow of water to the available dilated pore species of the rock. The swelling, and concomitant flow of water, can be time dependent as a function of gradual changes in permeability of the rock mass related to time-dependent change in the stored strain energy. Considering these results, it appears reasonable to assume that the perturbation of the stress field at the Cooling Tower fault did cause swelling in the bedrock. Therefore, the total expansion very likely may be the combined result of both factors: the separation along bedding planes and the internal volumetric changes. This internal dilation is relatively small or nonexistent on the footwall (excluding the rotated sliver), but may be considerable on the hanging wall. Hence, these postulated volumetric changes may be differential and could have enhanced and prolonged the deformation process by providing an additional source of incremental, distortional, strain energy (CEG, 1998).

Considering the observations and relationships provided above, buckling is the mechanism of reverse-slip deformation on the Cooling Tower fault. Buckling is also related to the bedding-plane-slip distortion of the normal fault observed in the excavations. It is important to note, therefore, that the direct shear displacement is only a secondary effect of the buckling instability (CEG, 1998).

The entire structure can actually be accurately described as a sequence of full-wave length (l) buckles in the upper part and a sequence of half-wave length (l/2) buckles in the lower part. These buckles are superimposed upon a preexisting normal fault that dips 60 degrees northward. The amplitudes and wavelengths of each type of buckle diminish progressively with depth. Concomitantly, 1) the reverse-slip displacements decrease to zero with depth, 2) the displacement decreases to zero in a lateral direction away from the structure, and 3) the zone of dilation on the hanging wall narrows with depth (CEG, 1998).

On the basis of the analysis of the deformation process and its origin, the following principal conclusions are drawn with respect to the Cooling Tower fault:

1. The development of the pre-Wisconsinan, reverse-slip deformation is attributed to the combined effects of three factors:

   a. In situ bedrock stress field.

   b. Changes in the stress field induced by the crustal downwarping caused by glacial loading.

   c. Pronounced anisotropy of the bedrock at the site.

2. In the present tectonic environment of the site area, it is not possible for the structure to propagate downward below its original depth of development. On this basis, the structure is considered to be presently incapable of generating vibratory ground motion (CEG, 1998).

3. The disturbance of the glaciolacustrine sediments (Lake Iroquois and Sandy Creek Stage of Lake Iroquois) is attributed to the excessive buildup of fluid pressure in the bedrock caused by postglacial fluctuations of the water level in the Ontario Basin. The present value of the fluid pressure has no significant influence on the stability of bedding adjoining the Cooling Tower fault. Hence, future movements of similar origin are unlikely.

4. Based on the present understanding of the site conditions and the mechanism of deformation, it cannot be ruled out that minor, subsurface adjustments may occur within the zone of buckling along the Cooling Tower fault. If these minor adjustments occur, they will involve a relatively low strain rate and only limited volumes of the rock mass, and thus should be considered to be inconsequential in terms of vibratory ground motion. These adjustments are expected to be restricted to the rock mass within the depth interval defined by the location of the Transition Zone (depth of approximately 50 ft, 15 m) and a depth of 200 ft (60 m). Furthermore, it is believed that the adjustments will not be expressed at the bedrock surface because of the presence of voids between layers that first must be closed (CEG, 1998).

5. As stated in the consultant report (Niagara Mohawk, 1980), "the faulting is not related to current tectonic processes that could introduce additional amounts of strain energy." In addition, it is stated that "it can be concluded that no increase in the amount of stored strain energy will occur during the coming centuries." (CEG, 1998)

In summary, site reconnaissance, coupled with literature review, do not provide evidence for the existence of capable faults at NMP Unit 2. There also is no pre-EPRI or post-EPRI (EPRI, 1986) study of seismicity spatially associated with these features. The high angle faults observed at NMP Unit 2 do not extend onto the NMP3NPP site and thus do not affect the NMP3NPP site.

2.5.3.2.3 NMP Unit 2 Thrust Faults

The following presents a summary of the shallow dipping thrust structures documented in the area of NMP Unit 2. Refer to Section 2.5.1.2 for detailed discussion of structural geology within a 5 mi (8 km) radius of the NMP3NPP site.

A series of shallowly dipping faults, referred to as thrust structures, are exposed in the bedrock excavations and tunnels at the NMP Unit 2 site. They appear to be interrelated because of striking similarities in structural style, mechanism of deformation, and relative age. A series of detailed structural, mineralogic, isotopic, and palynologic studies were conducted to investigate the nature of these thrust structures (CEG, 1998).

The faults are predominantly developed in the area of the erosional valley in the bedrock surface (Figure 2.5-73). All field evidence suggests that they are confined between the Cooling Tower fault and the Drainage Ditch fault. The Radwaste thrust fault was traced to the east with borings. The results indicate that the Radwaste fault thrust structure extends in its dip direction a minimum horizontal distance of 100 ft (30 m) to the east of its exposure in the North Radwaste Trench. The position of the thrust structures appears related to the presence of three prominent lithologic interfaces within the stratigraphic section penetrated by the site excavations. The Radwaste thrust structure was exposed in several shallow excavations at the site from the North Radwaste Trench to the Circulating Water Piping Trench. This structure is situated between the lower Oswego Sandstone and the upper portion of Unit A of the Pulaski Formation. The Unit B slip zone was exposed in the walls of the reactor containment excavation, and in rock cores from borings drilled in the vicinity of the reactor complex. It is located near the interface between Units B and C of the Pulaski Formation. The thrust faults in the tunnels are exposed at the base of the intake shaft and in both lake water tunnels. Stratigraphically, these structures are located within the upper portion of Unit C of the Pulaski Formation (CEG, 1998). Pulaski Formation Units A, B, and C are described in Section 2.5.1.2.

The thrust faults are all similar in overall appearance and display common structural characteristics. The structures consist of small zones of brecciation and folding that are at most several feet wide. The dips of these zones range from nearly horizontal to approximately 30 degrees from horizontal. The configuration of the thrust structures resembles a stack of tabular bedrock elements displaced to the west along bedding planes. These structures appear to be confined to specific stratigraphic units. They generally occur as planes of slip, parallel to bedding, with short intervals where the discontinuity transects the layering at a low angle and then merges with bedding at a higher stratigraphic level. The most intense deformation occurs along the inclined portions of the discontinuities. Locally, there may be no shear dislocation of the beds along the fault (CEG, 1998). The mode of displacement typically consists of:

1. Discontinuous shear dislocation of individual beds or groups of beds.

2. Rigid body rotation of beds to form small folds.

3. Broad arching of the hanging wall strata.

4. Dilation of the bedrock along bedding planes and variously oriented fractures.

Numerous indicators of dilation within the bedrock mass, such as voids, open fractures of various attitudes, and zones of loose bedrock rubble, were encountered during the investigation of the thrust structures. This is possibly the most important characteristic of the structures and is significant because it clearly indicates that an environment of low confining pressure was necessary for their development (CEG, 1998).

The results of detailed geologic investigation of the Radwaste fault resulted in the following conclusions regarding the nature and origin of the thrust structures. The following conclusions and results are supported by a panel of consultants (CEG, 1998).

1. Movements along the Radwaste fault (and similar thrust faults) have been recurrent.

2. The initial development of the structure is believed to be associated with crustal loading and unloading during episodes of glaciation. This suggests that the thrust was initiated sometime between 12,000 and 2,000,000 yr ago. Based on experience with similar structures, Drs. Jahns and Philbrick believe that the age of initial formation can be narrowed to between 150,000 and 400,000 yr B.P. (CEG, 1998).

3. The minimum age of development of the Radwaste fault is approximately 11,000 yr B.P. However, the exact age of the latest deformation is uncertain because the relationship of the lacustrine clays to the bedrock deformation does not provide certain resolution of the age of latest deformation (CEG, 1998).

4. The thrust faulting results from the release of stored strain energy caused by the reduction in vertical confining pressure by erosion. The faulting occurs on the flanks of the small bedrock valley. It is postulated that formation of the valley disturbed equilibrium conditions and removed the lateral restraint that had prevented the expansion of the strata on either side of the valley. Furthermore, the development of the thrust faults was facilitated by buckling across the lateral boundaries of the thrust sheet (i.e., Cooling Tower and Drainage Ditch faults). The buckling resulted in a significant reduction of the normal stress acting perpendicular to these boundaries, thus lowering the resistance to frictional sliding of the thrust sheet relative to the surrounding bedrock (CEG, 1998).

5. As stated in the consultant report (Niagara Mohawk, 1980), "the faulting is not related to current tectonic processes that could introduce additional amounts of strain energy." In addition, it is stated that "it can be concluded that no increase in the amount of stored strain energy will occur during the coming centuries." (CEG, 1998)"

6. Based on observations of analogous geologic structures, Drs. Philbrick and Jahns conclude that because of the inability of the structure to build up significant amounts of strain energy, the Radwaste structure is so nearly dead at present levels of exposure that its participation in such future movements would amount to no more than a small fraction of an inch (CEG, 1998).

Drs. Jahns and Philbrick also conclude that any future movements should not exceed 0.25 in (0.64 cm), based on their experience. Based on studies including mathematical modeling, it has been concluded that 1 inch (2.54 cm) is a conservative allowance for future maximum credible movement. Thus, an allowance of 1 in (2.54 cm) is used for design purposes (CEG, 1998). Maximum allowable movements for design purposes for NMP3NPP are presented in 2.5.4.

The magnitude of displacement also varies along both the strike and dip of the Radwaste fault. For example, 5 to 7 ft (1.5 to 2.1 m) of displacement is present near the upper limit of the ramp of the structure in the North Radwaste Trench; however, in the deepest part of the excavation, an apparent dip separation of 4.5 ft (1.4 m) was noted. The faults in the lake water tunnels exhibit small displacements typically less than several inches. The magnitude of displacement along the Unit B slip zone has not been established. However, one may infer that the displacement is at least equivalent to that of the tunnel faults because it occurs at a higher level in the stratigraphic section (CEG, 1998).

The age of development of the Radwaste fault (and other thrusts) was evaluated by considering the age and origin of the secondary filling materials. Specimens of calcite minerals were analyzed using geothermometry, isotope ratio analysis, and radiometric dating. These results were compared with similar data obtained from analyses of mineralization occurring in proximity to the high-angle faults. The paragenetic study of the calcite found in association

with the thrust structures strongly suggests that the four principal varieties identified may be different facies of the same depositional stage. Fluid inclusion analysis of this calcite indicated that it crystallized very near the ground surface at temperatures only slightly greater than present ambient temperatures, that is, 50 °F to 86 °F (10 °C to 30 °C). This calcite contrasts with the epigenetic calcite along the high-angle faults whose formation temperatures ranged from 158 °F to 320 °F (70 °C to 160 °C), indicating an origin at greater depth, and thus geologically older. Isotopic analysis confirmed the fresh water origin of the low temperature calcite and revealed that some of it (the calcitic breccias) probably formed below the groundwater table, whereas some (the travertine) apparently formed in the vadose zone. Radiometric dating of the former, using the Thorium-230/Uranium-234 technique, indicated only that the material is younger than 300,000 yr old. However, radiocarbon dating of the travertine yielded a C-14 age of 14,180 ±550 radiocarbon yr B.P. These radiometric dates confirm the interpretation that the low temperature calcite is younger than the high-temperature calcite and is likely Quaternary in age (CEG, 1998).

The interstitial sediment within openings in the bedrock is similar in appearance to surficial glaciolacustrine sediments of Pleistocene age (Section 2.5.1.2.). Therefore, it was suspected to be of similar origin. Specimens of the interstitial sediment were collected for grain size analysis, compositional and heavy mineral analysis, and pollen analysis. These results were compared with similar analyses of specimens from the surficial sediments. The conclusion of principal importance is that the tan, laminated sediment is derived from material of glaciolacustrine origin. This material contained pollen and spores similar to those found in portions of the Late-Pleistocene age surficial sediments. A Late-Pleistocene age of the interstitial sediment was confirmed by a C-14 date of 11,060 ± 360 radiocarbon yr B.P. for organic material in the sediment collected from within the Radwaste fault. The age of similar laminated clay encountered at a depth of 250 ft (76 m) in the borings is uncertain. However, palynologic analysis of this material also suggests a late-Quaternary age (CEG, 1998).

A minimum age of approximately 11,000 yr B.P. can be interpreted for the development of the Radwaste fault on the basis of the radiocarbon date of laminated clays encountered within the zone of deformation. Dilation of the bedrock associated with development of the structure clearly had to have occurred prior to emplacement of the clays. Nevertheless, the exact age of latest deformation is uncertain because the time of deformation of the laminated clay is unclear. Based on his observations in the North Radwaste Trench, Dr. L. Sirkin concluded that the lacustrine sediments were deposited in the bedrock openings and were subsequently deformed (NMPC, 1980). In contrast, the prevailing opinion is that of Drs. T. L. Pewe, R. H. Jahns, and S. S. Philbrick (NMPC, 1980), namely that the deformation in the bedrock had occurred prior to the deposition of the clays on the basis of observations of the clay overlying the hinge of a fold (CEG, 1998).

Field reconnaissance, coupled with interpretation of aerial photography (review and inspection of features preserved in aerial photos) determined that there are no geomorphic features indicative of potential Quaternary activity within the site area 5 mi (8 km) radius.

Based on EPRI (EPRI, 1986) earthquake data and more recent data for the region as described in Section 2.5.2, there is no seismicity spatially associated with features within the site vicinity 25 mi (40 km) radius (See Figures in Section 2.5.2) , nor is there geomorphic evidence to suggest that these features pose a surface-fault rupture hazard at the NMP3NPP site.

In summary, numerous investigations by government researchers, stratigraphers, and by consultants for Niagara Mohawk Power Corporation and NYSE&G, and by this study, have reported no visibly distinct signs of tectonic deformation as evidenced by their exposures near the NMP3NPP site, as shown in Figure 2.5-39.

NMP Unit 2 Mechanism of Postglacial Deformation

In light of the foregoing discussion, it is most likely that the disturbance of the overburden sediments reflects movements along the Cooling Tower fault caused by changes of fluid pressure in the bedrock. The disturbance of overburden sediments would be consistent with likely effects from the fluctuation of the water level in the Ontario Basin following glacial retreat. It seems very unlikely that the deformation of the overburden sediments indicates that the Cooling Tower fault buckles were propagating downward within the past 10,000 yr. The reasons for this are twofold. First, the postglacial movements occurred when the differential crustal downwarping was reduced due to glacioisostatic uplift or rebound. Hence, the amount of distortional strain energy stored in the bedrock was reduced during uplift due to glacial rebound. Consequently, the potential depth of development of the structure at this time was smaller than that to which the structure had already developed. Second, the dilated openings in the bedrock would prevent propagation of any movement to the surface from a depth of more than 140 ft (43 m). Hence, even if these movements had occurred at depth, one would not expect to find them expressed at the surface (CEG, 1998).

The maximum Lake Iroquois water level was approximately 300 ft (91 m) above the land surface at the NMPNS site. As the ice sheet receded to the north and opened the lowest lake outlet in the Thousand Islands region, Lake Iroquois was drained through the St. Lawrence Valley. The water level subsequently assumed a low stand commonly referred to as the Admiralty Stage. The water level of Lake Iroquois dropped approximately 450 ft (137 m) to reach this latter stage. The bedrock in the site area is covered by a thin, but relatively impervious veneer of unconsolidated sediments which would prevent a rapid flow of fluids to the surface or into the lake from the bedrock. Hence, it may be inferred that, at a time after deposition of the deformed lacustrine sediments, the fluid pressure in the bedrock could be much greater than the water pressure exerted by the lake. It may be further inferred that after the deposition of the unlithified sediments (including the upper sequence of Sandy Creek), this excess fluid pressure (DP) underwent incremental changes. Consequently, the effective stress normal to bedding was modified accordingly (CEG, 1998).

Such changes in the effective normal stress influenced the stability of the Cooling Tower feature by temporarily reducing the effective shear strength of bedding. The problem has been analyzed using a model showing a bedrock stratum with thickness (h) that is situated above a shear zone and that can move along this zone as a solid block. With the assumption that there was no change of in situ stress during the time between the completion of the preglacial movements on the Cooling Tower fault and the high stand of Lake Iroquois, the model presents the equilibrium conditions for sliding on bedding planes in the vicinity of the fault prior to the buildup of fluid pressure. The stratum modeled corresponds to a layer or sequence of layers forming one of the two limbs of the buckle feature. When the buckle feature was formed, stress-drop normal to the fault occurred. The modeled layer attained equilibrium for a particular value of the effective stress normal to bedding, and a point near the axial plane region of the fold was thereby displaced toward the region of greatest stress relief. If there was no change in DP until the end of the high stand of Lake Iroquois, then the equilibrium would endure until that time, and the displacement would remain constant. At the end of the high stand of Lake Iroquois, DP was progressively increasing, thereby causing an incremental reduction of the effective normal stress. This, in turn, caused an incremental reduction of the effective shear strength of bedding. Consequently, the equilibrium of the limb could not be maintained and additional incremental translations must have occurred toward the region of low stress, that is, toward the axial plane. The translation was greatest near the axial plane, and gradually decreased away from it (CEG, 1998).

One notable exception to this occurred in Trench 3 exposure where the north limb is unopposed by the south limb which was removed by glacial erosion. The north limb migrated

southward, displacing the older fault plane about 4 ft (1.2 m) leading to the folding of the unlithified sediments with ancillary faults. Conversely, if the margin of one limb was equally opposed by another, the lateral translations of this limb would be restricted, and most effectively so, if the axial plane (fault plane) separating the limbs were vertical. This situation existed during deformation of the overburden sediments at the Cooling Tower Piping Trench and Pit 1 (and other locations along the trace of the fault). Thus, at these locations, the lateral displacements at the margins of each limb could not be freely accomplished, and thereby resulted in an incremental buildup of layer-parallel normal stress in the strata contiguous with the fault. When this stress attained a certain value in conjunction with the high buildup of fluid pressure, both limbs of the structure buckled further, and formed a gentle arch with the fault along the crest (CEG, 1998).

Arching and compensatory normal faults developed in the overlying sediments in response to arching of the bedrock. The disturbance of the unlithified sediments very likely occurred as the result of a buildup of fluid pressure in the bedrock which equaled or exceeded the pressure due to the body weight of the rocks. The deformation does not, therefore, indicate that the Cooling Tower buckle was propagating downward during recent glacioisostatic uplift. The present maximum possible value of the fluid pressure in the bedrock is equal to approximately 40 percent of the pressure due to the body weight of the rock. Hence, it can be concluded that movements with a similar origin to those which caused the postglacial deformation are not likely to occur at the present time (CEG, 1998).}

2.5.3.3 Correlation of Earthquakes with Capable Tectonic Sources

{No reported historical earthquake epicenters with magnitude greater than M3 have been associated with bedrock faults within the 25 mi (40 km) radius of the NMP3NPP site vicinity (Daneshfar, 2002; Ebel, 2002; Fakundiny, 2002a; Fakundiny, 2002b; Frankel, 2002; Jacobi, 2002a; and Jacobi, 2002b ; Stover, 1987). Refer to Sections 2.5.1.2 and 2.5.2 for additional discussion and to the figures presented in Section 2.5.2.}

2.5.3.4 Ages of Most Recent Deformations

{As presented in Section 2.5.3.2, faults and folds within 5 mi (8 km) of the NMP3NPP site do not exhibit evidence of Quaternary activity. The USGS recently completed a compilation of all Quaternary faults, liquefaction features, and possible tectonic features in the eastern U.S. (Crone, 2000) (Wheeler, 2005) (Wheeler, 2006). These compilations do not show any Quaternary faults or related features within a 25 mi (40 km), and as a result the 5 mi (8 km), radius of the site as shown in Figure 2.5-73. It is interpreted that the NMP Unit 2 faults and Demster Zone Structures formed during the Paleozoic Era as part of the regional Taconic and Alleghenian orogenies and locally may have been reactivated during the Mesozoic. Based on a review of available published geologic literature, field reconnaissance, and interpretation of aerial photography faulting the NMP Unit 2 faults and Demster Zone Structures are not considered to be capable faults.}

2.5.3.5 Relationship of Tectonic Structures in the Site Area to Regional Tectonic Structures

{Neither major nor minor tectonic structures are present in the site area and no such structures are apparent in the site vicinity.

The Demster Structural Zone of folding and faulting trends northeastward. Its surface trace is approximately 2.8 mi (4.6 km) southeast of the NMPNS site. This zone is characterized by tight to broad, eastward-verging, asymmetric, locally-overturned folds; flexural slip; reverse faulting; normal faulting; and associated drag folding. The deformation resulted from at least two

phases of essentially contemporaneous movement, an initial stage of folding and reverse faulting followed by a stage of relaxation and normal faulting (CEG, 1998).

The Demster faults, both normal and reverse, strike northeasterly and dip steeply to the northwest; maximum throws are no more than a few feet. They occur in an elongate domain of closely jointed and highly broken rock that is transected by several zones of breccia-free gouge with trends both parallel and normal to the strike of bedding and the strike of the faults. In this ground there is no evidence of dilation such as that observed at NMP Unit 2, where the gouge and breccia are packed tightly along the nearly vertical faults. None of the faults offset the surface of bedrock or cut the overlying Quaternary glacial and lacustrine sediments. These faults are probably Paleozoic (possibly Alleghanian) in age, and certainly are no younger than Mesozoic in age. They are not capable faults (CEG, 1998).

The geologic structure at the NMP Unit 2 site (Section 2.5.1.2.3) is expressed by two steeply dipping, northwesterly striking normal faults that bound a block of gently dipping sedimentary rocks that are cut at shallow depths by a series of subparallel thrust faults grossly concordant with the host-rock bedding. The uppermost thrust fault dips southeastward at low angles across the bedrock strata where it is exposed in the excavation for the NMP Unit 2 Radwaste building. There the leading portion of the faulted rock is crumpled and dilated in very close similarity to the valley-bottom faults of the Upper Ohio River valley that were produced as a result of erosion of the bedrock in the river valley and the consequent reduction of the least principal stress in the bedrock . The relationships observed along the thrust zone also are similar to those associated with shallow-seated breaks noted in many New England granite quarries, where small thrust movements and numerous expressions of dilatancy also represent geologically young stress relief related to the ground surface (CEG, 1998).

The openwork along the NMP Unit 2 Radwaste fault contains in-fillings of lacustrine sediments containing pollen, which indicates a late-Wisconsinan age (10,000 to 13,500 yr B.P.) for those sediments. The faulting appears to have been geologically young, with movements that probably occurred during Pleistocene time in response to episodes of glacial loading and unloading. Holocene (post-Pleistocene) movements have been small if they have occurred at all. It cannot be demonstrated that no Holocene movements have occurred, as no dated infilling sediments or other reference features extend entirely across the zones of disturbance (CEG, 1998).

Displacement of late-Pleistocene lake sediments has occurred along the southerly bounding fault, the NMP Unit 2 Cooling Tower fault. Both of the normal faults are marked by thin zones of gouge, and both have displacements of a few feet or less (CEG, 1998).

The strata at the NMP Unit 2 site are essentially undisturbed except right at the faults, in contrast to the broken and highly disturbed strata in the Demster Zone. The faulting in the Demster Zone may well have been of direct tectonic origin, whereas the much younger faulting at the NMP Unit 2 site, and especially that along the NMP Unit 2 Radwaste thrust, is readily explainable as a result of local stress relief unrelated to major or contemporary tectonic activity. Such relief, as widely expressed in this and other regions, derives through failure, within a highly anisotropic stress field, of rocks containing a combination of residual strain energy and strain energy inherited from earlier tectonic activity (CEG, 1998).

As discussed in Section 2.5.1.2.3, reduction of the vertical load as a result of Pleistocene glacial erosion facilitated westward slip of the NMP Unit 2 Radwaste structure's hanging wall block by reducing the shear resistance of the block to stresses acting subhorizontally. This is similar to the mechanics of formation of the valley-bottom faults in the Upper Ohio River basin and of

sheet structure and associated exfoliation phenomena in more massive rocks of the northeastern United States (CEG, 1998).

Formation of the bounding normal faults at NMP Unit 2 probably resulted from adjustments during late stages of the Appalachian Basin as the bottom ceased to subside and oxidizing processes began. Minor Quaternary movements could be expected in the form of much younger readjustments associated with erosional unloading of the bedrock section (CEG, 1998).

The Demster folds and faults and the NMP Unit 2 Radwaste thrust faulting are quite different geologic structures in terms of respective sizes, extents, attitudes, degrees of brecciation, origins, and ages. The Demster Zone is tectonic in origin, whereas the NMP Unit 2 Radwaste structure is a result of much younger unloading by accelerated erosion. In both occurrences the causative processes are no longer active, and the faults are not capable (CEG, 1998).

The steeply dipping normal faults, striking northeasterly at New Haven and northwesterly at NMP Unit 2 , are related in origin to late-stage processes in the evolution of the Appalachian Basin, and perhaps to the extensional forces that opened near-vertical channels for emplacement of ultrabasic dikes in the adjacent Finger Lakes and Syracuse region during Mesozoic time. Deformation of the Quaternary lake sediments along the Cooling Tower fault at NMP Unit 2 evidently resulted from localized buckling related to removal of the ice load following recession of the Wisconsinan ice sheet. These normal faults are not tectonically capable (Section 2.5.1.2.3) (CEG, 1998).}

2.5.3.6 Characterization of Capable Tectonic Sources

{Based on previous discussions in Section 2.5.3.4, there are no capable tectonic sources within 5 mi (8 km) of the NMP3NPP site. Faults at the NMP Unit 2 site are not capable within the intent of Appendix A to 10 CFR 100 (CEG, 1998). Also, investigations regarding the Demster Structural Zone concluded that this feature is not a capable fault. (NYSG&E, 1978 and USGS, 2006) See Section 2.5.1.2 for additional discussion). The nearest capable fault appears to be the Clarendon-Linden Fault Zone located in western New York approximately 75 mi (120 km) from the NMP3NPP site. The lack of earthquake-induced liquefaction features suggests that the Clarendon-Linden Fault Zone did not generate large, moment magnitude, M> 6 earthquakes during the past 12,000 years (Tuttle, 2002). Section 2.5.1.1 presents a more detailed description of the Clarendon-Linden Fault Zone.}

2.5.3.7 Designation of Zones of Quaternary Deformation Requiring Detailed Fault Investigation

{Based on current investigations, there are no zones of Quaternary deformation requiring detailed investigation within the NMP3NPP site area. A review and interpretation of aerial photography, satellite imagery (EarthSat, 1997) and topographic maps identified a few discontinuous east to northeast-striking lineaments and northwest-striking lineaments. None of these lineaments is interpreted as fault-related at the NMP3NPP site. GEI interpreted lineaments at the NMP3NPP site to reflect glacial depositional and erosional features. In addition, geological reconnaissance studies (Section 2.5.3.2.2) have provided no evidence of Quaternary deformation in the site area.}

2.5.3.8 Potential for Tectonic or Non-Tectonic Deformation at the Site

{The potential for tectonic deformation at the site is negligible. This is based on:

1. The nearly flat-lying Paleozoic stratigraphy beneath the site interpreted from both existing and new borehole data,

2. The absence of significant surface faulting in Paleozoic rock exposed along Lake Ontario at the northwestern boundary of the NMP3NPP site.

3. The low level of seismic activity in the region

4. The interpretation of aerial photography data.

5. The interpretation of satellite imagery

6. Geologic field reconnaissance

Collectively, these data support the interpretation for the absence of Quaternary surface faults or capable tectonic sources within the site area. In addition, there is no evidence of nontectonic deformation at the NMP3NPP site, such as collapse structures, growth faults, salt migration, or volcanic intrusion. Quaternary non-tectonic deformation at the NMP Unit 2 site was attributable to fluctuation of the water level in the Ontario Basin following glacial retreat (CEG, 1998).

Popup structures or small scale buckling of excavated horizontal bedrock surfaces were noted in the foundation excavations for NMP Unit 2 all within the Pulaski Formation. These structures are very small scale. They are described in Sections 2.5.1.2 and considered for their impact on foundation stability in Section 2.5.4. These occurrences are not considered significant with respect to foundation stability. In addition, foundation excavations for NMP3NPP will all end above the top of the Pulaski in the Oswego Sandstone.}

2.5.3.9 References

{**Bretsky, 1978.** Benthic Marine Communities in the Upper Ordovician Clastics of the Tug Hill Region, New York, New York State Geological Association Guidebook 50th Annual Meeting, Syracuse New York, Pages 189-2003. P. Bretsky and D. Thomas, 1978.

CEG, 1998. Nine Mile Point Unit 2 Updated Safety Analysis Report, Docket No. 50-410, Constellation Energy Group, 1998

CFR, 2007a. Geologic and Seismic Siting Criteria, Title 10, Code of Federal Regulations, Part 100.23, 2007.

CFR, 2007b. Earthquake Engineering Criteria for Nuclear Power Plants, Title 10, Code of Federal Regulations, Part 50, Appendix S, 2007.

Crone, 2000. Data for Quaternary faults, liquefaction features, and possible tectonic features in the Central and Eastern United States, east of the Rocky Mountain front, Open File Report 00-260, U.S. Geological Survey, A. J. Crone and R. L. Wheeler, 2000.

Daneshfar, 2002. Spatial Relationships Between Natural Seismicity and Faults, Southeastern Ontario and North-Central New York State, Tectonophysics, B. Daneshfar and K. Benn, August, 2002.

EarthSat, 1997. Remote Sensing and Fracture Analysis for Petroleum Exploration of Ordovician to Devonian Fractured Reservoirs in New York State. New York State Energy Research and Development Authority, Albany NY, 1997.

Ebel, 2002. Earthquakes in the Eastern Great Lakes Basin From a Regional Perspective, Tectonophysics, J.E. Ebel and M. Tuttle, August 2002.

Engelder, 1979. The Nature and Deformation Within the Outer Limits of the Central Appalachian Foreland Fold and Thrust Belt in New York State, Tectonophysics, T. Engelder, June 1979.

Engelder, 1980. On the Use of Regional Joint Sets as Trajectories of Paleostress Fields During the Development of the Appalachian Plateau, New York, Journal of Geophysical Research, Volume 85, Number B11, Pages 6319-6341, T. Engelder and P. Geiser, November 1980.

Engelder, 1982a. Is There a Genetic Relationship Between Selected Regional Joints and Contemporary Stress Within the Lithosphere of North America?, Tectonics, Volume 1, Number 2, Pages 161-177, T. Engelder, April 1982.

Engelder, 1982b. Reply, Tectonics, T. Engelder, October 1982.

Engelder, 1985. Loading Paths to Joint Propagation During a Tectonic Cycle: an Example From the Appalachian Plateau, U.S.A., Journal of Structural Geology, Volume 7, Numbers 3 / 4, Pages 459-476, T. Engelder, 1985.

Engelder, 1993. Curving Cross joints and the Lithospheric Stress Field in Eastern North America, Geology, Volume 21, Pages 817-820, T. Engelder and M.R. Gross, September 1993.

Engelder, 2001. Horizontal Slip Along Alleghanian Joints of the Appalachian Plateau: Evidence Showing That Mild Penetrative Strain Does Little to Change the Pristine Appearance of Early Joints, Tectonophysics, Volume 336, Pages 31-41, T. Engelder, B.F. Haith and A. Yo, July 2001.

Engelder, 2006. Early Jointing in Coal and Black Shale: Evidence for an Appalachian-Wide Stress Field as a Prelude to the Alleghanian Orogeny, Geology, Volume 34, No 7, Pages 581-584, T. Engelder and A. Whitaker, July 2006.

Engelder, 2007. Propagation Velocity of Joints: A Debate Over Stable vs. Unstable Growth of Cracks in the Earth, in: Quinn, G.D.; Varner, J.R.; Wightman, M., eds., Fractography of Glasses and Ceramics V, American Ceramic Society, Westerville, OH, T. Engelder, 2007.

EPRI, 1986. Seismic Hazard Methodology for the Central and Eastern United States, EPRI Report NP-4726, Electric Power Research Institute, July 1986.

Evans, 1989a. Appalachian Stress Study 1. A Detailed Description of In Situ Stress Variations in Devonian Shales of the Appalachian Plateau, Journal of Geophysical Research, K.F. Evans, T. Engelder, and R.A. Plumb, June 1989.

Evans, 1989b. Appalachian Stress Study 2. Analysis of Devonian Shale Core: Some Implications for the Nature of Contemporary Stress Variations and Alleghanian Deformation in Devonian Rocks, Journal of Geophysical Research, K.F. Evans, G. Oertel and T. Engelder, June 1989.

Fakundiny, 2002a. Editorial: Neotectonics and Seismicity in the Eastern Great Lakes Basin: Introduction, Tectonophysics, R.H. Fakundiny, C.F.M. Lewis, and R.D. Jacobi, August 2002.

Fakundiny, 2002b. Seismic-Reflection Profiles of the Central Part of the Clarendon-Linden Fault System of Western New York in Relation to Regional Seismicity, Tectonophysics, R. H. Fakundiny and P.W. Pomeroy, August 2002.

Fisher, 1978. Engineering Geology at Nine Mile Point, New York, New York State Geological Association Guidebook 50th Annual Meeting, Syracuse New York, Pages 257-272, J.A. Fisher and H.S. Laird, 1978.

Frankel, 2002. Documentation for the 2002 Updated of the National Seismic Hazard Maps, Open File Report 02-420, U.S. Geological Survey, A.D. Frankel, M.D. Petersen, C.S. Mueller, K.M. Haller, R.L. Wheeler, E.V. Leyendecker, R.L. Wesson, S.C. Harmsen, C.H. Cramer, D.M. Perkins and K.S. Rukstales, 2002.

Gross, 1991. A Case for Neotectonic Joints Along the Niagara Escarpment, Tectonics, Volume 10, Number 3, Pages 631-641, M.R. Gross and T. Engelder, June 1991.

Hancock, 1989. Neotectonic Joints, Geological Society of America Bulletin, Volume 101, Pages 1197-1208, P.L Hancock and T. Engelder, October 1989.

Hickman, 1985. In Situ Stress, Natural Fracture Distribution, and Borehole Elongation in the Auburn Geothermal Well, Auburn, New York, Journal of Geophysical Research, S.H. Hickman, J.H. Healy and M.D. Zoback, June 1985.

Isachsen, 1977a. Preliminary Brittle Structures Map of New York – Adirondack Sheet, New York State Museum Map and Chart Series Number 31A, Y.W. Isachsen, and W.G. McKendree, 1977.

Isachsen, 1977b. Preliminary Brittle Structures Map of New York – Hudson-Mohawk Sheet, New York State Museum Map and Chart Series Number 31B, Y.W. Isachsen and W.G. McKendree, 1977.

Isachsen, 1977c. Preliminary Brittle Structures Map of New York – Lower Hudson Sheet, New York State Museum Map and Chart Series Number 31C, Y.W. Isachsen and W.G. McKendree, 1977.

Isachsen, 1977d. Preliminary Brittle Structures Map of New York – Niagara-Finger Lakes Sheet, New York State Museum Map and Chart Series Number 31D, Y.W. Isachsen and W.G. McKendree, 1977.

Isachsen, 1977e. Preliminary Brittle Structures Map of New York, New York State Museum Map and Chart Series Number 31E, Y.W. Isachsen and W.G. McKendree, 1977.

Isachsen, 1977f. Generalized Map of Recorded Joint Systems in New York, New York State Museum Map and Chart Series Number 31F, Y.W. Isachsen and W.G. McKendree, 1977.

Isachsen, 1977g. Sources of Information for Preliminary Brittle Structures Map of New York and Generalized Map of Recorded Joint Systems in New York, New York State Museum Map and Chart Series Number 31G, Y.W. Isachsen and W.G. McKendree, 1977.

Jacobi, 2002a. Basement Faults and Seismicity in the Appalachian Basin of New York State, Tectonophysics, R.D. Jacobi, August 2002.

Jacobi, 2002b. The Character and Reactivation History of the Southern Extension of the Seismically Active Clarendon-Linden Fault System, Western New York State, Tectonophysics, R.D. Jacobi and J. Fountain, August 2002.

Lash, 2007. Jointing within the Outer Arc of a Forebulge at the Onset of the Alleghanian Orogeny, Journal of Structural Geology, Volume 29, pages 774-786, G.G Lash and T. Engelder, May 2007.

NMPC, 1978a. Nine Mile Point Nuclear Station Unit 2, Geologic Investigation, Volume I, Geology, Syracuse, New York, Niagara Mohawk Power Corporation, April 1978.

NMPC, 1978b. Nine Mile Point Nuclear Station Unit 2, Geologic Investigation, Volume II, Geomorphology, Vertical Crustal Movement, Seismicity, Syracuse, New York, Niagara Mohawk Power Corporation, 1978.

NMPC, 1978c. Nine Mile Point Nuclear Station Unit 2, Geologic Investigation, Volume III, Stresses, Syracuse, New York, Niagara Mohawk Power Corporation, 1978.

NMPC, 1980. Nine Mile Point Nuclear Station Unit 2, Geologic Investigation, Radwaste Thrust Structure, Syracuse, New York, Niagara Mohawk Power Corporation, October 1980.

NRC, 1997. Identification and Characterization of Seismic Sources and Determination of Safe Shutdown Earthquake Ground Motion, Regulatory Guide 1.165, U.S. Nuclear Regulatory Commission, March 1997.

NRC, 1998. Investigation of Techniques for the Development of Seismic Design Basis Using the Probabilistic Seismic Hazard Analysis, NUREG/CR-6606, U.S. Nuclear Regulatory Commission, 1998.

NRC, 2007. A Performance Based Approach to Define the Site-Specific Earthquake Ground Motion, Regulatory Guide 1.208, U.S. Nuclear Regulatory Commission, March 2007.

NYSM, 1970a. Geologic Map of New York – Finger Lakes Sheet, New York State Museum and Science Service, Map and Chart Series Number 15, Rickard, L.V. and D.W. Fisher, 1970.]

NYSM, 1970b. Reprinted 1995, Geologic Map of New York – Adirondacks Sheet, New York State Museum and Science Service, Map and Chart Series Number 15, Y.W. Isachsen and D.W. Fisher.

NYSE&G, 1978. NYSE&G 1 and 2, Preliminary Safety Analysis Report, New Haven Site, Oswego County, New York, New York State Electric and Gas, November 1978.

Parker, 1942. Regional Systematic Jointing in Slightly Deformed Sedimentary Rocks, Geological Society of America Bulletin, Volume 53, pages 381-408, J.M Parker III, 1942.

Parker, 1969. Jointing in South-Central New York: Discussion, Geological Society of America Bulletin, Volume 80, Pages 919-922, J.M. Parker III, May 1969.

Patchen, 1978. Depositional Environments of the Oswego Sandstone (Upper Ordovician), Oswego County, New York, New York State Geological Association Guidebook 50th Annual Meeting, Syracuse New York, Pages 368-386, D.G. Patchen, 1978.

Plumb, 1985. Stress-Induced Borehole Elongation: A Comparison Between the Four-Arm Dipmeter and the Borehole Televiewer in the Auburn Geothermal Well, Journal of Geophysical Research, R. A. Plumb and S. H. Hickman, June 1985.

Plumb, 1991. Geophysical Log Responses and Their Correlation With Bed-to-Bed Stress Contrasts in Paleozoic Rocks, Appalachian Plateau, New York, Journal of Geophysical Research, R. A. Plumb, K.F. Evans, and T. Engelder, August, 1991.

Scheidegger, 1991. Neotectonic Joints: Discussion and Reply, Geological Society of America Bulletin, Volume 103, Pages 432-433, A.E. Scheidegger, March, 1991.

Stillwell, 2005. Fractures and Faults in the Eastern Lake Ontario Basin, Oswego County, New York, New York State Geological Association Guidebook 77th Annual Meeting, Oswego New York, Pages 29-44, S.M. Stillwell, J.D. Valentino, J.M. Gawron and D.W. Valentino, 2005.

Stover, 1987. Seismicity Map of the State of New York, USGS Map MF-1282, C.W. Stover, B.G. Reagor, L.M. Highland, and S.T. Algermissen, 1987.

Tuttle, 2002. Paleoliquefaction study of the Clarendon-Linden Fault System, Western New York State, Tectonophysics, M.P. Tuttle, K. Dyer-Williams, and N.L. Barstow, August 2002.

USGS, 2006. U.S. Geological Survey, 2006, Quaternary fault and fold database for the United States, accessed September, 2008, from USGS web site: http//earthquakes.usgs.gov/regional/qfaults/.

USGS, 2007a. Landsat Thematic Mapper, Landsat 5, Landsat Scene Identifier: LT50160302007214EDC00, U.S. Geological Survey, Date Acquired: August 2, 2007.

USGS, 2007b. Landsat Thematic Mapper, Landsat 5, Landsat Scene Identifier: LT50150302007223EDC00, U.S. Geological Survey, Date Acquired: August 11, 2007.

Wheeler, 2001. Known and Suggested Quaternary Faulting in the Midcontinent United States, Engineering Geology, R. L. Wheeler and A. J. Crone, October 2001.

Wheeler, 2005. Known or Suggested Quaternary Tectonic Faulting, Central and Eastern United States – New and Updated Assessments for 2005, Open File Report 2005-1336, U.S. Geological Survey, R.L. Wheeler, 2005.

Wheeler, 2006. Quaternary Tectonic Faulting in the Eastern United States, Engineering Geology, R. L. Wheeler, January 2006.

Whitaker, 2005. Characterizing Stress Fields in the Upper Crust Using Joint Orientation Distributions, Journal of Structural Geology, Volume 27, Pages 1778-1787, A.E. Whitaker and T. Engelde, October 2005.

Younes, 1999. Fringe Cracks: Key Structures for the Interpretation of the Progressive Alleghanian Deformation of the Appalachian Plateau, Geological Society of America Bulletin, A.I. Younes and T. Engelder, February 1999.

Zhao, 1997. Formation of Regional Cross-Fold Joints in the Northern Appalachian Plateau, Journal of Structural Geology, Volume 19, Number 6, Pages 817-834, M. Zhao and R. Jacobi, June 1997.

Zoback, 1985. Well Bore Breakouts and In Situ Stress, Journal of Geophysical Research, M.D. Zoback, D. Moos and L. Mastin, June 1985.

Zoback, 1989. Chapter 24: Tectonic Stress Field of the Continental United States, In: Pakiser, L.C.; Mooney, W.D., Geophysical Framework of the Continental United States, Geological Society of America Memoir 172, M.L. Zoback and M.D. Zoback, 1989.}

2.5.4 STABILITY OF SUBSURFACE MATERIALS AND FOUNDATIONS

The U.S. EPR FSAR includes the following COL Item for Section 2.5.4:

> A COL Applicant that references the U.S. EPR design certification will present site-specific information about the properties and stability of soils and rocks that may affect the nuclear power plant facilities, under both static and dynamic conditions including the vibratory ground motions associated with the CSDRS and the site-specific SSE.

This COL Item is addressed as follows:

This section addresses site-specific subsurface materials and foundation conditions. It was prepared based on the guidance in relevant sections of NRC Regulatory Guide 1.206, Combined License Applications for Nuclear Power Plants (LWR Edition) (NRC, 2007).

{References to elevation values in this subsection are based on the National Geodetic Vertical Datum of 1929 (NGVD29), unless stated otherwise.

The information presented in this section is based on the results of a subsurface investigation program implemented at the NMP3NPP site and evaluation of the collected data, unless otherwise noted.

Horizontal control is based on the Central Zone of the New York State Plane Coordinate System North American Datum of 1927 (NAD 27). NAD 27 was used instead of NAD 83 because NMP Unit 1 and Unit 2 were surveyed using NAD 27.

The following requirements for soil are identified in Table 2.0-1. Each requirement is satisfied for NMP3NPP as indicated.

Parameter (Table 2.0-1)	Requirement (Table 2.0-1)	Section in which Requirement is Documented
Minimum Bearing Capacity (Static)	22 kips/sf in localized areas at the bottom of the Nuclear Island basemat and 15 kips/sf on average across the total area of the bottom of the Nuclear Island basemat.	2.5.4.10 Safety-related structures will be founded on bedrock, or on concrete fill extending down to bedrock. The computed bearing capacity of the bedrock is 204 ksf, which exceeds the minimum value of 22 ksf.
Minimum Shear Wave Velocity (Low strain best estimate average value at bottom of basemat)	1000 ft/sec (300 m/sec)	2.5.4.2.1.8 Safety-related structures will be founded on bedrock, or on concrete fill extending down to bedrock. The shear wave velocity at the top of bedrock is significantly higher than 5000 ft/sec (1500 m/sec).
Liquefaction	None	2.5.4.8 The existing on-site soils that remain beneath and around safety-related structures and utilities after construction, i.e., glacial till soils at a depth of 2 feet or more below ground surface, are not susceptible to liquefaction. Existing on-site fill soils, surficial deposits, and glacial till to a depth of 2 feet below ground surface will be removed during construction from beneath and around safety-related structures, and will be replaced with compacted structural fill as required.

Parameter (Table 2.0-1)	Requirement (Table 2.0-1)	Section in which Requirement is Documented
Maximum Differential Settlement (across the basemat)	1/2 inch in 50 feet (1:1200) in any direction	2.5.4.10 Maximum computed differential settlement (across the basemat) is 1:7,200, which is less than the USEPR maximum of 1:1,200.
Slope Failure Potential	No slope failure potential is considered in the design of safety-related SSCs for U.S. EPR design certification.	2.5.5 No slope failure potential is present relevant to safety-related SSCs for NMP3NPP.
Maximum Ground Water	3.3 ft (1.0 m) below grade	2.4.12.5 The static elevation of groundwater in the Oswego Sandstone at NMP3NPP is more than 3.3 feet (1.0 m) below the proposed grade in the area of the power block.

}

2.5.4.1 Geologic Features

The U.S. EPR FSAR includes the following COL Item in Section 2.5.4.1:

Geologic features are site-specific and will be addressed by the COL applicant.

This COL Item is addressed as follows.

Section 2.5.1.1 addresses the regional geologic settings, including regional physiography and geomorphology, regional geologic history, regional stratigraphy, regional tectonic and non-tectonic conditions, and geologic hazards, as well as maps, cross-sections, and references. Section 2.5.1.2 addresses the geologic conditions specific to the site, including site structural geology, site physiography and geomorphology, site geologic history, site stratigraphy and lithology, site structural geology, seismic conditions, and site geologic hazard evaluation, accompanied by figures, maps, and references. Pre-loading influences on soil deposits, including estimates of consolidation, pre-consolidation pressures, and methods used for their estimation are addressed in Section 2.5.4.2. Related maps and stratigraphic profiles are also addressed in Section 2.5.4.2.

{Basic geologic and seismic information is presented in Section 2.5.1.1. Site specific geology is presented in Section 2.5.1.2.

The NMP3NPP site is located in the Central Lowlands physiographic province. The soils consist of glacial till with overlying minor lacustrine deposits. These soils were deposited during and after the most recent glaciation during the Wisconsinan period. Below the soils is Paleozoic sedimentary rock ranging in age from Middle to Late Ordovician and including the Oswego Sandstone, Pulaski Formation, Whetstone Gulf Formation, Trenton Group, and Black River Group. Paleozoic rock of the Oswego and Pulaski Formations are also exposed in the Lake Ontario lake bed. Metamorphic and igneous crystalline rock of Precambrian age underlies the Paleozoic rock.

Near surface bedrock in the region consists of nearly flat-lying Paleozoic sedimentary rock with horizontal homogeneity. The sedimentary rock formations dip regionally to the south-southwest with a gradient of approximately 50 ft per mile (9.5 m per km) which is equivalent to roughly 1 ft per hundred ft (1 m per 100 m).

Locally at the NMP3NPP site, the bedrock surface dips to the northwest, toward Lake Ontario, with a gradient of approximately 1.6 ft per hundred ft (1.6 m per 100 m). Bedrock formations immediately underlying the site dip to the south-southwest at about 1 foot per 100 feet (1 m per 100 m).

As determined by consistent field classifications of rock core borings, and a relatively narrow range of laboratory test properties, the soil and rock profile at the NMP3NPP site is laterally uniform. Individual layers within the profile have an angle of dip significantly less than 20 degrees, which corresponds to criterion 4 of Section 2.5.2.6 of the U.S. EPR for a uniform site condition.

The near-surface bedrock formations at the site are, from the surface down:

- Oswego Sandstone including Oswego Transition Zone (sandstone, Ordovician)
- Pulaski Formation (interbedded dark gray siltstone, gray sandstone, and dark gray argillaceous sandstone, Ordovician)
- Whetstone Gulf Formation (alternating dark gray siltstone, gray sandstone, and dark gray argillaceous sandstone, Ordovician)

The top elevations of the Oswego Sandstone, Pulaski Formation, and Whetstone Gulf Formation, as encountered in the borings, are presented in Table 2.5-41 and Table 2.5-42.

The estimated elevation of the top of the Trenton and Black River Groups at the site is 700 ft below mean sea level. The estimated elevation of the top of the Precambrian crystalline rock is 1500 feet below mean sea level, based on deep well data in the region.

The following subsections describe specific geologic features identified in NRC Regulatory Guide 1.206 (NRC 2007).

2.5.4.1.1 Subsidence, Solution, Uplift or Collapse

Based on review of literature and aerial photos, and on field reconnaissance, no large- or small-scale features indicative of collapse or subsidence occur in the area of the NMPNS site. The bedrock underlying the site is not subject to solution because the rocks are composed primarily of non-soluble materials. The only uplift occurring in the area is of regional extent (Section 2.5.1.1) and, as such, does not have a direct impact on the stability of the site foundations. This is confirmed by the uniformity and gentle dip of the rock strata at the site. Open dilations were not encountered at the NMP3NPP site. However, small voids were encountered within the rock mass at a number of locations in the area of the NMP Unit 2. The voids were associated with thrust structures and high-angle faults at NMP Unit 2 as discussed in Section 2.5.1.2. Voids, thrust structures and high-angle faults were not observed at NMP3NPP. Rock recoveries in the core borings were almost always greater than 90% and often were 100%. Rock quality designation (RQD) values were generally above 80%, indicating high quality rock.

2.5.4.1.2 Weathering, Alteration, and Bedrock Structure

Weathering and Alteration

Any major zones of surficial weathering that may have been present at the site were removed by erosion during the Wisconsinan glaciation. The bedrock surface is very clean and generally unweathered. Minor oxidation and development of clay are present in some near-surface joints. There are no zones of alteration or irregular weathering within the rock mass. During

construction at NMP Unit 2, rock surfaces in the strata composed largely of argillaceous material (Pulaski Formation) weathered fairly quickly upon exposure and tended to weaken and disintegrate over time (Section 2.5.4.2). However, in newly excavated exposures these strata were unweathered, competent bedrock. The Oswego Sandstone, which will be the formation excavated for NMP3NPP Structures, did not weather quickly upon exposure and remained unweathered, competent bedrock during NMP Unit 2 construction. The to of the Pulaski Formation is at least 30 ft below the bottom of excavations for NMP3NPP.

Bedrock Structures

Except where the minor faults are present at NMP Unit 2 (Section 2.5.1.2, Figure 2.5-55), the bedrock at the NMP3NPP site is only slightly to moderately fractured. A set of systematic fractures in the bedrock, which are consistent with regional trends, is discussed in Section 2.5.1.2. The systematic fractures are near-vertical, with one set oriented northeast to southwest, and a second set oriented northwest to southeast. Typical spacing between fractures is on the order of feet to tens of feet. These conjugate shear fractures may contain calcite and sulfide minerals, and are occasionally healed by this mineralization. The systematic fractures are most prevalent in the relatively brittle siliceous beds of the Oswego Sandstone within the stratigraphic section. Mineralization studies suggest that these fractures are older than Late-Cretaceous age (CEG, 1998).

Fracture density increases markedly near some minor faults at the NMP Unit 2 site. The nature of the fracturing at these locations is discussed in Section 2.5.1.2 and discussed in detail in prior reports (CEG, 1998). These fractures resulted from the development of the faults and associated minor folds. Some of these fractures are mineralized. Others are either open or filled with unconsolidated sediments, depending on their age of development.

At the NMP Unit 2 site, a few fractures along bedding planes are indicators that slip has occurred (Section 2.5.1.2). The fractures are sometimes filled with thin breccia and are frequently slickensided due to bedding-plane-slip. Near the thrust structures, these sub-horizontal fractures were often dilated and frequently filled with unconsolidated silt and clay, presumably of lacustrine origin (CEG, 1998). Bedding plane fractures filled with laminated silt and clay were detected within the rock mass to depths as great as 270 ft (82 m).

The high-angle faults and a series of thrust faults present at the NMP Unit 2 site are described in Section 2.5.1.2. Northeast-trending broad, low-amplitude folds, inferred to be of more regional extent, are discussed in Section 2.5.1.2.

Fractures filled with breccia, thrust faults, or high-angle faults have not been encountered at NMP3NPP. Isolated slickensides were noted on bedding -plane or higher-angle fractures at NMP3NPP and isolated, thin, clay-filled fractures were noted in land and offshore borings.

Of the minor faults identified at NMP Unit 2, only the cooling tower fault had a strike direction that would potentially intersect the NMP3NPP site. As discussed in Section 2.5.3.2.2, seven trenches and pits were dug to investigate the lateral extent of the cooling tower fault (CEG, 1998). The western extent of the fault (in the direction of NMP3NPP) is inferred, because Trenches 1 and 2 revealed no evidence of the fault (Figure 2.5-73 in Section 2.5.1.2).

Even though the two trenches at NMP Unit 2 located along the western projection of the cooling tower fault showed no evidence of the fault, offshore boring locations at NMP3NPP were positioned perpendicular to the possible extension of the cooling tower fault. No evidence of the cooling tower fault (e.g. significant sub vertical fracturing, fault gouge, slickensides or weathering) was noted in the borings.

Additionally, land-based and marine seismic refraction studies at NMP3NPP (Section 2.5.4.4) showed no anomalies that could be interpreted as faults or significant structures. Therefore, it does not appear that the cooling tower fault extends beyond the excavation mapping in Trench 1 and Trench 2 at NMP Unit 2.

While faults were not encountered during the land and marine boring program at NMP3NPP, the lithology at NMP3NPP is similar to that at NMP Unit 2. Based on the presence of non-capable faults in excavations at NMP Unit 2, it is possible that some non-capable faults or deformation zones may be encountered in some of the excavations at NMP3NPP. Structures encountered at NMP3NPP are likely to be similar in properties to those well documented at NMP Unit 2. The investigation of the structures at NMP Unit 2 is described in detail in Section 2.5.1.2

The uniform, nearly flat-lying, continuous rock strata at the NMP3NPP site can be traced from the southeastern-most portion of the site to the shore of Lake Ontario and then offshore along the length of the proposed cooling water tunnels. The continuity of the rock strata demonstrate the lack of significant vertical offset due to faulting, and the lateral and vertical uniformity of the NMP3NPP site.

2.5.4.1.3 Unrelieved Residual Stresses

Regional Stress Conditions

A discussion of regional stress conditions is presented in Section 2.5.1.1 and a discussion of site stress conditions is presented in Section 2.5.1.2.

Available hydrofracturing test data in western New York State are presented in Volume III of Niagara Mohawk, 1978. Maximum horizontal stresses of 1,495 to 2,275 psi (105 to 160 kg/sq cm) are reported from tests ranging from 500 to 1,700 ft (152 to 528 m) below the ground surface. The maximum principal stresses, as determined by hydrofracturing, generally trend east-northeast. Additionally, hydrofracturing tests were performed by the United States Geological Survey (USGS) in a well near Auburn, NY, (Hickman, 1985; Plumb, 1985). These tests were performed in the Paleozoic cover rock. Results of these tests show that the maximum horizontal stress is oriented approximately N85°E with a magnitude that varies from 141 kg/cm^2 ±10 kg/cm^2 at 593 m to 499 kg/cm^2 ±10 kg/cm^2 at 1482 m depth. These results agree in orientation and relative magnitude with other hydrofracturing results in western New York State.

A summary of near-surface overcore test sites and results in the region was presented in the NMP Unit 2 USAR (CEG, 1998). An outstanding characteristic of the data is the variability of the maximum and minimum horizontal stress magnitudes, stress differences, and stress orientations. The reported magnitude of maximum horizontal stress at depths of less than 85 ft (26 m) varies from -700 to 4,300 psi (-49 to 302 kg/sq cm) and averages approximately 1,200 psi (84 kg/sq cm). Despite the variability of stress magnitude and orientation, the regional data indicate a horizontal stress that is higher than the value that could be attributed to a simple gravitational loading by the present overburden (CEG, 1998).

Focal mechanism solutions of earthquakes that have occurred in the region are discussed in Section 2.5.2. Although indications of stresses at depth provided by earthquake focal plane analysis are limited in number, the results of these analyses support the conclusion of the presence of high horizontal stress. They indicate that the inferred maximum principal stress is subhorizontal and predominantly associated with thrust faulting. Furthermore, the average orientation of the inferred maximum principal stress is east-northeast to northeast, which

corresponds well with the average orientation determined by hydrofracturing test measurements (CEG, 1998).

Surface measurements of in situ strain are discussed in Volume III of Niagara Mohawk, 1978. While surface measurements of strain are indicators of regional stress, it is expected that they are strongly influenced by near-surface effects.

Postglacial deformational features in the region are discussed in Section 2.5.1.1. The axial trend of post-glacial folds shows a roughly northwest orientation. This suggests that the contemporary maximum horizontal stresses responsible for the formation of the folds are oriented northeast (perpendicular to the axial trends of the folds). The development of these post-glacial folds is a consequence of high horizontal stress. However, the maximum stress orientation inferred from these folds is considered to provide only an approximation of horizontal stress direction (CEG, 1998).

In summary, a review of the regional stress conditions indicates that the area is characterized by high horizontal rock stresses. The maximum measured horizontal stresses at NMP Unit 2 range from -700 to 4,300 psi (-49 to 302 kg/sq cm), and within the upper 200 ft (60 m) of bedrock, horizontal stresses can be expected to reach 1,000 psi (70 kg/sq cm) in the region (CEG, 1998).

Focal mechanism solutions and the results of hydrofracturing tests indicate that the orientation of the maximum horizontal stress is east-northeast. Surface strain measurements and the general orientation of post-glacial folds tend to confirm this orientation. However, overcoring measurements reveal a widespread variation of the orientation of the maximum horizontal stress (CEG, 1998).

Evolution of Regional Stresses

The evolution of regional stresses has been detailed as Appendix III-L of the 1978 Geologic Investigation (Niagara Mohawk, 1978). The principal features of this interpretation are that the relatively high stresses in the region are remnant gravitational and tectonic stresses resulting from burial in the Appalachian basin and subsequent uplift. "Ridge push" stresses transferred through the North American plate from the Mid-Atlantic Ridge also contribute to the contemporary stress regime (Section 2.5.1.1). The stress distribution from the weight and/or motion of the Wisconsinan glacier at NMP Unit 2 is represented locally by geologic structures such as the Drainage Ditch fault and Cooling Tower fault (Section 2.5.1.2, Figure 2.5-55). Glacial loading introduced additional stresses into the bedrock, with the shear stresses in the plane of bedding increasing with increasing flexure of the strata during glacial loading of the crust. These shear stresses decreased with crustal rebound (CEG, 1998).

These effects (basin subsidence, normal faulting, glacial loading) are common to large areas of the northeastern part of the Appalachian basin, and similar stresses to those measured at the NMP Unit 2 site exist at other locations in this sedimentary basin. Therefore, although the stresses measured at the NMP Unit 2 site are relatively high, they are not considered anomalous for the region and are significantly less than the strength of the bedrock (CEG, 1998).

NMP Unit 2 Site Stress Conditions

During the geologic investigations at NMP Unit 2, three series of overcoring tests to determine in situ stress conditions and one series of tests to evaluate residual strains by undercoring were conducted (CEG, 1998).

Because of the various stress measurements conducted, a number of conclusions have been drawn regarding the nature of in situ stress conditions at the NMP Unit 2 site. Generally, measured stress magnitudes and orientations differ between measurements taken outside the

fault block bounded by the Cooling Tower fault and the Drainage Ditch fault and within the fault block. Outside the fault block, the stresses measured are concluded to be typical of regional stress conditions at these depths. The direction of maximum normal stress is approximately northeast and the average magnitude of the maximum normal stress is greater than 1,700 psi (120 kg/sq cm).

Stress measurements taken between the Cooling Tower fault and the Drainage Ditch fault indicate that the fault block has experienced extensional relief parallel and perpendicular to the strike of the bounding faults (Section 2.5.1.2, Figure 2.5-55). This deformation is expressed by changes in both orientation and magnitude of stress relative to the pre-deformational stresses. This is manifest in a change in stress value and orientation in the hanging wall block of the Radwaste Thrust Structure relative to the footwall block. The orientation of the maximum stress in the hanging wall block is northeast and the magnitude is low, whereas in the footwall block the orientation is east-west and the magnitude is 1,200 to 1,300 psi (84 to 91 kg/sq cm). Additionally, stress measurements within the Radwaste Thrust block reveal the existence of stress gradients normal and parallel to the Cooling Tower fault. These gradients are postulated to have resulted from buckling in the vicinity of the Cooling Tower fault and fault-parallel translation associated with westward thrusting of the Radwaste fault.

In conjunction with other geologic evidence, the stress measurements indicate that the Cooling Tower fault is the southern boundary of the Radwaste Thrust Structure. The northern boundary is inferred to be either the Drainage Ditch fault or the outcrop of the strata in the lake, the western boundary coincides with the bedrock depression in the vicinity of the heater bay, and the eastern boundary is assumed to be coincident with the axial plane of a syncline. The base of the Radwaste Thrust Structure, as defined by an increase in stress magnitude and a change in the orientation of the maximum stress, lies approximately coincident with the illite layer in Unit A of the Pulaski Formation at least in the northern part of the fault block (CEG, 1998).

The magnitudes of stress measured in the vicinity of the NMP Unit 2 reactor excavation and the bedrock slot are low, not exceeding approximately 400 psi (28 kg/sq cm). The low recorded values are as expected because of the stress relief of the excavation and the close proximity of the western boundary of the Radwaste Thrust Structure (CEG, 1998). I f similar structures are encountered during excavation at NMP3NPP, it is expected that the excavation process would produce similar stress release.

Regional Rock Squeeze Considerations

Rock squeeze was recognized in the southern Ontario-western New York area as early as the beginning of this century. Since then, numerous cases of time-dependent rock displacements have been identified. Some of these have caused distress in engineering structures, such as pressure tunnels, bridges, and canals, while others are simply observations in open excavations or quarries. Most of the observations have been made in the area from Hamilton, Ontario, to Rochester, NY, particularly in the area of Niagara Falls. No specific problems or distress in engineered structures have been attributed to rock squeeze in the Oswego, NY, area (CEG, 1998).

A study of rock squeeze movements in western New York and southern Ontario has indicated that rock squeeze problems commonly occur in the Paleozoic sedimentary rocks (particularly shales) that are subjected to high horizontal stresses and are susceptible to swelling (CEG, 1998). While a similar swelling phenomenon is expected in shale dominant units at NMP3NPP, excavations for foundations are predominantly in the siliceous Oswego Sandstone where swelling is expected to be insignificant.

NMP Unit 2 Site Rock Squeeze Considerations

Based on a review of rock squeeze in the region and the occurrences of possible indicators of high horizontal stresses at the NMP Unit 2 site (offset drill holes and small buckles), it was decided to investigate the possibility of rock squeeze affecting the proposed structures at the NMP Unit 2 site were investigated. Stress measurements by overcoring were made and free swell tests were conducted on rock cores (CEG, 1998). Based on these tests, it was concluded that the NMP Unit 2 site did possess those characteristics (high in situ stress and rock units susceptible to swelling) that elsewhere in the region have caused time-dependent displacements in excavations. Because of this, it was decided to isolate Category 1 structures from the effects of rock squeeze. At that time, a single wall had been poured against the rock. This wall was analyzed for the effects of rock squeeze and subsequently redesigned to accommodate conservative estimates of potential rock movements. The design criteria developed from the various investigations are presented in Section 2.5.4.11 of the NMP Unit 2 USAR (CEG, 1998).

NMP Unit 2 Site Analysis

Rock squeeze studies at NMP Unit 2 were directed at analyzing the stability of the single wall and defining the amount of vertical and horizontal movement that may occur around Category 1 deep excavations so that adequate space could be provided and piping systems designed accordingly. A detailed description of finite element modeling is presented in the NMP Unit 2 USAR (CEG, 1998).

Rock Squeeze Potential at NMP3NPP

The potential for rock squeeze at NMP3NPP is considered small based on comparison to NMP Unit 2. Several minor buckles were observed in the excavation floors at NMP Unit 2 (CEG, 1998). The development of these buckles was attributed to the thinly bedded nature of the shale and sandstone units, the high horizontal stresses, and the removal of the overlying confining pressure. Structures were placed in the excavations, thereby increasing the vertical confining pressure, so the potential for further development of the buckles or the initiation of new buckles is unlikely (CEG, 1998). The argillaceous rock units (Pulaski Formation) at the site are susceptible to volumetric changes depending on the availability of moisture (CEG, 1998).

At NMP3NPP, the excavations will be made in Oswego Sandstone. The deepest excavations will be at least 30 feet above the top of the Pulaski formation, which experienced squeeze at NMP Unit 2. At NMP3NPP, rock squeeze of excavation walls in the Oswego Sandstone is unlikely due to the strength of the sandstone. Buckling of the excavation floor is less likely than at NMP Unit 2 because the NMP3NPP excavation floor is in the thickly bedded Oswego Sandstone and not in the thinly bedded Pulaski Formation as at NMP Unit 2. Furthermore, in-situ stress increases with depth and is greater in the Pulaski Formation than in the Oswego Sandstone (CEG, 1998).

Structures are founded in excavations in the Oswego Sandstone at NMP3NPP where the vertical confining pressure due to the structures will be equal to, or greater than, the existing vertical confining pressure of the bedrock. At NMP3NPP, the swelling of argillaceous rock units (Pulaski Formation) is not a concern, because excavations will not extend deeper than the siliceous Oswego Sandstone, which is not susceptible to significant volumetric changes due to moisture (CEG, 1998).

2.5.4.1.4 UNSTABLE ROCK AND SOIL

No safety-related structures are founded on the natural soils at the NMP3NPP site. Therefore, evaluations of stability characteristics of the soils are not required.

The rock samples recovered from the boreholes at the NMP3NPP site are fully lithified, generally unweathered, or rarely slightly weathered, and not subject to dissolution. Section 2.5.1.2 presents a complete discussion of rock type and characteristics.

The argillaceous rock units (Pulaski Formation) at the NMP3NPP site are susceptible to volumetric changes depending upon the availability of moisture. Several analyses have been completed that calculate the horizontal and vertical swelling capacities of the rock (CEG, 1998). Building designs at NMP3NPP do not extend deep enough to encounter the Pulaski Formation.

2.5.4.1.5 History of Deposition, Erosion, and Loading

No safety-related structures are founded on natural soils. Therefore, the loading history of the soils is not pertinent to this discussion.

A complete geologic history of the site is presented in Section 2.5.1.2 and regional geologic history is presented in Section 2.5.1.1. This section provides a synopsis of the bedrock loading history, focusing on its impact on the stability of the foundation materials.

The site bedrock strata were deposited in Late Ordovician time (450 million years ago). Continual regional subsidence until late in the Paleozoic era (250 to 300 million years ago) resulted in the burial of these units by 8,000 to 10,000 ft (2,438 to 3,048 m) of younger sedimentary rock. Throughout this period of subsidence, these sediments were subjected to diagenesis resulting in their induration and lithification. In Late Paleozoic time (200 million years ago), the more brittle siliceous strata were deformed by strike-slip faulting (Section 2.5.1.2). The process of regional uplift and erosion began in Late-Paleozoic time. Regional uplift continues today as remnant glacio-isostatic rebound. During the Mesozoic, normal faults due to extension, developed along the discontinuities resulting from the earlier Paleozoic deformation. Middle Paleozoic and younger stratigraphic units were eroded from the site in association with regional uplift. By Late-Tertiary time, much of the thick cover of sediments overlying the site was no longer present. During the Pleistocene Epoch, a series of glaciations dominated the active erosional and depositional processes in the site area.

Four main stages of glaciation have been identified in North America (Section 2.5.1.1). The last stage (Wisconsinan) removed any evidence of prior glaciation in the site area. Therefore, it is not known how prior stages of glaciation affected the site. It is certain that each glaciation resulted in a depression of the crust as an isostatic response to the load imposed by the ice. After the removal of the ice sheet during interglacial stages, the crust responded, at least partially, in an opposite manner by glacio-isostatic rebound. The maximum thickness of the Wisconsinan ice sheet at the site is estimated to have been about 6,500 ft (1,980 m), approximately 18,000 years ago. The depression of the crust from this load is estimated to have been between 1,500 and 1,800 ft (460 to 550 m) (CEG, 1998).

Downward flexing of the strata from glacial loading contributed to the deformation of the site bedrock as demonstrated by:

1. Breccia zones along bedding at NMP Unit 2 (Section 2.5.1.2).

2. Buckling associated with the north-dipping, high-angle faults at NMP Unit 2 (Section 2.5.1.2).

3. Shallow thrust structures at NMP Unit 2 (Section 2.5.1.2).

During Wisconsinan deglaciation, the site area was occupied by proglacial Lake Iroquois. It is estimated that the depth of water at the site was approximately 300 ft (90 m). From studies of the history of Lake Iroquois (Section 2.5.1.2), it is known that 11,000 years ago the lake level decreased to a level below the present level of Lake Ontario in only a few hundred years. A tendency for increasing uplift pressure might have developed, because the bedrock surface was covered at that time by a veneer of impermeable glacial sediments that prevented the fluid pressure in the rock mass from dissipating as the lake level was decreasing. This condition would have contributed to additional bedding-plane-slip where stress gradients were steep, such as at the NMP Unit 2 Cooling Tower fault and explains the deformation of overlying glacial sediments at the NMP Unit 2 fault (Section 2.5.1.2).

2.5.4.1.6 Consolidation and Preconsolidation

Section 2.5.4.1.3 and Section 2.5.4.1.4 address consolidation and preconsolidation. }

2.5.4.2 Properties of Subsurface Materials

The U.S. EPR FSAR includes the following COL Item in Section 2.5.4.2:

> A COL applicant that references the U.S. EPR design certification will reconcile the site-specific soil properties with those used for design of U.S. EPR Seismic Category I structures and foundations described in Section 3.8.

This COL Item is addressed as follows:

{All Seismic Category I structures at the NMP3NPP site are supported on bedrock, or on concrete fill extending down to bedrock. Portions of Seismic Category I and Category II-SSE utilities, and the cooling water pipe tunnel, are supported on structural fill extending down to bedrock.

These sections are added as a supplement to the U.S. EPR FSAR.

2.5.4.2.1 Static and Dynamic Engineering Properties of Soil and Rock

The static and dynamic properties of soil and bedrock at the NMP3NPP site are discussed in the following subsections.

2.5.4.2.1.1 Static Properties of Natural Soil

The predominant natural soil is glacial till that typically consists of silty sand with varying amounts of gravel, cobbles, and boulders. There are thin, intermittent layers of fill and surficial soils present at the NMP3NPP site; however, these soils are removed during the preliminary site preparation stage of the project and their engineering properties are not pertinent as no safety-related structures are founded on till. All Seismic Category I structures and utilities are supported on bedrock or on concrete fill or structural fill extending down to bedrock. The properties of glacial till are required for the site wide liquefaction analysis (section 2.5.4.8) and for the site wide analysis of the stability of slopes (section 2.5.5). The glacial till has the following static design properties:

- Unit Weight:
  - Saturated unit weight: 145.0 lbs/ft^3 (2,322.7 kg/m^3)
  - Moist unit weight: 140.0 lbs/ft^3 (2,242.6 kg/m^3)

The unit weights for glacial till are derived from published literature. Two published references contain soil property tables that provide typical ranges of soil unit weights. Table 1.4 titled "Porosity, Void Ratio, and Unit Weight of Typical Soils in Natural State" in (Peck, 1953) indicates a unit weight of glacial till as 132 lbs/ft^3 (2,114.4 kg/m^3) unsaturated, and 145 lbs/ft^3 (2,322.7 kg/m^3) saturated. Table 2-8 titled "Typical Soil Unit Weights" in (Kulhawy, 1990) presents a range of typical values for the normalized weights of dry and saturated soils of varying types. The NMP3NPP glacial till is most similar to the well graded gravel, sand, silt, and clay. The range of normalized saturated unit weight values (soil, saturated/water) for this soil type is 2.00 to 2.50, corresponding to a saturated unit weight of 125 to 156 lbs/ft^3 (2,000 to 2500 kg/m^3). The selected saturated unit weight of 145 lbs/ft^3 (2,320 kg/m^3) is slightly above the middle of this range.

Attempts were made to obtain undisturbed tube samples of the glacial till. However, these attempts were not successful due to the high density and high gravel content of the fill. Therefore, laboratory tests to measure the in situ unit weight could not be performed. For analyses related to lateral earth pressures on safety related structures, potential variation in the unit weight of the glacial till is not significant, because glacial till is not used as backfill around the structures. For slope stability analyses, potential variation in the unit weight of the glacial till does not significantly affect the results of the analyses, and the selected values of unit weight are relatively high (relatively conservative). Therefore, selection of glacial till unit weight based on values in the literature is considered appropriate.

- Specific gravity of solids: 2.74

  Specific gravity is based on the average of five laboratory tests performed on split spoon samples of glacial till collected from the borings. One specific gravity measurement on glacial till (2.683) was not included in the average. Specific gravity measurements are presented in Table 2.5-43. Table 3.1 titled “Specific Gravities of Minerals” (Lambe, 1989) provides specific gravities for various common soil minerals. The values range from 2.3 to 3.2, and confirm that the measured value of 2.74 is reasonable.

- Internal of angle of friction (phi): 36 degrees

  The angle of internal friction (phi) is based on the results of two consolidated undrained triaxial tests with pore pressure measurement performed on compacted specimens of glacial till. The test results indicated peak undrained friction angles of 38.2 degrees and 38.4 degrees. Test results are presented in Figure 2.5-155 and Figure 2.5-156. To be conservative, and to account for the potential variability of the glacial till soils, a lower undrained friction angle of 36 degrees is used for design. Table 11.3 titled “Summary of Friction Angel Data for Use in Preliminary Design” (Lambe, 1969) provides ranges of angle of internal friction for various soil types. For well-graded sand and for sand and gravel, which are the soil types most similar to the glacial till, the friction angles for medium dense to dense soil range from 34 to 48 degrees. This confirms that the selected value of 36 degrees is reasonable and conservative.

- Coefficient of friction acting on basemats: 0.7

  Coefficient of friction is calculated from the internal angle of friction using the following equation:

Coefficient of friction acting on basemats = tangent (phi) = 0.7

- Lateral earth pressure coefficients:
  - At-rest: K_0 = 1-sin(phi) = 0.41
  - Active: K_a = [1-sin(phi)]/ [1+sin(phi)] = 0.26
  - Passive: K_p = [1-sin(phi)]/ [1+sin(phi)] = 3.87

  These lateral earth pressure coefficients do not include lateral pressure due to hydrostatic loads.

2.5.4.2.1.2 Static Properties of Structural Fill

A source of structural fill was identified in an investigation of potential borrow pits performed in the vicinity of the NMP3NPP site. This investigation is discussed in Section 2.5.4.2.3.8. The structural fill consists of a widely graded sand and gravel containing less than 10 percent fines. Structural fill is used as backfill around the perimeter of Seismic Category I structures and beneath portions of Seismic Category I utilities at the NMP3NPP site. The structural fill has the following static design properties:

- Unit Weight:
  - Saturated unit weight: 147.2 lbs/ft^3 (2,358 kg/m^3)
  - Moist unit weight: 143.9 lbs/ft^3 (2,305 kg/m^3)
  - Dry unit weight: 134.7 lbs/ft^3 (2,158 kg/m^3)

  Unit weights for structural fill were derived from the results of a Modified Proctor compaction test. A plot of the compaction curve is presented as Figure 2.5-157. Table 3.2 titled "Maximum and Minimum Densities for Granular Soils" (Lambe, 1969) gives a range of 89 to 146 lbs/ft^3 for the dry unit weight of silty sand and gravel, confirming that the computed value of 134.7 lbs/ft^3 is reasonable.

- Specific gravity of solids: 2.70

  Specific gravity is based on the results of one laboratory test performed on a sample of structural fill. The specific gravity measurement data is presented in Table 2.5-44. Table 3.1 titled "Specific Gravities of Minerals" (Lambe, 1969) provides specific gravities for various common soil minerals. The values range from 2.3 to 3.2, and confirm that the measured value of 2.70 is reasonable.

- Internal angle of friction (phi): 35 degrees

  The angle of internal friction (phi) is based on the results of two consolidated undrained triaxial tests with pore pressure measurement performed on compacted specimens of structural fill. The test results indicated peak undrained friction angles of 37.5 degrees and 38.5 degrees. Test results are presented in Figure 2.5-158 and Figure 2.5-159. To be conservative, and to account for the potential variability of structural fill at the borrow pit, a lower undrained friction angle of 35 degrees is used for design. Table 11.3 titled "Summary Friction Angle Data for Use in Preliminary

Design" (Lambe, 1969) provides ranges of angle of internal friction for various soil types. For well-graded sand and for sand and gravel, which are the soil types from 34 to 48 degrees. This confirms that the selected value of 35 degrees is reasonable and conservative.

- Coefficient of friction acting on basemats: 0.7

  Coefficient of friction is calculated from the internal angle of friction using the following equation: Coefficient of friction acting on basemats = tangent (phi) = 0.73

- Lateral earth pressure:

  - At-rest: K_0 = 1-sin(phi) = 0.41
  - Active: K_a = [1-sin(phi)]/ [1+sin(phi)] = 0.26
  - Passive: K_p = [1-sin(phi)]/ [1+sin(phi)] = 3.87

  These lateral earth pressure coefficients do not include lateral pressure due to hydrostatic loads.

2.5.4.2.1.3 Dynamic Properties of Natural Soil

Dynamic properties of glacial till were measured using Resonant Column Torsional Shear (RCTS) tests on two specimens of recompacted glacial till. The complete test data are contained in (AREVA, 2008a). Each specimen was compacted in the laboratory to a moist total unit weight of 124.3 lb/ft^3 (1,989 kg/m^3) at a water content of 7.4 to 7.5%, and tested at five consolidation pressures ranging from 430 to 7,200 lb/ft^2 (21 to 345 kPa). Test results include the following data for five confining pressures for each sample:

- Low Amplitude Shear Wave Velocity
- Low Amplitude Shear Modulus
- Curves of Modulus Degradation vs. Shear Strain
- Curves of Damping vs. Shear Strain

Low-strain properties measured in the RCTS tests are presented below.

Low-Strain Dynamic Properties of Natural Soil from RCTS Tests						
Isotropic Confining Pressure, σ_o			Low-Strain-Amplitude Shear Modulus, G_{max}		Low-Strain-Amplitude Shear Wave Velocity, Vs	Low-Strain-Amplitude Material Damping Ratio, D_{min}
(psi)	(psf)	(kPa)	(ksf)	(MPa)	(fps)	(%)
Remolded Specimen 1						
3	432	21	1942	93	708	2.53
6	864	41	2359	113	780	2.38
13	1872	90	2831	136	854	2.21
25	3600	172	3577	172	958	2.03
50	7200	345	4610	221	1085	1.89
Remolded Specimen 2						
3	432	21	1916	92	704	2.39
6	864	41	2203	106	754	2.25

Low-Strain Dynamic Properties of Natural Soil from RCTS Tests						
Isotropic Confining Pressure, σ_o			Low-Strain-Amplitude Shear Modulus, G_{max}		Low-Strain-Amplitude Shear Wave Velocity, Vs	Low-Strain-Amplitude Material Damping Ratio, D_{min}
(psi)	(psf)	(kPa)	(ksf)	(MPa)	(fps)	(%)
13	1872	90	2681	129	831	2.13
25	3600	172	3443	165	940	1.98
50	7200	345	4504	216	1073	1.86

2.5.4.2.1.4 Dynamic Properties of Structural Fill

Dynamic properties of structural fill were measured using Resonant Column Torsional Shear (RCTS) tests on two specimens of recompacted structural fill. The complete test data are contained in (AREVA, 2008b). Each specimen was compacted in the laboratory to a to a moist total unit weight of 125.2 lb/ft^3 (2,006 kg/m^3) at a water content of 7.8 to 8.2%, and tested at five consolidation pressures ranging from 430 to 7,200 lb/ft^2 (21 to 345 kPa).

Low-strain properties measured in the RCTS tests are presented below.

Low-Strain Dynamic Properties of Structural Fill from RCTS Tests						
Isotropic Confining Pressure, σ_o			Low-Strain-Amplitude Shear Modulus, G_{max}		Low-Strain-Amplitude Shear Wave Velocity, Vs	Low-Strain-Amplitude Material Damping Ratio, D_{min}
(psi)	(psf)	(kPa)	(ksf)	(MPa)	(fps)	(%)
Remolded Specimen Pad 1-1						
3	432	21	1007	48	508.6	1.62
6	864	41	1363	65	591.3	1.47
13	1872	90	2016	97	718.7	1.22
25	3600	172	2976	143	872.0	1.10
50	7200	345	4405	211	1058.9	0.99
Remolded Specimen Pad 1-2						
3	432	21	932	45	489.0	1.59
6	864	41	1355	65	589.0	1.47
13	1872	90	2010	96	717.4	1.21
25	3600	172	2971	143	871.1	1.09
50	7200	345	4415	212	1059.9	0.99

2.5.4.2.1.5 Static Properties of Oswego Sandstone

The Oswego sandstone consists of hard, fresh to slightly weathered, fine to medium grained sandstone with minor interbedded siltstone and shale layers. All Seismic Category I structures at the NMP3NPP site are founded on the Oswego Sandstone, or on concrete fill extending down to the Oswego Sandstone. The Oswego Sandstone has the following static design properties:

- Unit Weight: 164 lbs/ft^3 (2,630 kg/m^3)

  This unit weight of Oswego Sandstone is the average of 22 unit weight measurements made on core samples collected from borings performed within the footprint of Seismic Category I Structures. The measured unit weights ranged from 157 lbs/ft^3 to 183 lbs/ft^3 (2,510 kg/m^3 to 2,930 kg/m^3). The test results are presented in Table 2.5-45 and Table 2.5-46.

Laboratory tests on two additional samples (Table 2.5-47 and Table 2.5-48) collected from the offshore borings indicated unit weights of the Oswego Sandstone of 159 and 165 pounds per cubic foot (pcf) (1,100 and 1,140 kPa) which are in the same range.

The spread in the data are indicative of normal variation. Most of the unit weights are close to the average value, and there is not trend of increasing or decreasing unit weight with depth. The values are within the anticipated range for sandstone.

- Unconfined compressive strength: 24,150 psi (166,500 kPa) onshore 14,500 psi (99,980 kPa) offshore

  The unconfined compressive strength of Oswego Sandstone is reported as the average of the results of 16 unconfined compression tests performed on core samples collected from borings performed within the footprint of Seismic Category I Structures. The measured unconfined compressive strengths ranged from 18,850 psi to 39,431 psi (130,000 kPa to 271,900 kPa). The test results are presented in Table 2.5-45 and Table 2.5-46.

  The spread in the data are indicative of normal variation. Most of the strengths are close to the average value, and there is not trend of increasing or decreasing strength with depth.

  Laboratory tests on two additional samples collected from the offshore borings (Table 2.5-47 and Table 2.5-48) indicated unconfined compression strengths of 11,734 and 17,267 pounds per square inch (psi) (80,803 to 119,050 kPa) with an average value of 14,500 psi (99,980 kPa).

  The average values and the range of values within the anticipated range for sandstones and siltstones.

- Poisson's ratio: 0.37

  This value of Poisson's ratio is calculated from shear wave velocities (V_s) and compression wave velocities (V_p) obtained from cross-hole measurements and refraction surveys. Depending on the method used to interpret the compression-wave data, the range in V_p/V_s ratio is 2.10 to 2.23, corresponding to a range in Poisson's ratio of 0.353 to 0.374. The best estimate is considered to be $V_p/V_s = 2.2$, with a corresponding Poisson's ratio of 0.37.

  V_p/V_s ratio is related to Poisson's ratio using the following equation (Fang, 1991):

  $$\text{Poisson's ratio} = [0.5(V_p/V_s)^2-1] / [(V_p/V_s)^2-1]$$

  Poisson's ratio was also measured in unconfined compression tests in the laboratory on 18 core samples. The laboratory test results are presented in Table 2.5-45, Table 2.5-46, Table 2.5-47 and Table 2.5-48. The laboratory test results indicated a Poisson's Ratio that ranged from 0.06 to 0.35. The measured value of Poisson's ratio for each specimen generally increased with increasing loading during the test. Poisson's ratio values are presented for stresses ranging from 0 to 15,000 psi (0 to 103,400 kPa). The laboratory test results are not considered representative of the in-situ Poisson's ratio because of stress relief and de-lamination of the horizontally bedded rock that occurs when the core samples are retrieved from the borehole.

- Young's Modulus

  Young's Modulus for Oswego Sandstone was measured during unconfined compressive strength tests performed on 16 core samples from onshore borings and 2 core samples from offshore borings. The value of Young's modulus is stress dependent. Test results correlated to specific stress ranges are presented in Table 2.5-47 and Table 2.5-48.

- Coefficient of friction acting on basemats: 0.7

  From published literature (NAVFAC, 1986); the coefficient of friction between mass concrete and clean sound rock is assumed to be equal to 0.7 based on the characteristics of that rock unit.

2.5.4.2.1.6 Static Properties of Pulaski Formation

The Pulaski Formation typically consists of medium hard, slightly weathered, interbedded layers of sandstone, argillaceous sandstone, siltstone, and shale. The top of the Pulaski Formation typically is encountered at depths of between 35 ft (10.7 m) to 80 ft (24.4 m) below the bottom of the foundations of the Seismic Category I structures at the NMP3NPP site. The Pulaski Formation has the following static design properties:

- Unit weight: 168 lbs/ft^3 (2,690 kg/m^3)

  This unit weight of the Pulaski Formation is the average of 18 unit weight measurements made on core samples collected from borings performed within the footprint of Seismic Category I Structures. The measured unit weights ranged from 161 lbs/ft^3 to 175 lbs/ft^3 (2,580 kg/m^3 to 2,800 kg/m^3). The test results are presented in Table 2.5-45 and Table 2.5-46.

  In addition, 28 unit weight measurements were made on samples recovered from the offshore borings. The unit weights ranged from 157 to 171 pounds per cubic foot (pcf) (2530 to 2740 kg/m^3) with an average value of 166 pcf (2660 kg/m^3). The test results are presented in Table 2.5-47 and Table 2.5-48.

  The spread in the data are indicative of normal variation. Most of the unit weights are close to the average value, and there is no trend of increasing or decreasing unit weight with depth. The values are within the anticipated range for sandstone and siltstone.

- Unconfined compressive strength: 17,430 psi (120,160 kPa) onshore 14,200 psi (97,890 kPa) offshore

  The unconfined compressive strength of the Pulaski Formation is reported as the average of the results of seven unconfined compression tests performed on core samples collected from borings performed within the footprint of Seismic Category I Structures. The measured unconfined compressive strengths ranged from 13,184 psi to 30,088 psi (90,000 kPa to 207,400 kPa), with an average of 17,430 psi (120,160 kPa). The test results are presented in Table 2.5-45 and Table 2.5-46.

  In addition, 13 unconfined compression tests on samples collected from the offshore borings indicated strengths in the range of 4,656 to 27,893 pounds per square inch (psi) (32,100 to 192,320 kPa) with an average value of 14,200 psi (97,890 kPa). The test results are presented in Table 2.5-47 and Table 2.5-48.

The spread in the data are indicative of normal variation. Most of the strengths are close to the average value, and there is not trend of increasing or decreasing strength with depth. The average values and the range of values are within the anticipated range for sandstones and siltstones.

- Poisson's ratio: 0.38

  Poisson's ratio for the Pulaski Formation is based on the value for the Oswego Sandstone, discussed above in 2.5.4.2.1.5. The Pulaski Formation is similar to the Oswego Sandstone (Ordovician clastic sedimentary rock), but has more siltstone and less sandstone. Therefore, one would expect the V_p/V_s ratio and Poisson's ratio to be slightly higher. The recommended value of V_p/V_s ratio is 2.3, and the corresponding Poisson's ratio is 0.38.

  Poisson's ratio was also measured in the laboratory on 20 core samples during unconfined compression tests. The test results are presented in Table 2.5-45, Table 2.5-46, Table 2.5-47 and Table 2.5-48. The laboratory test results indicated a Poisson's Ratio that ranged from 0.10 to 0.20.

  The measured value of Poisson's ratio for each specimen generally increased with increasing loading during the test. Poisson's ratio values are presented for stresses ranging from 0 to 15,000 psi (0 to 103,400 kPa). The laboratory test results are not considered representative of the in-situ Poisson's ratio because of stress relief and de-lamination of the horizontally bedded rock that occurs when the core samples are retrieved from the borehole.

- Young's Modulus - 1,950,000 psi - 2,200,000 psi (13,440,000 kPa - 15,170,000 kPa)

  Young's Modulus for the Pulaski Formation was measured during unconfined compressive strength tests performed on 7 core samples from onshore borings and 13 core samples from offshore borings. The value of Young's modulus is stress dependent. Test results correlated to specific stress ranges are presented in Table 2.5-46 and Table 2.5-48.

- Coefficient of friction acting on basemats: 0.7

  From published literature (NAVFAC, 1986), the coefficient of friction between mass concrete and clean sound rock is assumed to equal to 0.7 based on the characteristics of that rock unit.

2.5.4.2.1.7 Static Properties of Whetstone Gulf Formation

The Whetstone Gulf Formation typically consists of medium hard, slightly weathered, siltstone and shale with interbedded layers of sandstone. The top of the Whetstone Gulf Formation typically is encountered at depths of between 140 ft (43 m) and 160 ft (49 m) below the bottom of the foundations of the Seismic Category I structures at the NMP3NPP site. The Whetstone Gulf Formation has the following static design properties:

- Unit Weight: 167 lbs/ft^3 (2,675 kg/m^3)

  This unit weight of Whetstone Gulf Formation is the average of five unit weight measurements made on core samples collected from borings performed within the footprint of Seismic Category I Structures. The measured unit weights ranged from 157

lbs/ft^3 to 172 lbs/ft^3 (2,515 kg/m^3 to 2,755 kg/m^3). The test results are presented in Table 2.5-45 and Table 2.5-46.

In addition, three measurements on samples collected from offshore borings indicated unit weights that ranged from 167 to 175 pounds per cubic foot (pcf) (2680 to 2810 kg/m^3) with an average value of 170 pcf (2730 kg/m^3). The test results are presented in Table 2.5-47 and Table 2.5-48. These values are consistent with the onshore samples.

The spread in the data are indicative of normal variation. Most of the unit weights are close to the average value, and there is not trend of increasing or decreasing unit weight with depth. The average values and the range of values are within the anticipated range for sandstones and siltstones.

- Unconfined compressive strength: 20,328 psi (140,200 kPa)

  This unconfined compressive strength of Pulaski Formation is from one unconfined compression test performed on a core sample collected from a boring performed within the footprint of a Seismic Category I Structure. The test result is presented in Table 2.5-45 and Table 2.5-46.

  In addition, a test on a sample from offshore indicated a strength of 20,243 psi (139,570 kPa), which is consistent with the onshore measurement. The test result is presented in Table 2.5-47 and Table 2.5-48.

  The spread in the data are indicative of normal variation. Most of the strengths are close to the average value, and there is not trend of increasing or decreasing strength with depth. The average values and the range of values are within the anticipated range for sandstones and siltstones.

- Poisson's ratio: 0.38

  Poisson's ratio for the Whetstone Gulf Formation is based on the value for the Oswego Sandstone, discussed above in 2.5.4.2.1.5. The Pulaski Formation is similar to the Oswego Sandstone (Ordovician clastic sedimentary rock), but has more siltstone and less sandstone. Therefore, one would expect the V_p/V_s ratio and Poisson's ratio to be slightly higher. The recommended value of V_p/V_s ratio is 2.3, and the corresponding Poisson's ratio is 0.38.

  Poisson's ratio was also measured in the laboratory on two core samples during unconfined compression tests. The test results are presented in Table 2.5-45, Table 2.5-46, Table 2.5-47 and Table 2.5-48. The test results indicated a Poisson's Ratio that ranged from 0.04 to 0.30.

  The measured value of Poisson's ratio increased with increasing loading during the test. Poisson's ratio values are presented for stresses ranging from 0 to 15,000 psi (0 to 103,400 kPa). The laboratory test results are not considered representative of the in-situ Poisson's ratio because of stress relief and de-lamination of the horizontally bedded rock that occurs when the core samples are retrieved from the borehole.

- Young's Modulus: 850,000 psi – 1,500,000 psi (5,861,000 kPa – 10,340,000 kPa)

  Young's Modulus for the Whetstone Gulf Formation was measured during unconfined compressive strength tests performed on one core sample from an onshore boring,

and one core sample from as offshore boring. The value of Young's modulus is stress dependent. Test results correlated to specific stress ranges are presented in Table 2.5-46 and Table 2.5-48.

Coefficient of friction acting on basemats: 0.7

From published literature (NAVFAC, 1986); the coefficient of friction between mass concrete and clean sound rock is equal to 0.7.

2.5.4.2.1.8 Dynamic Properties of Rock

Dynamic properties of rock are presented in Table 2.5-49 and Table 2.5-50. The lab tests, field tests, and references used to obtain the dynamic properties are discussed as notes on the tables.

2.5.4.2.1.9 Permeability of Soil and Rock

Soil Permeability

Soil permeability values are discussed in 2.4.12.2.2. In summary, glacial till permeability values measured for NMP Unit 2 ranged from 3×10^{-5} to 6×10^{-4} cm/sec. Surface percolation tests performed for Unit 2 indicated an average vertical permeability of 1×10^{-5} cm/sec. Permeabilities ranging from 1×10^{-3} cm/sec to 1×10^{-5} cm/sec were measured at New Haven, New York. The till is descriptively similar to that at NMP Unit 2.

Rising head permeability tests were performed in soil at five locations at NMP3NPP. The test data are presented in Table 2.5-51. The permeabilities ranged from 6.3×10^{-6} cm/sec to 6.1×10^{-5} cm/sec. The permeabilities measured at NMP3NPP are similar to, but slightly lower than those measured at NMP Unit 2.

Rock Permeability

Permeability values of rock are based on water pressure (packer) tests and rising head tests discussed in Section 2.5.4.2.3.5. The test data are presented in Table 2.5-51, Table 2.5-52, and Table 2.5-53 and in Figure 2.5-174 and Figure 2.5-175. Permeability in rock is primarily a function of the fracturing of the rock. The relatively low measured permeabilities, generally less than 1×10^{-5} cm/sec, is consistent with the observed low degree of fracturing of the rock.

Oswego Sandstone - onshore

The results of in-situ permeability tests performed in the Oswego Sandstone indicated horizontal permeabilities in the range from $<1 \times 10^{-6}$ cm/sec to 8×10^{-4} cm/sec with a typical value of about 1×10^{-5} cm/sec. Measured permeabilities were generally higher near the top of the formation.

Oswego Sandstone - offshore

The results of in-situ permeability tests performed in the Oswego Sandstone indicated horizontal permeabilities in the range from $<1 \times 10^{-6}$ cm/sec to 1×10^{-5} cm/sec with a typical value of about 1×10^{-5} cm/sec.

Pulaski Formation - onshore

- The results of in-situ permeability tests in Unit A indicated horizontal permeabilities in the range from $<1 \times 10^{-6}$ cm/sec to 2×10^{-5} cm/sec with a typical value of about 5×10^{-6} cm/sec.

- The results of in-situ permeability tests in Unit B indicated horizontal permeabilities in the range from <1 x 10^{-6} cm/sec to 1 x 10^{-4} cm/sec with a typical value of about 1 x 10^{-5} cm/sec.

- The results of in-situ permeability tests in Unit C indicated horizontal permeabilities in the range from <1 x 10^{-6} cm/sec. to 8 x 10^{-5} cm/sec. with a typical value of about 1 x 10^{-6} cm/sec.

The Pulaski A is considered an aquitard to vertical flow based on the above results and observations of trapped natural gas in the Pulaski B, as discussed below in Section 2.5.4.2.5.4.

Pulaski Formation - offshore

The results of in-situ permeability tests in Units A and B indicated horizontal permeabilities in the range from <1 x 10^{-6} cm/sec to 2 x 10^{-4} cm/sec with a typical value of about 1 x 10^{-5} cm/sec. The results of in-situ permeability tests in Unit C indicated horizontal permeabilities in the range from 3 x 10^{-7} cm/sec to 2 x 10^{-4} cm/sec, with a typical value of about 1 x 10^{-5} cm/sec.

Whetstone Gulf Formation - onshore

The results of in-situ permeability tests in the Whetstone Gulf Formation indicated horizontal permeabilities in the range from <1 x 10^{-6} cm/sec to 2 x 10^{-5} cm/sec with a typical value of about 1 x 10^{-6} cm/sec.

Whetstone Gulf Formation - offshore

The results of in-situ permeability tests in the Whetstone Gulf indicated horizontal permeabilities in the range from <1 x 10^{-6} cm/sec to 5 x 10^{-5} cm/sec with a typical value of about 1 x 10^{-6} cm/sec.

2.5.4.2.2 Project and Site Information

2.5.4.2.2.1 Horizontal and Vertical Survey Datum

Vertical control for the project is based on the National Geodetic Vertical Datum of 1929 (NGVD 29). Horizontal control is based on the Central Zone of the New York State Plane Coordinate System North American Datum of 1927 (NAD 27). NAD 27 was used instead of NAD 83 because NMP Unit 1 and Unit 2 were surveyed using NAD 27.

C. T. Male Associates of Syracuse, New York surveyed initial and as-built locations for all field explorations including borings, test pits, and geophysical locations.

2.5.4.2.2.2 Site Description

The project site (Figure 2.5-59) is owned by Constellation Energy and is bounded to the north by Lake Ontario, to the east by NMP Unit 1 and Unit 2, to the south by Lake Road and by Constellation Energy property south of Lake Road, and to the west by private property, including the Ontario Bible Camp. NMP Unit 1 is located about 3000 feet (914.4 m) east of NMP3NPP and NMP Unit 2 is located about 3600 feet (1097.3 m) east of NMP3NPP (Figure 2.5-59).

The site topography in the area of plant structures (Figure 2.5-60, Figure 2.5-61, Figure 2.5-62) is flat, ranging from approximately El. 280 (on the south) to El. 260 feet (on the north). At the lake shore there is a small bluff that drops from the site to lake level of approximately El. 245 feet (as measured at NOAA Station ID 9052030 in Oswego, New York, which is approximately 8 miles (13 km) west of NMP3NPP). Several areas of wetlands exist on the site. There is a wetlands area

with a small pond located in the northern third of the site; the ground surface elevation in the area around the pond is generally about El. 254.

The site is generally covered by uplands forest with some woody shrubs. Areas of the site that were cleared during the construction of NMP Unit 1 and Unit 2 are generally covered with grass and scattered shrubs.

The beach along the lakeshore consists of cobbles and small boulders with frequent outcrops of Oswego Sandstone. The shoreline is exposed to an open westerly fetch off of Lake Ontario that at times produces significant waves. There is on-going erosion of the bluff exposing glacial till soils along this section of the shoreline. The elevation of the lake bottom ranges from about El. 245 ft (75 m) at the shoreline to about El. 200 ft (61.0 m) at a distance of 1500 (460 m) feet from the shoreline. The bathymetry of the lake bottom in the area of the cooling water intake tunnels is shown in Figure 2.5-160 and Figure 2.5-167.

During the construction of NMP Unit 1 and Unit 2, two softball fields were constructed and fenced. While now abandoned, these two fields are still generally intact. A communications tower is located just north of Lake Road. A meteorological tower serving Units 1 and 2 is located just east of the northerly baseball field. A gravel road traverses the property from Lake Road northeast to the meteorological tower. A rifle firing range is located on the Constellation Energy property on the south side of Lake Road.

2.5.4.2.2.3 Project Description

The layout of the proposed nuclear station structures is shown in Figure 2.5-59. The limits of the safety-related structures, and foundation elevation data, are included on subsurface profiles presented in Figure 2.5-63 through Figure 2.5-67. The limits of the offshore cooling water intake tunnels are included on subsurface profiles presented in Figure 2.5-161 and Figure 2.5-162.

The elevations of the foundation elements shown on the profiles include final site grade of El. 270.

2.5.4.2.3 Subsurface Exploration And Field Testing

2.5.4.2.3.1 General

The major tasks included in the subsurface exploration and field testing program for the NMP3NPP site characterization are listed below:

- Perform subsurface investigations including 108 borings and 3 test pits.
- Install groundwater monitoring wells in 38 of the completed borings.
- Perform field permeability tests in soil and rock.
- Perform seismic refraction and down-hole geophysics.
- Perform offshore seismic refraction survey.
- Perform monthly groundwater elevation surveys.
- Perform an investigation of potential sources of structural fill.

2.5.4.2.3.2 Quality Assurance Program

The subsurface explorations and field testing were performed under the AREVA NP, Inc. Quality Assurance (QA) program.

Personnel were trained on applicable procedures, work plans, and work instructions. Training records were maintained that document completed training for each person working on the project.

Records for specific field and laboratory equipment that required calibration based on applicable QA procedures are maintained in the AREVA project files, and can be accessed on the AREVA Intranet site. The calibrated equipment used in the field and laboratory are identified on the field boring logs and test data forms.

Personnel maintained sample inventory records and chain of custody records to track the soil, rock, and groundwater samples from the field to the temporary storage facility at the site, and to the testing laboratories.

2.5.4.2.3.3 Basis of Subsurface Investigation

The borehole locations and depths were selected based on a geological and hydrological interpretation of the site using available literature, including the Updated Safety Analysis Report for NMP Unit 2 (CEG, 1998), and were chosen to comply with the guidance in NRC Regulatory Guide 1.132 (NRC, 2003a). Adjustments to the program were made during the investigation to ensure thorough site characterization.

The borings were all performed as safety-related work, and were divided into four series. The locations of the 100-series borings were chosen to characterize the local geology and hydrology around the perimeter of the reactor complex. The locations of the 200-series borings were chosen to characterize the geology and hydrology within the footprint of the reactor complex. The locations of the 300-series borings were chosen to characterize the geology and hydrology along the alignment of the proposed cooling water pipeline tunnel between the reactor complex and the pump house located on the edge of Lake Ontario. The locations of the 400-series borings were chosen to characterize the geology at the pump house and along the alignment of the offshore cooling water intake tunnels.

The depths of the borings were based on two primary criteria: the depth required for geotechnical borings (200-, 300-, and 400-series) by Regulatory Guide 1.132 (NRC, 2003a), and the need to characterize the geological and hydrological variation (100-series) over three geological units (the Oswego Sandstone, the Pulaski Formation, and the Whetstone Gulf Formation). The 100-series borings were initially planned to be 200 feet (61.0 m) deep. About one third of the 100-series borings were drilled deeper than 200 feet (61.0 m) to verify the rock conditions in the Whetstone Gulf Formation.

The number and placement of the 200- 300- and 400- series borings were dictated by the guidance in Regulatory Guide 1.132 (NRC, 2003a). The relevant guidance included:

- Generally, all borings should extend at least 33 (10.0 m) feet below the lowest part of the foundation.
- If competent rock is encountered at lesser depths … borings should penetrate at least 20 feet (6.1 m) into sound rock.

- Along tunnel alignments, borings to penetrate 20 feet (6.1 m) into sound rock or to a minimum of five times the tunnel diameter below the invert elevation.
- At least one boring beneath every safety-related structure.
- For larger heavier structures, such as the containment and auxiliary structures, one boring per 10,000 ft^2 (929 m^2).
- Approximately 100-foot (30 m) spacing.
- A number of borings around the periphery, at corners, and other selected locations.
- At least one-fourth of the principal borings and a minimum of one boring per structure to penetrate into sound rock.
- Other borings to a depth below foundation elevation equal to the width of the structure, or to a depth equal to the foundation depth below the original ground surface, whichever is greater.
- Supplemental borings that are design-dependent, or necessary to define anomalies, critical conditions, etc.

The purpose of each boring performed for this investigation is summarized in Table 2.5-54, along with applicable references to the NRC Regulatory Guide criteria.

2.5.4.2.3.4 Test Borings

General

Seventy-nine test borings were performed from August 14 through October 30, 2007. The borings were numbered B101 through B124, B201 through B243, and B301 through B315 (exclusive of B303, B309, and B310). B303 was eliminated after a change in pump house location made it not applicable. B309 and B310 were omitted to preserve consistency with a federal wetlands permit which controlled the NMP3NPP site investigations. The homogeneity of site bedrock and its horizontal bedding and layering suggest that the area between borings B308 and B311 is highly unlikely to contain conditions or significant buried features unsuitable for the intended constructions. The scope of site investigation using numerous borings was supplemented by a detailed geophysical investigation to support the basis for this conclusion. Omission of borings B309 and 8 310 deviates from Regulatory Guide 1.132 (NRC, 2003a) guidance relative to borehole spacing.

An additional 29 borings were performed from April 18 through June 30, 2008. The borings were numbered B401 through B441 (exclusive of B403, B418 – B427, and B430). Boring B403 and B430 could not be performed because they were located in shallow water along the shoreline of Lake Ontario that was not accessible to barge mounted drilling equipment. The homogeneity of site bedrock and its horizontal bedding and layering suggest that the area between borings B402 and B404 and between boring B429 and B431 is highly unlikely to contain conditions or significant buried features unsuitable for the intended constructions. The scope of site investigation using numerous borings was supplemented by a detailed geophysical investigation to support the basis for this conclusion. Omission of borings B403 and B430 deviates from Regulatory Guide 1.132 (NRC.2003a) guidance relative to borehole spacing.Borings B418 – B427 were eliminated when the length of the cooling water intake tunnels were shortened at the start of the field investigation. B402a and B428a were drilled at an angle of roughly 60 degrees from horizontal.

Groundwater monitoring wells were installed in 38 of the borings, including 17 borings that were drilled without sampling to install shallow groundwater monitoring wells. These shallow wells were typically installed as part of a couplet, adjacent to a deep monitoring well that was installed in a sampled borehole. Table 2.5-55 provides a summary of the monitoring well installations.

Three borings were drilled without sampling to install inclinometer casing for cross-hole geophysical work.

Boring logs for all borings, including those drilled without sampling, are presented in Part 11E. The subsurface conditions at borings drilled without sampling were adequately characterized because the unsampled borings were close to sampled borings.

An engineer or geologist was present during all drilling, sampling, in situ testing, and installation of monitoring wells and inclinometer casing.

The "as-drilled" locations of all borings were surveyed. The "as-drilled" boring locations are shown on Figure 2.5-60 through Figure 2.5-62 and Figure 2.5-160. The "as-drilled" boring coordinates are presented in Table 2.5-54.

Drilling and Sampling

Test borings were generally advanced with 4.25-inch (10.8 cm) inside-diameter hollow stem augers to the top of bedrock. A few borings (as indicated on the individual boring logs) were advanced to bedrock by either driving or spinning 4-inch (10 cm) diameter casing and then cleaning out the casing by rotary drilling with water. The drilling bits were provided with bottom deflectors to discharge drilling fluid toward the side of the hole. Standard Penetration Tests (SPTs) were performed below the bottom of the auger or casing, generally at 5-foot intervals, to obtain split spoon samples and to obtain information on the density or consistency of the soils. In some of the borings, continuous split spoon samples were obtained.

Split spoon samples were placed in plastic bags and then sealed in glass jars to retain their natural moisture content.

All soil samples were classified in the field by an engineer or geologist. Soil descriptions shown on the boring logs represent the field classification modified, if required, based on laboratory classification and test results. Photographs were taken of each soil sample.

At the conclusion of laboratory testing the soil samples were transported to a final project storage warehouse managed by UniStar at the existing NMPNS.

Rock coring was performed using diamond-bit NQ-size (3-inch-O.D., 2-inch-I.D.) (7.6-cm-O.D., 5.1-cm-I.D.), double-tube core barrels with solid inner barrels. The first core run at the top of bedrock was generally 5 feet (1.5 m) in length, although shorter runs were occasionally used. Subsequent core runs were typically 10 feet (3.0 m) in length. Cores were placed in wooden core boxes for transport and storage.

The field engineer or geologist described the rock cores in the field on the field boring log. An experienced geologist reviewed the rock cores independently and prepared a separate geologic log. A geologist photographed each rock core box. Final typed boring logs were prepared based on both field data and a subsequent detailed examination by a qualified geologist.

Borings drilled using the NQ core barrel, in which groundwater wells were to be installed, were reamed with a 4-inch-diameter (10-cm-dia) air hammer. Borings drilled without sampling for installation of shallow bedrock wells were drilled using a 4-inch-diameter (10-cm-dia) air hammer.

Borehole Verticality

Borehole verticality surveys were performed in six 200-series boreholes used for cross-hole testing. The maximum deviation from vertical was 5.5 feet (1.7 m) over a depth of 205 feet. The five other measured holes averaged about 2 to 3 feet (0.6 to 0.9 m) deviation from vertical over about 200 (61.0 m) foot depths.

Borehole verticality surveys were performed in all of the 400-series borings. The results of the borehole verticality surveys performed on the 400-series borings indicated deviations of between 0.6 ft to 9.9 feet (0.2 to 3.0 m) from vertical over depths of between 150 and 200 feet (46 and 61 m). The average deviation from vertical for the 400 series borings was 3.4 feet (1.0 m).

Further verticality surveys of borings beyond the six of the 200 series and all of the 400 series were not conducted because of the minimal vertical deviations observed in the six 200 and all 400 series borings; the presence of homogeneous, horizontally bedded and layered site bedrock formations which favor vertical drilling; and the absence of drilling rig mechanical feedback indicative of vertical deviations. This deviates from Regulatory Guide 1.132 (NRC, 2003a) guidance relative to determination of vertical deviation for boreholes greater than 100 feet.

Borehole Grouting

All test borings, except those in which monitoring wells or inclinometer casing were installed, were backfilled upon completion with a bentonite-cement grout. Where monitoring wells were installed in the borings, the boreholes were typically backfilled with bentonite chips below the sanded zone of the well. Above the sanded zone, the boreholes were backfilled outside the well riser pipes with bentonite-cement grout. Where inclinometer casings were installed in the borings for geophysical testing, the boreholes were backfilled outside the inclinometer casing with bentonite-cement grout, and the inclinometer casings were protected with a steel surface casing. A borehole grouting form was completed for each boring.

2.5.4.2.3.5 In-Situ Soil and Rock Testing

Standard Penetration Testing

Standard Penetration Tests (SPTs) were performed to obtain soil samples for visual identification and laboratory testing and to measure the penetration resistance of the soil.

Automatic hammers were used for all SPTs. The drive weights for each automatic hammer was weighed at the start and completion of the work to verify that each of the drive weights weighed 140 pounds ± 2 pounds (63.5 kg ± 0.9 kg) in accordance with ASTM standards. During the performance of the SPTs, the drop height of the drive weight was spot checked through a sight glass on the side of the automatic hammer. The spot checks confirmed that the drive weights were dropping 30 inches ± 1 inch in accordance with ASTM standards.

The split spoon samplers had 24-inch-long (61 cm) barrels with an I.D. of 1.5 inches (3.8 cm). Liners were not used.

Borehole Permeability Testing

Eighty-one water pressure (packer) tests were performed in 14 borings advanced on-shore in the area of Category I structures. Forty-two water pressure (packer) tests were performed in 13 borings advanced offshore along the alignment of the cooling water intake tunnels. The tests provide a measurement of the permeability of the rock. The results of the packer tests are discussed in section 2.5.4.2.1.9 and presented in Table 2.5-52 and Table 2.5-53.

Permeability Testing in Wells

Thirteen rising head permeability tests were performed in monitoring wells screened in rock, and five were performed in soil. The data from the rising head permeability tests supplements the data from the packer tests. The results of the rising head tests are discussed in section 2.5.4.2.1.9 and summarized in Table 2.5-51.

Geophysics

Three geophysical investigations were performed as part of site characterization studies:

- Weston Geophysical conducted a land-based seismic refraction survey.
- Weston Geophysical conducted a land-based cross-hole seismic survey.
- Ocean Surveys, Inc. conducted an offshore seismic refraction survey.

The purposes of the geophysical surveys were 1) to provide a means to locate any low-velocity zone of poor quality rock that might require special investigation, 2) to measure the shear wave velocity and compression wave velocity of the rock in the area of the plant, and 3) to measure the bathymetry and refraction properties of the bedrock beneath Lake Ontario in the area of the proposed cooling water tunnels. The results of the geophysical studies are discussed in section 2.5.4.4.

2.5.4.2.3.6 Groundwater Wells

Well Installation

Groundwater monitoring wells were installed in 38 borings. The monitoring well locations are shown in Figure 2.5-60, Figure 2.5-61, and Figure 2.5-62. The screened sections of the monitoring wells are shown relative to the safety related structures on Figure 2.5-63 through Figure 2.5-67 and Figure 2.5-161 and Figure 2.5-162. Table 2.5-55 provides a summary of the monitoring well installations at the NMP3NPP site.

The monitoring well locations and depths were selected based on our geological and hydrological interpretation of the site using available literature, including the Updated Safety Analysis Report for NMP Unit 2 (CEG, 1998), and were chosen to comply with the guidance in NRC Regulatory Guide 1.132 (NRC, 2003a).

Monitoring wells were installed in all of the 100-series borings and some of the 200-series borings. The 100-series wells were selected to characterize the local hydrology and groundwater quality outside the footprint of the reactor complex, but within the boundary of the site. At most locations, a shallow boring with a well screen in the Oswego Sandstone was paired with a deep boring with a well screened in the Pulaski or Whetstone Gulf Formations to measure potential vertical groundwater gradients. B102 and B103, B104 and B105, and B106 and B107 are located to the north (down-gradient) of the reactor complex. B110 and B111 are located to the southwest of the reactor complex. B112 and B113, B114 and B115, and B118 and B119 are located to the southeast (up-gradient) of the reactor complex. Single borings B101,

B108, B109, B116, and B117 were located between the paired borings. The 100-series borings were generally spaced 1,000 feet (300 m) apart, around the periphery of the site, with variation to account for accessibility and avoidance of jurisdictional wetlands where possible.

Five 100-series wells were installed to characterize the overburden groundwater in the building footprint. B120 to B124 were drilled through the soil, terminating at bedrock. These borings were used to construct shallow wells to measure the seasonal presence and level of groundwater in the areas to be excavated for the foundations of the reactor complex.

The 200-series well locations were selected to characterize the hydrology and groundwater quality within the footprint of the reactor complex. The location of the wells and the depth of the screened intervals were chosen to provide representative lateral coverage across the site within each of the three stratigraphic units (Oswego, Pulaski, and Whetstone Gulf) being characterized. The actual depths of the screened interval was adjusted in the field to be within the targeted formation and, in some cases, to be in zones of relatively high permeability based on observed jointing and on the results of water pressure (packer) tests.

Each monitoring well was constructed of 2-inch-diameter (5-cm-dia) schedule 40 PVC riser and machine-slotted (0.010 inch (0.025 cm) slot) screen. The lengths of the screened intervals varied, but were typically 10 to 20 feet (3 to 6 m). At least four inches (10 cm) of filter sand was placed in the borehole below the PVC well screen. The filter sand pack extended up to at least 1.5 feet (0.5 m) above the top of the well screen. A bentonite seal or zone of extra fine sand was placed above the filter sand in the annular space between the PVC riser and borehole wall. Bentonite/cement grout was then placed by tremie tube to the ground surface. Each well was finished with a lockable steel casing and concrete pad.

All groundwater monitoring wells were developed after installation was complete. In general, the monitoring wells were developed until two criteria were satisfied: (1) a minimum specified volume of water was removed and (2) the water being pumped from the well appeared relatively clear and free from fines.

Groundwater Elevation Monitoring

Depth to groundwater was measured in the monitoring wells monthly from September 2007 through August 2008. The measured depths were converted to elevations, and are presented in Table 2.5-56. A complete discussion of the groundwater conditions at the NMP3NPP site is presented in subsection 2.5.4.6, and in Section 2.4.12.

2.5.4.2.3.7 Test Pits

Three test pits were excavated to collect bulk soil samples for laboratory testing. The test pits were excavated on November 13 and 14, 2007. The test pit locations are shown in Figure 2.5-60 and Figure 2.5-62. The test pit locations were selected to encompass the potential variability of the natural soils geographically across the site.

2.5.4.2.3.8 Structural Fill Investigation

Sand and gravel samples were collected from three borrow pits. The borrow pits with potential for providing granular soil structural fill for plant construction were chosen based on their proximity to the site and potential for suitable material. The borrow pits are located within approximately 10 miles (16 km) of the site. The names and locations of the pits are:

1. Northern Aggregates, Inc., Baldwin Road, Volney, NY

2. Lindsey Aggregates, Inc., Bateman Road, Volney, NY

3. Streeter-Rathburn Pit (SR), Rathburn Road, Oswego, NY

The surficial geology at each pit is shown in the Table below:

Borrow Pit	Surficial Geologic Unit
Lindsey - Bateman	Lacustrine Beach
Northern	Lacustrine Sand
Streeter - Rathburn	Kame deposits

Three locations in each borrow pit were selected to obtain representative samples of potential structural fill. At each sampling location, a sufficient quantity of material was excavated to create a sampling pad approximately 15 feet long by 8 feet wide by 3 feet deep (4.6 m long by 2.4 m wide by 0.9 m deep). A sample of material was obtained from each sampling pad consisting of five 5-gallon (19 L) buckets. Particles of material that would not pass a 3-inch (7.6 cm) sieve were not included.

A grain size analysis was performed on structural fill from each pad (9 pads total). The results of the grain size analysis are shown in Table 2.5-44.

The results of the grain size analysis tests indicated that all three pits contained sand and gravel mixtures that would be suitable for use as structural fill because they satisfied the criteria of being widely graded and containing less than 10 percent fines. The SR pit was selected as most suitable based on it's having a lower percentage of oversize material (cobbles and boulders) than the Lindsey-Bateman pit, and a smoother grain size curve (which is preferred for structural fill) than the Northern pit. From discussions with the pit owner we understand that there are over 200,000 cubic yards (150,000 cubic meters) of material available at the pit. Based on these considerations, the Streeter Rathburn Pit was selected for triaxial testing to measure friction angle. The results of the triaxial tests were discussed previously in section 2.5.4.2.1.2.

2.5.4.2.4 Laboratory Testing

2.5.4.2.4.1 General

The laboratory testing program for the NMP3NPP Site Characterization project consisted of the following:

- Index testing on split spoon samples of soil.
- Compaction and static triaxial strength testing on bulk samples of glacial till and structural fill.
- Dynamic properties testing on bulk samples of glacial till and structural fill.
- Corrosivity testing on bulk samples of glacial till and structural fill.
- Kd testing of soil and structural fill.
- Unit weight, unconfined strength, modulus, and Poisson's ratio testing on rock core samples
- Dynamic properties testing on rock core samples.
- Petrographic analysis of rock core specimens.

The laboratory test program performed for NMP3NPP sufficiently characterized the various soils encountered during the field drilling program, their degree of variability, and their range of index properties, as required by Regulatory Guides 1.132 and 1.138 (NRC, 2003a, NRC 2003b).

2.5.4.2.4.2 Index Tests on Split Spoon Samples of Soil

At the completion of the field investigation and sampling program all split spoon soil samples were transported to the GEI soils laboratory in Woburn, Massachusetts. A GEI laboratory technician inventoried all the soil samples and prepared a table that summarized the sampling information, number of jars of soil for each split spoon sample, and the weight of the soil collected for each sample.

A plan for laboratory testing for samples was based a review of the field boring logs and a sample information summary. Soil samples were selected for laboratory testing to satisfy the following objectives:

- To characterize the different soil types encountered in the borings.
- To collect data to assign index properties to the soils encountered in the borings.
- To observe if there was more than one major glacial soil layer present at the site.
- To check the accuracy and consistency of field soil descriptions on the boring logs.

Based on the above stated objectives GEI performed the following laboratory index tests:

- 33 grain size tests
- 17 Atterberg limit tests
- 6 specific gravity tests
- 35 water contents

The tests were performed on 37 samples:

- Glacial till: 30 samples obtained at various locations and depths around the site.
- Surficial soil: 5 samples obtained in and near wetland areas.
- Fill: 2 samples obtained from the central ball field area.

The test results are summarized in Table 2.5-43.

2.5.4.2.4.3 Tests on Bulk Soil Samples of Glacial Till and Structural Fill

The following tests were performed on bulk samples of glacial till and structural fill:

- 9 grain size tests
- 1 specific gravity test
- 2 modified compaction tests

- 4 consolidated undrained triaxial compaction tests with pore pressure measurement

Tests were performed on bulk samples of glacial till collected from test pits excavated on site and on bulk samples of Structural Fill collected from the potential borrow pit sources. Results of grain size analysis and specific gravity tests performed on structural fill are summarized in Table 2.5-44. The results of a compaction test on Structural Fill is presented in Figure 2.5-157. The results of consolidated undrained triaxial compression tests are presented in Figure 2.5-155, Figure 2.5-156, Figure 2.5-158, and Figure 2.5-159.

Tests were performed according to laboratory procedures based on ASTM standards. Triaxial tests were performed on specimens compacted in the laboratory to unit weights approximating field conditions. Specimens were back pressure saturated until a B-value of at least 0.95 was achieved. Specimens were then sheared using transducers to measure pore pressures during the test.

Test results are discussed in Section 2.5.4.2.1.2.

Glacial Till Testing. Disturbed samples of glacial till were obtained from the split spoon samples in the borings as discussed in Section 2.5.4.2.3.5. Bulk disturbed samples of glacial till were obtained from three test pits as discussed in Section 2.5.4.2.3.7. Attempts were made to obtain undisturbed tube samples, but the attempts were not successful because the glacial till was too dense and the gravel content was too high.

Samples from the borings were used for gradation testing, specific gravity testing, water content testing, and Atterberg limits testing as presented in Table 2.5-43.

Bulk samples from the test pits were used for grain size and triaxial testing as follows. One bulk sample of glacial till was collected from each test pit. Each of the three samples consisted of three 5-gallon (19-liter) buckets. For each of the three samples, all three of the buckets were mixed thoroughly in the laboratory on a sheet of plastic and spread into a circle. The circle was then divided into quarters. Two opposite quarters were mixed together for grain size testing and triaxial testing. The material for grain size testing was air-dried, and then the grain size test was performed. Material not used for the grain size test was used for triaxial testing.

The results of the grain size tests on the glacial till samples from the test pits are presented below.

		Grain Size Data		
Test Pit	Water Content (%)	Gravel (%)	Sand (%)	Fines (%)
TP 101	6.9	27.4	38.1	34.5
TP 102	7.7	11.7	39.7	48.6
TP 103	7.1	22.5	40.0	37.5

Two consolidated undrained triaxial compression tests were performed to measure the strength properties of the glacial till. The tests followed approved project procedures based on ASTM standards. Both tests were performed on till from Test Pit 102 located near the center of the site. The grain size distribution of that sample is generally representative of the till across the site as indicated in Table 2.5-43.

Because undisturbed samples of the till could not be obtained, it was necessary to prepare remolded, compacted specimens for triaxial compression testing. Particles larger than 3/8-inch

were screened out before preparing the triaxial specimens. Test specimens 6.3 inches (16 cm) high were compacted inside a 2.9-inch-dia (7.3-cm-dia) mold in eight lifts of equal height and weight.

The triaxial test specimens were compacted to a unit weight less than the expected in situ unit weight, to provide a conservative estimate of the strength of the till. As described in Section 2.5.4.2.1.1, the design value of in situ glacial till unit weight is 140 lb/ft^3 (21,980 N/m^3) moist and 145 lb/ft^3 (22,770 N/m^3) saturated. The actual saturated unit weights of the two triaxial test specimens, after consolidation and before shearing, were 135 lb/ft^3 (20,410 N/m^3) and 131 lb/ft^3 (20,570 N/m^3).

The effective isotropic consolidation pressure applied to each triaxial test specimen before shearing was 1 kg/cm^2 (2000 psf).

After being set up in the triaxial cell the specimens were backpressure saturated until a B-value of at least 0.95 was achieved, indicating full saturation. The specimens were sheared at a constant strain rate while load, deformation, and pore pressure were recorded.

The triaxial test data are presented in Figure 2.5-155 and Figure 2.5-156. The triaxial tests indicated a peak effective friction angle, phi, of 38.2 degrees and a cohesion of zero for R'1, and a peak effective friction angle of 38.4 degrees and a cohesion of zero for R?2. These values are conservatively low compared to the field condition because the tested specimens had a maximum particle size of 3/8 inch (10 mm) while the glacial till in the field will include larger gravel sizes, and because the triaxial specimens were compacted to a lower unit weight than the in situ unit weight. To add additional conservatism, and to account for potential variability of the glacial till in the field, a lower effective friction angle, phi, of 36 degrees is selected for the glacial till for design, with a cohesion of zero.

Structural Fill Testing. Selection and sampling of the structural fill borrow pits is discussed in Section 2.5.4.2.3.8. Three samples of structural fill were obtained at each of the three borrow pits (total of nine samples). Each of the nine samples consisted of five 5-gallon (19-liter) buckets.

For each of the nine samples, all five of the buckets were mixed thoroughly in the laboratory on a sheet of plastic and spread into a circle. The circle was then divided into quarters. Two opposite quarters were mixed together for compaction testing. The two remaining quarters were mixed together and used for grain size and other testing. The grain size portion of each sample was air-dried, and the grain size test was performed. Material not used for the grain size test was used for triaxial and specific gravity testing.

The results of the grain size analyses are presented in Figure 2.5-192, Figure 2.5-193, and Figure 2.5-194, and are summarized in Table 2.5-44.

The results of the grain size analyses indicated that all three borrow pits contained sand and gravel mixtures that would be suitable for use as structural fill because they satisfied the criteria of being widely graded and containing less than 10 percent fines. The Streeter-Rathburn pit was selected as most suitable based on its having a lower percentage of oversize material (cobbles and boulders) than the Lindsey-Bateman pit, and a smoother grain size curve (which is preferred for structural fill) than the Northern pit.

A compaction test was performed on the Streeter-Rathburn pad 1 sample in accordance with approved project procedures based on ASTM D 1557 (Standard Test Methods for Laboratory Compaction Characteristics of Soil Using Modified Effort (56,000 ft-lbf/ft3 (2,700 kN-m/m3)).

The measured maximum dry unit weight (minus ¾-inch fraction) was 130.4 pcf (20,470 N/m^3). The optimum water content corresponding to the maximum dry unit weight was 9.0%. This test is considered representative of the structural fill from all three pits because the grain size curves were all similar. Variation in the structural fill actually delivered for use is identified by testing during construction, as described in Section 2.5.4.5.3.3.

To obtain unit weight values for design, the dry unit weight and corresponding water content from the compaction test were adjusted to account for gravel larger than 3/4-inch size, for dry vs. moist vs. saturated conditions, and for compaction to 97% of maximum dry density (a conservative value based on specified compaction of 95%). The resulting adjusted values are used for design purposes for the unit weight of structural fill, as follows:

Dry Unit Weight: 134.7 pcf (21,150 N/m^3)

Moist Unit Weight: 143.9 pcf (22,590 N/m^3)

Saturated Unit Weight: 147.2 pcf (23,110 N/m^3)

These unit weights represent the maximum values of unit weight of the structural fill.

Two consolidated undrained triaxial compression tests were performed to measure the strength properties of the structural fill. The tests were performed on the Streeter Rathburn pad 1 sample in accordance with approved project procedures based on ASTM standards. Because the structural fill samples were collected as bulk samples, it was necessary to prepare a remolded, compacted specimen for triaxial compression testing.

The test specimens were obtained from the Streeter Rathburn pad 1 sample. Particles larger than 3/8-inch were screened out before preparing the triaxial specimens. Test specimens 6.3 inches (16 cm) high were compacted inside a 2.9-inch-dia (7.3-cm-dia) mold in eight lifts of equal height and weight.

As reported above, the maximum dry unit weight of the minus ¾-inch fraction of the Streeter Rathburn pad 1 sample is 130.4 pcf (20,470 N/m^3) (as measured in the compaction test). The calculated maximum dry unit weight of the minus 3/8-inch fraction of the Streeter Rathburn pad 1 sample is 121.9 pcf (19,140 N/m^3). The triaxial test was performed to approximate the soil density and in situ stress conditions that would be expected of compacted backfill placed during construction. Thus, the target dry unit weight of the test specimen as compacted in the laboratory was 95 percent (+/- 0.5%) of the maximum dry unit weight of the minus 3/8-inch fraction. This corresponds to a target test specimen dry unit weight range of 115.2 to 116.4 pcf (18,090 to 18,270 N/m^3), computed as follows:

Low end of target range = 0.945 x 121.9 pcf (19,140 N/m^3) = 115.2 pcf (18,090 N/m^3)

High end of target rage = 0.955 x 121.9 pcf (19,140 N/m^3) = 116.4 pcf (18,270 N/m^3)

The target effective confining stress for each triaxial test was 1800 psf (0.9 kg/ cm^2) ± 15%. This target effective confining stress corresponds to the effective vertical stress at a depth of 18 feet (5.5 m) of backfill, where the top 5 feet (1.5 m) are unsaturated and the bottom 13 feet (4 m) are saturated by groundwater (i.e., the groundwater table is located at a depth of 5 feet (1.5 m)). This stress was selected to be conservative over the range of expected thicknesses of backfill and groundwater conditions that may be present around the safety-related structures.

The actual effective isotropic confining stress applied to each triaxial test specimen prior to shearing was 1 kg/cm^2 (2000 psf), which falls within the target range.

The actual compacted dry unit weights of the triaxial test specimens were 116.2 pcf (18,240 N/m^3) for R?1 and 115.4 pcf (18,120 N/m^3) for R?2, which are both within the target range. After backpressure saturation and isotropic consolidation to the effective confining stress of 1 kg/cm^2 (2000 psf), the dry unit weights were 121.5 pcf (19,080 N/m^3) for R?1 and 118.5 pcf (18,600 N/m^3) for R?2.

After being set up in the triaxial cell the specimens were backpressure saturated until a B-value of at least 0.95 was achieved, indicating full saturation.

The specimens were sheared at a constant strain rate while load, deformation, and pore pressure were recorded.

The triaxial test data are presented in Figure 2.5-158 and Figure 2.5-159. The triaxial tests indicated a peak effective friction angle, phi, of 39.1 degrees and a cohesion of zero for R?1, and a peak effective friction angle of 37.8 degrees and a cohesion of zero for R?2. These values are conservatively low compared to the field condition because the tested specimens had a maximum particle size of 3/8 inch (10 mm) while the structural fill in the field will include larger gravel sizes. To add additional conservatism, and to account for potential variability of the structural fill in the field, a lower effective friction angle, phi, of 35 degrees is selected for the structural fill for design, with a cohesion of zero.

2.5.4.2.4.4 Dynamic Properties Tests on Bulk Soil Samples of Glacial Till and Structural Fill

Resonant column cyclic torsional shear tests (RCTS) were performed on bulk samples of glacial till collected from test pits excavated on-site and on bulk samples of Structural Fill collected from the borrow pit.

The test results are discussed in Sections 2.5.4.2.1.3 and 2.5.4.3.1.4.

2.5.4.2.4.5 Soil and Groundwater Testing for Corrosivity

Sampling and Testing Parameters

Seven soil samples were obtained for chemical testing for corrosion potential from three test pits on site and from the Streeter-Rathburn gravel pit. One sample was collected from each test pit (TP101, TP102, TP103), and four samples were collected from the Streeter-Rathburn gravel pit (SR). The samples from the test pits consisted of glacial till. The samples from SR were structural fill. The chemical testing on soil samples for corrosion potential includes testing for chlorides, sulfates, and pH. The results of these chemical tests are shown in Table 2.5-57.

Ten groundwater samples were collected from 10 different wells installed across the site. Five of the wells are shallow, and screened in soil (B120(MW) through B124(MW)). The five other wells are deeper, and are screened in bedrock (B107(MW), B11(MW), B202(MW), B217(MW), and B236(MW)). The chemical testing on groundwater samples for corrosion potential includes chlorides, sulfates, sulfides, and pH. The results of these chemical tests are shown in Table 2.5-58.

Results of Chemical Testing

Guidelines for soil and groundwater parameters that are potentially corrosive for concrete and reinforcing steel are shown in Table 2.5-59. According to ACI 318, Building Code Requirements

for Structural Concrete (ACI, 2005), sulfate concentrations in water of 0 – 150 ppm are considered negligible towards corrosion. Eight of the ten groundwater samples have concentrations within this range. Two groundwater samples have concentrations in the range 150 – 1500 ppm, which is considered moderately corrosive. B121(MW) has a concentration of 190 ppm, and B122(MW) has a concentration of 240 ppm. These two concentrations are very close to the lower limit of moderate corrosion potential. ACI 318 also defines corrosion potential based on water-soluble sulfates in soil. Sulfate concentrations of 0.00 – 0.10% by weight are considered negligibly corrosive. All of the soil samples have sulfate concentrations that fall within this range.

Soil or water with a pH in the range of 4.5 to 9.5 is considered to have a low corrosion potential for reinforcing steel. Nine of the ten groundwater samples have a pH that falls in this range. The groundwater sample from B107(MW) has a pH of 12.2, which could be considered highly corrosive. Each of the soil samples has a pH that falls within the low corrosion potential range.

Selection of cement for construction should consider the results of these chemical tests.

2.5.4.2.4.6 Kd Testing of Soil and Structural Fill

Five samples were obtained for Partitioning Coefficient (K_d) analyses. Three glacial till samples were obtained, one representative sample from each of the bulk samples from test pits TP101, TP102, and TP103. Two representative structural fill samples were obtained from the Streeter-Rathburn gravel pit.

Samples were spiked with the following isotopes: Sr-90, Fe-55, Mn-54, Co-60, Zn-65, Ru-106, Cs-134, and Cs-137. K_d was determined according to ASTM D4646-03 Standard Test Method for 24-h Batch-Type Measurement of Contaminant Sorption by Soils and Sediments (ASTM, 2003).

2.5.4.2.4.7 Unit Weight, Unconfined Compression, Modulus, and Poisson's Ratio Measurement on Rock

Unit weight, unconfined compression, modulus, and Poisson's ratio tests were performed in accordance with procedures based on ASTM standards.

Samples were selected for testing to encompass the potential variability of the rock both geographically across the site and with depth. Tests were performed to obtain representative properties for each of the major rock units (Oswego Sandstone, Pulaski Formation, and Whetstone Gulf Formation).

The selection of rock samples for testing was based on an understanding of the geology beneath the site developed during the boring program, and was guided by the following criteria:

- Obtaining typical samples spread across the area of the reactor complex to address lateral variability of properties.
- Obtaining typical samples at various depths to address vertical variability of properties, with particular emphasis on sampling below the bottom slab elevation of safety-related structures.
- Obtaining typical samples within the tunnel zone of the offshore cooling water intake tunnels.

- Obtaining typical samples at the vertical shafts for the offshore cooling water intake tunnels.

The results from tests on rock core samples collected from borings performed onshore within the footprint of Seismic Category I structures at the NMP3NPP site are presented in Table 2.5-45 and Table 2.5-46. The results from tests on rock core samples collected from borings performed offshore along the alignment of the cooling water intake tunnels are presented in Table 2.5-47 and Table 2.5-48.

Measurements needed to obtain modulus and Poisson's Ratio values were obtained by attaching strain gauges directly to the rock core specimens, and recording both vertical and lateral strain during shear.

2.5.4.2.4.8 Dynamic Properties Tests on Rock

Unconfined Free-Free Resonant Column laboratory tests were performed on 14 rock core specimens:

Samples were selected for testing from borings performed within the footprint of the reactor building. Tests were performed to obtain representative properties for each of the major rock units (Oswego Sandstone, Pulaski Formation, and Whetstone Gulf Formation). Test results are presented in Table 2.5-60 . A discussion of the test results is presented in Section 2.5.4.2.1.8.

Unconfined, free-free, resonant column (URC) tests were performed on 14 samples of rock collected during the NMP3NPP site characterization. URC tests were performed on rock from each formation. Three tests were performed on rock from the Oswego Sandstone Formation (including Oswego Transition Zone), five tests were performed on rock from the Pulaski Formation, and seven tests were performed on rock from the Whetstone Gulf Formation. The samples were selected from the rock cores collected from Borings B224 and B226. Boring B224 is located in the approximate center of the reactor, and boring B226 is also located within the footprint of the reactor (approximately 60 ft away from B224).

2.5.4.2.4.9 Petrographic Analysis

Fourteen samples from five boreholes were selected for petrographic analysis. At least one sample was taken from each geological unit: Oswego Sandstone, Oswego Transition Zone, Pulaski Formation Units A through C, and Whetstone Gulf Formation. The samples selected provided for a lateral and vertical representation of geologic units encountered while drilling. In addition, two samples from B207 and B238 (MW) targeted the green marker bed seen in several borings.

The results of the petrographic analyses are presented in Table 2.5-62.

2.5.4.2.5 Subsurface Conditions – Onshore (Nuclear Island and Pump House)

2.5.4.2.5.1 Soil and Rock Profiles

The minor amount of fill, the natural soils, and the bedrock encountered in the borings are described in the following paragraphs in order of increasing depth. The elevations of the top of the soil and bedrock layers encountered in the borings are presented in Table 2.5-41. Subsurface profiles at the locations of structures and along the alignment of the cooling water intake pipeline are presented in Figure 2.5-63 through Figure 2.5-67. Elevation contours of the top of the Oswego Sandstone (top of bedrock) and the top of the Pulaski Formation are presented in Figure 2.5-68and Figure 2.5-69.

2.5.4.2.5.2 Soil Descriptions

Fill

Fill was encountered at the ground surface in 11 of the 59 sampled land borings and ranged in thickness from 4 to 13.5 feet (1.2 to 4.1 m). Fill was encountered within a limited area in the borings located on and around the southern ball field (the area on the south side of the proposed reactor building) and in one boring advanced near the firing range (B116). Fill generally consisted of varying amount of silts, sands, and gravels with cobbles and boulders. Typically, the upper 6 to 12 inches (15 to 30 cm) of the fill layer was finer grained and had some organic material.

Soils were characterized as fill based on a higher quantity of cobbles and boulders, variability of SPT blowcounts, and the general surficial topography around the boring location. NMP Unit 1 and Unit 2 personnel indicated that rock fill from the construction of NMP Unit 2 might have been used to fill the area of the southern ball field. In general, we did not observe foreign matter or construction debris in the soils characterized as fill.

Surficial Deposits

Surficial deposits were encountered in 38 of the 59 sampled land borings at the ground surface and ranged in thickness from 0.5 to 10.6 feet (0.2 to 3.2 m). Surficial deposits can be broken down into two categories: topsoil and fine-grained soil near wetland areas.

The topsoil typically consisted of silty sand to sandy silt with varying amounts of organics and gravel. The topsoil was encountered throughout the site and typically ranged from 0.5 to about 2 feet (0.2 to 0.6 m) thick.

Fine grained soils were encountered to depths of up to 10.6 feet (3.2 m) in areas near wetlands to the north of the proposed reactor complex. These soils were typically observed in the 300-series borings that were performed along the proposed water intake alignment between the pump house and the nuclear island. The fine grained soils generally consisted of low plasticity silts and clays with varying amounts of sand and gravel. Occasional layers or pockets of organic materials were observed in these fine grained soils to depths of up to 10 feet (3.0 m).

Glacial Till

Glacial till was encountered at the ground surface in 10 of the 59 sampled borings, and was encountered below fill or surficial deposits in 45 of the 59 sampled borings. Where encountered, glacial till extended down to the top of bedrock. Glacial till was not encountered in four borings. In those four borings, the fill or surficial deposits extended to bedrock. The glacial till ranged in thickness from 2.1 to 21.3 feet (0.6 to 6.5 m) thick, but was typically between 5 and 15 feet (1.5 to 4.6 m) thick. The glacial till typically consisted of silty or clayey sand with gravel, with occasional cobbles and boulders. The results of grain size tests performed on glacial till samples indicated a widely graded soil with between 20 and 60% fines (passing the # 200 sieve). Atterberg limits tests performed on glacial till samples indicated the plasticity ranged from non-plastic to low plasticity. SPTs performed in the borings typically indicated a medium dense to very dense soil. Many of the SPTs encountered refusal on cobbles and boulders.

The upper portion of the glacial till layer was typically a light brown to tan color and the lower portion was light to dark gray. The grain size test results and the field classifications indicate that the gradations of the two different colored till soils are similar. The color difference appears to be related to site groundwater levels and the long-term degree of saturation of the soils.

Based on the descriptions of glacial till at NMP Unit 2 contained in CEG (1998), the brown and gray till at NMP3NPP is similar to the brown and gray till at NMP Unit 2

2.5.4.2.5.3 Rock Descriptions

General

The top of bedrock encountered in the borings varied between El. 283.2 ft (86.3 m) and El. 238.4 ft (72.7 m). The top of bedrock is highest in the southern portion of the site near the Strike Road and drops to the north-northwest towards Lake Ontario. Contours of the top of the Oswego Sandstone (top of bedrock) are presented in Figure 2.5-68.

Bedrock was cored with NQ coring equipment. Rock recoveries in the core runs were almost all greater than 90%, and often were 100%. Instances of low recoveries (less than 90%) were rare and may have been due to coring techniques that had not been adjusted to changes in rock quality or to rock core jamming in the core barrel.

Rock Quality Designation (RQD) was measured for all rock core samples. The RQD values are reported on the boring logs. In general, RQD values of the bedrock cored for this project were above 80%, indicating high quality rock.

The bedrock formations encountered in the borings were:

- Oswego Sandstone (including the Oswego Transition Zone at the base)
- Pulaski Formation (subdivided into Units A, B, and C)
- Whetstone Gulf Formation

All of these formations consist primarily of flat-lying sandstone, siltstone, and shale. The boundary between units is often gradational, and the units are lithologically similar. The engineering properties of all the units are also similar.

Oswego Sandstone

The Oswego Sandstone ranged in thickness from 29 to 79 feet (8.8 to 24.1 m) with typical thicknesses of about 45 to 60 feet (13.7 to 18.3 m). The Oswego Sandstone consisted of hard, fresh to slightly weathered, unfossiliferous, greenish-gray, fine to medium grained, massive to cross-bedded sandstone. Thin dark gray siltstone and shale beds were minor and siltstone clasts were common. The sandstone was typically composed of subangular to subrounded quartz grains, sometimes with well-rounded lithic fragments, feldspar crystals, and a clay matrix.

The lower portion of the Oswego Sandstone has been informally designated as the Oswego Transition Zone (CEG, 1998a). This sub-unit was found to range from 9 to 60 feet (2.7 to 18.3 m) thick in the borings with typical thicknesses of 15 to 30 feet (4.5 to 9.1 m). The Oswego Transition Zone consists of medium hard to hard, slightly weathered to fresh, alternating, laminated to thickly bedded, fine to medium-grained sandstone, argillaceous sandstone, and siltstone. Trace fossils are present. There is a general trend toward bed thinning and increasing clay content, downward through the sub-unit. A 3- to 12-inch-thick (7.6 to 30.5 cm) shale bed was often noted near the base of the Oswego Transition Zone.

Pulaski Formation

The Pulaski Formation was approximately 100 feet (30.5 m) thick at the NMP3NPP site. Elevation contours of the top of the Pulaski Formation are presented in Figure 2.5-69.

The Pulaski Formation was informally subdivided into Units A, B, and C during the investigation for NMP Unit 2 (CEG, 1998). Each unit was typically in the range of 20 to 35 feet (6.1 to 10.7 m) thick at the NMP3NPP site. All three units consisted of interbedded sandstone, siltstone, and shale. The relative amount of siltstone and shale increased in the lower portions of the Pulaski Formation. All three units contained marine fossil shell debris.

Unit A is the uppermost unit and consisted of slightly weathered, medium hard, dark gray argillaceous sandstone interbedded with light gray sandstone and a few beds of dark gray shale and siltstone. Unit A had abundant marine fossil debris and disturbed bedding layers indicating soft sediment deformation. A distinctive 1/2-inch to 2-inch-thick (1.3 to 5.0 cm) green layer of smectite and chlorite was noted near the base of Unit A or near the top of Unit B in many of the borings.

Unit B consisted of slightly weathered, medium hard, interbedded light gray sandstone, dark gray siltstone, and shale. Unit B had relatively more sandstone than Unit A and relatively less fossil debris than Unit A.

Unit C consisted of slightly weathered, medium hard dark gray siltstone and shale, interbedded with light gray sandstone. Unit C was darker and had more siltstone and shale than Units A and B.

Whetstone Gulf Formation

The Whetstone Gulf Formation is estimated to be approximately 770 feet (234.7 m) thick at the NMP3NPP site. Seventeen of the borings extended into the Whetstone Gulf Formation. The deepest boring (B101) extended to a depth of 255 feet (77.7 m), which penetrated 73 feet (22.3 m) into the Whetstone Gulf Formation.

The top of the Whetstone Gulf Formation is lithologically very similar to the Pulaski C. The differentiation among the formations is made in the literature based on the types of fossils in the rock (New York State, 1970a). The Whetstone Gulf Formation was informally subdivided into Units A and B during the investigation for NMP Unit 2 (CEG, 1998). The upper unit (Unit A) consisted of dark gray siltstone and shale with occasional light gray sandstone beds. The lower unit (Unit B) consisted of siltstone and shale interbedded with sandstone. Sandstone interbeds became more common in Unit B. One boring for NMP3NPP (B102) penetrated through Unit A into the top of Unit B. In B102, Unit A was observed to be 60 feet (18.3 m) thick.

2.5.4.2.5.4 Natural Gas Observations

Natural gas was encountered in at least 17 onshore borings. In general, gas was detected by either visual observations of drill water bubbling or being forced out of the drill casing under pressure or by measurement with a hand held gas multi-meter. The borings, depths, and rock formations where gas was observed are presented in Table 2.5-62. Gas was typically encountered between El. 150 ft (45.7 m) and El. 118 ft (36.0 m), which corresponds to the elevation range of the Pulaski Formation, Unit B.

Natural gas is present in many areas of central and western New York (CEG, 1998). It is not considered significant to the design of NMP3NPP because it was encountered at depths more than 60 feet (18.3 m) below the proposed deepest foundation mats.

2.5.4.2.6 Subsurface Conditions – Offshore (Cooling Water Intake Tunnels)

2.5.4.2.6.1 Soil and Rock Profiles

Geologic conditions along the alignment of the cooling water intake tunnels are consistent with conditions observed in the onshore borings except that there is a general lack of soil overlying the bedrock offshore. Subsurface profiles along the alignment of the cooling water tunnels are presented in Figure 2.5-161 and Figure 2.5-162.

2.5.4.2.6.2 Soil Descriptions

Sediment

Sediment was encountered at the lake bottom in 12 of the 25 offshore borings, and ranged in thickness from 0.5 to 3.2 feet (0.2 to 1.0 m). Sediment generally consisted of varying amounts of silts, sands, and gravel derived primarily from weathered Oswego Sandstone and glacial till. Sediments accumulated in minor depressions in the lake bottom. This is consistent with the data from the offshore geophysical investigation discussed in Section 2.5.4.4.2.

2.5.4.2.6.3 Rock Descriptions

General

The top of the bedrock encountered in the borings varied between El. 243.9 ft (74.3 m) and El. 203.8 ft (62.1 m). The top of bedrock is highest near the shoreline and drops gradually away from the shoreline into Lake Ontario.

Offshore rock formations and offshore rock quality are similar to that observed in the onshore borings.

Rock quality designation (RQD) values for each core run are reported on the boring logs. In general, RQD values of the bedrock cored for this project were above 80%, indicating high quality rock.

Fractures with northwest and east-northeast strikes were observed in bedrock outcrops. These fractures are generally nearly planar, and are approximately vertical (normal to the bedding).

The angles of fractures in rock cores, and descriptions of the fracture surfaces, are described in the boring logs. Fractures were generally planar and horizontal (parallel to the bedding), although occasional vertical and angled fractures were also encountered. The inclined and vertical fracture surfaces often contained calcite and sulfide mineralization.

The rock provides adequate foundation support for structures. The relationship of RQD and fracturing to bearing capacity and settlement are discussed in sections 2.5.4.10.1 and 2.5.4.10.2 respectively.

The rock is suitable for tunneling in terms of rock strength, fracturing, and potential water inflow during construction.

Oswego Sandstone

The Oswego Sandstone encountered in the offshore borings ranged in thickness from 0 to 19 feet (0 to 5.8 m) with typical thicknesses of about 8 to 17 feet (2.4 to 5.2 m). The sandstone layer thins and eventually pinches out at approximately 850 ft (259.1) from the shoreline.

The lower portion of the Oswego Sandstone has been informally designated as the Oswego Transition Zone (CEG, 1998). This sub-unit was found to range from 0 to 26 feet (0 to 7.9 m) thick in the borings with typical thicknesses of 13 to 19 feet (4.0 to 5.8 m).

Pulaski Formation

The Pulaski Formation was approximately 80 to 90 feet (24.4 to 27.4 m) thick as encountered in the offshore borings at the NMP3NPP site. The Pulaski Formation was informally subdivided into Units A, B, and C during the investigation for NMP Unit 2 (CEG, 1998). Each unit encountered in the offshore borings was typically in the range of 20 to 35 feet (6.1 to 9.1 m) thick. All three units consisted of interbedded sandstone, siltstone, and shale. The relative amount of siltstone and shale increased in the lower portions of the Pulaski Formation. All three units contained marine fossil shell debris.

Unit A is the uppermost unit and consists of slightly weathered, medium hard, dark gray argillaceous sandstone interbedded with light gray sandstone and a few beds of dark gray shale and siltstone. Unit A has abundant marine fossil debris and disturbed bedding layers indicating soft sediment deformation. A distinctive 1/2-inch to 2-inch-thick (1.3 to 5.1 m) green layer of smectite and chlorite was noted near the base of Unit A or near the top of Unit B in many of the borings.

Unit B consists of slightly weathered, medium hard, interbedded light gray sandstone, dark gray siltstone, and shale. Unit B has relatively more sandstone than Unit A and relatively less fossil debris than Unit A.

Unit C consists of slightly weathered, medium hard dark gray siltstone and shale, interbedded with light gray sandstone. Unit C is darker and had more siltstone and shale than Units A and B.

Whetstone Gulf Formation

The Whetstone Gulf Formation is estimated to be approximately 770 feet (234.7 m) thick at the NMP3NPP site (NRC, 2003a). The deepest 400 series boring (B401) extended to a depth of 249 feet (75.9 m), which penetrated 85.5 feet (25.9 m) into the Whetstone Gulf Formation.

The top of the Whetstone Gulf Formation is lithologically very similar to the Pulaski C. The differentiation among the formations is made in the literature based on the types of fossils in the rock (NRC, 2003a). The Whetstone Gulf Formation was informally subdivided into Units A and B during the investigation for NMP Unit 2 (CEG, 1998). The upper unit (Unit A) consists of dark gray siltstone and shale with occasional light gray sandstone beds. The lower unit (Unit B) consists of siltstone and black shale interbedded with sandstone. Sandstone interbeds become more common and siltstone clasts became more angular in Unit B.

2.5.4.2.6.4 Natural Gas Observations

Natural gas was encountered in at least six offshore borings. In general, gas was detected by either visual observations of drill water bubbling or being forced out of the drill casing under pressure or by measurement with a hand held gas multi-meter. The borings, depths, and rock formations where gas was observed are presented in Table 2.5-63. Gas was typically encountered between El. 180 and El. 149, which corresponds to the elevation range of the Pulaski Formation, Units A through C. Natural gas was observed at two elevations in B441; El.158.4 feet (Pulaski B) and El. 88.4 feet (Whetstone Gulf A Formation). It is probable that the natural gas observed when the boring was being advanced at El. 88.4 feet was actually from El. 158.4 and traveling up the annular space between the drill rods and the rock.

The elevations at which natural gas was encountered in the borings correspond to the approximate elevations at which the cooling water tunnels are designed for construction.

Natural gas is present in many areas of central and western New York (CEG, 1988) and was indicated as present during construction of the NMP Unit 2 cooling water tunnels (CEG, 1998). }

2.5.4.3 Foundation Interfaces

The U.S. EPR FSAR includes the following COL Item in Section 2.5.4.3:

> Foundation interfaces with underlying materials are site specific and will be addressed by the COL applicant. The COL applicant will confirm that the site soils have (1) sliding coefficient of friction equal to at least 0.7, (2) adequate shear strength to provide adequate static and dynamic bearing capacity, (3) adequate elastic and consolidation properties to satisfy the limits on settlement described in Section 2.5.4.10.2, and (4) adequate dynamic properties (i.e., shear wave velocity and strain-dependent modulus-reduction and hysteretic damping properties) to support the Seismic Category 1 structures of the U.S. EPR under earthquake loading.

This COL Item is addressed as follows:

{All Seismic Category I structures are supported on bedrock or on concrete fill extending down to bedrock.

The sliding coefficient of friction is equal to 0.7, as discussed in Sections 2.5.4.2.1.2 and 2.5.4.2.1.5.

The bedrock has adequate shear strength to provide adequate static and dynamic bearing capacity, as discussed in Section 2.5.4.10.2.

The bedrock has adequate elastic and consolidation properties to satisfy the limits on settlement described in U.S. EPR Section 2.5.4.10.2, as discussed in Section 2.5.4.10.3.

The bedrock has adequate dynamic properties (i.e. shear wave velocities and stain-dependent modulus-reduction and hysteretic damping properties) to support the Seismic Category I structures under earthquake loading, as described in Section 2.5.2.

Plans showing the locations of explorations, profiles, and excavations, with the safety-related facilities superimposed, are presented in Figure 2.5-60 through Figure 2.5-62 and Figure 2.5-168.

Profiles showing the relationship of foundations of safety-related facilities to subsurface materials are presented in Figure 2.5-63 through Figure 2.5-67.

Logs of core borings and test pits are presented in Part 11E.}

2.5.4.4 Geophysical Surveys

The U.S. EPR FSAR includes the following COL Item in Section 2.5.4.4:

> Geophysical surveys are site specific and will be addressed by the COL applicant.

This COL Item is addressed as follows:

2.5.4.4.1 {Geophysical Surveys performed Onshore

Seismic refraction surveys were performed along 12 profile lines totaling more than 15,000 linear feet of coverage. Cross-hole surveys were used to measure shear wave velocities in two borehole arrays, each array consisting of three boreholes drilled to depths of 210 feet below ground surface.

Locations of the seismic refraction lines and cross-hole arrays are shown in Figure 2.5-163. The results of the seismic refraction survey are shown in Figure 2.5-164 and Figure 2.5-165. The results of shear wave velocity measurements from the cross-hole surveys are shown in Figure 2.5-166.

Interpretations of geophysical data across the site support the following observations:

- The measured compression wave (P-wave) velocity at the top of bedrock across the site is in the range of 13,500 to 14,500 ft/sec and increased to greater than 15,000 ft/sec at depths of 30 to 60 feet below top of bedrock.
- Measured shear wave (S-wave) velocity increases from near 6,000 to 6,500 ft/sec at top of rock to greater than 7,000 to 7,500 ft/sec at 100 feet below top of bedrock.
- Only minor lateral changes in seismic P-wave velocity were observed along refraction profile lines.

Shear wave measurements made in the two cross-hole arrays separated by about 460 feet indicate nearly uniform shear wave profiles, support boring data that indicates the presence of uniform geologic conditions at the site.

2.5.4.4.2 Geophysical Surveys performed Offshore

A separate geophysical survey was performed just offshore of the NMP3NPP site in Lake Ontario. The survey consisted of hydrographic, sub-bottom reflection, and sub-bottom refraction methods performed in a rectangular shaped area (approximately 3,500 by 2,000 feet in size) centered on the alignment of the cooling water tunnels.

The results of the offshore survey are shown in Figure 2.5-167.

Data acquired in the survey area show the lake bed surface to be rough and gradually sloping offshore at an approximate 3% grade to a distance of about 2,900 feet offshore. Offshore at a distance of about 2,900 feet, the lake bed becomes smoother and appears almost flat lying with only a minor slope continuing to the northwest. The water depth is about 76 feet (El. 169 feet) along the cooling tunnel centerline at this offshore slope break point.

Sub-bottom seismic reflection and refraction data complemented each other and readily identified an "acoustic basement surface," interpreted as the upper surface of the Oswego Sandstone Formation. From the shoreline to approximate 2,900 feet offshore, the acoustic horizon is overlain by intermittent thin patches of surficial sediments. Offshore at a distance of 2,900 feet, the bedrock surface dips more steeply downward and appears to be overlain by a thickening sequence of unconsolidated sediments. An average acoustic velocity calculated for the upper surface of the basement is approximately 13,810 ft/sec. This acoustic velocity compares well with P-wave velocities measured onshore. The acoustic velocity analysis did not detect any large-scale lateral or vertical contrasts that might be indicative of major fractured or faulted zones in the subsurface throughout the area investigated. Such geophysical investigations however, would not identify small-scale joints and minor faults.}

2.5.4.5 Excavation and Backfill

The U.S. EPR FSAR includes the following COL Item in Section 2.5.4.5:

Excavations and backfill are site specific and will be addressed by the COL applicant.

This COL Item is addressed as follows:

2.5.4.5.1 {Source and Quantity of Backfill and Borrow

2.5.4.5.1.1 Type of Backfill

All major safety-related structures are founded on bedrock or, in a few cases, on concrete fill extending down to bedrock. Some utilities and the tunnel for cooling water pipeline are founded on structural fill extending down to bedrock. Major areas around safety-related structures that require backfill are shown on Figure 2.5-168 through Figure 2.5-173 and are summarized as follows:

Area Description	Type of Backfill
Areas of over-excavation outside of foundation walls (below top of bedrock)	Concrete Fill or Structural Fill
Areas of over-excavation outside of foundation walls (above top of bedrock)	Structural Fill
Area beneath Emergency Power Generating Building (Approx. El. 264 to top of bedrock)	Concrete Fill
Area beneath the Cooling Water Pipe Tunnel (Approx. El. 248 to top of bedrock)	Concrete Fill
Area of over-excavation outside the foundation walls of the Cooling Water Pipe Tunnel	Concrete Fill or Structural Fill

2.5.4.5.1.2 Quantity of Backfill

The volumes of materials needed to backfill safety-related structures are as follows:

Material Type	Backfill Volume (Cubic Yards)		
	Nuclear Island	Pump House	Pipeline
Concrete Fill	26,000	5,000	26,500
Structural Fill	82,000	45,500	36,000

2.5.4.5.1.3 Sources, Investigation, and Properties of Backfill

Excavated Natural Soil and Bedrock

Natural soils removed from excavations are not suitable for use as structural backfill. Excavated natural soils are used for general site grading away from all Category I structures.

Selected blast rock (Oswego Sandstone) is also used on-site for general site grading away from all Category I structures.

Structural Fill

Structural fill is obtained from offsite sources following a borrow pit study, described in Section 2.5.4.2.3.8, in which bulk samples from selected sources were obtained for the purpose of classification and grain size analysis. Based on the results of the borrow pit study, the Streeter-Rathburn Borrow Pit in Oswego, New York is identified as a source for structural fill. The static strength parameters of the structural fill are discussed in Section 2.5.4.2.1.2. The dynamic strength parameters of the structural fill are discussed in Section 2.5.4.2.1.3. The static and

dynamic strengths are based on laboratory testing of compacted samples from the Streeter-Rathburn Pit. Compaction criteria are discussed in Section 2.5.4.5.3.3.

Concrete Fill

Concrete fill is obtained from production facilities built for NMP3NPP. Concrete fill consists of a mixture of sand- and gravel-sized aggregate, water, Portland cement, and, potentially, other additives, such as retarders and accelerators. The type of cement and other additives are selected based on corrosion and construction requirements. Minimum strength criteria are discussed in section 2.5.4.5.3.4.

2.5.4.5.2 Extent of Excavations, Fills, and Slopes

Final site grade for the NMP3NPP site is El. 270 ft (82.3 m). As discussed in Section 2.5.4.2.2.2, the pre-construction site topography in the area of safety related structures was generally flat, with elevations ranging from approximately El. 280 ft (85.3 m) in the south to El. 260 (79.2 m) in the north. A listing of the safety-related structures with average bottom of foundation elevation is as follows:

Safety Related Structure	Bottom of Foundation elevation (ft) (NGVD 29)
Reactor Building	233.6
Safeguard Buildings	228.7
Fuel Building	228.7/224
Emergency Power Generating Building	264
ESWS Water Cooling Tower Structure	248
Ultimate Heat Sink Makeup Water Intake Structure (Pump House)	222
Makeup Water Pipeline Tunnel	245

Because bedrock is shallow and the site does not present special space constraints, excavation support systems are not required for the construction of the safety-related structures. In general, excavations made in soil are performed open cut with side slopes at 2 Horizontal to 1 Vertical (2H:1V) or flatter. Excavations in rock are vertical or close to vertical. There is a minimum 15-foot wide horizontal bench at the top of all rock excavations for working space and drainage control. Excavations in rock for safety related structures are extended 8 feet beyond the outside limit of the foundations walls. Excavations in soil for the makeup water pipe tunnel are extended 5 feet beyond the outside limit of the tunnel walls. Excavation plans and sections for the safety-related structures are shown in Figure 2.5-168 through Figure 2.5-173.

Along the Lake Ontario shorefront, the existing irregular slope is excavated from the top of rock to the top of existing site grade to create a stable 2H:1V slope. The slope is then covered with layers of graded stone bedding and riprap to create permanent shorefront slope protection.

Excavation for construction of the pump house requires removal of most of the existing soil along the north side between the excavation and Lake Ontario and construction of a temporary barrier to prevent lake water from entering the excavation. The barrier consists of steel interlocking sheet piles with the toe embedded in concrete and supported by rock fill on the inside and outside faces as needed to provide adequate stability against overturning and sliding. Final layout and design of the temporary barrier is developed during the detailed design stage of the project.

The excavation volumes for safety-related structures are as follows:

Material Type	Excavation Volume (Cubic Yards)		
	Nuclear Island	Pump House	Pipeline
Rock	248,000	20,000	0
Soil	345,500	41,500	34,100

2.5.4.5.3 Excavation and Compaction Specifications and Quality Control

2.5.4.5.3.1 Excavation Methods and Subgrade Preparation Criteria

The shallow soil materials overlying the Oswego Sandstone are removed by standard mechanical excavation equipment. The underlying bedrock is removed by blasting and standard mechanical excavation techniques. As required, the vertical rock faces of excavations for safety related structures are supported by a combination of rock dowels and welded wire fabric.

The locations, numbers, spacing, depths, and capacity of rock bolts are determined during construction based on observations of joint and bedding orientation in the exposed excavation faces.

Blast monitoring is performed to ensure that peak radial particle velocities are within specified limits. As excavation progresses, dewatering is provided as needed. The methods of dewatering are discussed in sections 2.5.4.5.4 and 2.5.4.6. Excavations to the final grades shown on the grading plans are performed carefully to remove any loosened or fractured bedrock without unnecessary over-excavation. All final subgrades are inspected and approved prior to being covered by a concrete mud mat, backfill, or concrete.

All blasting for excavation for structures is controlled by a systematic program. Methods for controlling over-break include line drilling and controlled perimeter blasting, such as cushion blasting, pre-splitting, and smooth-wall blasting. The control and monitoring of the blasting program are discussed below.

2.5.4.5.3.2 Rock Blasting Control Criteria

Blasting control procedures are addressed in a technical specification prepared during the detailed design stage of the project. It includes requirements for a pre-blast condition survey, a blasting and excavation plan, and a trial blasting program. The technical specification includes requirements for on-site monitoring of peak particle velocities and air blast overpressures for all blasts. The technical specification also provides criteria for maximum acceptable peak particle velocities and air blast overpressure.

2.5.4.5.3.3 Structural Fill Compaction and Placement Criteria

Moisture content for structural fill at the time of compaction and testing is specified between 3% above and 3% below the optimum moisture content as determined by ASTM D1557 (ASTM, 2007). The structural fill is placed and compacted to 95% of the maximum dry density as determined by ASTM D1557 (ASTM, 2007).

Structural Fill placement and compaction control procedures are addressed in a technical specification prepared during the detailed design stage of the project. The procedure includes requirements for suitable fill gradation and material properties, lift thickness, sufficient testing to address potential material variations, and in-place density and moisture content testing frequency, for example, a minimum of one test per 10,000 square ft (930 m^2) of fill placed. The

technical specification also includes requirements for an on-site testing laboratory for quality control, especially material gradation and plasticity characteristics, the achievement of specified moisture-density criteria, fill placement/compaction, and other requirements to ensure that the fill operations conform to the earthwork specification. The soil testing firm is required to be independent of the earthwork contractor and to have an approved quality program. A sufficient number of laboratory tests are required to be performed to ensure that variations in the fill material are accounted for. A trial fill program will be conducted to determine an optimum number of compactor coverages (passes), the maximum loose lift thickness, and other relevant data for optimum achievement of the specified compaction criteria.

2.5.4.5.3.4 Concrete Backfill Criteria

Concrete backfill below Category 1 structures, including mud mats to create construction working surfaces, is standard concrete with minimum 28-day compressive strengths of 3,000 pounds per square inch (psi). Concrete material specifications and testing requirements are addressed in a technical specification prepared during the detailed design stage of the project.

Concrete backfill around exterior foundation walls is lean concrete with minimum 28-day compressive strength of 2,000 psi. Lean concrete material specifications and testing requirements are addressed in a technical specification prepared during the detailed design stage of the project.

2.5.4.5.3.5 Excavated Natural Soil and Bedrock Compaction Criteria

Excavated natural soil and blast rock (Oswego Sandstone) are used, where acceptable, for general site grading away from all Category I structures. These materials are compacted or tamped using rollers or other standard construction equipment.

Placement and compaction control requirements are addressed in a technical specification prepared during the detailed design stage of the project. The requirements include suitable fill gradation and material properties, lift thickness, compaction equipment, and compaction effort.

2.5.4.5.4 Impact of Compaction on Structural Design

Loads due to compaction effort adjacent to foundation walls and other underground structures are included in the lateral load design criteria, as discussed in Section 3.8.4.

2.5.4.5.5 Control of Groundwater During Excavation

Construction dewatering is accomplished by conventional open sumps and pumps in the bottom of excavations in rock, and at the toe of soil slopes. A layer of crushed stone is placed over the lower portions of cut soil slopes as needed to prevent erosion due to seepage. Sumps and drains are constructed to maintain the groundwater level below the level of active excavation backfilling and foundation construction.

The top of the Oswego Sandstone bedrock may be grouted to reduce groundwater seepage through fractures from Lake Ontario into the pump house excavation.

Surface runoff from areas adjacent to excavations is prevented from entering excavations by sloping of the ground surface away from the top of the excavation and by installing interceptor ditches with sumps and pumps as needed.

All surface runoff and construction dewatering water is directed to the on-site storm water detention basins prior to discharge.

No permanent dewatering is required for the completed structures.

2.5.4.6 Groundwater Conditions

The U.S. EPR FSAR includes the following COL Item in Section 2.5.4.6:

The COL applicant will address site-specific groundwater conditions.

This COL Item is addressed as follows:

2.5.4.6.1 Groundwater conditions relative to foundation stability

Final site grade is El. 270 at all Category I structures.

Maximum potential static, non-transitory, groundwater level is El. 266.7, based on subsurface conditions and surface drainage incorporated in the site design, as discussed in Section 2.4.12.5.

These groundwater conditions are addressed for static and dynamic structural design of Category I structures as described in Sections 3.7 and 3.8, including lateral loading, uplift, and buoyancy.

All major safety-related structures are founded on bedrock (Oswego Sandstone) or on concrete fill extending down to bedrock. Some utilities are founded on structural backfill extending down to bedrock. The bedrock, concrete, and structural fill do not have potential for foundation instabilities due to groundwater flow or groundwater level fluctuations, as discussed in the following sections.

2.5.4.6.1.1 Stability of Bedrock

The following is a comparison of potential groundwater induced bedrock instabilities to conditions at NMP3NPP, as described in sections 2.5.1 and 2.5.4.1.

Settlement due to voids created by dissolution of rock mass is not a factor. The bedrock at NMP3NPP is not subject to dissolution.

Settlement due to voids created by erosion or consolidation of weathered zones is not a factor. The bedrock surface at NMP3NPP is clean and unweathered. Minor oxidation of near-surface joints is present at some locations. There are no zones of alteration or irregular weathering within the rock mass.

Swell due to expansive rock types, such as shales and argillaceous rock units is not a factor. All of the Category I structures are founded in the Oswego Sandstone, which is not an expansive rock type. The Pulaski formation underlying the Oswego Sandstone is argillaceous. However, building foundations do not extend deep enough to encounter the Pulaski formation and create conditions for potential swelling.

The outfall tunnels are largely constructed in the Pulaski, and potential swelling may occur during construction of the tunnels. However, the competed tunnel liners are designed to accommodate swell stresses.

2.5.4.6.1.2 Stability of Concrete Backfill

As discussed in Section 2.5.4.2.4.5, the soil and groundwater at the NMP3NPP site have chemical characteristics that are not corrosive to concrete.

2.5.4.6.1.3 Stability of Structural Backfill

The following is a comparison of potential groundwater induced structural backfill instabilities to conditions at NMP3NPP, as described in Sections 2.5.1 and 2.5.4.1.

Settlement or heave due to consolidation of fine-grained soils is not a factor. The structural fill is granular, free- draining, and contains less then eight percent fine-grained soils. As such, it is not subject to consolidation due to fluctuating groundwater levels.

Settlement due to voids created by subsurface erosion is not a factor. The structural fill is widely graded and free draining and thus functions as filter material and is not erodible by groundwater flow.

2.5.4.6.2 Plans for and Impact of Dewatering During Construction

Dewatering methods and criteria used during construction are discussed in Section 2.5.4.5.5.

The structural fill, concrete fill, and rock are not sensitive to groundwater flow or groundwater level changes, as discussed in Section 2.5.4.6.1. Therefore, the dewatering methods and criteria employed during construction will not affect the stability or settlement of temporary or permanent NMP3NPP structures.

2.5.4.6.3 Analysis and Interpretation of Seepage and Potential Piping During Construction

Current groundwater flow and seepage conditions are discussed in Section 2.4.12.

During construction, the primary sources of dewatering effluent are groundwater flow in the natural soils above the top of rock and groundwater flow within rock joints and fractures. As discussed in Section 2.5.4.2.3.6 the height of groundwater above the top of rock varies depending on the season. Combined with moderate permeability in the range of $1x10^{-4}$ cm/sec (section 2.5.4.2.1.9), the natural soils produce groundwater flows that can be readily managed with a combination of toe drains and filtered sumps. Likewise, the small fracture widths in bedrock result in groundwater flows that are readily managed with filtered sumps. In both the natural soil and bedrock, piping occurs only if the seepage flows induced by the groundwater gradients caused fine-grained material to erode out of the soil matrix or rock fractures. To prevent this, the dewatering methods discussed in section 2.5.4.5.5 include the use of sand, stone, or fabric filters on the sumps, and a layer of crushed stone placed over the lower portions of cut soil slopes in soil as needed to prevent erosion and piping due to seepage.

2.5.4.6.4 Permeability Testing

Testing for permeability of the foundation materials was performed using water pressure (packer) tests in rock. Rising head tests were performed in selected monitoring wells also. The data from the rising head permeability tests supplements the data from the packer tests. The results of the permeability tests are discussed in Section 2.5.4.2.1.9 and shown in Table 2.5-51, Table 2.5-52, and Table 2.5-53 and in Figure 2.5-174 and Figure 2.5-175.

2.5.4.6.5 History Of Groundwater Fluctuations

Groundwater monitoring records for 38 monitoring wells in soil and rock are discussed in Section 2.5.4.2.3.6, and in Section 2.4.12. }

2.5.4.7 Response of Soil and Rock to Dynamic Loading

The U.S. EPR FSAR includes the following COL Item in Section 2.5.4.7:

> The COL applicant will address site-specific response of soil and rock to dynamic loading, including the determination of strain-dependent modulus-reduction and hysteretic damping properties.

This COL Item is addressed as follows:

{ Detailed descriptions on response of site soils and rocks to dynamic loading are addressed in Section 2.5.2.

Sections 2.5.4.7.1 through 2.5.4.7.5 are added as a supplement to the U.S. EPR FSAR.

2.5.4.7.1 Site Seismic History

As presented in Section 2.5.3, faults and folds within 5 miles (8 km) of the NMP3NPP site do not exhibit evidence of Quaternary activity. The USGS recently completed a compilation of all Quaternary faults, liquefaction features, and possible tectonic features in the eastern United States. These compilations do not show any Quaternary faults or related features within a 25 mile (40 km) radius or a 5 mile (8 km) radius of the site. Faults older than Quaternary within 25 miles of NMP3NPP are the NMP Unit 2 faults and the Demster Zone Structures located about 8 miles from the site. These faults formed during the Paleozoic Era as part of the regional Taconic and Alleghenian orogenies, and may have been reactivated locally during the Mesozoic. Based on a review of available published geologic literature, field reconnaissance, and interpretation of aerial photography, the NMP Unit 2 faults and the Demster Zone Structures are not considered to be capable faults.

Based on current investigations, there are no zones of Quaternary deformation requiring detailed investigation within the NMP3NPP site area. A review and interpretation of aerial photography, satellite imagery, and topographic maps identified a few discontinuous east to northeast-striking lineaments and northwest-striking lineaments within 5 miles of NMP3NPP. As discussed in Section 2.5.3, none of these lineaments are interpreted as fault-related. These lineaments reflect glacial depositional and erosional features.

2.5.4.7.2 Site Investigations to Determine Dynamic Properties

The following site investigations and laboratory testing programs were performed to determine the dynamic properties of soil and rock at the NMP3NPP site:

- Geophysics, including seismic refraction surveys and crosshole shear (S) and compression (P) wave velocity measurements. The investigation methods and results are discussed in Sections 2.5.4.2 and 2.5.4.4.
- Reviews of relevant research.
- Laboratory testing of natural glacial till and structural fill. The laboratory testing programs and results are discussed in Section 2.5.4.2.

- Laboratory testing of rock. The laboratory testing programs and results are discussed in Section 2.5.4.2.

Based on these investigations and laboratory testing programs, dynamic properties for design for soil and rock are summarized below in sections 2.5.4.7.3 and 2.5.4.7.4.

2.5.4.7.3 Dynamic Properties of Soil and Rock

The dynamic properties of natural soil are discussed in Section 2.5.4.2.1.3.

The dynamic properties of structural fill are discussed in Section 2.5.4.2.1.4.

The dynamic properties of rock are presented in Table 2.5-49 and Table 2.5-50. Uncertainties in the values are quantified for use in site response analyses. The lab tests, field tests, and references used to obtain the dynamic properties are discussed as notes on the tables.

Seismic wave transmission characteristics of the site are discussed in Section 2.5.2.5

2.5.4.8 Liquefaction Potential

The U.S. EPR FSAR includes the following COL Item in Section 2.5.4.8:

> The COL applicant will address site-specific liquefaction potential. As stated in Section 2.5.2, the evaluation of liquefaction is performed for the seismic level of the site specific SSE.

This COL Item is addressed as follows:

{This section contains a summary of the liquefaction analysis for NMP3NPP.

2.5.4.8.1 Design Criteria and Analysis Methodology

The design of the US EPR assumes that the plant is not founded on liquefiable materials.

All Category I structures will be founded directly on rock, or on concrete fill or structural fill bearing on rock. These circumstances are inherently not subject to liquefaction. Therefore, the plant is not founded on liquefiable materials.

A liquefaction analysis was performed for the existing natural soil (glacial till) in accordance with guidance provided in NRC Regulatory Guide 1.198. As described below in Section 2.5.4.8.2, the existing natural soil (glacial till) is also not susceptible to liquefaction.

The liquefaction analysis included the following:

- The procedures described in Youd, 2001 were used to evaluate liquefaction potential based on SPT blowcounts corrected for overburden pressure, drilling methods, and percentage of fines (soil particles passing the No. 200 sieve). As stated in Youd, 2001, corrected N-values greater than 30 blows per foot are too dense to liquefy in an earthquake of any size and are classed as non-liquefiable.

- All N-value data from all borings performed at the site, except those indicating refusal, were initially considered, regardless of whether the soil would be removed during foundation construction.

- Based on the completed evaluation, any areas of potentially liquefiable soils that would not be removed during foundation construction were identified and evaluated.

2.5.4.8.2 SPT Data and Groundwater Levels

SPT data from seventy-nine onshore borings was used to assess liquefaction potential (this includes all onshore borings with SPT measurements except B401 and B428, which were performed at the pump house at the end of the field program). Boring logs are presented Part 11E.

For liquefaction calculations, all SPT blow counts in the overburden soils were evaluated, except those in which refusal was encountered before the full 18 inches of sampler penetration was reached. The SPT was considered to hit refusal based on one of the following two criteria:

- The sampler penetrated less than 6 inches with 50 blows of the hammer, or
- The sampler showed no penetration for 10 blows of the hammer.

The occurrence of refusal indicates that the material being sampled is very dense, and not susceptible to liquefaction. Therefore, it is appropriate and conservative to not consider the refusal blow counts in the liquefaction evaluation.

For the purpose of the liquefaction evaluation, the groundwater depth at the time the blow counts are obtained is of primary interest. Since the soils generally contained significant fines, and water was used as a drilling fluid, reliable indications of groundwater level could not be obtained during drilling of the boreholes. Groundwater levels were measured in five observation wells (B120 to B124) installed in the soils strata. Depths measured between October 2007 and August 2008 are shown in Table 2.5-56. These data indicate that the groundwater levels in the wells varied significantly in the first few months as the wells stabilized, but then were relatively stable from January through March 2008. Based on the stabilized readings, an average depth to groundwater of 5 feet was used for the liquefaction evaluation.

2.5.4.8.3 Liquefaction Potential Based on SPT Data

All standard penetration test (SPT) data were evaluated for liquefaction potential. Each SPT measurement was corrected to an equivalent clean sand N-value as described by Youd, 2001. The data are shown in Table 2.5-64.

As shown in Table 2.5-64, 7 out of 20 corrected blow counts in the fill and 24 out of 36 corrected blow counts in the surficial deposits were less than 30 blows per foot, and could potentially be susceptible to liquefaction during an earthquake. However, these soils will be removed from beneath and around safety-related structures and utilities during construction, and therefore will not affect the stability and performance of any safety-related structure or utility. Therefore, further evaluation of the liquefaction potential of these soils is not required.

In the glacial till, 9 of 88 corrected blow counts were less than 30 blows per foot. Of these 9 blow counts, 7 were at a depth of 1 foot, i.e., in locations where the glacial till was at the ground surface. During construction, the glacial till to a depth of 2 feet below ground surface will be removed from beneath and around safety-related structures and utilities, and therefore will not affect the stability and performance of any safety-related structure or utility. Therefore, further evaluation of the liquefaction potential of these soils is not required.

Two of the blow counts in glacial till, at depths of 3 feet below ground surface, had corrected blow counts of 29 blows per foot. These corrected blow counts are just marginally below the criterion of 30 blows per foot indicated in Youd, 2001 as the lower limit for soils to be considered not liquefiable during earthquakes of any size. In addition, as shown on Figure 2 in Youd, 2001, the asymptote for the corrected blow count for clean sand is actually about 29 blows per foot. Therefore, these two blow counts are not considered to indicate potential liquefaction of the till below a depth of 2 feet below ground surface.

For these calculations, the total unit weight of soil above the groundwater table is assumed to be 140 lbs/ft^3, and the total unit weight of soil below the groundwater table is assumed to be 145 lbs/ft^3. These soil unit weights were chosen as representative of the glacial till, since the fill and surficial soils will be removed during construction.

In the liquefaction analysis, the unit weight is used to determine the effective and total stresses in the soils at the time of sampling so the N-value can be corrected to a standard overburden pressure. The correction factor includes effective stress in the denominator, resulting in a lower correction factor with higher unit weights. Therefore, it is more conservative to use higher unit weights in the analysis. The unit weights used in the analyses are appropriately conservative. Based on the analysis described above, the existing natural soil (glacial till) is not susceptible to liquefaction.}

2.5.4.9 Earthquake Site Characteristics

The U.S. EPR FSAR includes the following COL Item in Section 2.5.4.9:

Site-specific earthquake site characteristics will be described by the COL applicant.

This COL Item is addressed as follows:

{Section 2.5.2.6 describes the derivation of the Safe Shutdown Earthquake (SSE) ground motion for the NMP3NPP site.

The selected SSE ground motion is based on the risk-consistent/performance-based approach of the NRC Regulatory Guide 1.208, "A Performance-Based Approach to Define the Site-Specific Earthquake Ground Motion" with reference to NUREG/CR-6728 and ASCE/SEI 43-05 (refer to Section 2.5.2.6 for references). Deviation from the guidance provided in Regulatory Guide 1.208 is discussed in Section 2.5.2.

Horizontal ground motion amplification factors are developed in Section 2.5.2.5 using site-specific data and estimates of near-surface geologic properties presented in Section 2.5.4.2 These amplification factors are then used to scale the hard rock spectra, presented in Section 2.5.2.4, to develop Uniform Hazard Response Spectra (UHRS), accounting for site-specific conditions using Approach 2A of NUREG/CR-6769. Horizontal GMRS spectra are developed from these site-specific UHRS, using the performance-based approach of ASCE/SEI 43-05, accepted by Regulatory Guide 1.208.

The SSE motion is defined at the free ground surface of a hypothetical outcrop at the base of the foundation. Section 2.5.2.6 also describes vertical SSE ground motion, which was developed by scaling the horizontal SSE by a frequency-dependent vertical-to-horizontal (V:H) factor, presented in Section 2.5.2.6.

2.5.4.10 Static Stability

{The table below contains a summary of static stability analyses for the nuclear island common basemat structure. All safety-related structures at the NMP3NPP site will be supported on rock or on concrete fill extending to rock. Therefore, the presence and properties of soils at the site do not affect computations of static stability analyses.

As discussed in the U.S. EPR FSAR, since the nuclear island common basemat structure is the largest and most heavily loaded structure at NMP3NPP, it represents the maximum loading and settlement design case for safety related structures at the site. Thus, by demonstrating that the nuclear island common basemat structure meets the US EPR static stability criteria at NMP3NPP, it is also demonstrated that all safety related structures meet the US EPR static stability criteria.

Static Stability Parameter	US EPR Criteria	Computed for NMP3NPP
Bearing Capacity on Rock	> 25,000 lb/ft^2	204,000 lb/ft^2
Total Settlement	< 3.0 inches	0.7 inches
Differential Settlement (angular distortion)	< 1:1,200	1:7,200
Rock Bedding Angle	< 20 degrees from horizontal	< 20 degrees from horizontal

The computed static stability parameters are within the U.S. EPR static stability criteria. Detailed discussion of each analysis is presented in the following sections.}

2.5.4.10.1 Bearing Capacity

The U.S. EPR FSAR includes the following COL Item in Section 2.5.4.10.1:

> A COL applicant that references the U.S. EPR design certification will verify that site-specific foundation soils beneath the foundation basemats of Seismic Category I structures have the capacity to support the bearing pressure with a factor of safety of 3.0 under static conditions.

This COL Item is addressed as follows:

{Sections 2.5.4.10.1.1 through 2.5.4.10.1.4 are added as a supplement to the U.S. EPR FSAR.

2.5.4.10.1.1 Analysis Methodology

The mat foundations for all Category I safety-related structures at NMP3NPP are founded directly on bedrock or on concrete fill extending to bedrock. The allowable bearing capacity for the mat foundations is based on the strength of the rock and the characteristics of the rock mass, as determined from the site explorations and laboratory testing on intact specimens of rock core. The properties of the soils at the site do not affect the stability of the Category I structures and are not considered in this analysis.

Allowable bearing capacity for foundations on rock is computed using the procedures outlined in the U.S. Army Corps of Engineers Manual EM 1110-1-2908, Rock Foundations. The analysis is based on the general Rankine bearing capacity model for a single layer foundation material with both cohesion and friction. The general form of the bearing capacity equation is:

$$q_{ult} = c\, N_c + 0.5\, \gamma_b\, B\, N_\gamma + \gamma_b\, D\, N_q$$

Where q_{ult} = ultimate bearing capacity

$c = c_{mass}$ = cohesion of rock mass,

γ_b = buoyant unit weight of rock

B = width of foundation

D = depth of foundation below finish grade

$N_c = 2\ N_\Phi^{1/2}\ (N_\Phi + 1)$

$N_\gamma = N_\Phi^{1/2}\ (N_\Phi^2 - 1)$

$N_q = N_\Phi^2$

$N_\Phi = \tan^2\ (45 + \Phi/2)$

Φ = angle of internal friction for rock mass

2.5.4.10.1.2 Key Assumptions

The following key assumptions were used:

The rock mass is isotropic and homogeneous. This assumption is supported by the similarity of the rock properties and fracturing observed in the explorations and laboratory testing. This is a standard assumption for bearing capacity calculations for good quality bedrock.

The rock mass has at least two primary nearly vertical fracture sets and horizontal bedding, which create a blocky structure that requires a failure to occur partially through intact rock. This assumption is supported by the rock characteristics observed in exposed outcrops at and near the site and in the rock cores.

The rock mass cohesion can be reasonably determined from the unconfined compressive strength on rock cores using the equations in U.S. Army Corps of Engineers, 1994. This assumption is supported by the facts that (1) the equations in U.S. Army Corps of Engineers, 1994 are based on empirical experience and (2) the resulting rock mass cohesion is small, equal to only 2.3% of the average intact rock unconfined strength.

The rock mass friction angle used for the bearing capacity analysis is taken as the average of the range for Class II rock shown on Table B- in U.S Army Corp of Engineers, 1994 based on the average Rock Mass Rating of 66 for rock a the NMP3NPP site, as discussed in Section 2.5.4.10.2.3.

2.5.4.10.1.3 Calculation Input

Pertinent information used in computing the bearing capacity of the rock mass is given below:

Subsurface Profile

The subsurface profile in the area of the safety related structures consists of about 10 to 20 feet of soil, overlying about 30 to 90 feet of Oswego Sandstone, about 100 feet of Pulaski Formation (interbedded sandstone, siltstone and shale), and then over 700 feet of the Whetstone Gulf Formation (siltstone and shale with varying amount of sandstone beds).

Foundation Size

The nuclear island is cruciform in shape, with overall dimensions of about 350 feet by 350 feet. The Emergency Power Generating Building (EPGB) mat is composed of approximately square sections, with overall dimensions of about 98 by 180 feet. The Essential Service Water Building (ESWB) is rectangular with overall dimensions of about 128 by 184 feet.

For the bearing capacity analysis, a foundation width of 100 feet is conservatively used.

Depth of Embedment

The depth of embedment of the bottom of the foundation mat below finished grade for the various structures varies from 6 feet to more than 30 feet (Figure 2.5-63 through Figure 2.5-67).

For the bearing capacity analysis, a conservative depth of embedment of 0 feet is used.

Intact Rock and Rock Mass Properties

For evaluation of bearing capacity, the average properties of the rock to a depth of about 1 times the width of the loaded area are considered, i.e., to a depth of up to 350 feet. Laboratory test results on intact specimens of rock from onshore borings are summarized in Table 2.5-45 and Table 2.5-46.

The Rock Mass Ratings for the Oswego Sandstone, Pulaski, and Whetstone Gulf formations are 65, 68, and 65, respectively, indicating Class II rock, which is good quality rock. Rock Mass Rating is used to rate a rock mass based on:

- Uniaxial compressive strength of intact rock
- Rock quality designation (RQD)
- Spacing of discontinuities
- Condition of discontinuities
- Groundwater conditions
- Orientation of discontinuities

Each of the six parameters is assigned a value based on field observations, descriptions of rock cores, and laboratory data. The sum of the six parameters is the Rock Mass Rating, which lies between 0 and 100.

Based on the field and laboratory studies, properties of the intact rock and the rock mass rating are sufficiently similar for all three rock strata that an average of the properties for the Oswego, Pulaski and Whetstone Gulf formations are used for the bearing capacity analysis.

As described below, key properties used in the analyses are:

a. Submerged unit weight, γ_b = 104 pcf

b. Rock mass cohesion, cmass = 112 psi = 16,250 psf

c. Friction angle for rock mass, Φ = 40 degrees

d. Average Rock Mass Rating = 66

The submerged unit weight is an average of the total unit weight of the Oswego Sandstone, Pulaski Formation and Whetstone Gulf Formation (164, 168, and 167 pcf, respectively) as reported in Sections 2.5.4.2.1.5, 2.5.4.2.1.6, and 2.5.4.2.1.7, minus the unit weight of water, 62.4 pcf.

The rock mass cohesion is 0.023 times the representative unconfined compressive strength of the intact rock core, 21,000 psi, which is computed as the average of the average strengths of each of the three rock formations as reported in Table 2.5-46. The mass reduction factor, 0.023, is determined from the procedure outlined in U.S. Army Corps of Engineers, 1994.

The rock mass friction angle used for the bearing capacity analysis, 40 degrees, is taken as the average of the range for Class II rock shown on Table B-2 in U.S. Army Corps of Engineers, 1994, based on the average Rock Mass Rating of 66 for the rock at the NMP3NPP site.

2.5.4.10.1.4 Bearing Capacity Calculation Results

Based on the specified equation and associated inputs, an ultimate bearing capacity, q_{ult} = 614,000 lb/ft^2 is calculated. Applying a factor of safety of 3.0, an allowable bearing pressure, q_{all} = 204,000 lb/ft^2 is determined. }

2.5.4.10.2 Settlement

The U.S. EPR FSAR includes the following COL Item in Section 2.5.4.10.2:

> A COL applicant that references the U.S. EPR design certification will verify that the differential settlement value of ½ inch per 50 ft in any direction across the foundation basemat of a Seismic Category I structure is not exceeded. Settlement values larger than this may be demonstrated acceptable by performing additional site specific evaluations.

This COL Item is addressed in the following section and in Section 3.8.5.

2.5.4.10.2.1 Analysis Approach

The nuclear island is approximately 350 ft by 350 ft in overall dimension and is shaped like a cruciform. Since the nuclear island is the largest and most heavily loaded structure at NMP3NPP, settlement calculated for the nuclear island foundation mat will provide a reasonable estimate of the maximum structure settlements expected for all safety-related structures at the site. All safety-related structures will be supported on rock or on concrete fill extending to rock. Therefore, the presence and properties of the soils at the site do not affect the estimated settlement of the safety-related structures.

The following approach was used to validate the calculation models and estimate the expected settlement of the nuclear island foundation mat:

1. Develop a subsurface profile based on data from the field exploration program

2. Utilize nuclear island foundation geometry and elevations and foundation mat loadings from the design of the nuclear island

3. Establish the engineering properties of the rock mass, including Poisson's ratio, Young's Modulus, joint spacing, rock quality designation (RQD), and rock mass rating (RMR), using the results of field investigations and laboratory testing.

4. Perform initial settlement hand calculations using two different formulations for settlement at the center of an uniformly loaded circular area at the surface of a semi-infinite, homogeneous elastic half-space

5. Perform initial 2-D finite element computer model (Sigma W) calculations using the same loading and half-space properties as the elastic calculations, to verify that the 2-D model was working properly and providing reasonable results.

6. Perform final 2-D finite element computer model calculations with horizontally layered rock foundation strata, and non-uniform structural loading on a flexible mat embedded at the design foundation mat depth below the rock surface, to obtain final settlement estimates for analysis.

2.5.4.10.2.2 Key Assumptions

The following key assumptions were used in the preparation of these calculations:

- The rock strata consist of the Oswego Sandstone, Oswego Transition Zone, Pulaski Formation, and Whetstone Gulf Formation. These rock strata are approximately horizontal and constant in thickness within the zone of influence of the nuclear island foundation mat.

- For the purpose of analysis, each rock stratum is considered horizontal, of constant thickness, homogeneous, and isotropic. This is a standard assumption for settlement calculations for good quality bedrock

- Accurate rock mass properties are determined from the laboratory tests on intact rock specimens using the empirical procedures outlined in Kulhawy and Carter (Kulhawy and Carter, 1992).

Based on these considerations, the final 2-D finite element model used the rock properties for each stratum as summarized in the following table:

	Oswego Sandstone	Oswego Transition	Pulaski	Whetstone Gulf
Depth to top of formation from bottom of foundation slab	0 ft	28 ft	55 ft	155 ft
Poisson's Ratio for rock mass, ν_m	0.37	0.37	0.37	0.37
Young's Modulus for rock mass, E_m	6.70E+07 psf	6.70E+07 psf	7.49E+07 psf	4.68E+07 psf
Unit Weight, γ	164 pcf	164 pcf	168 pcf	167 pcf

2.5.4.10.2.3 Settlement Analysis and Results

The foundation loads at the base of the nuclear island range from about 4 to 25 ksf, with most of the foundation area having loads in the range of 4 to 19 ksf.

For the elastic hand calculation models, an average uniform load of 15 ksf was used. The shape of the loaded area was circular, with a radius of approximately 178 feet, which provided a loaded area that encompassed the full maximum dimension of the cruciform shape, but resulted in an area about 24% larger than the mat area (99,800 ft^2 versus 81,000 ft^2 actual). Use

of the larger area in the computations is conservative because it results in greater computed settlement.

For the initial 2-D finite element analysis, a uniform foundation loading of 15 ksf on a 350-foot wide strip load was used.

For the final 2-D finite element analysis, a strip load with loads varying across the width of the strip was used. The applied loads ranged from 4 to 19 ksf.

The reactor building bears at El 233.6 and the adjoining safeguard buildings bear at El 228.7, both in the Oswego Sandstone formation. Final site grade is at approximately El. 270.

Based on the final 2-D finite element analyses, settlement of the reactor island foundation mat bearing on rock is calculated to be less than 0.7 inch, significantly below the design criteria of 3 inches maximum settlement. In addition, the differential settlement is calculated to be about 0.29 inches, significantly below the design criterion of 1.5 inches maximum. Also, the estimated angular distortion of 1:7,200 is well below the design criterion of 1:1,200.

The settlements computed using the hand calculation methods and the initial 2-D finite element model were within 20% of the settlements computed using the final finite element model. This verifies that the 2-D model works properly and provides reasonable results.

2.5.4.10.2.4 Uniformity and Variability of Foundation Support Media

Subsurface profiles are shown in Figure 2.5-63 through Figure 2.5-67. The soil and rock profile is laterally uniform. Individual layers within the profile have an angle of dip significantly less than 20 degrees.}

2.5.4.10.3 Uniformity and Variability of Foundation Support Media

The U.S. EPR FSAR includes the following COL Item in Section 2.5.4.10.3:

> A COL applicant that references the U.S. EPR design certification will investigate and determine the uniformity of the underlying layers of site specific soil conditions beneath the foundation basemats. The classification of uniformity or non-uniformity will be established by a geotechnical engineer.

These COL Item is addressed as follows:

{Subsurface profiles are shown in Figure 2.5-63 through Figure 2.5-67. The soil and rock profile is laterally uniform. Individual layers within the profile have an angle of dip significantly less than 20 degrees.}

2.5.4.10.4 Site Investigation for Uniform Sites

No departures or supplements.

2.5.4.10.5 Site Investigation for Non-uniform Sites

No departures or supplements.

2.5.4.11 Design Criteria

No departures or supplements.

2.5.4.12 Techniques to Improve Subsurface Conditions

The U.S. EPR FSAR includes the following COL Items in Section 2.5.4.12:

> Techniques used for improving subsurface conditions are site specific and will be addressed by the COL applicant.

This COL Item is addressed as follows:

{Category I structures are supported directly on the Oswego Sandstone bedrock, or on concrete fill extending to bedrock. The bedrock is a suitable support layer for all Category I structures, as discussed in Sections 2.5.4.1 through 2.5.4.10. Therefore, no ground improvement is anticipated for the foundations of Category I structures.

Controlled blasting, appropriate equipment and methods for excavation and subgrade preparation, placement of concrete mud mats, and ground water control by dewatering sumps are used to prevent disturbance to the bedrock below the bottom of excavations for Category I structures.

As discussed in Section 2.5.4.6, the Oswego Sandstone is grouted as needed to reduce inflow of groundwater during construction.

2.5.4.13 References

{This section is added as a supplement to the U.S. EPR FSAR.

ACI, 2005. ACI 318, Building Code Requirements for Structural Concrete, American Concrete Institute Committee, 2005.

AREVA, 2008a. Resonant Column Cyclic Torsional Shear Tests (RCTS) Report for Natural Soils - Nine Mile Point Site Characterization, 38-9086739-000, July 2008.

AREVA, 2008b. Resonant Column Cyclic Torsional Shear Tests (RCTS) Report - Nine Mile Point Site Characterization, 38-9084289-001, July 2008

ASTM, 2003. Standard Test Method for 24-h Batch-Type Measurement of Contaminant Sorption by Soils and Sediments, American Society for Testing and Materials, ASTM D4646-03, 2003.

ASTM, 2007. Standard Test Methods for Laboratory Compaction Characteristics of Soil Using Modified Effort (56,000 ft-lbf/ft^3 (2,700 kN-m/m^3)), American Society for Testing and Materials, ASTM D1557-07, 2007.

CEG, 1998. Nine Mile Point Unit 2 Updated Safety Analysis Report, Revision 10, Constellation Energy Group, 1998.

Fang, 1991. Foundation Engineering Handbook, 2nd Edition, Van Nostrand Reinhold.

Hickman, 1985. In Situ Stress, Natural Fracture Distribution, and Borehole Elongation in the Auburn Geothermal Well, Auburn, New York, Journal of Geophysical Research, June, 1985. S.H. Hickman, J.H. Healy and M.D. Zoback.

Kulhawy and Carter, 1992. Settlement and Bearing Capacity of Foundation on Rock Masses, Chapter 12 in Engineering in Rock Masses, F.G. Bell editor, Butterworth-Heinemann, Oxford, England, pp. 231-245.

Kulhawy, 1990. Manual on Estimating Soil Properties for Foundation Design, Pages 2-18, Kulhawy, F.H., et al, Cornel University Geotechnical Engineering Group. Ithaca, New York. 1990.

Lambe, 1969. Soil Mechanics, Lambe and Whitman, John Wiley & Sons, New York, 1969.

NAVFAC, 1986. Foundations & Earth Structures, Design Manual 7.02, Naval Facilities Engineering Command, September, 1986.

Niagara Mohawk, 1978. "Geologic Investigation, Nine Mile Point Nuclear Power Sta. Unit 2, Apr. 1978, Prepared by Dames & Moore for Niagara Mohawk Power Corp.

NRC, 2003a. Regulatory Guide 1.132, Site Investigations for Foundations of Nuclear Power Plants, Revision 2, U.S. Nuclear Regulatory Commission, October 2003.

NRC, 2003b. Regulatory Guide 1.138, Laboratory Investigations of Soils for Engineering Analysis and Design of Nuclear Power Plants, Revision 2, U. S. Nuclear Regulatory Commission, December 2003.

NRC, 2007. Regulatory Guide 1.206, Combined License Applications for Nuclear Power Plants (LWR Edition), U.S. Nuclear Regulatory Commission (NRC), June 2007

NYSM, 1970. Late Ordovician Benthic Marine Communities in North-Central New York, New York State Museum and Science Service, Bulletin 414, 1970.

Peck, 1953. Foundation Engineering, Page 13, Peck, R., et al, John Wiley & Sons, Inc. 1953

Plumb, 1985. Stress-Induced Borehole Elongation: A Comparison Between the Four-Arm Dipmeter and the Borehole Televiewer in the Auburn Geothermal Well, Journal of Geophysical Research, June, 1985. R. A. Plumb and S. H. Hickman.

U.S. Army Corps of Engineers, 1994. Manual EM 1110-1-2908, Rock Foundations, November 30, 1994.

Youd, 2001. Liquefaction Resistance of Soils: Summary Report from the 1996 NCEER and 1998 NCEER/NSF Workshops on Evaluation of Liquefaction Resistance of Soils, Journal of Geotechnical and Geoenvironmental Engineering, ASCE, Vol. 127, No. 10, Pages 817-833.}

2.5.5 STABILITY OF SLOPES

The U.S. EPR FSAR includes the following COL Item for Section 2.5.5:

> A COL applicant that references the U.S. EPR design certification will evaluate site-specific information concerning the stability of earth and rock slopes, both natural and manmade (e.g., cuts, fill, embankments, dams, etc.), of which failure could adversely affect the safety of the plant.

This COL Item is addressed as follows:

This section addresses the stability of constructed and natural slopes. It was prepared based on the guidance in relevant Section of NRC Regulatory Guide 1.206, "Combined License Applications for Nuclear Power Plants (LWR Edition)," (NRC, 2007). Constructed slopes evolve as part of the overall site development.

{The existing topography of the NMP3NPP site is fairly flat with a gentle slope down from south to north toward Lake Ontario, with an overall average slope of about 1 to 2% (10 to 20 ft in 1,000 ft (3 to 6 m in 300 m)) across the site area. The existing site topography is shown on the site grading and drainage plans (Figure 2.5-176). There is an existing natural wave-eroded slope along the Lake Ontario shorefront ranging from about 15 to 20 ft (4.5 to 6 m) in height. The existing slope sits directly on the top of bedrock and is primarily exposed soil consisting of natural glacial till, with local areas as steep as about 1H:1V. The limited amount of vegetation on the slope and its steepness indicates that the slope is in a state of ongoing gradual erosion. Although there is no direct measurement of the rate of erosion, the location of the site on a point strongly indicates that this local section of the lake shore is relatively resistant to erosion. During plant construction, the shorefront slope will be graded and protected with rip rap to provide appropriate long term stability and resistance to wave erosion.

The only safety-related structure affected by the shorefront slope is the raw water pump house and cooling water pipelines from the pump house to the plant area. The pump house is a rectangular concrete structure located at the top of the shorefront slope as shown on Figure 2.5-177. The bottom of the pump station mat bears on bedrock at elevation 228 ft (69.5 m) about 14 ft (4.3 m) below the bedrock surface.

The nuclear island and other safety related structures are located a distance of at least 1,000 ft (305 m) inland from the top of the shorefront slope, except for the fire protection storage tanks and building, which are about 950 ft (290 m) inland from the top of slope.

There are no other existing natural or man-made cuts or slopes in the site area that could affect the safety of the plant. The finished site grade around the nuclear island and other safety related structures is raised to about elevation 268 to 270 ft (81.7 to 82.3 m) requiring fills of about 5 to 10 ft (1.5 to 2 m) above existing grades. At the edges of these plant area fills, located at least 70 ft (21.3 m) from the edge of the safety related structures, the site grade slopes down at a 3H:1V slope or flatter to the existing ground surface or finished grade away from the plant area. The heights of these perimeter slopes are 3 to 12 ft (0.9 to 3.7 m). Also, there are three storm water detention basins in the general plant area, as shown on Figure 2.5-177. These basins have depths of 20 feet (6 m) with 3H:1V side slopes constructed in the glacial till and compacted fill. The nearest edges of the storm water basins are 300 to 600 ft (91 to 183 m) from safety related structures.

Section 2.5.5.1 through 2.5.5.5 are added as a supplement to the U.S. EPR FSAR.

2.5.5.1 Slope Characteristics

There are no natural slopes at the completed NMP3NPP site that could affect the safety of the plant.

Manmade slopes in the vicinity ofNMP3NPP are:

- Shorefront slope: 2H:1V slope up to 28 feet (805 m) in height
- Temporary construction excavation slopes: 2H:1V up to 22 feet (6.7 m) in height.
- Storm water detention basins: 3H:1V up to 20 feet (6.1 m) in height. Y
- General site grading: 3H: 1V up to 12 feet (3.7 m) in height.

All manmade slopes are in existing glacial till or compacted structural fill. The critical slope is at the Lake Ontario shorefront because it is the steepest and highest slope. Other manmade slopes do not need to be analyzed because they are shorter and/or flatter than the critical slope at the shorefront, and are therefore more stable than the critical slope at the shorefront.

The constructed shorefront slope is approximately at the location and follows approximately the alignment of the natural wave eroded slope prior to construction. The location and alignment of the constructed shorefront slope is shown on Figure 2.5-176.

The other slopes in the vicinity of safety related structures identified on Figure 2.5-176 and in above are lower in height, flatter and constructed in the same soils as the shorefront slope. Therefore, they have a higher factor of safety than the shorefront slope and are not analyzed further. Also, the other slopes are at sufficient distance that they do not affect the safety related structures.

The most important section of the shorefront slope is adjacent to the raw water pump station, located as shown on Figure 2.5-177. As discussed below, the height and subsurface conditions are uniform along the length of the slope. Therefore, the location of a typical section for analysis was chosen near the pump station, as shown on Figure 2.5-177.

The constructed shorefront slope has a 2H:1V slope, with a height of 28 ft (8.5 m). The top of slope elevation is at the finished plant grade, elevation 270 ft (82.3 m). The toe of slope is at the top of rock at the base of the existing slope. Existing soil over rock at the toe of slope is removed during construction. The top of rock at the slope is interpolated from the pump station and nearest offshore borings to be at elevation 242 ft (73.8 m). A cross section through the section of slope analyzed is shown in Figure 2.5-178.

The constructed slope consists of a surface layer of riprap 8 ft (2.4 m) thick, underlain by coarse and fine bedding layers each 2.5 ft (0.8 m) thick. The bedding rests on the natural glacial till or on compacted site fill above the till. The size and gradation of the riprap and bedding are determined to provide adequate protection against the design wave and storm conditions, and adequate filter criteria for preventing internal erosion and migration of particles by ground water seepage or wave action. For these analyses, the thin layer of soil over bedrock at the toe of the slope, which could be temporarily eroded during a severe storm, is not considered.

The shorefront slopes at the adjacent NMP Unit 2 Nuclear Power Plant, which have been in place for over 10 years, are visually in good condition and appear stable. The soil and rock exploration program, laboratory testing results, ground water elevations, evaluation of

liquefaction potential, and determination of material properties for the existing insitu glacial till and rock and for the site fill are discussed in detail in Section 2.5.4. The selection of properties for the riprap and coarse and fine bedding are discussed in Section 2.5.5.2.4.1 below.

2.5.5.2 Design Criteria and Analysis

2.5.5.2.1 Method of Slope Stability Analysis

The stability of the constructed shorefront slope is assessed using the simplified Bishop moment limit equilibrium method, (Bishop, 1955) which considers moment equilibrium of a potential sliding mass. The factor of safety (FS) of the slope is defined (Lambe, 1969) as:

$FS = M_R/M_D$ = Resisting Moment/Driving Moment

The simplified Bishop method of stability analysis is recognized as a reliable method of calculation, as indicated by comparisons of six methods of analysis (Ordinary Method, simplified Bishop method, Spencer method, Janbu simplified method, Janbu rigorous method, and Morganstern-Price method) reported by Fredlund and Krahn (Fredlund, 1977). Lambe and Whitman (Lambe, 1969) recommend the simplified Bishop method for general use in evaluating stability of slopes.

Dynamic analysis of the slope is performed using a pseudo-static approach, which represents the effects of seismic shaking by accelerations that create both horizontal and vertical inertial forces on the potential sliding mass. The pseudostatic approach provides a reasonable estimate of the seismic stability of slopes where the slope and foundation materials do not loose strength as a result of the earthquake shaking, which is the case for this slope (Kramer, 1996). The pseudo-static seismic forces are computed based on the design horizontal and vertical ground accelerations, a_h and a_v respectively, determined for the site as summarized in Section 2.5.5.2.4.3.

The glacial till and compacted site fill are not liquefiable as discussed in Section 2.5.4.8. Therefore, liquefaction potential was not considered in the stability analyses.

2.5.5.2.2 Criteria for Minimum Factor of Safety

The minimum acceptable value of FS under static loading for the shorefront slope is established based on recommendations in the U.S. Army Corps of Engineers Manual EM 1110-2-1902 Slope Stability, Table 3-1, (USACE, 2003) as:

$FS \geq 1.5$ for static (long-term) loading conditions.

The U.S. Army Corps of Engineers Manual EM 1110-2-1902 (USACE, 2003) does not provide a recommended minimum FS for seismic conditions. However, the Corps manual does provide a recommended minimum factor of safety for rapid drawdown from maximum surcharge pool, which is a very infrequent and short term event analogous to the design seismic event. Based on this recommendation, the minimum acceptable value of FS for pseudo-static under seismic loading is selected as:

$FS \geq 1.1$ for design seismic loading conditions.

During the life of the slope, temporary surcharge loading may be placed on the ground surface at the top of the slope as discussed in Section 2.5.5.2.4.4. For stability under the surcharge load, which may be in place for a longer time than seismic loading but does not represent a long

term loading condition, an intermediate factor of safety was selected based on the recommendations in EM 1110-2-1902 (USACE, 2003) for end of construction:

FS $\geq$ 1.3 for temporary loading conditions such as surcharge at top of slope.

2.5.5.2.3 Computer Software for Stability Analyses

The computer software program GeoStudio 2007, SLOPE/W (GEO-INTERNATIONAL, 2007) was used to perform the stability analysis calculations. This software is widely used and is representative of the state of practice for large civil projects. The program and platform were independently validated as part of the analysis as described below. The software searches for a critical slip surface by attempting several hundred combinations of surfaces of different shapes. Both static and pseudo-static analyses were performed for the design slope crosssection, allowing the program to search for the critical potential failure surface, i.e., the potential failure surface with minimum factor of safety.

Independent validation of the specific program and platform (software and computer) used for the analyses was performed by running three trial problems that have been previously solved and published to verify that the program produced the same results as published. The trial problems included static stability with circular surface, static stability with non-circular surface and pseudo-static stability with circular surface. The example problems were take from Lambe and Whitman (Lambe, 1969), Duncan and Wright (Duncan, 2005) and Kramer (Kramer, 1996). The validation runs matched the published factors of safety very closely (i.e., the factors of safety agree within ± 0.01), confirming that the program was operating properly. The first validation example was a calculation for the factor of safety for a simple slope, originally presented by Lambe and Whitman (1969). The simple slope example was used to verify the SLOPE/W solution for circular failures using the Bishop Method, a piezometric line, and grid and radius slip surface. With the same soil parameters and slope geometry, the factor of safety calculated by SLOPE/W of 1.34 was identical to the factor of safety calculated by Lambe and Whitman in the original problem. The second SLOPE/W validation problem was a static, non-circular search, originally presented by Duncan and Wright (2005). Using the Bishop Method with hlock specified slip surfaces and all the same input parameters, SLOPE/W calculated a factor of safety of 1.16. which is negligibly less than the factor of safety of 1.17 calculated by Duncan and Wright. The third SLOPE/W validation problem was a pseudo-static analysis, originally presented by Kramer (1996). This example was used to verify the SLOPE/W solution for circular slip surfaces under seismic conditions. The factor of safety calculated by SLOPE/W of 1.28 was the same as the factor of safety calculated by Kramer. In summary the validation problems matched the published factors of safety very closely (i.e., the factors of safety agree within ± 0.01), confirming that the program was operating properly.

2.5.5.2.4 Input Properties and Parameter for Stability Analyses

The input properties and parameters used for the stability analyses of the shorefront slope are summarized below.

2.5.5.2.4.1 Soil, Rock and Fill Properties

The properties of the various materials required for the stability analyses include unit weight, drained friction angle, and cohesion. The properties used in the analyses are as follows:

Material	Unit Weight		Friction Angle	Cohesion	
	(pcf)	kN/m^3	(degrees)	(psf)	kN/m^2
Glacial Till	140	22	36	0	
Bedrock	164	26	0	16,000	766
Site Fill	145	23	35	0	
Coarse and FIne Bedding	120	19	36	0	
Riprap	120	19	36	0	

The basis for these properties is summarized below:

1. Glacial Till

   The unit weight of glacial till is estimated from published ranges presented in Peck et al. (Peck, 1953) and Kulhawy et. al. (Kulhawy, 1990). A friction angle for the glacial till is estimated based on correlations to Standard Penetration Test N-values published in Peck et. al. (Peck, 1953). These values are slightly conservative compared to the density and friction angle measured on compacted samples of till, as reported in Section 2.5.4.2.1.

2. Bedrock

   The unit weight of bedrock is the average of the 45 measured values determined on intact specimens of rock core from the on-site explorations. The cohesion for the bedrock is determined for the rock mass based on the methodology recommended in the U.S. Army Corps of Engineers Manual EM 1110-1- 2908, Rock Foundations, (USACE, 1994) as discussed in Section 2.5.4.10. No friction was used for the rock mass because the confining pressure, and hence the friction component of rockstrength, is low compared to the rock mass cohesion value.

3. Site Fill

   The unit weight and friction angle for the site fill are determined based on laboratory tests on representative samples of the fill material, as discussed in Section 2.5.4.2.1. These values are slightly conservative compared to the density and friction angle measured on compacted samples of the site fill.

4. Coarse and Fine Bedding

   The coarse and fine bedding are angular to subangular processed quarry stone. Unit weight and friction angle of coarse and fine bedding are determined based on test data from similar types of materials previously used in large rock fill dams, as reported in Leps (Leps, 1970), Marachi et. al. (Marachi, 1972) and Hirschfeld and Poulos (Hirschfeld, 1973).

5. Riprap

The riprap is quarried stone with generally prismoidal shape. The dimensions and thickness vary depending on location. The riprap dimensions are described in the following table:

Riprap Design						
Location of Riprap	D_{50} of Riprap		Thickness of Riprap		Thickness of Bedding	
	(feet)	(meters)	(feet)	(meters)	(feet)	(meters)
Shoreline at Raw Water Pump House	2.50	0.76	3.75	1.14	1.50	0.46
Shoreline at other locations	2.00	0.61	3.00	0.91	1.50	0.46

The unit weight and friction angle for riprap are determined based on test data from similar types of materials previously used in large rock fill dams, as reported in Leps (Leps, 1970), Marachi et. al. (Marachi, 1972) and Hirschfeld and Poulos (Hirschfeld, 1973).

2.5.5.2.4.2 Groundwater

Groundwater levels in the soil at the NMP3NPP site vary during the year. The minimum depth to ground water below original site grade (prior to plant construction) was about 3 ft (0.91 m). For the stability analyses, it was conservatively assumed that the ground water in the soil behind the slope would be at a depth of 3 ft (0.91 m) below the finished site grade, which above the original site grade. This assumed depth to ground water is slightly conservative compared to the U.S. EPR design criteria for minimum depth to ground water, which is 3.3 ft (1.0 m).

2.5.5.2.4.3 Seismic Loading

The horizontal and vertical seismic ground accelerations (a_h and a_v, respectively) used in the stability analyses were equal to the rock surface values determined by the site specific seismic response analysis as follows:

$a_h = 0.071$ g

$a_v = 0.056$ g

No amplification in the soil above rock was considered due to the limited thickness of soil (14 ft (4.3 m) to mid-height of the slope) and the dense and granular nature of the till.

2.5.5.2.4.4 Temporary Surcharge

For evaluation of temporary loading conditions, a uniform ground surface surcharge of 300 lb/ft^2 (1465 kg/m^2) was added at the top of the slope. This surcharge is equivalent to an average of 2 ft (0.6 m) of temporary soil storage or to the distributed load of large construction equipment.

2.5.5.2.4.5 Results of Stability Analyses

The results of the stability analyses on the shorefront slope are shown in Figure 2.5-179 through Figure 2.5-187, for static and pseudo-static analyses using the circular arc and non-circular surface calculations. Because many of the critical failure surfaces were shallow, i.e., primarily through the bedding and riprap near the surface of the slope, additional analyses were

performed for deeper circular failure surfaces where a significant portion of the surface was forced to pass through the glacial till.

The Factor of Safety (FS) results are summarized in the table below:

Loading Condition	FS Criteria (Minimum Required)	FS for Circular Surface	FS for Non-Circular Surface	FS for Deep Circular Surface
Static	> 1.5	1.56	1.61	1.67
Static Plus Temporary Surcharge	> 1.3	1.47	1.59	1.47
Seismic (Pseudo-static)	> 1.1	1.33	1.39	1.39

The computed FS on the critical potential failure surface for each loading case exceeds the minimum required FS. These results demonstrate that the constructed shorefront slope is adequately stable under all design loading conditions to prevent adverse impact on safety related structures.

In addition, these results demonstrate that all other on-site temporary construction and permanent site grading slopes, which are not as high and are less steep, are adequately stable to prevent adverse impact on safety related structures.

2.5.5.3 Logs of Borings

The four borings located closest to the section of shorefront slope cross section analyzed are B-301 and B-302 onshore, and B-428 and B-431 offshore. The locations of these borings and the stratigraphy encountered at these borings are shown on the cross section in Figure 2.5-178. Logs of the borings are presented in Part 11E.

2.5.5.4 Compacted Fill

The properties of the compacted fill for the site are discussed in Section 2.5.4.5. Selection of design parameters for the compacted fill is discussed in Section 2.5.4.2.1 and 2.5.4.5.

The characteristics and properties of the riprap and coarse and fine bedding stone are discussed in Section 2.5.5.2. Specific gradations for the riprap and bedding layers are determined and specified based on the design wave forces and filter criteria. Material properties are specified to produce sound, durable stone, including angularity, aspect ratios (length to width to height requirements), durability, soundness and specific gravity. Quality control during construction is provided by field and laboratory testing of source materials, regular measurement of particle sizes of representative samples at the quarry prior to shipment to the site, and visual observation of the placement methods and in place gradation to ensure a dense, non-segregated layer.

2.5.5.5 References

Bishop, 1955. The Use of the Slip Circle in the Stability Analysis of Slopes, A. W. Bishop, Geotechnique, Volume 5, 1955.

Duncan, 2005. Soil Strength and Slope Stability, J. M. Duncan and S.G. Wright, John Wiley and Sons, 2005.

Fredlund, 1977. Comparison of Slope Stability Methods of Analysis, D.G. Fredlund and J. Krahn, Canadian Geotechnical Journal, National Research Council of Canada, Ottawa, Volume 14, Number 3, August 1977.

GEO-INTERNATIONAL, 2007. GeoStudio 2007, SLOPE/W, Version 7.11, Build 4199. GEOSLOPE International, Ltd., Calgary, Alberta, Canada, 2007.

Hirschfeld, 1973. Embankment Dam Engineering. R.C. Hirschfeld and S.J. Poulos, John Wiley and Sons, 1973.

Kulhawy, 1990. Kulhawy. F.R., Mayne, P.W., "Manual on Estimating Soil Properties for Foundation Design" Cornell University Geotechnical Engineering Group. Ithaca, New York, 1990, page 2-18.

Kramer, 1996. Geotechnical Earthquake Engineering, S.L. Kramer, Prentice Hall, 1996.

Lambe, 1969. Soil Mechanics, T.W. Lambe and R.V. Whitman, John Wiley and Sons, 1969.

Leps, 1970. Review of Shearing Strength of Rockfill, T.M. Leps, Journal of Soil Mechanics and Foundation Division, American Society of Civil Engineers, Volume 96, Number SM 4, Proceedings Paper 7394, July 1970.

Marachi, 1972. Evaluation of Properties of Rockfill Materials, N.D. Marachi, C.K. Chan, and H.B. Seed, Journal of the Soil Mechanics and Foundation Division, American Society of Civil Engineers, Volume 98, Number SM 1, Proceedings Paper 8672, January 1972.

NRC, 2007. Combined License Applications for Nuclear Power Plants (LWR Edition), Regulatory Guide 1.206, Revision 0, U.S. Nuclear Regulatory Commission, March 2007.

Peck, 19533. Peck. R. B., Hanson, W.E., Thombum, T.R., "Foundation Engineering" John Wiley & Sons, Inc. 1953. Pages 13, 87, and 310.

USACE, 1994. Rock Foundations, Manual EM 1110-1-2908, U.S. Army Corps of Engineers, November 30, 1994.

USACE, 2003. Slope Stability, Manual EM 1110-1-1902, U.S. Army Corps of Engineers, October 31, 2003.}

2.5.6 REFERENCES

No departures or supplements.

Table 2.5-1—{Earthquake Catalog for Earthquakes within 200 miles (320 km) of Site}

(Page 1 of 9)

YEAR	MONTH	DAY	HR	MIN	SEC	LAT	LON	DEPTH	MN	MLG	MD	m_b	INT	EMB	SMB	RMB	DISTANCE
1732	9	16	16			45.5	73.6					5.7	8	5.7	0.3	5.8	313
1796	12	26	11			42.9	79					4.3	6	4.3	0.55	4.65	220
1816	9	9				45.5	73.6					4.9	7	4.9	0.56	5.26	313
1818	12	7				44	76.5					3.11	4	3.11	0.56	3.47	54
1840	1	16	20			43	75					4	5.5	4	0.55	4.35	128
1840	9	10				43.2	79.85					3.4	4.5	3.4	0.56	3.76	279
1844	11					45.5	73.6					3.11	4	3.11	0.56	3.47	313
1853	3	12	7			43.7	75.5					4	5.5	4	0.55	4.35	76
1853	3	13	10			43.1	79.4					3.4	4.5	3.4	0.56	3.76	245
1855	12	17	19			43.3	73.7					3.11	4	3.11	0.56	3.47	219
1857	10	23	20	15		43.2	78.6					4.47	6	4.47	0.3	4.57	180
1858	1	1	7			42.9	78.5					3.11	4	3.11	0.56	3.47	182
1861	7	12				45.4	75.4					4.85	6	4.85	0.3	4.95	224
1861	10					45.6	73.7					3.7	5	3.7	0.56	4.06	316
1863	6	9	21	30		44.5	73					3.11	4	3.11	0.56	3.47	293
1864	10	21	9	10		45.5	73.6					3.11	4	3.11	0.56	3.47	313
1867	12	18	8			44.65	75.15					4.81	6	4.81	0.3	4.91	161
1871	1	3				45.6	74.6					3.7	5	3.7	0.56	4.06	272
1873	4	25	19			44.8	74.2					3.7	5	3.7	0.56	4.06	226
1873	4	30				45	74.7					3.11	4	3.11	0.56	3.47	214
1873	4	30				43.3	79.9					3.11	4	3.11	0.56	3.47	282
1873	7	6	14	30		43	79.5					4.58	5.5	4.58	0.24	4.65	256
1877	11	4				45.2	73.9					4.83	6	4.83	0.3	4.93	273
1877	12	18	10			45.7	76.85					3.7	5	3.7	0.56	4.06	245
1878	10	4	7	30		41.5	74					3.54	5	3.54	0.31	3.65	299
1879	8	21	8			43.2	79.2					3.51	4	3.51	0.3	3.61	227
1880	5	31				45.2	75.3					3.11	4	3.11	0.56	3.47	207
1880	9	6	5	30		45.2	73.8					3.11	4	3.11	0.56	3.47	279
1882	11	27	23	30		43	79.25					3.11	4	3.11	0.56	3.47	236
1883	3	12				45.1	74.5					3.11	4	3.11	0.56	3.47	232
1886	1	25		4		41.6	73.8					3.11	4	3.11	0.56	3.47	302
1888	1	11	9			45.8	77.1					3.11	4	3.11	0.56	3.47	260
1889	8	10				43.4	73.7					3.11	4	3.11	0.56	3.47	218
1894	12	17				42.5	73.8					3.11	4	3.11	0.56	3.47	240

Table 2.5-1—{Earthquake Catalog for Earthquakes within 200 miles (320 km) of Site}

YEAR	MONTH	DAY	HR	MIN	SEC	LAT	LON	DEPTH	MN	MLG	MD	m_b	INT	EMB	SMB	RMB	DISTANCE
1897	3	7				43.1	79.2					3.11	4	3.11	0.56	3.47	229
1897	3	23	23	7		45.5	73.6					4.55	6	4.55	0.3	4.65	313
1897	5	28	3	16		44.5	73.5					4.3	6	4.3	0.55	4.65	256
1898	1	7	6			45.1	74.3					3.11	4	3.11	0.56	3.47	243
1898	6	11	6	45		42.8	72.6					3.11	4	3.11	0.56	3.47	318
1903	12	25	12	30		44.7	75.5					3.7	5	3.7	0.56	4.06	150
1906	11	17	14			45.61	75.41					3.11	4	3.11	0.56	3.47	246
1907	1	10	9	45		41.2	77.1					3.11	4	3.11	0.56	3.47	266
1907	11	14	5			45.47	76.68					3.11	4	3.11	0.56	3.47	218
1908	6	16	20	41		45.1	74.8					3.7	5	3.7	0.56	4.06	218
1908	7	17	7	10		45.43	76.35					3.11	4	3.11	0.56	3.47	213
1909	2	1	8	20		45.51	73.57					3.11	4	3.11	0.56	3.47	316
1909	12	10	6	24	10	45.4	75.6					3.11	4	3.11	0.56	3.47	219
1910	2	25				43.2	79.8					3.11	4	3.11	0.56	3.47	275
1912	5	27	12	52		43.2	79.7					3.7	5	3.7	0.56	4.06	267
1913	4	29		28	57	44.87	75.33					4.14	5	4.14	0.24	4.21	173
1913	6	8	6	30		45.68	74.4					3.11	4	3.11	0.56	3.47	288
1913	8	10	5	15		44	74					3.65	4	3.65	0.3	3.75	200
1914	2	10	18	31		46	75					5.31	7	5.31	0.24	5.38	298
1915	2	21	23	41		44.7	73.4					3.11	4	3.11	0.56	3.47	273
1916	1	5	13	56		43.7	73.7					3.7	5	3.7	0.56	4.06	218
1916	2	3	4	26		43	74					4.1	5	4.1	0.3	4.2	203
1916	11	2	2	32		43.3	73.7					3.7	5	3.7	0.56	4.06	219
1917	5	22	9		26	45.1	75.6					4.16	4.5	4.16	0.3	4.26	188
1922	12	8	21	24		44.4	75.1					3.7	5	3.7	0.56	4.06	143
1924	7	15		10		45.7	76.5					4	5.5	4	0.55	4.35	243
1926	1	27				44.3	74.1					3.11	4	3.11	0.56	3.47	204
1926	8	23	16	40		45.8	77.1					3.11	4	3.11	0.56	3.47	260
1927	3	12	22	12		44.6	75.2					3.11	4	3.11	0.56	3.47	154
1927	10	24	11			44.7	73.8					3.11	4	3.11	0.56	3.47	246
1927	11	13		50		43.1	79.06					3.11	4	3.11	0.56	3.47	218
1928	3	18	15	25		44.5	74.3					4.31	5.5	4.31	0.24	4.38	201
1929	8	12	11	24	48.7	42.91	78.4					4.99	8	4.99	0.3	5.09	174
1931	4	20	19	54	30.6	43.47	73.78					4.81	7	4.81	0.3	4.91	211

Table 2.5-1—{Earthquake Catalog for Earthquakes within 200 miles (320 km) of Site}

(Page 3 of 9)

YEAR	MONTH	DAY	HR	MIN	SEC	LAT	LON	DEPTH	MN	MLG	MD	m_b	INT	EMB	SMB	RMB	DISTANCE
1931	4	22				42.9	78.9					3.11	4	3.11	0.56	3.47	212
1932	12	7	3	15		44.4	74.1					3.11	4	3.11	0.56	3.47	209
1933	1	21	16	4	39.5	45.3	74.65					3.74		3.74	0.41	3.93	243
1933	7	14	4	48	40	45.42	75.7					3.82		3.82	0.41	4.01	219
1933	10	29				43	73.7					3.11	4	3.11	0.56	3.47	226
1934	4	15	2	58		44.7	73.8					4.36	5.5	4.36	0.24	4.43	246
1935	1	28	6			44.8	74.3					3.11	4	3.11	0.56	3.47	220
1936	6	21	4	20		44.7	74.2					3.11	4	3.11	0.56	3.47	220
1937	3	10	5	29		44.6	75.2					3.11	4	3.11	0.56	3.47	154
1938	1	6	13	28	42.2	44.9	75.18					3.25		3.25	0.41	3.44	182
1938	1	24	5	29	2	45.57	76.27					3.09		3.09	0.41	3.28	229
1938	5	5		33	0.3	45.37	74.5					3.09		3.09	0.41	3.28	256
1938	9	7	23	18	18.9	45.87	74.9					2.81	3.5	2.81	0.56	3.17	288
1938	11	18	22	19	6	44.75	75.25					3.4	4.5	3.4	0.56	3.76	165
1939	1	14	8	10	16	43.25	79.85					3.34		3.34	0.41	3.53	278
1940	8	7	23	57	35.3	45.77	74.83					3.09		3.09	0.41	3.28	280
1941	3	5	7	29	23.2	46.27	75.5					3.09		3.09	0.41	3.28	314
1941	4	4	8	10	43.7	44.73	73.92					3.34		3.34	0.41	3.53	240
1941	10	21	6	10	41	44.77	74.8					3.34		3.34	0.41	3.53	189
1941	10	24	14	13	59.3	45.7	74.3					3.58		3.58	0.41	3.77	295
1942	5	20	12	19	22.8	45.77	74.67					4.23		4.23	0.41	4.42	286
1942	5	24	11	33		44.7	73.8					3.82		3.82	0.41	4.01	246
1942	10	2	22	29	50.5	42.57	73.8					3.09		3.09	0.41	3.28	236
1942	10	24	17	27	3.6	40.97	75.25					3.42		3.42	0.41	3.61	301
1943	5	9	11	3	12.5	44.77	73.83					3.25		3.25	0.41	3.44	248
1943	7	6	22	10	16	44.84	73.03					3.98		3.98	0.41	4.17	306
1944	1	22	21	55	9.1	45.83	76.78					4.15		4.15	0.41	4.34	259
1944	2	5	16	22		40.8	76.2					3.66		3.66	0.41	3.85	305
1944	9	5	4	38	45.7	44.96	74.72					5.71	8	5.71	0.2	5.76	209
1946	6	27	21	6	22	44.65	74.53					3.09		3.09	0.41	3.28	196
1946	10	28	20	36		41.5	76.6					3.58		3.58	0.41	3.77	227
1946	11	10	11	41	23.1	42.87	77.45					3.17		3.17	0.41	3.36	111
1948	6	9	3	4	12.2	45.23	73.87					3.66		3.66	0.41	3.85	277
1948	7	7	7	38	1.4	45.18	73.9					3.5		3.5	0.41	3.69	272

Table 2.5-1—{Earthquake Catalog for Earthquakes within 200 miles (320 km) of Site}

(Page 4 of 9)

YEAR	MONTH	DAY	HR	MIN	SEC	LAT	LON	DEPTH	MN	MLG	MD	m_b	INT	EMB	SMB	RMB	DISTANCE
1949	10	16	23	33	45.4	45.49	74.9					4.07		4.07	0.41	4.26	250
1950	3	6	16	14	11.8	46	74.5					3.9		3.9	0.41	4.09	315
1950	3	20	22	55	11.5	41.5	75.8					3.34		3.34	0.41	3.53	231
1950	8	4	14	29	28.7	45.2	74.72					3.9		3.9	0.41	4.09	230
1950	10	29	5	59	26	45.82	77.12					3.09		3.09	0.41	3.28	262
1951	8	8	9	36	24.1	45.93	74.67					3.34		3.34	0.41	3.53	302
1951	9	3	21	26	24.8	41.35	73.86					3.71	4	3.71	0.2	3.76	320
1951	9	25	15	45		46.22	75.37					3.66		3.66	0.41	3.85	312
1951	10	25	7	7	52.8	45.27	74.73					3.74		3.74	0.41	3.93	236
1951	11	6	17	54	45.9	44.92	73.55					4.01		4.01	0.2	4.06	276
1952	1	30	4			44.5	73.2					4.3	6	4.3	0.55	4.65	278
1952	8	25		7		43	74.5					3.44	5	3.44	0.31	3.55	164
1953	3	31	12	58	33.4	43.76	73.08					3.91	5	3.91	0.2	3.96	268
1953	4	26	1	17		44.7	73.5					3.72	4	3.72	0.33	3.85	266
1954	1	31	12	30		42.9	77.3					3.11	4	3.11	0.56	3.47	100
1954	2	1		37	50	43.03	76.65					3.34		3.34	0.41	3.53	58
1954	4	21	15	45		44.7	73.5					3.11	4	3.11	0.56	3.47	266
1954	4	27	2	14	8	43.1	79.2					3.98		3.98	0.41	4.17	229
1954	5	20	22			45	74.2					3.19	4	3.19	0.33	3.32	241
1954	12	13	3	53		44.6	74.6					3.66	4	3.66	0.33	3.79	188
1955	2	3	2	30		44.5	73.22					4.08	5	4.08	0.33	4.21	277
1955	6	29	1	17	40	43.77	79.63					3.35	4	3.35	0.33	3.48	259
1955	8	16	7	35		42.9	78.3					3.7	5	3.7	0.56	4.06	167
1955	10	7	18	9	52	45.22	73.9					3.5		3.5	0.41	3.69	275
1956	1	10	12	8	18	45.67	75.47					3.34		3.34	0.41	3.53	251
1956	2	2	19	24	16	45.45	74.82					3.17		3.17	0.41	3.36	249
1956	3	6	23	38	10	44.85	75.38					3.17		3.17	0.41	3.36	169
1956	7	27	1	34	44	44.7	73.78					3.42		3.42	0.41	3.61	247
1956	11	4	11	53	29.2	45.96	75.42					3.9		3.9	0.41	4.09	283
1957	2	20	15	45		44.9	74.9					3.11	4	3.11	0.56	3.47	195
1957	8	21	2	40	33	44.8	76.17					3.09		3.09	0.41	3.28	144
1958	1	11	16	36		44.9	74.9					3.11	4	3.11	0.56	3.47	195
1958	3	19	6	39	25	46	77.13					3.17		3.17	0.41	3.36	282
1958	7	22	1	46	40	43	79.5					4.23		4.23	0.41	4.42	256

Table 2.5-1—{Earthquake Catalog for Earthquakes within 200 miles (320 km) of Site}

(Page 5 of 9)

YEAR	MONTH	DAY	HR	MIN	SEC	LAT	LON	DEPTH	MN	MLG	MD	m_b	INT	EMB	SMB	RMB	DISTANCE
1958	8	4	20	25	58	43.13	80					3.82	4	3.82	0.33	3.95	292
1958	8	22	14	25	5	43	79					3.58		3.58	0.41	3.77	217
1958	9	30		13	58	45.18	73.73					3.66		3.66	0.41	3.85	282
1959	4	13	21	20	19	41.92	73.27					3.42		3.42	0.41	3.61	311
1961	3	13	10	55	45	45.17	75.28					3.66		3.66	0.27	3.74	205
1961	9	29	6	30		44.9	74.9					3.11	4	3.11	0.56	3.47	195
1962	1	27	12	11	17	45.92	74.85					3.71		3.71	0.2	3.76	294
1962	3	27	6	35		43	79.3					3.55	5	3.55	0.33	3.68	240
1962	4	10	14	30	45.2	44.11	72.97					4.1	5	4.1	0.3	4.2	283
1962	10	2	23	45		44.8	74.3					3.11	4	3.11	0.56	3.47	220
1963	1	30	14	50		44	75.9					3.35	4	3.35	0.33	3.48	67
1963	2	27	6			43.2	79.57					3.09		3.09	0.41	3.28	257
1963	3	2	20	24	32	41.51	75.73					3.42		3.42	0.41	3.61	232
1963	5	19	19	14		43.5	75.2					3.41	3	3.41	0.33	3.54	97
1963	7	1	19	59	12	42.37	73.75					3.34		3.34	0.41	3.53	251
1963	8	26	16	29	35	45.18	73.95					3.5		3.5	0.41	3.69	269
1964	3	29	9	16		44.9	74.9					4.24	5	4.24	0.33	4.37	195
1964	6	16	14			45	74.2					3.19	4	3.19	0.33	3.32	241
1965	7	16	11	6	57	43.04	78.08					3.61	4	3.61	0.33	3.74	145
1965	9	29	20	57		41.4	74.4					3.11	4	3.11	0.56	3.47	288
1966	1	1	13	23	39	42.84	78.25					4.58	6	4.58	0.1	4.59	167
1966	6	25		5	51	45.16	73.83					3.42		3.42	0.41	3.61	274
1967	6	13	19	8	55.5	42.84	78.23					4.38	6	4.38	0.1	4.39	165
1969	10	6				41.1	74.6					3.11	4	3.11	0.56	3.47	309
1971	5	23	6	24	27.9	43.9	74.48					4.08		4.08	0.1	4.09	160
1971	11	23	16	32	30	45.83	76.62					3.09		3.09	0.41	3.28	258
1971	12	18	15	36	24.5	46.01	74.67					3.98	5	3.98	0.1	3.99	309
1972	12	16	19	1	37.2	45.64	75.1					3.88		3.88	0.1	3.89	258
1973	7	15	8	20	30.7	43.87	74.47					3.45		3.45	0.2	3.5	160
1974	3	18	16	5		44.45	74.85					3.09		3.09	0.41	3.28	162
1974	6	9	18	39		44.9	73.6					3.4		3.4	0.3	3.5	271
1974	8	8	11	55	33	45.93	76.08					3.25		3.25	0.41	3.44	270
1974	10	23	22	52	57	46.08	75.48					3.25		3.25	0.41	3.44	294
1974	11	2	13	47	56	46.07	75.03					3.25		3.25	0.41	3.44	304

Table 2.5-1—{Earthquake Catalog for Earthquakes within 200 miles (320 km) of Site}

YEAR	MONTH	DAY	HR	MIN	SEC	LAT	LON	DEPTH	MN	MLG	MD	m_b	INT	EMB	SMB	RMB	DISTANCE
1975	6	9	18	39	22.7	44.87	73.65					3.4		3.4	0.3	3.5	266
1975	6	30	20	15	23	43.4	79.77					3.14	3	3.14	0.33	3.27	270
1975	11	3	20	54	55.3	43.91	74.65					3.9		3.9	0.3	4	147
1978	7	30	10	54	44	45.68	74.44					3.58		3.58	0.1	3.59	287
1978	8	21	8	47		44.52	74.51					3.17		3.17	0.41	3.36	188
1979	5	29	20	48	49.1	45	74.99					3.09		3.09	0.41	3.28	200
1979	6	7	13	45	53.3	44.43	73.86					3.17		3.17	0.41	3.36	227
1980	5	23	8	39	44	44.89	74.55					3.38		3.38	0.1	3.39	213
1980	6	6	13	15	51.96	43.56	75.23					3.48	5	3.48	0.1	3.49	95
1981	7	5	21	47	23	45.17	74.62					3.38		3.38	0.1	3.39	232
1981	9	18	7	16	7	46.11	75.02					3.48	3.5	3.48	0.1	3.49	309
1982	8	6	6	29	10	45.89	75.46					3.68	4	3.68	0.1	3.69	274
1982	9	3	23	14	3	45.67	76.61					3.68		3.68	0.1	3.69	240
1983	10	7	10	18	47	44.03	74.31					5.18	6	5.18	0.1	5.19	177
1983	10	11	4	10	55	45.21	75.77					4.18		4.18	0.1	4.19	195
1983	11	1	10	16	52	45.68	73.9					3.48		3.48	0.1	3.49	312
1984	10	23	6	26	21.92	43.59	73.93					3.43		3.43	0.3	3.53	199
1985	4	14	3	44	39	42.95	80.04	18	3.1					3.1	0	3.1	299
1985	8	24	6	4	2	45.68	76.65	18	3.1					3.1	0	3.1	241
1985	11	1	23	33	39	45.29	73.49	12.4	3.4					3.4	0	3.4	304
1986	1	10	9	59	48	45.8	77.32	18	3.3					3.3	0	3.3	264
1986	6	18	4	12	2	45.86	74.76	3.1	3					3.0	0	3.0	291
1986	8	13	4	55	18	45.1	74.25	7	3.3					3.3	0	3.3	246
1986	10	20	6	59	0	42.62	74.13	17.76	3					3.0	0	3.0	210
1987	7	23	9	32	28	43.49	79.47	6.8	3.4					3.4	0	3.4	246
1987	9	26	17	44	8	44.49	74.52	5	3.8					3.8	0	3.8	185
1987	10	23	12	31	2	45.76	74.51	14.8	3.7					3.7	0	3.7	291
1987	11	11	7	58	33	45.77	75.34	17.1	3.5					3.5	0	3.5	265
1988	3	10	14	42	55	46.34	75.67	12.5	3.7					3.7	0	3.7	319
1988	5	15	6	10	5	45.16	75.61	8.5	3.3					3.3	0	3.3	194
1988	8	9	13	57	27	45.01	74.99	9.5	3.4					3.4	0	3.4	201
1989	8	5	21	7	59	43.21	79.53	18	3.3					3.3	0	3.3	253
1989	8	5	21	7	58	43.29	79.76	5	3.2					3.2	0	3.2	271
1989	11	4	23	25	43	46.22	75.72	7.9	3.4					3.4	0	3.4	306

Table 2.5-1—{Earthquake Catalog for Earthquakes within 200 miles (320 km) of Site}

(Page 7 of 9)

YEAR	MONTH	DAY	HR	MIN	SEC	LAT	LON	DEPTH	MN	MLG	MD	m_b	INT	EMB	SMB	RMB	DISTANCE
1990	12	14	19	38	7	41.84	77.48	18	3					3.0	0	3.0	207
1991	2	16	0	46	41	44.66	74.08	5	3.3					3.3	0	3.3	225
1991	3	6	5	26	53	46.28	76.87	18	3.9					3.9	0	3.9	309
1991	5	17	18	8	47	45.5	74.4	18	4.4					4.4	0	4.4	272
1991	6	17	8	53	19	42.58	74.64	12.3	4.3					4.3	0	4.3	177
1991	7	5	1	47	36	45.2	73.85	18	3.8					3.8	0	3.8	276
1991	8	22	8	22	55	45.87	75.11	10.6	3.1					3.1	0	3.1	281
1991	9	2	0	58	0	42.49	74.21	5	3.1					3.1	0	3.1	212
1991	11	21	0	5	31	45.26	73.55	9.65	3.1					3.1	0	3.1	298
1992	6	7	0	59	16	42.58	74.11	7.05	3.4					3.4	0	3.4	213
1992	10	5	22	36	11	44.81	74.71	26.4	3					3.0	0	3.0	197
1992	11	17	3	58	1	45.77	74.93	16	4.4					4.4	0	4.4	277
1993	3	17	9	5	41	46.08	75.33	19.9	3.2					3.2	0	3.2	298
1993	4	4	1	5	17	45.34	74.04	18	3					3.0	0	3.0	276
1993	5	6	1	23	25	46.3	75.53	16.3	3.5					3.5	0	3.5	317
1993	7	30	22	30	54	45.26	74.12	8.1	3.8					3.8	0	3.8	266
1993	9	23	6	45	28	46.07	74.61	18	3.8					3.8	0	3.8	317
1993	11	16	9	31	44	45.19	73.46	15.1	4.3					4.3	0	4.3	299
1994	1	11	0	25	49	45.76	76.07	18	3.4					3.4	0	3.4	251
1994	3	12	10	43	16	42.78	77.88	1	3.6					3.6	0	3.6	145
1994	8	28	15	38	20	46.32	77.1	18	3.6					3.6	0	3.6	316
1994	12	15	21	44	6	45.92	75.24	13	3					3.0	0	3.0	283
1995	2	15	15	53	57	45.9	75.04	18	3.5					3.5	0	3.5	286
1995	3	2	5	33	52	44.24	74.43	5	3					3.0	0	3.0	177
1995	5	25	14	22	33	42.99	78.83	5	3					3.0	0	3.0	204
1995	7	28	5	47	37	46.16	74.95	18	3.3					3.3	0	3.3	316
1995	9	12	3	59	5	45.6	74.44	18	3.7					3.7	0	3.7	279
1995	9	21	23	3	28	45.09	74.21	18	3.1					3.1	0	3.1	247
1995	10	9	5	39	37	46.14	75.26	18	3.2					3.2	0	3.2	306
1996	2	20	6	13	17	45.96	74.78	18	3.1					3.1	0	3.1	301
1996	3	14	10	42	26	45.92	74.4	18	4.4					4.4	0	4.4	311
1997	4	3	18	32	15	42.92	75.71	10.53	3.5					3.5	0	3.5	88
1997	5	24	18	52	9	45.91	74.24	18	4.2					4.2	0	4.2	316
1997	7	10	13	57	50	45	74.78	10.1	3					3.0	0	3.0	210

Table 2.5-1—{Earthquake Catalog for Earthquakes within 200 miles (320 km) of Site}

(Page 8 of 9)

YEAR	MONTH	DAY	HR	MIN	SEC	LAT	LON	DEPTH	MN	MLG	MD	m_b	INT	EMB	SMB	RMB	DISTANCE
1997	7	21	22	49	51	46.05	75.42	19.7	3					3.0	0	3.0	292
1997	7	31	7	15	24	43.41	75.27	10	3.4					3.4	0	3.4	92
1997	10	12	8	28	21	44.91	74.55	18	3.1					3.1	0	3.1	214
1997	10	13	23	6	40	44.36	74.97	4.2	3					3.0	0	3.0	148
1998	2	26	14	20	31	46.08	76.36	18	3.7					3.7	0	3.7	285
1998	4	18	16	22	52	45.58	74.97	18	4.1					4.1	0	4.1	256
1998	5	18	15	39	20	45.18	74	18	3					3.0	0	3.0	266
1998	6	9	8	53	52	44.83	73.67	18	3.4					3.4	0	3.4	262
1998	8	24	19	27	33	43.87	75.76	18	3.1					3.1	0	3.1	65
1998	12	25	13	30	26	43.83	77.91	18	3.6					3.6	0	3.6	125
1999	1	19	6	23	20	45.44	74.53	18	3					3.0	0	3.0	261
1999	3	9	12	7	4	44.77	73.83	10	3					3.0	0	3.0	248
1999	3	25	14	6	8	45.96	74.86	18	3					3.0	0	3.0	298
1999	10	31	20	14	10	45.86	74.3	18	4.2					4.2	0	4.2	309
1999	11	26	22	33	1	43.7	78.98	5	3.8					3.8	0	3.8	207
2000	3	2	20	48	29	46.12	75.7	18	3					3.0	0	3.0	295
2000	4	20	8	46	56	44.01	74.32	18	4					4.0	0	4.0	176
2000	5	24	10	22	46	43.78	79.09	5	3.1					3.1	0	3.1	217
2000	8	6	8	52	24	46.19	74.97	18	4.2					4.2	0	4.2	318
2000	10	6	13	59	4	45.1	74.02	18	3.8					3.8	0	3.8	259
2000	10	10	19	46	36	46.28	76.9	18	3					3.0	0	3.0	310
2000	11	6	12	16	35	42.76	74.07	8	3.1					3.1	0	3.1	207
2000	11	10	7	40	53	45.74	75.3	18	3.3					3.3	0	3.3	262
2001	1	14	11	3	47	45.94	74.97	18	3.3					3.3	0	3.3	293
2001	2	3	0	32	43	46.05	74.99	18	3					3.0	0	3.0	303
2001	2	3	20	15	15	42.44	77.48	5	3.2					3.2	0	3.2	149
2001	2	6	14	44	47	46.05	75	18	3					3.0	0	3.0	303
2001	7	27	13	57	28	45.95	74.81	18	3.4					3.4	0	3.4	299
2002	2	24	21	38	33	45.29	75.17	18	3.1					3.1	0	3.1	220
2002	4	1	16	5	22	46.3	75.76	18	3.1					3.1	0	3.1	314
2002	4	20	10	50	47	44.53	73.73	18	5.5					5.5	0	5.5	241
2002	5	24	23	45	59	44.5	73.68	10	3.5					3.5	0	3.5	243
2002	5	28	9	15	38	45.63	76.62	18	3.4					3.4	0	3.4	236
2002	6	1	11	35	29	45.59	73.86	18	3.2					3.2	0	3.2	306

Table 2.5-1—{Earthquake Catalog for Earthquakes within 200 miles (320 km) of Site}

(Page 9 of 9)

YEAR	MONTH	DAY	HR	MIN	SEC	LAT	LON	DEPTH	MN	MLG	MD	m_b	INT	EMB	SMB	RMB	DISTANCE
2002	6	25	13	40	27	44.53	73.67	10	3.4					3.4	0	3.4	246
2002	11	7	16	55	6	44.07	77.44	5	3					3.0	0	3.0	103
2002	12	25	18	25	20	44.57	73.78	10.9	3.3					3.3	0	3.3	240
2003	1	28	16	52	18	45.31	74.92	18	3					3.0	0	3.0	232
2003	3	14	10	33	49	45.66	77.36	18	3.1					3.1	0	3.1	250
2003	4	8	15	6	13	44.62	74.37	11.9	3.7					3.7	0	3.7	204
2003	8	20	1	58	17	46.01	74.95	18	3.5					3.5	0	3.5	300
2003	9	19	17	22	34	45.79	74.85	18	3.3					3.3	0	3.3	281
2004	6	16	6	31	26	42.79	79.01	7	3.1					3.1	0	3.1	225
2004	8	4	23	55	26	43.68	78.24	4	3.8					3.8	0	3.8	148
2004	9	4	2	5	31	44.89	74.92	4	3.1					3.1	0	3.1	193
2005	3	3	2	22	1	45.06	74.2	18	3.5					3.5	0	3.5	245
2005	3	28	16	39	38	43.33	79.28	5	3.1					3.1	0	3.1	232
2005	3	31	15	13	8	46.28	75.64	18	3.4					3.4	0	3.4	313
2005	5	25	19	22	13	46.27	75.62	18	3.7					3.7	0	3.7	312
2005	6	23	18	32	8	46.06	75.04	19	3.3					3.3	0	3.3	303
2005	7	4	11	47	13	46.25	76.9	14.5	3.6					3.6	0	3.6	306
2005	9	6	14	10	51	46.28	75.29	18	3.5					3.5	0	3.5	320
2006	1	9	15	35	39	45.03	73.9	15	4.2					4.2	0	4.2	261
2006	2	25	1	39	22	45.65	75.23	20	4.5					4.5	0	4.5	255
2006	2	26	4	9	22	45.55	74.71	18	3.1					3.1	0	3.1	263
2007	6	2	2	19	55	46.09	74.96	14.64	3					3.0	0	3.0	308
2007	7	19	17	7	57	43.71	78.17	5	3.1					3.1	0	3.1	143
2007	7	24	1	56	49	42.6	74.12	15.15	3.1					3.1	0	3.1	212
2007	8	30	3	47	45	44.32	74.36	8	3.1					3.1	0	3.1	186

Table 2.5-2— {Earthquake Catalog for Earthquakes in Charlevoix Seismic Zone}

(Page 1 of 7)

YEAR	MONTH	DAY	HR	MIN	SEC	LAT	LON	DEPTH	MN	MLG	M	m_b	INT	EMB	SMB	RMB	DISTANCE
1663	2	5	17	30		47.6	70.1					6.1	9	6.1	0.48	6.36	668
1665	10	15	21	30		46.82	71.22					3.11	4	3.11	0.56	3.47	548
1668	4	13	13			47.1	70.5					4.3	6	4.3	0.55	4.65	610
1672	2					48.15	69.7					3.11	4	3.11	0.56	3.47	731
1744	5	27				46.8	71.2					3.11	4	3.11	0.56	3.47	547
1784	1	2	10			46.8	71.2					3.11	4	3.11	0.56	3.47	547
1791	12	6	20			47.4	70.5					5.67	7.5	5.67	0.34	5.8	631
1818	10	11				46.9	71.2					3.11	4	3.11	0.56	3.47	555
1831	5	8				47.3	70.5					4.9	7	4.9	0.56	5.26	624
1831	7	14				47.6	70.1					4.3	6	4.3	0.55	4.65	668
1833	3					47.65	70.17					3.11	4	3.11	0.56	3.47	668
1857	12	8	20			46.7	68					3.11	4	3.11	0.56	3.47	748
1860	10	17	11	15		47.5	70.1					5.92	7.5	5.92	0.3	6.02	661
1864	4	20	18	15		46.9	71.2					4.3	6	4.3	0.55	4.65	555
1866	11	9	16	10		46.8	71.2					3.11	4	3.11	0.56	3.47	547
1869	12					47.5	70.5					3.4	4.5	3.4	0.56	3.76	638
1870	10	20	16	30		47.4	70.5					6.3	8.5	6.3	0.3	6.4	631
1871	5	20	7			46.8	71.2					3.11	4	3.11	0.56	3.47	547
1874	7	31	9			48.6	69.1					3.11	4	3.11	0.56	3.47	798
1880	11	28	13	30		47.45	70.5					3.11	4	3.11	0.56	3.47	635
1881	10	1	6	40		47.6	70.2					3.11	4	3.11	0.56	3.47	663
1887	3	11				47.5	70.5					3.11	4	3.11	0.56	3.47	638
1887	5	27	6	15		47.45	70.5					3.4	4.5	3.4	0.56	3.76	635
1888	4	19	5	30		47.45	70.5					3.11	4	3.11	0.56	3.47	635
1888	12	7	14	25		48.5	68.7					3.11	4	3.11	0.56	3.47	813
1907	8	5	12	43		47.65	70.16					3.11	4	3.11	0.56	3.47	669
1908	3	10				47.45	70.5					3.11	4	3.11	0.56	3.47	635
1910	2					48	70					4.3	6	4.3	0.55	4.65	704
1910	10	25	9	30		47.6	69.8					3.4	4.5	3.4	0.56	3.76	686
1916	2	29	5	15		46.8	70.9					3.11	4	3.11	0.56	3.47	565
1917	6	12	2			49	68					3.4	4.5	3.4	0.56	3.76	888
1918	7	23	12			46.85	71.35					3.11	4	3.11	0.56	3.47	542
1919	10	26	10	28		47.6	70					3.11	4	3.11	0.56	3.47	674
1920	2	6				48.15	69.71					3.11	4	3.11	0.56	3.47	731

Table 2.5-2— {Earthquake Catalog for Earthquakes in Charlevoix Seismic Zone}

YEAR	MONTH	DAY	HR	MIN	SEC	LAT	LON	DEPTH	MN	MLG	M	m_b	INT	EMB	SMB	RMB	DISTANCE
1924	3	4	19	15		47.8	70.2					3.7	5	3.7	0.56	4.06	677
1924	9	30	8	52	30	47.8	69.8					5.04	7	5.04	0.24	5.11	700
1925	3	1	2	19	14.7	47.76	69.84					6.39	9	6.39	0.3	6.49	695
1925	10	9	5			46.82	71.22					3.11	4	3.11	0.56	3.47	548
1926	2	19	20	20		47.7	71					3.11	4	3.11	0.56	3.47	627
1926	7	18	6			47	71.5					3.11	4	3.11	0.56	3.47	545
1926	9	21	11	30		48	70.5					3.11	4	3.11	0.56	3.47	677
1927	7	25		56		47.3	71					3.4	4.5	3.4	0.56	3.76	596
1928	1	27				48	70.2					3.11	4	3.11	0.56	3.47	693
1930	7	13	4	52	39.3	47.5	69.83					3.17		3.17	0.41	3.36	677
1930	10	8	1	8	41	48.93	68.7					3.82		3.82	0.41	4.01	844
1930	12	13	23	18	23.7	47.65	70.17					3.5		3.5	0.41	3.69	668
1930	12	25	22	7	34	47.3	70.4					4.39		4.39	0.41	4.58	630
1931	1	8		13	0.36	47.3	70.4					5.04		5.04	0.42	5.24	630
1933	1	11	23	32		47.45	70.5					3.25		3.25	0.41	3.44	635
1933	2	25	9	43	2.7	47.43	69.93					3.42		3.42	0.41	3.61	666
1936	3	29		49	23.4	47.33	70.25					3.79		3.79	0.3	3.89	640
1938	5	17	18	32		49	68					3.69		3.69	0.3	3.79	888
1938	9	28	4	33	16	48.78	69.58					3.98		3.98	0.41	4.17	786
1939	6	24	17	20	18.3	47.59	69.98					4.29		4.29	0.3	4.39	675
1939	10	19	11	53	58	47.8	69.8					5.5	6	5.5	0.3	5.6	700
1939	12	8	1	17	47	47.97	71.4					3.66	4	3.66	0.33	3.79	629
1940	4	13	8	13	34	47.73	70.73					3.74		3.74	0.41	3.93	643
1940	9	11	1	6	55.4	47	71.13					3.5		3.5	0.41	3.69	566
1941	6	22	9	59	31	47.39	70.34					3.09		3.09	0.41	3.28	640
1941	9	6	17	4	56.5	47.43	70.52					3.74		3.74	0.41	3.93	632
1942	9	5	14	30	24.1	46.97	71.5					3.17		3.17	0.41	3.36	543
1943	9	25	5	52	36.1	47.55	70.65					3.34		3.34	0.41	3.53	634
1943	9	28	16	30	25.2	47.27	70.4					3.74		3.74	0.41	3.93	628
1945	6	18	15	20	4.7	47.34	71.09					4.47		4.47	0.41	4.66	594
1945	10	9	13	18	42	47.99	69.81					4.47		4.47	0.41	4.66	713
1946	9	1	4	39	41	47.33	71.47					3.34		3.34	0.41	3.53	573
1946	9	26	21	19	8.2	46.43	72.15					3.42		3.42	0.41	3.61	466
1947	2	2	16	50	32.3	47.67	70.53					4.07		4.07	0.41	4.26	650

Table 2.5-2— {Earthquake Catalog for Earthquakes in Charlevoix Seismic Zone}

(Page 3 of 7)

YEAR	MONTH	DAY	HR	MIN	SEC	LAT	LON	DEPTH	MN	MLG	M	m_b	INT	EMB	SMB	RMB	DISTANCE
1947	3	29	12	28	52.4	47.37	70.23					3.9		3.9	0.41	4.09	644
1948	1	1	18	33	45.3	47.3	70.4					4.31		4.31	0.41	4.5	630
1948	11	13	16	49	56.6	46.7	70.3					3.5		3.5	0.41	3.69	595
1949	10	30	20	51	13.7	46.47	72.12					3.42		3.42	0.41	3.61	470
1950	8	4	6	45	21	47.33	70.25					3.25		3.25	0.41	3.44	640
1951	7	25		22	51.5	47.2	71.37					3.34		3.34	0.41	3.53	568
1952	2	18	20	56	7	46.33	69.38					3.34		3.34	0.41	3.53	635
1952	2	26		56		46.8	70.2					3.66		3.66	0.41	3.85	608
1952	3	30	13	11	7	47.83	69.88					4.01		4.01	0.2	4.06	698
1952	4	19	2	50	52.8	47.47	70.58					3.74		3.74	0.41	3.93	632
1952	10	14	22	3	44.8	47.8	69.8					4.81	5	4.81	0.2	4.86	700
1954	2	7	20	24	16	47.6	70.25					3.74		3.74	0.41	3.93	660
1954	2	21	9		37	47.67	70.62					3.5		3.5	0.41	3.69	645
1954	6	30	7	41	7	47	70.12					3.66		3.66	0.41	3.85	626
1955	2	1	12	40	27	47.67	70.5					3.9		3.9	0.41	4.09	651
1955	10	20	20	58	32	48.93	70.2					3.25		3.25	0.41	3.44	767
1956	1	30	9	43	13	47.05	71.17					3.66		3.66	0.41	3.85	567
1956	10	27	14	40	6	48.25	69					3.42		3.42	0.41	3.61	778
1957	2	19	5	18	33	48.4	69.93					3.5		3.5	0.41	3.69	738
1957	8	6	23	50	38	47.48	70.42					3.9		3.9	0.41	4.09	641
1957	8	17	1	30	7	46.73	70.12					3.34		3.34	0.41	3.53	609
1957	10	9	14	16	58	48.42	69.9					3.17		3.17	0.41	3.36	741
1957	11	13	20	45	38	48.67	69.55					3.34		3.34	0.41	3.53	779
1958	5	6	16	2	49	48.57	70.32					3.66		3.66	0.41	3.85	732
1958	7	18	23	56	27	46.7	71.4					3.25		3.25	0.41	3.44	529
1958	7	27	8	58		47.32	70.3					3.09		3.09	0.41	3.28	637
1958	12	23	23	14	16	46.98	69.82					3.66		3.66	0.41	3.85	643
1959	4	16	16	36	25	47.12	70.33					3.5		3.5	0.41	3.69	621
1959	8	1	13	52	49	48.42	68.32					3.98		3.98	0.41	4.17	829
1959	8	22	3	52	30	46.95	70.78					3.25		3.25	0.41	3.44	583
1960	2	6		44	2	47.8	70.38					3.34		3.34	0.41	3.53	668
1960	4	23	11	47	47.1	47.88	70.34					3.9		3.9	0.41	4.09	676
1961	8	22	18	55	51	47.33	70.5					3.42		3.42	0.41	3.61	626
1962	3	23	2	2	21	47.18	69.47					3.34		3.34	0.41	3.53	678

Table 2.5-2— {Earthquake Catalog for Earthquakes in Charlevoix Seismic Zone}

(Page 4 of 7)

YEAR	MONTH	DAY	HR	MIN	SEC	LAT	LON	DEPTH	MN	MLG	M	m_b	INT	EMB	SMB	RMB	DISTANCE
1962	7	27	17	56	57	47.25	70.67					3.81		3.81	0.2	3.86	610
1962	8	11	3	5	16	47.53	70.05					3.51		3.51	0.2	3.56	666
1964	7	12			41	46.72	71.41					3.42		3.42	0.41	3.61	529
1965	3	1	2	22	8	47.5	71.25					3.17		3.17	0.41	3.36	598
1965	12	16	13	53	19	47.83	70.6					3.98		3.98	0.41	4.17	658
1966	7	20	20	8	29	47.75	70					3.25		3.25	0.41	3.44	685
1966	10	1	17	23	55	47.66	70.33					3.09		3.09	0.41	3.28	660
1966	12	12	21	4	12	49	68.17					3.42		3.42	0.41	3.61	878
1967	9	23	16	27	55	46.93	70.7					3.42		3.42	0.41	3.61	586
1968	4	11	9	18		47.6	70.4					3.5		3.5	0.41	3.69	651
1968	7	24	23	16	37	47.01	71.3					3.17		3.17	0.41	3.36	557
1969	7	14	3	6	59	47.83	70.09					3.78		3.78	0.1	3.79	686
1969	8	31	7	20	27	47.49	70.07					3.25		3.25	0.41	3.44	662
1975	8	21	4	29	37	47.44	70.18					3.17		3.17	0.41	3.36	652
1976	10	23	20	58	18	47.82	69.78					4.18		4.18	0.1	4.19	703
1979	8	19	22	49	30.4	47.67	69.9					4.58	5	4.58	0.1	4.59	685
1980	3	11	4	15	55	46.79	71.87					3.68		3.68	0.1	3.69	509
1980	7	1	3	6	38	47.56	70.75					3.38	3.5	3.38	0.1	3.39	629
1981	6	16	17	55	4	47.47	70					3.68		3.68	0.1	3.69	665
1982	8	29	2	7	11	47.37	70.38					3.38		3.38	0.1	3.39	636
1983	2	11	15	46	56	48.98	68.33					3.48		3.48	0.1	3.49	868
1983	5	16	2	1	57	47.7	69.89					3.78		3.78	0.1	3.79	688
1985	3	3	12	15	17	47.39	70.47	14.1	3.10					3.10	0.00	3.10	632
1985	4	10	5	52	56	47.52	69.96	12.7	3.10					3.10	0.00	3.10	671
1986	1	11	13	30	28	47.7	70.12	6.4	4.00					4.00	0.00	4.00	675
1986	7	12	20	32	48	46.11	68.22	8.8	3.40					3.40	0.00	3.40	706
1986	8	18	12	28	40	47.53	70.02	5.6	3.00					3.00	0.00	3.00	668
1986	9	19	15	53	1	47.3	70.32	21.9	4.20					4.20	0.00	4.20	634
1987	1	20	22	36	37	48.98	70.31	18	3.10					3.10	0.00	3.10	766
1987	3	18	19	44	48	47.72	70.19	4.2	3.30					3.30	0.00	3.30	672
1987	3	20	17	57	49	48.32	72.23	18	3.30					3.30	0.00	3.30	623
1987	5	3	0	21	53	48.75	68.23	18	3.60					3.60	0.00	3.60	857
1987	6	17	19	39	20	48.84	68.72	18	3.00					3.00	0.00	3.00	836
1987	8	6	20	41	5	47.43	70.28	18	3.40					3.40	0.00	3.40	646

Table 2.5-2— {Earthquake Catalog for Earthquakes in Charlevoix Seismic Zone}

(Page 5 of 7)

YEAR	MONTH	DAY	HR	MIN	SEC	LAT	LON	DEPTH	MN	MLG	M	m_b	INT	EMB	SMB	RMB	DISTANCE
1988	1	2	9	25	17	47.42	70.43	10.8	3.60					3.60	0.00	3.60	637
1988	1	24	4	33	35	47.44	70.46	10.5	3.10					3.10	0.00	3.10	636
1988	3	13	16	24	39	47.44	70.38	6.8	3.10					3.10	0.00	3.10	641
1988	5	12	6	16	19	47.03	70.82	14.1	3.10					3.10	0.00	3.10	586
1988	11	25	23	46	4	48.12	71.18	28.9			5.9			6.20	0.00	6.20	652
1989	1	19	21	36	38	48.06	71.01	24.8	3.60					3.60	0.00	3.60	655
1989	1	31	14	39	48	47.44	70.67	19.7	3.10					3.10	0.00	3.10	624
1989	3	9	9	41	32	47.72	69.86	10.5	4.30					4.30	0.00	4.30	691
1989	3	11	8	31	52	47.72	69.87	10.3	4.40					4.40	0.00	4.40	690
1989	10	13	14	4	42	47.39	70.13	22.7	3.20					3.20	0.00	3.20	652
1989	10	31	4	50	3	48.67	72.33	18	3.40					3.40	0.00	3.40	652
1989	11	22	23	2	51	47.46	70.34	7.6	3.40					3.40	0.00	3.40	645
1990	3	3	2	6	3	47.86	69.98	20.8	3.60					3.60	0.00	3.60	694
1990	3	13	19	10	39	47.53	70.14	15.3	3.20					3.20	0.00	3.20	661
1990	3	30	1	54	8	47.24	68.2	9.7	3.40					3.40	0.00	3.40	763
1990	4	21	1	23	4	47.55	70.07	9.6	3.10					3.10	0.00	3.10	667
1990	4	23	0	28	4	47.41	70.18	8.2	3.00					3.00	0.00	3.00	650
1990	9	21	19	33	1	47.58	70.24	4.1	3.20					3.20	0.00	3.20	659
1990	10	21	13	38	43	47.4	70.36	15.8	3.30					3.30	0.00	3.30	639
1990	10	26	9	13	51	47.57	69.98	10.9	3.10					3.10	0.00	3.10	673
1990	11	6	11	30	10	47.39	70.15	14.2	3.40					3.40	0.00	3.40	651
1990	11	19	0	0	0	47.23	70.7	9.14	3.00					3.00	0.00	3.00	607
1990	12	18	7	10	46	47.26	70.34	9.3	3.30					3.30	0.00	3.30	630
1991	7	3	9	26	42	47.53	70.15	18.4	3.00					3.00	0.00	3.00	661
1991	10	12	23	3	45	48.3	71.31	15	3.30					3.30	0.00	3.30	661
1991	12	8	3	0	30	47.78	69.86	23.2	4.30					4.30	0.00	4.30	695
1992	3	10	5	45	32	47.72	69.86	9.9	3.30					3.30	0.00	3.30	691
1992	5	1	0	37	51	47.45	70.41	2.7	3.20					3.20	0.00	3.20	640
1992	6	4	11	45	20	48.62	68.39	18	3.40					3.40	0.00	3.40	839
1992	6	28	12	31	0	46.84	71.52	18	3.30					3.30	0.00	3.30	532
1992	8	27	6	6	31	48.56	68.61	0	3.40					3.40	0.00	3.40	822
1992	8	28	23	0	36	46.71	71.12	18	3.60					3.60	0.00	3.60	546
1993	3	4	22	2	21	47.51	70.36	4.3	3.10					3.10	0.00	3.10	647
1993	8	7	21	25	31	47.67	69.89	5.5	3.10					3.10	0.00	3.10	685

Table 2.5-2— {Earthquake Catalog for Earthquakes in Charlevoix Seismic Zone}

(Page 6 of 7)

YEAR	MONTH	DAY	HR	MIN	SEC	LAT	LON	DEPTH	MN	MLG	M	m_b	INT	EMB	SMB	RMB	DISTANCE
1993	12	1	12	47	15	47.47	70.16	18	3.50					3.50	0.00	3.50	656
1993	12	30	23	1	47	47.45	70.36	6.2	3.80					3.80	0.00	3.80	643
1994	9	25	0	53	28	47.77	69.96	17	4.30					4.30	0.00	4.30	689
1994	12	1	13	2	47	47.44	70.31	10.8	3.00					3.00	0.00	3.00	645
1996	5	12	11	53	21	47.52	70.03	14.8	3.10					3.10	0.00	3.10	667
1996	6	7	9	41	42	47.53	69.94	13.3	3.10					3.10	0.00	3.10	673
1996	7	14	18	46	49	47.69	69.99	7.3	3.40					3.40	0.00	3.40	681
1996	9	24	23	41	2	47.55	70.24	12.5	3.10					3.10	0.00	3.10	657
1997	1	10	19	27	27	47.51	70.2	17	3.20					3.20	0.00	3.20	656
1997	1	14	4	47	32	47.66	69.88	14.6	3.10					3.10	0.00	3.10	685
1997	8	20	9	12	4	47.54	70.29	7.5	3.70					3.70	0.00	3.70	653
1997	10	28	11	44	18	47.67	69.91	11.3	4.70					4.70	0.00	4.70	684
1997	11	6	2	34	33	46.8	71.42	22.5	5.10					5.10	0.00	5.10	535
1998	1	10	1	51	4	48.19	70.91	18	3.60					3.60	0.00	3.60	671
1998	2	16	5	40	35	47.36	70.39	25.3	3.00					3.00	0.00	3.00	634
1999	10	2	9	45	36	47.42	70.12	8.7	3.00					3.00	0.00	3.00	654
2000	4	5	8	19	9	46.52	72.28	18	3.10					3.10	0.00	3.10	465
2000	6	15	9	25	54	47.67	69.8	11.4	3.70					3.70	0.00	3.70	691
2000	6	29	8	15	17	46.91	70.77	18	3.20					3.20	0.00	3.20	580
2000	7	12	15	1	49	47.56	71.06	18	4.20					4.20	0.00	4.20	612
2000	9	27	12	42	1	47.47	70.04	8.1	3.00					3.00	0.00	3.00	663
2001	5	22	0	33	29	47.65	69.92	11.4	3.50					3.50	0.00	3.50	682
2002	5	14	7	26	39	47.66	69.97	14.1	3.10					3.10	0.00	3.10	680
2002	6	12	17	14	18	47.51	70.02	7.8	3.10					3.10	0.00	3.10	667
2002	8	17	5	53	54	47.33	70.51	13.3	3.80					3.80	0.00	3.80	625
2003	2	28	9	40	47	47.5	70.03	8.6	3.30					3.30	0.00	3.30	665
2003	4	13	2	43	13	46.94	71.16	18	3.40					3.40	0.00	3.40	560
2003	6	13	11	34	40	47.7	70.09	11.1	4.10					4.10	0.00	4.10	676
2003	9	25	14	44	53	47.03	70.76	18	3.20					3.20	0.00	3.20	589
2003	10	11	0	10	2	47.53	69.86	23.2	3.10					3.10	0.00	3.10	677
2004	4	10	5	23	18	47.83	69.81	27.5	3.20					3.20	0.00	3.20	702
2004	5	4	15	41	15	47.94	70.67	22	3.50					3.50	0.00	3.50	663
2004	5	8	5	46	45	47.93	70.67	22	3.30					3.30	0.00	3.30	662
2004	5	24	12	18	43	47.64	70.18	13.6	3.00					3.00	0.00	3.00	667

Table 2.5-2— {Earthquake Catalog for Earthquakes in Charlevoix Seismic Zone}

YEAR	MONTH	DAY	HR	MIN	SEC	LAT	LON	DEPTH	MN	MLG	M	m_b	INT	EMB	SMB	RMB	DISTANCE
2004	5	29	21	21	16	47.44	70.17	6.5	3.30					3.30	0.00	3.30	653
2005	3	6	6	17	49	47.75	69.73	13.3	5.40					5.40	0.00	5.40	700
2006	4	7	8	31	41	47.38	70.46	24.5	4.10					4.10	0.00	4.10	632
2006	7	14	9	34	47	46.85	68.65	5	4.00					4.00	0.00	4.00	711
2006	10	31	2	41	41	47.62	70.18	14.4	3.00					3.00	0.00	3.00	665
2007	3	5	11	27	55	48.64	68.9	18	3.10					3.10	0.00	3.10	812
2007	9	27	11	31	8	47.41	70.37	14.5	3.30					3.30	0.00	3.30	639

Table 2.5-3—{Summary of Seismic Sources}

(Page 1 of 5)

Team	Source Zone	Description	Distance		Pa	M_{max} (m_b) and Wts	Smoothing Options and Wts	Contributed to 99% of EPRI Hazard	New Information to Suggest Change in Source
			(mi)	(km)					
Law Engineering	11	Ottawa-Bonnechere Graben	90	144	0.71	6.8 [0.50] 6.0 [0.50]	1c [1.00]	Yes	No
Law Engineering	12	Charlevoix - La Malbaie	370	595	1.00	6.4 [0.20] 7.4 [0.80]	1e [1.00]	Yes	No
Law Engineering	17	Eastern Tennessee - Eastern Basement	120	192	0.62	6.8 [0.80] 5.7 [0.20]	1b [1.00]	Yes	No
Law Engineering	111	Laurentian Block	0	0	0.90	6.0 [0.50] 5.5 [0.50]	1c [1.00]	Yes	No
Bechtel	3	Charlevoix	370	595	0.80	6.4 [0.10] 6.6 [0.10] 6.7 [0.40] 7.0 [0.40]	1 [0.33] 2 [0.34] 4 [0.33]	Yes	No
Bechtel	7	Bonnechere Graben	110	176	0.45	6.0 [0.10] 6.3 [0.40] 6.6 [0.50]	1 [0.33] 2 [0.34] 4 [0.33]	Yes	No
Bechtel	11	Clarendon-Linden	40	64	0.40	5.4 [0.10] 5.7 [0.40] 6.0 [0.40] 6.6 [0.10]	1 [0.33] 2 [0.34] 4 [0.33]	Yes	No
Bechtel	C	Western Quebec	70	112	0.35	6.0 [0.10] 6.3 [0.40] 6.6 [0.50]	1 [0.33] 2 [0.34] 4 [0.33]	Yes	No
Bechtel	D	Niagara area/peninsular	50	80	0.35	5.4 [0.10] 5.7 [0.40] 6.0 [0.40] 6.6 [0.10]	1 [0.33] 2 [0.34] 4 [0.33]	Yes	No
Bechtel	BZ5	Southern Appalachians Region	90	144	1.00	5.7 [0.10] 6.0 [0.40] 6.3 [0.40] 6.6 [0.10]	1 [0.33] 2 [0.34] 3 [0.33]	Yes	No
Bechtel	BZ6	Southern Eastern Craton Region	0	0	1.00	5.4 [0.10] 5.7 [0.40] 6.0 [0.40] 6.6 [0.10]	1 [0.33] 2 [0.34] 3 [0.33]	Yes	No

Table 2.5-3—{Summary of Seismic Sources}

(Page 2 of 5)

Team	Source Zone	Description	Distance (mi)	Distance (km)	Pa	M_{max} (m_b) and Wts	Smoothing Options and Wts	Contributed to 99% of EPRI Hazard	New Information to Suggest Change in Source
Bechtel	BZ7	Northern Eastern Craton Region	30	48	1.00	6.0 [0.10] 6.3 [0.40] 6.6 [0.50]	1 [0.33] 2 [0.34] 3 [0.33]	Yes	No
Bechtel	C05	Combination Zone 5 (D+11)	40	64	NA	5.4 [0.10] 5.7 [0.40] 6.0 [0.40] 6.6 [0.10]	1 [0.33] 2 [0.34] 4 [0.33]	No	No
Rondout	33	Niagara-by-the-Lake	30	48	0.79	5.2 [0.30] 6.3 [0.55] 6.5 [0.15]	1 [1.00] (a=-1.120, b=1.000)	Yes	No
Rondout	34	Nessmuk	70	112	0.30	5.2 [0.30] 6.3 [0.55] 6.5 [0.15]	1 [1.00] (a=-1.450, b=0.920)	Yes	No
Rondout	35	Tramblant	90	144	0.95	6.6 [0.30] 6.8 [0.60] 7.0 [0.10]	1 [1.00] (a=-0.730, b=1.040)	Yes	No
Rondout	37	La Malbaie	370	595	1.00	7.1 [0.10] 7.3 [0.80] 7.4 [0.10]	5 [1.00] (a=2.430, b=0.700)	Yes	No
Rondout	47	Cornwall/Massena/Montreal	90	144	0.89	6.6 [0.30] 6.8 [0.60] 7.0 [0.10]	1 [1.00] (a=-0.730, b=0.980)	Yes	No
Rondout	C02	Combination Zone 2 (Background 50, does not contain 12 or 33)	0	0	NA	4.8 [0.20] 5.5 [0.60] 5.8 [0.20]	3 [1.00]	Yes	No
Woodward-Clyde	15	Greater Western Quebec	100	160	0.06	5.9 [0.33] 6.3 [0.34] 7.0 [0.33]	2 [0.25] 3 [0.25] 4 [0.25] 5 [0.25]	Yes	No
Woodward-Clyde	18	Adirondack Dome/Uplift	40	64	0.33	5.4 [0.33] 6.3 [0.34] 6.9 [0.33]	2 [0.25] 3 [0.25] 4 [0.25] 5 [0.25]	Yes	No

Table 2.5-3—{Summary of Seismic Sources}

(Page 3 of 5)

Team	Source Zone	Description	Distance (mi)	Distance (km)	Pa	M_{max} (m_b) and Wts	Smoothing Options and Wts	Contributed to 99% of EPRI Hazard	New Information to Suggest Change in Source
Woodward-Clyde	19	Western Quebec Crustal Block	90	144	0.61	6.0 [0.33] 6.5 [0.34] 6.9 [0.33]	2 [0.25] 3 [0.25] 4 [0.25] 5 [0.25]	Yes	No
Woodward-Clyde	33	Western New York - Southern Ontario Trend	60	96	0.44	5.5 [0.33] 6.5 [0.34] 7.0 [0.33]	2 [0.25] 3 [0.25] 4 [0.25] 5 [0.25]	Yes	No
Woodward-Clyde	34	Attica, NY Intersection	80	128	0.49	5.6 [0.33] 6.3 [0.34] 7.4 [0.33]	3 [0.33] 4 [0.34] 5 [0.33]	Yes	No
Woodward-Clyde	C10	Combination Zone 10 (32+34)	70	112	NA	5.6 [0.33] 6.3 [0.34] 7.4 [0.33]	2 [0.25] 3 [0.25] 4 [0.25] 5 [0.25]	Yes	No
Woodward-Clyde	12	La Malbaie	370	595	0.894	6.5 [0.33] 7.0 [0.70] 7.5 [0.33]	2 [0.25] 3 [0.25] 4 [0.25 5 [0.25	Yes	No
Weston Geophysical	1	Charlevoix/ La Malbaie	370	595	1.00	7.2 [1.00]	[1.00]	Yes	No
Weston Geophysical	5	Western Quebec Zone	90	144	1.00	6.0 [0.61] 6.6 [0.36] 7.2 [0.03]	1b [0.50] 2b [0.50]	Yes	No
Weston Geophysical	7	Niagara Peninsula	70	112	0.36	5.4 [0.62] 6.0 [0.29] 6.6 [0.09]	1b [1.00]	Yes	No
Weston Geophysical	8	Clarendon-Linden Structure	60	96	0.83	5.4 [0.26] 6.0 [0.50] 6.6 [0.24]	1b [1.00]	Yes	No
Weston Geophysical	C12	Combination Zone 12 (101+7)	0	0	NA	5.4 [0.19] 6.0 [0.68] 6.6 [0.12]	1a [0.70] 2a [0.30]	Yes	No
Weston Geophysical	C13	Combination Zone 13 (101+8)	0	0	NA	5.4 [0.19] 6.0 [0.68] 6.6 [0.12]	1a [0.70] 2a [0.30]	Yes	No

Table 2.5-3—{Summary of Seismic Sources}

(Page 4 of 5)

Team	Source Zone	Description	Distance (mi)	Distance (km)	Pa	M_{max} (m_b) and Wts	Smoothing Options and Wts	Contributed to 99% of EPRI Hazard	New Information to Suggest Change in Source
Weston Geophysical	C14	Combination Zone 14 (101+29)	0	0	NA	5.4 [0.19] 6.0 [0.68] 6.6 [0.12]	1a [0.70] 2a [0.30]	Yes	No
Weston Geophysical	C16	Combination Zone 16 (101+7+8+29)	0	0	NA	5.4 [0.19] 6.0 [0.68] 6.6 [0.12]	1a [1.00]	Yes	No
Weston Geophysical	4	The St. Lawrence Rift	260	416	1.00	5.4 [0.55] 6.0 [0.28] 6.6 [0.14] 7.2 [0.03]	1b [1.00]	No	No
Dames and Moore	3	Adirondacks Zone	70	112	0.95	6.3 [0.80] 7.2 [0.20]	1 [0.75] 2 [0.25]	Yes	No
Dames and Moore	9	Clarendon-Linden Zone	90	144	0.51	6.5 [0.75] 7.2 [0.25]	1 [0.37] 2 [0.12] 3 [0.38] 4 [0.13]	Yes	No
Dames and Moore	38	Gloucester Fault	160	256	0.41	6.8 [0.75] 7.2 [0.25]	3 [0.75] 4 [0.25]	Yes	No
Dames and Moore	39B	Default Zone	160	256	0.18	6.8 [0.80] 7.2 [0.20]	1 [0.75] 2 [0.25]	Yes	No
Dames and Moore	59	La Malbaie/ Charlevoix	370	595	0.65	7.2 [1.00]	1 [0.26] 2 [1.09] 3 [0.48] 4 [0.17]	Yes	No
Dames and Moore	C09	Combination Zone 9 (1+38)	130	208	NA	6.6 [0.75] 7.2 [0.25]	1 [0.29] 2 [0.10] 3 [0.46] 4 [0.15]	Yes	No
Dames and Moore	C10	Combination Zone 10 (1+39)	130	208	NA	6.6 [0.75] 7.2 [0.25]	1 [0.29] 2 [0.10] 3 [0.46] 4 [0.15]	Yes	No
Dames and Moore	C11	Combination Zone 11 (1+39B)	130	208	NA	6.6 [0.75] 7.2 [0.25]	1 [0.29] 2 [0.10] 3 [0.46] 4 [0.15]	Yes	No

Table 2.5-3—{Summary of Seismic Sources}

(Page 5 of 5)

Team	Source Zone	Description	Distance (mi)	Distance (km)	Pa	M_{max} (m_b) and Wts	Smoothing Options and Wts	Contributed to 99% of EPRI Hazard	New Information to Suggest Change in Source
Dames and Moore	C02	Combination Zone 2 (8+9)	0	0	NA	5.6 [0.80] 7.2 [0.20]	1 [0.75] 2 [0.25]	No	No

Table 2.5-4— {Comparison of EPRI (1989) and Current Hazard Results Using EPRI (1989) Assumptions}

PGA cm/s^2	Hazard	EPRI-SOG	Current	% diff
100	mean	7.34E-05	7.34E-05	0%
	15%	6.61E-06	6.03E-06	-9%
	50%	4.99E-05	4.62E-05	-7%
	85%	1.35E-04	1.40E-04	3%
250	mean	6.89E-06	7.02E-06	2%
	15%	1.90E-07	1.60E-07	-16%
	50%	4.03E-06	4.27E-06	6%
	85%	1.50E-05	1.48E-05	-1%
500	mean	6.87E-07	7.15E-07	4%
	15%	3.09E-09	1.37E-09	-56%
	50%	2.98E-07	3.20E-07	7%
	85%	1.64E-06	1.74E-06	6%

Table 2.5-5—{Comparison of Seismicity Rates for M_b>6.8, 7.0, and 7.2 Using the Original EPRI (1989) Seismicity Catalog and the Updated Catalog}

Team	Catalog	Rate of m_b>6.8	Rate of m_b>7.0	Rate of m_b>7.2
Bechtel	Original	1.55E-03	1.12E-03	8.13E-04
	Updated	1.16E-03	8.08E-04	5.64E-04
	% diff.	-25.4%	-28.1%	-30.7%
Dames & Moore	Original	1.44E-03	9.95E-04	6.88E-04
	Updated	1.27E-03	8.67E-04	5.92E-04
	% diff.	-11.6%	-12.8%	-14.0%
Law	Original	1.63E-03	1.14E-03	8.00E-04
	Updated	1.47E-03	1.02E-03	7.03E-04
	% diff.	-9.7%	-10.9%	-12.1%
Rondout	Original	8.06E-04	5.30E-04	3.49E-04
	Updated	9.20E-04	6.08E-04	4.02E-04
	% diff.	14.1%	14.7%	15.2%
Weston	Original	6.79E-04	4.39E-04	2.83E-04
	Updated	8.99E-04	5.89E-04	3.85E-04
	% diff.	32.4%	34.2%	36.1%
Woodward	Original	9.48E-04	6.32E-04	4.22E-04
	Updated	1.02E-03	6.77E-04	4.52E-04
	% diff.	7.2%	7.2%	7.2%
Average	% diff.	1.2%	0.7%	0.3%

Table 2.5-6— {Mean and Fractile Seismic Hazard Curves for PGA, Rock, No CAV}

Amplitude	MEAN	0.05	0.16	0.5	0.84	0.95
1.00E-03	3.96E-02	1.48E-02	2.09E-02	3.39E-02	5.89E-02	8.32E-02
1.50E-03	3.01E-02	1.05E-02	1.38E-02	2.24E-02	4.79E-02	7.00E-02
2.00E-03	2.40E-02	7.41E-03	1.05E-02	1.82E-02	3.89E-02	5.89E-02
3.00E-03	1.67E-02	4.27E-03	6.46E-03	1.20E-02	2.75E-02	4.47E-02
5.00E-03	9.63E-03	1.93E-03	3.02E-03	6.03E-03	1.70E-02	2.66E-02
7.00E-03	6.30E-03	1.07E-03	1.74E-03	3.59E-03	1.05E-02	1.76E-02
1.00E-02	3.78E-03	5.96E-04	8.71E-04	2.07E-03	6.03E-03	1.12E-02
1.50E-02	1.96E-03	2.60E-04	4.07E-04	9.66E-04	3.02E-03	5.62E-03
2.00E-02	1.17E-03	1.40E-04	2.69E-04	5.75E-04	1.74E-03	3.35E-03
3.00E-02	5.35E-04	5.89E-05	1.18E-04	2.69E-04	7.59E-04	1.57E-03
5.00E-02	1.87E-04	1.29E-05	3.63E-05	1.02E-04	3.09E-04	5.37E-04
7.00E-02	9.24E-05	3.98E-06	1.95E-05	5.50E-05	1.45E-04	2.51E-04
1.00E-01	4.48E-05	9.66E-07	7.94E-06	2.75E-05	7.76E-05	1.10E-04
1.50E-01	2.05E-05	1.50E-07	2.46E-06	1.38E-05	3.63E-05	5.50E-05
2.00E-01	1.20E-05	3.27E-08	9.33E-07	7.41E-06	2.24E-05	3.76E-05
3.00E-01	5.70E-06	2.82E-09	2.69E-07	3.02E-06	1.20E-05	2.09E-05
5.00E-01	2.12E-06	8.32E-11	4.17E-08	1.00E-06	3.98E-06	8.22E-06
7.00E-01	1.04E-06	5.62E-12	9.77E-09	3.55E-07	1.74E-06	4.12E-06
1.00E+00	4.49E-07	2.34E-13	1.32E-09	1.02E-07	6.61E-07	1.80E-06
1.50E+00	1.53E-07	3.47E-18	8.32E-11	2.16E-08	1.91E-07	7.08E-07
2.00E+00	6.49E-08	5.50E-29	3.98E-12	5.43E-09	6.76E-08	3.31E-07
3.00E+00	1.65E-08	5.31E-29	1.45E-13	6.61E-10	1.70E-08	8.61E-08
5.00E+00	2.10E-09	1.82E-29	9.55E-29	3.16E-11	1.23E-09	1.20E-08
7.00E+00	4.31E-10	1.76E-29	7.76E-29	3.24E-12	1.55E-10	2.46E-09
1.00E+01	6.43E-11	6.03E-30	5.50E-29	2.34E-13	1.82E-11	3.67E-10

Table 2.5-7— {Mean and Fractile Seismic Hazard Curves for 25 Hz, Rock, No CAV}

Amplitude	MEAN	0.05	0.16	0.5	0.84	0.95
1.00E-03	5.13E-02	2.09E-02	2.95E-02	4.47E-02	7.76E-02	9.55E-02
1.50E-03	4.21E-02	1.59E-02	2.24E-02	3.63E-02	6.31E-02	8.61E-02
2.00E-03	3.58E-02	1.29E-02	1.82E-02	3.06E-02	5.13E-02	7.50E-02
3.00E-03	2.77E-02	8.81E-03	1.38E-02	2.16E-02	4.17E-02	6.10E-02
5.00E-03	1.90E-02	5.07E-03	7.94E-03	1.33E-02	2.95E-02	4.32E-02
7.00E-03	1.43E-02	3.35E-03	5.25E-03	9.44E-03	2.24E-02	3.51E-02
1.00E-02	1.03E-02	2.14E-03	3.24E-03	6.03E-03	1.59E-02	2.48E-02
1.50E-02	6.72E-03	1.15E-03	1.74E-03	3.47E-03	1.05E-02	1.64E-02
2.00E-02	4.81E-03	7.59E-04	1.07E-03	2.29E-03	6.92E-03	1.20E-02
3.00E-02	2.84E-03	3.67E-04	5.37E-04	1.23E-03	3.98E-03	6.92E-03
5.00E-02	1.34E-03	1.26E-04	2.51E-04	5.37E-04	1.62E-03	3.13E-03
7.00E-02	7.66E-04	6.31E-05	1.26E-04	3.09E-04	9.33E-04	1.74E-03
1.00E-01	4.05E-04	2.24E-05	5.89E-05	1.55E-04	5.01E-04	9.33E-04
1.50E-01	1.86E-04	6.24E-06	2.75E-05	7.76E-05	2.34E-04	4.22E-04
2.00E-01	1.04E-04	2.21E-06	1.29E-05	4.47E-05	1.26E-04	2.34E-04
3.00E-01	4.56E-05	4.68E-07	5.62E-06	2.24E-05	6.31E-05	1.10E-04
5.00E-01	1.63E-05	4.79E-08	1.23E-06	7.94E-06	2.57E-05	4.96E-05
7.00E-01	8.36E-06	9.12E-09	4.07E-07	3.98E-06	1.59E-05	2.85E-05
1.00E+00	4.15E-06	1.15E-09	1.35E-07	2.00E-06	8.51E-06	1.59E-05
1.50E+00	1.85E-06	9.55E-11	3.39E-08	7.08E-07	3.24E-06	7.16E-06
2.00E+00	1.01E-06	1.25E-11	9.77E-09	3.09E-07	1.62E-06	4.12E-06
3.00E+00	4.09E-07	4.84E-13	1.41E-09	8.04E-08	5.37E-07	1.74E-06
5.00E+00	1.15E-07	1.82E-17	7.76E-11	1.20E-08	1.18E-07	5.75E-07
7.00E+00	4.47E-08	7.00E-29	2.29E-12	2.72E-09	5.13E-08	2.43E-07
1.00E+01	1.47E-08	5.31E-29	2.04E-13	5.19E-10	1.12E-08	8.04E-08

Table 2.5-8— {Mean and Fractile Seismic Hazard Curves for 10 Hz, Rock, No CAV}

Amplitude	MEAN	0.05	0.16	0.5	0.84	0.95
1.00E-03	5.85E-02	2.85E-02	3.63E-02	5.50E-02	8.32E-02	1.02E-01
1.50E-03	4.77E-02	2.09E-02	2.75E-02	4.47E-02	6.76E-02	8.61E-02
2.00E-03	4.03E-02	1.70E-02	2.24E-02	3.63E-02	5.89E-02	7.50E-02
3.00E-03	3.05E-02	1.12E-02	1.59E-02	2.57E-02	4.47E-02	6.10E-02
5.00E-03	1.99E-02	6.24E-03	9.12E-03	1.59E-02	3.16E-02	4.32E-02
7.00E-03	1.43E-02	3.98E-03	6.03E-03	1.12E-02	2.24E-02	3.06E-02
1.00E-02	9.53E-03	2.21E-03	3.72E-03	6.92E-03	1.48E-02	2.16E-02
1.50E-02	5.63E-03	1.15E-03	1.86E-03	3.98E-03	9.12E-03	1.29E-02
2.00E-02	3.70E-03	7.33E-04	1.15E-03	2.46E-03	6.03E-03	8.51E-03
3.00E-02	1.91E-03	3.55E-04	5.37E-04	1.27E-03	3.02E-03	4.57E-03
5.00E-02	7.49E-04	1.22E-04	2.19E-04	4.68E-04	1.23E-03	1.80E-03
7.00E-02	3.83E-04	6.10E-05	1.18E-04	2.51E-04	6.17E-04	9.33E-04
1.00E-01	1.82E-04	2.16E-05	5.13E-05	1.22E-04	2.88E-04	4.52E-04
1.50E-01	7.75E-05	5.62E-06	2.09E-05	5.50E-05	1.26E-04	1.91E-04
2.00E-01	4.25E-05	2.07E-06	9.77E-06	2.95E-05	6.76E-05	1.02E-04
3.00E-01	1.86E-05	4.22E-07	3.72E-06	1.33E-05	3.16E-05	4.79E-05
5.00E-01	6.65E-06	3.89E-08	6.61E-07	4.42E-06	1.20E-05	2.02E-05
7.00E-01	3.29E-06	6.68E-09	2.19E-07	2.00E-06	6.92E-06	1.12E-05
1.00E+00	1.48E-06	8.41E-10	6.76E-08	7.08E-07	3.02E-06	5.82E-06
1.50E+00	5.42E-07	5.69E-11	1.29E-08	2.34E-07	1.07E-06	2.21E-06
2.00E+00	2.45E-07	6.92E-12	3.47E-09	8.61E-08	4.37E-07	1.04E-06
3.00E+00	7.03E-08	1.97E-13	4.37E-10	2.09E-08	1.18E-07	3.20E-07
5.00E+00	1.14E-08	2.51E-22	6.46E-12	2.82E-09	1.70E-08	5.50E-08
7.00E+00	2.95E-09	5.31E-29	6.17E-13	5.37E-10	4.27E-09	1.38E-08
1.00E+01	6.06E-10	5.13E-29	4.17E-14	7.24E-11	8.13E-10	2.72E-09

Table 2.5-9— {Mean and Fractile Seismic Hazard Curves for 5 Hz, Rock, No CAV}

Amplitude	MEAN	0.05	0.16	0.5	0.84	0.95
1.00E-03	5.74E-02	2.66E-02	3.63E-02	5.50E-02	8.32E-02	1.02E-01
1.50E-03	4.56E-02	1.88E-02	2.57E-02	4.17E-02	6.76E-02	8.32E-02
2.00E-03	3.76E-02	1.38E-02	1.95E-02	3.39E-02	5.89E-02	7.50E-02
3.00E-03	2.73E-02	9.12E-03	1.29E-02	2.24E-02	4.47E-02	5.89E-02
5.00E-03	1.66E-02	4.73E-03	6.46E-03	1.38E-02	2.75E-02	3.89E-02
7.00E-03	1.13E-02	2.82E-03	4.27E-03	9.12E-03	1.95E-02	2.66E-02
1.00E-02	7.05E-03	1.46E-03	2.46E-03	5.25E-03	1.20E-02	1.76E-02
1.50E-02	3.84E-03	6.84E-04	1.23E-03	2.72E-03	6.46E-03	1.01E-02
2.00E-02	2.38E-03	4.22E-04	7.08E-04	1.68E-03	4.27E-03	6.46E-03
3.00E-02	1.13E-03	1.91E-04	3.31E-04	7.85E-04	2.14E-03	3.13E-03
5.00E-02	4.05E-04	6.53E-05	1.18E-04	2.79E-04	6.61E-04	1.07E-03
7.00E-02	1.97E-04	2.85E-05	5.89E-05	1.35E-04	3.31E-04	5.01E-04
1.00E-01	8.94E-05	1.01E-05	2.57E-05	5.89E-05	1.35E-04	2.27E-04
1.50E-01	3.60E-05	2.82E-06	9.12E-06	2.40E-05	5.89E-05	8.61E-05
2.00E-01	1.88E-05	1.00E-06	3.98E-06	1.29E-05	3.16E-05	4.79E-05
3.00E-01	7.51E-06	1.66E-07	1.23E-06	4.90E-06	1.29E-05	2.16E-05
5.00E-01	2.27E-06	1.33E-08	2.19E-07	1.32E-06	4.57E-06	7.67E-06
7.00E-01	9.74E-07	2.00E-09	6.31E-08	5.01E-07	2.00E-06	3.59E-06
1.00E+00	3.70E-07	2.11E-10	1.48E-08	1.66E-07	7.59E-07	1.46E-06
1.50E+00	1.10E-07	1.25E-11	2.14E-09	3.63E-08	2.19E-07	4.68E-07
2.00E+00	4.29E-08	9.02E-13	3.80E-10	1.16E-08	8.32E-08	1.84E-07
3.00E+00	1.01E-08	3.47E-15	1.48E-11	1.86E-09	1.82E-08	4.32E-08
5.00E+00	1.31E-09	5.13E-29	6.31E-14	1.22E-10	1.62E-09	5.43E-09
7.00E+00	2.97E-10	1.82E-29	1.62E-15	1.70E-11	2.88E-10	1.15E-09
1.00E+01	5.45E-11	6.03E-30	8.91E-29	1.74E-12	3.89E-11	1.84E-10

Table 2.5-10—{Mean and Fractile Seismic Hazard Curves for 2.5 Hz, Rock, No CAV}

Amplitude	MEAN	0.05	0.16	0.5	0.84	0.95
1.00E-03	4.34E-02	1.53E-02	2.24E-02	3.89E-02	6.76E-02	8.32E-02
1.50E-03	3.20E-02	1.01E-02	1.48E-02	2.75E-02	5.13E-02	6.53E-02
2.00E-03	2.49E-02	7.41E-03	1.12E-02	2.09E-02	4.17E-02	5.31E-02
3.00E-03	1.65E-02	4.42E-03	6.46E-03	1.29E-02	2.75E-02	3.89E-02
5.00E-03	8.90E-03	2.00E-03	3.02E-03	6.92E-03	1.48E-02	2.24E-02
7.00E-03	5.59E-03	1.15E-03	1.86E-03	4.27E-03	1.05E-02	1.53E-02
1.00E-02	3.24E-03	5.96E-04	1.07E-03	2.29E-03	6.03E-03	8.81E-03
1.50E-02	1.64E-03	2.79E-04	4.68E-04	1.07E-03	3.02E-03	4.73E-03
2.00E-02	9.67E-04	1.50E-04	2.51E-04	6.38E-04	1.74E-03	2.72E-03
3.00E-02	4.34E-04	6.10E-05	1.10E-04	2.51E-04	7.08E-04	1.19E-03
5.00E-02	1.44E-04	1.82E-05	3.39E-05	8.04E-05	2.19E-04	3.94E-04
7.00E-02	6.58E-05	6.68E-06	1.48E-05	3.76E-05	1.02E-04	1.66E-04
1.00E-01	2.74E-05	2.37E-06	5.25E-06	1.53E-05	4.47E-05	7.24E-05
1.50E-01	9.64E-06	5.37E-07	1.62E-06	5.25E-06	1.59E-05	2.75E-05
2.00E-01	4.46E-06	1.60E-07	6.61E-07	2.37E-06	7.94E-06	1.48E-05
3.00E-01	1.45E-06	2.16E-08	1.66E-07	6.61E-07	2.29E-06	5.62E-06
5.00E-01	3.25E-07	8.41E-10	1.70E-08	1.02E-07	5.37E-07	1.41E-06
7.00E-01	1.15E-07	8.91E-11	3.02E-09	2.95E-08	1.78E-07	5.19E-07
1.00E+00	3.57E-08	7.16E-12	4.37E-10	6.92E-09	4.79E-08	1.60E-07
1.50E+00	8.63E-09	2.04E-13	3.63E-11	1.00E-09	9.12E-09	3.89E-08
2.00E+00	2.93E-09	6.92E-15	5.25E-12	2.11E-10	2.63E-09	1.20E-08
3.00E+00	5.73E-10	5.13E-29	2.34E-13	2.16E-11	3.80E-10	2.07E-09
5.00E+00	5.92E-11	6.24E-30	7.08E-16	8.71E-13	2.75E-11	1.60E-10
7.00E+00	1.15E-11	6.03E-30	8.91E-29	7.00E-14	3.98E-12	2.66E-11
1.00E+01	1.80E-12	6.03E-30	5.50E-29	3.72E-15	3.80E-13	3.24E-12

Table 2.5-11—{Mean and Fractile Seismic Hazard Curves for 1 Hz, Rock, No CAV}

Amplitude	MEAN	0.05	0.16	0.5	0.84	0.95
5.00E-04	3.16E-02	8.81E-03	1.48E-02	2.75E-02	5.13E-02	7.00E-02
7.00E-04	2.37E-02	6.03E-03	1.05E-02	1.95E-02	3.89E-02	5.50E-02
1.00E-03	1.69E-02	4.12E-03	6.92E-03	1.38E-02	2.75E-02	4.03E-02
1.50E-03	1.09E-02	2.46E-03	4.27E-03	8.51E-03	1.82E-02	2.75E-02
2.00E-03	7.82E-03	1.62E-03	2.82E-03	5.82E-03	1.29E-02	2.02E-02
3.00E-03	4.70E-03	7.85E-04	1.51E-03	3.35E-03	7.94E-03	1.25E-02
5.00E-03	2.33E-03	3.09E-04	6.61E-04	1.51E-03	3.98E-03	6.24E-03
7.00E-03	1.41E-03	1.55E-04	3.55E-04	8.71E-04	2.46E-03	3.85E-03
1.00E-02	7.93E-04	7.00E-05	1.66E-04	4.37E-04	1.32E-03	2.21E-03
1.50E-02	3.89E-04	2.66E-05	5.89E-05	2.04E-04	6.17E-04	1.15E-03
2.00E-02	2.24E-04	1.25E-05	3.16E-05	1.02E-04	3.55E-04	6.84E-04
3.00E-02	9.64E-05	3.47E-06	9.77E-06	3.89E-05	1.55E-04	3.09E-04
5.00E-02	2.95E-05	5.56E-07	1.86E-06	8.51E-06	3.89E-05	9.23E-05
7.00E-02	1.25E-05	1.72E-07	5.37E-07	3.02E-06	1.59E-05	3.76E-05
1.00E-01	4.67E-06	3.89E-08	1.35E-07	8.71E-07	5.25E-06	1.43E-05
1.50E-01	1.38E-06	5.25E-09	2.24E-08	1.97E-07	1.51E-06	4.57E-06
2.00E-01	5.47E-07	1.11E-09	6.03E-09	6.31E-08	5.37E-07	1.86E-06
3.00E-01	1.36E-07	9.55E-11	6.61E-10	1.01E-08	1.26E-07	4.52E-07
5.00E-01	2.11E-08	3.02E-12	2.75E-11	8.13E-10	1.48E-08	7.76E-08
7.00E-01	5.85E-09	1.97E-13	2.29E-12	1.35E-10	2.82E-09	1.95E-08
1.00E+00	1.44E-09	2.48E-17	1.78E-13	1.70E-11	4.68E-10	3.85E-09
1.50E+00	2.74E-10	5.31E-29	4.57E-15	1.15E-12	5.89E-11	6.17E-10
2.00E+00	8.03E-11	1.76E-29	1.02E-16	1.26E-13	1.05E-11	1.50E-10
3.00E+00	1.31E-11	6.03E-30	6.31E-29	3.24E-15	7.08E-13	1.82E-11
5.00E+00	1.14E-12	1.76E-29	6.31E-29	1.26E-28	1.70E-14	9.33E-13

Table 2.5-12—{Mean and Fractile Seismic Hazard Curves for 0.5 Hz, Rock, No CAV}

Amplitude	MEAN	0.05	0.16	0.5	0.84	0.95
5.00E-04	1.38E-02	3.59E-03	5.25E-03	1.12E-02	2.24E-02	3.39E-02
7.00E-04	9.79E-03	2.21E-03	3.47E-03	7.94E-03	1.70E-02	2.57E-02
1.00E-03	6.67E-03	1.37E-03	2.29E-03	5.07E-03	1.20E-02	1.76E-02
1.50E-03	4.21E-03	6.61E-04	1.32E-03	3.02E-03	7.41E-03	1.12E-02
2.00E-03	2.99E-03	3.94E-04	8.13E-04	2.14E-03	5.25E-03	7.94E-03
3.00E-03	1.79E-03	1.55E-04	4.07E-04	1.15E-03	3.47E-03	5.07E-03
5.00E-03	8.86E-04	4.32E-05	1.35E-04	4.37E-04	1.86E-03	2.63E-03
7.00E-03	5.36E-04	1.82E-05	5.89E-05	2.51E-04	1.00E-03	1.68E-03
1.00E-02	3.01E-04	6.68E-06	2.24E-05	1.18E-04	5.75E-04	9.02E-04
1.50E-02	1.47E-04	1.86E-06	6.92E-06	4.17E-05	2.34E-04	4.37E-04
2.00E-02	8.54E-05	6.61E-07	2.63E-06	1.82E-05	1.35E-04	2.51E-04
3.00E-02	3.74E-05	1.35E-07	5.37E-07	5.25E-06	5.50E-05	1.14E-04
5.00E-02	1.19E-05	1.20E-08	6.76E-08	8.71E-07	1.20E-05	3.63E-05
7.00E-02	5.23E-06	2.00E-09	1.38E-08	2.19E-07	4.57E-06	1.29E-05
1.00E-01	2.02E-06	2.79E-10	2.14E-09	5.13E-08	1.41E-06	3.98E-06
1.50E-01	6.09E-07	2.24E-11	1.66E-10	7.94E-09	2.69E-07	1.19E-06
2.00E-01	2.39E-07	3.13E-12	3.16E-11	1.93E-09	8.32E-08	5.01E-07
3.00E-01	5.62E-08	9.89E-14	1.74E-12	2.51E-10	1.38E-08	9.23E-08
5.00E-01	7.32E-09	2.69E-16	2.75E-14	1.12E-11	1.15E-09	1.16E-08
7.00E-01	1.70E-09	5.31E-29	7.08E-16	1.00E-12	1.78E-10	2.29E-09
1.00E+00	3.32E-10	5.13E-29	1.10E-28	4.17E-14	2.24E-11	3.55E-10
1.50E+00	4.88E-11	4.79E-29	6.31E-29	6.61E-16	9.33E-13	3.76E-11
2.00E+00	1.23E-11	1.82E-29	6.31E-29	1.30E-28	8.91E-14	7.94E-12
3.00E+00	1.72E-12	4.79E-29	6.31E-29	1.18E-28	2.00E-15	6.17E-13
5.00E+00	1.40E-13	5.31E-29	6.31E-29	9.23E-29	1.35E-28	1.70E-14

Table 2.5-13— {Mean Hard Rock UHRS Accelerations (g), No CAV Calculation}

ground motion	UHS results, g		
	mean 10^{-4}	mean 10^{-5}	mean 10^{-6}
PGA	0.0674	0.221	0.711
25 Hz	0.204	0.639	2.01
10 Hz	0.133	0.408	1.17
5 Hz	0.0951	0.264	0.693
2.5 Hz	0.0585	0.148	0.341
1 Hz	0.0295	0.0759	0.166
0.5 Hz	0.0184	0.0538	0.127

Table 2.5-14—{Percent Contribution to Low-Frequency Deaggregation for 10^{-4}}

Magnitude	Percent contribution by M-R bin							
	5.25	5.75	6.25	6.75	7.25	7.75	8.25	8.75
0-20 km	6.9	0.7	0.1	0.0	0.0	0.0	0.0	0.0
20-40 km	3.5	0.9	0.2	0.0	0.0	0.0	0.0	0.0
40-60 km	1.3	0.9	0.5	0.0	0.0	0.0	0.0	0.0
60-80 km	0.7	0.9	0.6	0.1	0.0	0.0	0.0	0.0
80-100 km	0.4	0.7	0.7	0.1	0.1	0.0	0.0	0.0
100-200 km	1.2	3.9	7.3	4.3	2.5	0.8	0.0	0.0
200-300 km	0.3	1.8	5.6	4.4	1.5	0.2	0.0	0.0
>300 km	0.0	0.5	3.8	8.7	19.9	13.4	0.2	0.0

Table 2.5-15—Percent Contribution to High-Frequency Deaggregation for 10^{-4}}

Magnitude	Percent contribution by M-R bin							
	5.25	5.75	6.25	6.75	7.25	7.75	8.25	8.75
0-20 km	17.2	0.9	0.1	0.0	0.0	0.0	0.0	0.0
20-40 km	14.0	1.5	0.3	0.0	0.0	0.0	0.0	0.0
40-60 km	5.9	1.6	0.6	0.0	0.0	0.0	0.0	0.0
60-80 km	3.0	1.5	0.7	0.1	0.0	0.0	0.0	0.0
80-100 km	1.9	1.4	0.9	0.1	0.1	0.0	0.0	0.0
100-200 km	6.0	7.0	7.8	3.6	2.0	0.7	0.0	0.0
200-300 km	1.0	2.2	4.0	2.6	0.9	0.1	0.0	0.0
>300 km	0.1	0.4	1.3	1.8	3.7	3.0	0.1	0.0

Table 2.5-16—{Percent Contribution to Low-Frequency Deaggregation for 10^{-5}}

Magnitude	Percent contribution by M-R bin							
	5.25	5.75	6.25	6.75	7.25	7.75	8.25	8.75
0-20 km	16.0	3.5	1.0	0.0	0.0	0.0	0.0	0.0
20-40 km	2.8	1.8	1.0	0.1	0.0	0.0	0.0	0.0
40-60 km	0.5	0.9	1.0	0.1	0.0	0.0	0.0	0.0
60-80 km	0.1	0.5	0.8	0.2	0.0	0.0	0.0	0.0
80-100 km	0.1	0.3	0.7	0.3	0.2	0.1	0.0	0.0
100-200 km	0.1	1.1	4.4	5.2	5.9	3.6	0.0	0.0
200-300 km	0.0	0.3	2.2	3.4	2.2	0.4	0.0	0.0
>300 km	0.0	0.0	0.9	3.8	16.7	17.2	0.4	0.0

Table 2.5-17—{Percent Contribution to High-Frequency Deaggregation for 10^{-5}}

Magnitude	Percent contribution by M-R bin							
	5.25	5.75	6.25	6.75	7.25	7.75	8.25	8.75
0-20 km	53.8	5.5	1.1	0.0	0.0	0.0	0.0	0.0
20-40 km	10.8	3.0	1.1	0.1	0.0	0.0	0.0	0.0
40-60 km	1.5	1.2	0.9	0.1	0.0	0.0	0.0	0.0
60-80 km	0.4	0.6	0.6	0.1	0.0	0.0	0.0	0.0
80-100 km	0.2	0.4	0.5	0.2	0.2	0.1	0.0	0.0
100-200 km	0.4	1.2	2.8	2.4	2.8	2.1	0.0	0.0
200-300 km	0.0	0.2	0.8	1.0	0.6	0.1	0.0	0.0
>300 km	0.0	0.0	0.1	0.3	1.1	1.6	0.1	0.0

Table 2.5-18— {Percent Contribution to Low-Frequency Deaggregation for 10^{-6}}

Magnitude	Percent contribution by M-R bin							
	5.25	5.75	6.25	6.75	7.25	7.75	8.25	8.75
0-20 km	22.5	9.8	4.4	0.3	0.0	0.0	0.0	0.0
20-40 km	1.2	1.7	1.9	0.2	0.1	0.0	0.0	0.0
40-60 km	0.1	0.4	1.0	0.2	0.1	0.0	0.0	0.0
60-80 km	0.0	0.1	0.5	0.2	0.1	0.0	0.0	0.0
80-100 km	0.0	0.1	0.3	0.3	0.5	0.5	0.0	0.0
100-200 km	0.0	0.2	1.5	3.4	7.5	8.4	0.0	0.0
200-300 km	0.0	0.0	0.5	1.6	1.9	0.4	0.0	0.0
>300 km	0.0	0.0	0.1	1.1	9.8	16.4	0.6	0.0

Table 2.5-19—{Percent Contribution to High-Frequency Deaggregation for 10^{-6}}

Magnitude	Percent contribution by M-R bin							
	5.25	5.75	6.25	6.75	7.25	7.75	8.25	8.75
0-20 km	69.7	13.7	4.3	0.2	0.0	0.0	0.0	0.0
20-40 km	2.4	1.7	1.3	0.1	0.0	0.0	0.0	0.0
40-60 km	0.1	0.2	0.4	0.1	0.0	0.0	0.0	0.0
60-80 km	0.0	0.1	0.1	0.1	0.0	0.0	0.0	0.0
80-100 km	0.0	0.0	0.1	0.1	0.1	0.2	0.0	0.0
100-200 km	0.0	0.1	0.3	0.5	1.3	2.2	0.0	0.0
200-300 km	0.0	0.0	0.0	0.1	0.1	0.0	0.0	0.0
>300 km	0.0	0.0	0.0	0.0	0.1	0.3	0.0	0.0

Table 2.5-20—{Controlling Magnitudes and Distances from Deaggregation (shaded cells indicate values used to construct UHRS)}

Struct. frequency	Annual Freq. Exceed.	Overall hazard		Hazard from R>100 km	
		M	R, km	M	R, km
1 & 2.5 Hz	1E-4	6.6	360	6.9	460
5 & 10 Hz	1E-4	5.7	150	6.3	270
1 & 2.5 Hz	1E-5	6.6	310	7.2	470
5 & 10 Hz	1E-5	5.4	62	6.9	250
1 & 2.5 Hz	1E-6	6.6	230	7.4	440
5 & 10 Hz	1E-6	5.3	25	7.4	190

Table 2.5-21— {Shear Wave Velocities and Other Properties for GMRS Profile}

Formation	thickness (ft)	V_s (ft/s)	Unit Wt. (pcf)
Oswego Sandstone	24.67	6500	164.0
Oswego Transition	26	6600	164.0
Pulaski A1	12	6600	168.0
Pulaski AB	44	7200	168.0
Pulaski C1	16	5800	168.0
Pulaski C2	22	6700	168.0
Whetstone Gulf 1	384	7000	167.0
Whetstone Gulf 2	245.08	7500	167.0
Whetstone-Trenton Transition 1	154.92	7806	167.8
Whetstone-Trenton Transition 2	154.92	8294	169.2
Trenton/Black River	490.16	8600	170.0
Trenton-Grenville Transition 1	154.92	9215	171.9
Trenton-Grenville Transition 2	154.92	10415	175.1
Grenville	—	11300	177.0

Table 2.5-22—{Shear Wave Velocities and Other Properties for FIRS Profile}

Formation	Thickness (ft)	V_s (ft/s)	Unit Wt. (pcf)
Oswego Sandstone 1	12	5900	164
Oswego Sandstone 2	38	6500	164.0
Oswego Transition	26	6600	164.0
Pulaski A1	12	6600	168.0
Pulaski AB	44	7200	168.0
Pulaski C1	16	5800	168.0
Pulaski C2	22	6700	168.0
Whetstone Gulf 1	384	7000	167.0
Whetstone Gulf 2	245.08	7500	167.0
Whetstone-Trenton Transition 1	154.92	7806	167.8
Whetstone-Trenton Transition 2	154.92	8294	169.2
Trenton/Black River	490.16	8600	170.0
Trenton-Grenville Transition 1	154.92	9215	171.9
Trenton-Grenville Transition 2	154.92	10415	175.1
Grenville	—	11300	177.0

Table 2.5-23—{Properties Used to Define Controlling Earthquakes}

Case	M	R (km)	Mo (dyne-cm)	fc (Hz)	T (sec)	Eff. Strain Ratio
1E-4 HF	5.7	150	3.98E+24	0.53	9.37	0.47
1E-4 LF	6.9	460	2.51E+26	0.13	30.46	0.59
1E-5 HF	5.4	62	1.41E+24	0.75	4.43	0.44
1E-5 LF	7.2	470	7.08E+26	0.09	34.04	0.62
1E-6 HF	5.3	25	1.00E+24	0.85	2.43	0.43
1E-6 LF	7.4	440	1.41E+27	0.08	35.26	0.64

Table 2.5-24— {Mean and Fractile Seismic Hazard Curves for PGA at GMRS Elevation, CAV}

Amplitude	MEAN	0.05	0.16	0.5	0.84	0.95
1.00E-03	3.25E-05	1.46E-06	3.98E-06	1.29E-05	5.13E-05	1.02E-04
1.50E-03	3.25E-05	1.46E-06	3.98E-06	1.29E-05	5.13E-05	1.02E-04
2.00E-03	3.25E-05	1.46E-06	3.98E-06	1.29E-05	5.13E-05	1.02E-04
3.00E-03	3.25E-05	1.46E-06	3.98E-06	1.29E-05	5.13E-05	1.02E-04
5.00E-03	3.25E-05	1.46E-06	3.98E-06	1.29E-05	5.13E-05	1.02E-04
7.00E-03	3.25E-05	1.46E-06	3.98E-06	1.29E-05	5.13E-05	1.02E-04
1.00E-02	3.25E-05	1.46E-06	3.98E-06	1.29E-05	5.13E-05	1.02E-04
1.50E-02	3.25E-05	1.46E-06	3.98E-06	1.29E-05	5.13E-05	1.02E-04
2.00E-02	3.25E-05	1.46E-06	3.98E-06	1.29E-05	5.13E-05	1.02E-04
3.00E-02	3.25E-05	1.46E-06	3.98E-06	1.29E-05	5.13E-05	1.02E-04
5.00E-02	3.14E-05	1.41E-06	3.98E-06	1.29E-05	5.13E-05	9.89E-05
7.00E-02	2.63E-05	1.07E-06	2.82E-06	1.05E-05	3.63E-05	8.61E-05
1.00E-01	1.80E-05	6.38E-07	2.00E-06	7.94E-06	2.40E-05	5.50E-05
1.50E-01	1.04E-05	3.20E-07	1.07E-06	4.90E-06	1.95E-05	3.16E-05
2.00E-01	7.08E-06	1.35E-07	6.61E-07	3.47E-06	1.20E-05	2.40E-05
3.00E-01	4.37E-06	2.32E-08	2.69E-07	2.14E-06	8.51E-06	1.64E-05
5.00E-01	2.28E-06	1.00E-09	6.31E-08	9.33E-07	3.98E-06	8.81E-06
7.00E-01	1.30E-06	9.23E-11	2.24E-08	4.37E-07	2.00E-06	5.07E-06
1.00E+00	6.18E-07	5.43E-12	4.27E-09	1.26E-07	1.07E-06	2.54E-06
1.50E+00	2.30E-07	1.14E-13	3.80E-10	2.57E-08	3.55E-07	1.11E-06
2.00E+00	1.03E-07	1.16E-17	5.89E-11	7.41E-09	1.26E-07	5.75E-07
3.00E+00	2.83E-08	5.31E-29	2.82E-12	9.02E-10	2.24E-08	1.72E-07
5.00E+00	3.92E-09	5.31E-29	1.70E-14	4.17E-11	1.51E-09	2.57E-08
7.00E+00	8.32E-10	5.13E-29	7.41E-21	3.85E-12	2.04E-10	5.43E-09
1.00E+01	1.28E-10	5.13E-29	5.50E-29	2.51E-13	2.24E-11	8.41E-10

Table 2.5-25— {Mean and Fractile Seismic Hazard Curves for 25 Hz at GMRS Elevation, CAV}

Amplitude	MEAN	0.05	0.16	0.5	0.84	0.95
1.00E-03	3.25E-05	1.46E-06	3.98E-06	1.29E-05	5.13E-05	1.02E-04
1.50E-03	3.25E-05	1.46E-06	3.98E-06	1.29E-05	5.13E-05	1.02E-04
2.00E-03	3.25E-05	1.46E-06	3.98E-06	1.29E-05	5.13E-05	1.02E-04
3.00E-03	3.25E-05	1.46E-06	3.98E-06	1.29E-05	5.13E-05	1.02E-04
5.00E-03	3.25E-05	1.46E-06	3.98E-06	1.29E-05	5.13E-05	1.02E-04
7.00E-03	3.25E-05	1.46E-06	3.98E-06	1.29E-05	5.13E-05	1.02E-04
1.00E-02	3.25E-05	1.46E-06	3.98E-06	1.29E-05	5.13E-05	1.02E-04
1.50E-02	3.25E-05	1.46E-06	3.98E-06	1.29E-05	5.13E-05	1.02E-04
2.00E-02	3.25E-05	1.46E-06	3.98E-06	1.29E-05	5.13E-05	1.02E-04
3.00E-02	3.25E-05	1.46E-06	3.98E-06	1.29E-05	5.13E-05	1.02E-04
5.00E-02	3.22E-05	1.41E-06	3.98E-06	1.29E-05	5.13E-05	1.02E-04
7.00E-02	3.14E-05	1.41E-06	3.98E-06	1.20E-05	4.79E-05	9.55E-05
1.00E-01	2.94E-05	1.27E-06	3.24E-06	1.12E-05	3.63E-05	8.61E-05
1.50E-01	2.47E-05	8.13E-07	2.29E-06	9.12E-06	2.95E-05	7.00E-05
2.00E-01	2.01E-05	6.17E-07	1.86E-06	7.94E-06	2.40E-05	5.69E-05
3.00E-01	1.36E-05	3.43E-07	1.07E-06	5.25E-06	2.09E-05	3.63E-05
5.00E-01	7.52E-06	1.02E-07	5.37E-07	3.02E-06	1.29E-05	2.32E-05
7.00E-01	5.00E-06	3.06E-08	3.09E-07	2.00E-06	8.51E-06	1.82E-05
1.00E+00	3.19E-06	5.43E-09	1.10E-07	1.23E-06	5.62E-06	1.29E-05
1.50E+00	1.79E-06	5.56E-10	4.17E-08	6.61E-07	2.82E-06	7.16E-06
2.00E+00	1.11E-06	8.91E-11	1.70E-08	3.09E-07	1.86E-06	4.57E-06
3.00E+00	5.12E-07	5.25E-12	3.72E-09	8.32E-08	8.71E-07	2.37E-06
5.00E+00	1.61E-07	7.00E-14	2.88E-10	1.48E-08	1.91E-07	9.02E-07
7.00E+00	6.66E-08	1.04E-15	4.17E-11	3.98E-09	5.89E-08	4.07E-07
1.00E+01	2.30E-08	1.48E-23	4.27E-12	6.61E-10	1.38E-08	1.45E-07

Table 2.5-26—{Mean and Fractile Seismic Hazard Curves for 10 Hz at GMRS Elevation, CAV}

Amplitude	MEAN	0.05	0.16	0.5	0.84	0.95
1.00E-03	3.25E-05	1.46E-06	3.98E-06	1.29E-05	5.13E-05	1.02E-04
1.50E-03	3.25E-05	1.46E-06	3.98E-06	1.29E-05	5.13E-05	1.02E-04
2.00E-03	3.25E-05	1.46E-06	3.98E-06	1.29E-05	5.13E-05	1.02E-04
3.00E-03	3.25E-05	1.46E-06	3.98E-06	1.29E-05	5.13E-05	1.02E-04
5.00E-03	3.25E-05	1.46E-06	3.98E-06	1.29E-05	5.13E-05	1.02E-04
7.00E-03	3.25E-05	1.46E-06	3.98E-06	1.29E-05	5.13E-05	1.02E-04
1.00E-02	3.25E-05	1.46E-06	3.98E-06	1.29E-05	5.13E-05	1.02E-04
1.50E-02	3.25E-05	1.46E-06	3.98E-06	1.29E-05	5.13E-05	1.02E-04
2.00E-02	3.25E-05	1.46E-06	3.98E-06	1.29E-05	5.13E-05	1.02E-04
3.00E-02	3.25E-05	1.46E-06	3.98E-06	1.29E-05	5.13E-05	1.02E-04
5.00E-02	3.22E-05	1.46E-06	3.98E-06	1.29E-05	5.13E-05	9.89E-05
7.00E-02	3.11E-05	1.41E-06	3.98E-06	1.29E-05	5.13E-05	9.55E-05
1.00E-01	2.77E-05	1.32E-06	3.47E-06	1.12E-05	3.63E-05	8.32E-05
1.50E-01	2.10E-05	9.02E-07	2.29E-06	9.12E-06	2.95E-05	6.10E-05
2.00E-01	1.56E-05	6.61E-07	1.86E-06	7.94E-06	2.24E-05	4.47E-05
3.00E-01	9.37E-06	3.67E-07	1.07E-06	4.57E-06	1.82E-05	2.85E-05
5.00E-01	4.79E-06	1.06E-07	4.68E-07	2.46E-06	8.51E-06	1.64E-05
7.00E-01	3.00E-06	2.75E-08	2.51E-07	1.51E-06	6.03E-06	1.16E-05
1.00E+00	1.67E-06	4.57E-09	8.91E-08	8.13E-07	3.24E-06	6.68E-06
1.50E+00	7.28E-07	4.22E-10	2.24E-08	2.88E-07	1.32E-06	2.92E-06
2.00E+00	3.58E-07	6.76E-11	8.51E-09	1.26E-07	6.17E-07	1.51E-06
3.00E+00	1.11E-07	3.47E-12	1.74E-09	3.16E-08	1.78E-07	5.01E-07
5.00E+00	1.92E-08	3.16E-14	1.26E-10	4.12E-09	2.95E-08	8.91E-08
7.00E+00	5.13E-09	5.89E-17	1.59E-11	8.71E-10	7.41E-09	2.48E-08
1.00E+01	1.09E-09	5.19E-25	1.62E-12	1.30E-10	1.41E-09	5.43E-09

Table 2.5-27— {Mean and Fractile Seismic Hazard Curves for 5 Hz at GMRS Elevation, CAV}

Amplitude	MEAN	0.05	0.16	0.5	0.84	0.95
1.00E-03	3.25E-05	1.46E-06	3.98E-06	1.29E-05	5.13E-05	1.02E-04
1.50E-03	3.25E-05	1.46E-06	3.98E-06	1.29E-05	5.13E-05	1.02E-04
2.00E-03	3.25E-05	1.46E-06	3.98E-06	1.29E-05	5.13E-05	1.02E-04
3.00E-03	3.25E-05	1.46E-06	3.98E-06	1.29E-05	5.13E-05	1.02E-04
5.00E-03	3.25E-05	1.46E-06	3.98E-06	1.29E-05	5.13E-05	1.02E-04
7.00E-03	3.25E-05	1.46E-06	3.98E-06	1.29E-05	5.13E-05	1.02E-04
1.00E-02	3.25E-05	1.46E-06	3.98E-06	1.29E-05	5.13E-05	1.02E-04
1.50E-02	3.25E-05	1.46E-06	3.98E-06	1.29E-05	5.13E-05	1.02E-04
2.00E-02	3.25E-05	1.46E-06	3.98E-06	1.29E-05	5.13E-05	1.02E-04
3.00E-02	3.24E-05	1.46E-06	3.98E-06	1.29E-05	5.13E-05	1.02E-04
5.00E-02	3.10E-05	1.37E-06	3.98E-06	1.29E-05	5.13E-05	9.55E-05
7.00E-02	2.81E-05	1.23E-06	3.47E-06	1.20E-05	4.47E-05	8.91E-05
1.00E-01	2.28E-05	9.33E-07	2.46E-06	9.77E-06	3.16E-05	7.00E-05
1.50E-01	1.54E-05	6.17E-07	1.62E-06	7.41E-06	2.24E-05	4.47E-05
2.00E-01	1.06E-05	4.07E-07	1.15E-06	5.07E-06	1.82E-05	3.16E-05
3.00E-01	5.67E-06	1.91E-07	7.08E-07	2.92E-06	1.12E-05	1.88E-05
5.00E-01	2.28E-06	3.76E-08	1.91E-07	1.23E-06	3.98E-06	8.22E-06
7.00E-01	1.15E-06	9.12E-09	8.32E-08	5.37E-07	2.29E-06	4.27E-06
1.00E+00	4.97E-07	1.37E-09	2.95E-08	2.04E-07	1.00E-06	1.93E-06
1.50E+00	1.65E-07	1.10E-10	4.57E-09	5.89E-08	3.31E-07	6.84E-07
2.00E+00	6.85E-08	1.59E-11	1.07E-09	1.95E-08	1.35E-07	2.99E-07
3.00E+00	1.73E-08	6.84E-13	1.26E-10	3.35E-09	3.16E-08	7.50E-08
5.00E+00	2.43E-09	7.59E-16	6.03E-12	2.60E-10	3.47E-09	1.05E-08
7.00E+00	5.81E-10	2.48E-26	6.17E-13	3.89E-11	6.17E-10	2.37E-09
1.00E+01	1.13E-10	5.13E-29	1.48E-14	4.42E-12	8.91E-11	4.07E-10

Table 2.5-28—{Mean and Fractile Seismic Hazard Curves for 2.5 Hz at GMRS Elevation, CAV}

Amplitude	MEAN	0.05	0.16	0.5	0.84	0.95
1.00E-03	3.25E-05	1.46E-06	3.98E-06	1.29E-05	5.13E-05	1.02E-04
1.50E-03	3.25E-05	1.46E-06	3.98E-06	1.29E-05	5.13E-05	1.02E-04
2.00E-03	3.25E-05	1.46E-06	3.98E-06	1.29E-05	5.13E-05	1.02E-04
3.00E-03	3.25E-05	1.46E-06	3.98E-06	1.29E-05	5.13E-05	1.02E-04
5.00E-03	3.25E-05	1.46E-06	3.98E-06	1.29E-05	5.13E-05	1.02E-04
7.00E-03	3.25E-05	1.46E-06	3.98E-06	1.29E-05	5.13E-05	1.02E-04
1.00E-02	3.25E-05	1.46E-06	3.98E-06	1.29E-05	5.13E-05	1.02E-04
1.50E-02	3.23E-05	1.46E-06	3.98E-06	1.29E-05	5.13E-05	1.02E-04
2.00E-02	3.19E-05	1.37E-06	3.98E-06	1.29E-05	5.13E-05	9.89E-05
3.00E-02	3.03E-05	1.27E-06	3.72E-06	1.20E-05	4.79E-05	9.55E-05
5.00E-02	2.50E-05	9.02E-07	2.82E-06	1.05E-05	3.89E-05	8.04E-05
7.00E-02	1.96E-05	6.61E-07	2.00E-06	7.94E-06	2.95E-05	6.10E-05
1.00E-01	1.32E-05	4.07E-07	1.07E-06	5.25E-06	1.82E-05	4.03E-05
1.50E-01	7.10E-06	1.91E-07	6.17E-07	3.02E-06	1.05E-05	2.09E-05
2.00E-01	4.11E-06	9.23E-08	3.55E-07	1.74E-06	6.46E-06	1.25E-05
3.00E-01	1.67E-06	2.48E-08	1.35E-07	6.61E-07	2.63E-06	5.82E-06
5.00E-01	4.55E-07	2.29E-09	2.57E-08	1.45E-07	7.59E-07	1.93E-06
7.00E-01	1.76E-07	3.31E-10	6.03E-09	4.17E-08	2.69E-07	7.85E-07
1.00E+00	5.94E-08	2.40E-11	1.00E-09	1.05E-08	8.91E-08	2.69E-07
1.50E+00	1.55E-08	8.13E-13	8.91E-11	2.00E-09	1.82E-08	6.76E-08
2.00E+00	5.55E-09	4.95E-14	1.29E-11	5.37E-10	5.25E-09	2.40E-08
3.00E+00	1.16E-09	8.04E-17	7.08E-13	5.50E-11	8.71E-10	4.57E-09
5.00E+00	1.32E-10	9.33E-28	7.94E-15	2.07E-12	6.76E-11	3.94E-10
7.00E+00	2.74E-11	1.82E-29	1.02E-16	1.97E-13	1.12E-11	6.76E-11
1.00E+01	4.56E-12	6.46E-30	4.17E-20	1.12E-14	1.32E-12	9.44E-12

Table 2.5-29—{Mean and Fractile Seismic Hazard Curves for 1 Hz at GMRS Elevation, CAV}

Amplitude	MEAN	0.05	0.16	0.5	0.84	0.95
5.00E-04	3.25E-05	1.46E-06	3.98E-06	1.29E-05	5.13E-05	1.02E-04
7.00E-04	3.25E-05	1.46E-06	3.98E-06	1.29E-05	5.13E-05	1.02E-04
1.00E-03	3.25E-05	1.46E-06	3.98E-06	1.29E-05	5.13E-05	1.02E-04
1.50E-03	3.25E-05	1.46E-06	3.98E-06	1.29E-05	5.13E-05	1.02E-04
2.00E-03	3.25E-05	1.46E-06	3.98E-06	1.29E-05	5.13E-05	1.02E-04
3.00E-03	3.25E-05	1.46E-06	3.98E-06	1.29E-05	5.13E-05	1.02E-04
5.00E-03	3.22E-05	1.37E-06	3.98E-06	1.29E-05	5.13E-05	1.02E-04
7.00E-03	3.16E-05	1.37E-06	3.72E-06	1.20E-05	5.13E-05	9.89E-05
1.00E-02	3.04E-05	1.19E-06	3.47E-06	1.12E-05	5.13E-05	9.89E-05
1.50E-02	2.78E-05	9.66E-07	2.63E-06	9.77E-06	4.47E-05	9.23E-05
2.00E-02	2.49E-05	7.08E-07	2.00E-06	7.94E-06	3.89E-05	8.32E-05
3.00E-02	1.94E-05	4.07E-07	1.23E-06	5.25E-06	3.16E-05	6.53E-05
5.00E-02	1.17E-05	1.40E-07	4.68E-07	2.72E-06	1.70E-05	3.76E-05
7.00E-02	7.23E-06	5.69E-08	1.91E-07	1.46E-06	8.51E-06	2.40E-05
1.00E-01	3.77E-06	1.70E-08	6.76E-08	6.17E-07	3.98E-06	1.20E-05
1.50E-01	1.49E-06	3.47E-09	1.82E-08	1.84E-07	1.41E-06	4.73E-06
2.00E-01	6.88E-07	9.33E-10	5.62E-09	7.00E-08	6.61E-07	2.29E-06
3.00E-01	1.99E-07	1.02E-10	9.33E-10	1.48E-08	1.91E-07	7.08E-07
5.00E-01	3.41E-08	4.27E-12	4.79E-11	1.32E-09	2.57E-08	1.22E-07
7.00E-01	9.80E-09	3.55E-13	5.25E-12	2.11E-10	5.25E-09	3.16E-08
1.00E+00	2.48E-09	1.38E-14	4.07E-13	2.75E-11	8.71E-10	6.92E-09
1.50E+00	4.89E-10	8.32E-17	1.29E-14	2.14E-12	1.18E-10	1.15E-09
2.00E+00	1.48E-10	9.44E-24	8.71E-16	2.34E-13	2.24E-11	2.99E-10
3.00E+00	2.53E-11	3.27E-29	2.82E-18	9.12E-15	1.74E-12	4.03E-11
5.00E+00	2.35E-12	6.46E-30	6.76E-29	4.79E-17	4.79E-14	2.37E-12

Table 2.5-30—{Mean and Fractile Seismic Hazard Curves for 0.5 Hz at GMRS Elevation, CAV}

Amplitude	MEAN	0.05	0.16	0.5	0.84	0.95
5.00E-04	3.25E-05	1.46E-06	3.98E-06	1.29E-05	5.13E-05	1.02E-04
7.00E-04	3.25E-05	1.46E-06	3.98E-06	1.29E-05	5.13E-05	1.02E-04
1.00E-03	3.24E-05	1.41E-06	3.98E-06	1.29E-05	5.13E-05	1.02E-04
1.50E-03	3.21E-05	1.37E-06	3.98E-06	1.29E-05	5.13E-05	1.02E-04
2.00E-03	3.17E-05	1.27E-06	3.72E-06	1.20E-05	5.13E-05	9.89E-05
3.00E-03	3.06E-05	1.11E-06	3.24E-06	1.12E-05	5.13E-05	9.89E-05
5.00E-03	2.81E-05	7.85E-07	2.29E-06	9.77E-06	4.79E-05	9.23E-05
7.00E-03	2.55E-05	5.75E-07	1.86E-06	7.41E-06	4.17E-05	8.32E-05
1.00E-02	2.21E-05	3.55E-07	1.23E-06	5.82E-06	3.63E-05	7.50E-05
1.50E-02	1.76E-05	1.60E-07	5.75E-07	3.59E-06	2.75E-05	5.89E-05
2.00E-02	1.43E-05	7.50E-08	3.09E-07	2.54E-06	1.95E-05	4.62E-05
3.00E-02	9.83E-06	2.09E-08	9.55E-08	1.19E-06	9.77E-06	2.95E-05
5.00E-02	5.15E-06	3.02E-09	1.95E-08	3.09E-07	3.02E-06	1.38E-05
7.00E-02	2.96E-06	6.17E-10	5.25E-09	1.10E-07	1.74E-06	7.41E-06
1.00E-01	1.44E-06	1.02E-10	1.07E-09	2.95E-08	8.71E-07	3.24E-06
1.50E-01	5.36E-07	9.77E-12	1.45E-10	5.62E-09	2.19E-07	9.66E-07
2.00E-01	2.35E-07	1.51E-12	2.75E-11	1.62E-09	6.31E-08	3.43E-07
3.00E-01	6.22E-08	8.32E-14	2.14E-12	2.04E-10	1.38E-08	9.55E-08
5.00E-01	8.90E-09	5.75E-16	2.24E-14	1.05E-11	1.32E-09	1.33E-08
7.00E-01	2.15E-09	5.07E-18	1.07E-15	1.07E-12	2.04E-10	2.63E-09
1.00E+00	4.31E-10	5.89E-29	1.12E-17	5.89E-14	2.75E-11	4.68E-10
1.50E+00	6.43E-11	5.31E-29	1.18E-28	1.51E-15	1.32E-12	4.95E-11
2.00E+00	1.62E-11	5.13E-29	6.31E-29	5.89E-17	1.35E-13	1.05E-11
3.00E+00	2.30E-12	5.13E-29	6.31E-29	7.50E-26	3.98E-15	8.71E-13
5.00E+00	1.91E-13	5.13E-29	6.31E-29	1.10E-28	6.92E-18	2.66E-14

Table 2.5-31— {Horizontal 10^{-5} and 10^{-6} UHRS Amplitudes (in g) at GMRS and FIRS Elevation}

Freq	GMRS elevation		FIRS elevation	
	10^{-5}	10^{-6}	10^{-5}	10^{-6}
100	1.54E-1	7.93E-1	1.58E-1	8.07E-1
25	3.91E-1	2.12E+0	4.15E-1	2.22E+0
10	2.85E-1	1.29E+0	2.90E-1	1.29E+0
5	2.08E-1	7.42E-1	2.12E-1	7.49E-1
2.5	1.20E-1	3.67E-1	1.23E-1	3.71E-1
1	5.58E-2	1.74E-1	5.62E-2	1.73E-1
0.5	2.94E-2	1.16E-1	3.00E-2	1.17E-1

Table 2.5-32—{Mean and Fractile Seismic Hazard Curves for PGA at FIRS Elevation, CAV}

Amplitude	MEAN	0.05	0.16	0.5	0.84	0.95
1.00E-03	3.38E-05	1.51E-06	4.27E-06	1.38E-05	5.50E-05	1.06E-04
1.50E-03	3.38E-05	1.51E-06	4.27E-06	1.38E-05	5.50E-05	1.06E-04
2.00E-03	3.38E-05	1.51E-06	4.27E-06	1.38E-05	5.50E-05	1.06E-04
3.00E-03	3.38E-05	1.51E-06	4.27E-06	1.38E-05	5.50E-05	1.06E-04
5.00E-03	3.38E-05	1.51E-06	4.27E-06	1.38E-05	5.50E-05	1.06E-04
7.00E-03	3.38E-05	1.51E-06	4.27E-06	1.38E-05	5.50E-05	1.06E-04
1.00E-02	3.38E-05	1.51E-06	4.27E-06	1.38E-05	5.50E-05	1.06E-04
1.50E-02	3.38E-05	1.51E-06	4.27E-06	1.38E-05	5.50E-05	1.06E-04
2.00E-02	3.38E-05	1.51E-06	4.27E-06	1.38E-05	5.50E-05	1.06E-04
3.00E-02	3.38E-05	1.51E-06	4.27E-06	1.38E-05	5.50E-05	1.06E-04
5.00E-02	3.26E-05	1.46E-06	3.98E-06	1.29E-05	5.13E-05	1.02E-04
7.00E-02	2.72E-05	1.11E-06	2.82E-06	1.12E-05	3.63E-05	8.61E-05
1.00E-01	1.86E-05	6.84E-07	2.00E-06	7.94E-06	2.57E-05	5.89E-05
1.50E-01	1.07E-05	3.31E-07	1.15E-06	5.25E-06	2.09E-05	3.27E-05
2.00E-01	7.33E-06	1.45E-07	6.61E-07	3.47E-06	1.20E-05	2.40E-05
3.00E-01	4.52E-06	2.32E-08	2.88E-07	2.14E-06	8.51E-06	1.76E-05
5.00E-01	2.36E-06	1.04E-09	6.31E-08	1.00E-06	3.98E-06	9.12E-06
7.00E-01	1.34E-06	9.23E-11	2.40E-08	4.68E-07	2.14E-06	5.07E-06
1.00E+00	6.40E-07	5.62E-12	4.57E-09	1.35E-07	1.15E-06	2.72E-06
1.50E+00	2.38E-07	1.18E-13	4.07E-10	2.66E-08	3.80E-07	1.19E-06
2.00E+00	1.07E-07	1.29E-17	5.89E-11	7.67E-09	1.26E-07	5.75E-07
3.00E+00	2.95E-08	5.31E-29	3.02E-12	9.66E-10	2.40E-08	1.84E-07
5.00E+00	4.11E-09	5.31E-29	2.24E-14	4.32E-11	1.51E-09	2.66E-08
7.00E+00	8.77E-10	5.13E-29	7.94E-21	4.27E-12	2.04E-10	6.03E-09
1.00E+01	1.35E-10	5.13E-29	5.50E-29	2.79E-13	2.40E-11	8.71E-10

Table 2.5-33—{Mean and Fractile Seismic Hazard Curves for 25 Hz at FIRS Elevation, CAV}

Amplitude	MEAN	0.05	0.16	0.5	0.84	0.95
1.00E-03	3.38E-05	1.51E-06	4.27E-06	1.38E-05	5.50E-05	1.06E-04
1.50E-03	3.38E-05	1.51E-06	4.27E-06	1.38E-05	5.50E-05	1.06E-04
2.00E-03	3.38E-05	1.51E-06	4.27E-06	1.38E-05	5.50E-05	1.06E-04
3.00E-03	3.38E-05	1.51E-06	4.27E-06	1.38E-05	5.50E-05	1.06E-04
5.00E-03	3.38E-05	1.51E-06	4.27E-06	1.38E-05	5.50E-05	1.06E-04
7.00E-03	3.38E-05	1.51E-06	4.27E-06	1.38E-05	5.50E-05	1.06E-04
1.00E-02	3.38E-05	1.51E-06	4.27E-06	1.38E-05	5.50E-05	1.06E-04
1.50E-02	3.38E-05	1.51E-06	4.27E-06	1.38E-05	5.50E-05	1.06E-04
2.00E-02	3.38E-05	1.51E-06	4.27E-06	1.38E-05	5.50E-05	1.06E-04
3.00E-02	3.37E-05	1.51E-06	4.27E-06	1.38E-05	5.50E-05	1.06E-04
5.00E-02	3.34E-05	1.51E-06	4.27E-06	1.29E-05	5.50E-05	1.02E-04
7.00E-02	3.27E-05	1.46E-06	3.98E-06	1.29E-05	5.13E-05	1.02E-04
1.00E-01	3.07E-05	1.37E-06	3.47E-06	1.20E-05	3.89E-05	9.23E-05
1.50E-01	2.60E-05	9.33E-07	2.46E-06	9.77E-06	3.16E-05	7.50E-05
2.00E-01	2.13E-05	6.38E-07	2.00E-06	7.94E-06	2.57E-05	5.89E-05
3.00E-01	1.45E-05	3.80E-07	1.15E-06	5.25E-06	2.24E-05	3.89E-05
5.00E-01	8.08E-06	1.18E-07	6.17E-07	3.47E-06	1.38E-05	2.48E-05
7.00E-01	5.39E-06	3.51E-08	3.55E-07	2.14E-06	9.12E-06	1.88E-05
1.00E+00	3.45E-06	6.46E-09	1.26E-07	1.41E-06	6.03E-06	1.38E-05
1.50E+00	1.95E-06	6.84E-10	5.13E-08	7.08E-07	3.24E-06	7.67E-06
2.00E+00	1.22E-06	1.18E-10	1.95E-08	3.55E-07	2.00E-06	4.90E-06
3.00E+00	5.62E-07	6.92E-12	4.90E-09	9.55E-08	9.33E-07	2.54E-06
5.00E+00	1.78E-07	9.89E-14	3.80E-10	1.70E-08	2.19E-07	9.66E-07
7.00E+00	7.40E-08	1.86E-15	5.50E-11	4.57E-09	6.76E-08	4.68E-07
1.00E+01	2.58E-08	2.85E-23	5.25E-12	7.59E-10	1.48E-08	1.72E-07

Table 2.5-34—{Mean and Fractile Seismic Hazard Curves for 10 Hz at FIRS Elevation, CAV}

Amplitude	MEAN	0.05	0.16	0.5	0.84	0.95
1.00E-03	3.38E-05	1.51E-06	4.27E-06	1.38E-05	5.50E-05	1.06E-04
1.50E-03	3.38E-05	1.51E-06	4.27E-06	1.38E-05	5.50E-05	1.06E-04
2.00E-03	3.38E-05	1.51E-06	4.27E-06	1.38E-05	5.50E-05	1.06E-04
3.00E-03	3.38E-05	1.51E-06	4.27E-06	1.38E-05	5.50E-05	1.06E-04
5.00E-03	3.38E-05	1.51E-06	4.27E-06	1.38E-05	5.50E-05	1.06E-04
7.00E-03	3.38E-05	1.51E-06	4.27E-06	1.38E-05	5.50E-05	1.06E-04
1.00E-02	3.38E-05	1.51E-06	4.27E-06	1.38E-05	5.50E-05	1.06E-04
1.50E-02	3.38E-05	1.51E-06	4.27E-06	1.38E-05	5.50E-05	1.06E-04
2.00E-02	3.38E-05	1.51E-06	4.27E-06	1.38E-05	5.50E-05	1.06E-04
3.00E-02	3.38E-05	1.51E-06	4.27E-06	1.38E-05	5.50E-05	1.06E-04
5.00E-02	3.34E-05	1.51E-06	4.27E-06	1.38E-05	5.50E-05	1.02E-04
7.00E-02	3.22E-05	1.46E-06	3.98E-06	1.29E-05	5.13E-05	9.89E-05
1.00E-01	2.86E-05	1.37E-06	3.47E-06	1.20E-05	3.89E-05	8.32E-05
1.50E-01	2.16E-05	9.66E-07	2.29E-06	9.77E-06	2.95E-05	6.10E-05
2.00E-01	1.60E-05	6.84E-07	2.00E-06	7.94E-06	2.24E-05	4.79E-05
3.00E-01	9.59E-06	3.94E-07	1.15E-06	4.90E-06	1.82E-05	3.06E-05
5.00E-01	4.90E-06	1.06E-07	5.01E-07	2.63E-06	8.51E-06	1.70E-05
7.00E-01	3.06E-06	2.85E-08	2.69E-07	1.62E-06	6.03E-06	1.16E-05
1.00E+00	1.70E-06	4.57E-09	8.91E-08	8.13E-07	3.24E-06	6.92E-06
1.50E+00	7.38E-07	4.22E-10	2.24E-08	3.09E-07	1.32E-06	2.92E-06
2.00E+00	3.61E-07	6.76E-11	9.12E-09	1.35E-07	6.17E-07	1.51E-06
3.00E+00	1.12E-07	3.47E-12	1.86E-09	3.27E-08	1.78E-07	5.01E-07
5.00E+00	1.93E-08	3.16E-14	1.26E-10	4.27E-09	2.95E-08	8.91E-08
7.00E+00	5.14E-09	5.89E-17	1.59E-11	8.71E-10	7.41E-09	2.48E-08
1.00E+01	1.10E-09	5.19E-25	1.62E-12	1.30E-10	1.51E-09	5.43E-09

Table 2.5-35— {Mean and Fractile Seismic Hazard Curves for 25 Hz at FIRS Elevation, CAV}

Amplitude	MEAN	0.05	0.16	0.5	0.84	0.95
1.00E-03	3.38E-05	1.51E-06	4.27E-06	1.38E-05	5.50E-05	1.06E-04
1.50E-03	3.38E-05	1.51E-06	4.27E-06	1.38E-05	5.50E-05	1.06E-04
2.00E-03	3.38E-05	1.51E-06	4.27E-06	1.38E-05	5.50E-05	1.06E-04
3.00E-03	3.38E-05	1.51E-06	4.27E-06	1.38E-05	5.50E-05	1.06E-04
5.00E-03	3.38E-05	1.51E-06	4.27E-06	1.38E-05	5.50E-05	1.06E-04
7.00E-03	3.38E-05	1.51E-06	4.27E-06	1.38E-05	5.50E-05	1.06E-04
1.00E-02	3.38E-05	1.51E-06	4.27E-06	1.38E-05	5.50E-05	1.06E-04
1.50E-02	3.38E-05	1.51E-06	4.27E-06	1.38E-05	5.50E-05	1.06E-04
2.00E-02	3.37E-05	1.51E-06	4.27E-06	1.38E-05	5.50E-05	1.06E-04
3.00E-02	3.36E-05	1.51E-06	4.27E-06	1.38E-05	5.50E-05	1.02E-04
5.00E-02	3.21E-05	1.46E-06	3.98E-06	1.29E-05	5.13E-05	1.02E-04
7.00E-02	2.92E-05	1.32E-06	3.47E-06	1.20E-05	4.79E-05	9.23E-05
1.00E-01	2.37E-05	9.66E-07	2.63E-06	1.05E-05	3.39E-05	7.24E-05
1.50E-01	1.60E-05	6.61E-07	1.74E-06	7.94E-06	2.40E-05	4.96E-05
2.00E-01	1.10E-05	4.37E-07	1.23E-06	5.25E-06	1.82E-05	3.27E-05
3.00E-01	5.86E-06	1.91E-07	7.59E-07	3.02E-06	1.12E-05	1.88E-05
5.00E-01	2.35E-06	4.03E-08	2.04E-07	1.23E-06	4.27E-06	8.22E-06
7.00E-01	1.17E-06	9.77E-09	8.91E-08	5.37E-07	2.29E-06	4.42E-06
1.00E+00	5.04E-07	1.46E-09	2.95E-08	2.19E-07	1.00E-06	1.93E-06
1.50E+00	1.66E-07	1.18E-10	4.57E-09	5.89E-08	3.31E-07	6.84E-07
2.00E+00	6.87E-08	1.64E-11	1.07E-09	1.95E-08	1.35E-07	2.99E-07
3.00E+00	1.72E-08	7.08E-13	1.35E-10	3.35E-09	3.16E-08	7.50E-08
5.00E+00	2.41E-09	8.41E-16	6.03E-12	2.51E-10	3.47E-09	1.01E-08
7.00E+00	5.78E-10	2.75E-26	6.17E-13	3.76E-11	6.17E-10	2.29E-09
1.00E+01	1.13E-10	5.13E-29	1.38E-14	4.27E-12	8.91E-11	4.07E-10

Table 2.5-36—{Mean and Fractile Seismic Hazard Curves for 2.5 Hz at FIRS Elevation, CAV}

Amplitude	MEAN	0.05	0.16	0.5	0.84	0.95
1.00E-03	3.38E-05	1.51E-06	4.27E-06	1.38E-05	5.50E-05	1.06E-04
1.50E-03	3.38E-05	1.51E-06	4.27E-06	1.38E-05	5.50E-05	1.06E-04
2.00E-03	3.38E-05	1.51E-06	4.27E-06	1.38E-05	5.50E-05	1.06E-04
3.00E-03	3.38E-05	1.51E-06	4.27E-06	1.38E-05	5.50E-05	1.06E-04
5.00E-03	3.38E-05	1.51E-06	4.27E-06	1.38E-05	5.50E-05	1.06E-04
7.00E-03	3.38E-05	1.51E-06	4.27E-06	1.38E-05	5.50E-05	1.06E-04
1.00E-02	3.37E-05	1.51E-06	4.27E-06	1.38E-05	5.50E-05	1.06E-04
1.50E-02	3.35E-05	1.51E-06	4.27E-06	1.38E-05	5.50E-05	1.02E-04
2.00E-02	3.31E-05	1.46E-06	4.27E-06	1.29E-05	5.50E-05	1.02E-04
3.00E-02	3.14E-05	1.37E-06	3.98E-06	1.29E-05	5.13E-05	9.89E-05
5.00E-02	2.59E-05	9.66E-07	2.82E-06	1.05E-05	4.17E-05	8.32E-05
7.00E-02	2.03E-05	6.84E-07	2.00E-06	8.51E-06	3.16E-05	6.31E-05
1.00E-01	1.37E-05	4.37E-07	1.15E-06	5.62E-06	1.95E-05	4.03E-05
1.50E-01	7.33E-06	1.97E-07	6.61E-07	3.02E-06	1.05E-05	2.32E-05
2.00E-01	4.24E-06	9.89E-08	3.80E-07	1.86E-06	6.46E-06	1.29E-05
3.00E-01	1.73E-06	2.66E-08	1.45E-07	6.84E-07	2.82E-06	6.03E-06
5.00E-01	4.68E-07	2.54E-09	2.75E-08	1.45E-07	8.13E-07	2.07E-06
7.00E-01	1.81E-07	3.43E-10	6.46E-09	4.47E-08	2.88E-07	8.13E-07
1.00E+00	6.10E-08	2.57E-11	1.00E-09	1.12E-08	8.91E-08	2.79E-07
1.50E+00	1.59E-08	8.71E-13	8.91E-11	2.00E-09	1.95E-08	7.24E-08
2.00E+00	5.71E-09	5.50E-14	1.38E-11	5.37E-10	5.62E-09	2.48E-08
3.00E+00	1.20E-09	9.23E-17	7.08E-13	5.69E-11	9.33E-10	4.73E-09
5.00E+00	1.36E-10	1.64E-26	8.51E-15	2.14E-12	7.24E-11	4.22E-10
7.00E+00	2.83E-11	1.82E-29	1.10E-16	2.11E-13	1.12E-11	7.24E-11
1.00E+01	4.72E-12	6.46E-30	4.47E-20	1.16E-14	1.32E-12	1.01E-11

Table 2.5-37—{Mean and Fractile Seismic Hazard Curves for 1 Hz at FIRS Elevation, CAV}

Amplitude	MEAN	0.05	0.16	0.5	0.84	0.95
5.00E-04	3.38E-05	1.51E-06	4.27E-06	1.38E-05	5.50E-05	1.06E-04
7.00E-04	3.38E-05	1.51E-06	4.27E-06	1.38E-05	5.50E-05	1.06E-04
1.00E-03	3.38E-05	1.51E-06	4.27E-06	1.38E-05	5.50E-05	1.06E-04
1.50E-03	3.38E-05	1.51E-06	4.27E-06	1.38E-05	5.50E-05	1.06E-04
2.00E-03	3.37E-05	1.51E-06	4.27E-06	1.38E-05	5.50E-05	1.06E-04
3.00E-03	3.37E-05	1.51E-06	4.27E-06	1.38E-05	5.50E-05	1.06E-04
5.00E-03	3.34E-05	1.46E-06	4.27E-06	1.29E-05	5.50E-05	1.02E-04
7.00E-03	3.28E-05	1.37E-06	3.98E-06	1.29E-05	5.50E-05	1.02E-04
1.00E-02	3.15E-05	1.27E-06	3.72E-06	1.20E-05	5.13E-05	9.89E-05
1.50E-02	2.86E-05	9.66E-07	2.82E-06	1.05E-05	4.79E-05	9.23E-05
2.00E-02	2.55E-05	7.33E-07	2.14E-06	8.51E-06	4.17E-05	8.32E-05
3.00E-02	1.99E-05	4.22E-07	1.23E-06	5.62E-06	3.16E-05	6.53E-05
5.00E-02	1.19E-05	1.45E-07	4.68E-07	2.82E-06	1.70E-05	4.03E-05
7.00E-02	7.28E-06	5.69E-08	1.91E-07	1.46E-06	8.51E-06	2.40E-05
1.00E-01	3.76E-06	1.70E-08	6.76E-08	6.17E-07	3.98E-06	1.20E-05
1.50E-01	1.48E-06	3.47E-09	1.82E-08	1.84E-07	1.41E-06	4.57E-06
2.00E-01	6.78E-07	9.33E-10	5.62E-09	7.00E-08	6.61E-07	2.21E-06
3.00E-01	1.95E-07	1.02E-10	9.33E-10	1.48E-08	1.91E-07	7.08E-07
5.00E-01	3.32E-08	4.27E-12	4.79E-11	1.32E-09	2.40E-08	1.18E-07
7.00E-01	9.50E-09	3.55E-13	5.25E-12	1.97E-10	5.25E-09	3.16E-08
1.00E+00	2.40E-09	1.33E-14	4.07E-13	2.75E-11	8.71E-10	6.92E-09
1.50E+00	4.73E-10	8.04E-17	1.38E-14	2.14E-12	1.10E-10	1.15E-09
2.00E+00	1.42E-10	9.44E-24	8.13E-16	2.19E-13	2.09E-11	2.99E-10
3.00E+00	2.43E-11	3.27E-29	2.46E-18	8.51E-15	1.62E-12	3.89E-11
5.00E+00	2.25E-12	6.46E-30	6.76E-29	4.17E-17	4.47E-14	2.14E-12

Table 2.5-38— {Mean and Fractile Seismic Hazard Curves for 0.5 Hz at FIRS Elevation, CAV}

Amplitude	MEAN	0.05	0.16	0.5	0.84	0.95
5.00E-04	3.37E-05	1.51E-06	4.27E-06	1.38E-05	5.50E-05	1.06E-04
7.00E-04	3.37E-05	1.51E-06	4.27E-06	1.38E-05	5.50E-05	1.06E-04
1.00E-03	3.36E-05	1.51E-06	4.27E-06	1.38E-05	5.50E-05	1.06E-04
1.50E-03	3.33E-05	1.46E-06	3.98E-06	1.29E-05	5.50E-05	1.06E-04
2.00E-03	3.28E-05	1.37E-06	3.98E-06	1.29E-05	5.50E-05	1.02E-04
3.00E-03	3.17E-05	1.19E-06	3.24E-06	1.20E-05	5.13E-05	9.89E-05
5.00E-03	2.90E-05	8.41E-07	2.46E-06	9.77E-06	4.79E-05	9.23E-05
7.00E-03	2.63E-05	5.75E-07	2.00E-06	7.94E-06	4.17E-05	8.32E-05
1.00E-02	2.27E-05	3.67E-07	1.23E-06	5.82E-06	3.63E-05	7.50E-05
1.50E-02	1.80E-05	1.60E-07	5.75E-07	3.85E-06	2.75E-05	6.10E-05
2.00E-02	1.46E-05	7.50E-08	3.09E-07	2.72E-06	1.95E-05	4.62E-05
3.00E-02	9.99E-06	2.09E-08	9.55E-08	1.19E-06	9.77E-06	2.95E-05
5.00E-02	5.22E-06	2.82E-09	1.95E-08	3.09E-07	3.24E-06	1.43E-05
7.00E-02	3.00E-06	5.96E-10	5.25E-09	1.10E-07	1.74E-06	7.41E-06
1.00E-01	1.47E-06	9.89E-11	1.07E-09	2.95E-08	8.71E-07	3.24E-06
1.50E-01	5.44E-07	9.77E-12	1.45E-10	5.82E-09	2.34E-07	1.00E-06
2.00E-01	2.39E-07	1.51E-12	2.75E-11	1.62E-09	6.76E-08	3.67E-07
3.00E-01	6.33E-08	7.76E-14	2.14E-12	2.19E-10	1.38E-08	9.89E-08
5.00E-01	9.06E-09	5.37E-16	2.24E-14	1.05E-11	1.41E-09	1.33E-08
7.00E-01	2.18E-09	4.73E-18	1.07E-15	1.15E-12	2.19E-10	2.72E-09
1.00E+00	4.37E-10	5.89E-29	1.12E-17	6.31E-14	2.75E-11	4.68E-10
1.50E+00	6.51E-11	5.31E-29	1.18E-28	1.86E-15	1.51E-12	5.50E-11
2.00E+00	1.64E-11	5.13E-29	6.31E-29	7.76E-17	1.45E-13	1.05E-11
3.00E+00	2.32E-12	5.13E-29	6.31E-29	1.30E-22	4.57E-15	9.02E-13
5.00E+00	1.93E-13	5.13E-29	6.31E-29	1.10E-28	8.51E-18	2.66E-14

Table 2.5-39—{Horizontal 10^{-5} UHRS (at GMRS Elevation) and GMRS, and Vertical GMRS (in g)}

Freq.	Horiz 1E-5	Horiz GMRS	V/H	Vert GMRS
100	1.54E-01	6.93E-02	0.78	5.41E-02
90	1.58E-01	7.13E-02	0.82	5.88E-02
80	1.71E-01	7.66E-02	0.87	6.64E-02
70	1.99E-01	8.94E-02	0.89	7.99E-02
60	2.36E-01	1.06E-01	0.89	9.48E-02
50	2.74E-01	1.24E-01	0.86	1.06E-01
45	3.04E-01	1.36E-01	0.85	1.15E-01
40	3.46E-01	1.55E-01	0.83	1.28E-01
35	3.80E-01	1.71E-01	0.79	1.36E-01
30	3.91E-01	1.76E-01	0.77	1.34E-01
25	3.91E-01	1.75E-01	0.74	1.31E-01
20	3.74E-01	1.68E-01	0.71	1.20E-01
15	3.50E-01	1.57E-01	0.69	1.08E-01
12.5	3.21E-01	1.44E-01	0.68	9.80E-02
10	2.85E-01	1.29E-01	0.67	8.63E-02
9	2.75E-01	1.24E-01	0.67	8.30E-02
8	2.60E-01	1.17E-01	0.67	7.84E-02
7	2.43E-01	1.09E-01	0.67	7.31E-02
6	2.29E-01	1.03E-01	0.67	6.88E-02
5	2.08E-01	9.25E-02	0.67	6.20E-02
4	1.66E-01	7.48E-02	0.67	5.01E-02
3	1.37E-01	6.15E-02	0.67	4.12E-02
2.5	1.20E-01	5.39E-02	0.67	3.61E-02
2	1.09E-01	4.92E-02	0.67	3.30E-02
1.5	9.01E-02	4.04E-02	0.67	2.71E-02
1.25	7.55E-02	3.38E-02	0.67	2.26E-02
1	5.58E-02	2.55E-02	0.67	1.71E-02
0.9	5.31E-02	2.39E-02	0.67	1.60E-02
0.8	4.81E-02	2.17E-02	0.67	1.45E-02
0.7	4.22E-02	1.90E-02	0.67	1.27E-02
0.6	3.60E-02	1.61E-02	0.67	1.08E-02
0.5	2.94E-02	1.31E-02	0.67	8.79E-03
0.4	2.29E-02	1.04E-02	0.67	6.96E-03
0.3	1.69E-02	7.58E-03	0.67	5.08E-03
0.2	1.11E-02	5.05E-03	0.67	3.38E-03
0.15	8.31E-03	3.73E-03	0.67	2.50E-03
0.125	6.76E-03	3.03E-03	0.67	2.03E-03
0.1	4.42E-03	1.99E-03	0.67	1.33E-03

Table 2.5-40— {Horizontal 10^{-5} UHRS (at FIRS Elevation) and FIRS, and Vertical FIRS (in g)}

Freq.	Horiz 1E-5	Horiz FIRS	V/H	Vert FIRS
100	1.58E-01	7.11E-02	0.78	5.55E-02
90	1.63E-01	7.32E-02	0.82	6.04E-02
80	1.76E-01	7.90E-02	0.87	6.85E-02
70	2.03E-01	9.15E-02	0.89	8.18E-02
60	2.49E-01	1.13E-01	0.89	1.01E-01
50	3.03E-01	1.36E-01	0.86	1.16E-01
45	3.11E-01	1.40E-01	0.85	1.18E-01
40	3.27E-01	1.47E-01	0.83	1.22E-01
35	3.62E-01	1.62E-01	0.79	1.29E-01
30	3.99E-01	1.79E-01	0.77	1.37E-01
25	4.15E-01	1.86E-01	0.74	1.38E-01
20	3.89E-01	1.75E-01	0.71	1.24E-01
15	3.58E-01	1.61E-01	0.69	1.11E-01
12.5	3.27E-01	1.47E-01	0.68	1.00E-01
10	2.90E-01	1.31E-01	0.67	8.79E-02
9	2.83E-01	1.27E-01	0.67	8.53E-02
8	2.66E-01	1.20E-01	0.67	8.02E-02
7	2.48E-01	1.11E-01	0.67	7.47E-02
6	2.32E-01	1.04E-01	0.67	6.98E-02
5	2.12E-01	9.43E-02	0.67	6.32E-02
4	1.68E-01	7.60E-02	0.67	5.09E-02
3	1.39E-01	6.23E-02	0.67	4.18E-02
2.5	1.23E-01	5.53E-02	0.67	3.70E-02
2	1.12E-01	5.04E-02	0.67	3.38E-02
1.5	9.13E-02	4.09E-02	0.67	2.74E-02
1.25	7.61E-02	3.41E-02	0.67	2.29E-02
1	5.62E-02	2.57E-02	0.67	1.72E-02
0.9	5.36E-02	2.41E-02	0.67	1.61E-02
0.8	4.87E-02	2.19E-02	0.67	1.47E-02
0.7	4.28E-02	1.93E-02	0.67	1.29E-02
0.6	3.66E-02	1.63E-02	0.67	1.09E-02
0.5	3.00E-02	1.34E-02	0.67	8.97E-03
0.4	2.34E-02	1.06E-02	0.67	7.10E-03
0.3	1.73E-02	7.74E-03	0.67	5.19E-03
0.2	1.14E-02	5.16E-03	0.67	3.46E-03
0.15	8.49E-03	3.81E-03	0.67	2.56E-03
0.125	6.91E-03	3.10E-03	0.67	2.07E-03
0.1	4.52E-03	2.03E-03	0.67	1.36E-03

Table 2.5-41—{Summary of Geologic Units of 100, 200, and 300 Series Borings}

(Page 1 of 2)

Boring No.	Ground Surface Elevation (ft)	Elevation Top of Geologic Unit (ft)							Bottom of Boring Elevation (ft)
		Glacial Till	Oswego Sandstone	Oswego Transition Zone	Pulaski Formation			Whetstone Gulf Formation	
					Unit A	Unit B	Unit C		
B101 (MW)	265.3	262.3	242.8	202.8	180.3	150.3	137.8	83.3	10.3
B102 (MW)	255.6	252.1	240.0	205.6	193.1	151.1	115.6	83.1	10.0
B103 (MW)	256.0	NM	240.4	NM	NM	NM	NM	NM	192.4
B104 (MW)	255.9	253.4	238.4	205.9	195.4	139.4	118.4	82.9	52.4
B105 (MW)	255.9	NM	238.4	NM	NM	NM	NM	NM	194.9
B106 (MW)	256.0	NE	248.0	201.0	185.0	153.5	136.5	91.0	61.0
B107 (MW)	256.2	NM	248.7	NM	NM	NM	NM	NM	187.2
B108 (MW)	259.8	259.8	257.6	209.8	183.8	128.8	NE	NE	109.8
B109 (MW)	262.5	261.5	260.0	206.5	197.5	149.5	130.0	NE	112.5
B110 (MW)	267.1	267.1	264.6	199.6	179.6	146.1	111.6	67.6	41.9
B111 (MW)	266.9	NM	264.4	NM	NM	NM	NM	NM	179.4
B112 (MW)	282.9	279.4	264.9	225.4	165.4	132.4	115.9	98.9	79.4
B113 (MW)	283.0	NM	265.0	NM	NM	NM	NM	NM	172.0
B114 (MW)	274.0	NE	273.2	195.0	183.5	141.5	130.0	84.0	80.5
B115 (MW)	274.3	NM	273.5	NE	NE	NE	NE	NE	180.8
B116 (MW)	294.8	282.3	275.9	239.8	214.8	184.8	149.8	NE	139.3
B117 (MW)	279.0	279.0	277.0	229.0	186.5	141.0	98.5	NE	94.5
B118 (MW)	293.5	293.0	283.2	243.5	213.5	178.0	148.0	118.0	88.0
B119 (MW)	293.5	NM	283.2	NM	NM	NM	NM	NM	223.3
B120 (MW)	267.0	NM	252.5	NE	NE	NE	NE	NE	252.5
B121 (MW)	266.6	NM	249.1	NE	NE	NE	NE	NE	249.1
B122 (MW)	282.5	NM	262.9	NE	NE	NE	NE	NE	262.9
B123 (MW)	272.2	NM	264.2	NE	NE	NE	NE	NE	264.2
B124 (MW)	263.3	NM	251.3	NE	NE	NE	NE	NE	251.3
B201 (MW)	255.9	254.9	249.1	219.9	175.4	150.9	110.9	77.9	55.9
B202 (MW)	256.2	NM	250.2	NM	NM	NM	NM	NM	225.2
B203	257.2	NE	250.5	196.7	171.7	151.7	122.2	NE	107.2
B204	259.8	256.3	248.3	189.3	172.3	149.3	113.3	NE	109.8
B205	261.2	260.7	252.7	190.7	173.2	151.2	120.7	NE	110.2
B206	260.5	260.0	251.6	203.5	177.0	151.5	113.5	NE	110.5
B207	262.1	261.6	251.5	194.6	173.6	151.1	117.1	NE	111.1
B208 (MW)	265.3	264.3	250.3	218.8	176.3	159.3	121.3	NE	114.3
B209 (MW)	266.0	NM	251.0	NM	NM	NM	NM	NM	214.0
B210	266.7	266.7	247.7	213.7	184.7	152.2	123.2	NE	116.7
B211	268.3	268.3	246.3	198.3	179.8	153.3	122.3	NE	118.3
B212	269.4	268.4	251.9	214.4	181.9	128.9	NE	NE	119.4
B213	265.6	264.6	251.6	203.1	180.6	148.1	125.1	NE	115.1
B214	267.8	264.3	253.3	210.8	187.8	153.8	127.8	NE	117.8
B215	262.5	261.5	257.5	202.0	181.5	147.5	127.5	NE	112.5
B216 (MW)	265.8	265.8	258.8	203.3	185.3	156.8	130.8	85.8	60.8
B217 (MW)	265.1	NM	258.1	NM	NM	NM	NM	NM	215.1
B218	265.2	264.7	249.2	197.2	171.2	149.2	120.2	NE	115.2
B219 (MW)	274.4	273.4	256.4	211.9	186.9	147.9	NE	NE	120.2
B220 (MW)	275.0	NM	257.0	NM	NM	NM	NM	NM	194.0
B221 (MW)	280.2	267.7	253.6	214.2	175.7	149.2	118.7	79.7	64.2
B222	281.3	273.3	255.3	210.3	174.8	150.8	140.3	NE	130.3
B223	280.4	266.9	250.4	205.4	175.9	150.4	NE	NE	130.4
B224	274.2	270.2	258.3	205.7	178.2	143.2	123.7	83.7	64.21

Table 2.5-41—{Summary of Geologic Units of 100, 200, and 300 Series Borings}

(Page 2 of 2)

Boring No.	Ground Surface Elevation (ft)	Elevation Top of Geologic Unit (ft)							Bottom of Boring Elevation (ft)
		Glacial Till	Oswego Sandstone	Oswego Transition Zone	Pulaski Formation			Whetstone Gulf Formation	
					Unit A	Unit B	Unit C		
B225	275.8	NM	257.8	NM	NM	NM	NM	NM	65.8
B226	275.8	275.8	258.3	210.8	187.8	154.8	130.8	78.3	65.8
B227	281.7	269.2	260.6	199.2	176.7	NE	NE	NE	131.4
B228	281.7	271.2	259.2	207.7	176.2	149.2	NE	NE	131.7
B229	282.8	269.3	257.3	195.3	177.8	147.8	NE	NE	132.8
B230 (MW)	282.6	270.1	263.1	199.1	175.1	149.6	128.1	98.6	78.6
B231	280.9	272.4	262.6	197.4	179.4	153.4	NE	NE	130.9
B232	282.1	274.1	263.6	207.1	175.6	149.6	128.1	101.6	82.1
B233 (MW)	275.5	275.5	259.5	212.0	179.0	154.5	146.5	NE	125.3
B234	271.8	269.8	263.3	198.3	180.8	157.3	127.8	NE	121.8
B235 (MW)	271.9	268.4	261.9	201.9	181.9	155.9	128.4	NE	118.4
B236 (MW)	272.1	NM	262.1	NM	NM	NM	NM	NM	236.1
B237	272.5	271.5	258.9	194.5	171.0	147.5	123.5	NE	122.5
B238 (MW)	279.2	276.2	260.5	197.2	173.2	148.2	119.2	90.2	63.4
B239	280.3	280.3	259.0	199.8	174.3	146.8	NE	NE	125.0
B240	283.0	282.0	261.0	208.0	172.5	NE	NE	NE	128.0
B241	272.5	NM	258.5	NM	NM	NM	NM	NM	62.5
B242	272.4	NM	259.4	NM	NM	NM	NM	NM	62.4
B243	270.5	270.5	259.4	195.5	175.0	147.5	117.0	73.0	60.5
B301	262.1	261.6	244.1	202.6	187.6	NE	NE	NE	142.1
B302	262.5	259.0	242.0	202.5	187.5	162.5	NE	NE	142.5
B303									
B304	262.5	259.0	249.0	207.5	NE	NE	NE	NE	187.5
B305	260.9	260.4	250.3	205.9	NE	NE	NE	NE	185.9
B306	256.3	255.8	249.1	203.8	186.3	NE	NE	NE	181.3
B307	254.7	253.7	241.7	202.2	185.7	NE	NE	NE	179.7
B308	254.4	244.9	242.8	203.9	184.9	NE	NE	NE	179.4
B309	Not Drilled								
B310	Not Drilled								
B311	255.4	245.4	244.9	200.4	183.4	NE	NE	NE	180.4
B312	256.2	248.7	241.7	200.7	182.2	NE	NE	NE	181.2
B313	257.2	NE	244.7	202.2	183.2	NE	NE	NE	182.2
B314	258.4	254.9	245.9	207.9	190.9	NE	NE	NE	183.4
B315	262.7	261.2	248.4	207.7	193.7	NE	NE	NE	187.7

Notes:

Elevations are based on the National Geodetic Vertical Datum of 1929 (NGVD 29).

Abbreviations:

MW Monitoring Well

NM Not measured. Boring drilled without sampling using rotary percussion tools. Only the top of bedrock was identified

NE Not encountered. Where glacial till was not encountered, other soils were present above bedrock. Where rock formations were not encountered, the boring was terminated before encountering the formation.

Table 2.5-42—{Summary of Geologic Units of 400 Series Borings}

Boring No.	Ground Surface Elevation (ft)	Elevation Top of Geologic Unit (ft)							Bottom of Boring Elevation (ft)
		Glacial Till	Oswego Sandstone	Oswego Transition Zone	Pulaski Formation			Whetstone Gulf Formation	
					Unit A	Unit B	Unit C		
B401	262.7	243.7	205.4	191.3	150.8	134.2	103.9	65.7	13.7
B402a	263.5	243.6	207.5	192.2	156.2	141.9	105.8	70.8	49.2
B403	Not Drilled								
B404	241.3	241.3	224.4	204.7	165.8	153.8	115.3	69.3	38.8
B405	238.3	238.3	226.6	208.1	166.3	149.8	111.2	78.0	39.8
B406	237.3	237.3	227.9	200.1	163.5	149.8	113.9	88.9	49.8
B407	236.6	236.6	217.1	199.8	168.9	155.5	117.9	84.0	40.6
B408	237.1	235.8	214.8	200.3	171.7	156.0	116.0	90.8	39.3
B409	232.8	232.8	218.3	201.3	169.3	156.8	117.8	84.8	48.8
B410	229.6	226.4	216.4	202.7	174.2	157.6	120.1	92.1	47.6
B411	226.0	226.0	217.7	203.5	170.9	153.2	121.0	88.0	48.0
B412	222.0	222.0	219.8	203.7	161.7	151.0	118.3	83.0	43.3
B413	217.3	NE	216.0	206.6	177.0	161.3	120.8	87.3	57.3
B414	214.1	NE	212.6	206.1	168.6	157.0	121.3	85.9	52.1
B415	210.7	NE	208.7	206.6	179.0	158.6	121.4	92.9	51.7
B416	207.5	NE	NE	206.8	165.0	149.7	111.7	77.5	52.5
B417	204.3	NE	NE	204.3	176.7	163.0	120.9	88.6	54.3
B428	260.7	243.2	203.1	188.7	154.4	136.5	100.6	62.2	21.4
B429a	261.3	238.3	198.1	184.6	150.1	135.0	91.0	66.3	53.6
B430	Not Drilled								
B431	240.1	238.1	220.6	200.3	167.8	153.1	116.6	88.3	40.1
B432	239.4	239.4	222.4	203.3	164.6	144.9	117.5	79.9	39.4
B433	237.3	233.8	227.0	209.8	167.8	150.1	110.0	77.8	48.8
B434	238.3	238.3	224.9	208.3	172.2	153.8	120.4	93.6	42.2
B435	236.4	234.5	221.6	198.8	161.5	150.3	120.0	93.6	46.5
B436	234.8	234.3	225.2	198.0	172.6	155.3	117.1	94.5	50.8
B437	233.2	233.2	223.4	197.7	167.3	148.9	108.2	72.0	57.3
B438	230.1	227.8	215.8	198.4	161.9	147.8	114.0	84.1	51.8
B439	227.5	227.5	217.0	200.4	172.0	153.0	120.8	96.4	52.5
B440	223.1	221.6	218.4	201.6	169.2	150.2	120.7	96.6	52.1
B441	218.7	NE	218.7	205.5	167.4	152.2	123.9	83.7	60.7

Notes:

Elevations are based on the National Geodetic Vertical Datum of 1929 (NGVD 29).
B402a and B429a were drilled at angles and elevations are corrected.
B401, B402a, B428, and B429a were drilled onshore. All other 400 Series Borings were drilled offshore.
Ground surface elevation corresponds with mudline for offshore borings.

Abbreviation:

NE Not Encountered

Table 2.5-43—{Laboratory Soil Test Data}

(Page 1 of 2)

Sample Identification					Index Properties							
Boring Number	Sample Number	Sample Depth (feet)	Sample Elevation (feet)	Layer Name	Water Content (%)	Liquid Limit	Plastic Limit	Plasticity Index	Specific Gravity	Gravel (%)	Sand (%)	Fines (%)
B101(MW)	S2	5.0	260.3	Glacial Till	10.8	—	—	—	—	1.2	45.0	53.8
B102(MW)	S4 (0″-13″)	10.0	245.6	Glacial Till	5.7	15	12	3	—	8.0	39.1	52.8
B104(MW)	S3 (3.5″-13″)	10.0	245.9	Glacial Till	3.4	—	—	—	—	21.9	48.2	29.8
B106(MW)	S2 (8″-24″)	5.0	251.0	Surficial Deposits	15.6	23	12	11	—	8.7	30.9	60.4
B112(MW)	S2	5.0	277.9	Glacial Till	8.0	—	—	—	—	27.8	41.5	30.7
B112(MW)	S3	10.0	272.9	Glacial Till	12.9	NV	NA	NP	—	11.8	41.0	47.2
B116(MW)	S4	15.0	279.8	Glacial Till	7.9	15	13	2	—	4.0	46.9	49.1
B118(MW)	S2 (0″-17″)	5.0	288.5	Glacial Till	8.6	NV	NA	NP	—	12.7	44.5	42.8
B208(MW)	S4	6.0	259.3	Glacial Till	6.0	—	—	—	2.74	15.9	38.2	45.9
B208(MW)	S5	8.0	257.3	Glacial Till	6.2	18	11	7	—	—	—	—
B208(MW)	S6	10.0	255.3	Glacial Till	7.8	17	11	6	—	52.3	22.9	24.8
B213	S1 (3″-14″)	0.0	265.6	Glacial Till	6.7	—	—	—	—	35.9	33.0	31.2
B213	S3	10.0	255.6	Glacial Till	8.9	—	—	—	2.75	8.1	39.3	52.6
B214	S2	5.0	262.8	Glacial Till	7.0	—	—	—	—	6.8	42.1	51.1
B214	S3	10.0	257.8	Glacial Till	8.7	—	—	—	—	8.5	36.2	55.2
B219(MW)	S3 (0″-16″)	4.0	270.4	Glacial Till	7.5	17	13	4	—	8.9	45.9	45.1
B221(MW)	S4	15.0	265.0	Glacial Till	15.3	24	15	9	—	5.0	33.8	61.2
B224	S3	4.0	270.2	Glacial Till	8.0	24	15	9	—	1.1	32.6	66.3
B224	S7	12.0	262.2	Glacial Till	6.0	17	11	6	—	13.6	39.4	47.1
B227	S3	10.0	271.7	Fill	9.1	—	—	—	2.74	—	—	—
B229	S2	5.0	277.8	Fill	6.0	—	—	—	—	5.4	39.6	55.0
B229	S5	20.0	262.8	Glacial Till	5.6	—	—	—	—	13.5	39.0	47.5
B231	S3	10.0	270.9	Glacial Till	6.7	15	12	3	—	9.3	46.0	44.7
B234	S4	6.0	265.8	Glacial Till	4.9	25	14	11	2.68	9.5	47.1	43.4
B238(MW)	S3	4.0	275.2	Glacial Till	11.1	—	—	—	—	12.1	46.0	41.9
B238(MW)	S9	16.0	263.2	Glacial Till	5.7	—	—	—	—	5.9	43.6	50.5

Table 2.5-43—{Laboratory Soil Test Data}

(Page 2 of 2)

Sample Identification					Index Properties							
Boring Number	Sample Number	Sample Depth (feet)	Sample Elevation (feet)	Layer Name	Water Content (%)	Liquid Limit	Plastic Limit	Plasticity Index	Specific Gravity	Gravel (%)	Sand (%)	Fines (%)
B240	S3	9.0	274.0	Glacial Till	5.7	13	12	1	—	20.8	40.2	39.0
B240	S5	19.0	264.0	Glacial Till	4.9	17	11	6	2.75	8.8	41.1	50.1
B301	S5	8.0	254.1	Glacial Till	8.1	—	—	—	2.74	8.3	39.9	51.8
B305	S2	4.0	256.9	Glacial Till	9.9	—	—	—	—	37.5	33.9	28.6
B306	S2	4.0	252.3	Glacial Till	7.4	—	—	—	—	36.4	39.2	24.4
B308	S3	4.0	250.4	Surficial Deposits	10.9	—	—	—	—	10.0	30.8	59.1
B311	S4	6.0	249.4	Surficial Deposits	5.6	—	—	—	—	44.1	31.4	24.5
B313	S2 (0″-11″)	5.0	252.2	Surficial Deposits	12.6	22	10	12	—	—	—	—
B313	S2 (11″-23″)	5.0	252.2	Surficial Deposits	—	—	—	—	—	1.3	42.0	56.6
B314	S2 (0″-8″)	5.0	253.4	Glacial Till	—	—	—	—	—	53.9	25.0	21.1
B314	S2 (8″-16″)	5.0	253.4	Glacial Till	6.0	24	15	9	—	—	—	—

Notes:

"Sample Depth" and "Sample Elevation" refer to the top depth of the split-spoon sample
"—" Indicates test was not performed

Abbreviations:

NV No Value
NA Not Applicable
NP Non-plastic
MW Monitoring Well

Table 2.5-44— {Laboratory Structural Fill Test Data}

Sample Identification		Water Content (%)	Specific Gravity	Grain Size Data		
Borrow Pit	Sample Number			Gravel (%)	Sand (%)	Fines (%)
Lindsey - Bateman	Pad 1	4.1	NM	67.6	29.9	2.5
Lindsey - Bateman	Pad 2	2.6	NM	62.9	34.4	2.7
Lindsey - Bateman	Pad 3	4.0	NM	66.7	30.8	2.6
Northern	Pad 1	7.9	NM	49.4	47.0	3.6
Northern	Pad 2	8.7	NM	52.1	43.2	4.7
Northern	Pad 3	9.2	NM	53.4	41.8	4.7
Streeter - Rathburn	Pad 1	5.7	2.70	54.9	42.6	2.5
Streeter - Rathburn	Pad 2	7.5	NM	54.6	42.6	3.1
Streeter - Rathburn	Pad 3	7.1	NM	59.5	37.5	3.0

Abbreviation:

NM Not Measured

Table 2.5-45—{Laboratory Rock Test Data - Onshore}

(Page 1 of 2)

Sample Identification				Test Results [1]			
Formation	**Boring Number**	**Sample Number**	**Top of Sample Elevation (feet)**	**Unconfined Compressive Strength (psi)**	**Unit Weight (pcf)**	**Range of Young's Modulus (ksi)**	**Range of Poisson's Ratio**
Oswego Sandstone and Oswego Transition Zone	B201 (MW)	C3	230.8	22,207	183	1,200 to 1,600	0.09 to 0.20
	B201 (MW)	C6	199.7	23,239	159	1,100 to 2,000	0.07 to 0.21
	B208 (MW)	C2	243.1	19,881	161	1,200 to 1,700	0.07 to 0.29
	B210	C6	220.1	—	169	—	—
	B216 (MW)	C5	230.4	21,090	161	960 to 1,800	0.05 to 0.14
	B216 (MW)	C9	190.3	39,431	170	3,300 to 4,400	0.04 to 0.11
	B219 (MW)	C7	198.0	22,127	160	1,200 to 1,600	0.08 to 0.33
	B221 (MW)	C3	240.0	18,816	163	1,000 to 1,600	0.05 to 0.20
	B223	C2	243.7	—	170	—	—
	B224	C3	245.1	—	163	—	—
	B224	C3	242.9	21,996	164	3,100 to 3,900	0.15 to 0.41
	B224	C6	216.9	22,993	161	930 to 1,600	0.07 to 0.24
	B224	C9	189.4	—	168	—	—
	B229	C3	240.8	24,203	161	710 to 1,500	0.04 to 0.20
	B232	C8	191.0	28,025	166	1,100 to 2,200	0.03 to 0.14
	B233 (MW)	C3	241.3	29,758	160	800 to 2,100	0.02 to 0.12
	B235 (MW)	C3	243.0	27,535	160	740 to 2,100	0.03 to 0.15
	B238 (MW)	C6	221.2	18,550	157	640 to 1,800	0.03 to 0.46
	B238 (MW)	C9	183.9	—	168	—	—
	B301	C1-C2	239.5	21,833	162	1,400 to 1,600	0.07 to 0.35
	B301	C6	196.7	—	167	—	—
	B311	C2	239.5	24,728	166	1,300 to 1,700	0.06 to 0.16

Table 2.5-45—{Laboratory Rock Test Data - Onshore}

(Page 2 of 2)

Sample Identification				Test Results[1]			
Formation	Boring Number	Sample Number	Top of Sample Elevation (feet)	Unconfined Compressive Strength (psi)	Unit Weight (pcf)	Range of Young's Modulus (ksi)	Range of Poisson's Ratio
Pulaski Formation	B201 (MW)	C10	158.5	30,088	167	2,700 to 3,200	0.09 to 0.13
	B201 (MW)	C13	129.9	—	167	—	—
	B201 (MW)	C16	91.9	13,184	170	2,500 to 2,600	0.10 to 0.13
	B216 (MW)	C10-C11	171.7	—	169	—	—
	B216 (MW)	C16	115.0	—	171	—	—
	B219 (MW)	C11	158.6	18,333	169	2,000 to 2,300	0.14 to 0.20
	B219 (MW)	C13-C14	131.4	—	171	—	—
	B224	C12	159.2	—	163	—	—
	B224	C15	135.5	—	167	—	—
	B224	C18	106.9	15,587	161	950 to 1,400	0.07 to 0.14
	B232	C11	163.0	—	166	—	—
	B232	C14	131.0	—	169	—	—
	B232	C16	111.3	—	170	—	—
	B238 (MW)	C12	160.3	—	169	—	—
	B238 (MW)	C14	134.7	—	167	—	—
	B238 (MW)	C17	105.9	—	175	—	—
	B301	C8	178.1	—	172	—	—
	B301	C10	151.7	15,308	168	1,300 to 1,500	0.09 to 0.26
	B428	C13	129.3	14,256	167	1,300 to 1,600	0.11 to 0.18
	B428	C14	118.6	—	168	—	—
	B428	C15	110.2	15,235	165	2,000 to 2,700	0.08 to 0.11
Whetstone Gulf Formation	B201 (MW)	C19	77.8	—	168	—	—
	B216 (MW)	C20-C21	71.3	—	170	—	—
	B224	C21	74.2	—	172	—	—
	B232	C18	91.3	—	168	—	—
	B238 (MW)	C20	75.8	20,328	157	840 to 1,500	0.08 to 0.30

Notes:

1 Young's Modulus and Poisson's Ratio are calculated for the range of Axial Stress from 2,500 psi to 15,000 psi.

"—" Indicates test was not performed

Elevations are based on the National Geodetic Vertical Datum of 1929 (NGVD 29)

Abbreviations:

MW Monitoring Well

Table 2.5-46—{Range and Average of Laboratory Rock Test Data - Onshore}

Formation	Unit weight			Unconfined Compressive Strength			Average Value of Young's Modulus (ksi) for Specific Stress Ranges			Average Value of Poisson's ratio for Specific Stress Ranges			Number of Data Points
	Average (pcf)	Range (pcf)	Number of Data Points	Average (psi)	Range (psi)	Number of Data Points	Low Range 2.0-4.0 or 2.5-5.0 or 0.0-5.0 (ksi)	Mid Range 6.0-8.0 or 7.5-10.0 or 5.0-10.0 (ksi)	High Range 10.0-12.0 or 12.5-15.0 or 10.0-15.0 (ksi)	Low Range 2.0-4.0 or 2.5-5.0 or 0.0-5.0 (ksi)	Mid Range 6.0-8.0 or 7.5-10.0 or 5.0-10.0 (ksi)	High Range 10.0-12.0 or 12.5-15.0 or 10.0-15.0 (ksi)	
Oswego Sandstone and Oswego Transition Zone	165	157-183	22	24,151	18,550-39,431	16	1382 Max 4400 Min 710	1856 Max 3600 Min 1300	2031 Max 3900 Min 1500	0.06 Max 0.15 Min 0.02	0.014 Max 0.28 Min 0.07	0.23 Max 0.23 Min 0.11	16
Pulaski Formation	168	161-175	21	17,427	13,184-30,888	7	1864 Max 2700 Min 950	2057 Max 2900 Min 1400	2 180 Max 3200 Min 1400	0.10 Max 0.16 Min 0.07	0.13 Max 0.16 Min 0.09	0.18 Max 0.26 Min 0.11	7[(a)]
Whetstone Gulf Formation	167	157-172	5	20,328	20,328	1	840 Max only one Min	1300 Max only one Min	1500 Max only one Min	0.08 Max only one Min	0.16 Max only one Min	0.30 Max only one Min	16

Note:

a Five data points were used to compute the averages of Poisson's Ratio and Young's Modulus for the 12.5-15.0 or 10.0-15.0 ksi stress range

Table 2.5-47—{Laboratory Rock Test Data - Offshore}

(Page 1 of 2)

Formation	Sample Identification			Test Results[1]			
	Boring Number	Sample Number	Top of Sample Elevation (feet)	Unconfined Compressive Strength (psi)	Unit Weight (pcf)	Range of Young's Modulus (ksi)	Range of Poisson's Ratio
Oswego Transition Zone	B413	C2	210.5	17,267	159	520 to 1,200	0.07 to 0.44
	B441	C1	214.4	11,734	165	1,900 to 2,700	0.09 to 0.25
Pulaski Formation	B406	C16	129.6	13,204	166	1,200 to 1,600	0.10 to 0.14
	B409	C11	144.6	14,202	162	660 to 1,500	0.02 to 0.14
	B409	C12	132.8	18,389	162	610 to 1,100	0.02 to 0.10
	B413	C4	197.2	—	167	—	—
	B413	C5	185.7	21,828	161	1,300 to 1,900	0.09 to 0.13
	B413	C7	177.5	7,192	166	1,200 to 2,900	0.22 to 0.47
	B413	C9	153.3	12,757	159	1,400 to 2,200	0.05 to 0.10
	B413	C10	148.2	—	167	—	—
	B413	C11	135.3	—	168	—	—
	B413	C12	127.2	11,724	163	900 to 1,300	0.06 to 0.14
	B417	C2	194.2	—	168	—	—
	B417	C3	183.9	—	167	—	—
	B417	C5	176.6	27,893	167	2,600 to 3,900	0.13 to 0.37
	B417	C6	164.2	—	167	—	—
	B417	C7	152.2	—	168	—	—
	B417	C8	143.5	22,454	164	1,500 to 1,900	0.10 to 0.24
	B431	C15	123.7	4,656	170	2,600 to 3,500	0.27 to 0.33
	B433	C12	131.2	—	169	—	—
	B433	C13	126.9	—	168	—	—
	B437	C10	147.3	14,330	157	730 to 1,400	0.13 to 0.29
	B441	C4	198.4	9,245	171	1,300 to 1,500	0.12 to 0.16

Table 2.5-47—{Laboratory Rock Test Data - Offshore}

Formation	Sample Identification			Test Results[1]			
	Boring Number	Sample Number	Top of Sample Elevation (feet)	Unconfined Compressive Strength (psi)	Unit Weight (pcf)	Range of Young's Modulus (ksi)	Range of Poisson's Ratio
	B441	C4	189.3	—	168	—	—
	B441	C5	179.1	—	168	—	—
	B441	C7	168.4	—	166	—	—
	B441	C8	155.9	—	168	—	—
	B441	C9	147.2	11,685	161	750 to 1,100	0.03 to 0.10
	B441	C9	141.9	—	169	—	—
	B441	C10	130.8	—	165	—	—
Whetstone Gulf Formation	B413	C13	118.1	20,243	167	920 to 2,100	0.04 to 0.28
	B441	C11	119.9	—	169	—	—
	B441	C12	109.9	—	175	—	—

Notes:

1 Young's Modulus and Poisson's Ratio are calculated for the range of Axial Stress from 2,000 psi to 15,000 psi.
"—" Indicates test was not performed
Elevations are based on the National Geodetic Vertical Datum of 1929 (NGVD 29).

Table 2.5-48—{Range and Average of Laboratory Rock Test Data - Offshore}

Formation	Unit weight			Unconfined Compressive Strength			Average Value of Young's Modulus (ksi) for Specific Stress Ranges			Average Value of Poisson's ratio for Specific Stress Ranges			Number of Data Points
	Average (pcf)	Range (pcf)	Number of Data Points	Average (psi)	Range (psi)	Number of Data Points	Low Range 2.0-4.0 or 2.5-5.0 or 0.0-5.0 (ksi)	Mid Range 6.0-8.0 or 7.5-10.0 or 5.0-10.0 (ksi)	High Range 10.0-12.0 or 12.5-15.0 or 10.0-15.0 (ksi)	Low Range 2.0-4.0 or 2.5-5.0 or 0.0-5.0 (ksi)	Mid Range 6.0-8.0 or 7.5-10.0 or 5.0-10.0 (ksi)	High Range 10.0-12.0 or 12.5-15.0 or 10.0-15.0 (ksi)	
Oswego Sandstone and Oswego Transition Zone	162	159-165	2	14,501	11,734-17,267	2	1260 Max 2000 Min 520	1950 Max 2700 Min 1200	No data Max No data Min	0.08 Max 0.09 Min 0.07	0.35 Max 0.44 Min 0.25	No data Max No data Min	2[a]
Pulaski Formation	166	157-171	28	14,581	4,656-27,893	13	1182 Max 2600 Min 610	1600 Max 2900 Min 1000	1743 Max 2900 Min 11	0.10 Max 0.33 Min 0.02	0.14 Max 0.47 Min 0.07	0.16 Max 0.29 Min 0.10	13[b][c]
Whetstone Gulf Formation	170	167-175	3	20,243	20,243	1	920 Max only one Min	1400 Max only one Min	1900 Max only one Min	0.04 Max only one Min	0.07 Max only one Min	0.13 Max only one Min	1

Notes:

a No data points for the high stress range
b Twelve data points were used to compute the averages of Poisson's Ratio and Young's Modulus for the mid stress range
c Twelve data points were used to compute the averages of Poisson's Ratio and Young's Modulus for the high stress range

Table 2.5-49—{Rock Profile and Rock Properties}

Layer Name	Elevation Range (ft, NGVD 1929)	Unit Weight (lbs/ft^3)	Shear Wave Velocity at Small Strains (Note 6)	Poisson's Ratio
Oswego Sandstone (Including Oswego Transition Zone)	Top of Rock to El. 178	164 (Note 4)	Top of Rock to El. 242: 5,900 ft/sec El. 242 to 204: 6,500 ft/sec El. 204 to 178: 6,600 ft/sec Standard deviation is 10%. (Note 7)	0.37 ±0.03 (Note 10)
Pulaski Formation	El. 178 to El. 84 (Note 2)	168 (Note 4)	El. 178 to 166: 6,600 ft/sec El. 166 to 122: 7,200 ft/sec El. 122 to 106: 5,800 ft/sec El. 106 to 84: 6,700 ft/sec Standard deviation is 10%. (Note 7)	0.38 ±0.03 (Note 11)
Whetstone Gulf Formation	El. 84 to El. -700 (Notes 2,3)	167 (Note 4)	El. 84 to El. -300: 7,000 ft/sec El. -300 to El. -700: 7,500 ft/sec Standard deviation is 10%. (Note 8)	0.38 ±0.03 (Note 11)
Trenton Group / Black River Group	Top of formation at El. -700 ft plus or minus 200 ft (Note 3)	170 (Note 5)	Best estimate: 8,600 ft/sec Standard deviation is 10%. (Note 9)	0.31 ±0.03 (Note 12)
Precambrian Grenville crystalline basement rock	Top of formation at El. -1500 ft plus or minus 200 ft (Note 3)	177 (Note 5)	Best estimate: 11,300 ft/sec Standard deviation is 10%, but minimum value is 9,200 ft/sec. (Note 9)	0.28 ±0.03 (Note 12)

Notes:

1. Not used.
2. Elevations of the top of the Pulaski and Whetstone Gulf formations are based on the final log for Boring B224 located at the center of the reactor building.
3. Elevations of the top and bottom of the Trenton Group / Black River Group, and the top of the Precambrian Grenville are based on published data.
4. Unit weights of the Oswego Sandstone, Pulaski, and Whetstone Gulf Formations are based on laboratory test data.
5. Unit weight of the Trenton Group / Black River Group and unit weight of the Precambrian Grenville crystalline basement rock are based on published data.
6. Shear wave velocity values at small strains are valid for shear strains of $1x10^{-4}$ percent or less.
7. Shear wave velocities of the Oswego Sandstone and the Pulaski Formation are based on cross-hole test measurements. The recommended standard deviation is based on engineering judgment, such that values within two standard deviations are reasonable.
8. Shear wave velocities for the Whetstone Gulf formation are based on cross-hole test measurements. The cross-hole measurements extended about 10 feet into the Whetstone Gulf Formation. However, the Whetstone Gulf formation consists of sandstones and siltstones lithologically similar to the Pulaski formation. The difference between the two formations is predominantly paleontological. Therefore, the shear wave velocities should be essentially the same. An increase in shear wave velocity is estimated for the bottom half of the Whetstone Gulf formation to account for the increase in overburden stresses with depth. The recommended standard deviation is based on engineering judgment, such that values within two standard deviations are reasonable.
9. Shear wave velocity of the Trenton Group / Black River Group and shear wave velocity of the Precambrian Grenville crystalline basement rock are based on published data. The recommended standard deviation is based on engineering judgment, such that values within two standard deviations are reasonable.
10. Poisson's ratio for the Oswego Sandstone is based on Ref. 6, Weston Geophysical Engineers Inc. That report provides representative values of P-wave velocity and S-wave velocity for the Oswego Sandstone. Based on the method of interpreting the P-wave data, the range in Vp/Vs ratio is 2.10 to 2.23, corresponding to a range in Poisson's ratio of 0.353 to 0.374. The best estimate is considered to be Vp/Vs = 2.2, with a corresponding Poisson's ratio of 0.37. The recommended range of Poisson's ratio (±0.03) is based on engineering judgment.
11. Poisson's ratio for the Pulaski and Whetstone Gulf formations are based on the value for the Oswego Sandstone, discussed above in Note 10. The Pulaski and Whetstone Gulf Formations are similar to the Oswego Sandstone (Ordovician clastic sedimentary rock), but have more siltstone and less sandstone. Therefore, one would expect the Vp/Vs ratio and Poisson's ratio to be slightly higher. The recommended value of Vp/Vs ratio is 2.3, and the corresponding Poisson's ratio is 0.38. The recommended range of Poisson's ratio (±0.03) is based on engineering judgment.
12. Poisson's ratio for the Trenton/Black River Groups and the Grenville Precambrian are based on published Vp/Vs ratios. Representative Vp/Vs ratios are 1.9 and 1.8 for the Trenton/Black River Groups and the Grenville Precambrian, respectively, corresponding to Poisson's ratios of 0.31 and 0.28. The recommended range of Poisson's ratio (±0.03) is based on engineering judgment.

Table 2.5-50—{Representative Modulus Reduction and Damping for Rock}

Shear Strain, Percent	G / G_{max}	Damping, Percent[1]
0.0001	1	0.4
0.0003	1	interpolate
0.001	0.99	0.6
0.003	0.97	interpolate
0.01	0.93	1
0.03	0.85	interpolate
0.1	0.75	3
1	0.55	4.6

Notes:

1 Standard deviation is 25%.

- In analyses, values of damping should be capped at 1.0 percent for conservatism.
- The recommended standard deviation for damping values is based on engineering judgment.
- Values of modulus reduction vs. shear strain, and damping vs. shear strain are based on the following references:
  - Schnabel, P.B., Lysmer, J., and Seed, H.B. (1972). "SHAKE: A Computer Program for Earthquake Response Analysis of Horizontally Layered Sites," Report No. EERC 72-12, Earthquake Engineering Research Center, University of California, Berkeley, California.
  - Dynamic Properties of Ash-Flow Tuffs, by Won Kyoung Choi, Dissertation presented to the faculty of the Graduate School of the University of Texas at Austin in partial fulfillment of the requirements for the degree of Doctor of Philosophy, University of Texas at Austin, May 2008.
  - Results of free-free laboratory testing on rock core specimens from borings at the NMP3NPP site (University of Texas, 2008)

Table 2.5-51—{Rising Head Permeability Tests}

Geologic Formation	Boring	Test Interval				Horizontal Permeability (k_h)	
		Depth Below Ground Surface(ft)		Elevation Range (ft)		(cm/sec)	(ft/min)
Soil	B120 (MW)	4.5	14.5	262.5	252.5	1.0E-04	8.7E-05
	B121 (MW)	4.5	17.5	262.1	249.1	2.0E-05	1.3E-05
	B122 (MW)	4.5	19.6	278.0	262.9	2.0E-05	1.2E-05
	B123 (MW)	4.2	8.0	268.0	264.2	1.0E-04	1.2E-04
	B124 (MW)	5.0	12.0	258.3	251.3	3.0E-05	2.3E-05
Oswego Sandstone	B202 (MW)	18.0	31.0	238.2	225.2	4.7E-06	9.3E-06
	B209 (MW)	22.5	52.0	243.5	214.0	1.0E-08	2.0E-08
	B217 (MW)	26.0	50.0	239.1	215.1	1.4E-04	2.7E-04
	B236 (MW)	23.0	36.0	249.1	236.1	3.3E-04	6.5E-04
Oswego Transition Zone /Pulaski A	B111 (MW)	71.0	87.5	195.9	179.4	1.0E-05	2.0E-05
Pulaski A & B	B102 (MW)	104.0	125.0	151.6	130.6	4.8E-06	9.4E-06
Pulaski B	B109 (MW)	113.0	132.0	149.5	130.5	1.1E-04	2.2E-04
	B116 (MW)	118.0	142.0	176.8	152.8	6.6E-07	1.3E-06
	B117 (MW)	140.0	167.0	139.0	112.0	1.2E-06	2.4E-06
	B201 (MW)	112.0	138.0	143.9	117.9	1.9E-05	3.7E-05
Pulaski B & C	B101 (MW)	117.9	134.5	147.4	130.8	1.1E-05	2.2E-05
	B208 (MW)	135.5	151.0	129.8	114.3	3.8E-06	7.5E-06
	B235 (MW)	132.9	146.9	139.0	125.0	5.4E-05	1.1E-04

Notes:

Tests performed in Monitoring Wells.
Test interval corresponds to the sanded zone of the groundwater monitoring well.
Horizontal permeability was computed assuming a ratio of horizontal to vertical permeability (k_h/k_v) of nine.
Elevations are based on the National Geodetic Vertical Datum of 1929 (NGVD 29).

Abbreviation:

MW Monitoring Well

Table 2.5-52—{Onshore Water Pressure Tests}

(Page 1 of 12)

Geologic Formation	Boring	Test Interval				Applied Pressure at Ground Surf.	Horizontal Permeability (k_h)	Representative Permeability (k_h) at Test Interval		
		Depth Below Ground Surface		Elevation Range						
		(ft)		(ft)		(psi)	(cm/sec)	(ft/min)	(cm/sec)	(ft/min)
Oswego Sandstone	B101 (MW)	30.0	51.3	235.3	214.1	15	< 2.0E-06	< 3.9E-06	< 1 E-06	< 2 E-06
						30	< 1.3E-06	< 2.5E-06		
						45	< 9.4E-07	< 1.8E-06		
						30	< 1.3E-06	< 2.5E-06		
						15	< 2.0E-06	< 4.0E-06		
Oswego Sandstone	B106 (MW)	12.5	32.5	243.5	223.5	4	1.3E-05	2.6E-05	1 E-05	2 E-05
						8	1.4E-05	2.8E-05		
						12	7.5E-06	1.5E-05		
Oswego Sandstone	B108 (MW)	24.3	45.0	235.4	214.8	8	6.5E-04	1.3E-03	5 E-04	1 E-03
						12	5.6E-04	1.1E-03		
						16	5.1E-04	1.0E-03		
						25	4.3E-04	8.5E-04		
						16	4.5E-04	9.0E-04		
						8	4.9E-04	9.7E-04		
Oswego Sandstone	B114 (MW)	49.9	70.9	224.1	203.1	15	2.7E-05	5.2E-05	3 E-05	6 E-05
						31	2.5E-05	4.9E-05		
						45	3.5E-05	6.8E-05		
						31	2.0E-05	3.9E-05		
						15	< 2.5E-06	< 4.9E-06		
Oswego Sandstone	B216 (MW)	24.0	44.0	241.8	221.8	8	9.6E-04	1.9E-03	9 E-04	2 E-03
						12	8.9E-04	1.8E-03		
						15	9.1E-04	1.8E-03		
						10	7.9E-04	1.6E-03		
						5	7.6E-04	1.5E-03		
Oswego Sandstone	B224	45.0	65.8	229.2	208.4	15	2.3E-06	4.5E-06	4 E-06	7 E-06
						30	2.8E-06	5.6E-06		
						45	5.1E-06	1.0E-05		

Table 2.5-52—{Onshore Water Pressure Tests}

(Page 2 of 12)

Geologic Formation	Boring	Test Interval				Applied Pressure at Ground Surf.	Horizontal Permeability (k_h)	Representative Permeability (k_h) at Test Interval		
		Depth Below Ground Surface		Elevation Range						
		(ft)		(ft)		(psi)	(cm/sec)	(ft/min)	(cm/sec)	(ft/min)
Oswego Sandstone	B230 (MW)	45.0	65.0	237.6	217.6	15	3.1E-04	6.1E-04	2 E-04	5 E-04
						30	2.8E-04	5.6E-04		
						45	2.5E-04	4.8E-04		
						31	1.8E-04	3.5E-04		
						15	1.4E-04	2.8E-04		
Oswego Sandstone	B238 (MW)	50.0	70.8	229.2	208.4	15	6.3E-06	1.2E-05	8 E-06	2 E-05
						30	6.8E-06	1.3E-05		
						45	1.6E-05	3.2E-05		
						30	1.7E-05	3.3E-05		
						15	1.6E-05	3.1E-05		
Oswego Sandstone	B401	20.0	40.0	242.9	222.9	6	< 3.6E-06	< 7.1E-06		
						12	5.2E-06	1.0E-05		
						18	1.0E-05	2.0E-05	5 E-05	1 E-04
						12	2.6E-06	5.2E-06		
						6	< 3.6E-06	< 7.1E-06		
Oswego Sandstone	B401	35.0	55.0	227.9	207.9	15	< 2.3E-06	< 4.5E-06		
						30	< 1.4E-06	< 2.8E-06	< 1 E-06	< 2 E-06
						45	< 1.1E-06	< 2.1E-06		
Oswego Sandstone	B428	20.0	40.0	241.0	221.0	6	< 4.0E-06	< 7.8E-06		
						12	< 2.8E-06	< 5.5E-06	2 E-06	4 E-06
						18	2.2E-06	4.3E-06		
Oswego Sandstone / Oswego Transition Zone	B104 (MW)	38.8	60.0	217.2	195.9	15	< 2.4E-06	< 4.7E-06	2 E-06	4 E-06
						30	1.4E-06	2.8E-06		
						45	1.0E-06	2.0E-06		
						30	< 1.4E-06	< 2.8E-06		
						15	< 2.4E-06	< 4.6E-06		

Table 2.5-52—{Onshore Water Pressure Tests}

(Page 3 of 12)

Geologic Formation	Boring	Test Interval				Applied Pressure at Ground Surf.	Horizontal Permeability (k_h)	Representative Permeability (k_h) at Test Interval		
		Depth Below Ground Surface		Elevation Range						
		(ft)		(ft)		(psi)	(cm/sec)	(ft/min)	(cm/sec)	(ft/min)
Oswego Sandstone / Oswego Transition Zone	B108 (MW)	49.3	70.0	210.4	189.8	15	< 2.7E-06	< 5.3E-06	1 E-05	2 E-05
						30	7.9E-06	1.5E-05		
						45	1.0E-05	2.0E-05		
Oswego Sandstone / Oswego Transition Zone	B112 (MW)	36.9	57.9	246.0	225.0	15	1.5E-05	2.9E-05	1 E-05	2 E-05
						30	1.7E-05	3.4E-05		
						45	1.1E-04	2.1E-04		
						30	1.9E-05	3.7E-05		
						15	1.9E-05	3.8E-05		
Oswego Sandstone / Oswego Transition Zone	B201 (MW)	20.0	40.0	235.9	215.9	7	2.7E-04	5.4E-04	2 E-04	5 E-04
						14	2.6E-04	5.1E-04		
						20	2.3E-04	4.5E-04		
						14	2.0E-04	4.0E-04		
						7	1.6E-04	3.2E-04		
Oswego Sandstone / Oswego Transition Zone	B216 (MW)	51.0	71.0	214.8	194.8	16	< 2.5E-06	< 5.0E-06	< 1 E-06	< 2 E-06
						32	< 1.5E-06	< 3.0E-06		
						46	< 1.1E-06	< 2.2E-06		
Oswego Sandstone / Oswego Transition Zone	B238 (MW)	75.0	95.8	204.2	183.4	15	< 3.1E-06	< 6.2E-06	< 1 E-06	< 2 E-06
						30	< 1.7E-06	< 3.3E-06		
						45	< 1.2E-06	< 2.3E-06		
Oswego Sandstone / Oswego Transition Zone / Pulaski Formation Unit A	B102 (MW)	45.0	65.8	210.6	189.8	15	5.3E-05	1.0E-04	6 E-05	1 E-04
						30	8.9E-05	1.8E-04		
						45	1.1E-04	2.2E-04		
						30	2.2E-05	4.3E-05		
						15	1.3E-05	2.6E-05		
Oswego Sandstone / Oswego Transition Zone / Pulaski Formation Unit A	B114 (MW)	78.3	99.3	195.7	174.7	16	< 2.3E-06	< 4.5E-06	1 E-05	2 E-05
						30	2.9E-06	5.7E-06		
						46	2.3E-05	4.4E-05		

Table 2.5-52—{Onshore Water Pressure Tests}

(Page 4 of 12)

Geologic Formation	Boring	Test Interval				Applied Pressure at Ground Surf.	Horizontal Permeability (k_h)	Representative Permeability (k_h) at Test Interval		
		Depth Below Ground Surface		Elevation Range						
		(ft)		(ft)		(psi)	(cm/sec)	(ft/min)	(cm/sec)	(ft/min)
Oswego Transition Zone	B112 (MW)	84.3	105.3	198.6	177.6	16	1.9E-06	3.8E-06	1 E-05	2 E-05
						30	2.6E-06	5.2E-06		
						47	2.1E-05	4.2E-05		
						30	1.3E-05	2.6E-05		
						15	< 2.1E-06	< 4.1E-06		
Oswego Transition Zone / Pulaski Formation Unit A	B101 (MW)	65.2	86.6	200.1	178.8	16	3.9E-05	7.7E-05	4 E-06	8 E-06
						31	7.5E-06	1.5E-05		
						46	5.6E-06	1.1E-05		
						30	2.6E-06	5.1E-06		
						15	< 2.1E-06	< 4.1E-06		
Oswego Transition Zone / Pulaski Formation Unit A	B101 (MW)	82.5	103.8	182.8	161.6	15	6.2E-06	1.2E-05	8 E-06	2 E-05
						30	3.9E-06	7.7E-06		
						45	1.8E-05	3.6E-05		
						30	9.1E-06	1.8E-05		
						15	4.1E-06	8.1E-06		
Oswego Transition Zone / Pulaski Formation Unit A	B106 (MW)	55.0	75.0	201.0	181.0	15	9.1E-05	1.8E-04	7 E-05	1 E-04
						30	5.3E-05	1.0E-04		
						45	4.6E-05	9.0E-05		
						30	5.7E-05	1.1E-04		
						15	3.6E-05	7.0E-05		
Oswego Transition Zone / Pulaski Formation Unit A	B112 (MW)	109.7	130.7	173.2	152.2	15	< 2.1E-06	< 4.1E-06	7 E-06	1 E-05
						30	1.3E-06	2.6E-06		
						45	2.2E-05	4.4E-05		
						30	1.3E-06	2.6E-06		
Oswego Transition Zone / Pulaski Formation Unit A	B201 (MW)	65.0	85.0	190.9	170.9	15	< 3.0E-06	< 6.0E-06	5 E-06	1 E-05
						30	3.4E-06	6.7E-06		
						45	8.2E-06	1.6E-05		

Table 2.5-52—{Onshore Water Pressure Tests}

(Page 5 of 12)

Geologic Formation	Boring	Test Interval				Applied Pressure at Ground Surf.	Horizontal Permeability (k_h)	Representative Permeability (k_h) at Test Interval		
		Depth Below Ground Surface		Elevation Range						
		(ft)		(ft)		(psi)	(cm/sec)	(ft/min)	(cm/sec)	(ft/min)
Oswego Transition Zone / Pulaski Formation Unit A	B216 (MW)	80.0	100.0	185.8	165.8	15	< 2.7E-06	< 5.4E-06	< 1 E-06	< 2 E-06
						30	< 1.6E-06	< 3.2E-06		
						47	< 1.1E-06	< 2.2E-06		
Oswego Transition Zone / Pulaski Formation Unit A	B224	76.0	96.8	198.2	177.4	15	2.3E-06	4.5E-06	< 1 E-06	< 2 E-06
						30	< 1.4E-06	< 2.8E-06		
						45	< 1.0E-06	< 2.0E-06		
Oswego Transition Zone / Pulaski Formation Unit A	B230 (MW)	105.0	125.0	177.6	157.6	15	2.4E-05	4.8E-05	2 E-05	3 E-05
						30	1.4E-05	2.8E-05		
						45	1.2E-05	2.3E-05		
						30	1.5E-05	2.9E-05		
						15	2.0E-05	4.0E-05		
Oswego Transition Zone / Pulaski Formation Unit A	B238 (MW)	100.0	120.8	179.2	158.4	15	< 3.1E-06	< 6.2E-06	< 1 E-06	< 2 E-06
						30	< 1.7E-06	< 3.3E-06		
						45	< 1.2E-06	< 2.3E-06		
Pulaski Formation Unit A	B102 (MW)	80.0	100.8	175.6	154.8	15	5.3E-06	1.1E-05	1 E-05	2 E-05
						30	1.4E-05	2.8E-05		
						46	1.4E-05	2.8E-05		
						30	1.2E-05	2.4E-05		
						15	1.6E-05	3.2E-05		
Pulaski Formation Unit A	B104 (MW)	78.8	100.0	177.2	155.9	15	2.4E-06	4.8E-06	5 E-06	1 E-05
						31	1.4E-06	2.8E-06		
						44	7.3E-06	1.4E-05		
						30	7.3E-06	1.4E-05		
						16	4.7E-06	9.3E-06		
Pulaski Formation Unit A	B106 (MW)	80.0	100.0	176.0	156.0	15	3.0E-06	5.9E-06	2 E-06	4 E-06
						30	1.8E-06	3.6E-06		
						45	1.3E-06	2.6E-06		

Table 2.5-52—{Onshore Water Pressure Tests}

(Page 6 of 12)

Geologic Formation	Boring	Test Interval				Applied Pressure at Ground Surf.	Horizontal Permeability (k_h)	Representative Permeability (k_h) at Test Interval		
		Depth Below Ground Surface		Elevation Range						
		(ft)		(ft)		(psi)	(cm/sec)	(ft/min)	(cm/sec)	(ft/min)
Pulaski Formation Unit A	B114 (MW)	100.5	121.5	173.5	152.5	15	< 2.4E-06	< 4.8E-06	2 E-05	4 E-05
						30	< 1.5E-06	< 2.9E-06		
						45	1.8E-05	3.5E-05		
Pulaski Formation Unit A	B201 (MW)	85.0	105.0	170.9	150.9	15	< 3.0E-06	< 6.0E-06	2 E-06	5 E-06
						30	1.7E-06	3.3E-06		
						45	2.4E-06	4.6E-06		
Pulaski Formation Unit A	B224	100.0	120.8	174.2	153.4	15	4.6E-06	9.1E-06	5 E-06	1 E-05
						30	5.7E-06	1.1E-05		
						45	5.1E-06	1.0E-05		
Pulaski Formation Unit A	B428	85.0	105.0	176.0	156.0	15	< 2.4E-06	< 4.8E-06		
						30	< 1.5E-06	< 2.9E-06	< 1 E-06	< 2 E-06
						45	< 1.1E-06	< 2.1E-06		
Pulaski Formation Unit A / Pulaski Formation Unit B	B108 (MW)	115.0	135.0	144.8	124.8	15	< 2.8E-06	< 5.5E-06	8 E-06	2 E-05
						30	6.5E-06	1.3E-05		
						46	1.1E-05	2.2E-05		
Pulaski Formation Unit A / Pulaski Formation Unit B	B112 (MW)	140.3	161.3	142.6	121.6	15	< 2.1E-06	< 4.0E-06	< 1 E-06	< 2 E-06
						30	< 1.3E-06	< 2.6E-06		
						45	< 9.8E-07	< 1.9E-06		
Pulaski Formation Unit A/ Pulaski Formation Unit B	B401	100.0	120.0	162.9	142.9	15	< 2.3E-06	< 4.5E-06		
						30	< 1.4E-06	< 2.8E-06	< 1 E-06	< 2 E-06
						45	< 1.1E-06	< 2.1E-06		
Pulaski Formation Unit A/ Pulaski Formation Unit B	B428	100.0	120.0	161.0	141.0	15	< 2.4E-06	< 4.8E-06		
						30	< 1.5E-06	< 2.9E-06	< 1 E-06	< 2 E-06
						45	< 1.1E-06	< 2.1E-06		
Pulaski Formation Unit A / Pulaski Formation Unit B / Pulaski Formation Unit C	B114 (MW)	130.7	151.7	143.3	122.3	16	2.4E-05	4.6E-05	2 E-05	4 E-05
						30	1.9E-05	3.7E-05		
						45	1.8E-05	3.5E-05		

Table 2.5-52—{Onshore Water Pressure Tests}

(Page 7 of 12)

Geologic Formation	Boring	Test Interval				Applied Pressure at Ground Surf.	Horizontal Permeability (k_h)	Representative Permeability (k_h) at Test Interval		
		Depth Below Ground Surface		Elevation Range						
		(ft)		(ft)		(psi)	(cm/sec)	(ft/min)	(cm/sec)	(ft/min)
Pulaski Formation Unit A / Pulaski Formation Unit B / Pulaski Formation Unit C	B224	130.0	150.8	144.2	123.4	15	4.6E-06	9.1E-06	4 E-06	7 E-06
						30	4.3E-06	8.4E-06		
						45	2.1E-06	4.1E-06		
Pulaski Formation Unit B	B102 (MW)	105.0	125.8	150.6	129.8	15	2.7E-06	5.3E-06	1 E-06	2 E-06
						30	< 1.6E-06	< 3.1E-06		
						45	1.1E-06	2.2E-06		
						30	< 1.6E-06	< 3.1E-06		
						15	< 2.7E-06	< 5.3E-06		
Pulaski Formation Unit B	B108 (MW)	136.0	150.0	123.8	109.8	15	1.1E-04	2.2E-04	2 E-06	5 E-06
						30	2.2E-06	4.3E-06		
						45	1.2E-04	2.3E-04		
						30	< 2.2E-06	< 4.3E-06		
						15	3.7E-06	7.4E-06		
Pulaski Formation Unit B	B201 (MW)	115.0	135.0	140.9	120.9	15	1.8E-04	3.5E-04	1 E-04	3 E-04
						30	8.2E-05	1.6E-04		
						45	9.0E-05	1.8E-04		
						45	9.0E-05	1.8E-04		
						30	1.0E-04	2.0E-04		
						15	1.4E-04	2.7E-04		
Pulaski Formation Unit B	B216 (MW)	115.0	135.0	150.8	130.8	15	2.6E-06	5.0E-06	5 E-06	9 E-06
						31	4.6E-06	9.0E-06		
						46	6.5E-06	1.3E-05		
Pulaski Formation Unit B / Pulaski Formation Unit C	B101 (MW)	115.0	136.3	150.3	129.1	14	1.5E-05	2.9E-05	1 E-05	3 E-05
						30	1.3E-05	2.5E-05		
						45	1.6E-05	3.1E-05		
						30	1.4E-05	2.8E-05		
						15	1.4E-05	2.8E-05		

Table 2.5-52—{Onshore Water Pressure Tests}

(Page 8 of 12)

Geologic Formation	Boring	Test Interval				Applied Pressure at Ground Surf.	Horizontal Permeability (k_h)	Representative Permeability (k_h) at Test Interval		
		Depth Below Ground Surface		Elevation Range						
		(ft)		(ft)		(psi)	(cm/sec)	(ft/min)	(cm/sec)	(ft/min)
Pulaski Formation Unit B / Pulaski Formation Unit C	B104 (MW)	123.3	144.5	132.7	111.4	15	2.4E-06	4.8E-06	2 E-06	5 E-06
						30	2.9E-06	5.6E-06		
						45	2.0E-06	4.0E-06		
						30	2.8E-06	5.6E-06		
						15	< 2.4E-06	< 4.7E-06		
Pulaski Formation Unit B / Pulaski Formation Unit C	B106 (MW)	105.0	125.0	151.0	131.0	15	1.3E-04	2.6E-04	1 E-04	2 E-04
						30	1.3E-04	2.6E-04		
						45	1.1E-04	2.1E-04		
						30	8.7E-05	1.7E-04		
						15	6.7E-05	1.3E-04		
Pulaski Formation Unit B / Pulaski Formation Unit C	B230 (MW)	136.0	156.0	146.6	126.6	15	< 2.0E-06	< 4.0E-06	< 1 E-06	< 2 E-06
						31	< 1.3E-06	< 2.5E-06		
						45	< 9.6E-07	< 1.9E-06		
Pulaski Formation Unit B / Pulaski Formation Unit C	B238 (MW)	145.0	165.8	134.2	113.4	15	< 3.1E-06	< 6.2E-06	1 E-06	2 E-06
						30	< 1.7E-06	< 3.3E-06		
						45	1.2E-06	2.3E-06		
Pulaski Formation Unit B/ Pulaski Formation Unit C	B401	113.0	133.0	149.9	129.9	15	1.6E-05	3.2E-05		
						30	1.7E-05	3.4E-05		
						45	1.9E-05	3.7E-05	2 E-05	4 E-05
						30	1.6E-05	3.1E-05		
						15	< 2.3E-06	< 4.5E-06		
Pulaski Formation Unit B/ Pulaski Formation Unit C	B401	120.0	140.0	142.9	122.9	15	3.0E-05	5.9E-05		
						30	2.5E-05	4.8E-05		
						45	2.4E-05	4.8E-05	3 E-05	6 E-05
						30	2.2E-05	4.3E-05		
						15	< 2.3E-06	< 4.5E-06		

Table 2.5-52—{Onshore Water Pressure Tests}

(Page 9 of 12)

Geologic Formation	Boring	Test Interval				Applied Pressure at Ground Surf.	Horizontal Permeability (k_h)	Representative Permeability (k_h) at Test Interval		
		Depth Below Ground Surface		Elevation Range						
		(ft)		(ft)		(psi)	(cm/sec)	(ft/min)	(cm/sec)	(ft/min)
Pulaski Formation Unit B/ Pulaski Formation Unit C	B428	120.0	140.0	141.0	121.0	15	7.3E-06	1.4E-05		
						30	1.2E-05	2.4E-05	1 E-05	2 E-05
						45	1.6E-05	3.2E-05		
Pulaski Formation Unit C	B101 (MW)	145.0	166.3	120.3	99.1	15	< 2.0E-06	< 4.0E-06	1 E-06	2 E-06
						29	1.3E-06	2.6E-06		
						45	9.4E-07	1.9E-06		
						30	< 1.3E-06	< 2.5E-06		
						15	< 2.1E-06	< 4.0E-06		
Pulaski Formation Unit C	B102 (MW)	140.0	160.8	115.6	94.8	15	< 2.7E-06	< 5.3E-06	< 1 E-06	< 2 E-06
						30	< 1.6E-06	< 3.1E-06		
						45	< 1.1E-06	< 2.2E-06		
						30	< 1.6E-06	< 3.1E-06		
						15	< 2.6E-06	< 5.2E-06		
Pulaski Formation Unit C	B104 (MW)	143.8	165.0	112.2	90.9	16	2.3E-06	4.5E-06	2 E-06	5 E-06
						30	2.8E-06	5.6E-06		
						45	2.0E-06	4.0E-06		
						30	2.8E-06	5.6E-06		
						15	< 2.4E-06	< 4.6E-06		
Pulaski Formation Unit C	B106 (MW)	128.0	148.0	128.0	108.0	15	< 3.2E-06	< 6.3E-06	2 E-06	5 E-06
						30	1.9E-06	3.7E-06		
						45	1.3E-06	2.6E-06		
Pulaski Formation Unit C	B114 (MW)	161.5	182.5	112.5	91.5	16	< 2.4E-06	< 4.8E-06	< 1 E-06	< 2 E-06
						30	< 1.5E-06	< 2.9E-06		
						45	< 1.0E-06	< 2.1E-06		
Pulaski Formation Unit C	B224	160.0	180.8	114.2	93.4	15	< 2.3E-06	< 4.5E-06	< 1 E-06	< 2 E-06
						31	< 1.4E-06	< 2.7E-06		
						45	< 1.0E-06	< 2.0E-06		

Table 2.5-52—{Onshore Water Pressure Tests}

(Page 10 of 12)

Geologic Formation	Boring	Test Interval				Applied Pressure at Ground Surf.	Horizontal Permeability (k_h)	Representative Permeability (k_h) at Test Interval		
		Depth Below Ground Surface		Elevation Range						
		(ft)		(ft)		(psi)	(cm/sec)	(ft/min)	(cm/sec)	(ft/min)
Pulaski Formation Unit C	B230 (MW)	158.0	178.0	124.6	104.6	14	1.0E-04	2.0E-04	8 E-05	2 E-04
						30	6.8E-05	1.3E-04		
						45	7.4E-05	1.5E-04		
						30	7.5E-05	1.5E-04		
						15	8.1E-05	1.6E-04		
Pulaski Formation Unit C	B401	133.0	153.0	129.9	109.9	15	< 2.3E-06	< 4.5E-06		
						30	< 1.4E-06	< 2.8E-06	< 1 E-06	< 2 E-06
						45	< 1.1E-06	< 2.1E-06		
Pulaski Formation Unit C	B428	130.0	150.0	131.0	111.0	15	< 2.4E-06	< 4.8E-06		
						30	< 1.5E-06	< 2.9E-06	< 1 E-06	< 2 E-06
						45	< 1.1E-06	< 2.1E-06		
Pulaski Formation Unit C / Whetstone Gulf Formation Unit A	B104 (MW)	169.3	190.5	86.7	65.4	15	4.7E-06	9.3E-06	4 E-06	7 E-06
						30	4.3E-06	8.4E-06		
						45	3.0E-06	6.0E-06		
						30	4.3E-06	8.5E-06		
						15	2.4E-06	4.6E-06		
Pulaski Formation Unit C / Whetstone Gulf Formation Unit A	B112 (MW)	172.0	193.0	110.9	89.9	15	2.1E-05	4.1E-05	2 E-05	4 E-05
						30	2.2E-05	4.3E-05		
						45	2.0E-05	3.9E-05		
Pulaski Formation Unit C / Whetstone Gulf Formation Unit A	B201 (MW)	170.0	190.0	85.9	65.9	15	1.5E-04	3.0E-04	1 E-05	3 E-05
						30	1.7E-05	3.3E-05		
						45	1.1E-05	2.2E-05		
Pulaski Formation Unit C / Whetstone Gulf Formation Unit A	B216 (MW)	165.0	185.0	100.8	80.8	15	< 2.7E-06	< 5.3E-06	< 1 E-06	< 2 E-06
						30	< 1.6E-06	< 3.1E-06		
						45	< 1.1E-06	< 2.2E-06		
Pulaski Formation Unit C / Whetstone Gulf Formation Unit A	B224	185.0	205.8	89.2	68.4	15	< 2.3E-06	< 4.5E-06	< 1 E-06	< 2 E-06
						30	< 1.4E-06	< 2.8E-06		
						46	< 1.0E-06	< 2.0E-06		

Table 2.5-52—{Onshore Water Pressure Tests}

(Page 11 of 12)

Geologic Formation	Boring	Test Interval				Applied Pressure at Ground Surf.	Horizontal Permeability (k_h)	Representative Permeability (k_h) at Test Interval		
		Depth Below Ground Surface		Elevation Range						
		(ft)		(ft)		(psi)	(cm/sec)	(ft/min)	(cm/sec)	(ft/min)
Pulaski Formation Unit C / Whetstone Gulf Formation Unit A	B230 (MW)	179.5	199.5	103.1	83.1	14	< 2.1E-06	< 4.2E-06	1 E-06	2 E-06
						30	1.3E-06	2.6E-06		
						46	9.6E-07	1.9E-06		
Pulaski Formation Unit C / Whetstone Gulf Formation Unit A	B238 (MW)	170.0	190.8	109.2	88.4	15	3.1E-06	6.2E-06	3 E-06	6 E-06
						30	3.4E-06	6.7E-06		
						45	3.5E-06	6.9E-06		
Pulaski Formation Unit C/ Whetstone Gulf Formation Unit A	B401	140.0	160.0	122.9	102.9	15	2.3E-06	4.5E-06		
						30	2.9E-06	5.7E-06	3 E-06	6 E-06
						45	3.2E-06	6.2E-06		
Pulaski Formation Unit C/ Whetstone Gulf Formation Unit A	B428	150.0	170.0	111.0	91.0	15	< 2.4E-06	< 4.8E-06		
						30	< 1.5E-06	< 2.9E-06	< 1 E-06	< 2 E-06
						45	< 1.1E-06	< 2.1E-06		
Whetstone Gulf Formation Unit A	B101 (MW)	185.0	206.3	80.3	59.1	15	2.0E-06	3.9E-06	< 1 E-06	< 2 E-06
						29	2.6E-06	5.1E-06		
						45	< 9.3E-07	< 1.8E-06		
						47	9.0E-07	1.8E-06		
						30	< 1.3E-06	< 2.5E-06		
						15	< 2.0E-06	< 3.9E-06		
Whetstone Gulf Formation Unit A	B102 (MW)	180.0	200.8	75.6	54.8	15	1.3E-06	2.6E-06	< 1 E-06	< 2 E-06
						30	< 1.6E-06	< 3.1E-06		
						45	< 1.1E-06	< 2.2E-06		
						30	< 1.6E-06	< 3.1E-06		
						15	< 2.7E-06	< 5.3E-06		
Whetstone Gulf Formation Unit A	B106 (MW)	172.0	192.0	84.0	64.0	15	3.2E-06	6.4E-06	2 E-06	4 E-06
						30	1.9E-06	3.7E-06		
						46	1.3E-06	2.6E-06		

Table 2.5-52—{Onshore Water Pressure Tests}

(Page 12 of 12)

Geologic Formation	Boring	Test Interval				Applied Pressure at Ground Surf.	Horizontal Permeability (k_h)	Representative Permeability (k_h) at Test Interval		
		Depth Below Ground Surface		Elevation Range						
		(ft)		(ft)		(psi)	(cm/sec)	(ft/min)	(cm/sec)	(ft/min)
Whetstone Gulf Formation Unit A	B216 (MW)	182.0	202.0	83.8	63.8	15	< 2.6E-06	< 5.1E-06	< 1 E-06	< 2 E-06
						30	< 1.6E-06	< 3.1E-06		
						45	< 1.1E-06	< 2.2E-06		
Whetstone Gulf Formation Unit A	B238 (MW)	190.0	210.8	89.2	68.4	15	< 3.1E-06	< 6.2E-06	< 1 E-06	< 2 E-06
						30	< 1.7E-06	< 3.3E-06		
						45	< 1.2E-06	< 2.3E-06		
Whetstone Gulf Formation Unit A	B401	175.0	195.0	87.9	67.9	15	< 2.3E-06	< 4.5E-06		
						30	< 1.4E-06	< 2.8E-06	< 1 E-06	< 2 E-06
						45	< 1.1E-06	< 2.1E-06		
Whetstone Gulf Formation Unit A	B428	170.0	190.0	91.0	71.0	15	< 2.4E-06	< 4.8E-06		
						30	< 1.5E-06	< 2.9E-06	< 1 E-06	< 2 E-06
						45	< 1.1E-06	< 2.1E-06		
Whetstone Gulf Formation Unit B	B401	216.0	236.0	46.9	26.9	15	2.3E-06	4.5E-06		
						30	2.9E-06	5.7E-06	2 E-06	4 E-06
						45	2.1E-06	4.1E-06		
Whetstone Gulf Formation Unit B	B428	215.0	235.0	46.0	26.0	15	< 2.4E-06	< 4.8E-06	1 E-06	2 E-06
						30	< 1.5E-06	< 2.9E-06		
						45	1.1E-06	2.1E-06		

Notes:

Tests with measured flow less than 1 gallon per minute were stopped at maximum pressure.
Horizontal permeability was computed assuming a ratio of horizontal to vertical permeability (k_h / k_v) of nine.
Permeabilities reported with a "less than" symbol (<) indicate that the measured flow during the test was less than the smallest increment of flow we could measure.
Elevations are based on the National Geodetic Vertical Datum of 1929 (NGVD 29).
Representative permeability is based on engineering judgment.

Abbreviation:

MW Monitoring Well

Table 2.5-53— {Offshore Water Pressure Tests}

(Page 1 of 9)

Geologic Formation	Boring	Test Interval				Applied Pressure at Ground Surf.	Horizontal Permeability (k_h)		Representative Permeability (k_h) of Test Interval	
		Depth Below Ground Surface		Elevation Range						
		(ft)		(ft)		(psi)	(cm/sec)	(ft/min)	(cm/sec)	(ft/min)
Oswego Transition Zone/ Pulaski Formation Unit A	B406	30.0	51.0	207.3	186.3	10	2.3E-04	4.5E-04	2 E-04	4 E-04
						20	1.8E-04	3.5E-04		
						30	1.6E-04	3.2E-04		
						20	1.3E-04	2.6E-04		
						10	1.4E-04	2.8E-04		
Oswego Transition Zone/ Pulaski Formation Unit A	B409	30.0	51.0	202.8	181.8	10	6.2E-04	1.2E-03		
						21	4.6E-04	9.1E-04		
						30	4.2E-04	8.3E-04	5 E-04	9 E-04
						20	4.2E-04	8.2E-04		
						10	4.8E-04	9.4E-04		
Oswego Transition Zone/ Pulaski Formation Unit A	B413	10.0	31.0	207.3	186.3	4	7.3E-04	1.4E-03		
						10	6.8E-04	1.3E-03	7 E-04	1 E-03
						7	7.1E-04	1.4E-03		
Oswego Transition Zone/ Pulaski Formation Unit A	B437	15.0	36.0	218.2	197.2	5	4.2E-06	8.2E-06		
						11	5.7E-06	1.1E-05	5 E-06	1 E-05
						15	5.0E-06	9.8E-06		
Pulaski Formation Unit A	B405	30.0	51.0	208.3	187.3	10	2.3E-04	4.5E-04		
						20	1.7E-04	3.3E-04		
						30	1.6E-04	3.1E-04	2 E-04	4 E-04
						20	1.4E-04	2.8E-04		
						10	1.4E-04	2.8E-04		

Table 2.5-53— {Offshore Water Pressure Tests}

(Page 2 of 9)

Geologic Formation	Boring	Test Interval				Applied Pressure at Ground Surf.	Horizontal Permeability (k_h)		Representative Permeability (k_h) of Test Interval	
		Depth Below Ground Surface		Elevation Range						
		(ft)		(ft)		(psi)	(cm/sec)	(ft/min)	(cm/sec)	(ft/min)
Pulaski Formation Unit A	B433	40.0	60.0	197.3	177.3	5	7.9E-05	1.6E-04		
						10	8.5E-05	1.7E-04		
						16	1.0E-04	2.0E-04	8 E-05	2 E-04
						10	8.0E-05	1.6E-04		
						6	6.5E-05	1.3E-04		
Pulaski Formation Unit A	B441	30.0	51.0	188.7	167.7	15	9.2E-06	1.8E-05		
						30	1.8E-05	3.5E-05	2 E-05	3 E-05
						45	1.6E-05	3.2E-05		
Pulaski Formation Unit A/ Pulaski Formation Unit B	B409	55.0	76.0	177.8	156.8	15	< 2.3E-06	< 4.6E-06		
						31	1.4E-06	2.8E-06	1 E-06	2 E-06
						45	< 1.0E-06	< 2.0E-06		
Pulaski Formation Unit A/ Pulaski Formation Unit B	B433	64.6	84.6	172.7	152.7	16	4.0E-06	7.8E-06		
						30	2.8E-06	5.4E-06	4 E-06	8 E-06
						45	5.6E-06	1.1E-05		
Pulaski Formation Unit A/ Pulaski Formation Unit B	B437	56.5	77.5	176.7	155.7	15	< 2.2E-06	< 4.4E-06		
						30	< 1.4E-06	< 2.7E-06	< 1 E-06	< 2 E-06
						44	< 1.0E-06	< 2.0E-06		

Table 2.5-53— {Offshore Water Pressure Tests}

(Page 3 of 9)

Geologic Formation	Boring	Test Interval				Applied Pressure at Ground Surf.	Horizontal Permeability (k_h)		Representative Permeability (k_h) of Test Interval	
		Depth Below Ground Surface		Elevation Range						
		(ft)		(ft)		(psi)	(cm/sec)	(ft/min)	(cm/sec)	(ft/min)
Pulaski Formation Unit A/ Pulaski Formation Unit B	B441	45.0	66.0	173.7	152.7	15	4.4E-05	8.6E-05		
						30	5.5E-05	1.1E-04		
						45	3.9E-05	7.7E-05	4 E-05	8 E-05
						30	1.5E-05	2.9E-05		
						15	1.4E-05	2.7E-05		
Pulaski Formation Unit A/ Pulaski Formation Unit B/ Pulaski Formation Unit C	B405	69.0	90.0	169.3	148.3	15	3.2E-06	6.3E-06		
						30	1.3E-06	2.6E-06	2 E-06	4 E-06
						45	< 1.0E-06	< 2.0E-06		
Pulaski Formation Unit A/ Pulaski Formation Unit B/ Pulaski Formation Unit C	B406	69.0	90.0	168.3	147.3	15	9.1E-06	1.8E-05		
						30	8.9E-06	1.7E-05	1 E-05	2 E-05
						45	1.1E-05	2.1E-05		
Pulaski Formation Unit A/ Pulaski Formation Unit B/ Pulaski Formation Unit C	B417	25.0	46.0	179.3	158.3	8	6.2E-04	1.2E-03		
						16	4.9E-04	9.6E-04		
						25	3.9E-04	7.7E-04	5 E-04	9 E-04
						16	3.9E-04	7.7E-04		
						8	4.5E-04	8.9E-04		

Table 2.5-53— {Offshore Water Pressure Tests}

Geologic Formation	Boring	Test Interval				Applied Pressure at Ground Surf.	Horizontal Permeability (k_h)		Representative Permeability (k_h) of Test Interval	
		Depth Below Ground Surface		Elevation Range						
		(ft)		(ft)		(psi)	(cm/sec)	(ft/min)	(cm/sec)	(ft/min)
Pulaski Formation Unit B/ Pulaski Formation Unit C	B407	80.0	100.0	156.6	136.6	15	< 2.4E-06	< 4.8E-06		
						30	< 1.5E-06	< 2.9E-06	1 E-06	2 E-06
						45	1.1E-06	2.1E-06		
Pulaski Formation Unit B/ Pulaski Formation Unit C	B413	43.0	64.0	174.3	153.3	15	3.4E-05	6.8E-05		
						30	3.0E-05	5.9E-05		
						43	3.8E-05	7.5E-05	4 E-05	7 E-05
						30	3.6E-05	7.0E-05		
						15	3.5E-05	6.9E-05		
Pulaski Formation Unit B/ Pulaski Formation Unit C	B435	85.0	106.0	151.4	130.4	15	4.7E-05	9.2E-05		
						30	4.8E-05	9.4E-05		
						45	4.3E-05	8.5E-05	5 E-05	9 E-05
						30	4.5E-05	8.8E-05		
						15	4.6E-05	9.1E-05		
Pulaski Formation Unit B/ Pulaski Formation Unit C	B437	79.5	100.5	153.7	132.7	15	2.1E-05	4.0E-05		
						30	1.7E-05	3.4E-05		
						45	1.7E-05	3.4E-05	2 E-05	4 E-05
						30	1.5E-05	3.0E-05		
						15	1.5E-05	3.0E-05		

Table 2.5-53— {Offshore Water Pressure Tests}

(Page 5 of 9)

Geologic Formation	Boring	Test Interval				Applied Pressure at Ground Surf.	Horizontal Permeability (k_h)		Representative Permeability (k_h) of Test Interval	
		Depth Below Ground Surface		Elevation Range						
		(ft)		(ft)		(psi)	(cm/sec)	(ft/min)	(cm/sec)	(ft/min)
Pulaski Formation Unit B/ Pulaski Formation Unit C	B441	60.0	81.0	158.7	137.7	15	9.6E-05	1.9E-04		
						30	6.2E-05	1.2E-04		
						45	5.7E-05	1.1E-04	6 E-05	1 E-04
						30	4.5E-05	8.9E-05		
						15	5.0E-05	9.7E-05		
Pulaski Formation Unit C	B405	90.0	111.0	148.3	127.3	15	5.1E-05	1.0E-04		
						30	3.9E-05	7.7E-05		
						45	3.6E-05	7.2E-05	4 E-05	7 E-05
						30	3.0E-05	5.9E-05		
						15	3.0E-05	6.0E-05		
Pulaski Formation Unit C	B406	89.0	110.0	148.3	127.3	15	1.5E-05	2.9E-05		
						30	1.1E-05	2.1E-05		
						45	9.2E-06	1.8E-05	1 E-05	2 E-05
						30	8.4E-06	1.7E-05		
						14	9.1E-06	1.8E-05		
Pulaski Formation Unit C	B408	85.0	105.0	152.1	132.1	15	3.0E-05	6.0E-05		
						30	3.8E-05	7.4E-05		
						45	4.6E-05	9.0E-05	4 E-05	8 E-05
						30	3.5E-05	7.0E-05		
						15	4.0E-05	7.9E-05		
Pulaski Formation Unit C	B409	80.0	101.0	152.8	131.8	16	2.3E-04	4.6E-04		
						30	1.7E-04	3.3E-04		
						45	1.4E-04	2.8E-04	2 E-04	3 E-04
						30	1.3E-04	2.5E-04		

Table 2.5-53— {Offshore Water Pressure Tests}

(Page 6 of 9)

Geologic Formation	Boring	Test Interval				Applied Pressure at Ground Surf.	Horizontal Permeability (k_h)		Representative Permeability (k_h) of Test Interval	
		Depth Below Ground Surface		Elevation Range						
		(ft)		(ft)		(psi)	(cm/sec)	(ft/min)	(cm/sec)	(ft/min)
Pulaski Formation Unit C	B413	58.0	79.0	159.3	138.3	15	6.2E-05	1.2E-04		
						30	5.1E-05	1.0E-04		
						45	5.3E-05	1.0E-04	6 E-05	1 E-04
						30	5.1E-05	1.0E-04		
						15	6.1E-05	1.2E-04		
Pulaski Formation Unit C	B415	55.0	76.0	155.7	134.7	15	1.5E-04	2.9E-04		
						30	1.6E-04	3.1E-04		
						45	1.4E-04	2.7E-04	1 E-04	3 E-04
						30	1.2E-04	2.4E-04		
						15	1.2E-04	2.4E-04		
Pulaski Formation Unit C	B417	45.0	66.0	159.3	138.3	15	2.2E-04	4.4E-04		
						30	1.9E-04	3.7E-04		
						45	1.7E-04	3.3E-04	2 E-04	4 E-04
						30	1.8E-04	3.5E-04		
						15	2.1E-04	4.1E-04		
Pulaski Formation Unit C	B433	91.0	111.0	146.3	126.3	15	2.4E-06	4.7E-06		
						30	6.1E-07	1.2E-06	1 E-06	2 E-06
						45	3.3E-07	6.5E-07		
Pulaski Formation Unit C	B434	90.0	110.0	148.3	128.3	15	6.4E-05	1.3E-04		
						30	5.3E-05	1.0E-04		
						45	4.9E-05	9.7E-05	5 E-05	1 E-04
						30	4.8E-05	9.4E-05		
						15	4.9E-05	9.6E-05		

FSAR Section 2.5

Table 2.5-53— {Offshore Water Pressure Tests}

(Page 7 of 9)

Geologic Formation	Boring	Test Interval				Applied Pressure at Ground Surf.	Horizontal Permeability (k_h)		Representative Permeability (k_h) of Test Interval	
		Depth Below Ground Surface		Elevation Range						
		(ft)		(ft)		(psi)	(cm/sec)	(ft/min)	(cm/sec)	(ft/min)
Pulaski Formation Unit C	B437	100.5	121.5	132.7	111.7	15	3.4E-06	6.6E-06		
						30	8.5E-06	1.7E-05	1 E-05	2 E-05
						45	1.2E-05	2.4E-05		
Pulaski Formation Unit C/ Whetstone Gulf Formation Unit A	B406	109.0	130.0	128.3	107.3	15	5.7E-06	1.1E-05		
						31	1.3E-06	2.5E-06	1 E-06	2 E-06
						45	5.8E-07	1.1E-06		
Pulaski Formation Unit C/ Whetstone Gulf Formation Unit A	B407	100.0	120.0	136.6	116.6	15	4.3E-05	8.6E-05		
						30	5.9E-05	1.2E-04		
						45	4.7E-05	9.3E-05	4 E-05	8 E-05
						30	4.1E-05	8.2E-05		
						15	3.6E-05	7.1E-05		
Pulaski Formation Unit C/ Whetstone Gulf Formation Unit A	B409	110.0	131.6	122.8	101.2	16	6.5E-06	1.3E-05		
						30	4.2E-06	8.2E-06	4 E-06	8 E-06
						44	3.1E-06	6.0E-06		
Pulaski Formation Unit C/ Whetstone Gulf Formation Unit A	B413	79.0	100.0	138.3	117.3	15	2.6E-05	5.1E-05		
						30	2.6E-05	5.1E-05		
						45	2.8E-05	5.6E-05	3 E-05	6 E-05
						30	2.8E-05	5.5E-05		
						15	3.2E-05	6.2E-05		

Table 2.5-53— {Offshore Water Pressure Tests}

(Page 8 of 9)

Geologic Formation	Boring	Test Interval				Applied Pressure at Ground Surf.	Horizontal Permeability (k_h)		Representative Permeability (k_h) of Test Interval	
		Depth Below Ground Surface		Elevation Range						
		(ft)		(ft)		(psi)	(cm/sec)	(ft/min)	(cm/sec)	(ft/min)
Pulaski Formation Unit C/ Whetstone Gulf Formation Unit A	B417	65.0	86.0	139.3	118.3	15	4.9E-06	9.6E-06		
						30	5.7E-06	1.1E-05	6 E-06	1 E-05
						45	9.2E-06	1.8E-05		
Pulaski Formation Unit C/ Whetstone Gulf Formation Unit A	B433	111.0	131.0	126.3	106.3	15	8.0E-05	1.6E-04		
						30	7.0E-05	1.4E-04		
						45	7.1E-05	1.4E-04	7 E-05	1 E-04
						30	3.2E-05	6.3E-05		
Pulaski Formation Unit C/ Whetstone Gulf Formation Unit A	B441	80.0	101.0	138.7	117.7	15	1.5E-04	3.0E-04		
						30	1.2E-04	2.4E-04		
						45	1.0E-04	2.0E-04	1 E-04	2 E-04
						30	9.2E-05	1.8E-04		
						15	9.1E-05	1.8E-04		
Whetstone Gulf Formation Unit A	B413	109.0	130.0	108.3	87.3	15	2.1E-05	4.0E-05		
						30	1.6E-05	3.2E-05	2 E-05	3 E-05
						45	1.3E-05	2.6E-05		
Whetstone Gulf Formation Unit A	B441	110.0	131.0	108.7	87.7	15	1.3E-05	2.6E-05		
						30	1.2E-05	2.3E-05	1 E-05	2 E-05
						45	9.8E-06	1.9E-05		
Whetstone Gulf Formation Unit A/ Whetstone Gulf Formation Unit B	B409	135.0	156.6	97.8	76.2	15	4.5E-06	8.9E-06	3 E-06	6 E-06
						30	1.4E-06	2.7E-06		
						46	3.0E-06	5.8E-06		

Table 2.5-53— {Offshore Water Pressure Tests}

Geologic Formation	Boring	Test Interval				Applied Pressure at Ground Surf.	Horizontal Permeability (k_h)		Representative Permeability (k_h) of Test Interval	
		Depth Below Ground Surface		Elevation Range						
		(ft)		(ft)		(psi)	(cm/sec)	(ft/min)	(cm/sec)	(ft/min)
Whetstone Gulf Formation Unit A/ Whetstone Gulf Formation Unit B	B417	105.0	126.0	99.3	78.3	15	1.1E-05	2.2E-05	1 E-05	2 E-05
						30	1.0E-05	2.0E-05		
						45	2.7E-05	5.4E-05		
						30	3.9E-06	7.6E-06		
						15	2.3E-06	4.5E-06		
Whetstone Gulf Formation Unit B	B406	154.0	175.0	83.3	62.3	15	4.4E-06	8.6E-06	3 E-06	5 E-06
						31	2.5E-06	5.0E-06		
						45	7.7E-07	1.5E-06		
Whetstone Gulf Formation Unit B	B417	127.0	148.0	77.3	56.3	15	5.5E-05	1.1E-04	4 E-05	7 E-05
						31	3.8E-05	7.5E-05		
						45	3.3E-05	6.5E-05		
						31	2.9E-05	5.7E-05		
						15	3.2E-05	6.3E-05		

Notes:

Tests with measured flow less than 1 gallon per minute were stopped at maximum pressure.
Horizontal permeability was computed assuming a ratio of horizontal to vertical permeability (k_h / k_v) of nine.
Permeabilities reported with a "less than" symbol (<) indicate that the measured flow during the test was less than the smallest increment of flow we could measure.
Elevations are based on the National Geodetic Vertical Datum of 1929 (NGVD 29).
Representative permeability is based on engineering judgment.

Abbreviation:

MW Monitoring Well

Table 2.5-54— {Basis of Subsurface Investigation}

(Page 1 of 4)

Location	As-Built Coordinates		Depth (ft)	Purpose for Boring
	Northing	Easting		
B101 (MW)	1,282,173.9	543,489.0	255.0	Characterize the site geology and hydrology
B102 (MW)	1,281,119.1	542,988.4	245.6	Characterize the site geology and hydrology
B103 (MW)	1,281,133.2	542,986.1	63.6	Shallow bedrock well installed as a couplet to B102 (MW)
B104 (MW)	1,281,396.9	543,483.1	203.5	Characterize the site geology and hydrology
B105 (MW)	1,281,404.3	543,488.9	61.0	Shallow bedrock well installed as a couplet to B104 (MW)
B106 (MW)	1,282,272.9	544,173.3	195.0	Characterize the site geology and hydrology
B107 (MW)	1,282,275.5	544,161.8	69.0	Shallow bedrock well installed as a couplet to B106 (MW)
B108 (MW)	1,280,487.7	543,437.5	150.0	Characterize the site geology and hydrology
B109 (MW)	1,281,864.9	544,562.3	150.0	Characterize the site geology and hydrology
B110 (MW)	1,279,838.6	543,552.2	225.2	Characterize the site geology and hydrology
B111 (MW)	1,279,841.1	543,563.3	87.5	Shallow bedrock well installed as a couplet to B110 (MW)
B112 (MW)	1,280,382.8	544,368.5	203.5	Characterize the site geology and hydrology
B113 (MW)	1,280,379.7	544,381.4	111.0	Shallow bedrock well installed as a couplet to B112 (MW)
B114 (MW)	1,280,763.3	544,983.0	193.5	Characterize the site geology and hydrology
B115 (MW)	1,280,775.0	544,989.7	93.5	Shallow bedrock well installed as a couplet to B114 (MW)
B116 (MW)	1,279,550.8	544,655.3	155.5	Characterize the site geology and hydrology
B117 (MW)	1,280,280.0	545,532.7	184.5	Characterize the site geology and hydrology
B118 (MW)	1,279,283.8	545,652.1	205.5	Characterize the site geology and hydrology
B119 (MW)	1,279,282.6	545,639.9	70.2	Shallow bedrock well installed as a couplet to B118 (MW)
B120 (MW)	1,281,137.8	544,051.0	14.5	Groundwater observation well in soil, no samples
B121 (MW)	1,280,926.9	543,909.4	17.5	Groundwater observation well in soil, no samples
B122 (MW)	1,280,694.8	544,110.8	19.6	Groundwater observation well in soil, no samples
B123 (MW)	1,280,883.9	544,313.3	8.0	Groundwater observation well in soil, no samples
B124 (MW)	1,280,799.2	543,866.6	12.0	Groundwater observation well in soil, no samples
B201 (MW)	1,280,776.2	543,669.7	200.0	Bldg UKS (135x135 = 18,225 sq ft) (1 of 4 boreholes)
B202 (MW)	1,280,779.1	543,673.3	31.0	Shallow bedrock well installed as a couplet to B201 (MW)
B203	1,280,824.6	543,738.8	150.0	Bldg UKS (135x135 = 18,225 sq ft) (1 of 4 boreholes)
B204	1,280,695.3	543,724.7	150.0	Bldg UKS (135x135 = 18,225 sq ft) (1 of 4 boreholes)
B205	1,280,754.1	543,806.7	151.0	Bldg UKS (135x135 = 18,225 sq ft) (1 of 4 boreholes)
B206	1,280,860.5	543,825.2	150.0	Bldg UKA (120x145 = 17,400 sq ft) (1 of 2 boreholes)
B207	1,280,806.6	543,863.7	151.0	Bldg UKA (120x145 = 17,400 sq ft) (1 of 2 boreholes)
B208 (MW)	1,280,921.3	543,897.4	151.0	Bldg UKH (90x130 = 11,700 sq ft) (1 of 2 boreholes)
B209 (MW)	1,280,924.5	543,901.5	52.0	Shallow bedrock well installed as a couplet B208 (MW)

Table 2.5-54— {Basis of Subsurface Investigation}

(Page 2 of 4)

Location	As-Built Coordinates		Depth (ft)	Purpose for Boring
	Northing	Easting		
B210	1,280,878.4	543,932.8	150.0	Bldg UKH (90x130 = 11,700 sq ft) (1 of 2 boreholes)
B211	1,280,976.9	543,972.8	150.0	Bldg UFA (75x100 = 7,500 sq ft) (1 of 2 boreholes)
B212	1,280,938.8	544,013.9	150.0	Bldg UFA (75x100 = 7,500 sq ft) (1 of 2 boreholes)
B213	1,281,129.8	544,047.2	150.5	Bldg 2URB (165x110 = 18,150 sq ft) (1 of 2 boreholes)
B214	1,281,058.0	544,085.3	150.0	Bldg 2URB (165x110 = 18,150 sq ft) (1 of 2 boreholes)
B215	1,281,214.5	544,162.3	150.0	Bldg 1URB (165x110 = 18,150 sq ft) (1 of 2 boreholes)
B216 (MW)	1,281,146.8	544,210.4	205.0	Bldg 1URB (165x110 = 18,150 sq ft) (1 of 2 boreholes)
B217 (MW)	1,281,155.3	544,206.5	50.0	Shallow bedrock well installed as a couplet to B216 (MW)
B218	1,280,643.2	543,825.0	150.0	Bldg 3UBP/4UBP (180x90 = 16,200 sq ft) (1 of 2 boreholes)
B219 (MW)	1,280,570.9	543,875.9	154.2	Bldg 3UBP/4UBP (180x90 = 16,200 sq ft) (1 of 2 boreholes)
B220 (MW)	1,280,574.3	543,880.2	81.0	Shallow bedrock well installed as a couplet to B219 (MW)
B221 (MW)	1,280,735.3	543,922.7	216.0	Bldg 4UJH/4UJK (80x100 = 8,000 sq ft)
B222	1,280,655.1	543,963.9	151.0	Bldg UKE (80x90 = 7,200 sq ft)
B223	1,280,778.6	543,968.0	150.0	Bldg UJA reactor (πr^2 r=90, 25,400 sq ft) (1 of 4 boreholes)
B224	1,280,831.1	544,021.9	210.0	Bldg UJA reactor (πr^2 r=90, 25,400 sq ft) (1 of 4 boreholes)
B225	1,280,843.5	544,036.7	210.0	Boring for cross-hole testing
B226	1,280,869.8	544,068.6	210.0	Bldg UJA reactor (πr^2 r=90, 25,400 sq ft) (1 of 4 boreholes)
B227	1,280,769.4	544,067.8	150.3	Bldg UJA reactor (πr^2 r=90, 25,400 sq ft) (1 of 4 boreholes)
B228	1,280,728.2	543,999.7	150.0	Bldg 3UJH/3UJK (90x110 = 9,900 sq ft) (1 of 3 boreholes)
B229	1,280,653.5	544,055.4	150.0	Bldg 3UJH/3UJK (90x110 = 9,900 sq ft) (1 of 3 boreholes)
B230 (MW)	1,280,698.5	544,118.4	204.0	Bldg 3UJH/3UJK (90x110 = 9,900 sq ft) (1 of 3 boreholes)
B231	1,280,831.5	544,126.6	150.0	Bldg 2UJH/2UJK (90x110 = 9,900 sq ft) (1 of 2 boreholes)
B232	1,280,743.1	544,178.7	200.0	Bldg 2UJH/2UJK (90x110 = 9,900 sq ft) (1 of 2 boreholes)
B233 (MW)	1,280,918.8	544,142.4	150.2	Bldg 1UJH/1UJK (80x100 = 8,000 sq ft)
B234	1,280,964.0	544,262.5	150.0	Bldg 1UBP/2UBP (180x95 = 17,100 sq ft) (1 of 2 boreholes)
B235 (MW)	1,280,889.9	544,316.3	153.5	Bldg 1UBP/2UBP (180x95 = 17,100 sq ft) (1 of 2 boreholes)
B236 (MW)	1,280,883.8	544,319.0	36.0	Shallow bedrock well installed as a couplet to B235 (MW)
B237	1,280,357.7	543,838.5	150.0	Bldg 4URB (165x110 = 18,150 sq ft) (1 of 2 boreholes)
B238 (MW)	1,280,285.2	543,890.3	215.8	Bldg 4URB (165x110 = 18,150 sq ft) (1 of 2 boreholes)
B239	1,280,444.2	543,957.5	155.3	Bldg 3URB (165x110 = 18,150 sq ft) (1 of 2 boreholes)
B240	1,280,372.3	544,008.8	155.0	Bldg 3URB (165x110 = 18,150 sq ft) (1 of 2 boreholes)
B241	1,280,399.3	543,844.8	210.0	Boring for cross-hole testing
B242	1,280,416.0	543,833.6	210.0	Boring for cross-hole testing

Table 2.5-54— {Basis of Subsurface Investigation}

(Page 3 of 4)

Location	As-Built Coordinates		Depth (ft)	Purpose for Boring
	Northing	Easting		
B243	1,280,448.1	543,810.1	210.0	Boring for cross-hole testing
B301	1,282,261.0	543,340.8	120.0	Bldg: Water Pumphouse - Forebay (20x125 = 2,500 sq ft.)
B302	1,282,204.9	543,374.5	120.0	Bldg: Essential Service Water Make-Up Pumphouse (75x125 = 9,375.0 sq ft.)
B303	Not drilled - ESW Pumphouse location moved.			
B304	1,282,115.9	543,438.4	75.0	Water Intake Pipeline to Bldg 2URB/1URB (1 boring per 100 linear ft)
B305	1,282,032.5	543,496.0	75.0	Water Intake Pipeline to Bldg 2URB/1URB (1 boring per 100 linear ft)
B306	1,281,951.5	543,551.8	75.0	Water Intake Pipeline to Bldg 2URB/1URB (1 boring per 100 linear ft)
B307	1,281,868.2	543,609.7	75.0	Water Intake Pipeline to Bldg 2URB/1URB (1 boring per 100 linear ft)
B308	1,281,785.2	543,665.4	75.0	Water Intake Pipeline to Bldg 2URB/1URB (1 boring per 100 linear ft)
B309	Not drilled - in wetland, not permitted.			
B310	Not drilled - in wetland, not permitted.			
B311	1,281,531.2	543,835.6	75.0	Water Intake Pipeline to Bldg 2URB/1URB (1 boring per 100 linear ft)
B312	1,281,454.1	543,892.3	75.0	Water Intake Pipeline to Bldg 2URB/1URB (1 boring per 100 linear ft)
B313	1,281,372.8	543,946.0	75.0	Water Intake Pipeline to Bldg 2URB/1URB (1 boring per 100 linear ft)
B314	1,281,291.5	543,995.6	75.0	Water Intake Pipeline to Bldg 2URB/1URB (1 boring per 100 linear ft)
B315	1,281,197.5	544,059.5	75.0	Water Intake Pipeline to Bldg 2URB/1URB (1 boring per 100 linear ft)
B401	1,282,352.3	543,373.9	249.0	Characterize Intake A Pumphouse geology and hydrology
B402a	1,282,385.1	543,414.1	214.3	Characterize Tunnel A geology and hydrology
B403	Not drilled - Inaccessible to barge.			
B404	1,282,643.9	543,302.3	202.5	Characterize Tunnel A geology and hydrology
B405	1,282,777.8	543,199.3	198.5	Characterize Tunnel A geology and hydrology
B406	1,282,832.4	543,228.4	187.5	Characterize Tunnel A geology and hydrology
B407	1,282,907.5	543,142.6	196.0	Characterize Tunnel A geology and hydrology
B408	1,283,016.0	543,151.0	197.8	Characterize Tunnel A geology and hydrology
B409	1,283,086.4	543,070.2	184.0	Characterize Tunnel A geology and hydrology
B410	1,283,206.9	543,072.0	182.0	Characterize Tunnel A geology and hydrology
B411	1,283,277.4	542,989.4	178.0	Characterize Tunnel A geology and hydrology
B412	1,283,391.2	543,005.4	178.7	Characterize Tunnel A geology and hydrology
B413	1,283,462.7	542,911.4	160.0	Characterize Intake A Offshore geology and hydrology
B414	1,283,574.6	542,924.3	162.0	Characterize Tunnel A geology and hydrology
B415	1,283,648.5	542,844.7	159.0	Characterize Tunnel A geology and hydrology
B416	1,283,761.3	542,848.9	155.0	Characterize Tunnel A geology and hydrology

Table 2.5-54— {Basis of Subsurface Investigation}

(Page 4 of 4)

Location	As-Built Coordinates		Depth (ft)	Purpose for Boring
	Northing	Easting		
B417	1,283,832.6	542,768.2	150.0	Characterize Discharge A Offshore geology and hydrology
B428	1,282,227.8	543,307.2	239.3	Characterize Intake B Pumphouse geology and hydrology
B429a	1,282,219.5	543,253.1	207.7	Characterize Tunnel B geology and hydrology
B430	Not drilled - Inaccessible to barge.			
B431	1,282,454.4	543,106.6	200.0	Characterize Tunnel B geology and hydrology
B432	1,282,565.6	543,096.8	200.0	Characterize Tunnel B geology and hydrology
B433	1,282,624.5	542,997.8	188.5	Characterize Tunnel B geology and hydrology
B434	1,282,742.0	542,988.3	196.1	Characterize Tunnel B geology and hydrology
B435	1,282,797.2	542,892.0	189.9	Characterize Tunnel B geology and hydrology
B436	1,282,908.1	542,881.9	184.0	Characterize Tunnel B geology and hydrology
B437	1,282,964.3	542,790.8	175.9	Characterize Tunnel B geology and hydrology
B438	1,283,074.0	542,775.5	178.3	Characterize Tunnel B geology and hydrology
B439	1,283,141.1	542,680.9	175.0	Characterize Tunnel B geology and hydrology
B440	1,283,244.9	542,676.2	170.0	Characterize Tunnel B geology and hydrology
B441	1,283,307.4	542,583.3	158.0	Characterize Intake B Offshore geology and hydrology
TP101	1,282,274.0	543,334.3	5.5	Characterize Bulk Soil Samples
TP102	1,280,872.3	544,050.8	8.0	Characterize Bulk Soil Samples
TP103	1,280,418.6	544,378.9	7.5	Characterize Bulk Soil Samples

Notes:

See the legend on Figure 2.5-60 for an explanation of the building acronyms.
Horizontal control is based on the Central Zone of the New York State Plane Coordinate System North American Datum of 1927 (NAD 27).

Abbreviation:

MW Monitoring Well

Table 2.5-55—{Monitoring Well Details}

(Page 1 of 2)

Monitoring Well Number	Well Depth (ft)	Screened Interval[1]				
		Depth Range (ft)		Elevation Range (ft)		Geologic Formation
B101 (MW)	134.5	117.9	134.5	147.4	130.8	Pulaski B & C
B102 (MW)	125.0	104.0	125.0	151.6	130.6	Pulaski A & B
B103 (MW)	63.6	45.5	63.6	210.5	192.4	Oswego Sandstone, Oswego Transition & Pulaski A
B104 (MW)	200.1	176.5	200.1	79.4	55.9	Whetstone Gulf
B105 (MW)	60.0	41.0	60.0	214.9	195.9	Oswego Sandstone & Oswego Transition
B106 (MW)	195.0	170.0	195.0	86.0	61.0	Whetstone Gulf
B107 (MW)	69.0	53.8	69.0	202.4	187.2	Oswego Sandstone & Oswego Transition
B108 (MW)	150.0	136.6	150.0	123.2	109.8	Pulaski B
B109 (MW)	132.0	113.0	132.0	149.5	130.5	Pulaski B
B110 (MW)	225.2	201.8	225.2	65.3	41.9	Whetstone Gulf
B111 (MW)	87.5	71.0	87.5	195.9	179.4	Oswego Transition & Pulaski A
B112 (MW)	191.8	167.7	191.8	115.2	91.1	Pulaski C & Whetstone Gulf
B113 (MW)	91.5	78.2	91.5	204.8	191.5	Oswego Transition
B114 (MW)	146.0	130.4	146.0	143.6	128.0	Pulaski A, B & C
B115 (MW)	93.5	80.0	93.5	194.3	180.8	Oswego Transition & Pulaski A
B116 (MW)	142.0	118.0	142.0	176.8	152.8	Pulaski B
B117 (MW)	167.0	140.0	167.0	139.0	112.0	Pulaski B
B118 (MW)	203.0	177.5	203.0	116.0	90.5	Whetstone Gulf
B119 (MW)	70.2	47.5	70.2	246.0	223.3	Oswego Sandstone & Oswego Transition
B120 (MW)	14.5	4.5	14.5	262.5	252.5	Soil
B121 (MW)	17.5	4.5	17.5	262.1	249.1	Soil
B122 (MW)	19.6	4.5	19.6	278.0	262.9	Soil
B123 (MW)	8.0	4.2	8.0	268.0	264.2	Soil
B124 (MW)	12.0	5.0	12.0	258.3	251.3	Soil
B201 (MW)	138.0	112.0	138.0	143.9	117.9	Pulaski B
B202 (MW)	31.0	17.0	31.0	239.2	225.2	Oswego Sandstone
B208 (MW)	151.0	135.5	151.0	129.8	114.3	Pulaski B & C
B209 (MW)	52.0	22.5	52.0	243.5	214.0	Oswego Sandstone & Oswego Transition
B216 (MW)	205.0	182.0	205.0	83.8	60.8	Whetstone Gulf
B217 (MW)	50.0	26.0	50.0	239.1	215.1	Oswego Sandstone
B219 (MW)	146.4	127.5	146.4	146.9	128.0	Pulaski B
B220 (MW)	81.0	65.5	81.0	209.5	194.0	Oswego Transition

FSAR Section 2.5

Table 2.5-55—{Monitoring Well Details}

Monitoring Well Number	Well Depth (ft)	Screened Interval[1]				
		Depth Range (ft)		Elevation Range (ft)		Geologic Formation
B221 (MW)	211.0	197.0	211.0	83.2	69.2	Pulaski C & Whetstone Gulf
B230 (MW)	204.0	183.0	204.0	99.6	78.6	Pulaski C & Whetstone Gulf
B233 (MW)	150.0	135.0	150.0	140.5	125.5	Pulaski C
B235 (MW)	146.9	131.9	146.9	140.1	125.0	Pulaski B & C
B236 (MW)	36.0	23.0	36.0	249.1	236.1	Oswego Sandstone
B238 (MW)	211.0	187.5	211.0	91.7	68.2	Pulaski C & Whetstone Gulf

Notes:

1 The screened interval corresponds to the upper and lower limits of the sanded zone. Monitoring Wells are 2 inches in diameter and have a screen slot size of 0.010 inches. Elevations are based on the National Geodetic Vertical Datum of 1929 (NGVD 29).

Abbreviation:

MW Monitoring Well

Table 2.5-56—{Groundwater Elevation Data}

(Page 1 of 2)

Monitoring Well Number	Elevation of Measuring Point	October 2007		November 2007		December 2007		January 2008		February 2008		March 2008		April 2008		May 2008		June 2008		July 2008		August 2008	
		Depth	Elevation	Depth	Elevation	Depth	Elevation	Depth	Elevation	Depth	Elevation	Depth	Elevation	Depth	Elevation	Depth	Elevation	Depth	Elevation	Depth	Elevation	Depth	Elevation
	(ft)	(ft)	(ft)	(ft)	(ft)	(ft)	(ft)	(ft)	(ft)	(ft)	(ft)	(ft)	(ft)	(ft)	(ft)	(ft)	(ft)	(ft)	(ft)	(ft)	(ft)	(ft)	(ft)
B101 (MW)	267.5	24.0	243.5	25.9	241.6	22.6	244.9	26.4	241.1	24.8	242.7	24.6	242.9	24.3	243.2	23.3	244.2	23.3	244.2	23.6	244.0	23.6	243.9
B102 (MW)	258.0	17.2	240.8	15.5	242.5	16.5	241.4	16.0	242.0	10.0	247.9	10.3	247.7	11.9	246.1	10.1	247.9	9.7	248.3	13.3	244.7	12.4	245.6
B103 (MW)	258.1	51.7	206.4	42.7	215.4	33.3	224.8	7.2	250.8	4.4	253.7	4.9	253.2	4.6	253.4	4.6	253.4	6.0	252.1	7.1	251.0	6.4	251.6
B104 (MW)	258.1	23.5	234.6	51.8	206.3	37.9	220.2	28.8	229.3	25.8	232.3	24.6	233.6	23.7	234.4	23.1	235.0	22.5	235.6	22.3	235.8	22.2	235.9
B105 (MW)	258.3	55.7	202.6	54.0	204.3	52.3	206.1	49.5	208.9	46.7	211.6	44.0	214.3	40.0	218.3	37.4	220.9	34.7	223.6	32.4	226.0	30.0	228.3
B106 (MW)	258.2	78.8	179.4	128.0	130.2	116.5	141.7	89.2	169.1	61.3	197.0	50.8	207.4	86.1	172.1	76.8	181.4	64.6	193.6	131.0	127.2	94.7	163.5
B107 (MW)	258.4	59.5	198.9	53.0	205.4	46.5	211.9	60.9	197.5	49.2	209.2	40.8	217.6	62.9	195.5	53.2	205.2	43.7	214.7	63.2	195.2	52.1	206.3
B108 (MW)	262.4	26.4	236.0	18.4	244.0	17.3	245.0	17.9	244.5	16.6	245.8	16.6	245.8	16.3	246.1	15.5	246.9	15.3	247.0	15.4	247.0	15.5	246.9
B109 (MW)	265.0	23.5	241.5	23.0	242.0	25.4	239.6	25.0	240.0	23.5	241.5	23.2	241.8	23.1	241.9	22.4	242.6	22.1	242.9	22.3	242.7	22.2	242.8
B110 (MW)	270.0	179.3	90.7	161.8	108.2	145.3	124.7	187.6	82.5	163.5	106.5	146.3	123.8	168.6	101.5	151.2	118.8	134.5	135.6	146.1	123.9	131.5	138.5
B111 (MW)	269.8	8.2	261.6	7.4	262.4	6.9	262.9	6.3	263.5	5.5	264.3	5.9	263.9	5.9	263.9	6.1	263.7	6.7	263.1	8.5	261.3	6.4	263.4
B112 (MW)	285.1	42.9	242.2	76.8	208.3	48.8	236.3	45.4	239.7	44.1	241.0	43.9	241.2	43.8	241.4	43.1	242.0	42.7	242.4	42.6	242.5	42.3	242.8
B113 (MW)	284.4	87.0	197.4	88.3	196.1	85.2	199.3	70.4	214.0	51.4	233.0	37.1	247.4	19.0	265.5	13.1	271.3	10.6	273.8	11.1	273.4	11.2	273.2
B114 (MW)	275.8	14.0	261.8	11.1	264.7	9.9	265.9	9.8	266.0	9.8	266.0	9.9	265.9	9.7	266.1	9.9	265.9	10.3	265.5	10.8	265.0	9.8	266.0
B115 (MW)	276.8	88.0	188.8	93.2	183.6	92.8	184.0	92.0	184.7	91.3	185.5	90.8	186.0	90.1	186.7	88.7	188.1	89.2	187.6	88.7	188.0	88.3	188.5
B116 (MW)	297.0	30.8	266.2	30.0	267.0	29.5	267.5	28.1	268.9	26.4	270.6	25.5	271.5	25.2	271.8	25.6	271.4	26.1	270.9	26.9	270.1	26.6	270.4
B117 (MW)	281.3	25.5	255.8	24.9	256.4	25.1	256.2	24.9	256.4	23.7	257.6	23.6	257.7	23.8	257.6	23.7	257.6	24.0	257.4	32.0	249.4	23.1	258.2
B118 (MW)	296.0	19.3	276.7	16.6	279.4	12.6	283.4	11.2	284.8	11.2	284.8	11.2	284.7	11.1	284.9	11.5	284.4	12.7	283.3	13.4	282.5	11.7	284.3
B119 (MW)	296.0	20.8	275.2	19.6	276.4	18.1	277.9	15.2	280.8	14.7	281.2	14.9	281.0	15.7	280.2	16.4	279.6	18.0	278.0	18.7	277.3	17.8	278.2
B120 (MW)	269.3	NA	NA	Dry	Dry	Dry	Dry	4.4	264.9	4.2	265.2	4.7	264.6	4.9	264.4	4.7	264.6	6.1	263.2	5.3	264.1	6.0	263.3
B121 (MW)	269.4	NA	NA	17.6	251.8	15.5	253.9	5.8	263.5	4.7	264.7	5.4	263.9	4.5	264.9	4.9	264.5	6.7	262.7	5.2	264.2	6.0	263.3
B122 (MW)	284.9	NA	NA	3.6	281.3	3.5	281.5	3.2	281.7	2.6	282.3	2.7	282.2	3.3	281.6	3.1	281.8	7.2	277.8	5.8	279.2	5.0	279.9
B123 (MW)	274.6	NA	NA	Dry	Dry	9.9	264.7	4.4	270.2	3.2	271.4	4.7	269.9	4.5	270.1	4.6	270.1	7.3	267.3	6.8	267.8	6.6	268.0
B124 (MW)	265.6	NA	NA	9.9	255.7	3.4	262.2	3.4	262.2	2.5	263.1	3.2	262.4	3.5	262.1	2.9	262.7	4.4	261.2	3.2	262.4	4.1	261.5
B201 (MW)	258.9	15.8	243.1	17.7	241.2	18.1	240.8	16.4	242.4	14.1	244.7	13.7	245.2	13.7	245.2	12.9	246.0	12.6	246.3	13.8	245.1	12.7	246.2
B202 (MW)	258.8	8.5	250.3	7.6	251.2	4.9	253.9	4.4	254.4	3.6	255.2	3.8	255.1	3.8	255.0	4.0	254.9	4.4	254.4	4.4	254.4	4.4	254.5

Table 2.5-56—{Groundwater Elevation Data}

(Page 2 of 2)

Monitoring Well Number	Elevation of Measuring Point	October 2007		November 2007		December 2007		January 2008		February 2008		March 2008		April 2008		May 2008		June 2008		July 2008		August 2008	
		Depth	Elevation	Depth	Elevation	Depth	Elevation	Depth	Elevation	Depth	Elevation	Depth	Elevation	Depth	Elevation	Depth	Elevation	Depth	Elevation	Depth	Elevation	Depth	Elevation
	(ft)	(ft)	(ft)	(ft)	(ft)	(ft)	(ft)	(ft)	(ft)	(ft)	(ft)	(ft)	(ft)	(ft)	(ft)	(ft)	(ft)	(ft)	(ft)	(ft)	(ft)	(ft)	(ft)
B208 (MW)	267.4	29.0	238.4	28.2	239.2	28.4	239.0	28.6	238.8	27.0	240.4	26.6	240.8	27.7	239.7	27.0	240.4	26.6	240.8	27.1	240.3	27.0	240.4
B209 (MW)	268.2	41.1	227.1	29.0	239.2	19.3	248.9	7.6	260.6	7.1	261.1	7.4	260.8	7.3	260.9	20.2	248.0	8.2	260.0	8.1	260.1	7.3	260.9
B216 (MW)	268.3	171.1	97.2	158.9	109.4	148.8	119.5	187.1	81.2	169.0	99.4	155.7	112.7	191.9	76.5	174.4	93.9	155.4	112.9	154.7	113.6	136.0	132.4
B217 (MW)	267.7	11.4	256.3	10.3	257.4	8.9	258.9	8.8	258.9	8.3	259.4	8.7	259.0	8.7	259.0	8.7	259.0	9.5	258.2	9.4	258.4	9.1	258.6
B219 (MW)	276.6	26.1	250.5	22.7	253.9	22.0	254.5	22.1	254.5	23.8	252.7	23.5	253.0	18.7	257.9	17.3	259.2	18.1	258.5	37.7	238.8	16.8	259.8
B220 (MW)	277.1	71.1	206.0	18.7	258.4	17.6	259.5	16.2	260.9	15.5	261.6	15.2	261.9	15.3	261.8	15.3	261.8	15.4	261.7	16.1	261.0	15.8	261.3
B221 (MW)	282.4	48.7	233.7	19.3	263.1	14.5	267.9	12.6	269.8	10.8	271.7	10.4	272.0	8.9	273.5	10.9	271.5	14.2	268.2	13.3	269.1	11.7	270.7
B230 (MW)	284.8	43.3	241.5	42.2	242.6	41.6	243.2	49.0	235.8	45.1	239.7	44.0	240.8	50.2	234.6	47.3	237.5	46.3	238.5	69.0	215.8	48.6	236.2
B233 (MW)	277.7	51.4	226.3	64.7	213.0	35.4	242.3	34.2	243.5	32.9	244.8	32.6	245.1	32.7	245.0	32.1	245.6	31.9	245.8	32.0	245.7	32.0	245.7
B235 (MW)	274.4	35.4	239.0	34.7	239.7	35.9	238.5	36.1	238.4	34.9	239.5	34.7	239.7	34.8	239.6	34.4	240.0	34.1	240.4	34.1	240.3	34.0	240.4
B236 (MW)	274.3	12.4	261.9	11.3	263.0	9.3	265.1	8.9	265.4	8.4	265.9	8.8	265.5	8.6	265.7	8.6	265.7	9.2	265.2	9.0	265.3	8.9	265.4
B238 (MW)	281.3	97.2	184.1	68.0	213.3	33.5	247.8	5.2	276.2	3.3	278.0	4.8	276.6	4.5	276.8	3.7	277.6	6.1	275.2	5.0	276.4	5.1	276.3

Notes:

Elevations are based on the National Geodetic Vertical Datum of 1929 (NGVD 29).
Measuring Point is from the top of the PVC well riser. Measuring Point is typically 2 feet above ground surface.
Depth refers to depth below the top of the PVC well riser.
Dry indicates there was no measurable water in the monitoring well at the time of the measurement.

Abbreviations:

NA Not applicable. The monitoring well was not installed at the time of the measurement.
MW Monitoring Well

Table 2.5-57—{Chemical Testing Results for Soil Concrete Parameters}

	Sample Location:		TP101-S1	TP102-S1	TP103-S1	SR-S1	SR-S2	SR-S3	SR-S3
	Sample Name:		TP101-S1-2	TP102-S1-2	TP103-S1-2	SR-S1-2	SR-S2-2	SR-S3-2	SR-S4-2
	Sample Date:		11/13/2007	11/14/2007	11/14/2007	2/7/2008	2/7/2008	2/7/2008	2/7/2008
Analyte	**Method**	**Unit**							
Chloride	Ion Chromatography	mg/kg	< 1	< 1	1	< 1	2	6 G	< 1 G
Sulfate	Ion Chromatography	mg/kg	2	2	4	1	< 1	2 G	< 1 G
pH	pH Specific Electrode	s.u.	8.6	8.8	8.2	8.8	8.7	8.7 G	8.8 G

Notes:

1. s.u. = standard units.
2. mg/kg = milligrams per kilogram.
3. "<" = Analyte not detected at a concentration above the specified laboratory reporting limit.
4. Chloride, sulfate, and pH analyzed by NSL Analytical, Cleveland, Ohio.
5. Samples names preceded by 'TP' were collected from test pits at Nine Mile Point. Samples preceded by 'SR' were collected from the Streeter-Rathburn Borrow Pit in Oswego, New York.

Qualifying Notes:

G The result is estimated due to duplicate precision outside control limits.

Table 2.5-58—{Chemical Testing Results for Groundwater Concrete Parameters}

Sample Location			B107(MW)	B111(MW)	B120(MW)	B121(MW)	B122(MW)	B123(MW)	B124(MW)	B202(MW)	B217(MW)	B236(MW)
Sample Name:			B107(MW)	B111(MW)	B120(MW)	B121(MW)	B122(MW)	B123(MW)	B124(MW)	B202(MW)	B217(MW)	B236(MW)
Sample Date			3/6/2008	3/5/2008	3/7/2008	3/7/2008	3/7/2008	3/7/2008	3/7/2008	3/5/2008	3/5/2008	3/6/2008
Screen Depth			57.7-67.7	74-84	6-14	6-17	6-19	5.7-7.7	6.5-11.5	19.8-29.8	28-48	24.7-34.7
Analyte	**Method**	**Unit**										
Chloride	Ion Chromatography	mg/L	6,200	9,900	5.7	10	7.2	210	12	130	77	55
Sulfate	Ion Specific Electrode	mg/L	12	1.8	120	190	240	43	120	3.1	6.4	33
Sulfide	Ion Chromatography	mg/L	< 1	< 1	< 1	< 1	< 1	< 1	< 1	< 1	< 1	< 1
pH	pH Specific Electrode	s.u.	12.22	7.23	7.00	6.81	7.33	7.10	7.53	9.26	6.98	6.66

Table 2.5-59—{Guidelines for Soil and Groundwater Chemistry Evaluation}

Sulfate Exposure	Water soluble sulfate in soil, % by weight	Sulfate in water, ppm	Cement Type	Maximum Water-Cementitious material ratio	Resistivity Ω-cm	pH	Chlorides[1]
Negligible/Low	0.00 - 0.10	0 - 150	—	—	5,000 - 10,000	4.5 < pH < 9.5	
Moderate	0.10 - 0.20	150 - 1500	II, IP(MS), IS(MS), P(MS), II(PM)(MS), I(SM)(MS)	0.50	2,000 - 5,000	—	
Severe	0.20 - 2.00	1500 - 10,000	V	0.45	700 - 2,000	<4 or >10	
Very Severe	> 2.00	> 10,000	V plus pozzolan	0.45	< 700	—	

Notes:

1 Guidelines for corrosion due to chloride exposure not provided at this time.
1 mg/kg = 0.0001% by weight.
1 ppm = 1 mg/L

(ACI, 2005)

Table 2.5-60—{Summary of Unconfined, Free-Free, resonant Column (URC) Tests of Rock}

(Page 1 of 2)

	UT Sample ID	Geologic Formation	Sample No.	Depth	Length	Dia.	Weight	Total Unit Weight	V_C	E_{max}	D_C	V_S	G_{max}	D_S	V_P	M_{max}	Poisson's Ratio ν		
				(ft)	(in.)	(in.)	(gram)	(lbf/ft^3)	(ft/sec)	(lbf/ft^2)	(%)	(ft/sec)	(lbf/ft^2)	(%)	(ft/sec)	(lbf/ft^2)	(MG)[1]	(EG)[2]	(ME)[3]
1st 1st	UTA-61-1	Oswego Sandstone	C3	33.3-33.82	4.82	1.99	613.8	156.1	10,620[4]	5.47E+08[4]	0.92	5,900	1.69E+08	0.72	9,920	4.77E+08	0.23	0.62[5]	Undefined[6]
	UTA-61-2	Oswego Sandstone	C6	58.75-59.3	4.66	2.00	612.9	160.0	10,100[4]	5.07E+08[4]	0.82	5,710	1.62E+08	0.71	9,890	4.86E+08	0.25	0.56[5]	Undefined[6]
	UTA-61-3	Oswego Transition Zone	C9	84.1-84.58	4.44	1.99	602.6	165.8	9,650	4.8E+08	3.54	6,520	2.19E+08	4.94	10,090	5.24E+08	0.14	0.10	0.19
	UTA-61-4	Pulaski Formation Unit A	C12	113.86-114.95	4.66	2.00	644.4	168.5	15,300[4]	1.23E+09[4]	0.73	8,710	3.97E+08	0.77	14,710	1.13E+09	0.23	0.54[5]	Undefined[6]
	UTA-61-5	Pulaski Formation Unit B	C15	139.9-141.2	4.69	2.00	622.2	161.7	13,510[4]	9.16E+08[4]	0.82	7,970	3.19E+08	0.51	13,160	8.70E+08	0.21	0.43	Undefined[6]
	UTA-61-6	Pulaski Formation Unit C	C18	167.7-168.16	4.65	2.00	616.7	161.4	11,710[4]	6.87E+08	0.92	6,720	2.27E+08	1.38	11,760	6.93E+08	0.26	0.52[5]	0.06
	UTA-61-7	Pulaski Formation Unit C	C18	169.96-170.70	4.64	1.99	620.9	163.3	12,030[4]	7.34E+08	0.91	6,780	2.33E+08	1.50	12,060	7.38E+08	0.27	0.58[5]	0.05
	UTA-61-8	Whetstone Gulf Formation Unit A	C21	198.5-198.89	3.25	1.99	445.6	168.0	9,970	5.18E+08	2.83	6,260	2.05E+08	2.94	10,110	5.33E+08	0.19	0.27	0.11
	UTA-61-9	Whetstone Gulf Formation Unit A	C21	199.42-199.75	1.98	1.99	273.1	168.9	12,560[4]	8.27E+08[4]	1.38	6,690	2.35E+08	2.23	12,210	7.82E+08	0.29	0.76[5]	Undefined[6]

FSAR Section 2.5

Table 2.5-60—{Summary of Unconfined, Free-Free, resonant Column (URC) Tests of Rock}

(Page 2 of 2)

	UT Sample ID	Geologic Formation	Sample No.	Depth	Length	Dia.	Weight	Total Unit Weight	V_C	E_{max}	D_C	V_S	G_{max}	D_S	V_P	M_{max}	Poisson's Ratio ν		
				(ft)	(in.)	(in.)	(gram)	(lbf/ft^3)	(ft/sec)	(lbf/ft^2)	(%)	(ft/sec)	(lbf/ft^2)	(%)	(ft/sec)	(lbf/ft^2)	(MG)[1]	(EG)[2]	(ME)[3]
2nd Set	UTA-61-10	Oswego Transition Zone	C6	69.5-70.08	4.43	1.87	513.7	160.4	9,470	4.47E+08	2.61	5,520	1.52E+08	1.24	11,230	6.28E+08	0.34	0.47	0.31
	UTA-61-11	Pulaski Formation Unit C	C19	196.04-196.51	2.86	1.87	341.3	164.5	11,310	6.53E+08	1.93	7,770	3.08E+08	1.40	11,480	6.74E+08	0.08	0.06	0.11
	UTA-61-12	Whetstone Gulf Formation Unit A	C19	203.41-203.99	2.37	1.87	282.3	165.4	10,070[4]	5.21E+08	1.38	5,970	1.83E+08	4.98	10,540	5.71E+08	0.26	0.42	0.19
	UTA-61-13	Whetstone Gulf Formation Unit A	C20	206.08-206.65	4.36	1.87	528.9	168.1	9,590	4.8E+08	1.63	5,870	1.80E+08	1.62	10,920	6.23E+08	0.30	0.34	0.29
	UTA-61-14	Whetstone Gulf Formation Unit A	C20	209.14-209.72	4.55	1.87	540.3	164.6	15,050[4]	1.16E+09[4]	1.96	8,600	3.78E+08	1.75	14,310	1.05E+09	0.22	0.53[5]	Undefined[6]

(1)

$$\nu_{MG} = \frac{M_{max} - 2G_{max}}{2(M_{max} - G_{max})} = \frac{V_p^{\,2} - 2V_s^{\,2}}{2(V_p^{\,2} - V_s^{\,2})}$$

(2)

$$\nu_{EG} = \frac{E_{max} - 2G_{max}}{2G_{max}} = \frac{V_c^{\,2} - 2V_s^{\,2}}{2V_s^{\,2}}$$

(3)

$$\nu_{ME} = \frac{1}{4M_{max}}(-M_{max} + E_{max} + \sqrt{(9M_{max} - E_{max})(M_{max} - E_{max})}) = \frac{1}{4V_p^{\,2}}(-V_p^{\,2} + V_c^{\,2} + \sqrt{(9V_p^{\,2} - V_c^{\,2})(V_p^{\,2} - V_c^{\,2})})$$

Table 2.5-61—{Petrography Results}

(Page 1 of 2)

Formation	Boring	Sample Interval				Boring Log Description	Petrographic Description	Texture	Mineralogy
		Depth Below Ground (feet)		Elevation Range (feet)					
Oswego Sandstone/ Oswego Transition Zone	B301	23.2	23.7	238.9	238.4	Sandstone to sandstone with interbedded siltstone and shale	Altered Sandstone	No alteration and none to a weakly directed fabric, typically quartz, potassium feldspar and plagioclase grains in a clay matrix held together by dolomite/ferroan dolomite cement.	Quartz – 31 to 62% Dolomite – up to 42% Clay – 5% to 25% Potassium Feldspar – 12 to 15% Minor amounts (<10%) –plagioclase, ferroan dolomite, opaques and zircon.
	B224	26.0	26.1	248.2	248.1				
	B224	60.6	60.9	213.6	213.3				
	B301	66.0	66.4	196.1	195.7				
	B224	84.6	84.8	189.6	189.4				
Pulaski A	B201(MW)	97.1	97.5	158.8	158.5	Argillaceous sandstone interbedded with siltstone and sandstone	Altered Siltstone and Sandstone	Thinly bedded sedimentary rock with quartz, potassium feldspar and plagioclase grains held together in a clay matrix by ferroan dolomite cement.	Quartz – 42% Clay(illite?) – 20% Potassium feldspar – 15% Ferroan dolomite – 15% Plagioclase, opaques, and zircon – 5% or less of each
	B224	115.6	116.0	158.6	158.2	Argillaceous sandstone with mottling	Altered Mudstone	Weakly directed fabric with no alteration features, and was an equal amount of ferroan dolomite cement.	Clay – 50% Quartz – 27% Potassium feldspar – 18% Plagioclase, ferroan dolomite, and opaques – 5% or less of each
Green Marker Bed	B207	110.9	110.9	151.2	151.2	Sandstone with layers of siltstone and shale	Altered Claystone	Altered sedimentary rock with moderately directed fabric, and mostly clay matrix/cement with grains of various forms of potassium feldspar and quartz.	Clay – 83 to 89% Potassium feldspar, quartz, biotite, chlorite, rutile, zircon, and opaques <10% of some or all
	B238 (MW)	132.2	132.2	147.0	147.0	Argillaceous sandstone and siltstone			
Pulaski B	B224	138.5	138.8	135.7	135.5	Siltstone interbedded with sandstone and argillaceous sandstone	Altered Sandy Mudstone	Altered (deformed) and weakly directed equal amounts of quartz/potassium feldspar/plagioclase grains and clay matrix, with a very minor amount of ferroan dolomite cement.	Clay – 50% Quartz – 35% Potassium feldspar – 12% Plagioclase, ferroan dolomite, and opaques – 3% or less of each

Table 2.5-61—{Petrography Results}

(Page 2 of 2)

Formation	Boring	Sample Interval				Boring Log Description	Petrographic Description	Texture	Mineralogy
		Depth Below Ground (feet)		Elevation Range (feet)					
Pulaski C	B224	167.1	167.4	107.1	106.9	Siltstone interbedded with sandstone and argillaceous sandstone	Altered Clayey Sandstone	Altered (deformed) with a weakly directed fabric and quartz, potassium feldspar, and plagioclase grains in a clay matrix held together by ferroan dolomite cement.	Clay – 45% Quartz – 35% Potassium feldspar – 13% Ferroan dolomite, plagioclase, zircon, and opaques <10%
	B238 (MW)	174.0	174.1	105.3	105.1	Siltstone with interbedded sandstone	Claystone	Unaltered but had a moderately directed fabric and was almost all clay matrix/cement with a minor amount of quartz and potassium feldspar grains.	Clay – 93% Unidentifiable opaques, quartz, and potassium feldspar – 3% or less
Whetstone A	B201 (MW)	188.2	188.8	67.7	67.2	Alternating sandstone and siltstone	Altered Siltstone	Slightly altered and deformed with weakly directed clay minerals with quartz, potassium feldspar, and plagioclase grains held together in a clay matrix by ferroan dolomite cement.	Clay (illite?) – 40% Quartz – 30% Potassium feldspar – 15% Ferroan dolomite, plagioclase, and opaques – 10% or less
Whetstone A	B224	200.8	200.9	73.4	73.3	Siltstone with occasional layers of argillaceous sandstone	Silty Claystone	Unaltered but moderately directed fabric with mostly a clay matrix/cement and minor amounts of quartz and potassium feldspar.	Clay – 85% Quartz, potassium feldspar, opaques, and carbonaceous matter <5% each

Notes:

Elevations are based on the National Geodetic Vertical Datum of 1929 (NGVD 29).

Abbreviation:

MW Monitoring Well

Table 2.5-62—{Onshore Natural Gas Observations}

Boring Number	Observations During Drilling			Observations During Groundwater Sampling
	Depth (feet)	Formation	Observation	
B102 (MW)	NA	NA	NA	Measured gas levels at top of well after initial opening reached 40% LEL, dissipated within 1 minute.
B106 (MW)	130.0	Pulaski C	Drill water bubbling at the top of the casing, measured gas levels over 10% LEL	Measured gas levels at top of well after initial opening reached 12% LEL, dissipated within 1 minute.
B108 (MW)	135.5	Pulaski B	Drill water forced out of the top of casing, slight sulfuric odor.	NA
B114 (MW)	NM	NM	Measured gas levels exceed 100% LEL	NA
B117 (MW)	149.5	Pulaski B	Drill water forced out of top of drill casing.	Measured gas levels at top of well after initial opening reached 8% LEL, dissipated within 1 minute.
B201 (MW)	121.0	Pulaski B	Drill water forced out of top of casing, measured gas level at 15% LEL, water bubbling at top of drill casing into next day.	NA
B206	117.0	Pulaski B	Measured gas level of 46% LEL	NA
B208 (MW)	119.0	Pulaski B	Encountered gas	NA
B211	150.0	Pulaski C	Encountered gas	NA
B213	116.0	Pulaski A/B	Encountered gas	NA
B214	126.5	Pulaski B	Encountered gas	NA
B215	116.0	Pulaski B	Drill water forced out of top of casing. Measured gas levels above 10% LEL	NA
B216 (MW)	116.0	Pulaski B	Measured gas level above 10% LEL	NA
B218	126.0	Pulaski B	Encountered gas, Measured gas levels above 100% LEL.	NA
B230 (MW)	144.0	Pulaski B	Encountered gas, Measured gas levels above 100% LEL.	NA
B235 (MW)	123.5	Pulaski B	Encountered gas, Measured gas level above 25% LEL.	NA
B238 (MW)	154.8	Pulaski B	Encountered gas, after 5 hours measured levels above 50% LEL	NA
B240	155.0	Pulaski A	Encountered gas, Measured gas levels dropped below 10% LEL within the hour.	NA
B243	135.5	Pulaski B	Encountered gas, gas vented overnight.	NA

Notes:

Gas levels measured with a VRAE Hand Held 5 Gas Surveyor manufactured by RAE Systems, Inc. of San Jose, California.
Data in this table for borings B106 (MW), B114 (MW), B206, B213, B215, B216 (MW), B218, B230 (MW), B235 (MW), B240, and B243 were collected from non-safety related documents.

Abbreviations:

LEL Lower Explosive Limit
NA Not Applicable
MW Monitoring Well

FSAR Section 2.5

Table 2.5-63—{Offshore Natural Gas Observations}

Boring Number	Observations During Drilling		
	Depth (feet)	Formation	Observation
B407	71.0	Pulaski B	Encountered natural gas.
B408	75.0	Pulaski B	Encountered natural gas.
B413	68.0	Pulaski C	Encountered natural gas (9% LEL).
B414	51.0	Pulaski B	Encountered natural gas.
B431	59.5	Pulaski A	Encountered natural gas near bottom of C8
B441	60.3	Pulaski B	Encountered natural gas (6% LEL).
	130.3	Whetstone A	Encountered natural gas (18 % LEL).

Note:

Gas levels measured with a VRAE Hand Held 5 Gas Surveyor manufactured by RAE Systems, Inc. of San Jose, California.

Abbreviations:

LEL Lower Explosive Limit
NA Not Applicable

Table 2.5-64— {Liquefaction Resistance Analysis of Site Soils}

(Page 1 of 6)

Soil Zone	Boring	Sample	Estimated USCS	Depth (ft)	Elevation (ft)	N_{raw} Field	Sigma (psf)	U (psf)	Sigma' (psf)	C_N	N_1	C_R	C	$N_1[60]$	Fines Content	a	b	Equivalent $N_1[60]_{cs}$
							[1]	[1]	[1]	[2]	[3]		[4]	[5]	FC [6]	[7]	[8]	[9]
Surf. Dep.	B101(MW)	S1	SM	0.75	264.6	35	105	—	105	1.70	59.50	0.75	0.86	51.32	25	4.29	1.12	62
G. Till	B101(MW)	S2	ML	5.75	259.6	27	809	47	762	1.39	37.57	0.75	0.86	32.41	54	5.00	1.20	44
Surf. Dep.	B102(MW)	S1	ML	1.00	254.6	19	140	—	140	1.70	32.30	0.75	0.86	27.86	60	5.00	1.20	38
G. Till	B102(MW)	S4	ML/GC	11.00	244.6	76	1570	374	1196	1.22	93.00	0.80	0.92	85.56	53	5.00	1.20	108
Surf. Dep.	B104(MW)	S1	SM	0.75	255.2	19	105	—	105	1.70	32.30	0.75	0.86	27.86	25	4.29	1.12	35
G. Till	B104(MW)	S2	SM	5.75	250.2	30	809	47	762	1.39	41.75	0.75	0.86	36.01	25	4.29	1.12	44
G. Till	B104(MW)	S3	SM	11.00	244.9	29	1570	374	1196	1.22	35.49	0.80	0.92	32.65	30	4.71	1.15	42
G. Till	B104(MW)	S4	GP	16.00	50.0	31	2295	686	1609	1.10	34.03	0.85	0.98	33.26	0	0.00	1.00	33
Surf. Dep.	B106(MW)	S1	SM	1.00	255.0	10	140	—	140	1.70	17.00	0.75	0.86	14.66	25	4.29	1.12	21
Surf. Dep.	B106(MW)	S2	SM	6.00	250.0	7	845	62	783	1.38	9.68	0.75	0.86	8.35	60	5.00	1.20	15
G. Till	B108(MW)	S1	GW-GM	1.00	258.8	51	140	—	140	1.70	86.70	0.75	0.86	74.78	10	0.87	1.02	77
Surf. Dep.	B109(MW)	S1	SM	1.00	261.5	15	140	—	140	1.70	25.50	0.75	0.86	21.99	25	4.29	1.12	29
G. Till	B110(MW)	S1	SM	1.00	266.1	36	140	—	140	1.70	61.20	0.75	0.86	52.79	20	3.61	1.08	61
Surf. Dep.	B112(MW)	S1	SM	1.00	281.9	11	140	—	140	1.70	18.70	0.75	0.86	16.13	15	2.50	1.05	19
G. Till	B112(MW)	S2	SM	6.00	276.9	54	845	62	783	1.38	74.66	0.75	0.86	64.39	31	4.77	1.16	80
G. Till	B112(MW)	S3	SM	11.00	271.9	70	1570	374	1196	1.22	85.66	0.80	0.92	78.81	47	5.00	1.20	100
G. Till	B112(MW)	S4	SM	16.00	266.9	29	2295	686	1609	1.10	31.83	0.85	0.98	31.12	47	5.00	1.20	42
Fill	B116(MW)	S1	ML	1.00	293.8	56	140	—	140	1.70	95.20	0.75	0.86	82.11	50	5.00	1.20	104
Fill	B116(MW)	S2	ML	6.00	288.8	8	845	62	783	1.38	11.06	0.75	0.86	9.54	50	5.00	1.20	16
Fill	B116(MW)	S3	ML	11.00	283.8	20	1570	374	1196	1.22	24.47	0.80	0.92	22.52	70	5.00	1.20	32
G. Till	B117(MW)	S1	GM	1.00	278.0	35	140	—	140	1.70	59.50	0.75	0.86	51.32	20	3.61	1.08	59
G. Till	B118(MW)	S1	SM	1.00	292.5	48	140	—	140	1.70	81.60	0.75	0.86	70.38	40	5.00	1.20	89
G. Till	B118(MW)	S2	SM	6.00	287.5	64	845	62	783	1.38	88.48	0.75	0.86	76.31	43	5.00	1.20	97
Surf. Dep.	B201(MW)	S1	SM	1.00	254.9	33	140	—	140	1.70	56.10	0.75	0.86	48.39	40	5.00	1.20	63
G. Till	B201(MW)	S2	ML	3.00	252.9	46	420	—	420	1.56	71.77	0.75	0.86	61.90	55	5.00	1.20	79
G. Till	B201(MW)	S3	SM/GW-GM	5.00	250.9	65	700	0	700	1.42	92.26	0.75	0.86	79.57	20	3.61	1.08	90
Surf. Dep.	B203(MW)	S1	SP-SM	1.00	256.7	12	140	—	140	1.70	20.40	0.75	0.86	17.60	10	0.87	1.02	19
Surf. Dep.	B203(MW)	S2	SP-SM	3.00	254.2	17	420	—	420	1.56	26.52	0.75	0.86	22.88	10	0.87	1.02	24

Table 2.5-64— {Liquefaction Resistance Analysis of Site Soils}

(Page 2 of 6)

Soil Zone	Boring	Sample	Estimated USCS	Depth (ft)	Elevation (ft)	N_{raw} Field	Sigma (psf)	U (psf)	Sigma' (psf)	C_N	N_1	C_R	C	$N_1[60]$	Fines Content	a	b	Equivalent $N_1[60]_{cs}$
							[1]	[1]	[1]	[2]	[3]		[4]	[5]	FC [6]	[7]	[8]	[9]
Surf. Dep.	B203(MW)	S3	CL	5.00	252.2	13	700	0	700	1.42	18.45	0.75	0.86	15.91	60	5.00	1.20	24
Surf. Dep.	B204	S1	SM	1.00	258.8	15	140	—	140	1.70	25.50	0.75	0.86	21.99	35	5.00	1.20	31
G. Till	B204	S2	SM	6.00	253.8	48	845	62	783	1.38	66.36	0.75	0.86	57.24	40	5.00	1.20	74
G. Till	B208(MW)	S1	SM	1.00	264.3	20	140	—	140	1.70	34.00	0.75	0.86	29.33	15	2.50	1.05	33
G. Till	B208(MW)	S2	SC	3.00	262.3	66	420	—	420	1.56	102.98	0.75	0.86	88.82	45	5.00	1.20	112
G. Till	B208(MW)	S3	SC	5.00	259.3	47	700	0	700	1.42	66.71	0.75	0.86	57.54	45	5.00	1.20	74
G. Till	B208(MW)	S4	SC	7.00	258.3	49	990	125	865	1.35	66.03	0.75	0.86	56.95	46	5.00	1.20	73
G. Till	B208(MW)	S5	SC	9.00	256.3	58	1280	250	1030	1.28	74.39	0.75	0.86	64.16	45	5.00	1.20	82
G. Till	B208(MW)	S6	GC	11.00	254.3	85	1570	374	1196	1.22	104.02	0.80	0.92	95.69	25	4.29	1.12	111
G. Till	B208(MW)	S7	SC	13.00	252.3	67	1860	499	1361	1.17	78.39	0.85	0.98	76.62	46	5.00	1.20	97
G. Till	B210	S2	SM	6.00	260.7	59	845	62	783	1.38	81.57	0.75	0.86	70.35	30	4.71	1.15	86
G. Till	B211	S1	SM	1.00	267.3	26	140	—	140	1.70	44.20	0.75	0.86	38.12	25	4.29	1.12	47
G. Till	B211	S2	SW	6.00	262.3	32	845	62	783	1.38	44.24	0.75	0.86	38.16	5	0.00	1.00	38
G. Till	B211	S3	SM	11.00	257.3	59	1570	374	1196	1.22	72.20	0.80	0.92	66.42	30	4.71	1.15	81
G. Till	B211	S4	SM	16.00	252.3	54	2295	686	1609	1.10	59.27	0.85	0.98	57.94	25	4.29	1.12	69
G. Till	B211	S5	SM	21.00	247.3	20	3020	998	2022	1.00	19.90	0.95	1.09	21.74	30	4.71	1.15	30
G. Till	B212	S1	SM	1.00	268.4	16	140	—	140	1.70	27.20	0.75	0.86	23.46	15	2.50	1.05	27
G. Till	B212	S3	SM	11.00	258.4	58	1570	374	1196	1.22	70.98	0.80	0.92	65.30	15	2.50	1.05	71
G. Till	B212	S4	SM	16.00	253.4	34	2295	686	1609	1.10	37.32	0.85	0.98	36.48	15	2.50	1.05	41
G. Till	B213	S1	SM/GM	1.00	264.6	19	140	—	140	1.70	32.30	0.75	0.86	27.86	31	4.77	1.16	37
G. Till	B213	S2	ML	6.00	259.6	52	845	62	783	1.38	71.89	0.75	0.86	62.01	50	5.00	1.20	79
G. Till	B213	S3	ML	11.00	254.6	54	1570	374	1196	1.22	66.08	0.80	0.92	60.79	53	5.00	1.20	78
Surf. Dep.	B214	S1	SM	1.00	266.8	8	140	—	140	1.70	13.60	0.75	0.86	11.73	15	2.50	1.05	15
G. Till	B214	S2	CL	6.00	261.8	67	845	62	783	1.38	92.63	0.75	0.86	79.89	51	5.00	1.20	101
G. Till	B214	S3	CL	11.00	256.8	41	1570	374	1196	1.22	50.17	0.80	0.92	46.16	55	5.00	1.20	60
G. Till	B216(MW)	S1	SM	1.00	264.8	20	140	—	140	1.70	34.00	0.75	0.86	29.33	30	4.71	1.15	39
G. Till	B218	S1	ML	1.00	264.2	15	140	—	140	1.70	25.50	0.75	0.86	21.99	50	5.00	1.20	31
G. Till	B218	S2	ML	6.00	259.2	56	845	62	783	1.38	77.42	0.75	0.86	66.78	50	5.00	1.20	85
G. Till	B218	S3	CL	11.00	254.2	67	1570	374	1196	1.22	81.99	0.80	0.92	75.43	55	5.00	1.20	96

Table 2.5-64— {Liquefaction Resistance Analysis of Site Soils}

(Page 3 of 6)

Soil Zone	Boring	Sample	Estimated USCS	Depth (ft)	Elevation (ft)	N_{raw} Field	Sigma (psf)	U (psf)	Sigma' (psf)	C_N	N_1	C_R	C	$N_1[60]$	Fines Content	a	b	Equivalent $N_1[60]_{cs}$
							[1]	[1]	[1]	[2]	[3]		[4]	[5]	FC [6]	[7]	[8]	[9]
G. Till	B219(MW)	S1	ML	1.00	273.4	13	140	—	140	1.70	22.10	0.75	0.86	19.06	70	5.00	1.20	28
G. Till	B219(MW)	S2	SM	3.00	271.4	33	420	—	420	1.56	51.49	0.75	0.86	44.41	45	5.00	1.20	58
G. Till	B219(MW)	S3	SM	5.00	269.4	67	700	0	700	1.42	95.10	0.75	0.86	82.02	45	5.00	1.20	103
Fill	B221(MW)	S1	SM	1.00	279.0	16	140	—	140	1.70	27.20	0.75	0.86	23.46	20	3.61	1.08	29
Fill	B221(MW)	S2	SM	6.00	274.0	3	845	62	783	1.38	4.15	0.75	0.86	3.58	20	3.61	1.08	7
Fill	B221(MW)	S3	CL	11.00	269.0	3	1570	374	1196	1.22	3.67	0.80	0.92	3.38	60	5.00	1.20	9
G. Till	B221(MW)	S4	CL	16.00	264.0	58	2295	686	1609	1.10	63.66	0.85	0.98	62.23	61	5.00	1.20	80
Fill	B222	S1	SM	1.00	280.3	23	140	—	140	1.70	39.10	0.75	0.86	33.72	25	4.29	1.12	42
Fill	B222	S2	SM	6.00	275.3	27	845	62	783	1.38	37.33	0.75	0.86	32.20	25	4.29	1.12	40
Fill	B223	S1	SM	1.00	279.4	88	140	—	140	1.70	149.60	0.75	0.86	129.03	20	3.61	1.08	143
Fill	B223	S2	SM	6.00	274.4	7	845	62	783	1.38	9.68	0.75	0.86	8.35	20	3.61	1.08	13
Fill	B223	S3	SM	11.00	269.4	20	1570	374	1196	1.22	24.47	0.80	0.92	22.52	30	4.71	1.15	31
G. Till	B223	S6	SM	26.00	254.4	53	3745	1310	2435	0.91	48.24	0.95	1.09	52.70	30	4.71	1.15	66
Fill	B224	S1	ML	1.00	273.2	16	140	—	140	1.70	27.20	0.75	0.86	23.46	60	5.00	1.20	33
G. Till	B224	S2	ML	3.00	271.2	15	420	—	420	1.56	23.40	0.75	0.86	20.19	60	5.00	1.20	29
G. Till	B224	S3	CL	5.00	269.2	40	700	0	700	1.42	56.77	0.75	0.86	48.97	66	5.00	1.20	64
G. Till	B224	S6	ML	11.00	263.2	86	1570	374	1196	1.22	105.24	0.80	0.92	96.82	50	5.00	1.20	121
G. Till	B224	S7	ML	13.00	261.2	73	1860	499	1361	1.17	85.41	0.85	0.98	83.49	47	5.00	1.20	105
G. Till	B226	S1	SM	1.00	274.8	46	140	—	140	1.70	78.20	0.75	0.86	67.45	25	4.29	1.12	79
G. Till	B226	S2	SM	6.00	269.8	78	845	62	783	1.38	107.84	0.75	0.86	93.01	25	4.29	1.12	108
Fill	B227	S1	ML	1.00	280.6	42	140	—	140	1.70	71.40	0.75	0.86	61.58	70	5.00	1.20	79
Fill	B228	S1	SM	1.00	280.7	36	140	—	140	1.70	61.20	0.75	0.86	52.79	25	4.29	1.12	63
Fill	B228	S2	SM	6.00	275.7	10	845	62	783	1.38	13.83	0.75	0.86	11.92	30	4.71	1.15	18
G. Till	B228	S3	SM	11.00	270.7	46	1570	374	1196	1.22	56.29	0.80	0.92	51.79	30	4.71	1.15	64
Fill	B229	S1	SW-SM	1.00	281.8	33	140	—	140	1.70	56.10	0.75	0.86	48.39	10	0.87	1.02	50
Fill	B229	S3	ML/SM	11.00	271.8	79	1570	374	1196	1.22	96.67	0.80	0.92	88.94	40	5.00	1.20	112
Fill	B230(MW)	S1	SM	1.00	281.6	35	140	—	140	1.70	59.50	0.75	0.86	51.32	25	4.29	1.12	62
Fill	B231	S2	SM	6.00	274.9	11	845	62	783	1.38	15.21	0.75	0.86	13.12	45	5.00	1.20	21
Fill	B232	S1	SM	1.00	281.1	36	140	—	140	1.70	61.20	0.75	0.86	52.79	20	3.61	1.08	61

Table 2.5-64— {Liquefaction Resistance Analysis of Site Soils}

(Page 4 of 6)

Soil Zone	Boring	Sample	Estimated USCS	Depth (ft)	Elevation (ft)	N_{raw} Field	Sigma (psf)	U (psf)	Sigma' (psf)	C_N	N_1	C_R	C	$N_1[60]$	Fines Content	a	b	Equivalent $N_1[60]_{cs}$
							[1]	[1]	[1]	[2]	[3]		[4]	[5]	FC [6]	[7]	[8]	[9]
G. Till	B233(MW)	S1	SM	1.00	274.5	29	140	—	140	1.70	49.30	0.75	0.86	42.52	25	4.29	1.12	52
G. Till	B233(MW)	S2	SM	6.00	269.5	33	845	62	783	1.38	45.62	0.75	0.86	39.35	25	4.29	1.12	48
Surf. Dep.	B234	S1	GM	1.00	270.8	12	140	—	140	1.70	20.40	0.75	0.86	17.60	30	4.71	1.15	25
G. Till	B234	S2	SM	3.00	268.8	28	420	—	420	1.56	43.69	0.75	0.86	37.68	35	5.00	1.20	50
G. Till	B234	S3	SC	5.00	266.8	42	700	0	700	1.42	59.61	0.75	0.86	51.42	40	5.00	1.20	67
Surf. Dep.	B235(MW)	S1	SM	1.00	270.9	17	140	—	140	1.70	28.90	0.75	0.86	24.93	25	4.29	1.12	32
G. Till	B235(MW)	S2	SM	6.00	265.9	25	845	62	783	1.38	34.56	0.75	0.86	29.81	30	4.71	1.15	39
G. Till	B237	S1	ML	1.00	271.5	6	140	—	140	1.70	10.20	0.75	0.86	8.80	40	5.00	1.20	16
Surf. Dep.	B238(MW)	S1	ML	1.00	278.2	21	140	—	140	1.70	35.70	0.75	0.86	30.79	50	5.00	1.20	42
G. Till	B238(MW)	S2	ML	3.00	276.2	15	420	—	420	1.56	23.40	0.75	0.86	20.19	50	5.00	1.20	29
G. Till	B238(MW)	S3	SM	5.00	274.2	47	700	0	700	1.42	66.71	0.75	0.86	57.54	42	5.00	1.20	74
G. Till	B238(MW)	S5	SM	9.00	270.2	70	1280	250	1030	1.28	89.79	0.75	0.86	77.44	42	5.00	1.20	98
G. Till	B239	S1	ML	1.00	279.3	15	140	—	140	1.70	25.50	0.75	0.86	21.99	55	5.00	1.20	31
G. Till	B239	S2	ML	5.00	275.3	40	700	0	700	1.42	56.77	0.75	0.86	48.97	50	5.00	1.20	64
G. Till	B240	S1	ML	1.00	282.0	8	140	—	140	1.70	13.60	0.75	0.86	11.73	80	5.00	1.20	19
G. Till	B240	S2	ML	5.00	278.0	52	700	0	700	1.42	73.81	0.75	0.86	63.66	60	5.00	1.20	81
G. Till	B243	S1	ML	1.00	269.5	21	140	—	140	1.70	35.70	0.75	0.86	30.79	60	5.00	1.20	42
G. Till	B301	S1	SM	1.00	261.1	22	140	—	140	1.70	37.40	0.75	0.86	32.26	20	3.61	1.08	38
G. Till	B301	S2	SM	3.00	259.1	71	420	—	420	1.56	110.78	0.75	0.86	95.55	40	5.00	1.20	120
G. Till	B301	S3	SM	5.00	257.1	75	700	0	700	1.42	106.45	0.75	0.86	91.81	40	5.00	1.20	115
G. Till	B301	S4	SM	7.00	255.1	69	990	125	865	1.35	92.98	0.75	0.86	80.20	40	5.00	1.20	101
G. Till	B301	S5	ML	9.00	253.1	79	1280	250	1030	1.28	101.33	0.75	0.86	87.40	52	5.00	1.20	110
Surf. Dep.	B302	S1	SM	1.00	261.5	17	140	—	140	1.70	28.90	0.75	0.86	24.93	35	5.00	1.20	35
Surf. Dep.	B304	S1	SM	1.00	261.5	15	140	—	140	1.70	25.50	0.75	0.86	21.99	35	5.00	1.20	31
Surf. Dep.	B305	S1	ML/SM	1.00	259.9	9	140	—	140	1.70	15.30	0.75	0.86	13.20	45	5.00	1.20	21
G. Till	B305	S2	GM	5.00	255.9	37	700	0	700	1.42	52.52	0.75	0.86	45.30	29	4.64	1.15	57
G. Till	B306	S1	ML/SM	1.00	255.3	3	140	—	140	1.70	5.10	0.75	0.86	4.40	40	5.00	1.20	10
G. Till	B307	S1	ML	1.00	253.7	5	140	—	140	1.70	8.50	0.75	0.86	7.33	60	5.00	1.20	14
Surf. Dep.	B308	S1	ML	1.00	253.4	2	140	—	140	1.70	3.40	0.75	0.86	2.93	80	5.00	1.20	9

Table 2.5-64— {Liquefaction Resistance Analysis of Site Soils}

(Page 5 of 6)

Soil Zone	Boring	Sample	Estimated USCS	Depth (ft)	Elevation (ft)	N_{raw} Field	Sigma (psf)	U (psf)	Sigma' (psf)	C_N	N_1	C_R	C	$N_1[60]$	Fines Content	a	b	Equivalent $N_1[60]_{cs}$
							[1]	[1]	[1]	[2]	[3]		[4]	[5]	FC [6]	[7]	[8]	[9]
Surf. Dep.	B308	S2	ML	3.00	251.4	6	420	—	420	1.56	9.36	0.75	0.86	8.07	65	5.00	1.20	15
Surf. Dep.	B308	S3	ML	5.00	249.4	10	700	0	700	1.42	14.19	0.75	0.86	12.24	59	5.00	1.20	20
Surf. Dep.	B308	S4	ML	7.00	247.4	6	990	125	865	1.35	8.09	0.75	0.86	6.97	60	5.00	1.20	13
Surf. Dep.	B311	S1	SM	1.00	254.4	18	140	—	140	1.70	30.60	0.75	0.86	26.39	20	3.61	1.08	32
Surf. Dep.	B311	S2	SM	3.00	252.4	18	420	—	420	1.56	28.09	0.75	0.86	24.22	15	2.50	1.05	28
Surf. Dep.	B311	S3	SM	5.00	250.4	32	700	0	700	1.42	45.42	0.75	0.86	39.17	15	2.50	1.05	44
Surf. Dep.	B311	S4	GC	7.00	248.4	26	990	125	865	1.35	35.04	0.75	0.86	30.22	25	4.29	1.12	38
Surf. Dep.	B311	S5	ML/SM	9.00	246.4	20	1280	250	1030	1.28	25.65	0.75	0.86	22.13	20	3.61	1.08	27
Surf. Dep.	B312	S1	SM	1.00	255.1	3	140	—	140	1.70	5.10	0.75	0.86	4.40	15	2.50	1.05	7
Surf. Dep.	B312	S2	SM	6.00	250.1	20	845	62	783	1.38	27.65	0.75	0.86	23.85	20	3.61	1.08	29
G. Till	B312	S3	GM	11.00	245.1	42	1570	374	1196	1.22	51.40	0.80	0.92	47.28	15	2.50	1.05	52
Surf. Dep.	B313	S1	SM	1.00	256.2	5	140	—	140	1.70	8.50	0.75	0.86	7.33	15	2.50	1.05	10
Surf. Dep.	B313	S2	CL	6.00	251.2	0	845	62	783	1.38	0.00	0.75	0.86	0.00	57	5.00	1.20	5
Surf. Dep.	B313	S3	GM/CL	11.00	246.2	10	1570	374	1196	1.22	12.24	0.80	0.92	11.26	55	5.00	1.20	19
Surf. Dep.	B314	S1	SM	1.00	257.4	10	140	—	140	1.70	17.00	0.75	0.86	14.66	15	2.50	1.05	18
G. Till	B314	S2	GM/SC	6.00	252.4	48	845	62	783	1.38	66.36	0.75	0.86	57.24	21	3.78	1.09	66
G. Till	B314	S3	GM	11.00	247.4	24	1570	374	1196	1.22	29.37	0.80	0.92	27.02	15	2.50	1.05	31
G. Till	B315	S1	ML	1.00	261.7	12	140	—	140	1.70	20.40	0.75	0.86	17.60	60	5.00	1.20	26
G. Till	B315	S2	ML	3.00	259.7	85	420	—	420	1.56	132.62	0.75	0.86	114.39	60	5.00	1.20	142
G. Till	B315	S3	ML	5.00	257.7	26	700	0	700	1.42	36.90	0.75	0.86	31.83	60	5.00	1.20	43
G. Till	B315	S4	ML	7.00	255.7	90	990	125	865	1.35	121.28	0.75	0.86	104.60	60	5.00	1.20	131
G. Till	B315	S6	ML	11.00	251.7	33	1570	374	1196	1.22	40.38	0.80	0.92	37.15	60	5.00	1.20	50

Notes

[1] Total stress, pore water pressure, and effective stress based on depth of groundwater and estimated unit weights.

[1A] Ground water depth based on five observation wells in soil (B120 (MW) through B124 (MW)). Data from January and February, 2008, which are first stabilized readings after time of drilling. Depth to water ranged from 2.5 to 5.8 feet below ground surface. Depth = 5 ft used as typical at time of drilling.

[2] C_N - Overburden correction factor from Youd et. al. (2001), where $C_N = 2.2/(1.2 + \sigma'_{vo}/P_a)$ with a maximum value of $C_N = 1.7$, and where Pa is 1.0 tons per square foot.

[3] N_1 is $N_{raw} \times C_N$

Table 2.5-64— {Liquefaction Resistance Analysis of Site Soils}

Soil Zone	Boring	Sample	Estimated USCS	Depth (ft)	Elevation (ft)	N_{raw} Field	Sigma (psf)	U (psf)	Sigma' (psf)	C_N	N_1	C_R	C	$N_1[60]$	Fines Content	a	b	Equivalent $N_1[60]_{cs}$
							[1]	[1]	[1]	[2]	[3]		[4]	[5]	FC [6]	[7]	[8]	[9]

Notes continued

[4] Correction factor for sampling, $C = C_H * C_L * C_D * C_R$, where

C_H =	correction for hammer type	1.00	(cal. automatic trip)
C_L =	correction for liner	1.15	(No liner)
C_D =	correction for borehole diameter	1.00	4-inch OD hole
C_R =	correction for drill rod length	0.75	(depth < 10')
		0.80	(10'< depth <13')
		0.85	(13'< depth < 20')
		0.95	(20'< depth < 33')
		1.00	(33'< depth)

[5] $N_1[60] = N_1 \times C$

[6] 31 Percent fines from laboratory testing 25 Percent fines estimated from boring logs (no box)

[7] α from equations 6a through 6c of Youd et. al. (2001), where $\alpha = 0$ for FC<=5%; $\alpha = 5.0$ for FC>=35%, else $\alpha = \exp[1.76-(190/FC^2)]$

[8] β from equations 7a through 7c of Youd et. al. (2001), where $\beta = 1.0$ for FC<=5%; $\beta = 1.2$ for FC>=35%, else $\beta = [0.99 + (FC^{1.5}/1000)]$

[9] $N_1[60]_{cs} = \alpha + \beta(N_1[60])$

Samples of glacial till with corrected blowcount ($N_1[60]_{cs}$)less than 30 blows/foot.

Depth to Groundwater (See Note 1A):	5	ft
Estimated Unit Weight of Soil Above Groundwater:	140	pcf
Estimated Unit Weight of Soil Below Groundwater:	145	pcf

Figure 2.5-1—{Site Location Map 200-Mile (322 km) Radius}

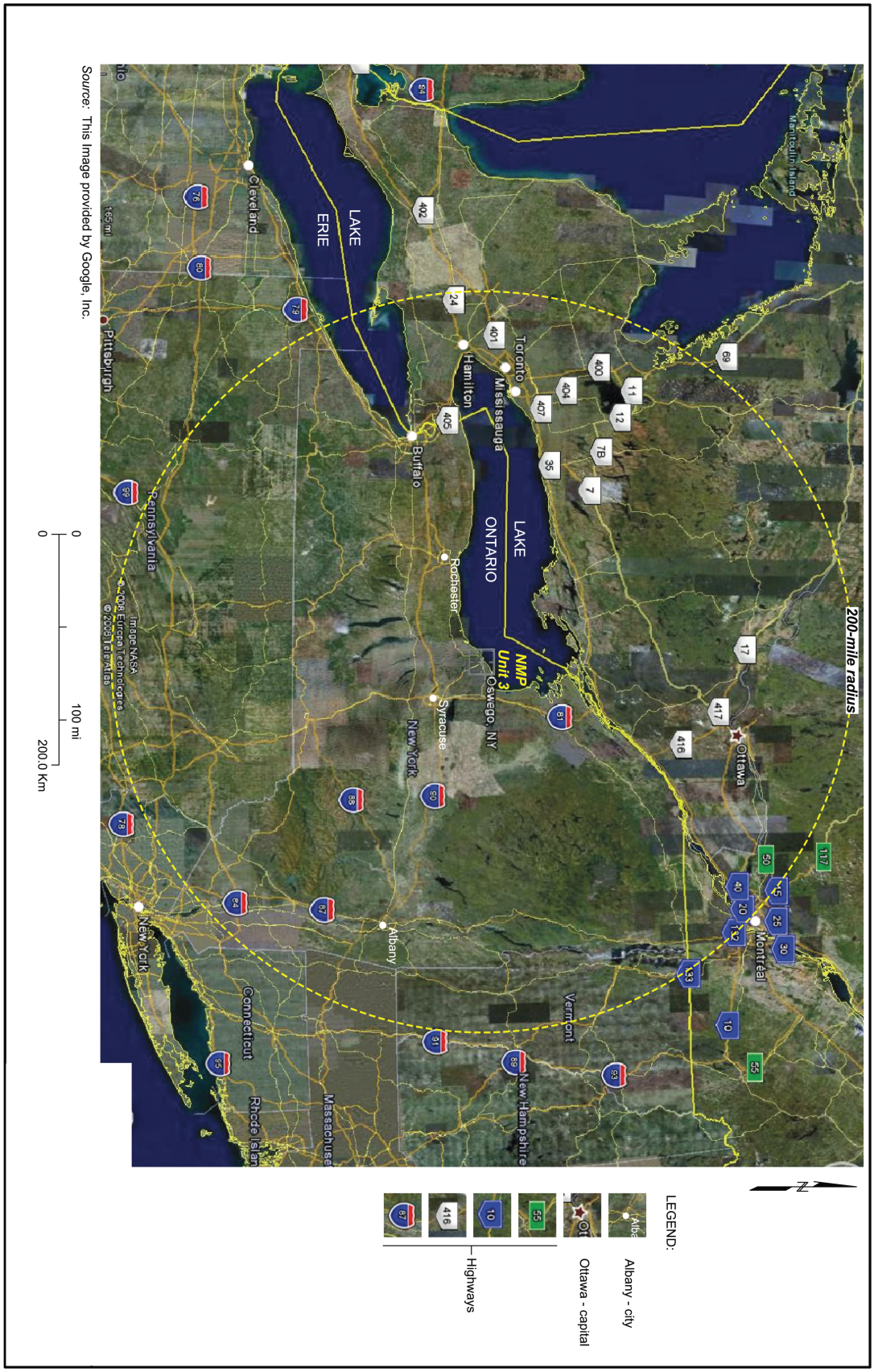

Figure 2.5-2—{Regional Geologic Map}

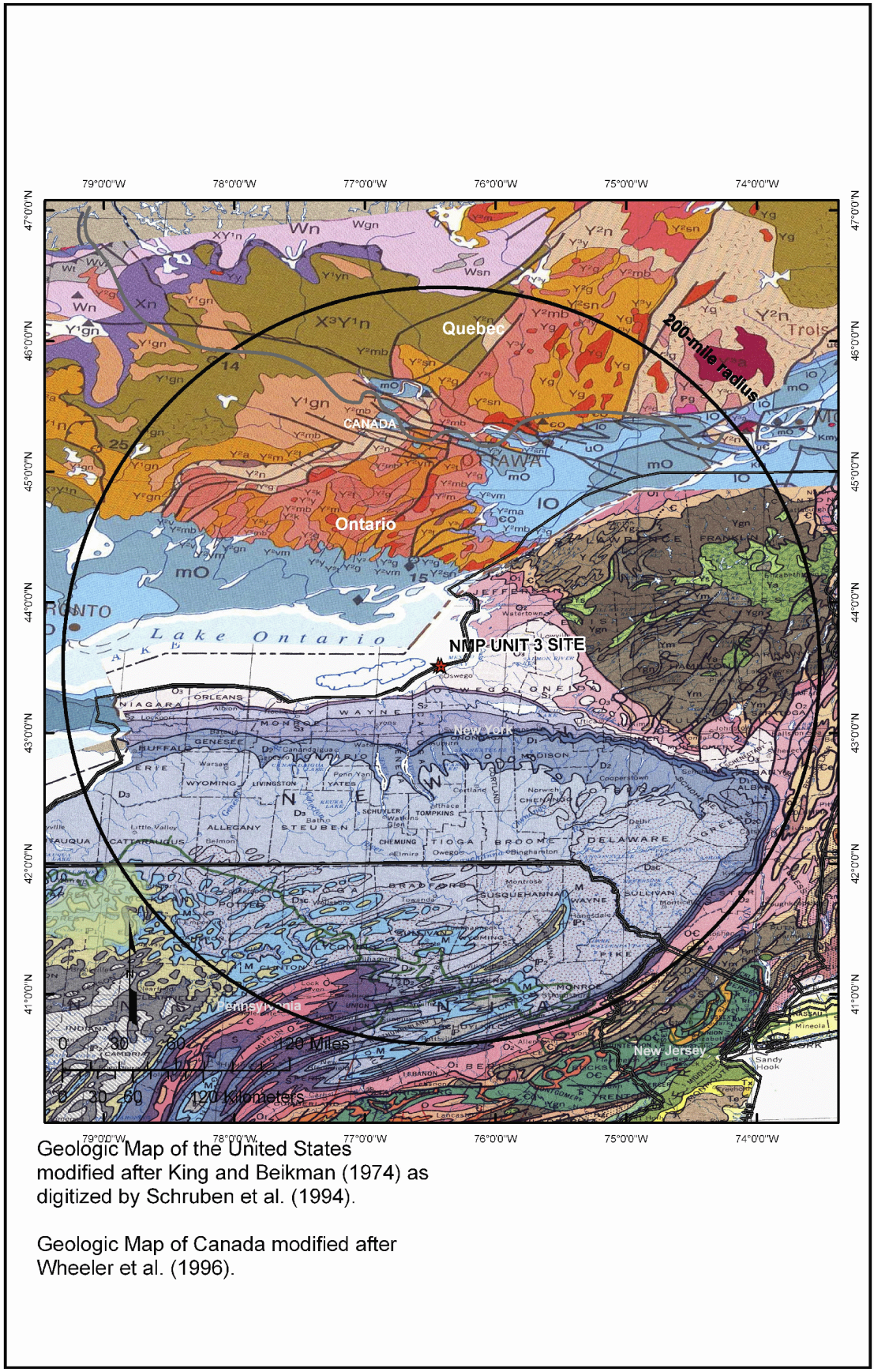

Geologic Map of the United States modified after King and Beikman (1974) as digitized by Schruben et al. (1994).

Geologic Map of Canada modified after Wheeler et al. (1996).

Figure 2.5-2a—{Regional Geologic Map}

Figure 2.5-2b—{Regional Geologic Map}